NONLINEAR ANALYSES OF COMPOSITE PREFLEX STEEL BEAMS ENCASED IN CONCRETE

Dr. Raad K. Al-Azawi
Lecturer. /Civil Eng. Dept.
College of Eng. / University of Baghdad.

Yousif S. Jafar
Master research student /Civil Eng. Dept.
College of Eng. / University of Baghdad.

ABSTRACT:

In the present study, a nonlinear three-dimensional finite element analysis has been used to predict the load-deflection and moment-rotation behaviors of composite encased beams consisting of preflex steel sections using the finite element computer program (**ANSYS V. 10**). Composite encased beams are analyzed and a comparison is made with available experimental moment-rotation curves, good agreement with the experimental results is observed. Camber of steel section is introduced on the steel section of the composite beams encased in concrete. It is found that using of preflex section can increase the ultimate load capacity of the composite encased beam by relatively (15%) and also it is found that rotations are nearly (65% to 80%) the rotations of the same beam without preflex steel section. Parametric studies have been carried out to study the increasing of the moment-carrying capacity due to the use of encased concrete for the laminated partially encased beams; meanwhile the slip along the composite partially encased beams length is studied. The strain distributions along the steel section and encased concrete depth are also examined. Poisson's ratio of concrete, the effect of cambering of steel-section and the effect of mesh refinement are also investigated.

KEYWORDS: Concrete Encasement, Finite Element Analyses, ANSYS Computer Program, Preflexing, Headed Studs.

الخلاصة:

أستخدم في الدراسة الحالية، طريقة العناصر المحددة للتحليل اللاخطي ثلاثي الابعاد و ذلك لغرض تحري علاقة منحنى كل من الحمل – الهطول و كذلك العزم – الدوران للعتبات المركبة و التي تحتوي على عنصر فولاذي مثني مغلف بالخرسانة وباستخدام برنامج العناصر المحددة للتحليل الانشائي الـ(**ANSYS V. 10**). تم تحليل العتبات المركبة ذوات المقاطع المغلفة و تمت مقارنة نتائج منحنيات العزم –الدوران مع النتائج العملية المتوفرة، تم ملاحظة توافق جيد بين النتائج المستحصلة من البرنامج و النتائج العملية. تم توليد تحديب (أنثناء) في المقطع الفولاذي للعتبات المركبة المغلفة بالخرسانة. لقد لوحظ بأن استخدام المقاطع المثنية في العتبات المركبة و المغلفة بالخرسانة يؤدي الى زيادة قابلية تحمل تلك العتبات بمقدار (١٥٪)، و كذلك لوحظ بأن الدوران يتراوح مابين (٦٥٪ الى ٨٠٪) من الدوران للعتبات التي تحتوي على مقاطع مثنية. تم دراسة تأثير وجود الخرسانة المغلفة على زيادة قابلية تحمل العزوم للعتبات القشرية المركبة و المغلفة جزئياً بالخرسانة، في تلك الاثناء تم دراسة التزحلق الذي يحدث في سطح الاتصال و على طول العتب للعتبات المركبة أيضاً. بالاظافة الى ذلك تم دراسة نمطية توزيع الانفعالات على العمق الكامل للمقاطع الفولاذية و كذلك الخرسانة المغلفة. و اخيراً، تم التحقق من تاثير كل من (Poisson's ratio)، مقدار تحدب (ثني) المقطع الفولاذي و مقدار نعومة (دقة) النموذج المعمول بالـ(**ANSYS**) على قابليات تحمل العتبات المركبة.

INTRODUCTION

In civil engineering construction fields, the merits of materials are based on many factors such as availability, structural strength, durability and workability. It is hardly surprising to know that there is no naturally occurring material "till now" possessed all these properties to a certain desired level, and from this fact, the engineer's efforts foxed on combining more than one material to each other to form a structural member with the aim that only the desirable properties of each material will be utilized by virtue of designated position. Structural member consist of two or more materials is known as "composite member" [1]. In present study, the term composite member refer to the steel beam (section) mantled (fully and partially encased) to reinforced concrete by mechanisms of natural bond (adhesion and friction) with or without the presence of mechanical connector (shear connectors). Encasement of a steel shape increases its stiffness, energy absorption, and drastically reduces the possibility of local buckling of the encased steel. This type of composite member has been used in Japan for more than (4 decades)-(**Wakabayashi 1987**). It also becomes increasingly popular to use the concrete encased steel members in building construction in Taiwan after the **Ji-Ji** earthquake in (1999). A design guide for this type of structural member can be found from the latest edition of the steel reinforced concrete **(SRC)** structures design standards published by **Architectural Institute of Japan** (**AIJ** 2001). Past studies of composite concrete encased steel members have concentrated on the strength and behavior of columns or beam columns **(Procter 1967; Furlong 1968; Naka et al. 1977 Johnson and May 1978; Mirza 1989; Ricles and Paboojian 1994; El-Tawila et al. 1995; Mirza et al. 1996; Munoz and Hsu 1997a, b; El-Tawil and Deievlein 1999**).

<u>Composite Beams Of Concrete Encased Structural Steel Section:</u>

The earliest known form of steel-concrete composite construction, dating from the late (1800s), comprised a steel beam fully or partially encased in concrete, as shown in (Fig. 1). The arrangement was first used in a bridge in **Iowa** and a building in **Pittsburgh**. The encasement provides fire protection but also enhances the bending strength of the steel beam [2].

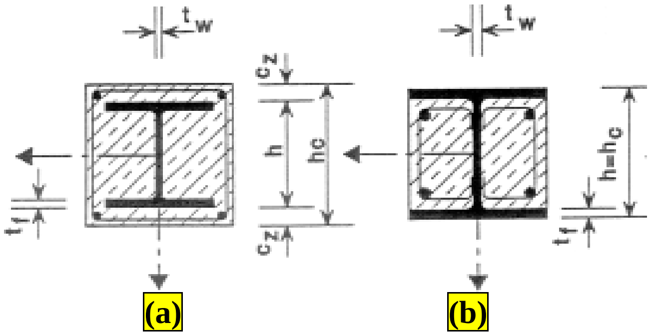

<u>Fig. 1.</u>Composite Beam of Concrete Encased Steel Section [3]:
(a) Fully Encased Composite Beam, (b) Partially Encased Composite Beam.

The local buckling strength also increases in relation to the steel section, and the overall height of both composite beam and composite floor is reduced. In addition, lower construction cost compared to reinforced concrete construction or steel frame system and also shorter construction time can be obtained through the using of encased beams. Therefore, the concrete cast within the flanges of the steel beam is an innovative and interesting alternative that needs to be investigated in details [4]. (Fig. 2). shows different form of composite beam encased (fully or partially) steel section that used nowadays.

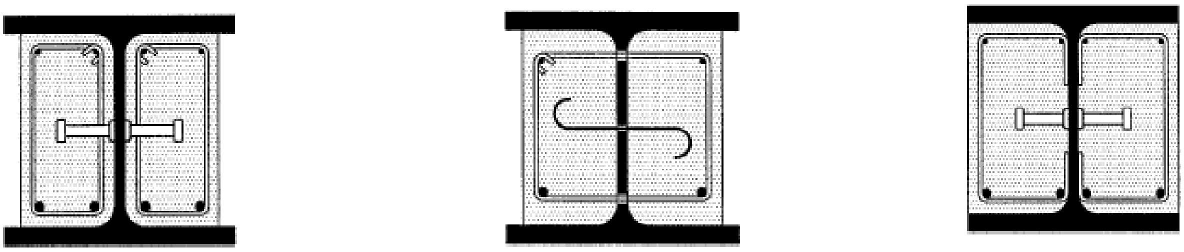

(a) (b) (c)

Fig. 2. Different Form of Steel–Concrete Composite Encased Beams [4, 5]: (a) Steel Profile with Studs and Closed Stirrups, (b) Steel Profile with Stirrups through the Web, (c) Steel Profile with Studs and Open Stirrups Welded to the Web.

Preflex Beam:

Preflex beam is a composite beam, which is maximizing the structural advantage of both steel frame and reinforced concrete; it is produced by cambering the steel beam upwards over the span using suitable propping or jacking systems. Preflex beams have been used successfully in a number of road bridges as well as building structures. The typical construction sequence of a precambered beam is as follows [6], see (Fig. 3):

a. In the plant, setup a straight steel I-girder.
b. Prebend the steel girder by applying two concentrated loads at one-third of the span from both sides by using suitable propping or jacking systems.
c. Cast the concrete in form of fully or partially encasement around the steel girder while keeping in place the loads of the prebending phase of the girder.
d. after the hardening of concrete, remove the prebending loads. As a result, the beam goes down, the precamber becomes smaller than the original precamber and the concrete is now subjected to compression [6].

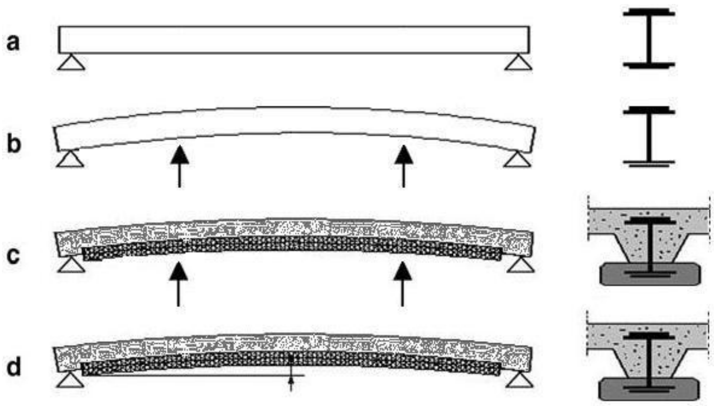

Fig. 3. Schematic Showing Construction Stages of Preflex (precambered) Beam [6].

AVAILABLE EXPERIMENTAL RESEARCH:

Works on encased composite beams dates back to the beginning of the last century, a series of testes have been conducted on this type of composite beam to study the influence of the concrete encasement on the behavior of steel beam section under different loading conditions. In the present study, **Hegger and Goralski, in (2006) [7]**, tested specimens (S1, S2, S3 and S4) are chosen to verify the applicability of **ANSYS** computer program to analyze the encased composite beams and also to investigate the main parameters that affected it's the behavior.

DETAILS OF THE TEST SPECIMENS:

A total of eight simply support (full-scale) laminated composite beams composed of structural steel beam (rolled section) partially encased in high strength concrete were tested under two concentrated loads [7]. Variables of the beams were the studs connecting the encasement with the steel profile. The beams (S1, S3, H1 and H3) were fully shear connected according to (**EURO CODE 1994**); the remaining beams (S2, S4, H2, and H4) contained only one stud above each support for fixing reasons. For the present study the tested specimens (S1, S2, S3, and S4) are chosen. The headed studs of (19 mm) diameter and total post-weld height (125 mm-connect the steel section with the laminated slab) and (120 mm to 80 mm-connect the steel section with the concrete encasement) were directly welded on each side of the web or top flange of the steel section. The aim of studing these experimental beams were to investigate the effectiveness of the high strength concrete encasement (C80/95)-(compression strength equal to 95 N/mm2) under positive and negative bending moment. The cross-sections and loading arrangement for the tested specimens are shown in (Fig. 4), and (Fig. 5). The dimensions of the steel sections, gross-sections and failure mode are given in (Table 1). The material properties are given in (Table 2).

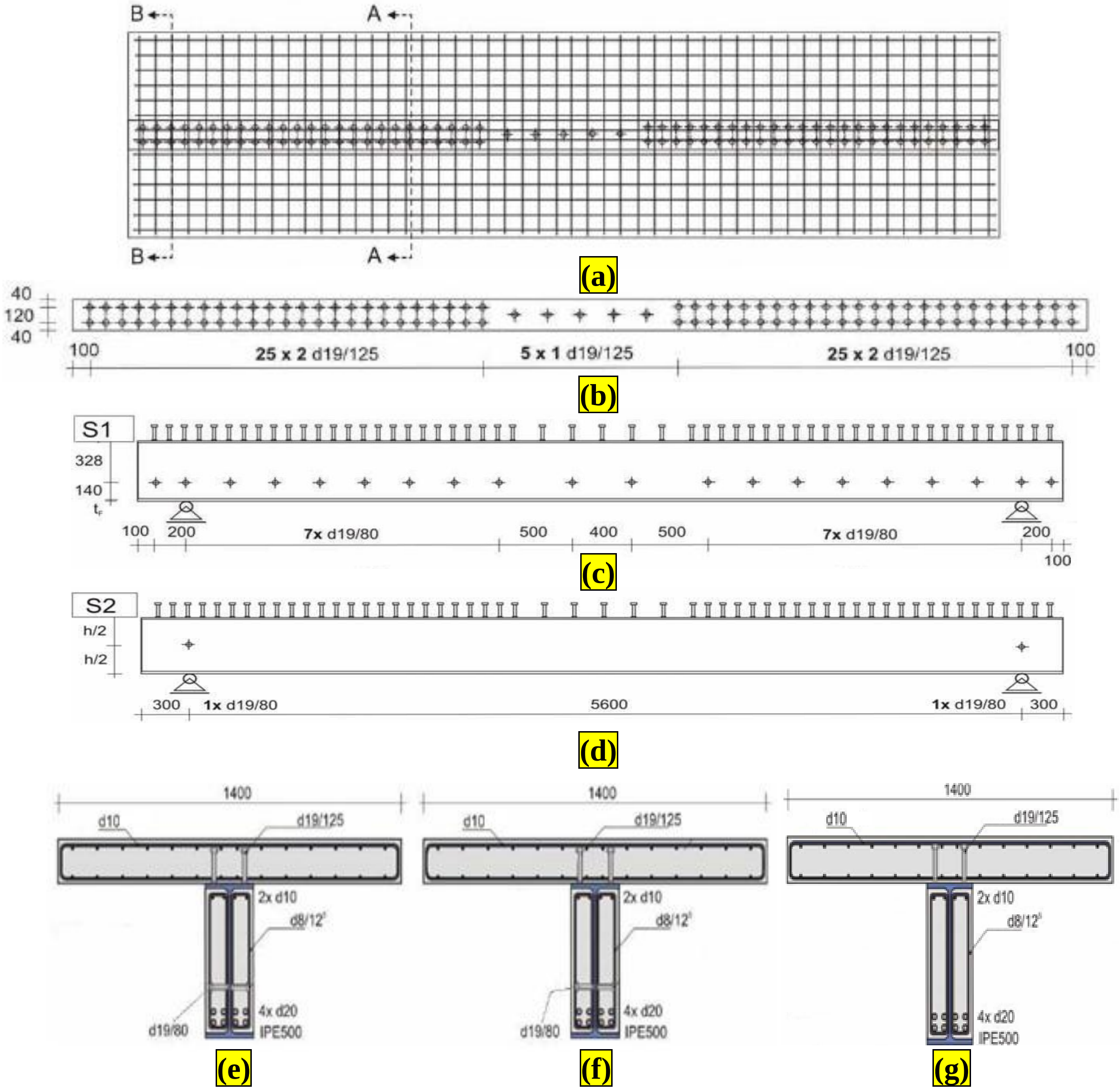

Fig. 4. **Geometry of the Laminated Partially Encased Tested Specimens [7]: (a) Flexural and Shear Reinforcement Distributions in the Top Slab (S1+S2), (b) Studs Distribution on the Top Flange (S1+S2), (c) Studs Distribution on the Web (S1), (d) Studs Distribution on the Web (S2), (e) Section (A-A) Specimens (S1+S2), (f) Section (B-B) Specimen (S1), (g) Section (B-B) Specimen (S2), (All dimensions in mm).**

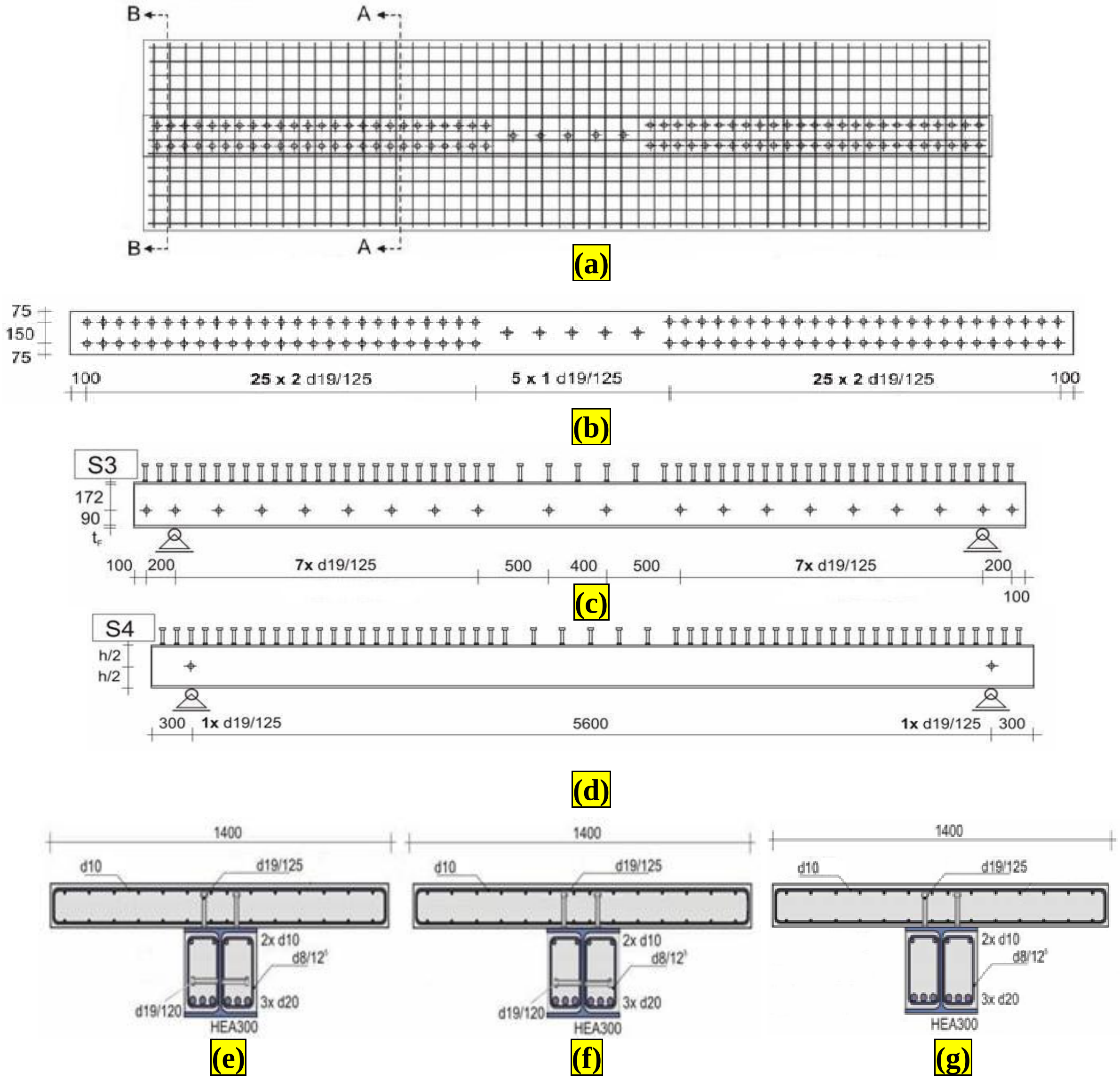

Fig. 5. Geometry of the Laminated Partially Encased Tested Specimens [7]: (a) Flexural and Shear Reinforcement Distributions in the Top Slab (S3+S4), (b) Studs Distribution on the Top Flange (S3+S4), (c) Studs Distribution on the Web (S3), (d) Studs Distribution on the Web (S4), (e) Section (A-A) Specimens (S3+S4), (f) Section (B-B) Specimen (S3), (g) Section (B-B) Specimen (S4), (All dimensions in mm).

Table 1: Descriptions, Dimensions of Steel Sections and Dimensions of Gross-Sections of the Tested Specimens.

Analyzed (Tested) specimen	Steel shape (ds×bf×tw×tf) (mm)	Cross-Section Dimensions(mm)
S1	{500X200X10.2X16}	SLAB(1400X140)
		BEAM(500X200)
S2	{500X200X10.2X16}	SLAB(1400X140)
		BEAM(500X200)
S3	{290X300X8.5X14}	SLAB(1400X140)
		BEAM(290X300)
S4	{290X300X8.5X14}	SLAB(1400X140)
		BEAM(290X300)

Table 2: **Material Properties of the Analyzed (Tested) Specimens.**

Analyzed (Tested) specimen	**S1**		**S2**		**S3**		**S4**	
	BEAM	**SLAB**	**BEAM**	**SLAB**	**BEAM**	**SLAB**	**BEAM**	**SLAB**
Concrete								
Compressive strength-(f'c)-(N/mm2)(♦)	89.000	55.000	83.000	52.000	85.000	53.000	89.000	48.000
Tensile strength-(f_{cr})-(N/mm2)(♥)	5.860	4.610	5.660	4.480	5.730	4.520	5.860	4.300
Young modulus- (Ec)-(N/mm2)(♣)	44651.0	35100.9	43119.7	34130.1	43636.1	34456.8	44651.0	32791.2
Poisson's ratio-(ν)(♠)	0.2	0.2	0.2	0.2	0.2	0.2	0.2	0.2
Steel section								
Yield stress of steel-(fy)-(N/mm2)(♦)	553		553		504		504	
Ultimate stress of steel-(fy)(N/mm2)(♦)	650		650		528		528	
Young modulus- (Es)-(N/mm2)(♠)	200000	200000	200000	200000	200000	200000	200000	200000
Poisson's ratio-(ν)(♠)	0.3	0.3	0.3	0.3	0.3	0.3	0.3	0.3
Flexural reinforcement	D20 mm D10 mm	D10 mm	D20 mm D10 mm	D10 mm	D20 mm D10 mm	D10 mm	D20 mm D10 mm	D10 mm
Yield stress of steel-(fy)-(N/mm2)(♦)	529 565	565	529 565	565	529 565	565	529 565	565
Ultimate stress of steel-(fy)-(N/mm2)(♦)	659 641	641	659 641	641	659 641	641	659 641	641
Young modulus- (Es)-(N/mm2)(♠)	200000	200000	200000	200000	200000	200000	200000	200000
Poisson's ratio-(ν)(♠)	0.3	0.3	0.3	0.3	0.3	0.3	0.3	0.3
Shear reinforcement (stirrups)	D8 mm	D10 mm	D8 mm	D10 mm	D8 mm	D10 mm	D8 mm	D10 mm
Yield stress of steel-(fy)-(N/mm2)(♦)	619	565	619	565	619	565	619	565
Ultimate stress of steel-(fy)-(N/mm2)(♦)	699	641	699	641	699	641	699	641
Young modulus- (Es)-(N/mm2)(♠)	200000	200000	200000	200000	200000	200000	200000	200000
Poisson's ratio-(ν)(♠)	0.3	0.3	0.3	0.3	0.3	0.3	0.3	0.3
Shear connector (studs)	D19 mm	D19 mm	D19 mm	D19 mm	D19 mm	D19 mm	D19 mm	D19 mm

Yield stress of steel-(fy)-(N/mm2)(♠)	550	550	550	550	550	550	550	550
Young modulus- (Es)-(N/mm2)(♠)	200000	200000	200000	200000	200000	200000	200000	200000
Poisson's ratio-(ν)(♠)	0.3	0.3	0.3	0.3	0.3	0.3	0.3	0.3

Notation

Symbol	Description
(♣)	Equation (1)
(♠)	Assumed
(♥)	Equation (2)
(♦)	From test

- $E_c = 4733\sqrt{f'_c}$ ……………………………………………………………………… (1)
- $f_{cr} = 0.622\sqrt{f'_c}$ ……………………………………………………………………… (2)

Where:

E_c = Modulus of elasticity of concrete in (MPa).
f'_c= Cylinder uniaxial compressive strength (MPa).
f_{cr}= tensile strength of concrete (MPa).

FINITE ELEMENT MODEL:
SOFTWARE, ELEMENT TYPES AND MESH CONSTRUCTION:

Advances in computational features and software have brought the finite element method within reach of both academic research and engineers in practice by means of general-purpose nonlinear finite element analysis packages, with one of the most used nowadays being **ANSYS**. The program offers a wide range of options regarding element types, material behaviors and numerical solution controls, as well as graphic user interfaces (known as GUIs), auto-meshers [8], and sophisticated postprocessors and graphics to speed the analyses. In the present study, the structural system modeling is based on the use of this commercial software. The finite element types considered in the model are as follows: elastic-plastic shell **(SHELL43)** and solid **(SOLID65)** elements for the steel section and the concrete slab, respectively, and nonlinear springs **(COMBIN39)** to represent the shear connectors. Both longitudinal and transverse reinforcing bars are modeled as discrete using **(LINK8)** element. Rigid-to-flexible contact mechanisms are used to model the interface contact surface between the structural steel section and the encased concrete. The rigid target surface (encased steel section which is represented by **(SHELL43)** element) modeled with **(TARGE170)** elements, while the contact flexible surface (concrete encasement which is represented by **(SOLID65)** elements) modeled with **(CONTA173)** elements. The element **(SHELL43)** is defined by four nodes having six degrees of freedom at each node. The deformation shapes are linear in both in-plane directions. The element allows for plasticity, creep, stress stiffening, large deflections, and large strain capabilities [8]. The element **(SOLID65)** is used for three dimensional modeling of solids with or without reinforcing bars (rebars capability). The element has eight nodes and three degrees of freedom (translations) at each node. The concrete is capable of cracking (in three orthogonal directions), crushing, plastic deformation, and creep [8]. The rebars **(LINK8)** element are capable of sustaining tension and compression forces, but not shear, being also capable of plastic deformation and creep and have two nodes with three translation degrees of freedom at each node. The element **(COMBIN39)** is defined by two node points and a generalized force–deflection curve and has longitudinal or torsional capability. The longitudinal option is a uniaxial tension–compression element with up to three degrees of freedom (translations) at each node. A typical finite element mesh for a composite encased beam is shown in (Fig. 6).

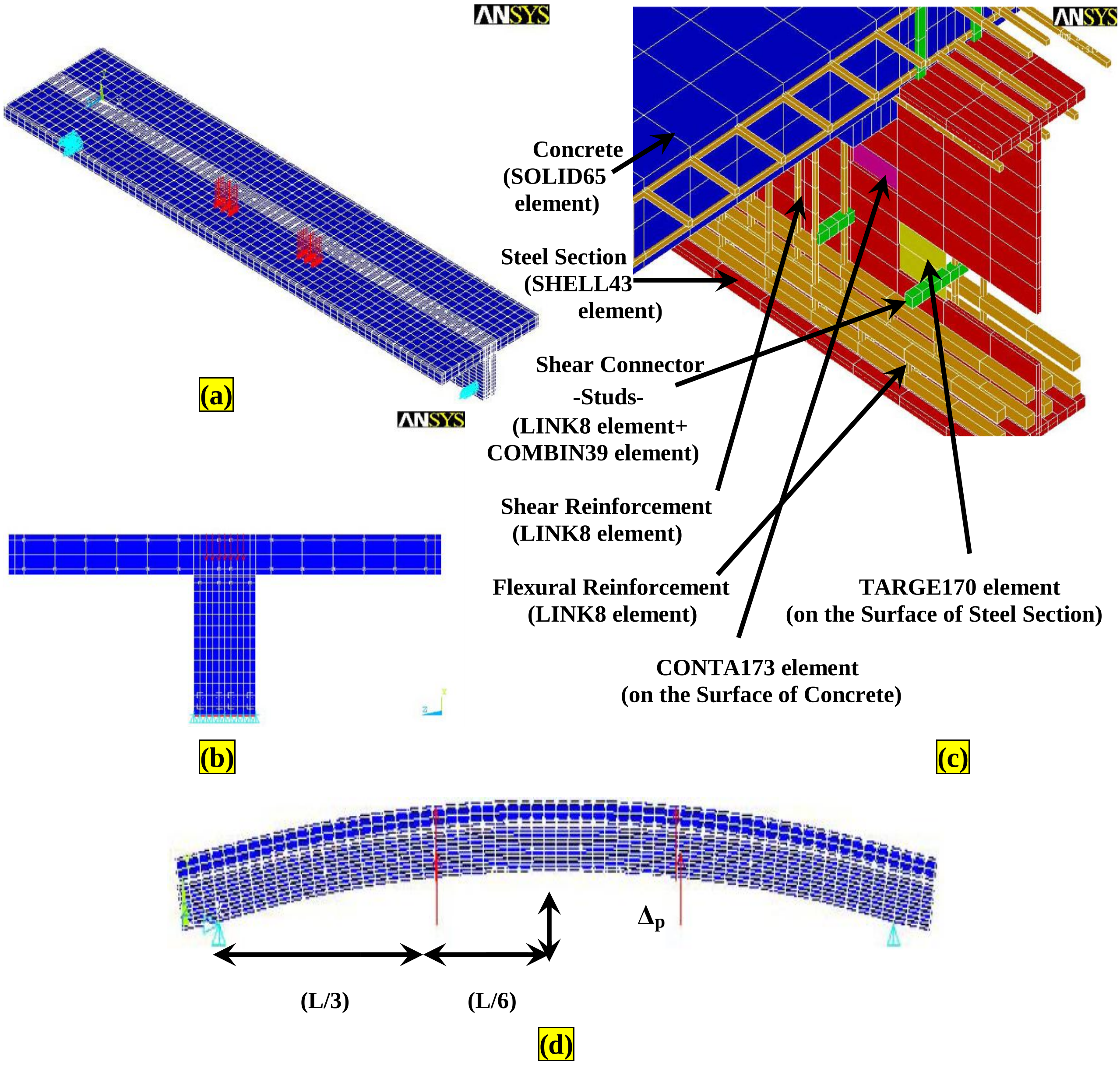

Fig. 6. Finite Element Mesh for (S1) Model:
(a) Isometric-View, (b) Front-View, (c) Internal Section, (d) Preflexing Shape.

The following equations are used to calculate the amount of forces required to produce the upward movement (cambering) of simply support steel section subjected into two forces at distance (L/3) from its two ends for a given allowable compressive stress in the steel beam [9].

Upward deflection $\Delta_p = \dfrac{23PL^3}{648EI}$ ………………………………………………… (3)

Bending moment $M = \dfrac{PL}{3}$ ………………………………………………………… (4)

Compression flange stress $\sigma = \dfrac{My}{I}$ ……………………………………………… (5)

By substituting in equation (3):

$$\Delta_p = \frac{23\sigma L^2}{216Ey} \quad \text{...} (6)$$

$$P = \frac{3\sigma I}{Ly} \quad \text{...} (7)$$

Where:

Δ_p in **(mm)**= cambering produced in the steel section.

P= force applied to the a steel section to produced cambering.

σ= Allowable compressive stress in the steel beam - (N/mm2) are given in (Table 2).

L= Clear span of the tested specimens-(mm).

E=Es= (Young modulus of steel=200,000 N/mm2).

y= Distance from the steel section centroid to the top surface of compression flange in (mm).

MATERIAL MODELIND:

The von Mises yield criterion with isotropic hardening rule (multilinear work-hardening material) is used to represent the steel beam (flanges and web) behavior. The stress–strain relationship is linear elastic up to yielding, perfectly plastic between the elastic limit and the beginning of strain hardening. The von Mises yield criterion with isotropic hardening rule is also used for the reinforcing steel. An elastic-linear-work hardening material is considered, with tangent modulus being equal to (1/10000) of the elastic modulus, in order to avoid numerical problems. The values measured in the experimental tests for the material properties of the steel components (steel beam and reinforcing bars) are used in the finite element analyses. The concrete encasement behavior is modeled by a multilinear isotropic hardening relationship, using the von Mises yield criterion coupled with an isotropic work hardening assumption. The uniaxial behavior is described by a piece-wise linear total stress–total strain curve, starting at the origin, with positive stress and strain values, considering the concrete compressive strength (f'_c) corresponding to a compressive strain of (0.2%). The stress–strain curve also assumes a total increase of (0.05 N/mm2) in the compressive strength up to the concrete strain of (0.35%) to avoid numerical problems due to an unrestricted yielding flow. The concrete element shear transfer coefficients considered are: (0.25) for open crack and (0.8) for closed crack. Typical values range from (0 to 1), where (0) represents a smooth crack (complete loss of shear transfer) and (1) a rough crack (no loss of shear transfer). The default value of (0.6) is used as the stress relaxation coefficient (a device that helps accelerate convergence when cracking is imminent). The crushing capability of the concrete element is also disabled to improve convergence. The concrete encasement compressive strength is taken as the actual cylinder strength test value. The concrete tensile strength and the Poisson's ratio are assumed as (1/10) of its compressive strength and (0.2), respectively. The concrete elastic modulus is evaluated according to equation (1) mentioned above. The model allows for any pattern of stud distribution to be considered. In all analyses, the number/spacing of studs adopted in the experimental programmers is utilized. As far as the shear connector behavior is concerned, the load–slip curves for the studs are used (obtained from available push-out tests) by defining a table of force values and relative displacements (slip) as input data for the nonlinear springs. These springs are modeled at the steel–concrete interface [10], as shown in (Fig. 7). the behavior of the interface surface of contact between the steel section and concrete encasement is modeled according to the basic **Coulomb friction model**, in which, two contacting surfaces can carry shear stresses up to a certain magnitude across their interface before they start sliding relative to each other. This state is known as sticking. The **Coulomb friction model** defines an equivalent shear stress (τ), at which sliding on the surface begins as a fraction of the contact pressure (p) as [8]:

$$\tau_{lim} = \mu p + COHE, \quad |\tau| \leq \tau_{lim} \quad \text{.......................................} (8)$$

where:

τ_{lim} = limit shear stress, τ= equivalent shear stress, μ= the friction coefficient, P= constant normal pressure, COHE= cohesion sliding resistance (stress unite).

Once the shear stress is exceeded, the two surfaces will slide relative to each other. This state is known as sliding. The sticking/sliding calculations determine when a point transitions from sticking to sliding, see (Fig. 8). **ANSYS** provides two models for Coulomb friction [8]: Isotropic friction (2-D and 3-D contact): which is based on a single coefficient of friction (MU) and the orthotropic friction (3-D contact): which is based on two coefficients of friction (MU1 and MU2). In the present study, (3-D) Isotropic friction model is used with single coefficient of friction (MU), and the cohesion sliding resistance (COHE) set to (0.00) making (Fig. 9(a)) change to (Fig. 9(b)).

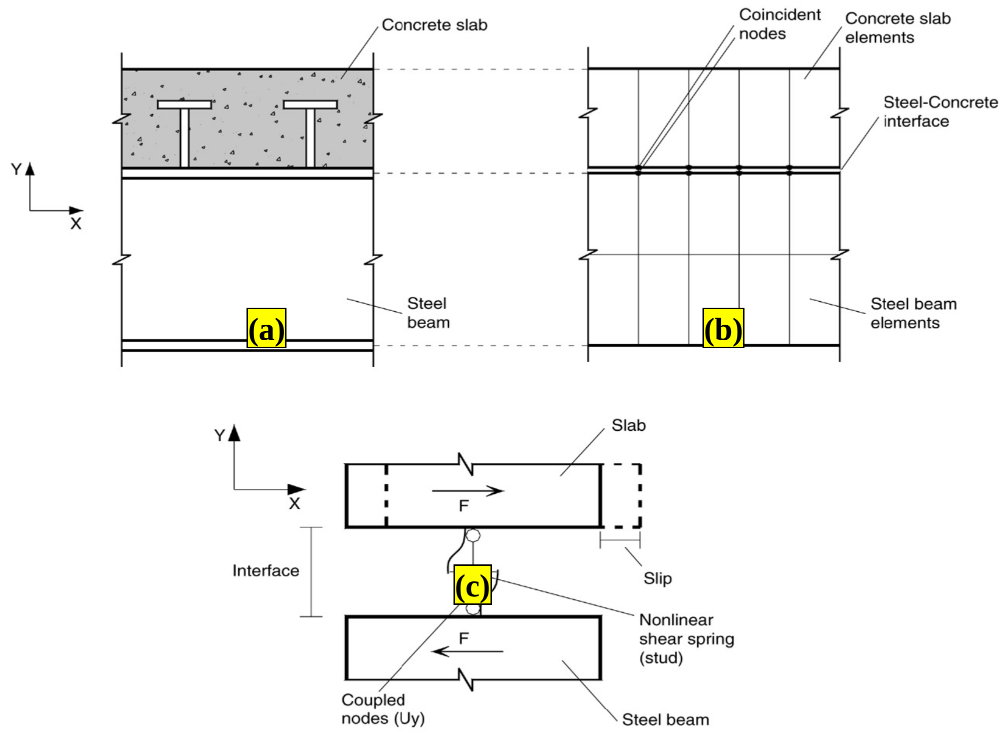

Fig. 7. Modeling of shear connectors (longitudinal view) [10]:

(a) Shear studs in a typical composite beam. (b) Shear studs in a typical composite beam finite element mesh. (c) Representation of the shear stud model.

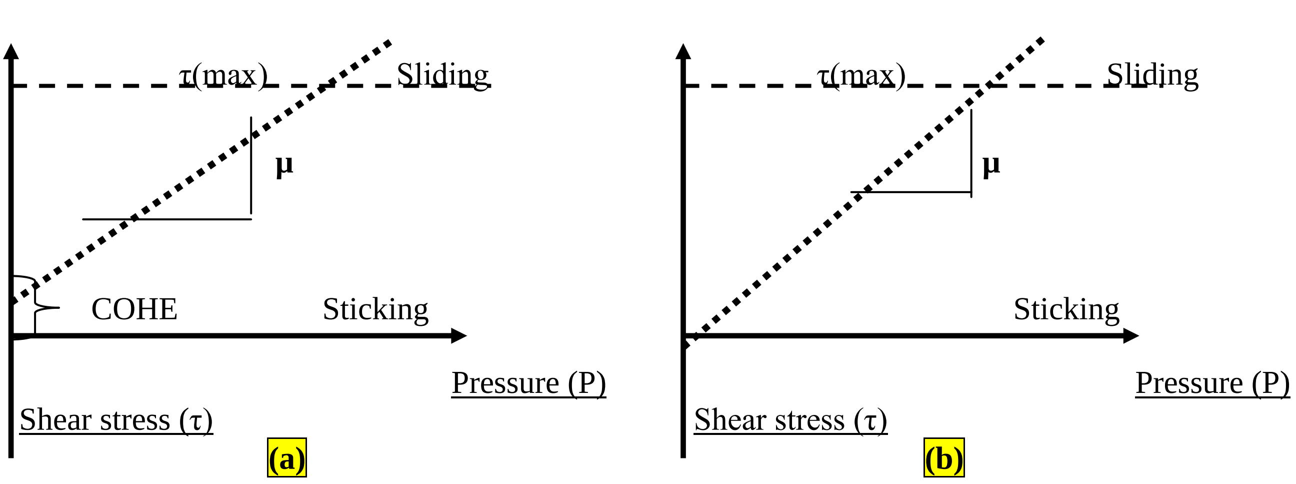

Fig. 8. Frictional Models [8].

APPLICATION OF THE LOAD AND NUMERICAL CONTROL:

Regarding application of the load, concentrated loads are incrementally applied to the model by means of an equivalent displacement to overcome convergence problems (displacement control). For the convergence criterion, the **L2-Norm** (square root sum of the squares) of displacements is considered. Concentrated loads are represented by means of point loads applied at nodes. These concentrated loads are also applied to the model incrementally using the load control strategy and the **L2-Norm**. The tolerance associated with this convergence criterion (**CNVTOL** command of **ANSYS**) and the load step increments are varied in order to solve potential numerical problems. Whenever the solution does not converge for the set of parameters considered, as far as load step size and converge criterion are concerned, the **RESTART** command is used in conjunction with the **CNVTOL** option [1]. **ANSYS** allows two different types of restart: the single-frame restart and the multi-frame restart, which can be used for static or full transient structural analyses. The single-frame restart only allows the user to resume a job at the point it stopped. The multi-frame restart can resume a job at any point in the analysis for which information is saved. This capability enables multiple model analyses, presenting more options for data retrieval after an undesired aborted solution. The second approach is used throughout the present analyses. For the case in which only one point load is applied to the system, there is a direct relationship between force and displacement, making the displacement control method easier to be utilized. The load control method is, however, less efficient than the displacement control method in nonlinear analyses. This fact is observed especially when the applied load approaches the ultimate load of the system, as an incremental increase in the load leads to a significant increase in the corresponding displacements, causing difficulties in terms of numerical convergence. For the type and size of the finite element problem investigated, the load control method demanded, on average, (70%) more disk space and took (150%) longer to be processed than similar displacement control solutions. The finite element analysis of the models was set up to examine two main behaviors: (initial cracking of the composite encased beams and the strength limit state). The Full Newton-Raphson method of analysis is used to compute the nonlinear response. The application of the loads up to failure was done incrementally as required by the Newton-Raphson procedure [1].

ANALYSIS PROCESS FOR THE ANALYZED FINITE ELEMENT MODELS:

ANALYSIS OF THE STRAIGHT ENCASED COMPOSITE BEAMS:

The finite element analyses for the straight simply support composite encased beams under concentrated forces have been carried out using static analysis type. The solution controls command dictates the use of a linear or non-linear solution for the finite element model. The program behavior upon non-convergence for this analysis was set such that the program will terminate but not exit. The most important typical commands utilized in a nonlinear static analysis are shown in Table (3). The rest of the commands were set to defaults.

Table 3: The Most Important Commands Used to Control Nonlinear Analysis.

Commands	Description
solution printout controls	all solution items such as {nodal DOF solution, nodal reaction loads, element solution (element nodal stresses+element elastic and plastic strains…etc),…etc}
print frequency	write every substep
controls for database and results file written.	all solution items such as {nodal DOF solution, nodal reaction loads, element solution (Element nodal stresses+element elastic and plastic strains…etc),…etc}
print frequency	write every substep

time at end of loadstep	**(experimental failure load)X(1.1)**
time Step size	**(1%) from the time at end of loadstep**
automatic time stepping	**on**
max no. of substeps	**time Step size**
min no. of substeps	**(10%) from the max no. of substeps**

At first trials for the analysis, the values for the convergence criteria (force and displacement) are set to defaults except for the tolerances. The tolerances for force and displacement are set as (15 times) the default values. However, when the composite encased beams began cracking, convergence for the non-linear analysis was impossible with the default values. The displacements converged, but the forces did not. Therefore, the convergence criterion for force was dropped and the reference value for the Displacement criteria was changed to (5), this value is then multiplied by the tolerance value of (0.01) to produce a criterion of (0.05) during the nonlinear solution for convergence. A small criterion must be used to capture correct response. Table (4) represents the commands used for the nonlinear algorithm and convergence criteria.

Table 4: Nonlinear Algorithm and Convergence Criteria Parameters.

Commands	**Description**	
equilibrium iteration	**100**	
criteria to stop an analysis	**stop and stay**	
Set Convergence Criteria		
Label	F (force)	U (displacements)
reference value	**calculated**	**calculated**
convergence tolerance	**0.001**	**0.010**
Norm	**L2 (SRSS value)**	**L2(SRSS value)**
Minimum reference value	**Default**	**Default**

ANALYSIS OF THE PREFLEX ENCASED COMPOSITE BEAMS:

Analyses for the preflex encased composite beams were similar to the analyses of the straight encased composite beams. However, different load steps were used. The first load step taken was to produce camber in the steel beam only in which the upward movement of the beam resulted, meanwhile all others element consisting the encased beams except the shear connector element **(COMBIN39** element) considered to be a **(DEAD ELEMENTS)** according to **(ELEMENT BIRTH AND DEATH OPTION)** supported by **ANSYS** commands. **RESTART** command then used to re-analyze the beams due to its original state of loading (Experimental Researches papers), during this, the flexural reinforcement, shear reinforcement and concrete element are re-activated **(BIRTH**) and the two preflexing forces are neutralized by two forces having the same magnitude but opposite direction. The preflexing loads are removed. As a result, the beam goes down a little due to self weight (**gravity-loads**) and the stress recovery of the steel beam, the precamber amount becomes smaller than the original cambering, and the concrete is now subjected to compression. The moment-rotation curves for analyzed laminated composite partially encased beams {{(S1+S2+S3+S4) **Hegger** and **Goralski**, (2006) [7]}} which were obtained numerically by the finite element method using **ANSYS (V.10)** computer program for straight and preflex steel section are compared with the experimental results and presented in (Fig. 10) through (Fig. 13); respectively. The goal of the comparison of the finite element models and the beams experimental works is to ensure that the elements types, meshing, material properties, real constants and convergence criteria are adequate to model the response of the beams. The angle of rotation (φ_s)-(which is idealized the X-axis of the moment-rotation curves for the analyzed specimens (S1, S2, S3 and S4) is obtained by the secant angle of the displacement at mid span and represent the rotation of cross-section of the laminated partially encased composite beams at mid span [7]. see (Fig. 9).

φ_s= Secant Angle = **ARCTAN (Δ/0.5L)** .... (9)

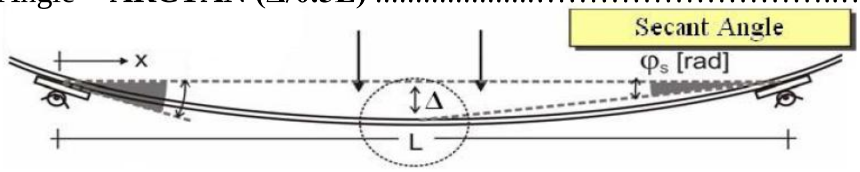

Fig. 9. Definition of the Secant Angle (φ_s) [7].

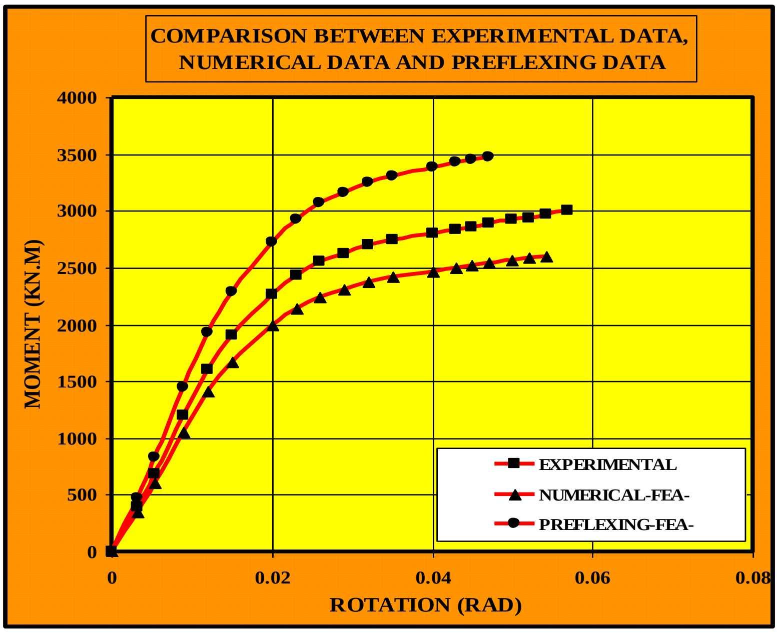

Fig. 10. Finite Element Analysis Result for Model (S1).

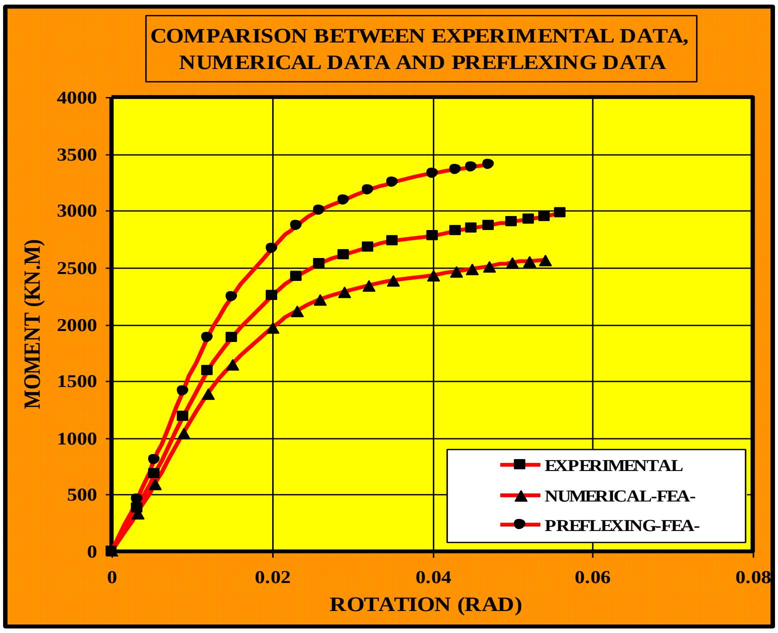

Fig. 11. Finite Element Analysis Result for Model (S2).

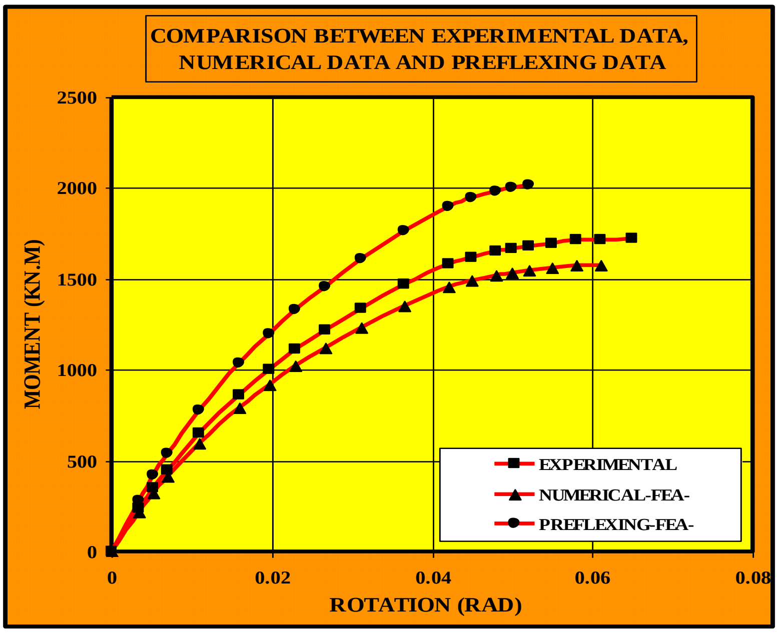

Fig. 12. Finite Element Analysis Result for Model (S3).

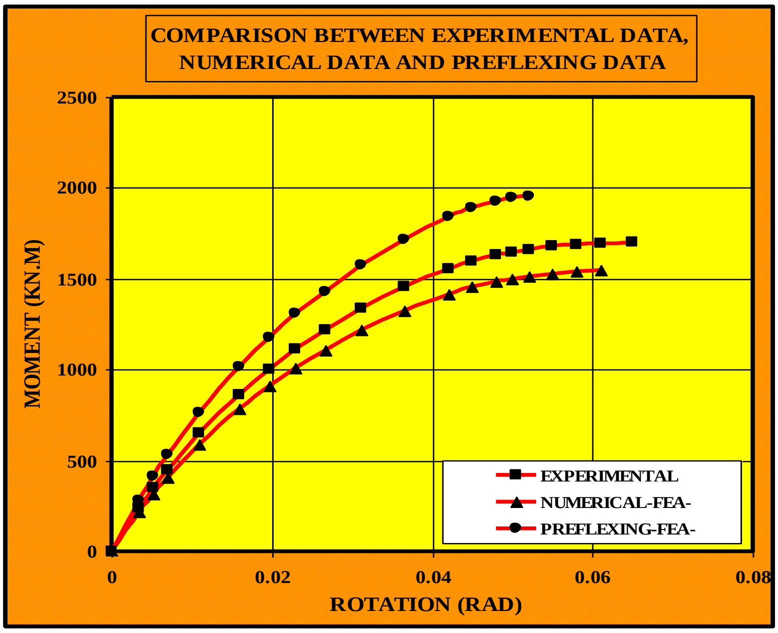

Fig. 13. Finite Element Analysis Result for Model (S4).

BEHAVIOR AT ULTIMATE MOMENTS:

The analytical and experimental values of the maximum moments for straight and preflex composite encased beams which presented in (Fig. 10) through (Fig. 13); respectively, are summarized in (Table 5). Table 5 showed that the preflexed moment of models (S1+S3)-(fully shear connection specimens) are higher than the models (S2+S4)-(partially shear connection specimens) this is due to the numerous presence of shear studs in models (S1+S3), were the longitudinal shear force occurred mainly by friction forces acting at the interface among the concrete encasement and the structural steel are well transfer by shear studs, and also the confinement effect of the steel profile in some areas of the concrete increases the preflexing capacity of the encased beams. The analyses finished (Done) for the laminated partially encased composite analyzed specimens (S1+S2+S3+S4) due to the crushing of concrete in the compression zone.

Table 5: **Comparison between Analytical and Experimental Values of the Ultimate Moments.**

Tested specimen	Experimental (maximum moments)	Analytical (maximum moments)-straight beams	A%	Analytical (maximum moments)-preflex beams	B%
S1	3001	2595	13.5	3473.78	13.6
S2	2981	2564	14	3408.89	12.5
S3	1723	1578	8.4	2014.6	14.4
S4	1703	1544	9.3	1955.8	13
Notation					
Symbol	Description				
A%	$\frac{(M_u)_{exp} - (M_u)_{\mathbf{ANSYS\text{-}Straight}}}{(M_u)_{exp}}$				
B%	$\frac{(M_u)_{\mathbf{ANSYS\text{-}Preflex}} - (M_u)_{exp}}{(M_u)_{\mathbf{ANSYS\text{-}Preflex}}}$				

BEHAVIOR AT MAXIMUM ROTATIONS:

The analytical and experimental values of the maximum rotations for straight and preflex composite encased beams are summarized in (Table 6). The moment rotations curves which presented in (Fig. 10) through (Fig. 13); respectively, for the analyzed specimens in which the corresponding experimental, theoretical and preflexing curves are superimposed, show that the curves are lie very close to each other at initial stages for all the specimens. However, there seems to be some deviation between the results near the failure. The discrepancy may be due to the inadequacy in concrete and interface behavior modeling. It was found that the rotations are nearly (85% to 95%) the rotations of the same experimental beam for straight beam situation, and (65% to 80%) of the same experimental beam for preflexed beam situation.

Table 6: Comparison between Analytical and Experimental Values of the Maximum Rotations.

Tested specimen	Experimental Rotations	Analytical (Rotations) straight beams	Analytical (Rotations) preflex beams
S1	0.057	0.054	0.046
S2	0.057	0.055	0.048
S3	0.065	0.061	0.05
S4	0.066	0.062	0.052

THE PARAMETRIC STUDY:

A parametric study has been done on the same samples that have been analyzed. Many parameters can be studied to examine the effect of each parameter on the behavior of the models results. Some models were chosen to study the effect of encased concrete in the increasing of moment-bearing capacity, meanwhile other are chosen to study the slip along the composite partially encased beams length. The strain distributions along the steel section and encased concrete depth are also examined. The Poisson's ratio of concrete and the effect of cambering of steel-section are also investigated.

EFFECT OF THE ENCASED CONCRETE IN THE INCREASING OF THE LOAD-CARRYING CAPACITY:

The partially laminated encased beams (S1) and (S3), which were described in details in (Fig. 4) and (Fig. 5), are chosen to examine the influence of the encased concrete in the steel-section on the moment-rotation capacity behavior. It is observed that the moment- rotation capacity for the composite beams (S1) and (S3) are reduced by (28.3%) and (27.4%) respectively, with the absence of the encased concrete as shown in Fig. (14) and Fig. (14) respectively. It should be mentioned that the analyses made for the composite beams (S1) and (S3) in the presence of the laminated slab and shear studs distribution on the top flange of the steel section but without encased concrete in the steel-section.

Fig. (14) and Fig. (15) respectively, shows that the moment- rotation capacity for the composite beams are reduced by (57.6%) and (63.5%) for the beams (S1) and (S3) respectively with the absence of the encased concrete and the laminated reinforced slab (steel section only).

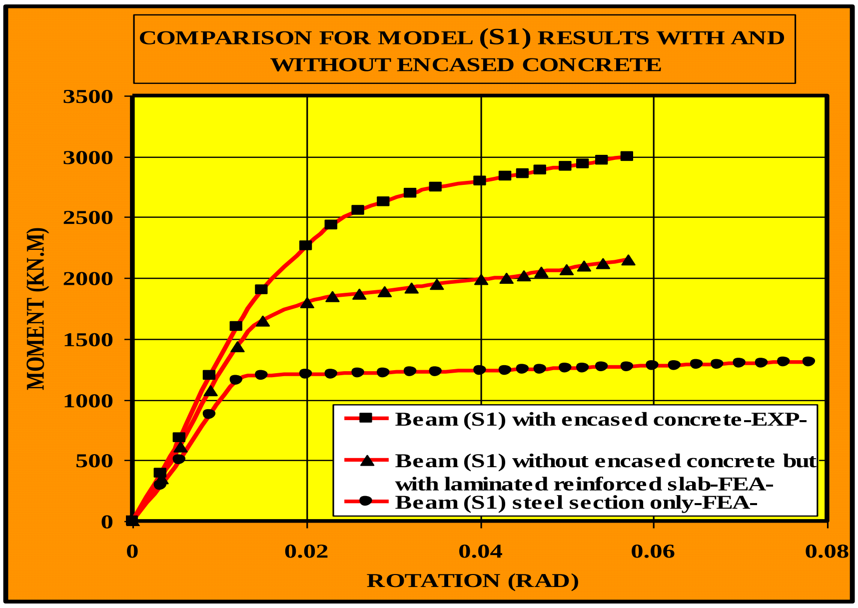

Fig. 14. **Finite Element Results of Model (S1) with and without the Encased Concrete in the Steel Section.**

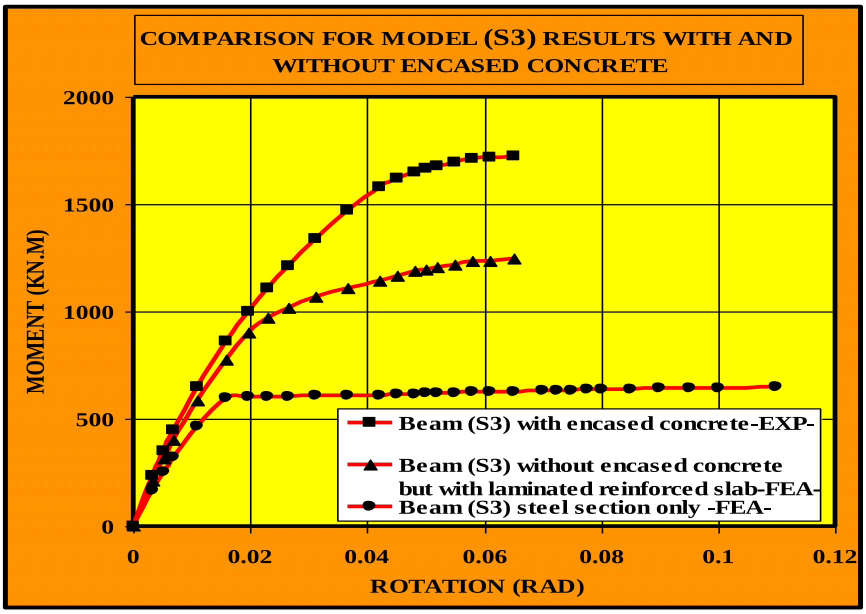

<u>Fig. 15.</u> Finite Element Results of Model (S3) with and without Encased Concrete in the Steel Section.

<u>THE EVALUATION OF SLIPS ALONG THE COMPOSITE ENCASED BEAMS INTERFACE:</u>

The partially laminated encased beams (S1), (S2), (S3) and (S4) which were described in (Fig. 4) and (Fig. 5) are chosen for the evaluation of the slip along the steel-encased concrete interface surface length under different loading magnitudes (0.5 Mu and 0.85 Mu). It is observed that the value of slips near the point of load application is more than the other values along the steel-encased concrete interface surface.

It is also observed that the values of slips for the composite encased beams (S1) and (S3) are less than (S2) and (S4) due to the presence of shear studs (full shear connections) as shown in Fig. (16) and Fig. (17) respectively. It should be mentioned that the values of the slips were obtained from the (DOF solution, X-component of displacement).

<u>Note:-</u> the slips behavior along the beams length take a nonlinear configuration, but in Fig. (16) and Fig. (17) respectively, are drawing linearly for simplifying reasons.

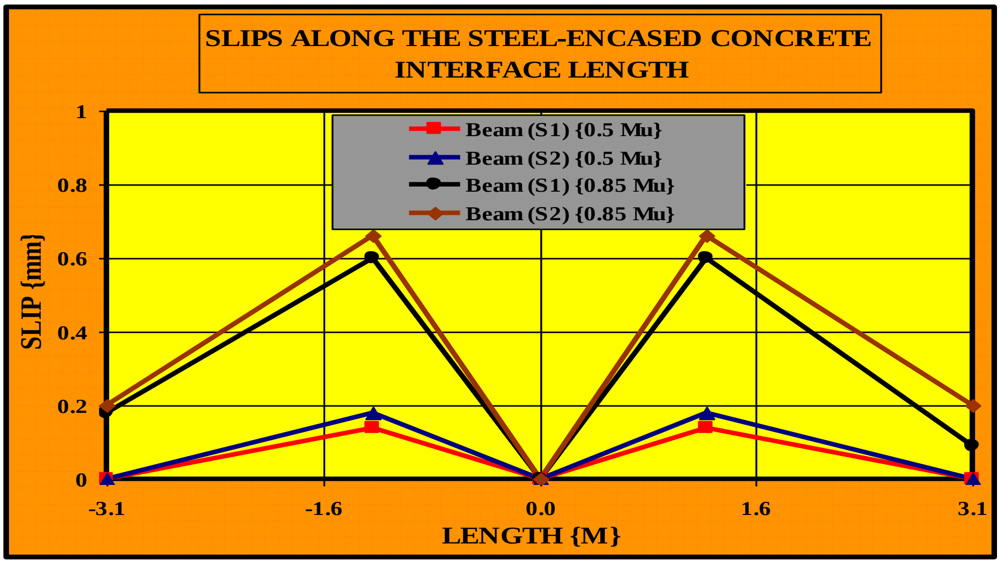

<u>Fig. 16.</u> Finite Element Results of Model (S1 and S2) to Show the Slips along the Steel-Encased Concrete Interface.

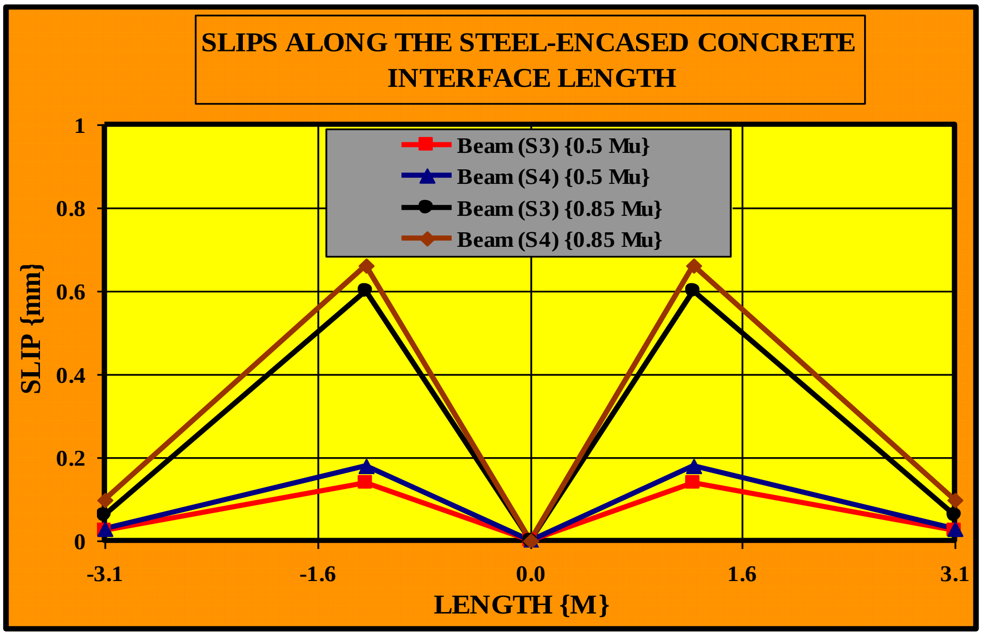

Fig. 17. **Finite Element Results of Model (S3 and S4) to Show the Slips along the Steel-Encased Concrete Interface.**

THE EVALUATION OF STRAIN DISTRIBUTIONS ALONG THE STEEL SECTION AND ENCASED CONCRETE DEPTH:

The partially laminated encased beams (S1) and (S2) which were described in details in (Fig. 4) are chosen to examine the strain distributions along the depth of both steel section and concrete encasement under different loading magnitudes as shown in (Fig. 18) through (Fig. 21).

It is observed that the values of strains at the steel-encased concrete surface (contact plane) for the model (S1) are nearly the same due to the fully shear connection of this model in comparative with the model (S2) were the strains values at the contact plane between the steel section and concrete encasement showing miner diverging due to the partially shear connection, see (Fig. 22).

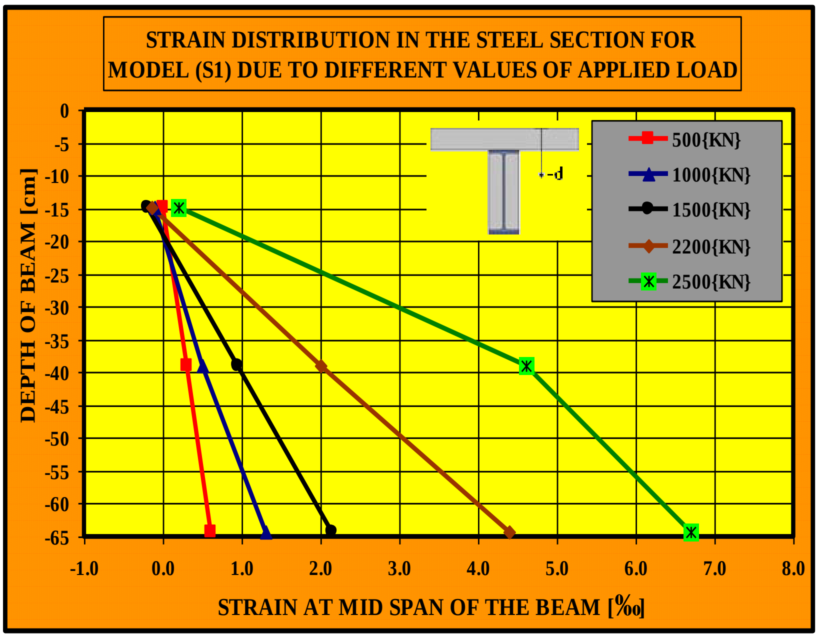

Fig. 18. **Strain Distribution along the Depth of Steel Section for Model (S1).**

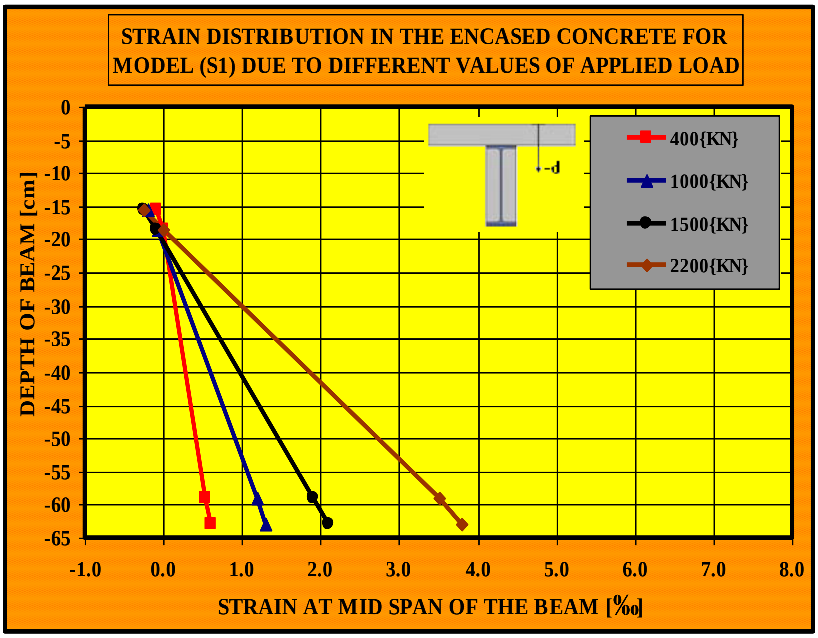

Fig. 19. Strain Distribution along the Depth of Concrete Encasement for Model (S1).

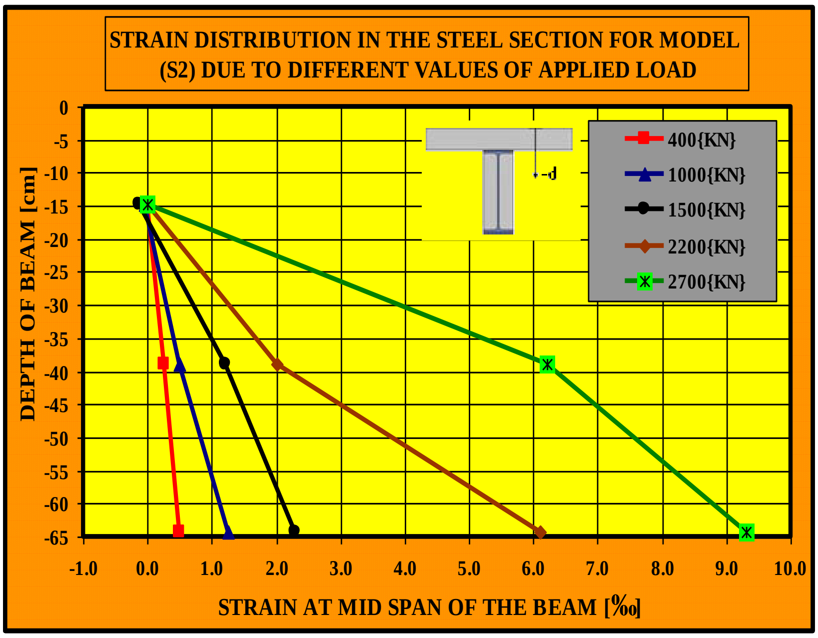

Fig. 20. Strain Distribution along the Depth of Steel Section for Model (S2).

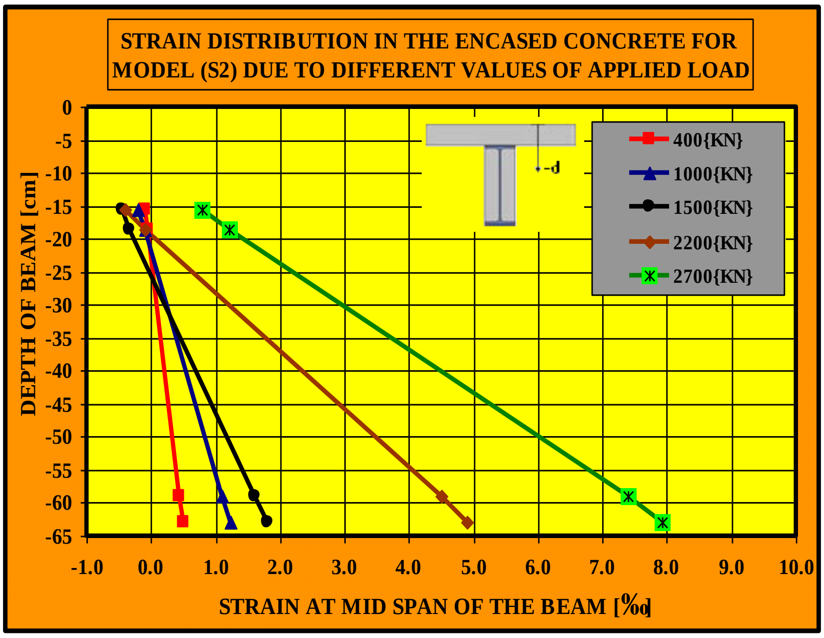

Fig. 21. Strain Distribution along the Depth of Concrete Encasement for Model (S2).

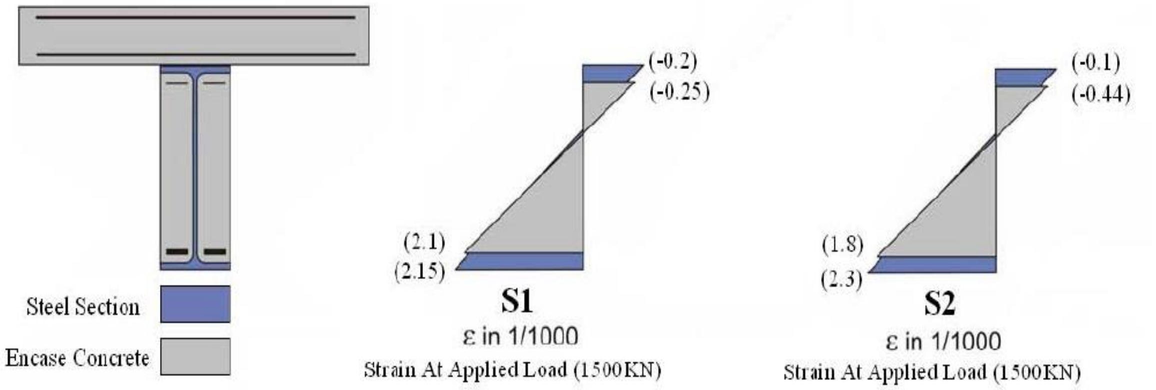

Fig. 22. Strain Difference between Models (S1) and (S2) along the Depth of Concrete Encasement and Steel Section.

Effect Of Concrete Poisson's Ratio On The Behavior Of Model (S3):

The composite encased beam (S3) has been chosen to study the effect of variation of the concrete Poisson's Ratio on its behavior. This beam is described in details in (Fig. 5). The beam has an assumed concrete Poisson's Ratio equal to (ν=0.2**)** and it has been reanalyzed for values of (0.17 and 0.15). As shown in (Fig. 23). the ultimate load capacity of this beam has also insignificant effect with reduction of Poisson's ratio value, and the ratio of reduction in the ultimate load capacity is (2.5% and 4%) for the concrete Poisson's ratio values (0.17 and 0.15) respectively.

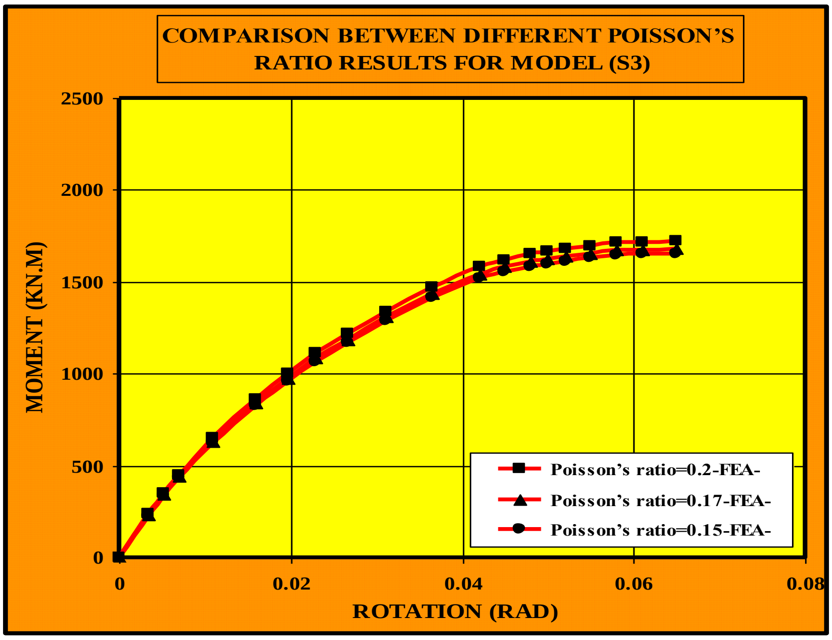

Fig. 23. **Effect of Poisson's Ratio on the Behavior of Model (S3).**

Effect Of Cambering Of Steel Section For The Model (S4):

The composite laminated partially encased beam (S4) has been chosen to study the effect of cambering of the I-steel section on its behavior. This beam is described in details in (Fig. 5). When the model is preflexed for a given allowable compressive stress in the steel equal to its yield stress (504 N/mm2), the predicted ultimate load of this beam is increased by (13%) due to an amount of upward deflection (57.989 mm) obtained by Equation (6). When the beam is reanalyzed using (250 N/mm2) for the yield stress of steel, the predicted ultimate load of this beam is increased by (6.1%) due to preflex deflection (28.78 mm), as shown in (Fig. 24).

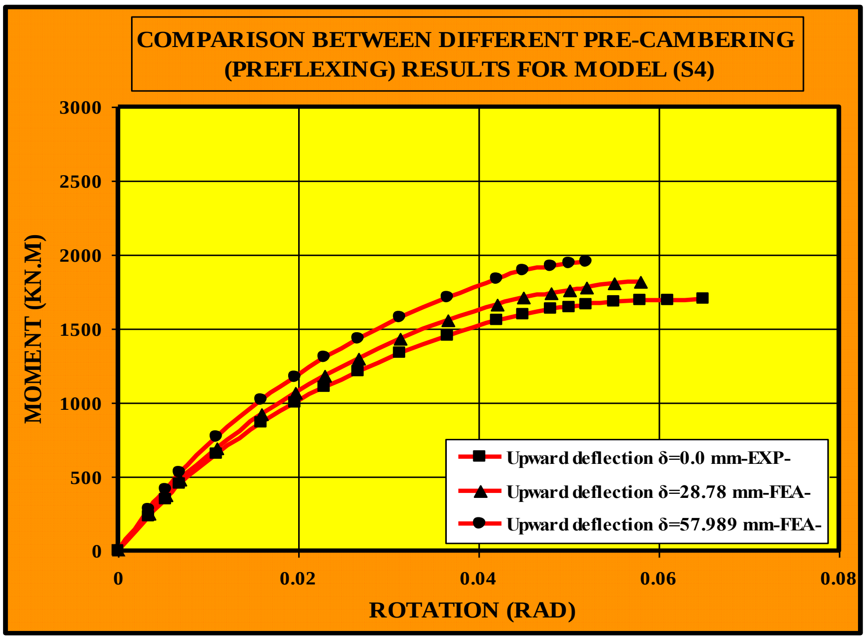

Fig. 24. **Effect of Cambering of Steel Section on the Behavior of Beam (S4).**

CONCLUSIONS:

Based on the results of this investigation, the following conclusions can be drawn:

- The modeling of the investigated beams by the finite element method gives results which are close to the experimental results for the analysis of composite encased beams consisting of preflex steel section.
- The failure load given by **ANSYS** computer program are close to that measured during experimental test.
- Preflexing of the steel I-beam by introducing initial cambering enhances the strength in comparison with the same simply supported composite beam consisting of steel section encased into concrete without preflexing by relatively (15%) and also it is found that the rotations are nearly (65% to 80%) the rotations of the same beam but without preflex.
- The load carrying capacity is higher for larger profiles than small profiles; this is due to the larger contact surface between the flange and the concrete encasement which is led to an increasing in the contact surface (bond area) between the steel section and the encased concrete and also by the lower shortening of the concrete due to the shrinkage. The confinement effect of the steel profile in some areas of the concrete also increases the load carrying capacity. When reinforcing bars and headed shear studs are combined to provide the composite action, the longitudinal shear force transfer occurred mainly by friction forces acting at the interface among the concrete encasement and the structural steel.
- The values of strains at the steel-encased concrete surface (contact plane) for the models with full shear connection are nearly the same in comparison with the same model without shear studs were the strains values at the contact plane showing miner divergence.
- The finite element results show that the Poisson's ratio has insignificant effect on the increasing or decreasing the ultimate load of the composite encased beams.

NOTATIONS:

1-D	One Dimensional Mode
2-D	Two Dimensional Mode
3-D	Three Dimensional Mode
Ec	Modulus of Elasticity of Concrete
Es	Modulus of Elasticity of Steel
f	Function
f'_c	Uniaxial Compressive Strength of Concrete
f_t	Uniaxial Tensile Strength of Concrete
P	Applied Concentrated Load
ε	Strain
ε_{cu}	Ultimate Strain
ν	Poisson’s Ratio
τ	Shear Stress
φ_s	Secant Angle
Δ_p	Cambering Produced in the Steel Section
Δ	Deflection
y	Distance from the Steel Section Centroid to the Top Surface of Compression Plange
I	Moment of Inertia
M	Bending Moment

REFEENCES:

- Yousif S. J., " Nonlinear Analysis of Composite Preflex Steel Beams Encased in Concrete", M.Sc., Thesis, University of Baghdad, Iraq, 2008.
- Airil Y. Mohd Yassina, and David A. Nethercotb, "Cross-Sectional Properties of Complex Composite Beams", Engineering Structures, Vol. 29 , 2007, pp.212–195 .
- "Steel-Concrete Composite Construction Using Rolled Sections"ARCELOR Sections Commercial S.A., Web-site:www.sections.arcelor.com, January-2005.
- Silvana De Nardin, and Ana Lucia H.C. El Debs, "Study of Partially Encased Composite Beams with Innovative Position of Stud Bolts"Journal of Constructional Steel Research, March-2008, pp.1–9 .
- Eurocode1994: Design of Composite Steel and Concrete Structures- Part 1-1: General rules And rules for buildings, English version, September 2002.
- [N. Roussel, S. Staquet, L. D'Aloia Schwarzentruber, R. Le Roy, and F. Toutlemonde, "SCC Casting Prediction for the Realization of Prototype VHPC-Precambered Composite Beams", Materials and Structures, Vol. 40, 2007, pp.877–887 .
- Josef Hegger, and Clause Goralski, "Structural Behavior of Partially Concrete Encased Composite Sections with High Strength Concrete", Composite construction in steel and Concrete, 2006, pp.346–355 .
- Swanson Analysis Systems, ANSYS. Online manual, version10.0 (2005) and Theory Reference.10th ed. Swanson Analysis Systems, s.1., s.d.
- Method of Manufacturing Preflex Beams", World Intellectual Property Organization (International Bureau), International Publication Number: WO 01/18319 A1, International Publication Date: 15 March 2001, pp 1-56.
- F.D. Queiroza, P.C.G.S. Vellascob, and D.A. Nethercota, "Finite Element Modeling of Composite Beams with Full and Partial Shear Connection", Journal of Constructional Steel Research, Vol.63, 2007, pp.505–521.

Number 3 Volume 15 September 2009 Journal of Engineering

EXPERIMENTAL INVESTIGATION OF REINFORCED CONCRETE FLEXURAL BEAMS STRENGTHENED OR REPAIRED WITH CFRP

Prof. Dr. Husain M. Husain* Assist. Prof. Dr. Nazar K. Al-Oukaili** DAWLAT D. ALI

* Building and Construction Department/ University of Technology
** College of Engineering/University of Baghdad

ABSTRACT
Fiber reinforced polymers are typically comprised of high strength fibers (e.g. carbon and glass) impregnated with an epoxy (often termed the matrix). Experimental investigations of the behavior of reinforced concrete beams, strengthened or repaired by CFRP for flexural case have been presented in this paper. The experimental program consisted of 14 test beams. The study took into account strengthened and repaired cases in using CFRP; therefore, similar beams were used once for strengthening and once for repairing to make a comparison between them. All beams had been tested in a simply supported span and subjected to two-point loading while the main variable is the quantity, distribution and location of CFRP. The beams included additional anchorage at the ends of the main CFRP sheet reinforcement to prevent end separation of CFRP sheet. The results of experiments show that the use of CFRP as external strengthening has significant enhancement on ultimate load, crack pattern and deflection. It is observed that the use of external CFRP in strengthening or repairing beams could enhance the ultimate load capacity up to 160% over the capacity of the identical reference (untreated) beam.

KEYWORDS: reinforced concrete beam, strengthening of concrete structures, repairing of R.C. structures, CFRP, Epoxy.

التحري العملي لعتبات الانثناء الخرسانية المسلحة المقواة أو المعاد تصليحها بالCFRP

الخلاصة:
الياف التقوية بالبوليمر تتالف بصورة مثالية من الياف عالية المقاومة (على سبيل المثال الكاربون او الزجاج) منغمسة بالايبوكسي. التحريات العملية لسلوك العتبة الخرسانية المسلحة المقواة او المعاد تصليحها بهذه الالياف لحالة انثناء العتبة تم تقديمها في هذا البحث. البرنامج العملي تالف من 14 عتبة فحص (عتبات انثناء) لدراسة اخذت بنظر الاعتبار حالتي التقوية واعادة التصليح لذلك صنعت عتبات متشابهه ستستعمل واحدة منها للتقوية واخرى لاعادة التصليح لعمل مقارنة بينهما. كل العتبات تم فحصها بفضاء بسيط الاسناد ومتعرضة الى نقطتي تحميل بينما المتغيرات الرئيسية كانت كمية توزيع وموقع شرائح الالياف. مجموعة عتبات الانثناء تضمنت تثبيت اضافي في نهايات صفيحة تقوية الCFRP الرئيسي لمنع انفصال صفيحة CFRP . نتائج الفحوصات العملية بينت أن استعمال CFRP كتقوية خارجية له تاثير كبير على الحمل الاقصى، شكل التشقق والهطول. تم الاستنتاج بان استعمال الCFRP الخارجي في التقوية او اعادة تصليح عتبات الانثناء يمكن ان تعزز سعة الحمل الاقصى الى 160% من سعة العتبة المصدرية المثالية.

الكلمات الدالة : عتبة خرسانية مسلحة، تقوية خرسانة مسلحة، أعادة تصليح المنشات الكونكريتية، CFRP ، غراء

INTRODUCTION

The need to develop economic and efficient methods to upgrade, repair, or strengthen existing reinforced concrete structures, Fiber Reinforced Polymer (FRP) plates or sheets or laminates have been found to be successful for flexural and shear strengthening and for ductility enhancement of concrete structures.

Strengthening of reinforced concrete beams with (FRP) composite is becoming an attractive alternative in the construction industry. These laminates offer the advantages of composite materials, such as immunity to corrosion, and allowing a high strength to weight ratio [1].

Due to the usually high cost of new construction there is an increasing need for repair, strengthening, or retrofit of (RC) structures. The concrete repair manufacturing industry is responding by producing new and more advanced materials for concrete repair and retrofit. A new structure composite technology that uses FRP has recently emerged as a very practical tool for strengthening and/or retrofitting of concrete structures, because of FRP's excellent strength to weight ratios. Reduced FRP material costs, relatively unlimited material length, comparably simpler construction and immunity to corrosion are some advantages of FRP. There are many types of FRP such as Carbon Fiber Reinforced Polymer, Glass Fiber Reinforced Polymer and Aramid Fiber Reinforced Polymer.

Carbon Fiber Reinforced Polymer (CFRP) sheets are used for strengthening and rehabilitation of beams. The advantages of using CFRP include reduced installation time, corrosion resistance and ease of application [1, 2, 3]. Also, externally bonded CFRP can be used to repair and strengthen damaged prestressed concrete girder bridges [1].

The objective of the present study is to investigate, experimentally and analytically, the behavior of reinforced concrete beams externally strengthened or repaired simple beams with Carbon Fiber Reinforced Polymer sheets (CFRP) attached to their flexural or shear sides.

EXPERIMENTAL PROGRAM:

The experimental program included fourteen beams that were designed to fail in bending (flexural). Table 1 shows the properties of these beams (with their designations).

MATERIAL PROPERTIES OF TEST SPECIMENS:

Normal weight concrete was used to cast all concrete components in the test program. Mix design was based on several trial mixes in order to have the most suitable fractions of components, and it arrives at the following proportions by weight: 1 cement; 1.5 sand; 3.0 gravel, to give a 28-day cylinder compressive strength of 41 N/mm^2 approximately. The water/cement ratio was 0.4 giving a slump of 80mm-100mm (medium workable mix). The mix design was according to ACI 211.1-91 [4].

Table 1 Concrete material properties of test beams (flexural failure)

Type of test / Beam name	**1** f_c' (N/mm^2)	**2** f_{cu} (N/mm^2)	**3** f_t (N/mm^2)	**4** f_r (N/mm^2)	**5** f_r (N/mm^2)	**6** E_c (N/mm^2)
BB1, BB2	41.3	49.2	3.62	4.88	4.49	30204
BB3, BB4	42.9	51.8	4.16	5.31	4.58	30784
BB5, BB6	42.5	55.3	3.68	5.19	4.56	30640
BB7, BB8	40.8	49	3.47	4.79	4.47	30021
BB9, BB10	44.1	53.1	3.48	4.87	4.64	31211
BB11, BB12	42.8	51	4.12	4.76	4.57	30748
BB13, BB14	40.8	49	3.6	4.85	4.47	30021

Notes (type of test):

- Concrete compressive strength by cylinder of 150mm*300mm in dimensions (adopted in the calculations of this study).
- Concrete compressive strength by cube of 150mm*150mm*150mm in dimensions.
- Concrete splitting tensile strength by cylinder of 150mm*300mm in dimensions.
- Concrete modulus of rupture (flexural strength) by prism of 100mm*100mm*500mm and loaded at third points (adopted in the calculations of this study).
- Concrete modulus of rupture according to ACI 318 [5], $f_r = 0.7\sqrt{f_c'}$ (N/mm^2).
- Concrete modulus of elasticity according to ACI 318 [5], $E_c = 4700\sqrt{f_c'}$ (N/mm^2), (adopted in the calculations of this study).

REINFORCMENT BARS

Tensile tests were conducted on several specimens, at least three specimens, prepared from steel reinforcing bars which were used in the tested beams. Static yield stress and ultimate strength are summarized in Table 2. All steel reinforcement, used in this study, is assumed to have a modulus of elasticity equals to 210000 N/mm^2. The tensile tests were performed using the testing machine available at the Building Material Laboratory in the College of Engineering, Al-Mustansiriya University. The load and elongation readings were obtained from a digital computer complementary with the testing machine.

Table 2 Specifications and test results of steel reinforcement bars.

Reinforcement bar diameter (mm)	Yield Stress f_y (N/mm^2)	Ultimate Strength f_u (N/mm^2)	Modulus of Elasticity E * (N/mm^2)
6	348	420	210000
8	355	422	210000
10	580	680	210000
12	596	685	210000
16	598	688	210000

* Assumed value.

CFRP

The uniaxial behavior of Carbon Fiber Reinforced Polymer (CFRP) sheets used in this study was assumed to be linear up to failure. Properties for the Carbon Fiber Reinforced Polymer and Epoxy systems were not determined in the laboratory. However, the properties published by the manufacturer (FOSROC) Nitowrap FRC were used to define the material properties for the analytical studies. Values of the parameters of the carbon fiber reinforced polymer are summarized in Table 3 for the specifications of the CFRP used in the present study.

Table 3 Specifications of the CFRP used in the present study (Fosroc/Nitorap)

Properties	CFRP 300HS(FRC)
Weight (g/m^2)	300
Thickness (mm)	0.167
Tensile strength (N/mm^2)	3550
Modulus of Elasticity (N/mm^2)	235000

DETAILS OF TEST BEAMS

Details of the strengthened and repaired beams by CFRP sheets are given in Table 4. Figures 1 and 2 show the general details of loading and the cross section.

Table 4 Specification of tested beams (Flexural Group)

Beam's Symbol	CFRP Locations	Working Status	Form's type
BB1 BB2	No strengthening	No strengthening	Control
BB3 BB9	External Longitudinal CFRP bonded on bottom face of beam	Strengthening	A_B
BB4 BB10	External longitudinal CFRP bonded on bottom & side faces of beam	Strengthening	B_B
BB5	External longitudinal CFRP bonded on side	Strengthening	C_B

BB11	faces of beam		
BB6 BB12	External longitudinal CFRP bonded on bottom face of beam	Repairing	A_B
BB7 BB13	External longitudinal CFRP bonded on bottom & side faces of beam	Repairing	B_B
BB8 BB14	External longitudinal CFRP bonded on sides faces of beam	Repairing	C_B

The form (A_B) represents strengthening or repairing of the flexural beams (BB) by gluing a sheet of CFRP at the bottom face of the beam (maximum tension region). This sheet has a length of 2350mm, width of 120mm, and thickness of 0.167mm. One layer of paste was used by a suitable epoxy. Two anchorage supports had been placed at the ends of the main longitudinal CFRP sheets by using a suitable epoxy as shown in Figure 3.a and b that clarify the details of form (A_B). Figures 4.a and b show the details of beams B_B and Figures 5.a and b show the details of C_B.

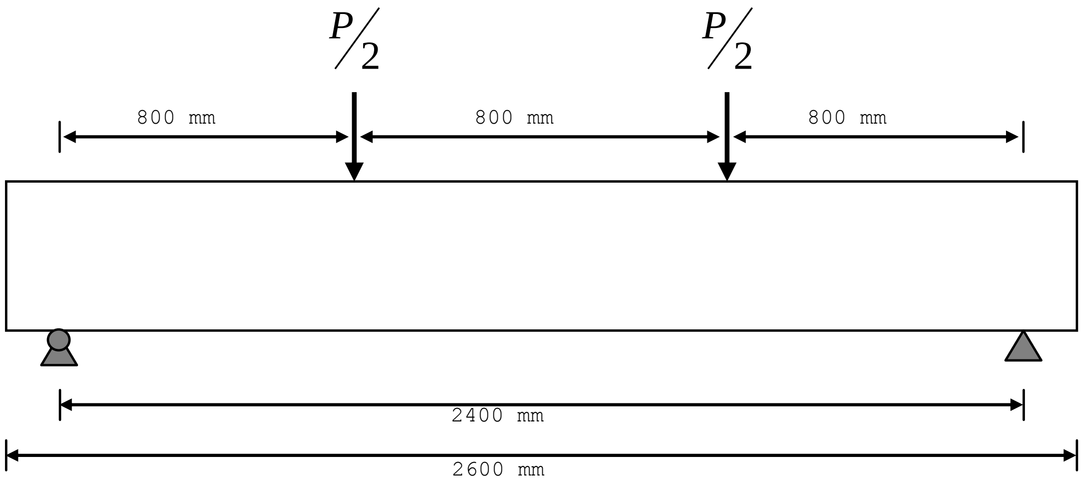

FIGURE 1 Dimensions and details of flexural beams

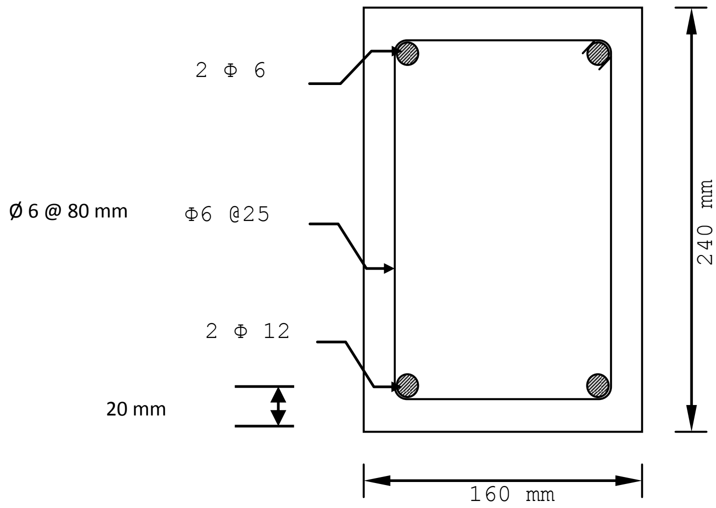

FIGURE 2 Cross section of flexural beam in shear span

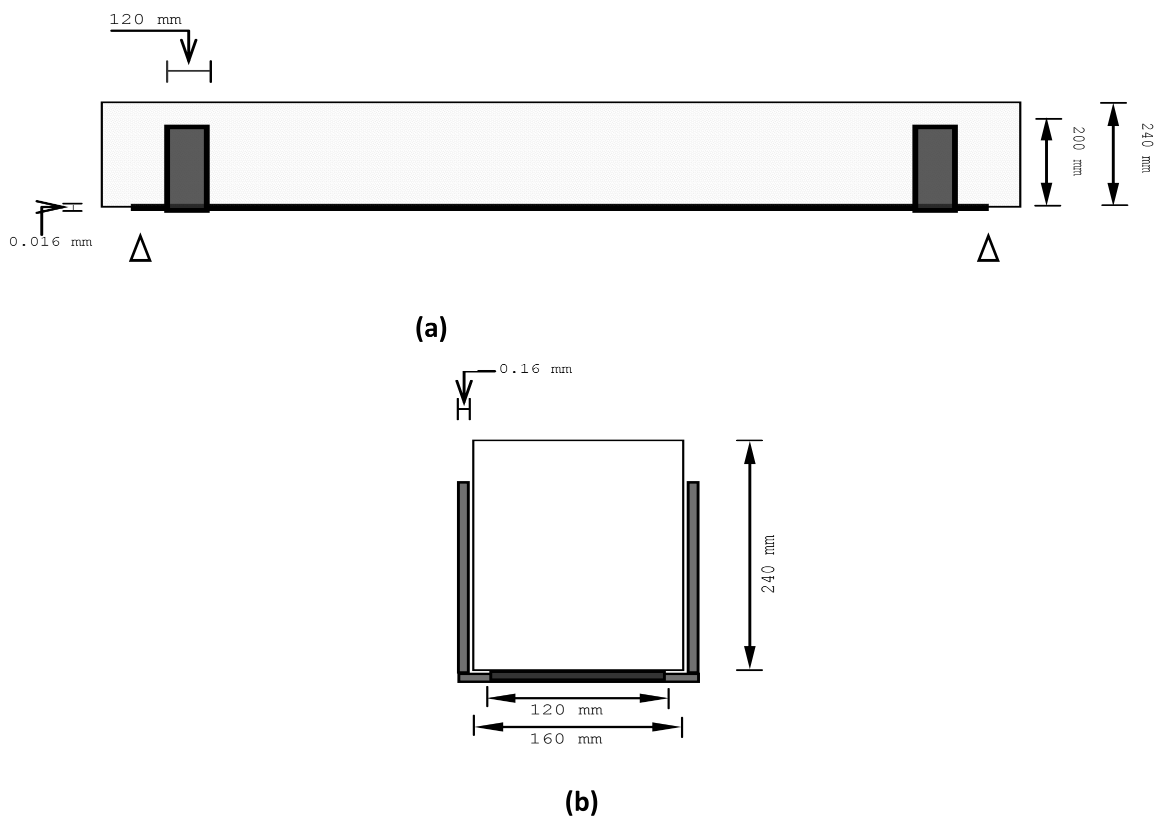

Figure 3 Specification and details of CFRP locations of beams A_B. **(a)** Front side view. **(b)** End side view

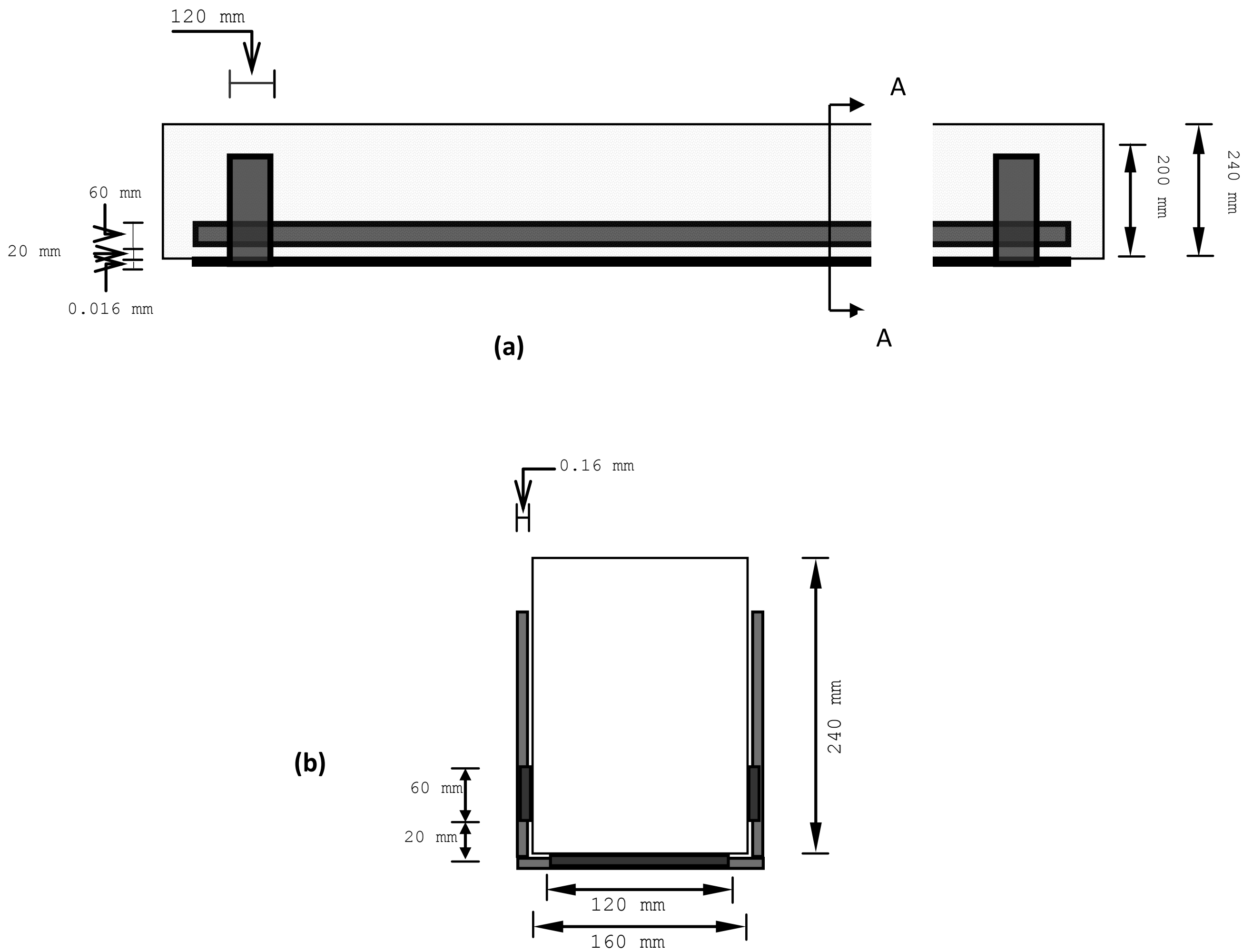

Figure 4 Specification and details of CFRP locations of beams B_B. **(a)** Front side view. **(b)** End side view (Section A-A)

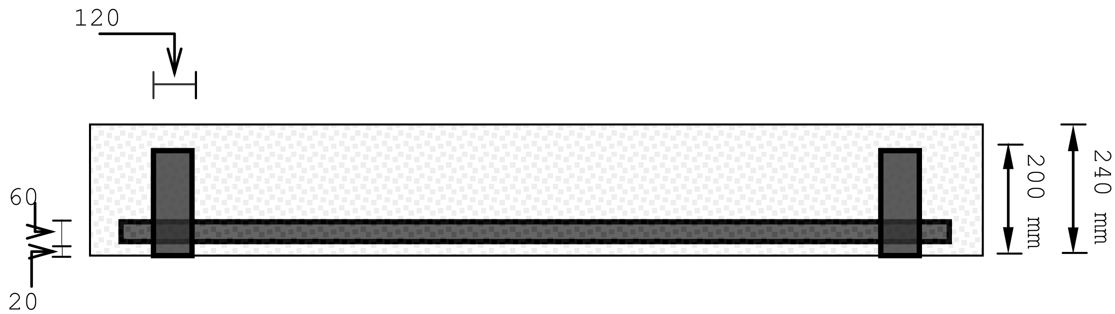

(a)

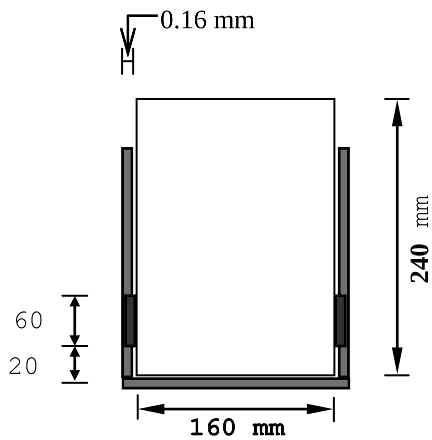

(b)

Figure 5 Specification and details of CFRP locations of beams C_B. **(a)** Front side view. **(b)** End side view

SUPPORT AND LOADING CONDITIONS

All beams were tested in a universal testing machine, model 8551 M. F. L. system, with maximum capacity of 3000kN. The adjustable supports were changed to suit the span of the test beams. The test beams were simply supported over a span of 2600mm and 2000mm (for flexural and shear groups respectively) and loaded with two-point loads (knife edge load, K.E.L.) applied and distributed across the entire width of the beams by using a solid rod. The beams were tested under static loads, loaded in successive increments, up to failure. For each increment, the load was kept constant until the required readings were recorded [6].

INSTRUMENTATION AND TEST PROCEDURE

During the test, the applied load and the corresponding deflections, at mid-span and under load (third-span of beam), were measured from the universal testing machine and the dial gauges (reading to 0.01mm); then, the outputs from each test beam were collected and used in plotting the load-deflection curves. Longitudinal strains, over the depth of the concrete layer at mid-span, were measured using 100mm demec gauge and the extensometer.

FLEXURAL GROUP

GENERAL BEHAVIOR

All beams were designed so that failure would occur in flexure. All the details were according to ACI building code requirements. The steel reinforcement and the concrete strength were selected to satisfy this demand. The general behavior of the tested beams can be summarized as below,

For the control beams, at early stages of loading, the deformations were initially within the elastic ranges, then the applied load was increased until the first crack occurred which was observed by a magnifying glass in the maximum moment region between the two-point loads. As the load was increased further, several flexural cracks initiated in the tension face at intervals along the span.

When the load was increased further, one mode of failure appeared which can be classified as flexural failure in tension by yielding of the main steel reinforcement.

The strengthened beams also showed similar behavior, but when the load level attained the value at which the steel is yielding, the CFRP contributed mainly in resisting the loads and increased the stiffness of the concrete beams up to failure. The failure was usually recorded due to sudden cut (rupture) of main longitudinal CFRP sheet at mid-span (maximum moment region). In case of repaired beams, the failure was similar to that observed in strengthened beams [6].

CONCRETE CRACKING

In the present study, the cracks initiated from the bottom concrete surface at the maximum moment region and moved upwards but did not reach the top fiber compression zone. Figures 6 and 7 show photographs for crack patterns for the control beams (BB1) and (BB2).

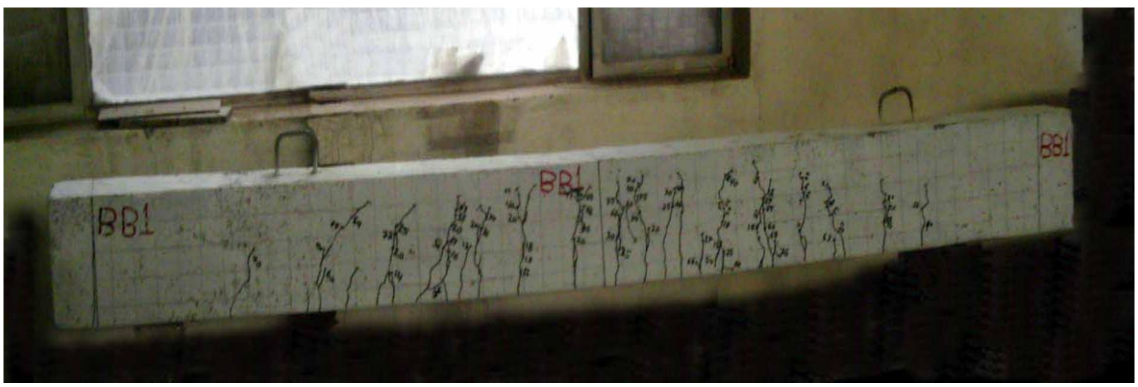

Figure 6 Crack pattern for beam BB1- control beam

Figure 7 Crack pattern for beam BB2- control beam

Figures 8 and 9 show the crack pattern for a beam strengthened with CFRP located at the bottom face of the beam. No major shear crack was noticed. Failure occurred by yielding of reinforcement and followed by CFRP rupture.

(a)

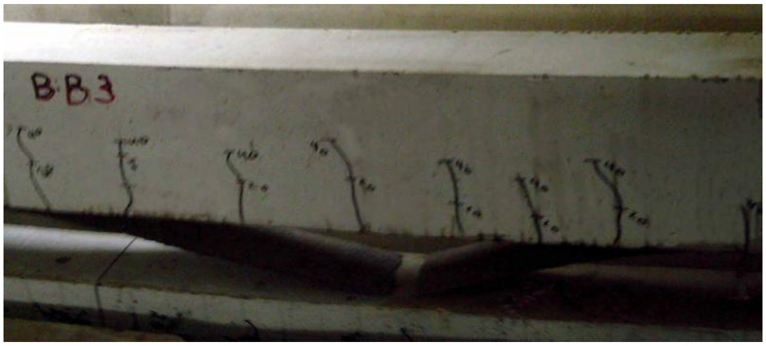

(b)

Figure 8 Crack pattern for beam BB3- strengthened beam (bottom face). **(a)** Cracks on overall beam. **(b)** Magnified picture for cracks at mid-span.

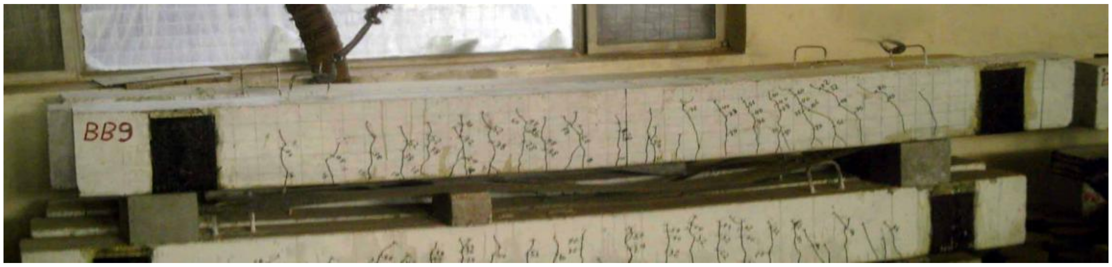

Figure 9 Crack pattern for beam BB9- strengthened beam (bottom face)

Figures 10 and 11 show the crack pattern for a beam strengthened with CFRP located at the bottom and side faces of the beam. The crack initially developed at bottom (tension zone). It is seen that the number of cracks has been reduced significantly due to presence of side face CFRP sheets. The beam failed before the cracks reach the top fiber. Failure occurred by yielding of reinforcement and followed by CFRP failure at the maximum moment zone (cut of the bottom CFRP and followed in the side CFRP sheets).

(a)

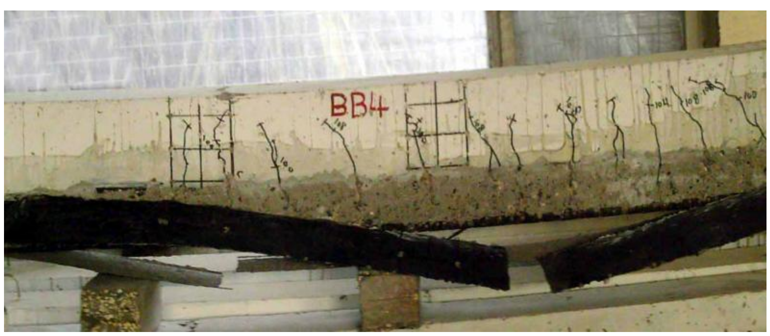

(b)

Figure 10 Crack pattern for beam BB4- strengthened beam (at bottom and side face by CFRP sheets)**. (a)** Cracks on overall beam. **(b)** Magnified picture for cracks at mid-span.

Figure 11 Crack pattern for beam BB10- strengthened beam (at bottom and side face by CFRP sheets)

Figures 12 and 13 show the crack pattern for a beam strengthened with CFRP located at the sides of the beam only. Also, the cracks started in the (tension zone) and moved towards compression zone while the number of cracks was reduced due to presence of side face CFRP sheets. The beam failed before the cracks reach to the top fiber. Failure developed by yielding of reinforcement and followed by CFRP failure.

(a)

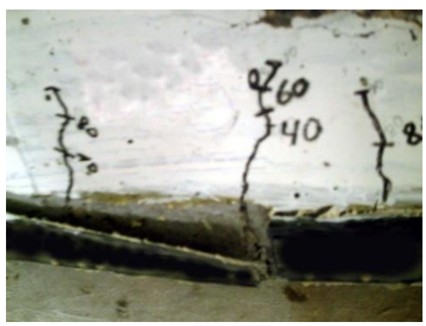

(b)

Figure 12 Crack pattern for beam BB5- strengthened beam (at sides of beam). **(a)** Cracks on overall beam. **(b)** Magnified picture for cracks at mid-span.

Figure 13 Crack pattern for beam BB11- strengthened beam (at sides of beam)

Figure 14 shows the crack pattern for the beam at 50% of failure loading and then repaired and loaded up to failure. The crack started at the bottom face (tension zone) and exceeded the middle of the beam. The crack width did not exceed 2mm.

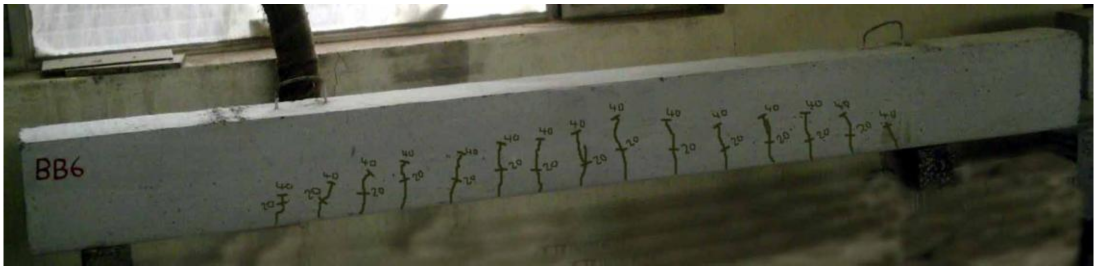

Figure 14 Crack pattern for beam BB6- (holding 50% of failure loading) before repairing.

Figures16 to20 show the crack pattern for the repaired cracked beams holding 50% of failure load, and then repaired and loaded up to failure. The failure mode and crack pattern are the same as in strengthened beams except that the load at failure in the repaired beams was less than the load at failure of the strengthened beams.

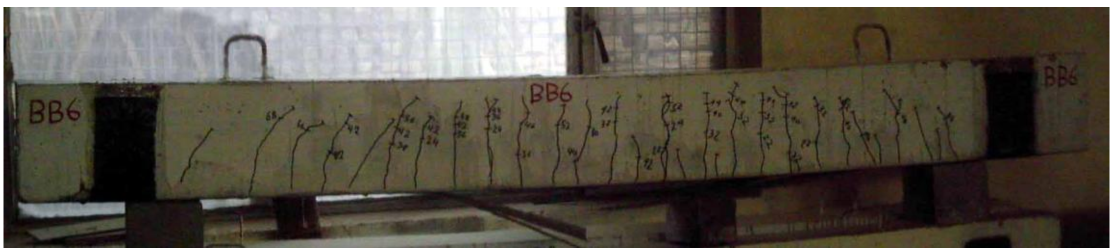

Figure 15 Crack pattern for beam BB6- (beam repaired by CFRP in bottom face)

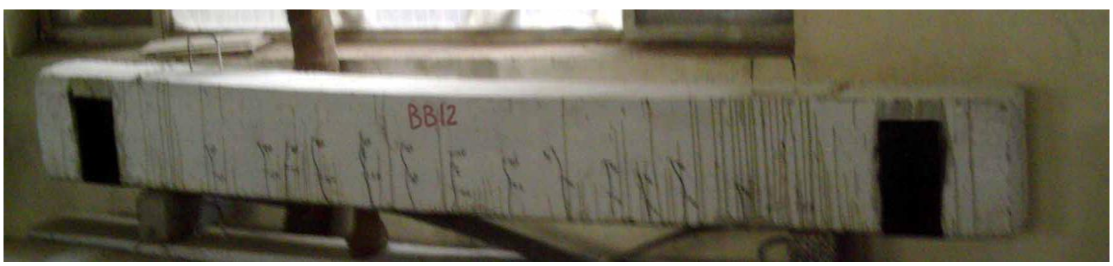

Figure 16 Crack pattern for beam BB12- (beam repaired by CFRP in bottom face)

Figure 17 Crack pattern for beam BB7- (beam repaired by CFRP in bottom and sides)

Figure 18 Crack pattern for beam BB13- (beam repaired by CFRP in bottom and sides)

Figure 19 Crack pattern for beam BB8- (beam repaired by CFRP in side faces)

Figure 20 Crack pattern for beam BB14- (beam repaired by CFRP in side faces)

LOAD-DEFLECTION CURVES

Load versus central deflection curves for the tested beams that had been constructed and tested to fail in flexure are shown in Figures 21 and 22. Figure 21 shows the load-deflection curves for the control and strengthened beams. Figure 22 show the load deflection curves for the control and repaired beams. The enhancement in stiffness and ultimate load by CFRP sheets is clear in these figures.

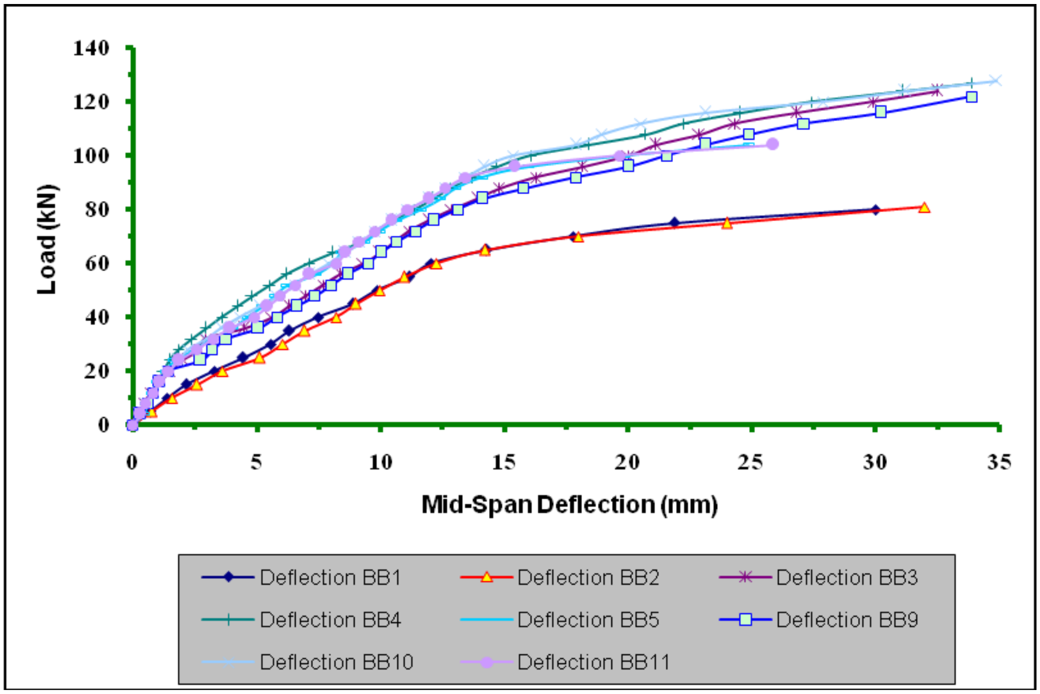

Figure 21 Load-deflection comparisons between strengthened and control beams

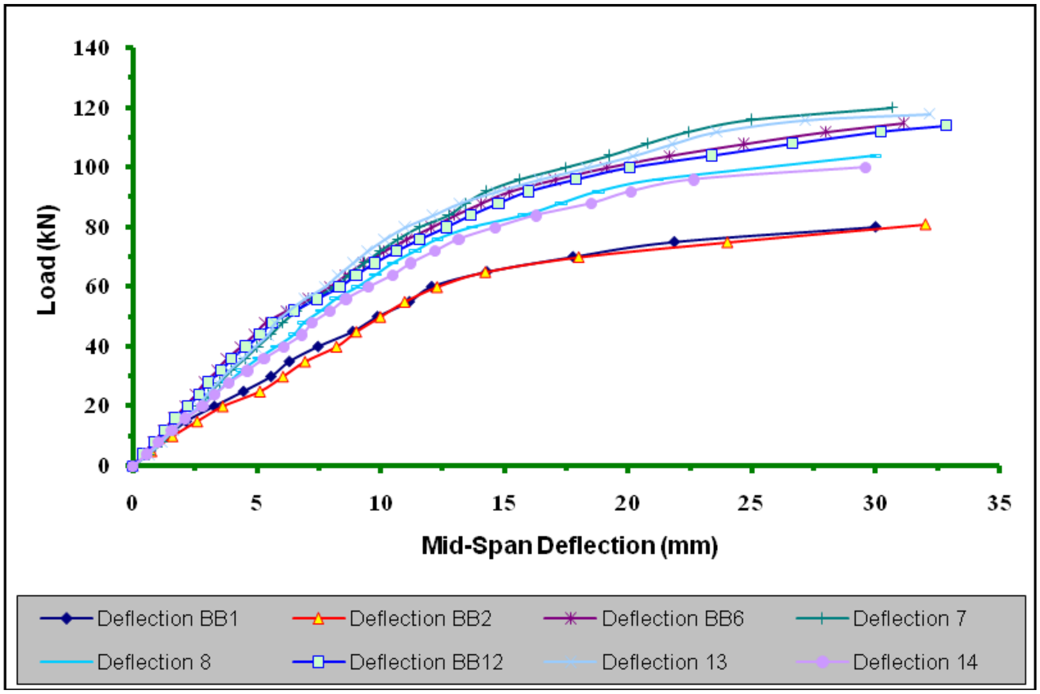

Figure 22 Load-Deflection Comparison between repaired and control beams

Conclusions

From test results and observations, the following major conclusions can be drawn:

- In all cases in the present work (flexural group), the failure in strengthened beams is caused by steel yielding fallowed by CFRP rupture.
- The presence of external CFRP bonded to concrete beams increases the ultimate load at failure to a significant value. The maximum increase in the ultimate strength of externally strengthened beams by CFRP depends on the amount of the area and configuration of the external CFRP sheet added.
- The use of external CFRP sheet connected to the tension sides of beams could enhance the ultimate load capacity by (160%) in flexure over the capacity of the identical unstrengthened control beam.
- Same behavior for strengthened and repaired beams is noticed except that the ultimate load in repaired beams reaches (95 % to 97 %) of ultimate load of strengthened beams.

REFRENCES:

- Klaiber, F.W., Wipf, J.J. and Kempers, B.J., **"Repair of Damaged Prestressed Concrete Bridges using CFRP"**, Proceedings of the 2003 Mid Transportation Research Symposium, Ames, Iowa, August 2003 by Iowa State University, www.ctre.iastate.edu. .

- Sergio, F. B., Regan M. B., Sharon L. Wood, and Michael E. K., **"Use of Carbon Fiber Reinforced Polymer Composites to Increase the Flexural Capacity of Reinforced Concrete Beams"**, Research Project 0-1776 by the Center for Transportation Research Bureau of Engineering Research, the University of Texas at Austin, U.S.A., April 2001.

- Khan, A. R., **"Repair and Strengthening of Reinforced Concrete Structures using CFRP Plates"**, FEST Hamadard University, India, 2002.

- ACI Committee 211, **"Standard Practice for Selecting Proportions for Normal, Heavyweight, and Mass Concrete (ACI 211.1-91 Code)"**, Reapproved 1997, American Concrete Institute, Michigan, U.S.A.

- ACI Committee 318**, "Building Code Requirements for Structural Concrete (318M-02) and Commentary (318RM-02)"**, American Concrete Institute, Michigan, USA, 2002.

- Ali, D. D., **“Experimental and Theoretical Investigation of the Behavior of Reinforced Concrete Beams Strengthened by Fiber Reinforced Polymer”,** Ph.D. Thesis, Baghdad University, 2007.

MOIDIEFIED VERSION OF ADJUSTED STEP SIZE LMS ALGORITHIM (MASSLMS) FOR ADAPTIVE LINEAR FIR EQUALIZER

Dr. Thamer M. Jamel
University of Technology, Department of Electrical Engineering, Baghdad –Iraq

ABSTRACT

In this paper a Modified version of Adjusted Step Size Least Mean Square algorithm (MASSLMS) is proposed which overcome and avoid one of the drawback of the standard LMS and our previous proposed algorithm Adjusted Step Size Least Mean Square algorithm (ASSLMS). This drawback is the requirement of a statistical knowledge of the input signal prior to the starting training of the algorithm which is necessary to determine the fixed value of the maximum step size (i.e. the upper bound value) in the initialization stage of the ASSLMS algorithm. In this proposed algorithm an appropriate time varying value of the maximum step size was calculated based on inversely proportional of the instantaneous energy of the input signal vector. Then this time varying upper bound value of the step size is used to guarantee the stability of adjusted step size of the algorithm which is a recursively adjusted based on rough estimate of the performance surface gradient square . The proposed algorithm does not need trial and error for choosing the value of the maximum step size (μ_{MAX}) compared with ASSLMS and standard LMS algorithms. The proposed algorithm shows through computer simulation results faster and low level of miss-adjustment in the steady state compared with LMS and ASSLMS for three different types of channel in adaptive linear equalizer system.

KEYWORS: Linear Adaptive Equalizer, LMS Adaptive algorithm, Variable Step Size LMS algorithm.

نسخة معدلة من خوارزمية اقل معدل للتربيع ذات معامل الخطوة المتغيرة زمنيا لمنظومة المكافىء الخطية

الخلاصة

هذا البحث يركز على اقتراح نسخة معدلة من خوارزمية اقل معدل للتربيع ذات معامل الخطوة المتغيرة زمنيا لمنظومة المكافىء الخطية وسميت الخوارزمية المقترحة الجديدة باسم (MASSLMS) وهي نسخة مطورة من اصل الخوارزمية التي سبق ان تم اقتراحها مسبقا من قبل الباحث نفسه وسميت في حينها باسم (ASSLMS) . والهدف الاساسي من هذه الخوارزمية الجديدة هو حل مشكلة اختيار اعظم قيمة لمعامل الخطوة المتغيرة زمنيا (μ_{MAX}) حيث كان سابقا يتم اختيار قيمة ثابتة لها وعن طريق التجربة والخطاء . أما الان في هذه الخوارزمية المقترحة الجديدة فانه يتم تغيريها زمنيا وحسابها لكل عينة عن طريق حساب معكوس القدرة الكهربائية للاشارة الداخلة للمرشح المتكيف . وبعد ذلك يتم استخدام هذه القيمة المتغيرة زمنيا للـ(μ_{MAX}) في تنفيذ بقية الخطوات اللازمة للخوارزمية . تعتبر عملية حساب الـ(μ_{MAX}) بهذه الطريقة مناسبة ومفضلة لانها ستتمكن من تعقب اي تغيير قد يحصل بالاشارة الداخلة مقارنة بالطريقة السابقة . اثبتت الخوارزمية المقترحة الجديدة من خلال برنامج المحكاة كفاءة بالاداء

وخصوصا السرعة في التعلم افضل من خوارزمية اقل معدل للتربيع التقليدية المسماة بـ (LMS) وكذلك الخوارزمية المساة بـ (ASSLMS) لمنظومة المكافىء الخطية وباستخدام ثلاثة انواع مختلفة من قنوات الاتصال .

INTRODUCTION

Adaptive equalizer was widely used in digital communication systems in order to reduce or eliminate the channel distortions or intersymbol interference ISI before demodulation at the receiver. The simple structure for adaptive equalizer was the Finite Impulse Response filter (FIR) which can be trained by the Least Mean Square adaptive algorithm (LMS). This LMS algorithm, which was first proposed by Widrow and Hoff at Stanford University, Stanford, CA in 1960 [B.Farhang Boranjrncy, 1999]. This LMS algorithm is regarded as special case of the Gradient Search algorithm and is regarded as one of the most popular algorithms in adaptive signal processing due to the simplicity in the number of calculations required for its update. Furthermore, it does not require matrix inversion, nor does it require measurements of the pertinent correlation functions [B.Farhang Boranjrncy, 1999]. But this algorithm suffers from slow convergence adaptation process since the convergence time of LMS algorithm is inversely proportional to the step size [B. Widrow and S. Stearns, 1985]. Also it suffers from trade off between low level of miss-adjustment and fast convergence i.e. If large step size is selected, then fast convergence will be obtained but this selection results in deterioration of the steady state performance (i.e. increased the miss-adjustment (excess error). Also small value of the step size will cause slow convergence but will enhance or decrease the steady state error level [B. Widrow and S. Stearns, 1985].

Therefore, a lot of modifications of the LMS algorithm have been reported. One technique of these modifications is using time varying step size i.e. the step size will be adjusted in each iteration according to the specific rules. Several time varying step size LMS algorithm were reported [,R.W.Harris, D.M. Chadries, 1986 , Long Le, Ozgu Ozun, and Phiipp Steurer, 2002, Charles Q. Hoang, 2000, J.J. Chen, R.R. Priemer, Feb.1995, Bozo K. ,Zdravko U. , and Ljubisa S., April 2003, S.K., G. Zeng. July 1989, R.H.Kang, E.W.Johnstone, July 1992, R.W. Wies, A. Balasubramanian, J. W. Pierre, 2006 and Yonggang Zhang, Ning Li, Jonathon A. Chambers, and Yanling Hao, 2008]. In this paper time varying step size is chosen due to its powerful effect on the performance of the system also the structure of the adaptive equalizer will not be changed and this technique require less overhead in computations which is an important factor for hardware implementation. The proposed algorithm in this paper is called MASSLMS algorithm (Modified Adjusted Step Size LMS) which is regard as modified version of previous ASSLME algorithm [Thamer M.Jamel, 2007]. This new proposed algorithm shows good performance and also gets rid of the main drawback of the previous algorithm which is the trial and error in selection of the maximum value of the step size (μ_{MAX}). The value of the maximum of the step size in this paper is adjusted according to the input power of the signal instead of the fixed value. This step size is proportional to the inverse of the total expected energy of the instantaneous values of the coefficients of the input vector.

ADAPTIVE LINEAR EQUALIZER WITH LMS ALGORITHM

Linear Equalizer LE is one type of adaptive equalization techniques which use only received signal symbols in their calculations and do not use any previously detected symbols. Fig.1 shows the classical model of the LE .As shown in this figure there are two modes of operations, namely, the training mode and decision-directed mode [Simon Haykin , 1983]. During the training mode, the transmitter generates a data symbol sequence known to the receiver.

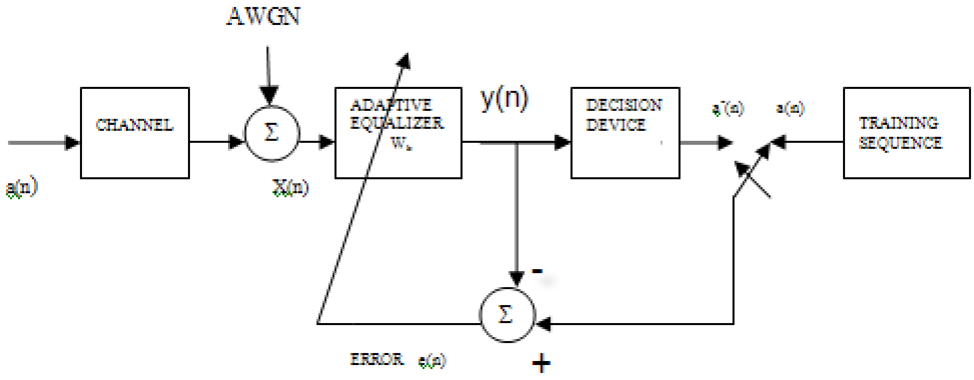

Fig. 1 Classical Model of LE

The receiver therefore, substitutes this known training signal in place of the decision device output. Once an agreed time has elapsed, the decision device output is substituted and the actual data transmission begins. When the training process is completed, the adaptive equalizer is switched to its second mode of operation: the decision-directed mode. In this mode of operation, the error signal is defined by [R.W. Wies, A. Balasubramanian, J. W. Pierre, 2006]:

$$e(n) = a^{\wedge}(n) - y(n) \tag{1}$$

Where y (n) is the equalizer output and $a^{\wedge}(n)$ is the final correct estimate of the transmitted symbol $a(n)$. The linear transversal equalizer(i.e. FIR) Fig.2 is the simplest equalization techniqe available. It is made up of tapped-delay line with tap spacing equal to the symbol time. The equalizer input consists of sampled output of the matched filter that preceds the equalizer. These samples are placed in shift register and shifited once every sample period. The contents of each register is multiplied by a tap gain and added togother to form the output of the equalizer. This output is the estimate of the current symbol, this operation can be described by the following equation [John M. Morton, 1998].

$$\hat{d}_k = \sum_{k=-N_1}^{N_2-1} w_k y_{n-k} \tag{2}$$

In this equation, y_n is the input sequance to the equalizer, w_k is the set of tunable complex multipliers called tap weights, N_1 is the number of the non-caus equalizer taps, N_2 is the number of causal taps, the total nunmer of equalizer taps is therfore $N_1+N_2=N$. The Ts blocks indicate a delay of one symbol period

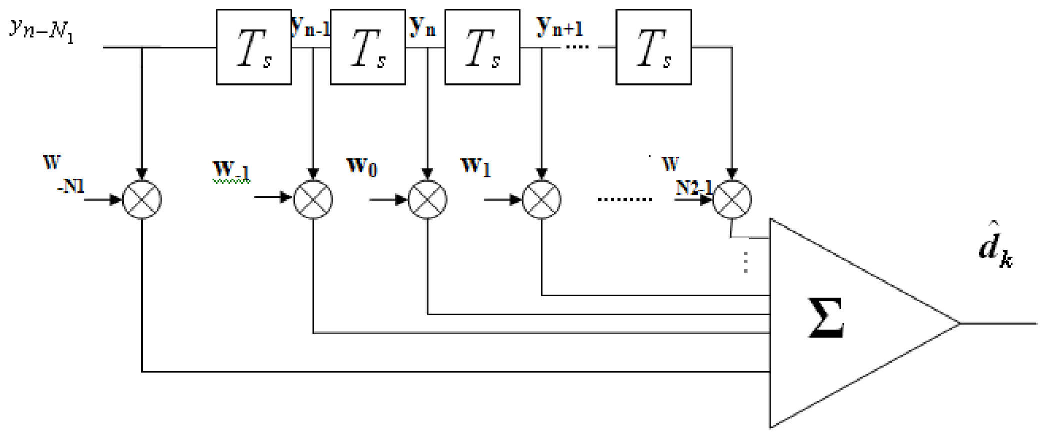

Fig. 2 The linear transversal equalizer structure of the LTE

Under the mean square error criterion, the tap weights of the equalizer are adjusted to minimize the mean-square error between the original data symbol and the output of the equalizer. This error includes both ISI as well as the additive noise. It follows that when the desired equalizer output is known (i.e., $d_k = x_k$) the error signal e_k is given by [Rappaport T.S. 2002, B. Widrow and S. Stearns, 1985]

$$e_k = d_k - \hat{d}_k = x_k - \hat{d}_k \tag{3}$$

The squared error is defined as [R.W.Harris, D.M. Chadries, 1986]

$$|e_k|^2 = |d_k - \hat{d}_k|^2 = |x_k - \hat{d}_k|^2 \tag{4}$$

To compute the mean square error $|e_k|^2$ at time instant k, from eq. (3) the following obtained

$$|e_k|^2 = x_k^2 + w_k^T y_k y_k^T w_k - 2 x_k y_k^T w_k \tag{5}$$

Taking the expected value of $|e_k|^2$ over k (which in practice amounts to computing a mean squared) yields [B. Widrow and S. Stearns, 1985]

$$E\left[|e_k|^2\right] = E\left[x_k^2\right] + w_k^T E\left[y_k y_k^T\right] w_k - 2E\left[x_k y_k^T\right] w_k \tag{6}$$

Where E is the expectation operator. To find the set of equalizer coefficients those minimize the mean squared error for this linear equalizer. The following sets of computations are made. Let R be defined as the (N+1)×(N+1) square matrix

$$R = E\left[y_k y_k^T \right] = E \begin{bmatrix} y_k^2 & y_k y_{k-1} & y_k y_{k-2} & \cdots & y_k y_{k-N} \\ y_{k-1} y_k & y_{k-1}^2 & y_{k-1} y_{k-2} & \cdots & y_{k-1} y_{k-N} \\ \cdots & \cdots & \cdots & \cdots & \cdots \\ y_{k-N} y_k & y_{k-N} y_{K-1} & y_{k-N} y_{k-2} & \cdots & y_{k-N}^2 \end{bmatrix} \tag{7}$$

Where $(.)^T$ denotes the transpose operation. This matrix is designated the "input correlation matrix." The main diagonal terms are the mean squares of the input signal, and the cross terms are the cross correlations among the input signal. Let P be similarly defined as the column vector

$$P = E[\ x_k y_k\ ] = E\ [\ x_k y_k \quad x_k y_{k-1} \quad x_k y_{k-2} \quad \ldots \quad x_k y_{k-N}\ ]^T \tag{8}$$

This vector is the set of cross correlations between the desired response and the input signal. Using eq. (7) and eq.(8), equation (6) may be written as [R.W.Harris, D.M. Chadries, 1986]

$$MSE = \xi = E\left[x_k^2\right] + w^T R w - 2P^T w \tag{9}$$

By minimizing eq. (9) in terms of the weight vector w_k, it becomes possible to adaptively tune the equalizer to provide a flat spectral response (minimal ISI) in the received signal. This is due to the fact that when the input signal y_k and the desired response x_k are stationary, the mean square error (MSE) is quadratic on w_k, and minimizing the MSE leads to optimal solutions for w_k.

To determine the minimum MSE (MMSE), the gradient of (9) can be used. As long as R is nonsingular (has an inverse), the MMSE occurs when w_k are such that the gradient is zero. The gradient of ξ is defined as [Rappaport T.S. 2002, B. Widrow and S. Stearns, 1985]

$$\nabla \cong \frac{\partial \xi}{\partial w} \cong \left[\frac{\partial \xi}{\partial w_0} \frac{\partial \xi}{\partial w_1} \cdots \frac{\partial \xi}{\partial w_L} \right]^T \tag{10}$$

Where L is number of weight coefficients. By expanding (9) and differentiating with respect to each signal in the weight vector, it can be shown that eq.(10) yields [Rappaport T.S. 2002, B. Widrow and S. Stearns, 1985]

$$\nabla = 2RW - 2P \tag{11}$$

Setting $\nabla = 0$ in eq. (11), the optimum weight vector w_{opt} for MMSE is given by [Rappaport T.S. 2002, B. Widrow and S. Stearns, 1985]

$$w_{opt} = R^{-1} P \tag{12}$$

Using equation (12) to substitute w_{opt} for w in eq. (9) $\xi_{\min}$ is found to be [Rappaport T.S. 2002, B. Widrow and S. Stearns, 1985]

$$\xi_{\min} = MMSE = \mathrm{E}[\ x_k^2\ ] - P^T R^{-1} P = \mathrm{E}[\ x_k^2\ ] - P^T w_{opt} \qquad (13)$$

Eq. (13) solves the MMSE for optimal tap weights w_{opt}.

The LMS algorithm is an iterative procedure that continuously updates a vector of equalizer coefficients. It updates these coefficients based on the mean-square error cost function given in eq. (9). This cost function is dependant on the output of the equalizer which is dependant on the tap coefficients. Each vector of equalizer coefficients will have a certain mean square error associated with it. One such vector will produce the minimum mean-square error. The LMS algorithm attempts to find the desired vector [B. Widrow and S. Stearns, 1985, John M. Morton, 1998]. The change in weights vector is represented as [B. Widrow and S. Stearns, 1985]:-

$$W_{k+1} = W_k + \mu(-\nabla_k) \qquad (14)$$

Where μ is constant called the step size that regulates the stability and convergence time of the adaptive process. To develop the LMS algorithm, e_k^2 itself is taken as an estimate of ξ_k. Then, at each iteration in the adaptive process, a gradient estimate of the following form has been obtained [B. Widrow and S. Stearns, 1985],

$$\hat{\nabla}_k = \begin{bmatrix} \dfrac{\partial e_k^2}{\partial w_0} \\ \vdots \\ \dfrac{\partial e_k^2}{\partial w_L} \end{bmatrix} = 2e_k \begin{bmatrix} \dfrac{\partial e_k}{\partial w_0} \\ \vdots \\ \dfrac{\partial e_k}{\partial w_L} \end{bmatrix} = -2e_k y_k \qquad (15)$$

Put eq. (15) into eq. (14) then the updating weights vector became [B. Widrow and S. Stearns, 1985]:-

$$W_{k+1} = W_k - \mu\ \hat{\nabla}_k$$
$$W_{k+1} = W_k + 2\mu e_k y_k \qquad (16)$$

This is the LMS algorithm and it is also known as the "stochastic gradient algorithm", and μ is the step size that regulates the speed and stability of adaptation. Since the weight changes at each iteration are based on imperfect gradient estimates, one would expect the adaptive process to be noisy, also the iterative procedure start with initial guess which may be a null vector [Qureshi S.U. 1985, B. Widrow and S. Stearns, 1985]. If the step size is made too large, the algorithm can become unstable and will not converge to the optimal tap vector. The main drawback of the LMS algorithm is the slow convergence rate. To overcome this limit, a modified version of the LMS algorithm is presented which used time varying step size instead of the fixed step size as shown in the next section.

MODIFIED ADJUSTED STEP SIZE LMS (MASSLMS) ALGORITHM:-

As explained previously this paper propose algorithm which is called Modified Adjusted Step Size LMS (MASSLMS) algorithm. MASSLMS regards as modified version of the ASSLMS algorithm

[Thamer M.Jamel, 2007]. ASSLMS algorithm used variable step size that will be adjusted according to the square of the gradient of the performance surface (i.e. $e_k y_k)^2$ as follows:-

$$\mu_{k+1} = \alpha\mu_k + \delta(e_k.y_k)^2 \qquad (17)$$

Where $0\langle\alpha\langle 1$ and $\delta\rangle 0$, then:-

$$\mu_{k+1} = \mu_{MAX} \quad \text{if} \quad \mu_{k+1}\rangle\mu_{MAX} \quad , \text{ or} \quad \mu_{k+1} = \mu_{\min} \quad \text{if} \quad \mu_{k+1}\langle\mu_{\min}, \qquad (18)$$
$$\text{Otherwise} \quad \mu_{k+1} = \mu_{k+1}$$

Eq. (17) is a formula to adjust the step size in each iteration and it is modified from the original equation of in [R.H.Kang, E.W.Johnstone, July 1992]. In this equation the step size will be adjusted according to the square of the gradient of the performance surface (i.e. $e_k y_k)^2$ as shown in eq. (17). To ensure stability, the variable step size μ(*n*) is constrained to the pre-determined maximum and minimum step size values while α and δ are the parameters controlling the recursion . 0< α<1, and δ>0 , and μ(n+1) is set to μmin or μmax when it falls below or above these lower and upper bounds, respectively. The constant μmax is normally selected near the point of instability of the conventional LMS to provide the maximum possible convergence speed. The value of μmin is chosen as a compromise between the desired level of steady state misadjustment and the required tracking capabilities of the algorithm. The parameter δ controls the convergence time as well as the level of misadjustment of the algorithm at steady state. However there is no any formula or equation to calculate α and δ in all papers including the original paper [R.W. Wies, A. Balasubramanian, J. W. Pierre, 2006] but usually they assigned high value for α which is very close to 1 (i.e. 0.97-to-0.99) and very small value for δ.
Then the update eq. (16) for the weight vector will be:-

$$w_{k+1} = w_k + 2\mu_k e_k y_k \qquad (19)$$

Where $\mu_{\min}$ is chosen to provide minimum level of miss-adjustment at steady state, and μ_{MAX} ensures the stability of this algorithm []R.H.Kang, E.W.Johnstone, July 1992]. This proposed algorithm (ASSLMS) algorithm regard as modified version of the VSSLMS algorithm [Thamer M.Jamel, 2007]. Involving the term (y_k) which represents the input signal in the updating step size formula in addition to error factor is favorite choice in order to speed up the estimation and adaptation process. The main drawback of the ASSLMS algorithm is how to select the value of the upper bound of step size i.e. μ_{MAX} . In other words this drawback is the requirement of a statistical knowledge of the input signal prior to the starting training of the algorithm which is necessary to determine the fixed value of the maximum step size μ_{MAX} (i.e. the upper bound value) in the initialization stage of the ASSLMS algorithm.
In this proposed algorithm an appropriate time varying value of the maximum step size is calculated based upon inversely proportional of the instantaneous energy of the input signal vector .

$$\mu_{MAX} = \frac{1}{2y_k^T y_k} \qquad (20)$$

This sum of the expected energies of the input samples is also equivalent to the dot product of the input vector with itself. Then this time varying upper bound value of the step size is used to guarantee the stability of adjusted step size of the algorithm eq. (17) which is a recursively adjusted based on rough estimate of the performance surface gradient square.

Eq. (20) is used in Normalized LMS (NLMS) algorithm which is an extension of the LMS algorithm that overcomes the drawback of the LMS algorithm by selecting a different step size value, $\mu(k)$, for each samples of the input signal. [Scott C. Douglas, march 1994]. Eq. (20) is implemented as follows:-

$$\mu_{MAX} = \frac{\beta}{2y_k^T y_k + \Psi} \qquad (21)$$

Where the value of ψ is a small positive constant in order to avoid division by zero when the values of the input vector are zero and β is within the range of $0<\beta>2$, usually it is equal to 1. In the MASSLMS algorithm the upper bound available to each element of the step size vector, μ_{MAX} , is calculated for each iteration.

SIMULATION RESULTS

Case 1:- In this case LE was simulated with different algorithms. The channel used here is called channel 1 which is raised cosine function. The order of FIR adaptive filter for all simulation was 11 taps and signal to noise ratio was 26 dB, the additive noise was Gaussian noise with zero mean, and variance $\sigma^2 = 0.001$. The training samples were 1000 samples then the adaptive process is switched to decision mode. Fig.3 shows the learning curves for this case with different algorithms. The optimum step size for LMS algorithm was chosen by trial and error to be 0.03. The optimum values (by trial and error) of μ_{max} and μ_{min} was chosen to be 0.05 and 0.0001 respectively for ASSLMS algorithm. The values of α and δ was chosen to be 0.97 and 0.001 respectively for all algorithms. The β is equal 1 and ψ is equal 0.1 for MASSLMS algorithm.

As shown in Fig. 3 the proposed algorithm has fast convergence time than LMS and ASSLMS algorithms. The convergence time from Fig.3 is equal to 1000, 600 and 500 iterations for LMS, ASSLMS and MASSLMA algorithms respectively. Also the proposed algorithm has smooth descending towards the minimum point compared with the LMS and ASSLMS algorithms. This is because the upper bound of the step size is time varying value which can track any change in the input signal as shown in eq. (21).

Case 2:- The channel used here is called channel 2 which has frequency response with two spectral null in the middle region. The impulse response of this channel is (h = [0.2, -0.15, 1.0, 0.21, 0.03]) and is shown in Fig.4.

The same parameters of the case 1 are used in this case except that the optimum value of the upper bound of the μ_{MAX} of the ASSLMS algorithm was found by trial and error to be equal 0.03. Fig.5 shows the learning curves for different algorithms for this 2nd channel. As shown in figure (5) the proposed algorithm has fast convergence time than both LMS and ASSLMS algorithms. The convergence time from Fig.5 is equal to 250, 200 and 100 iterations for LMS, ASSLMS and MASSLMA algorithms respectively. Notice that the parameters of the MASSLMS algorithm are kept the same without any need to be changed by trial and error and this fact is also present in the next case i.e. case 3.

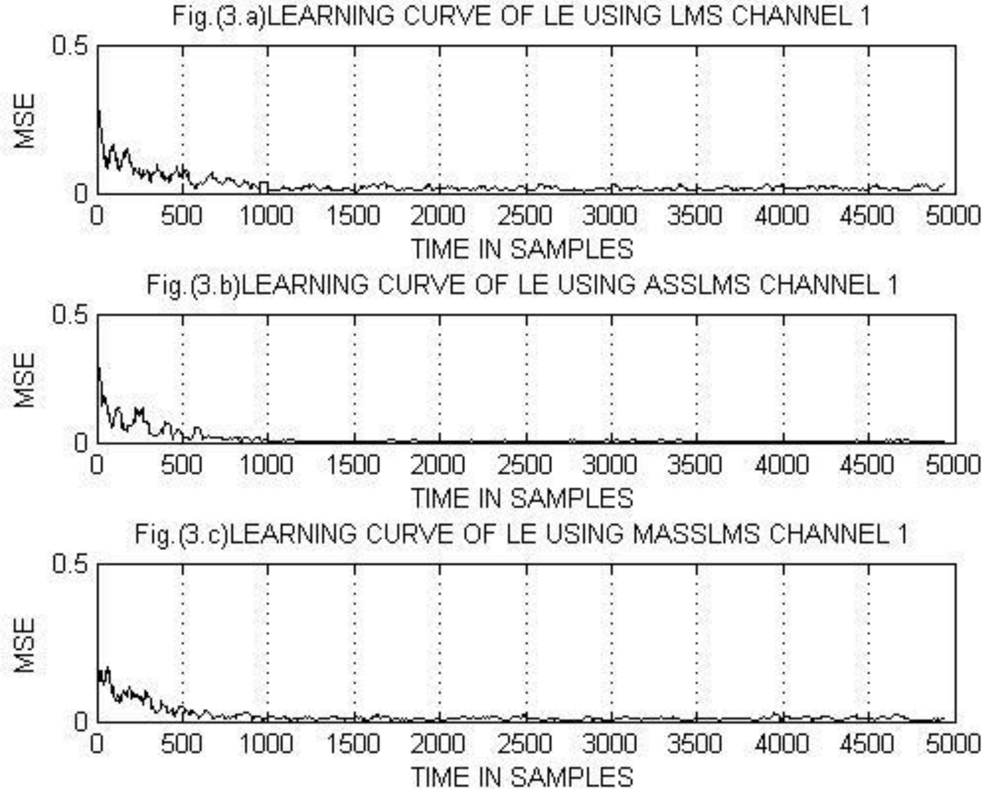

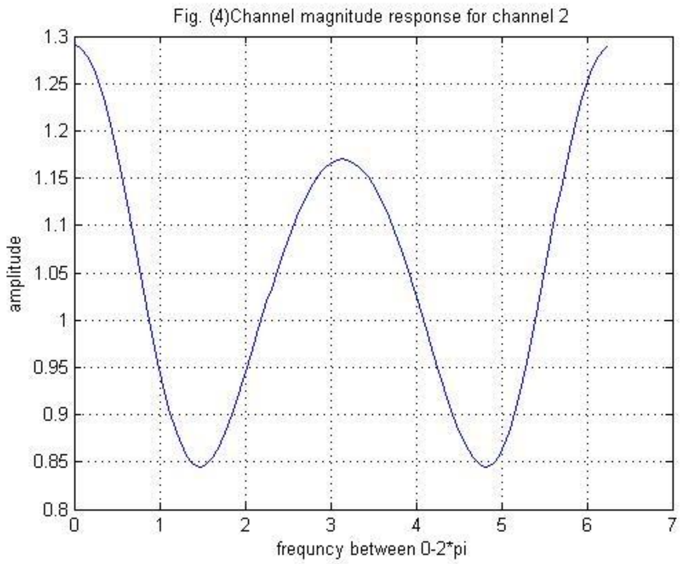

Case 3:- The channel used here is called channel 3 which has the following impulse response h=[0.01,0.08,-0.126,-0.25,0.7047,0.25,-0.02,0.016,0.0]; and shown in Fig.6. Fig.7 shows the learning curves of different algorithms using the same parameters as in case 2 above for all algorithms.

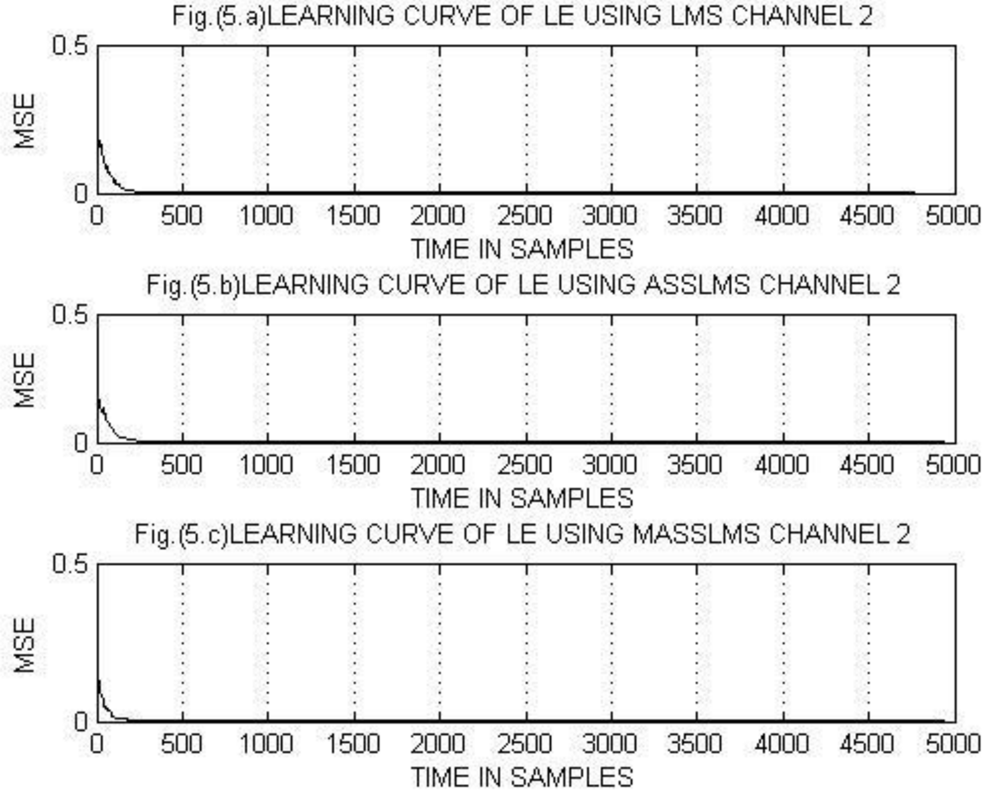

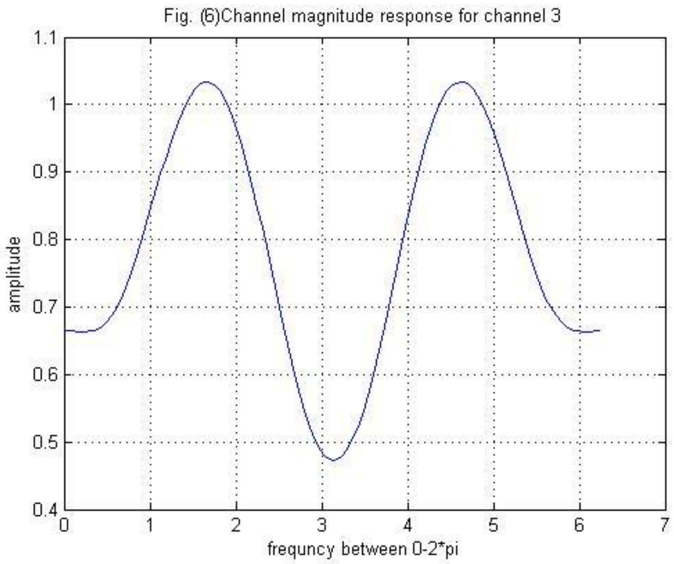

As shown in Fig.7 the proposed algorithm has fast convergence time than LMS and ASSLMS algorithm. The convergence time from Fig.7 is equal to 500, 400 and 200 iterations for LMS, ASSLMS and MASSLMA algorithms respectively. Also as seen in Fig.7.b , the learning curve of the ASSLMS algorithm has the same performance compared with the LMS algorithm due to that , the same parameters of the ASSLMS algorithm are used as in case 2 . So in order to enhance the performance of the ASSLMS algorithm the parameters of this algorithm must be optimized by trial and error which in turns represents the main draw back point of the ASSLMS algorithm. This draw back is overcome with the proposed algorithm (i.e. MASSLMS) which does not need any optimizations of its parameters.

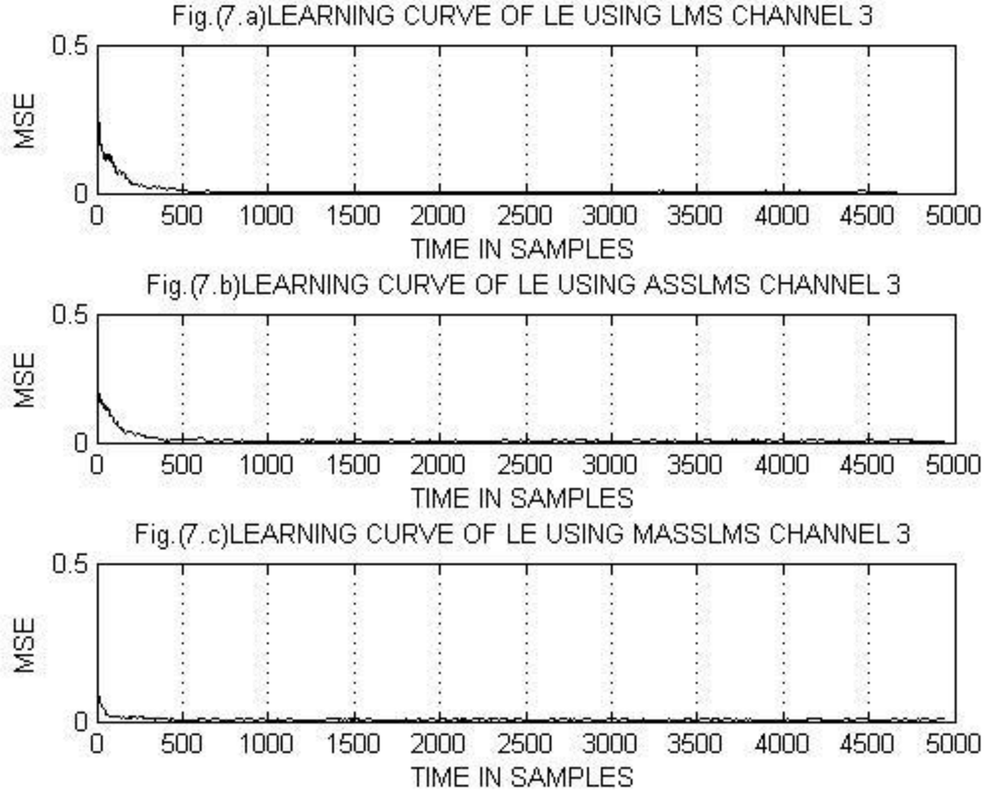

CONCLUSIONS

This paper focused on enhance the performance of our previous proposed algorithm (ASSLMS) which suffer from choosing the suitable value of the upper bound of the step size μ_{MAX}. The upper bound of the step size μ_{MAX} needs a statistical knowledge of the input signal prior to the starting training of the algorithm which is necessary to determine the fixed value of the maximum step size (i.e. the upper bound value) in the initialization stage of the ASSLMS algorithm. The proposed algorithm called Modified Adjusted Step Size LMS (MASSLMS) which used an appropriate time varying value of the maximum step size μ_{MAX} that is calculated based upon inversely proportional of the instantaneous energy of the input signal vector . This method is favorite choice because the time varying μ_{MAX} will track any chang in the input signal power. Then this time varying μ_{MAX} is used to guarantee the stability of adjusted step size of the algorithm which is a recursively adjusted based on rough estimate of the performance surface gradient square (i.e. $e_k y_k)^2$.

The proposed algorithm MASSLMS shows fast convergence time through the simulation of the adaptive linear equalizer using three different channels compared with the LMS and ASSLMS algorithms in spite of using the same parameters for all different cases.

REFERENCES

- B.Farhang Boranjrncy, 1999, “**Adaptive Filters**” John Wileys & Sonc,.
- B. Widrow and S. Stearns, 1985” **Adaptive Signal Processing**” Prentic-Hall, Inc..
- R.W.Harris, D.M. Chadries, 1986 , F.A. Bishop “ **A variable Step (VS) Adaptive filter algorithm**” IEEE Trans. On ASSP-34, No.2, pp.309-316,April.

- Long Le, Ozgu Ozun, and Phiipp Steurer, 2002, " **Adaptive Channel Estimation for Sparse Channels**", submitted for the degree of Bachelor of Eng. (Honors) in the Division of Elect. And Electronic Eng. , university of Queensland,..

- Charles Q. Hoang, 2000," **LMS Modeling and Estimation of Non-stationary Telecommunication Channels**", submitted for the degree of Bachelor of Eng. (Honors) in the Division of Elect. And Electronic Eng. , university of Queensland,.

- J.J. Chen, R.R. Priemer, Feb.1995 ," **An in Inequality by which to adjust the LMS algorithm Step Size**" IEEE Trans. On COMM-43,No.2/3/4,pp1477-1483.

- Bozo K. ,Zdravko U. , and Ljubisa S., April 2003,"**Adaptive Equalizer with Zero-Noise Constrained LMS algorithm** ", In Elec. Eng. of FACTA University, vol.16, , 1-xx.

- S.K., G. Zeng. July 1989," **A new Convergence Factor for Adaptive Filters**" IEEE Trans. On CAS-36,No.7,pp.1011-1012,.

- R.H.Kang, E.W.Johnstone, July 1992,"**A variable Step Size LMS algorithm"** IEEE Trans. On Signal Processing, Vol.40, No.7, pp.1633-1642,.

- R.W. Wies, A. Balasubramanian, J. W. Pierre, 2006,"**Using Adaptive Step-Size Least Mean Squares (ASLMS) for Estimating Low- Frequency Electromechanical Modes in Power Systems** ", In 9th International Conference on Probabilistic Methods Applied to Power Systems KTH, Stockholm, Sweden – June 11- 15,

- Yonggang Zhang, Ning Li, Jonathon A. Chambers, and Yanling Hao, 2008 , ""**New Gradient- Based Variable Step Size LMS Algorithms**" Research Article in Hindawi Publishing Corporation EURASIP Journal on Advances in Signal Processing Volume, Article ID 529480, 9 pages doi: 10.1155/ 2008/ 529480 .

- Thamer M.Jamel, 2007," **Performance Improvements of Adaptive FIR Equalizer Using Modified Version of VSSLMS Algorithm**" , In Journal of Engineering , Baghdad University ,No.4 , Vol. 13, December 2007.

- Simon Haykin , 1983, " **Communication Systems**" John Wiley & Sons, Inc., New York,.

- John M. Morton, 1998 , "**Adaptive Equalization for Indoor Wireless Channels**" M.Sc. Thesis, Faculty of the Virginia polytechnic institute and state university, Blacksburg, Virginia, August.

- Rappaport T.S. 2002, "**Wireless Communications Principles and Practice**", 2nd Edition, Prentice-Hall Inc.,.

- Qureshi S.U. 1985, "**Adaptive Equalization**", Proceeding of IEEE, vol. 37, no. 9, pp. 1340-1387, September.

- Scott C. Douglas, march 1994, "**A Family of Normalized LMS Algorithms**" IEEE signal processing letters, Vol. SPL-1, No.3, pp. 49-51,.

HYDROISOMERIZATION OF *n*-ALKANE OVER ZEOILTE SUPPORTED CATALYST

Abdul-Halim A.K. Mohamed and Mohamed Kamel

College of Engineering/University of Baghdad

ABSTRACT

The conversion of *n*C5-*n*C7 over 0.32wt%Pt/HY-Zeolite catalyst was studied with temperature range 240-270ºC, liquid hourly space velocity range 1-3h^{-1}, hydrogen to n-alkane mole ratio 8-24 and atmospheric total pressure. The effect of the P_{H2}, P_{nC5}, P_{nC6}, and P_{nC7} orders on the overall reaction rate was studied. For *n*C7, the reaction order with respect to hydrogen varied between -0.998 and -0.948 while with respect to *n*C7 varied between 0.154 and 0.156. For *n*C6, the reaction order varied between -0.811 and -0.808 while with respect to *n*C6 varied between 0.332 and 0.337. For *n*C5, the reaction order with respect to hydrogen varied between -0.652 and -0.620 while the reaction order with respect to *n*C5 was varied between 0.336 and 0.339. The values of apparent activation energy were obtained and found to be varied between 110 and 111 kJ/mol for *n*C7, 120 to 122 kJ/mol for *n*C6, and 145 to 148 kJ/mol for *n*C5.

الخلاصة

تم دراسة تحول البنتان الأعتيادي ،الهكسان الأعتيادي والهبتان الأعتيادي على العامل المساعد من نوع زيولايت والحاوي على نسبة 0.32% وزنا من البلاتين والمحضر بطريقة الترطيب . تم إجراء التجارب بضغط جوي في منظومة مختبريه تحتوي على مفاعل ذو حشوة ثابتة وبدرجات حرارة بين 240 -270°م وباستخدام سرع فراغية بين 1- 3 سا$^{-1}$ وبنسب مولية للهيدروجين إلى البنتان والهكسان والهبتان بين 8 - 24 . درس تأثير مرتبة التفاعل بالنسبة للهيدروجين والبنتان والهكسان والهبتان الأعتيادي بالنسبة لتفاعل الهبتان الأعتيادي لوحظ ان مرتبة التفاعل بالنسبة للهيدروجين تتراوح بين -0.998 و -0.948، بينما كانت مرتبة التفاعل بالنسبة للهبتان الاعتيادي تتراوح بين 0.154 و 0.156 . بالنسبة لتفاعل تحول الهكسان الأعتيادي كانت مرتبة التفاعل بالنسبة للهيدروجين تتراوح بين -0.811 و -0.808، بينما كانت مرتبة التفاعل بالنسبة للهكسان الاعتيادي تتراوح بين 0.332 و 0.337. بالنسبة لتفاعل تحول البنتان الأعتيادي كانت مرتبة التفاعل بالنسبة للهيدروجين تتراوح بين -0.652 و -0.620، بينما كانت مرتبة التفاعل بالنسبة للبنتان الاعتيادي تتراوح بين 0.336 و 0.339. تم دراسة قيم طاقات التنشيط و وجدت بانها تتراوح بين 110- 111 كيلوجول/مول بالنسبة للهبتان الاعتيادي ، 120-122 كيلو جول/مول بالنسبة للهكسان الاعتيادي ، و 145 - 148 كيلو جول/مول بالنسبة للبنتان الاعتيادي ،

KEYWORDS

Isomerization, HY-Zeolite, Heptane, Hexane, Pentane

INTRODUCTION

Hydroisomerization of light alkanes is becoming extremely important as an alternative for octane upgrading. Since the branched alkanes products have high research octane numbers (RON) and burn cleanly they are the only acceptable alternative as octane booster. The interest in improving the environmental protection and to promote the efficiency of the automotive motors encourages the formulation of new catalysts and development of new processes for gasoline. Considering that branched-chain alkanes posse the greatest octane numbers, the use of gasoline containing higher content of these compounds is one alternative to obtain fuel with high antiknock characteristics [Kuchar et al.,1993]. Usually, branched chain alkane can be obtained by isomerization reaction employing bifunctional catalysts formed by metal supported over acid zeolite [Kouwenhoven and Zijll, 1971]. The isomerization is a catalytic processes involveing rearrangement of the molecular structure of a hydrocarbon without gain or loss of any of its components [Meyers,1996]. The interest in the isomerization process heightened with the phase out of tetraethyl lead in 1970's, following the phase out of leaded gasoline due to the introduction of Clean Air Act Amendments of 1990 in the USA and similar legislation in other countries.

The aim of this work is to provide:

(1) An integrated experimental data on the skeletal isomerization of *n*C5, *n*C6 and *n*C7 on zeolite catalysts in a continues reaction unit containing a fixed bed of a catalyst and at atmospheric pressure;

(2) A study on the effect of operating conditions (Temperature, LHSV, ($H_2/nC_{5,6,7}$) mole ratio, n-alkane and H_2 partial pressures) on the isomerization rate and selectivity;

(3) A comparison between the conversion of *n*-C5, *n*-C6, and *n*-C7 over platinum loaded zeolite

EXPERIMENTAL

<u>Catalyst Preparation</u>

HY-zeolite as a powder was mixed with montmorillonite clay as binder. The preferred binder content is between (15-30 wt %) as noticed by Allain et al.(1997) and Cañizares et al.(2000) . The resulting mixture was mixed with water to form a paste. An extrudates with 3~5 mm length and about 2 mm diameter were formulated and dried over night at 110°C. The value of Pt required to obtain acid reaction as the limiting step is between 0.15-2wt%, as reported by Lanewala et al.(1967), Ribeiro et al.(1982), and Runstraat et al.(1997a). In this study a Pt/HY-zeolite catalysts with 0.32wt% Pt were prepared using impregnation method. To prepare a 0.32wt% Pt/HY-Zeolite catalyst the impregnation process requires proper solution of hexchlorplatinic acid. The impregnated extrudates were then dried at 110°C over night and calcinated at 300°C for 3 hours in a furnace with dry air. The calcinated catalyst were then reduced with hydrogen at 350°C for 3 hours [Runstraat et al.,1997a, Exner et al., 1989]. The impregnation process was carried out under vacuum and the solution was added as drop wise with mixing for homogenous distribution at fixed temperature 40°C.

TEST METHODES

Catalyst Composition

The analysis of platinum in the prepared catalyst was achieved using atomic absorption spectrophotometer type (PYE UNICAM SP9) at Ibn-Sina State Company.The surface area and pore volume tests where done by the Petroleum Research and Development Center. It is found that the surface area decreases to 545.96 m^2/gm after adding the binder and formulate the particles, while it falls down to 435.59 m^2/gm with the pore volume 0.3735 ml/gm after adding platinum.

GC Analysis

The separation and analysis of reaction product into their components were carried out by gas chromatographic analysis on packed model 438Aa-VSA from Agilent Technologies Company. All the gas chromatograph analysis was done in AL DURA refinery.

PROCEDURE AND CONDITION

Thirty cubic centimeters of fresh catalyst was charged to the reactor between two layers of inert materials. The charged reactor was flushed with nitrogen to purge the air from the system. Meanwhile, the reactor is heated to the desired temperature. After reaching the reaction temperature, the nitrogen valve was closed. A pre-specified flow rate of feedstock was set on, vaporization of the feed occurs in the evaporator, and the vapor feed is mixed with the hydrogen and nitrogen in the mixing section at a specified flow rates .The mixture entered the reactor from the top, distributed uniformly by the inert materials and reacted on the catalyst charged inside. The product gases passed through down to the condenser and the final condensates were collected only after steady state operation was established and initial products were discarded. **Figure 1** shows the catalytic hydro-conversion unit process flow digrame.

The isomerization reaction conditions, employed are temperature 240-270ºC, liquid hourly space velocity of 1-3 h^{-1}, hydrogen to n-alkane mole ratio 8 to 24 and the total pressure kept atmospheric. *n*C5, *n*C6 and *n*C7 partial pressures were kept constant at 7.3 kPa while hydrogen pressure varied between 47.7-90.2 kPa using nitrogen as a make-up gas varied between 3.75-46.3 kPa to obtain the final reaction pressure of atmospheric. Another set of experiments were done by keeping the hydrogen partial pressure constant at 90.2 kPa while *n*C5, *n*C6 and *n*C7 partial pressures varied between 3.6-11 kPa, and the nitrogen partial pressure varied between 0-7.4 kPa to give the final reaction pressure of atmospheric pressure.

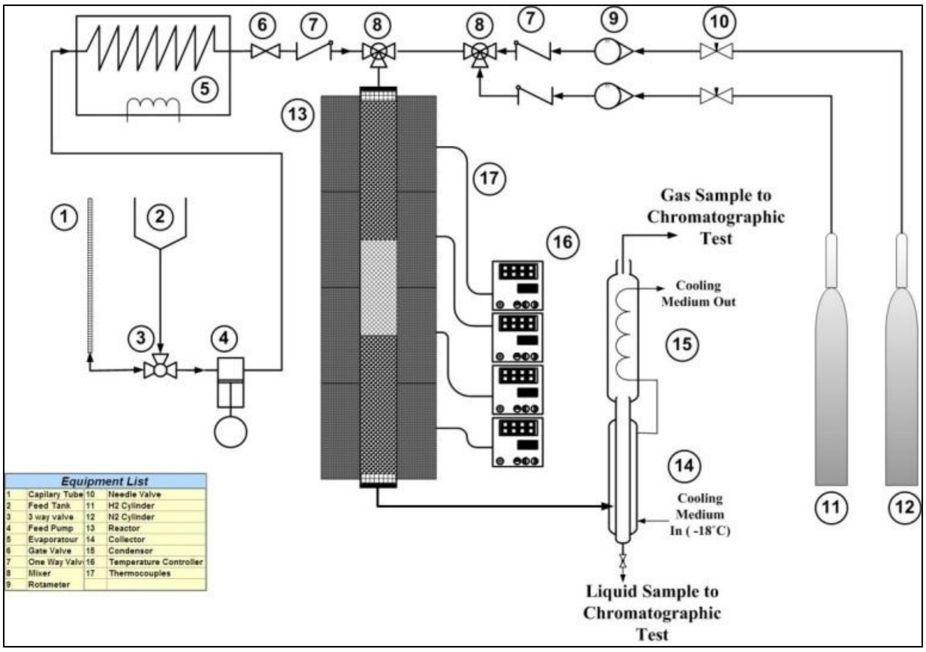

Figure 1 The catalytic hydro-conversion unit process flow digrame

RESULTS & DISCUSSION

Effect of Temperature

Figures 2, shows that the increasing of temperature of isomerization process at a constant LHSV increases the conversion of n-pentane, n-hexane and, n-heptane ,that is due to the number of sites that can be used for the reaction increased when the temperature increases, in agreement with Ahari et al.(2006), Asuquo et al.(1997), Martens et al.(2000) and and Narbeshuber et al. (1997).

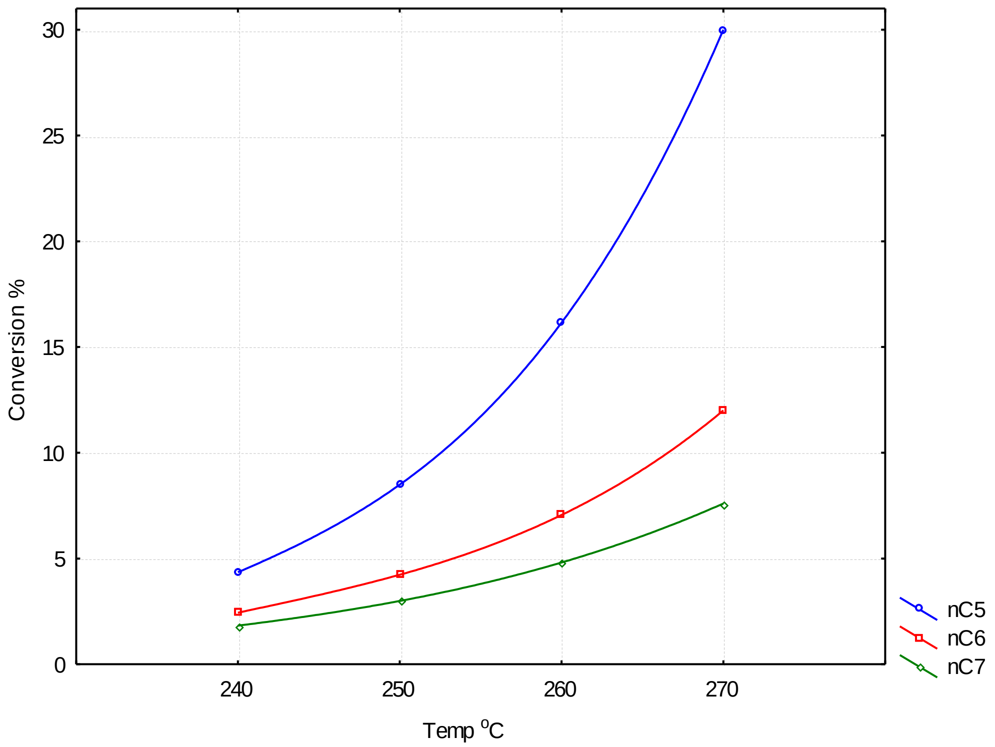

Figure 2 Conversion of nC5, nC6, and, nC7 at different temperature and LHSV=1hr-1

EFFECT OF LHSV

Figures 3 shows the changes of *n*C5,*n*C6 and, *n*C7 conversion as a function of a space time(1/LHSV). As LHSV decreases the conversion increases. This means that increasing in the residence time, which leads to offer a plenty of contact time of feed stock with catalyst inside the reactor. All results indicate that low LHSV is favored for isomerization process.

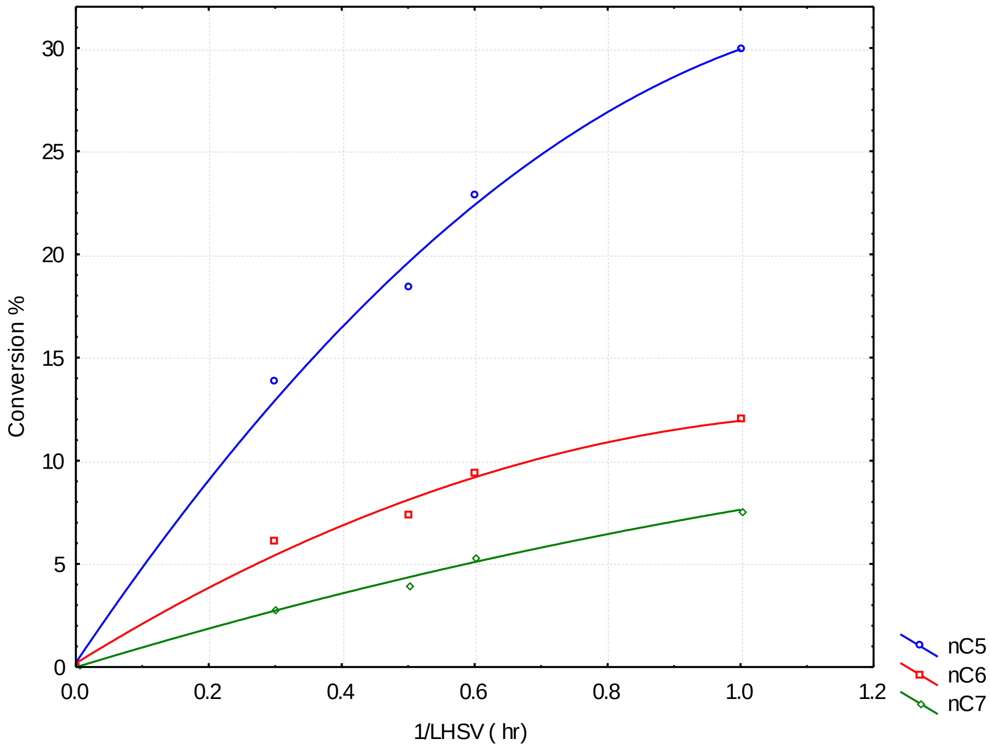

Figure 3 Conversion of nC5, nC6, and, nC7 at different contact time and T=270˚C

Rate of Reaction

According to the differential method, the rate of reaction can be estimated by finding the slop of the line tangent to the curve which represents the relationship between n-alkane conversion and (W/F_{Ao}) at any given point. **Figures 4 - 5** shows the plots of %conversion vs. the(W/F_{Ao}) for nC5, nC6, and nC7.

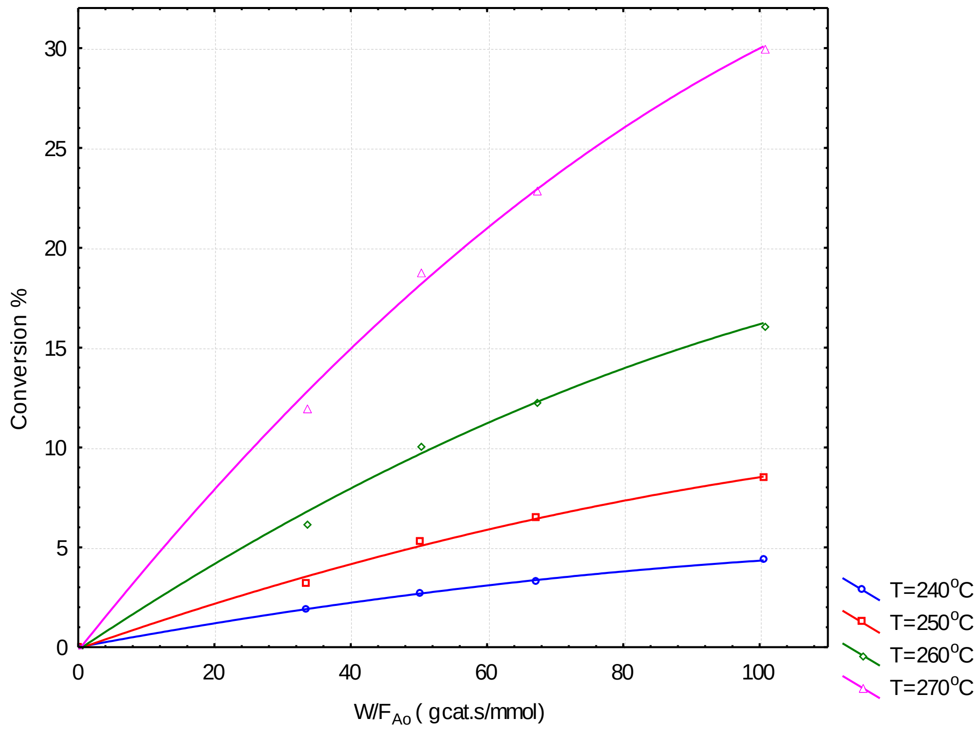

Figure 4 Experimental conversion of nC5 vs W/FAo

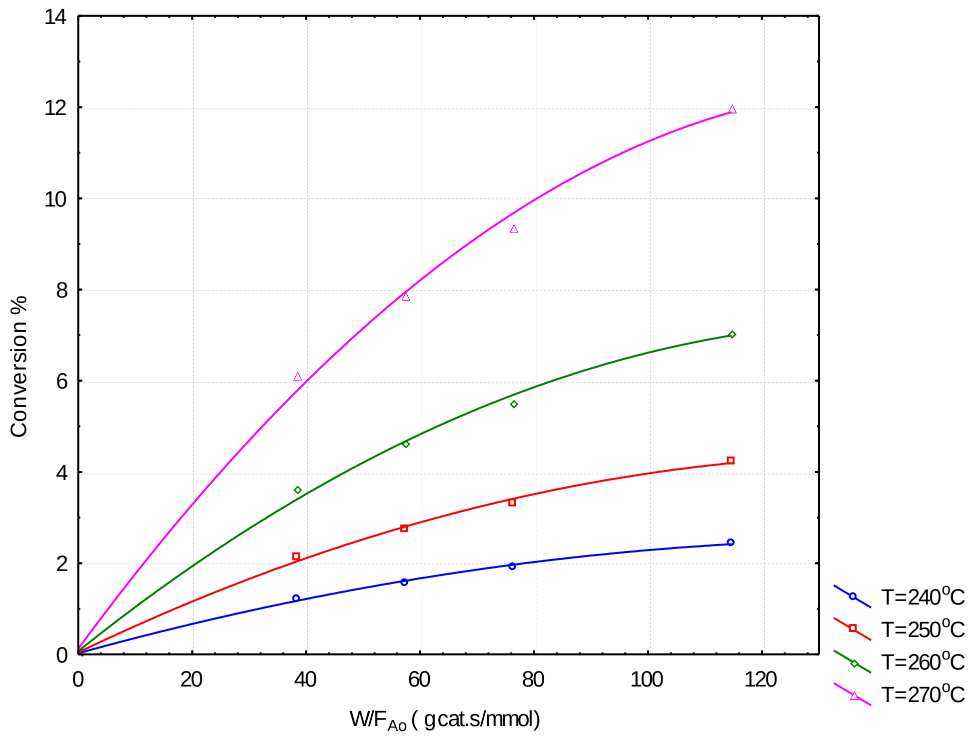

Figure 5 Experimental conversion of nC6 vs W/FAo

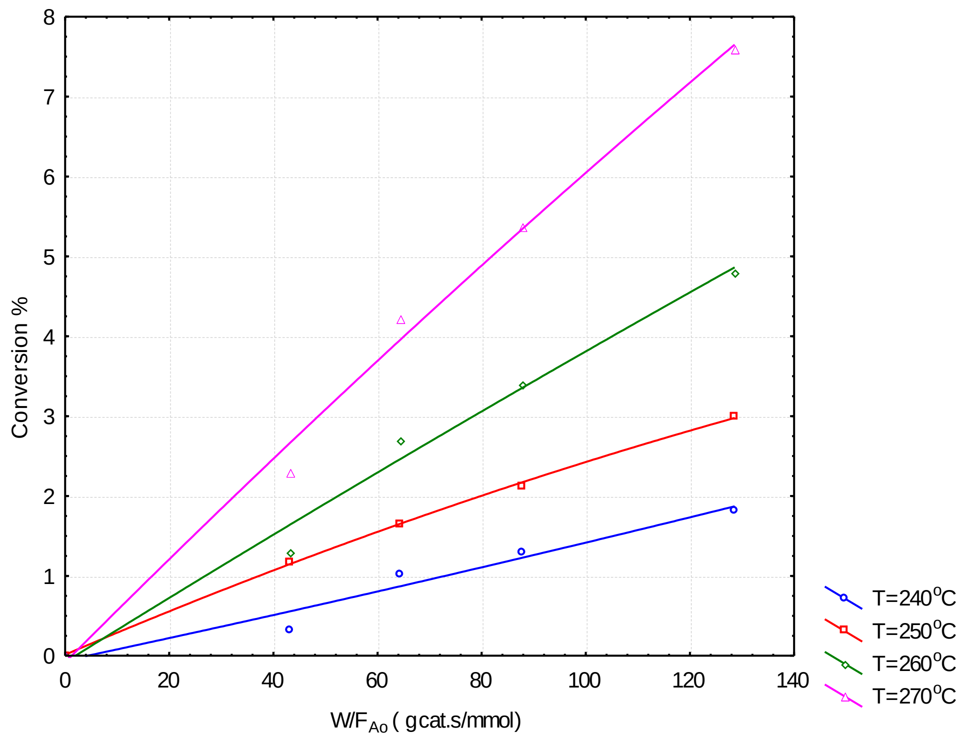

Figure 6 Experimental conversion of nC7 vs W/FAo

The Apparent Activation Energy Measurements

The activation energy (E_{act}) is usually determined by measuring the rate of reaction (***r***) as a function of temperature and fitting the data to Arrhenius equation.

$$r = z\exp(-E_{act} / RT) \qquad \textbf{(1)}$$

Rewriting equation (**1**) gives equation (**2**):

$$\ln(r) = \ln(z) - \frac{E_{act}}{RT} \qquad \textbf{(2)}$$

Table 1 shows the apparent activation energies for *n*C5, *n*C6, and *n*C7 conversions over the temperature range 240-270ºC. These values are determined from the slopes of the straight lines of plots of figures 7 to 9 and according to equation (**2**).

Table 1 Apparent activation energy(kJ/mol) for C5,C6and C7

LHSV hr^{-1}	*n*-C5	*n*-C6	*n*-C7
1	145	119.9	110
1.5	147	120.9	110
2	148	122	110
3	148	122	111

As shown in Table 1 the apparent activation energy decreases with decreasing LHSV, since the rate of reaction increases with decreasing space time. Also, these values are decreases as the carbon number increases. The difference in the apparent activation energies possibly resulted from the different adsorption enthalpy since the experimentally determined activation energy consists of the sum of the true activation energy and the adsorption enthalpy. Additionally, variation of temperature and n-alkane partial pressures can lead to a variation of surface coverage which corresponds to a higher or lower degree of adsorption sides occupied and therefore different adsorption energy is observed

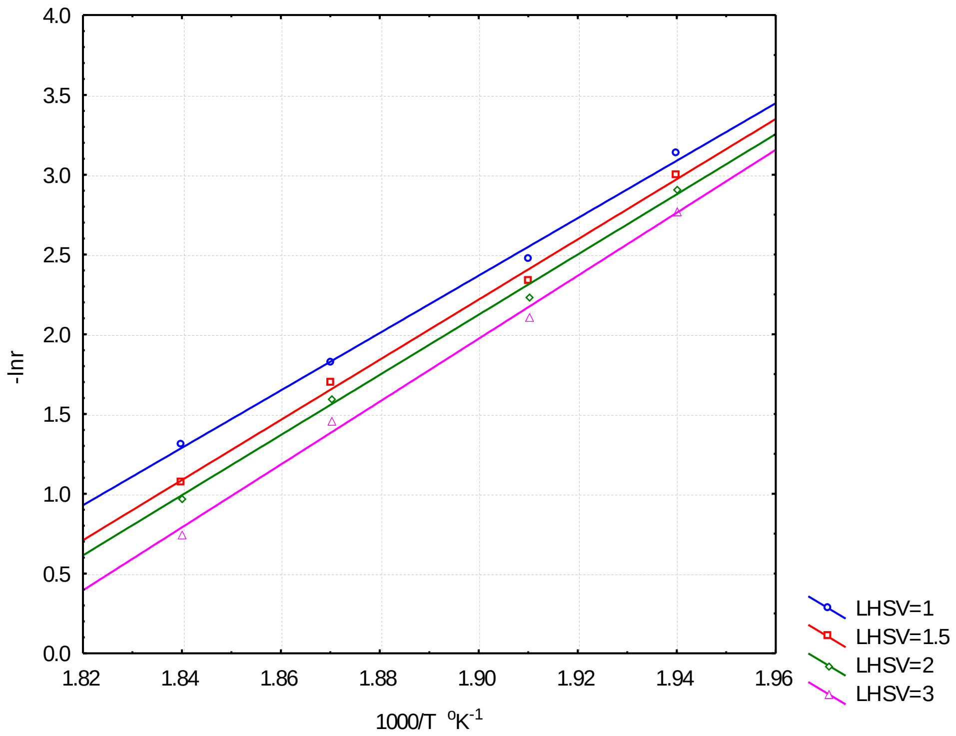

Figure 7 Arrhenius plots for isomerization process of nC5

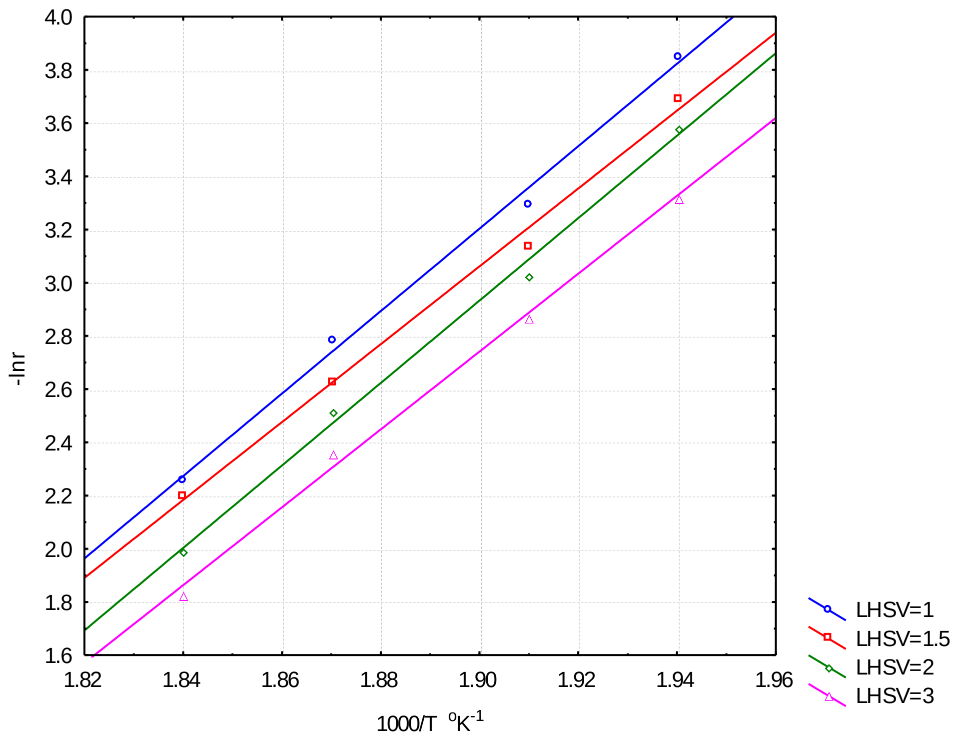

Figure 8 Arrhenius plots for isomerization process of nC6

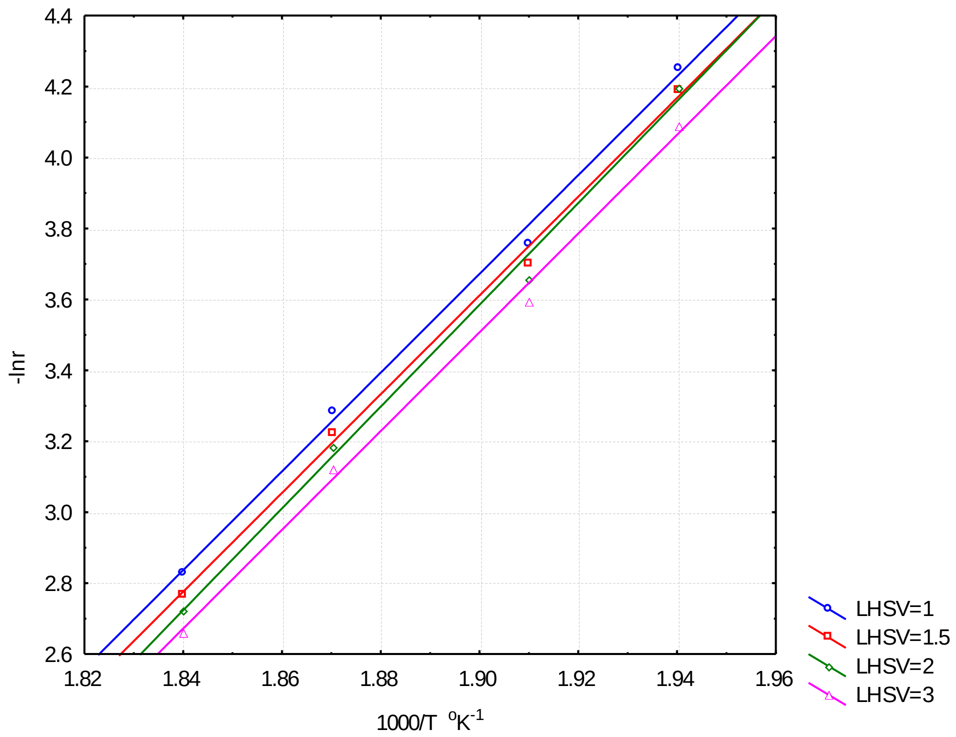

Figure 9 Arrhenius plots for isomerization process of nC7

The reaction order with respect to hydrogen and n-alkane pressure

The effect of deactivation on common empirical kinetic parameters, namely the reaction order with respect to n-alkane (***m***) and hydrogen (***n***) and the apparent activation energy ($E_{act,app}$) is represented in equation 3 [Alvarez et al.,1996]:

$$TOF = k_{re}\ P^{m}_{n-alkane}\ P^{n}_{H2} \quad (\mathbf{3})$$

Where, TOF is the turnover frequency and is defined as the rate of reaction per acid site [Runstraat et al., 1997b], k_{re} is effective reaction rate coefficient. From equation 2.1 it can be gathered that m and n are function of $P_{n\text{-}alkane}$ and P_{H2} ranging from 0 to 1 for (***m***) and -1 to 0 for (***n***). However, in many studies the absolute values of ***m*** and ***n*** is found both ***m***<-***n*** and ***m***> -***n***. These differences are usually attributed to deactivation effects [Alvarez et al.,1996, Santen et al.,1997].Since the TOF is defined as the rate of reaction of n-alkane per acid site, equation (**3**) can be rewritten into the following empirical form:

$$-r = k\ P^{m}_{n-alkane}\ P^{n}_{H2} \quad (\mathbf{4})$$

Where, ***k*** is constant and equal to the effective reaction rate coefficient multiplied by the number of acid site. Rewriting equation (**4**) gives equation (**5**):

$$\ln(-r) = \ln k + m \ln P_{n-alkane} + n \ln P_{H2} \quad (\mathbf{5})$$

The order of reaction with respect to hydrogen at given temperature can be calculated by simulating the reaction at different hydrogen partial pressure and fixed n-alkane partial pressure. According to equation (**5**), plotting ln(-***r***) vs. ln($\mathbf{P_{H2}}$) must gives a straight line with slop equal to ***n***. The order of reaction with respect to n-alkane was achieved by simulation the reaction in variable n-alkane partial pressure and constant hydrogen partial pressure. According to equation (**5**), plotting ln(-***r***) vs. ln($\mathbf{P_{n\text{-}alkane}}$) should gives a straight line with slop equal to ***m***.

Alkane Order Measurement

Table 2 shows the order of reaction with respect to nC5, nC6, and nC7 at different temperature. As shown in table 2, no significant change in the reaction order was detected when the temperature increases from 240-270ºC. The values of the reaction order with respect to n-alkane are arranged in the following manner:

$$\mathbf{C_7 < C_6 < C_5}$$

Table 2 Reaction order with respect to n-alkane(m) at different temperature

Temp ˚K	*n*-C5	*n*-C6	*n*-C7
513	0.339	0.337	0.156
523	0.338	0.335	0.155
533	0.335	0.332	0.154
543	0.336	0.332	0.154

The most likely reason for slight change in the order of reaction may be due to the active sites elimination resulted from deactivation increase with increasing $P_{n\text{-}alkane}$. This is enhanced by the fact that coking involves bimolecular reactions. The extent to which (***m***) is decreased depends on the rate of deactivation which itself is a function of, among other things, temperature and catalyst characteristics. Hence the variation in the deviations from the intrinsic (***m***) values caused by deactivation.

Hydrogen Order Measurement

The orders of reaction with respect to hydrogen (***n***) are tabulated in **table 3**. These values are vary with the n-alkane carbon number, and arranged in the following order:

$$C_5>C_6>C_7$$

Also, it seems that these values are slightly affected when the temperature rises from 240 to 270ºC, the decrease of ***n*** values can be attributed to the change in the number of active sites resulting from coke deposition. The steady state level of deactivation increases with decreasing P_{H2}. These results show that the effect of deactivation on hydrogen order is stronger than on the n-alkane order, indicating that the rate of deactivation is more sensitive to P_{H2} than to $P_{n\text{-alkane}}$. The reason for this is probably that a decrease of P_{H2} not only results in a higher concentration of alkene, but also in a lower rate of decoking reaction.

Table 3 Reaction order with respect to hydrogen (n) at different temperature

Temp ˚K	*n*-C5	*n*-C6	*n*-C7
513	-0.652	-0.811	-0.998
523	-0.640	-0.809	-0.981
533	-0.631	-0.810	-0.968
543	-0.620	-0.808	-0.948

Selectivity and Product Distribution

n-Heptane

Figure 10 shows the distribution of three main products : methylhexane and ethylpentane (monobranched isomers(**MB**)); dimethylpentane (dibranched isomers(**DB**)); and cracked products(**CP**), as a function of the total conversion.

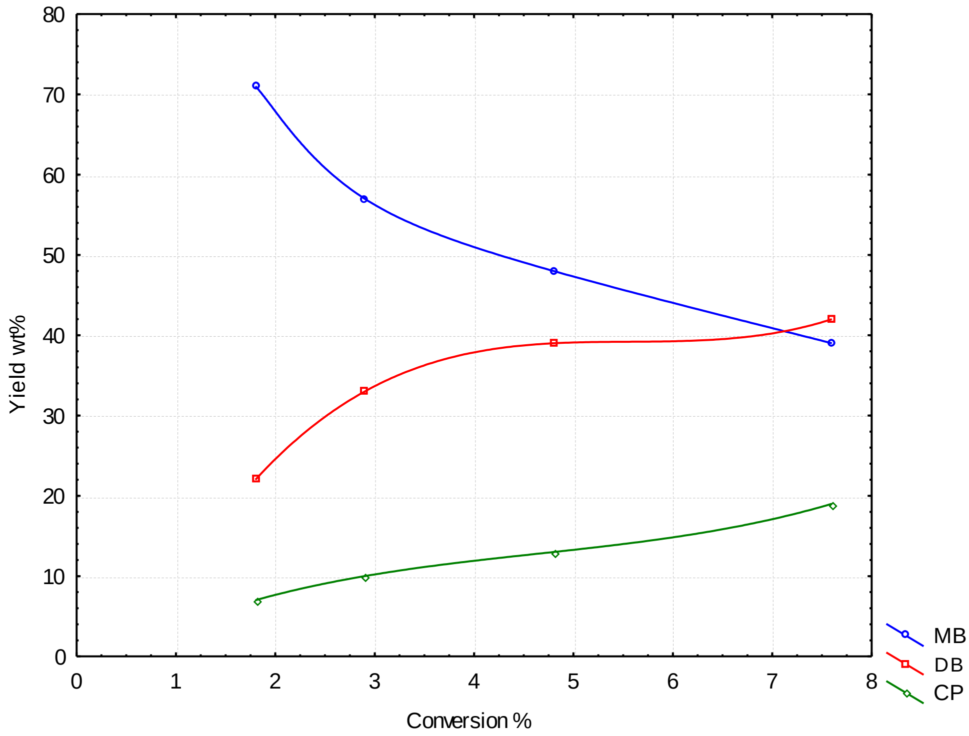

Figure 10 Product distribution for nC7 conversion (LHSV=1hr-1)

Figure 11 shows that Methylhexane constitute over 97% of the mono branched products,and that 2- and 3- methylhexane seems to be in a ratio close to equilibrium value that is around 1.2 (**figure 12**) .

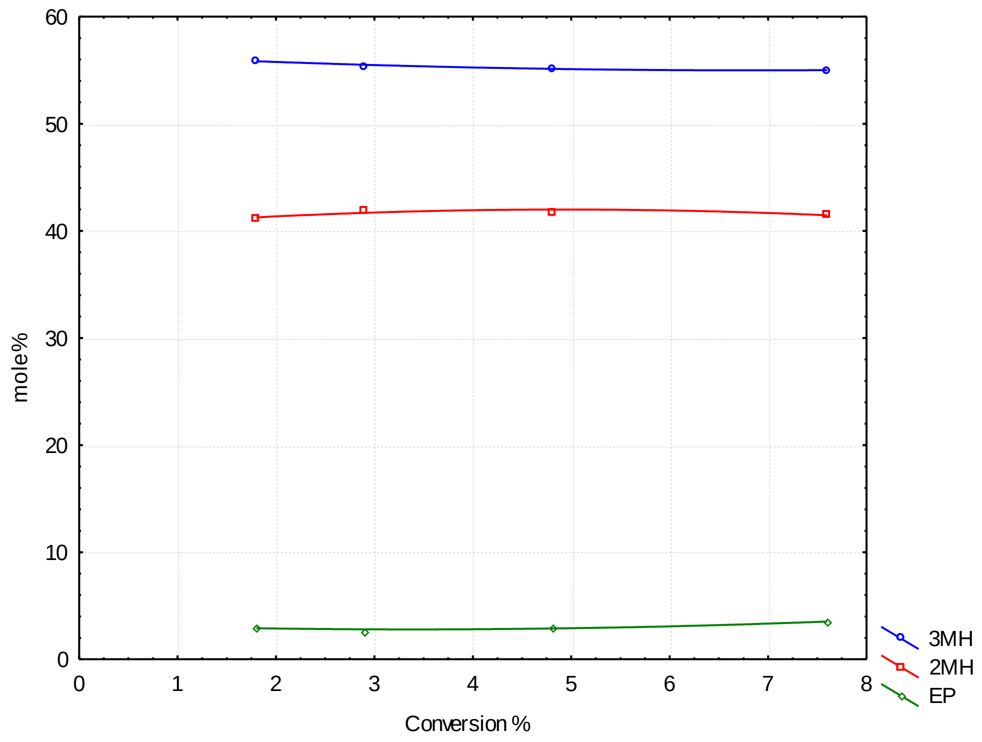

Figure 11 Distribution of monobranched isomers for nC6 conversion (LHSV=1 hr-1)

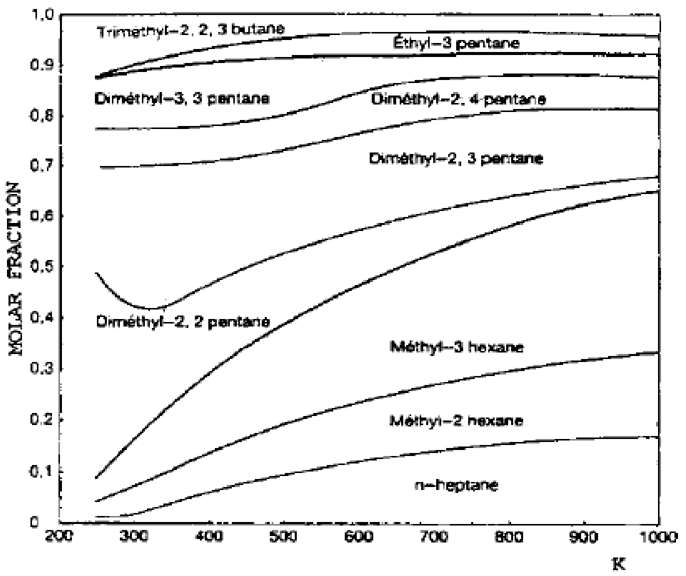

Figure 12 Thermodynamic equiliberium for Heptane isomerization (Pins et al. 1984)

The dibranched isomers distribution changes also very noticeably with the conversion (**figure 13**). 2,3-Dimethylpentane is initially highly favored but disappears for the benefit of 2,2- and 3,3-dimethylpentanes. 2,2,3-Trimethylbutane formed with negligible amount, moreover, its only formed like cracking products for very high conversion. This results are in agreement with the results published by Giusepp et al.(1986).

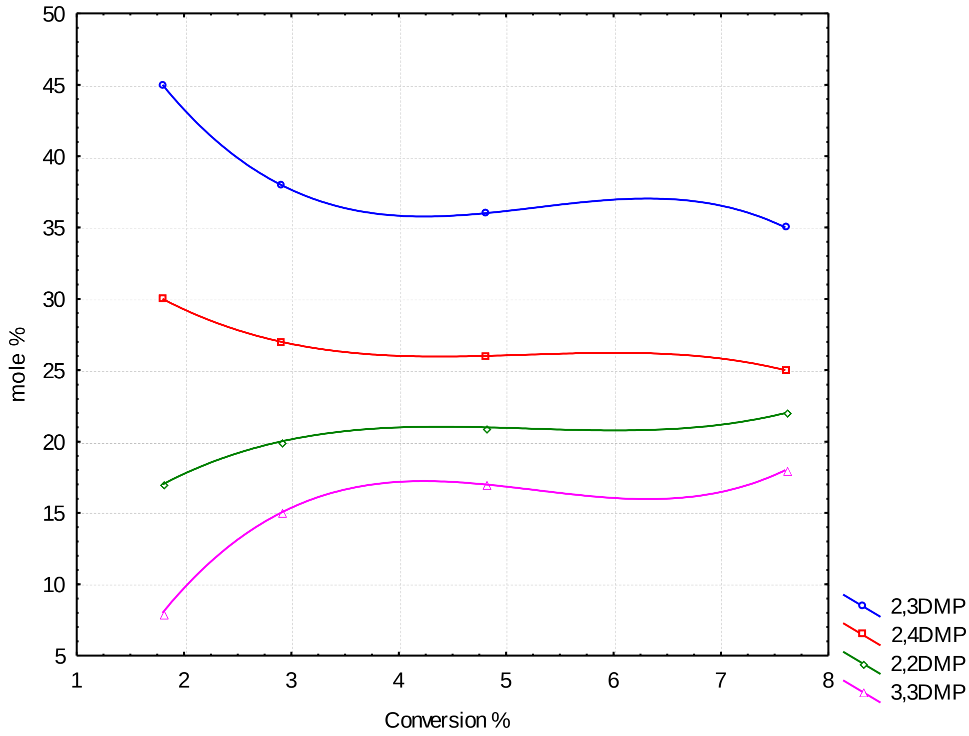

Figure 13 Distribution of dibranched isomers for nC7 conversion (LHSV=1 hr-1)

***n*-Hexane**

Figure 14 shows the distribution of three main products: methylpentane (monobranchedisomers(**MB**)); dimethyl-butane (dibranched isomers (**DB**)); and cracked products(**CP**), as a function of the total conversion.

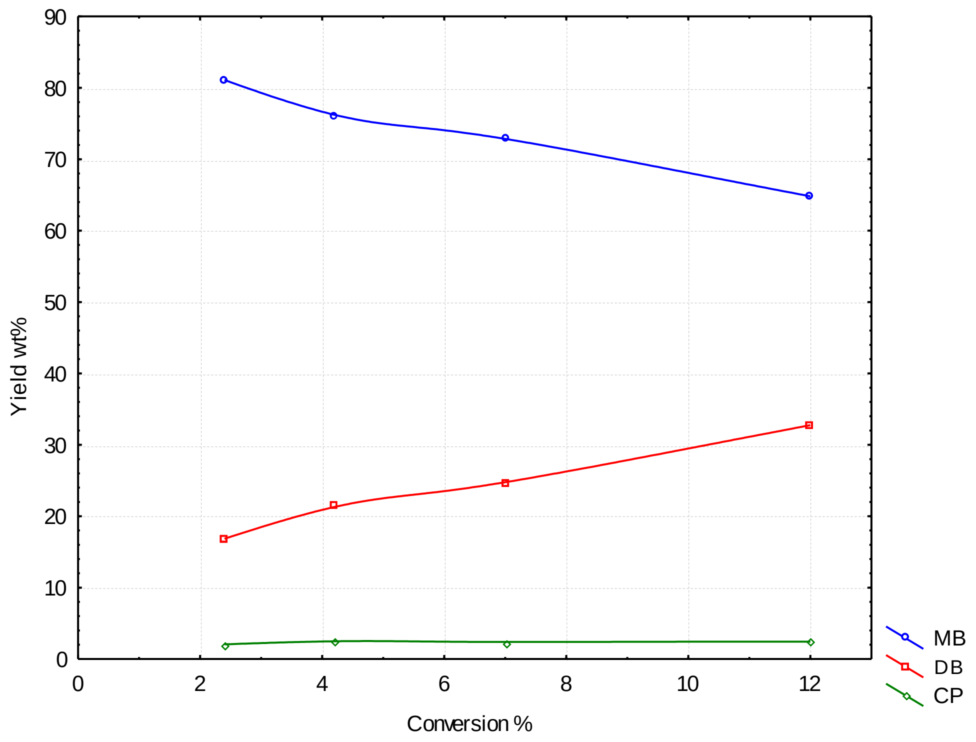

Figure 14 Product distribution for nC6 conversion (LHSV=1hr-1)

Figure 14 shows that the monobranched isomers are the main products. **Figure 15** shows that the 2-methylpentane (2MP)/ 3-methylpentane(3MP) ratio is found to be around the thermodynamic equilibrium value (~1.6) (**figure 16**).

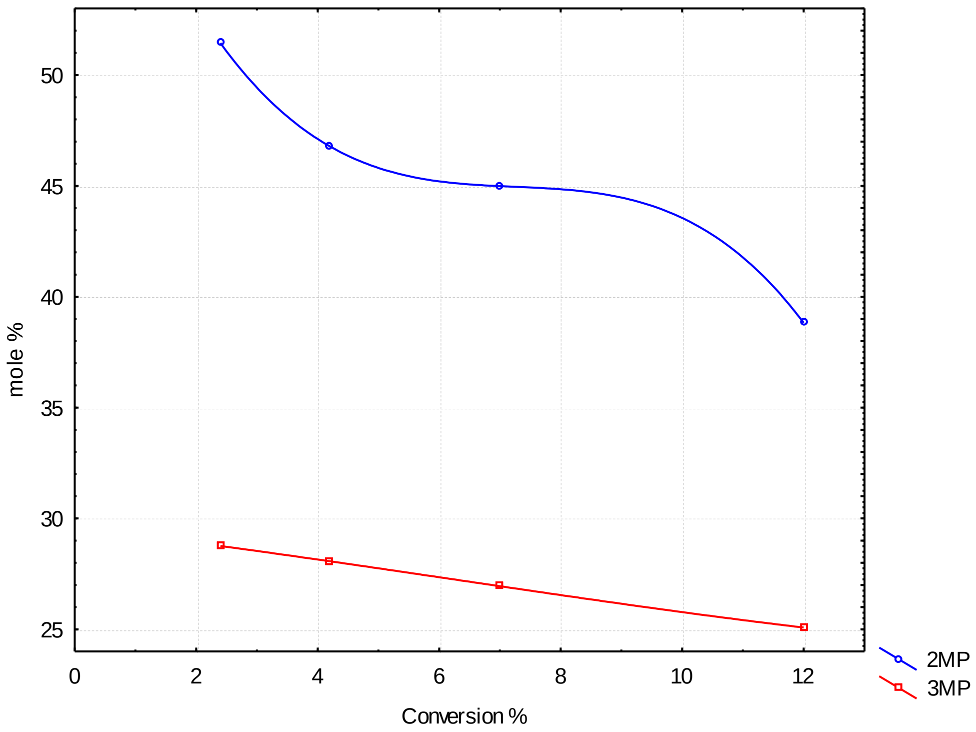

Figure 15 Distribution of monobranched isomers for nC6 conversion (LHSV=1 hr-1)

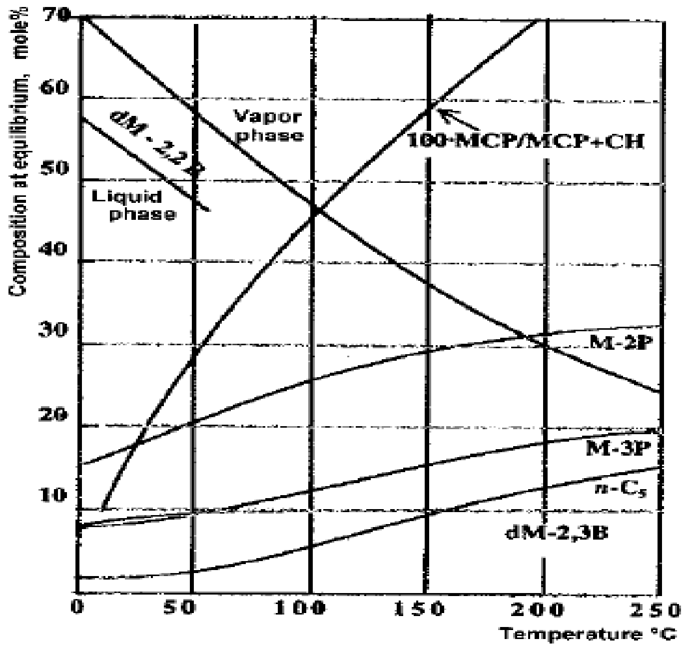

Figure 16 Thermodynamic equiliberium for Hexane isomerization(Serge, 2003)

The ratio of 2-methylpentane (2MP) /2,3-dimetylbutane (2,3DMB) is also reached the thermodynamic equilibrium value as seen in **figure 17**. Further more 2,3DMB should be formed more rapidly than 2,2DMB since 2,3DMB formation involves tertiary cation [Allain et al.,1997]. However, the transformation of 2,3DMB to 2,2DMB is slow because it is required the passage through a tertiary carbocation which is less stable.

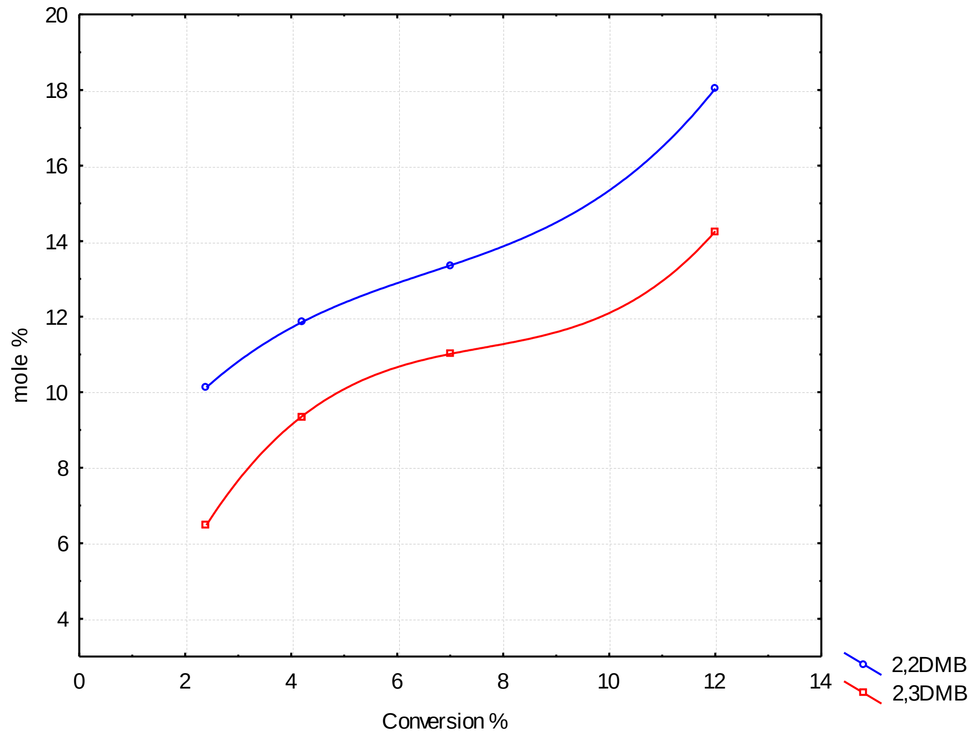

Figure 17 Distribution of dibranched isomers for nC6 conversion (LHSV=1 hr-1)

n-Pentane

Figure 18 show that the iso-pentanes is the main product for n-pentane conversion over Pt/HY-Zeolite, the n-pentane molecules are easily penetrated into the catalyst pore so that the conversion is higher than that for n-hexane and n-heptane reaction.

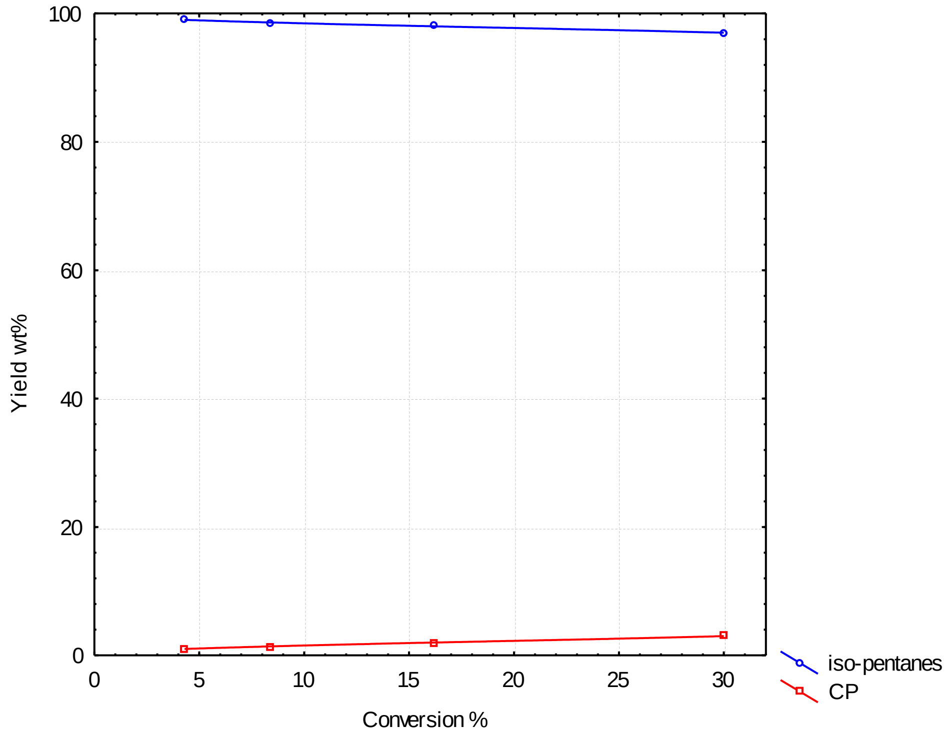

Figure 18 Product distribution for nC5 conversion (LHSV=1hr-1)

CONCLUSION

- It was observed that the isomerization of n-heptane occurs as follows:

  nC7↔(3MH,2MH,EP)↔(2,3DMP,2,4DMP)↔(2,2DMP,3,3DMP)

  and the that the isomerization of n-hexane occur as follows:

  n-C6↔(2MP,3MP)↔(2,3DMB)↔(2,2DMB)

- The conversion of n-pentane, n-hexane, and n-heptane increases as pressure of n-alkane increases and hydrogen pressure decreases. This leads to positive order with respect to n-pentane, n-hexane, and n-heptane , and negative order with respect to hydrogen.
- It was observed that the values of apparent activation energy for hydroisomerization of n-pentane, n-hexane, and n-heptane over the prepared catalyst take the following order

  E_{act} of *n*-Heptane < E_{act} of *n*-Hexane < E_{act} of *n*-Pentane

  And the apparent activation energy decreases with decreasing LHSV since the rate of reaction increases with decreasing space time
- the selectivity to iso-alkanes increases as the n-alkanes chain become shorter. This illustration can be seen in **Figure 19** show a comparison between the selectivity of n-pentane, n-hexane, and n-heptane to the total isomers as a function of temperature. Okuhara (2004) reported that if the number of carbon

atom is 7 or higher, the β-scission of the carbenium ion can take place to form alkenes and carbenium ion with less number of carbon atoms. As a result, a smaller hydrocarbon chains are formed. This is one of the important reasons for the low selectivity in the isomerization of n-heptane especially when the reaction temperature increases. **Figure 20** show a comparison between the selectivity of n-pentane, n-hexane, and n-heptane to the cracked products as a function of temperature.

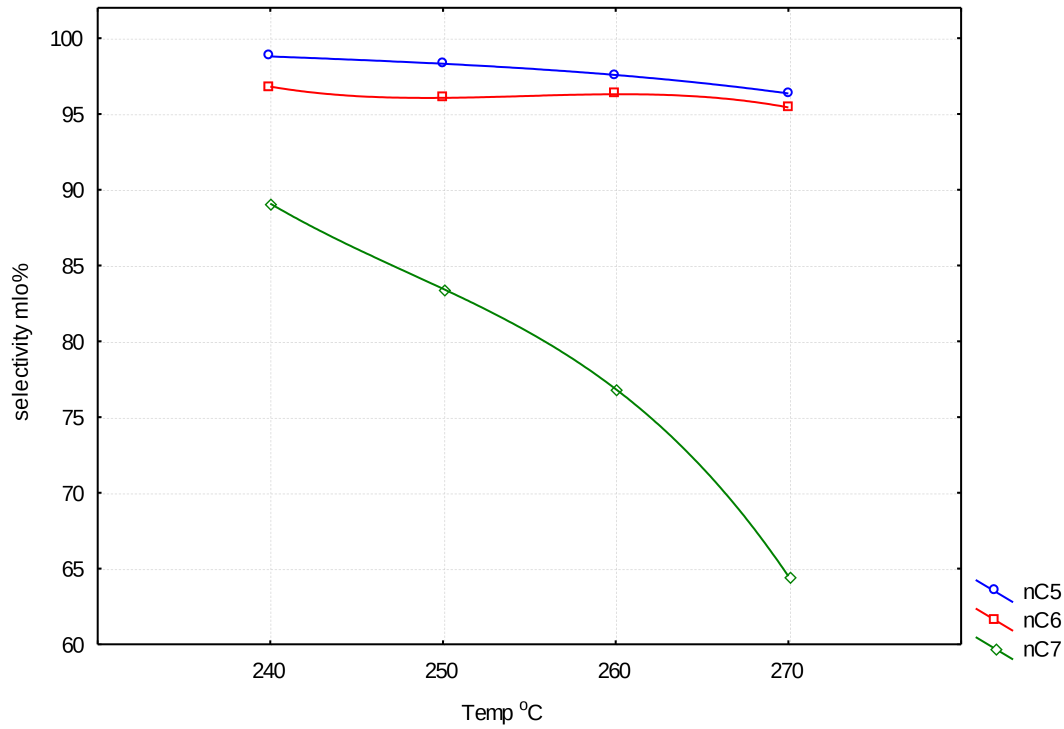

Figure 19 Selectivity to total isomers for nC5, nC6, and nC7 at different temperature (LHSV=1 hr-1)

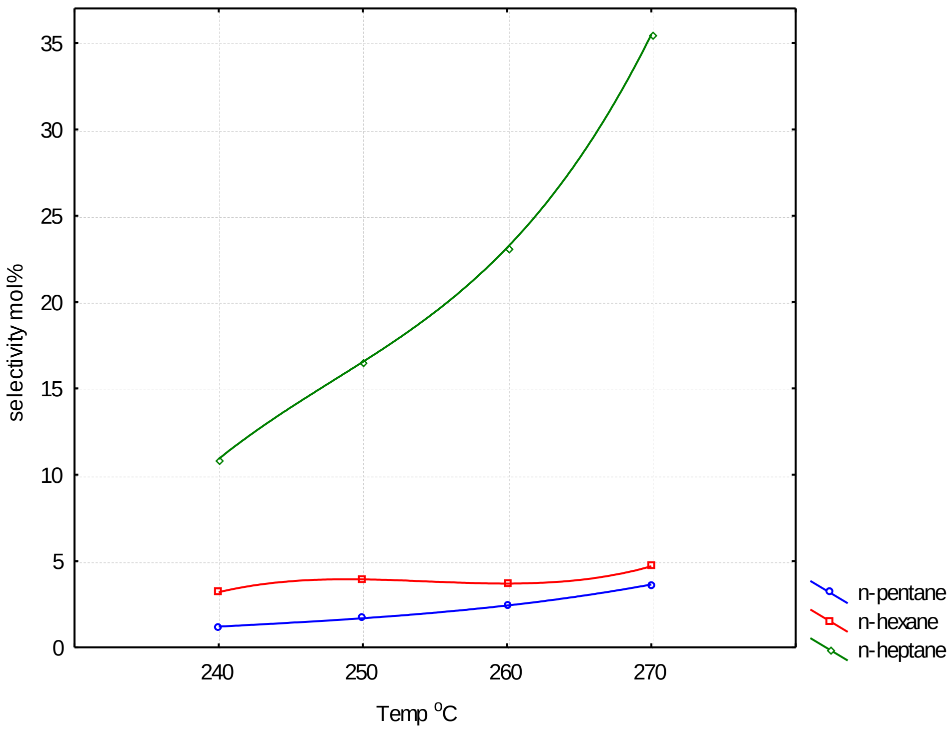

Figure 20 Selectivity to cracked products for nC5, nC6, and nC7 at different temperature (LHSV=1 hr-1)

REFERENCES

- Jafar Sadeghzadeh **Ahari**, Kayvan Khorsand, Azita A Hosseini, Amir Farshi ," EXPERIMENTAL STUDY OF C5/C6 ISOMERIZATION IN LIGHT STRAIGHT RUN GASOLINE (LSRG) OVER PLATINUM MORDENITE ZEOLITE", Pet. & Co. 48 (3), 42-50, 2006.

- **Allain** J. F., P. Magnoux, Ph. Schulz and M. Guisnet," *Hydroisomerization of n-hexane over platinum mazzite and platinum mordenite catalysts kinetics and mechanism*", App. Cat. Vol.152, (2) , 221-235,1997
- **Alvarez**, F., Ribeiro, F.R., Perot, G., Thomazeau, C., Guisnet, M., Jour.of Cat., Vol. 162,(2, 179-189), 1996.
- **Asuquo** R.A.,G.Eder-Mirth, K. Seshan, J. A. Z. Piterse, and J. A. Lercher " *Improving the stability of H-mordenite for n-butane isomerization*" , Jour.of Cat.,168,292-300(1997).
- **Cañizares** P., A. Durán, F. Dorado and M. Carmona, App.Clay Sci.Vol.16, 273-287,2000

- **Exner** H., E. Nagy, F. Fetting, and L. Gubicza, conf. of app. Chem. Vol 2 420-425(1989).
- **Giuseppe** E. Glannetto, Guy R. Perot, and Michel I., *Ind. Eng. Chem. Prod. Res. D8V.* 1986, 25, 481-490
- **Kouwenhoven** H.W. and W.C. Van Zijll Langhout, ,.*Chem .Eng. Prog*., v.67, p.65, 1971

- **Kuchar** P. J., J. C. Bricker, M. E. Reno, R. S. Haizmann, Fuel Pro. Tech., Vol.35, . 1-2, 183-200,1993

- **Lanewala** M. A., P. E. Pickert and A. P. Botton, Journal of CatalysisVolume 9, Issue 1, September 1967, Pages 95-97.
- **Meyers**, A. Robert, "*Handbook of Petroleum Refining Process*." McGraw Hill, New York (1996).
- **Martens** G.G., G.B.Marin, J.A.Martens, P.A. Jacobs, and G.V. Baron" *A fundemental kinetic model for hydrocracking of C8 to C12 alkanes on Pt/US-Yzeolites*", jor.of cat.195,253-267 (2000).
- **Narbesshuber** Thomas F., Axel Brait, Kulathuyiedr Seshan, and Johannes A. Lercher "*Dehydrogenation of light alkanes over zeolite*" , jor. of cat. 172,127-136(1997).
- **OKUHARA** Toshio, *Skeletal Isomerization of n-Heptane to Clean Gasoline*,jour. Of jap.petr.inst. 47,(1),1-10, 2004
- **Pine** L. A., P. J. Maher, W. A. Wachter," *Prediction of cracking catalyst behavior by a zeolite unit cell size model*" Jour. of Cat., Vol. 85, .2, 466-476,1984.
- **Ribeiro** F., C. Marcilly, M. Guisnet, Jour. of Cat., Vol. 78, 2, , Pages 267-274,1982.
- **Runstraat** A. van de, J. A. Kamp, P. J. Stobbelaar, J. van Grondelle, S. Krijnen, and R. A. van Santen, Jour. of Cat. 171, 77–84 (1997a)

- **Runstraat** A. van de, Joop van Grondelle, and Rutger A. van santen, Ind. Eng. Chem. Res.,36,3116-3125. (1997b)
- **Santen** R. A. van, Runstraat A. van de, J. van Grondelle, , Jour.of Cat., Volume 167, .2, Pages 460-463 ,1997.
- **Serge** Raseev, "***Catalytic processes in petroleum refining***", *New York* 2003.

Number 3 Volume 15 September 2009 Journal of Engineering

HYDROGENATION OF D-GLUCOSE TO D-MANNITOL USING RANEY NICKEL CATALYST

Muthanna J. Ahmed
Chemical Engineering Department-College of Engineering-University of Baghdad-Iraq

ABSRACT

Hydrogenation of D-glucose in the presence of Raney nickel as a catalyst was employed for the preparation of D-mannitol. The effects of the reaction time (15-115 min), reaction temperature (15-65 ^{o}C), and catalyst to D-glucose ratio (3-11 %) on the yield of D-mannitol were studied. The experimental design of Box-Wilson method was adopted to find a useful relationship between the effecting variables and the D-mannitol yield. The experimental data collected by this design was successively fitted to a second order polynomial mathematical model. The analysis of variance shows that the reaction time had the greatest effect on the yield of D-mannitol among other variables. An optimum operating conditions of 115 min reaction time, 50 ˚C reaction temperature, and 3 % catalyst to D-glucose ratio gave 14.01 % D-mannitol yield, 81.34 % D-sorbitol yield, and 94.9 % D-glucose conversion. D-Mannitol of purity 99.7 % was obtained after its separation from D-sorbitol, the second product of the hydrogenation process, using the fractional crystallization method.

الخلاصة

يهدف البحث إلى إنتاج المانيتول من الكلوكوز بطريقة الهدرجة و باستعمال (Raney Nickel) كعامل مساعد. تمت دراسة تأثير زمن التفاعل (15- 115 دقيقة)، درجة الحرارة (15- 65 ˚م)، ونسبة العامل المساعد إلى الكلوكوز (3 - 11 %) على إنتاجية المانيتول. استخدمت طريقة (Box-Wilson) لتكوين علاقة رياضية تربط المتغيرات الثلاثة بإنتاجية المانيتول، وتم تمثيل هذه العلاقة بشكل ناجح بمعادلة من الدرجة الثانية (Second-Order Polynomial) وقد بين التحليل الإحصائي (F-test) إن زمن التفاعل هو المتغير ذو التأثير الأكبر على إنتاجية المانيتول. إن الظروف التشغيلية المثلى التي أعطت إنتاجية مانيتول عالية هي زمن تفاعل (115دقيقة)، درجة حرارة (50˚م)، ونسبة عامل مساعد (3%). عند هذه الظروف كانت إنتاجية المانيتول (14,01%)، إنتاجية السوربيتول (81,34%)، ونسبة تحول الكلوكوز (94,9%). تم استخدام طريقة البلورة التجزيئية لفصل المانيتول من السوربيتول، الذي يعتبر الناتج الثاني لعملية الهدرجة، والحصول على مانيتول بنقاوة (99,7%).

KEYWORDS
D-Mannitol, Catalytic Hydrogenation, D-glucose, Raney-Nickel, Box-Wilson Design

INTRODUCTION

D-Mannitol, $C_6H_{14}O_6$, is a hexahydric alcohol with a straight chain of six carbon atoms and six hydroxyl groups. As a pure solid, it is a white, odorless, nontoxic, crystalline material. D-Mannitol has been widely used in the food, pharmaceutical, medicine, and chemical industries. An important use of D-mannitol is for the preparation of mannitol hexanitrate which is a well known vasodilator used in the treatment of hypertension (Von Weymarn, 2002).

D-Mannitol can be extracted from many plant raw materials such as manna, seaweed, and algae. However, the extraction of D-mannitol from these raw materials is not a good commercial source. Both fermentation and catalytic hydrogenation processes are used. The catalytic hydrogenation process has been widely used for the commercial production of D-mannitol (Ojamo et al., 2000).

D-mannitol can be made by the catalytic hydrogenation of three naturally occurring hexoses, D-glucose, D-fructose, and D-mannose. Pure D-mannitol is obtained by the hydrogenation of D-mannose, while an equal portions mixture of both D-mannitol and D-sorbitol is obtained by the hydrogenation of D-fructose. A low portion of D-mannitol as compared with D-sorbitol is obtained when D-glucose is used as the raw material, where a portion of D-glucose is isomerizes to D-fructose and D-mannose. However, D-glucose or a mixture of D-glucose and D-fructose is the practical source because of its greater availability and low cost. Raney nickel catalysts, to which various promoters have been added, are widely used in the hydrogenation process. These catalysts, which are prepared from nickel -aluminum alloys, are approximately as effective as platinum catalysts for promoting many hydrogenations at low pressures and temperatures (Schwarz, 1994).

Different separation processes have been used for the separation of D-mannitol from D-sorbitol. D-Mannitol is readily separated from D-sorbitol by a fractional crystallization from aqueous solutions, in which D-sorbitol is soluble (Devose, 1995). Both D-mannitol and D-sorbitol can be separated chromatographically on a column of calcium poly styrenesulfonate, which professionally retains D-sorbitol (Melaja and Hamalainen, 1975).

Experimental designs are frequently performed in the study of empirical relationships between one or more measured responses and a number of variables. Having such relations, it can specify a combination of variables that will achieve some practical benefit. In the chemical industry, experimental designs are particular applied to the study of process variables and how they affect the product. The basic types of experimental design are factorial design, fractional factorial design, and Box-Wilson design (Montogomary, 1976).

The catalytic hydrogenation process was used by different researchers to prepare D-mannitol from different feedstocks using different catalysts. Makkee et al. (1980) used a platinum metal catalyst for the preparation of D-mannitol by catalytic hydrogenation of a mixture of D-glucose and D-fructose. Makkee et al. (1985) prepared D-mannitol by catalytic hydrogenation of D-glucose over a copper on silica catalyst. Toukoniitty et al., (2005) used Raney nickel catalyst for the preparation of D-mannitol by catalytic hydrogenation of D-fructose.

The aim of the present work is to study the catalytic hydrogenation of D-glucose to D-mannitol using Raney nickel catalyst, and the effect of reaction time, reaction temperature, and catalyst ratio on the yield of D-mannitol.

EXPERIMENTAL WORK

Materials

D-Glucose: D-Glucose (supplied by Hopkin and Williams, Searle Company) of purity 99% was used for the preparation of D-mannitol.
Hydrogen: Hydrogen (supplied by Al-Mansour Factory) of purity 99.9% was used for D-glucose hydrogenation.
Catalyst: Highly active Raney nickel catalyst (supplied by Aldrich Company) of pore size 50 μ and surface area 90 m^2/g was used for the hydrogenation of D-glucose to D-mannitol. It was stored as 50% slurry in water. Its nickel content was 75.11%.

Apparatus

A schematic diagram of laboratory experimental unit used for the hydrogenation of D-glucose is shown in Fig.1. This unit consists of a reaction flask which was a pyrex three-necked 500ml glass flask. The feed was charged to the reaction flask through a glass dropping funnel with a capacity of 100ml, and the hydrogen gas was fed to the reaction flask by means of a special perforated bulb tube (Sparser) in order to keep the solution in considerable agitation and to prevent settling of the catalyst. The loss of vapor from the reaction flask was prevented by using a pyrex double pipe glass condenser with an inner pipe of spiral shape. The reaction flask temperature was measured by a glass thermometer range from 0 to 100˚C, and maintained at the desired value by the use of a water bath. The hydrogen gas flow rate was controlled by a needle valve (Micro Hooke mite) and measured by a rotameter (GEC-Elliott). The composition of product was measured by a shimadzu Lc-6A high performance liquid chromatography (HPLC) system consist of: 6mm ID x 150mm L column (Shim-Pack CLC-ODS) and spectrophotometric detector (SPD-6A at 63nm).

Experimental Procedure

20 wt% D-glucose solution was prepared by dissolving 40 g D-glucose in 160 ml distilled water. This solution was brought to pH value of 9 by the addition of 0.01 g calcium hydroxide per 40 g D-glucose and mixed with 2-6 g Raney nickel catalyst to form the reaction slurry. The resultant slurry was charged through the dropping funnel into the reaction flask. When the required temperature was reached, hydrogen gas was fed continuously at a flow rate of 1.86 liter/min through the reaction slurry by means of the perforated glass bulb tube to keep the slurry in considerable agitation during the reaction time. At the end of duration time, the solution was cooled and the catalyst was allowed to settle at the bottom of the reaction flask. The supernatant solution was filtered and by HPLC method for its D-mannitol, D-sorbitol, and D-glucose content. The above procedure was applied at the optimum operating conditions and the D-mannitol was separated from the product solution as follows:

The alkaline product solution (filterate) was first neutralized with dilute sulfuric acid and then concentrated to about 33ml at a temperature of 45 ˚C and under a pressure of 50 mmHg using a glass evaporation-vacuum system. To this solution, 50 ml of 90% ethanol was added and the precipitated salts were removed by filtration. The solution was cooled to 15 ˚C and seeded with D-mannitol. After 2 hours, D-mannitol crystallized in the form of fine needle-like crystals whish were separated by filtration, washed with cold 80% ethanol, and dried at 40 ˚C and 600 mmHg.

The dried D-mannitol crystals were recrystallized twice from ethanol, filtered and dried. Then the purity (assay) of D-mannitol was 99.7.

The D-mannitol yield, D-sorbitol yield, and D-glucose conversion are defined mathematically as follows:

$$\text{D-Mannitol yield}\,(\%) = \frac{W_m}{W_{gf}} * 100 \tag{1}$$

$$\text{D-Sorbitol yield}\,(\%) = \frac{W_s}{W_{gf}} * 100 \tag{2}$$

$$\text{D-Glucose conversion}\,(\%) = \frac{W_{gf} - W_{gp}}{W_{gf}} \tag{3}$$

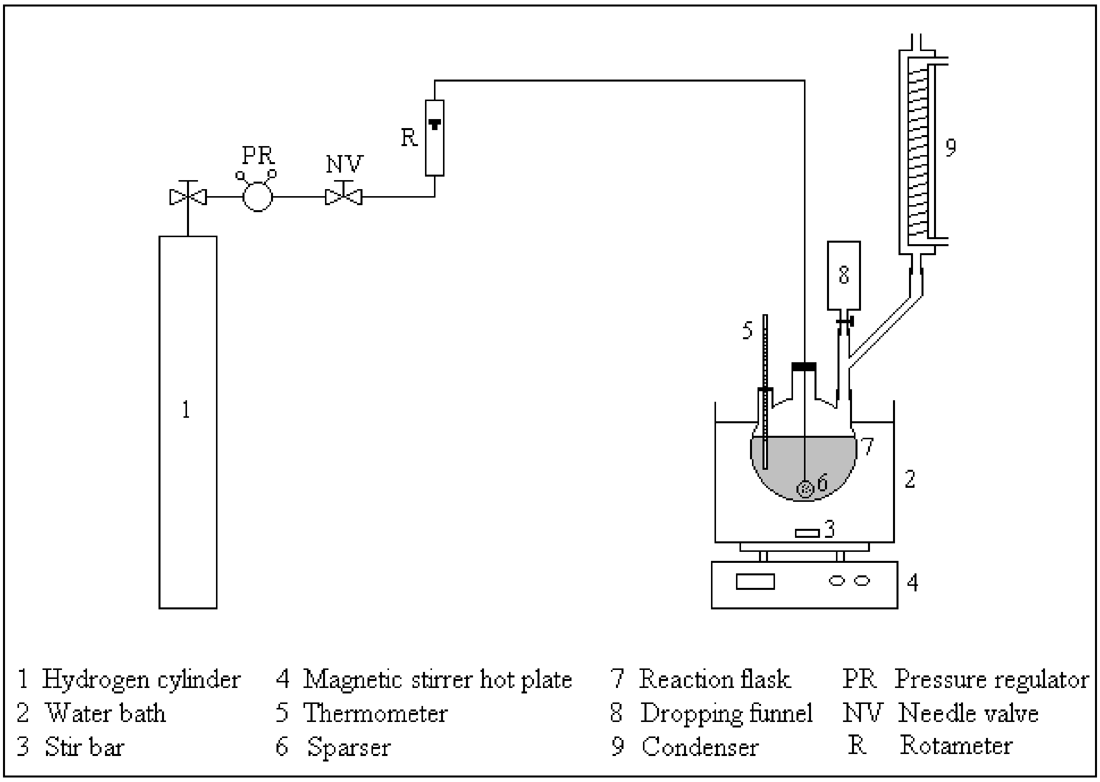

Fig. 1, Schematic diagram of D-Glucose Hydrogenation Unit

Mathematical Modeling

A second order polynomial mathematical model was employed to represent the yield of D-mannitol y as a function of reaction time X_1, reaction temperature X_2, and catalyst ratio X_3. The general form of this model for three variables is represented by the following equation:

$$\begin{aligned} y &= B_o + B_1X_1 + B_2X_2 + B_3X_3 + B_4X_1X_2 + B_5X_1X_3 \\ &\quad + B_6X_2X_3 + B_7X_1^2 + B_8X_2^2 + B_9X_3^2 \end{aligned} \tag{4}$$

An experimental design based on Box-Wilson central composite method was used to organize the experiments. In order to design the experiments, the operating range of the variables is first specified, thus:

X_1=reaction time from 15 to 115 min.
X_2=reaction temperature from 15 to 65 ˚C.
X_3=catalyst ratio from 3 to 11 %.

The total number of experiments N is computed according to the following equation:

$$N = 2^P + 2P + 1 \tag{5}$$

Then:

$$N = 2^3 + 2(3) + 1 = 15$$

The relationship between the coded variable and the corresponding real variable is as follows:

$$X_{coded} = \left(\frac{X_{actual} - X_{center}}{X_{center} - X_{min}}\right) * \sqrt{P} \tag{6}$$

Then:

$$X_{1coded} = \left(\frac{X_{1actual} - 65}{50}\right) * \sqrt{3} \tag{7}$$

$$X_{2coded} = \left(\frac{X_{2actual} - 40}{25}\right) * \sqrt{3} \tag{8}$$

$$X_{3coded} = \left(\frac{X_{3actual} - 0.07}{0.04}\right) * \sqrt{3} \tag{9}$$

RESULTS AND DISCUSSION

Analysis of Box-Wilson Experimental Results

Table 1 shows the coded and real values of independent variables for the experiments to be conducted according to Box-Wilson method, and the experimental response represented by D-mannitol yield.

A nonlinear least-squares regression program based on Gauss-Newton method was used to fit Eq. (4) to the coded data and experimental D-mannitol yield given in Table 1. This fitting gave the predicted D-mannitol yield y, the residual error e, and the coefficients B of this equation as shown in Table 2. The fitted response surface of Eq. (4) is:

$$\begin{aligned} y &= 9.30 + 2.28X_1 + 1.14X_2 - 2.27X_3 - 0.078X_1X_2 + 0.017X_1X_3 \\ &\quad + 0.037X_2X_3 - 0.638X_1^2 - 0.799X_2^2 - 0.639X_3^2 \end{aligned} \qquad (10)$$

The analysis of variance (F-test) was used for testing the significance of each effect in Eq. (2). The calculations are given in Table 3.

An estimate of the variance S_b^2 is obtained by dividing the experimental error variance S_r^2 by the sum of squares of each effect ΣX^2 ,as follows:

$$S_b^2 = S_r^2 / \Sigma X^2$$

Where

$$S_r^2 = (\Sigma e^2) / \gamma$$

$$\gamma = N - n$$

The significance of effects may be estimated by comparing the values of the ratio (B^2/Sb^2) with the critical value of the F-distribution at 95 % confidence level ($F_{0.95}$=6.61). If the ratio B^2/Sb^2 > 6.61 then the effect is significant. Thus, according to the results shown in Table 3, it appears that the interaction effects are not significant. The best response function is then conveniently written as follows:

$$y = 9.30 + 2.28X_1 + 1.14X_2 - 2.27X_3 - 0.638X_1^2 - 0.799X_2^2 - 0.639X_3^2 \qquad (11)$$

This equation represents the best form of the mathematical model that relates the D-mannitol yield y to the three variables in terms of coded levels. An equivalent equation, in terms of the actual levels will be more useful in estimating the response for any desired conditions in the range of the independent variables. The new equation with a correlation coefficient of 97 % is obtained as follows:

$$\begin{aligned} y &= -7.89313 + 0.181469X_1 + 0.398825X_2 + 75.29651X_3 - 0.000789X_1^2 \\ &\quad - 0.003984X_2^2 - 1239.08X_3^2 \end{aligned} \qquad (12)$$

The optimum operating conditions was determined by differentiating both sides of Eq. (12) for each independent variable and equating the derivative to zero. Thus, the optimum conditions corresponding to a maximum D-mannitol yield are 115 min reaction time, 50 ˚C reaction temperature, and 3 % catalyst ratio. At these conditions the optimum theoretical D-mannitol yield calculated from Eq. (12) is 13.66 % and the experimental yield is 14.01 %. Also the experimental D-sorbitol yield is 81.34 % and D-glucose conversion is 94.9 %.

Effect of Reaction Time

Figures 2 and 3 show the effect of reaction time on the theoretical D-mannitol yield at different reaction temperatures and catalyst ratios, respectively.

Figure 2 shows that the yield of D-mannitol increases with increasing reaction time. An increase in reaction time from 15 to 115 min at 50 ˚C and 3 % catalyst ratio leads to an increase in D-mannitol yield from 5.77 to 13.66 %. Figure 3 together with Fig. 2 show that there is no interaction between reaction time and catalyst ratio, and also between reaction time and temperature as summarized in Table 3. The results of this table show that the reaction time has the greatest effect on D-mannitol yield.

Effect of Reaction Temperature

The effect of reaction temperature on the theoretical yield of D-mannitol at different reaction times and catalyst ratios is shown in Figs. 4 and 5, respectively.

These figures indicate that at lower temperature, longer reaction time and smaller amounts of catalyst are necessary to obtain comparable values of D-mannitol yield. At 45 ˚C and 3 % catalyst ratio, 8.2 % D-mannitol yield is achieved in 35 min, while at 19 ˚C and 3 % catalyst ratio, 75 min is needed to achieve the same yield, as shown in Fig. 4. Figure 5 shows that at 45 ˚C and 115 min, 8.2 % D-mannitol yield is obtained using 9 % catalyst ratio, while at 19 ˚C and 115 min it is necessary to use 6 % catalyst ratio in order to reach the same yield.

Figures 5 and 6 also show that the use of high temperatures (above 50 ˚C) reduces D-mannitol yield, because at high temperatures, Raney nickel catalyst losses its activity as explained by Jianping et al. (2004).

Effect of Catalyst Ratio

Figures 6 and 7 show the effect of catalyst ratio on the theoretical D-mannitol yield at different reaction times and temperatures, respectively.

In Fig. 6, the yield of D-mannitol yield decreases with the increase of catalyst ratio. An increase in the catalyst ratio from 3 to 11 % at 50 ˚C and 115 min causes a decrease in the yield of D-mannitol from 13.66 to 5.81 %. The use of low catalyst ratio increases D-mannitol yield, because the rate of isomerization of D-glucose will be greater than its hydrogenation rate, as explained by Makkee et al. (1985). This figure also shows that the time required to reach 8.2 % yield can be reduced from 75 to 35 min by decreasing the catalyst ratio from 9 to 5 %.

Figure 7 shows that there is no interaction between the catalyst ratio and the reaction temperature, as explained in Table 3. This table shows that the catalyst ratio and reaction time have nearly the same effect on the yield of D-mannitol.

Table 1, D-Mannitol Yields of Box-Wilson Method Experiments

Run No.	Coded Variables			Real Variables			D-Mannitol Yield (%)
	X_1	X_2	X_3	X_1	X_2	X_3	
1	-1	-1	-1	36	26	0.0469	6.05
2	1	-1	-1	94	26	0.0469	10.29
3	-1	1	-1	36	54	0.0469	8.86
4	1	1	-1	94	54	0.0469	13.01
5	-1	-1	1	36	26	0.0931	1.89
6	1	-1	1	94	26	0.0931	6.42
7	-1	1	1	36	54	0.0931	5.07
8	1	1	1	94	54	0.0931	9.07
9	-1.732	0	0	15	40	0.07	2.57
10	1.732	0	0	115	40	0.07	11.25
11	0	-1.732	0	65	15	0.07	5.09
12	0	1.732	0	65	65	0.07	7.76
13	0	0	-1.732	65	40	0.03	11.52
14	0	0	1.732	65	40	0.11	2.29
15	0	0	0	65	40	0.07	9.30

Table 2, Statistical Analysis Results of Fitting Eq. (4)

No.	X_1	X_2	X_3	Y(%)	y(%)	e(%)	Coefficient B	
1	-1	-1	-1	6.05	6.05	0	B_0	9.30
2	1	-1	-1	10.29	10.73	-0.44	B_1	2.28
3	-1	1	-1	8.86	8.41	0.45	B_2	1.14
4	1	1	-1	13.01	12.78	0.23	B_3	-2.27
5	-1	-1	1	1.89	1.40	0.49	B_4	-0.078
6	1	-1	1	6.42	6.16	0.27	B_5	0.017
7	-1	1	1	5.07	3.91	1.16	B_6	0.037
8	1	1	1	9.07	8.36	0.71	B_7	-0.638
9	-1.732	0	0	2.57	3.43	-0.86	B_8	-0.799
10	1.732	0	0	11.25	11.34	-0.09	B_9	-0.639
11	0	-1.732	0	5.09	4.93	0.16		
12	0	1.732	0	7.76	8.88	-1.12		
13	0	0	-1.732	11.52	11.31	0.21		
14	0	0	1.732	2.29	3.46	-1.17		
15	0	0	0	9.30	9.30	0		

Table 3, Variance Analysis of Variable Effects*

Effect	$\sum X^2$	Coefficient B		Variance $S_b^2 = S_r^2 / \sum X^2$	F-value $= B^2/S_b^2$	$F_{0.95}$ =6.61
	15	B_0	9.30			
X_1	14	B_1	2.28	0.086	60.45	S
X_2	14	B_2	1.14	0.086	15.11	S
X_3	14	B_3	-2.27	0.086	59.92	S
X_1X_2	8	B_4	-0.078	0.151	0.040	NS
X_1X_3	8	B_5	0.017	0.151	0.002	NS
X_2X_3	8	B_6	0.037	0.151	0.009	NS
X_1^2	26	B_7	-0.638	0.047	8.66	S
X_2^2	26	B_8	-0.799	0.047	13.58	S
X_3^2	26	B_9	-0.639	0.047	8.69	S

* S= Significant, NS= Not Significant

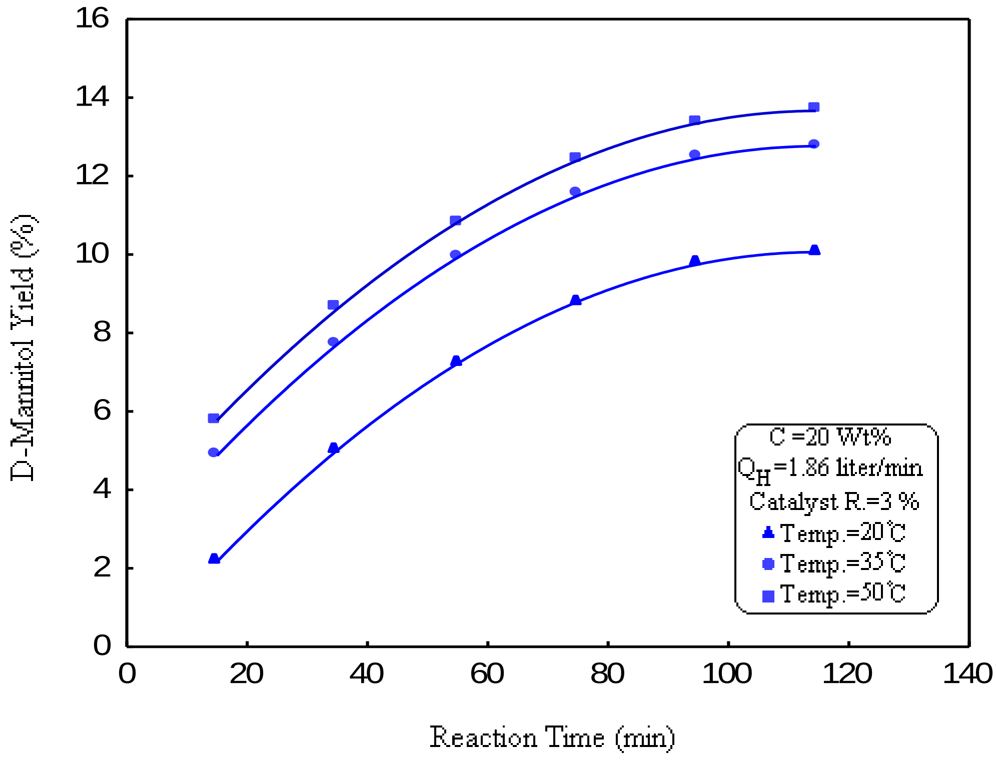

Fig. 2, D-Mannitol Yield Vs. Reaction Time at Different Temperatures

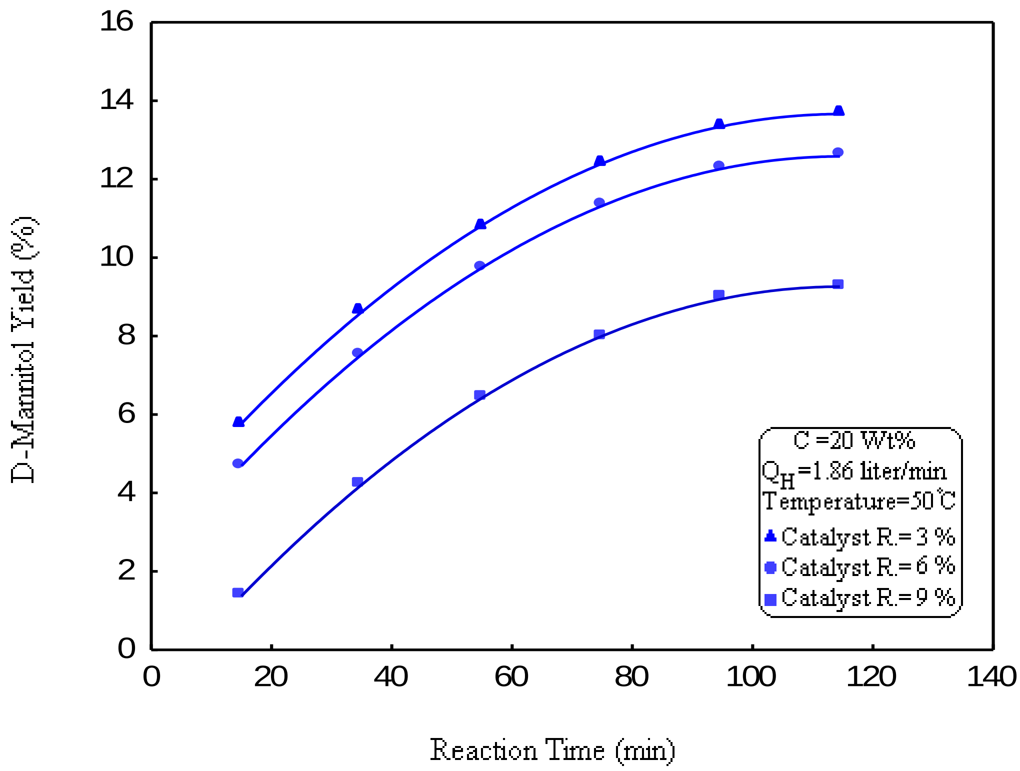

Fig. 3, D-Mannitol Yield Vs. Reaction Time at Different Catalyst Ratios

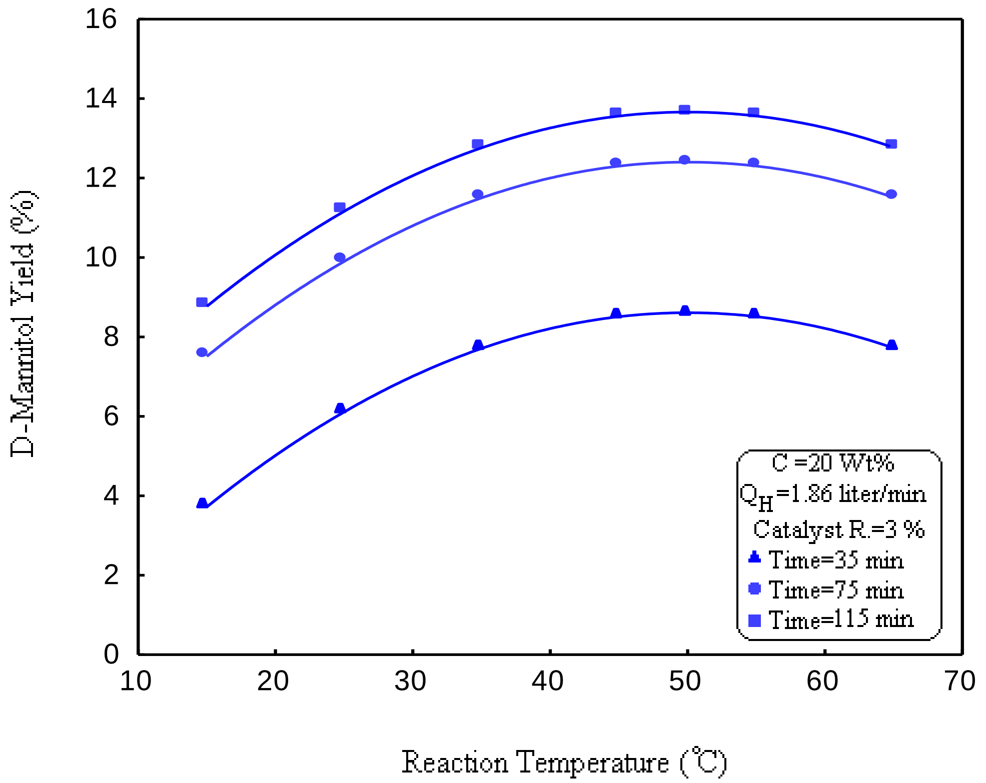

Fig. 4, D-Mannitol Yield Vs. Reaction Temperature at Different Times

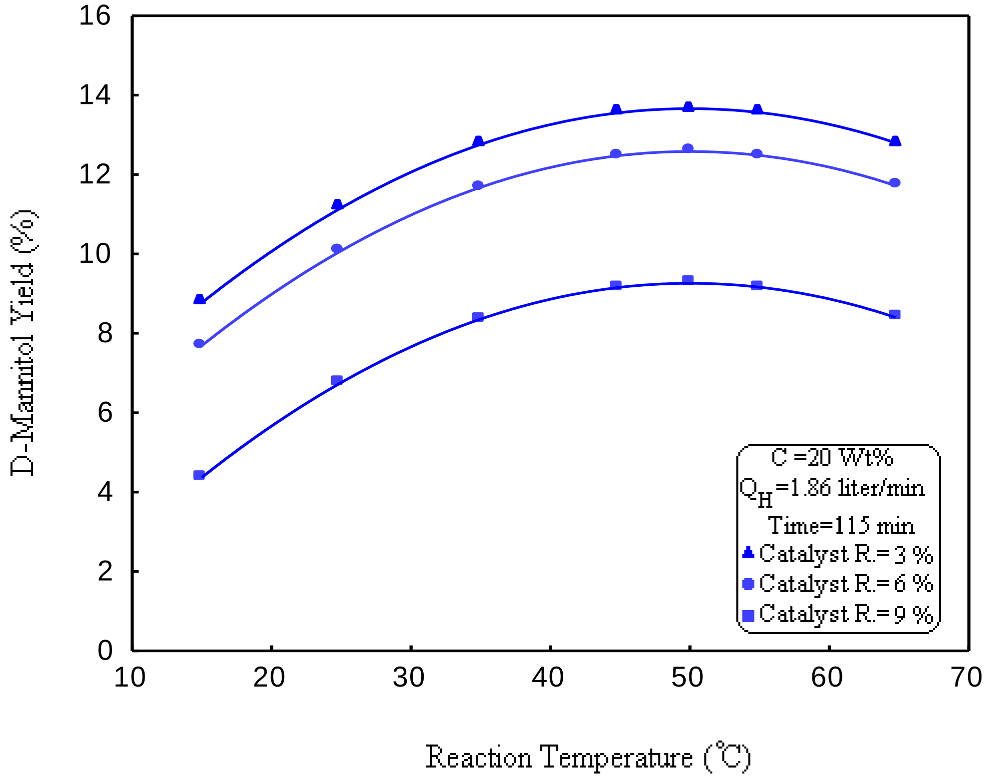

Fig. 5, D-Mannitol Yield Vs. Reaction Temperature at Different Catalyst Ratios

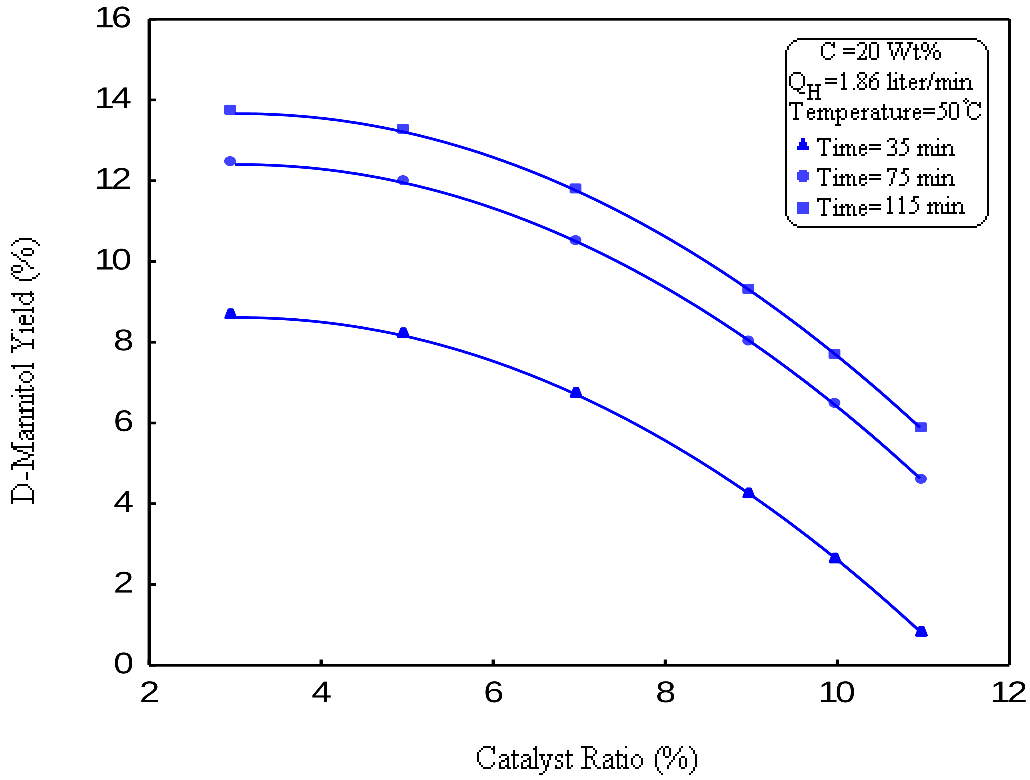

Fig. 6, D-Mannitol Yield Vs. Catalyst Ratio at Different Times

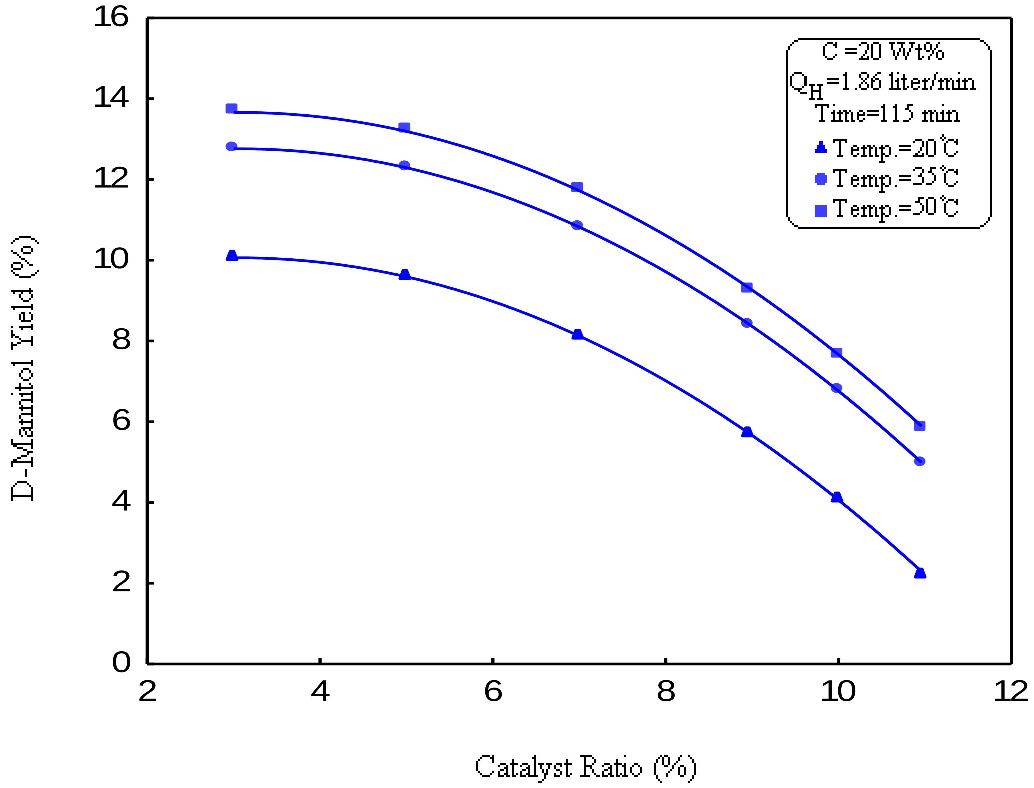

Fig. 7, D-Mannitol Yield Vs. Catalyst Ratios at Different Temperatures

CONCLUSSIONS

- The reaction time had the greatest effect on D-mannitol yield, as compared with the other variables.
- There was no interaction between the reaction time, reaction temperature, and catalyst ratio.
- A quantitative relationship between D-mannitol yield and the three variables was well represented by a second order polynomial mathematical model.
- A maximum D-mannitol yield of 13.66% was obtained at 115 min reaction time, 50˚C reaction temperature, and 3 % catalyst ratio.

REFERENCES

Devose, F., (1995), "Process for the Production of Mannitol", U.S. Patent, US 5466795.

Jianping, W., Changlin, W., and Yanxin, L., (2004), "The Preparation of D-Glucitol in A Multi-Tube Airlift Loop Reactor with Low H/D Ratio, Chem. Biochem. Eng. Q., 18, 3, 273-277.

Makkee, M., Kieboom, A.P.G., and Van Bekkum, H. (1980), "Combined Action of Enzyme and Metal Catalyst, Applied to the Preparation of D-Mannitol", J.Chem.Soc., Chem.Commun., 930-931.

- Makkee, M., Kieboom, A.P.G., and Van Bekkum, H., (1985), "Production Methods of D-Mannitol", Starch, 37, 4, 136-141.

- Melaja, A.J. and Hamalainen, L., (1975), "Process for the Production of Mannitol and Sorbitol", U.S. Patent, US 3864406.

- Montogomary, D.G., (1976), "Design and Analysis of Industrial Experiments", John Wiley & Sons, New York.

- Qjamo, H., Koivikko, H., and Heikkila, H., (2000), "Process for the Production of Mannitol by Immobilized Micr-Organisms", Patent Application, WO 0004181.

- Schwarz, E., (1994), "Sugar Alcohols: Mannitol", Ulmans Encyclopedia of Industrial Chemistry, 5 th ed., A25, VCH, Weinheim, 423-426.

- Toukoniitty, B., T., Kuusisto, J., and Mikkola, J.-P., (2005), "Effect of Ultrasound on Catalytic Hydrogenation of D-Fructose to D-Mannitol", Ind. & Eng. Chem. Res., 44, 25, 9370-9375.

- Von Weymarn, N., (2002), “Process Development for Mannitol Production by Lactic Acid Bacteria”, Ph.D. Thesis, Helsinki University of Technology.

NOMENCLATURE

Notation

B Coefficient of estimated model (%)
C Initial concentration of D-glucose solution (wt. %)
e Residual error (%)
n Number of coefficients in the model
N Number of experiments
NS Not significant
P Number of variables
Q_H Volumetric flow rate of hydrogen (liter/min)
S Significant
S_b^2 Variance of coefficient B
S_r^2 Residual variance
W_{gf} Weight of D-glucose in the feed (g)
W_{gp} Weight of D-glucose in the product (g)
W_m Weight of D-mannitol in the product (g)
W_s Weight of D-sorbitol in the product (g)
X_1 Reaction time (min)
X_2 Reaction temperature (˚C)
X_3 Catalyst ratio (%)
y Theoretical or predicted value of D-mannitol yield (%)
Y Experimental or observed value of D-mannitol yield (%)

Greek Leters

γ Number of degree of freedom

A DEVELOPED MODIFIED OSAP CONTROLLER WITH REPETITIVE CONTROL ACTION FOR UPS

Azzam A. Marouf
Alkhwarizmi College of engineering
University of Baghdad

Sameer A. Abdel Razzak
College of engineering
University of Baghdad

ABSTRACT

In this work, a developed modified one sampling ahead preview **(OSAP)** controller with repetitive control action for single – phase voltage source **PWM** inverters used in **(UPS)** systems is proposed. The proposed technique minimizes largely the plant modeling errors resulted from simplification made to obtain a linear discrete - time plant model. In addition, due to the repetitive control action, this digital control scheme can minimize the steady-state error and periodic distortions caused by nonlinear cyclic loads. Hence, the Total Harmonic Distortion **(THD)** will be reduced. This technique utilizes a switching frequency greater than the sampling frequency, yielding additional minimization in the plant modeling errors. As the sampling frequency is less than the switching frequency, it is possible to implement this controller on a low speed microcontroller. Plant model and theoretical analysis of the control scheme are discussed. Simulation results are presented to verify the performance of the proposed approach under different load conditions.

KEYWORDS

Uninterruptible power supply (UPS), PWM inverters, repetitive controller, one sampling ahead preview (OSAP) controller, digital control, and microcontroller.

الخلاصة

في هذا العمل تم اقتراح نظام سيطرة يسمى (Developed Modified OSAP Controller) وبالاشتراك مع المسيطر التكراري (Repetitive Controller) للسيطرة على عمل العاكس ذو مصدر الفولتية متغير التجهيز (PWM) أحادي الطور (Single-Phase) والمستعمل في أنظمة مصدر القدرة الغير منقطع (UPS).

إن التقنية المقترحة تقلل إلى حد كبير مقدار الخطأ المتولد من التبسيط المستخدم في تحويل النظام إلى النوع الخطي، وكما أن الخطأ يقل أكثر في حالة زيادة تردد عمل مفاتيح المعدل (Switching Frequency) فقد تم زيادة هذا التردد مع بقاء تردد أخذ العينات (Sampling Frequency) ثابتا مما يفيد من إمكانية استعمال المسيطر الدقيق (Microcontroller) المنخفض السرعة والقيمة في تنفيذ مثل هذا النوع من السيطرة.

قد بينت النتائج أن وجود المسيطر التكراري يخفض إلى الحد الأدنى من مقدار الخطأ الموجود في حالة الاستقرار وكما يقلل من التشوهات المتكررة الناتجة من الأحمال الدورية اللاخطية مما يسبب انخفاضاً في نسبة مجموع المركبات المشوهة (THD).
تم تحليل المنظومة بشكل نظري (رياضي)، كما تم تمثيل النتائج على الحاسوب لتقييم أداء التقنية المقترحة تحت عدة حالات مختلفة من الأحمال.

INTRODUCTION

The uninterruptible power supply (UPS) systems have been widely used as backup for critical load applications such as computers and life support systems in hospitals.

The widespread availability of low cost microcontrollers and DSP processors has yielded possible of use digital control techniques to improve the performance of UPS systems. Digital control techniques should generate the pulse width modulated (PWM) signal to produce the sinusoidal output voltage of the UPS system with low total harmonic distortion (THD) for linear and nonlinear loads. The microprocessor – based deadbeat control scheme had been used in [1, 2]. The PWM signal is determined at each sampling instant by the microprocessor, based on output measurements and the reference signal. This approach can result in a low (THD) sinusoidal output with fast transient response. The drawback of this scheme is the detection of both output voltage and output capacitor current required at each sampling instant. Thus, a deadbeat control algorithm using only a voltage sensor, which may be called one sampling ahead preview (OSAP) controller, was proposed to reduce the cost of the overall system and the computation time of the controller [3]. Although this technique demonstrates quick response for load disturbances and nonlinear loads, the output voltage waveform normally presents high (THD) for nonlinear cyclic loads such as AC phase–controlled loads and rectifier loads in computer systems. Thus, a repetitive controller was added to OSAP controller to minimize the steady–state error and periodic distortions caused by nonlinear cyclic loads [4]. In spite of this, the pulsewidth in these schemes is limited by the computation time of the microprocessor.

A modified OSAP controller [5] was proposed to increase the maximum available pulsewidth. In this approach, the pulsewidth in the (***k-th***) sampling interval is computed by using the output voltage sampled at the previous sampling instants. Hence, the pulsewidth is determined during the previous interval in order to extend the pulsewidth to the entire sampling interval ($\boldsymbol{T}$). However, this digital control technique is very sensitive to parameter variations and plant modeling errors.

An improved modified OSAP controller [6] was implemented to reduce the effects of the plant modeling errors resulting from the simplifications made to obtain a linear discrete–time plant model. This digital control scheme employs a switching frequency greater than the sampling frequency, minimizing the plant modeling errors.

In this work, a developed modified OSAP controller with a repetitive control action is proposed for voltage source PWM inverter used in (UPS) systems. The proposed scheme differs from the aforementioned previous scheme, presented by reference [6], by the positions of the switching pulses within the sampling interval. Applying this scheme minimizes the effects of the plant modeling errors produced by linearization of the discrete–time plant model more than that obtained with the previous scheme. The switching frequency used in the proposed scheme is also greater than the sampling frequency, which minimizes the undesirable effects of the plant modeling errors too. As the sampling frequency is smaller than the switching frequency, it is possible to implement this controller on a low cost microcontroller.

Plant modeling and stability analysis for the proposed system are presented. Simulation results (for 110 $\boldsymbol{V_{rms}}$, 60 Hz, 1 KVA system) are carried out to demonstrate the performance of the proposed control approach due to sudden changes at load, linear and nonlinear cyclic loads, and unmodeled dynamics. Finally, conclusions and suggestions for future work are reported.

PLANT MODEL

Figure (1) shows the single–phase PWM inverter circuit of the UPS, where the full–bridge inverter, (***LC***) filter and pure resistive load (R) are considered as the plant to be controlled. The state and the output equations of such a second–order system, with state vector $[v_c(t) \quad \dot{v}_c(t)]^T$, are:

$$\begin{aligned} \dot{x}(t) &= Ax(t) + Bu(t) \\ y(t) &= Cx(t) \end{aligned} \tag{1}$$

where

$$\left.\begin{aligned} x(t) &= \begin{bmatrix} v_c(t) \\ \dot{v}_c(t) \end{bmatrix}, A = \begin{bmatrix} 0 & 1 \\ -\omega_p^2 & -2\zeta_p\omega_p \end{bmatrix}, B = \begin{bmatrix} 0 \\ \omega_p^2 \end{bmatrix}, \\ C &= \begin{bmatrix} 1 & 0 \end{bmatrix}, \omega_p = \frac{1}{\sqrt{L_f C_f}}, \zeta_p = \frac{1}{2R}\sqrt{\frac{L_f}{C_f}} \end{aligned}\right\} \tag{2}$$

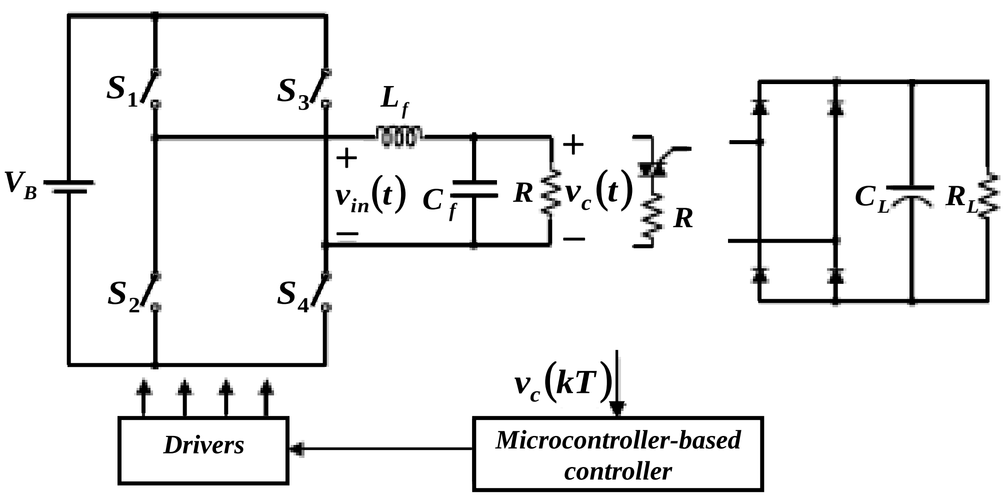

Figure (1) [7]
Digitally controlled PWM inverter

The proposed control scheme is very similar to the control scheme presented by [6]. The only difference between them is that *the train of input pulses in the sampling period for the proposed* *system is positioned in the center of these sections instead of being in the beginning*. Figures (2) and (3) demonstrate the train of pulses for the two schemes.

For the proposed controller the sampled–data state equation can be written as:

$$x(k+1) = e^{AT}x(k) + \int_{\frac{T-\Delta T(k)}{2n_p}}^{\frac{T+\Delta T(k)}{2n_p}} e^{A(T-\tau)}BV_B d\tau + \int_{\frac{3T-\Delta T(k)}{2n_p}}^{\frac{3T+\Delta T(k)}{2n_p}} e^{A(T-\tau)}BV_B d\tau + \cdots + \int_{\frac{(2n_p-1)T-\Delta T(k)}{2n_p}}^{\frac{(2n_p-1)T+\Delta T(k)}{2n_p}} e^{A(T-\tau)}BV_B d\tau \qquad (3)$$

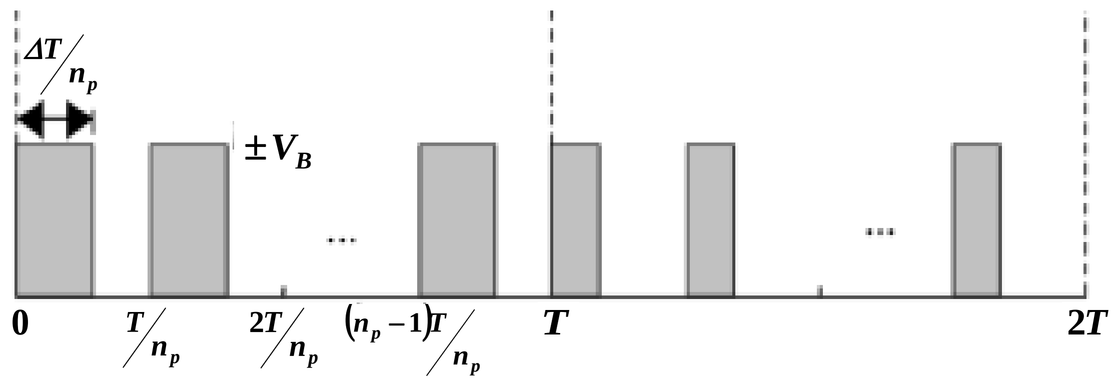

Figure (2) [7]
Multiple–Pulse Width Modulation (MPWM) pattern for the improved modified OSAP controller. Each pulse placed in the beginning of its section

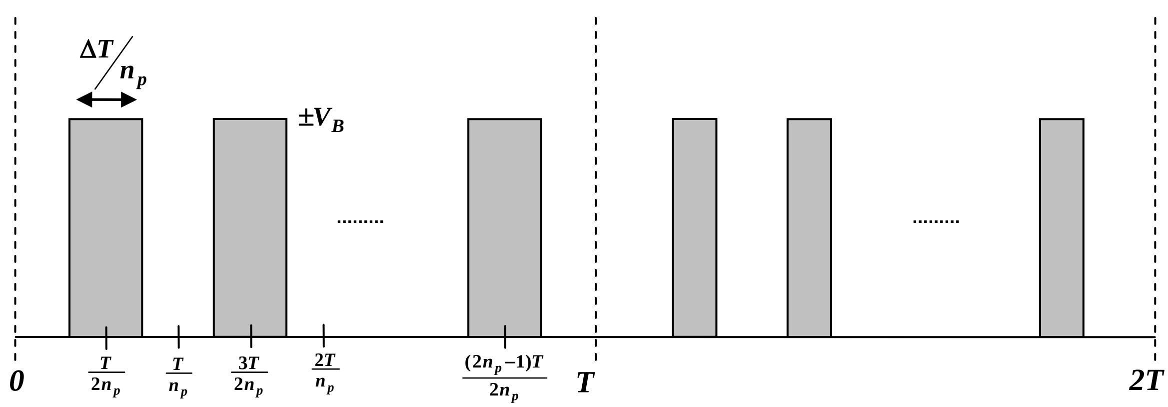

Figure (3)
MPWM pattern for the proposed (developed modified OSAP) controller each pulse placed in the center of its section

Integrating Eq.(3) and taking $\left(e^{\frac{A\Delta T(k)}{2n_p}} - e^{\frac{-A\Delta T(k)}{2n_p}}\right)$ as a common term, the nonlinear discrete–time state equation can be obtained:

$$x(k+1) = e^{AT}x(k) + \begin{bmatrix} h_{d_{non}1}(k) \\ h_{d_{non}2}(k) \end{bmatrix} \tag{4}$$

where:

$$\begin{bmatrix} h_{d_{non}1}(k) \\ h_{d_{non}2}(k) \end{bmatrix} = \left(\sum_{i=1,2,\cdots}^{n_p} e^{\frac{(2i-1)AT}{2n_p}}\right)\left(e^{\frac{A\Delta T(k)}{2n_p}} - e^{\frac{-A\Delta T(k)}{2n_p}}\right)A^{-1}BV_B \tag{5}$$

It is possible to obtain a linear discrete–time model by computing the term $\left(e^{\frac{A\Delta T(k)}{2n_p}} - e^{\frac{-A\Delta T(k)}{2n_p}}\right)$ using Taylor series and neglecting terms of higher than (ΔT^2), yields:

$$x(k+1) = G_d x(k) + H_d \Delta T(k) \tag{6}$$

where:

$$G_d = \begin{bmatrix} g_{d11} & g_{d12} \\ g_{d21} & g_{d22} \end{bmatrix} = e^{AT}, \qquad H_d = \begin{bmatrix} h_{d1} \\ h_{d2} \end{bmatrix} = \frac{1}{n_p}\left(\sum_{i=1,2,\cdots}^{n_p} e^{\frac{(2i-1)AT}{2n_p}}\right)BV_B \tag{7}$$

Figure (4) shows the normalized errors between the parameters of the input matrix H_d (h_{d1} and h_{d2}) and respective parameters of the nonlinear model for different values of (n_p). The normalized errors can be calculated using the following Equations:

$$\text{Normalized error of } (h_{d1}) = \frac{h_{d1} - h_{d_{non}1}(k)/\Delta T(k)}{h_{d_{non}1}(k)/\Delta T(k)} \tag{8}$$

and

$$\text{Normalized error of } (h_{d2}) = \frac{h_{d2} - h_{d_{non}2}(k)/\Delta T(k)}{h_{d_{non}2}(k)/\Delta T(k)} \tag{9}$$

Figure (4) demonstrates the superiority of the proposed approach upon the previous one (improved modified OSAP controller presented by reference [6]) in modeling errors amount. Moreover, it is very clear from the Figure that modeling error decreased significantly as the switching frequency of the PMW inverter increased.

Using Eq. (6), the input–output equation in the (z–domain) can be obtained:

$$y(z) = \frac{h_{d1} + (h_{d2}g_{d12} - h_{d1}g_{d22})z^{-1}}{z - (g_{d11} + g_{d22}) + (g_{d11}g_{d22} - g_{d12}g_{d21})z^{-1}}\Delta T(z) \tag{10}$$

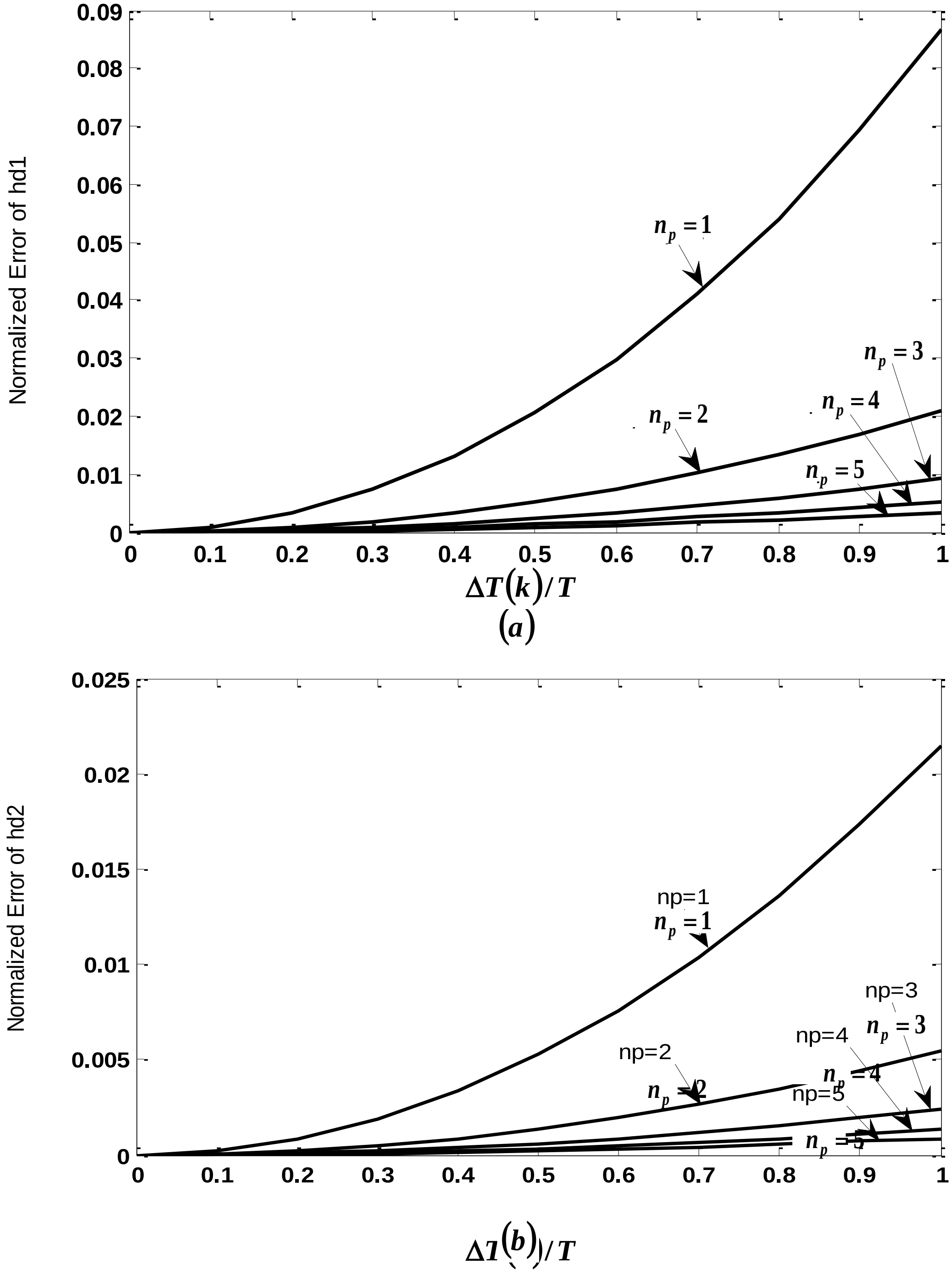

Figure (4)

Modeling error for different values of $n_p\left(\omega_p = 11550\, rad / s, \zeta_p = 0.25\right)$

(b) Normalized error of h_{d1}. (a) Normalized error of h_{d2}.

Thus, the input–output difference equation can be written as:

$$y(k+1)+a_{d1}y(k)+a_{d2}y(k-1)=b_{d1}u(k)+b_{d2}u(k-1) \tag{11}$$

where

$$\left.\begin{aligned} &a_{d1} = -(g_{d11} + g_{d22}),\ a_{d2} = g_{d11}g_{d22} - g_{d12}g_{d21},\ b_{d1} = h_{d1}T/V_B,\\ &b_{d2} = (h_{d2}g_{d12} - h_{d1}g_{d22})T/V_B,\ u(k) = \frac{\Delta T(k)}{T}V_B \end{aligned}\right\} \tag{12}$$

CONTROL LAW

The OSAP control law can be obtained from Eq.(11) considering that the output is equal to the reference signal at the next sampling instant, ***y(k+1)*** is substituted by ***r(k+1)***. Then, the following control law can be obtained:

$$u_{OSAP}(k) = \frac{r(k+1) + p_1 y(k) + p_2 y(k-1) - q_2 u(k-1)}{q_1} \tag{13}$$

If the OSAP controller gains p_1, p_2, q_1 and q_2 are equal to the plant parameters a_1, a_2, b_1 and b_2, respectively, it becomes a deadbeat control law which forces the output voltage to be equal to the reference signal at the next sampling interval. However, if the plant parameters change after the controller gains in Eq.(13) have been determined; the deadbeat response is no longer obtained [3].

Moreover, the maximum available pulsewidth is limited by the delay time caused by the output voltage (***A/D***) conversion and control law computation. To solve this problem a modified OSAP controller is presented[5]. The modified OSAP controller equation becomes:

$$u_{dMOSAP}(K)=\frac{r(k+1)+P_{d1}y(k-1)+P_{d2}y(k-2)-Q_{d2}u(k-1)-Q_{d3}u(k-2)}{Q_{d1}} \tag{14}$$

where the developed controller gains are:

$$\left.\begin{aligned} P_{d1} &= -(g_{d11}^2 + g_{d11}g_{d22} + g_{d12}g_{d21} + g_{d22}^2)\\ P_{d2} &= -(g_{d11}g_{d12}g_{d21} - g_{d11}^2 g_{d22} + g_{d12}g_{d21}g_{d22} - g_{d11}g_{d22}^2)\\ Q_{d1} &= h_{d1}T/V_B\\ Q_{d2} &= (h_{d1}g_{d11} + h_{d2}g_{d12})T/V_B\\ Q_{d3} &= (-h_{d1}(g_{d11}g_{d22} + g_{d22}^2) + h_{d2}(g_{d11}g_{d12} + g_{d12}g_{d22}))T/V_B \end{aligned}\right\} \tag{15}$$

Equation (14) shows that the pulse width determination can be completed during the previous interval, and the pulse width can be extended to the theoretically maximum limit, that is, the sampling interval (***T***).

To minimize the steady – state error and periodic distortions, a repetitive controller is added to this developed modified OSAP controller, as shown in Figure (5), such that the control law becomes:

$$u(k) = u_{dMOSAP}(k) + u_{RP}(k) \tag{16}$$

The repetitive control law can be written as [4]:

$$u_{RP}(k) = c_{r1}e(k + N - n) + c_{r2}\sum_{i=1}^{\infty} e(k + N - i.n) \tag{17}$$

where $e(k)$ is the tracking error, c_{r1} and c_{r2} are the gains of the repetitive controller, N is the time advance step size and n is the number of samples in a period of reference voltage which equal to the ratio of the sampling frequency f_s to that of the reference sinusoidal waveform f_r. In this control system, each pulse width $u_{RP}(k)$, and as a result $u(k)$, is determined by referring the output voltage in the previous cycle. The repetitive controller gains are designed to guarantee a good steady – state response for any resistive load and fast convergence of the output error for nonlinear cyclic loads [6].

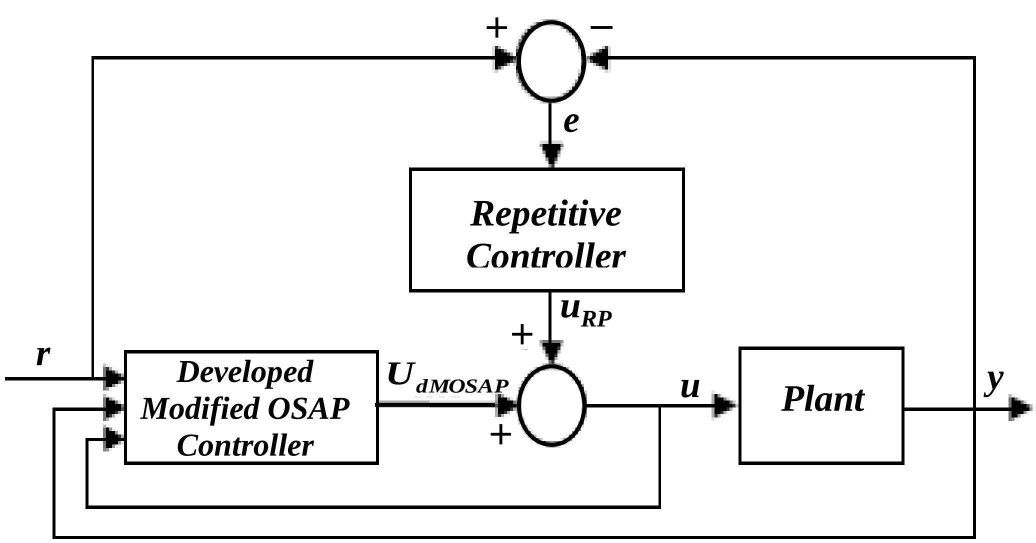

Figure (5)
Control system block diagram using
the developed modified OSAP controller with repetitive control action

STABILITY ANALYSIS

Figure (6) shows the developed control system before adding the repetitive controller. The transfer function ($G_{dMOSAP}(z) = y(z)/r(z)$) can be obtained by taking the z – transformation of Eqs. (11) and (14), and elimination the plant input ($u_{dMOSAP}(z)$), yields:

$$\frac{y(z)}{r(z)} = \frac{(b_{d1}z + b_{d2})z^3}{(z^2 + a_{d1}z + a_{d2})(Q_{d1}z^2 + Q_{d2}z + Q_{d3}) - (P_{d1}z + P_{d2})(b_{d1}z + b_{d2})} \tag{18}$$

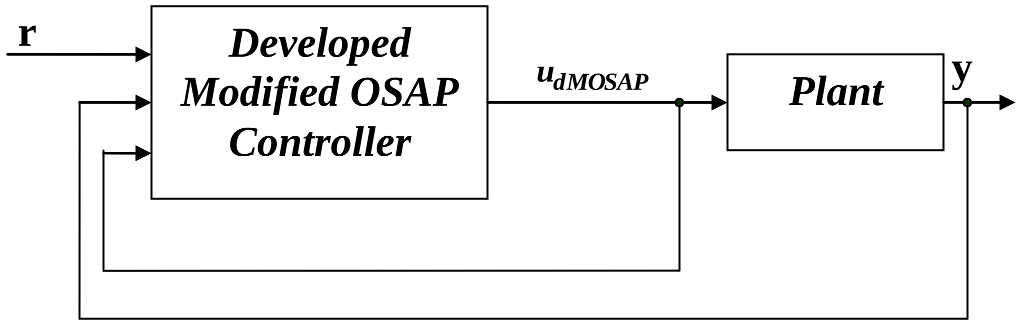

Figure (6)
Block diagram of the developed control system without the repetitive controller.

Figure (7) shows the stability region of the developed modified OSAP controller in the $|\,\omega_p - \zeta_p\,|$ plane for two nominal values of filter parameters (case ***(a)*** $L_f = 0.5mH, C_f = 15\mu F$, case ***(b)*** $L_f = 0.35mH, C_f = 10\mu F$). This is performed from the localization of the closed-loop poles (the denominator of Eq.(18)) with the variation of plant parameters ($R, L_f,$ and C_f). Figure (7) also shows the trajectories of the plant parameters in this plane. The trajectory of one parameter is done maintaining the other two parameters constant at their nominal values. From the Figure, it is clear that stability is expected for load changes from no load to rated load. In addition, an accepted stability region with a good range of output filter parameters is obtained.

On another hand the choices of the filter parameters must be governed by the sampling frequency choice

If a repetitive controller is added to the system, the z–transform of the repetitive controller Eq. (17) can be written as:

$$u_{RP}(z) = e(z)z^N z^{-n}\left(\frac{c_{r1} + c_{r2} - c_{r1}z^{-n}}{(1 - z^{-n})}\right) \tag{19}$$

The transfer function ($e(z)/r(z)$) of the system shown in Figure (5) can be obtained, using Eq.(19) and the z–transform of Eqs. (11), (14), and (16). Then:

$$\frac{e(z)}{r(z)} = \frac{(1 - G_{dMOSAP}(z))(1 - z^{-n})}{1 - z^{-n}H_{dMOSAP}(z)} \tag{20}$$

where $e(z), r(z)$ are the z–transform of the output error and the reference input respectively, and:

$$H_{dMOSAP}(z) = 1 - Q_{d1} z^{N-1}\left(c_{r1} + c_{r2} - c_{r1} z^{-n}\right) G_{dMOSAP}(z) \tag{21}$$

Since the stability of Eq.(18) is established, the repetitive controller determines the overall system stability. From Eq.(20), a sufficient condition for stability [4] is:

$$|\ H_{dMOSAP}(j\omega)\ | \leq 1 \tag{22}$$

where ω is the angular frequency of the reference input: $\omega = 2\pi\ m\ f$, (m=0, 1, 2 … n/2).

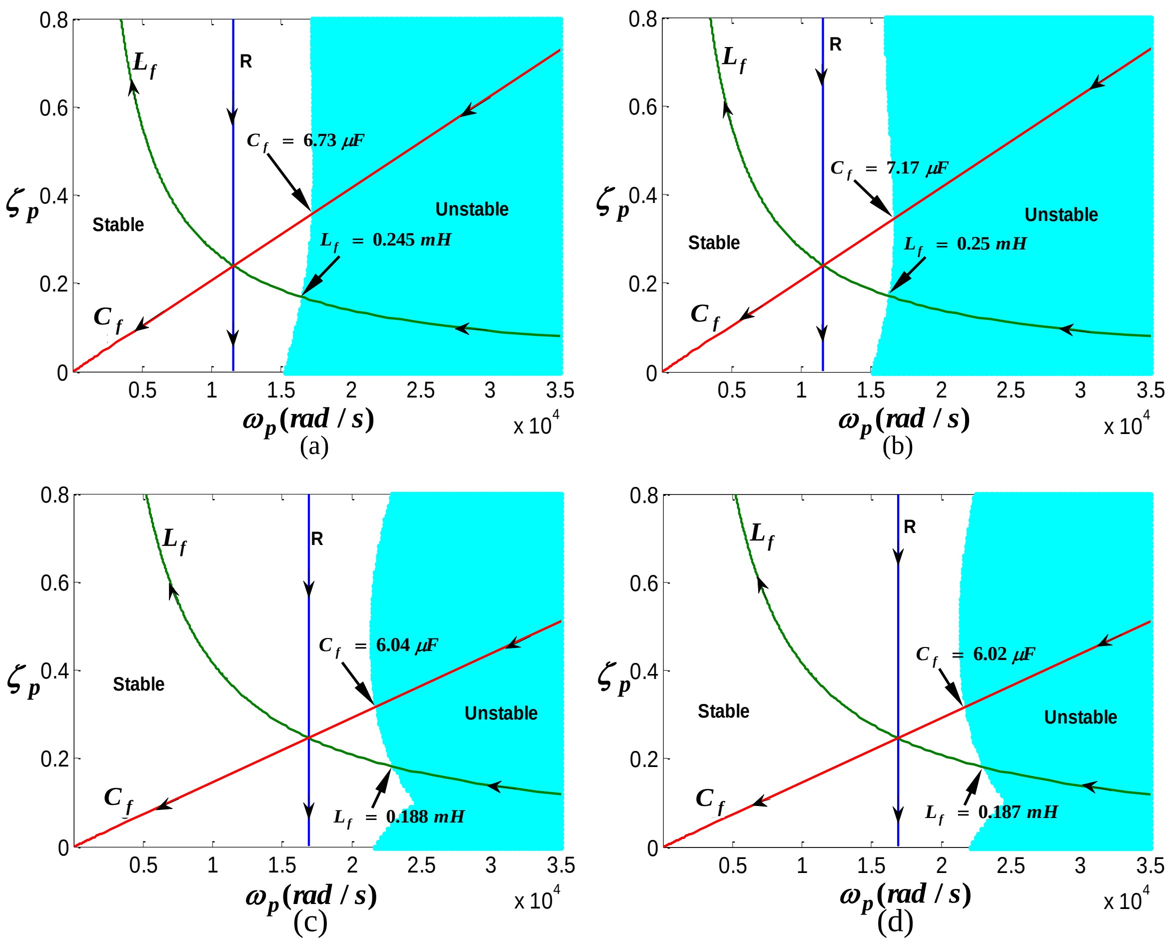

Figure (7)

Stability region of the modified OSAP controller in $|\omega_p - \zeta_p|$ plane with:

a) $(f_{sw} = f_s)$, controller parameters: $L_f = 0.5\ mH,\ C_f = 15\ \mu F,\ and\ R = 12\Omega$.

b) $(f_{sw} = 3 f_s)$, controller parameters: $L_f = 0.5\ mH,\ C_f = 15\ \mu F,\ and\ R = 12\Omega$.

c) $(f_{sw} = f_s)$, controller parameters: $L_f = 0.35\ mH,\ C_f = 10\mu F,\ and\ R = 12\Omega$.

d) $(f_{sw} = 3 f_s)$, controller parameters: $L_f = 0.35\ mH,\ C_f = 10\mu F,\ and\ R = 12\Omega$.

5- Simulation Results

The performance of the developed modified OSAP controller with repetitive control action is evaluated using the digital computer simulation by writing some programs (with MATLAB ®, version (7.4)). Table (1) summarizes the parameters of the single – phase PWM inverter system used in simulation. The simulation results for three different cases (1), (2), and (3) of filter parameters and switching frequency values are presented according to the load conditions.

Table (1)

Parameters of the single-phase PWM inverter used in simulation

PARAMETER	VALUE
DC input voltage	$V_B = 200\,V$
Reference voltage & frequency	$V_{ref} = 110\,V,\; f_r = 60Hz$
Nominal resistive load	$R = 12\Omega$
Sampling frequency	$f_s = 10.8KHz$
Sampling period	$T = 92.6\mu s$
Repetitive controller gains	$c_{r1} = 0,\; c_{r2} = 0.3$
OUTPUT FILTER PARAMETERS	
Case (1)	$L_f = 0.5mH, C_f = 15\mu F$ Switching frequency ($f_{sw} = 10.8KHz$) PWM (one pulse in the center)
Case (2)	$L_f = 0.5mH, C_f = 15\mu F$ Switching frequency ($f_{sw} = 32.4KHz$) MPWM (three pulses, each one is in the center of its section of the sampling interval)
Case (3)	$L_f = 0.35mH, C_f = 10\mu F$ Switching frequency ($f_{sw} = 32.4KHz$) MPWM (three pulses, each one is in the center of its section of the sampling interval)

NOMINAL LOAD CONDITION

The developed modified OSAP controller with and without repetitive control action is simulated using nominal resistive load (R=12Ω). The waveforms of the output voltage $v_c(t)$, reference voltage $v_{ref}(t)$, and load current $i_L(t)$ for the three different cases (1), (2), and(3) are shown in Figure (8).

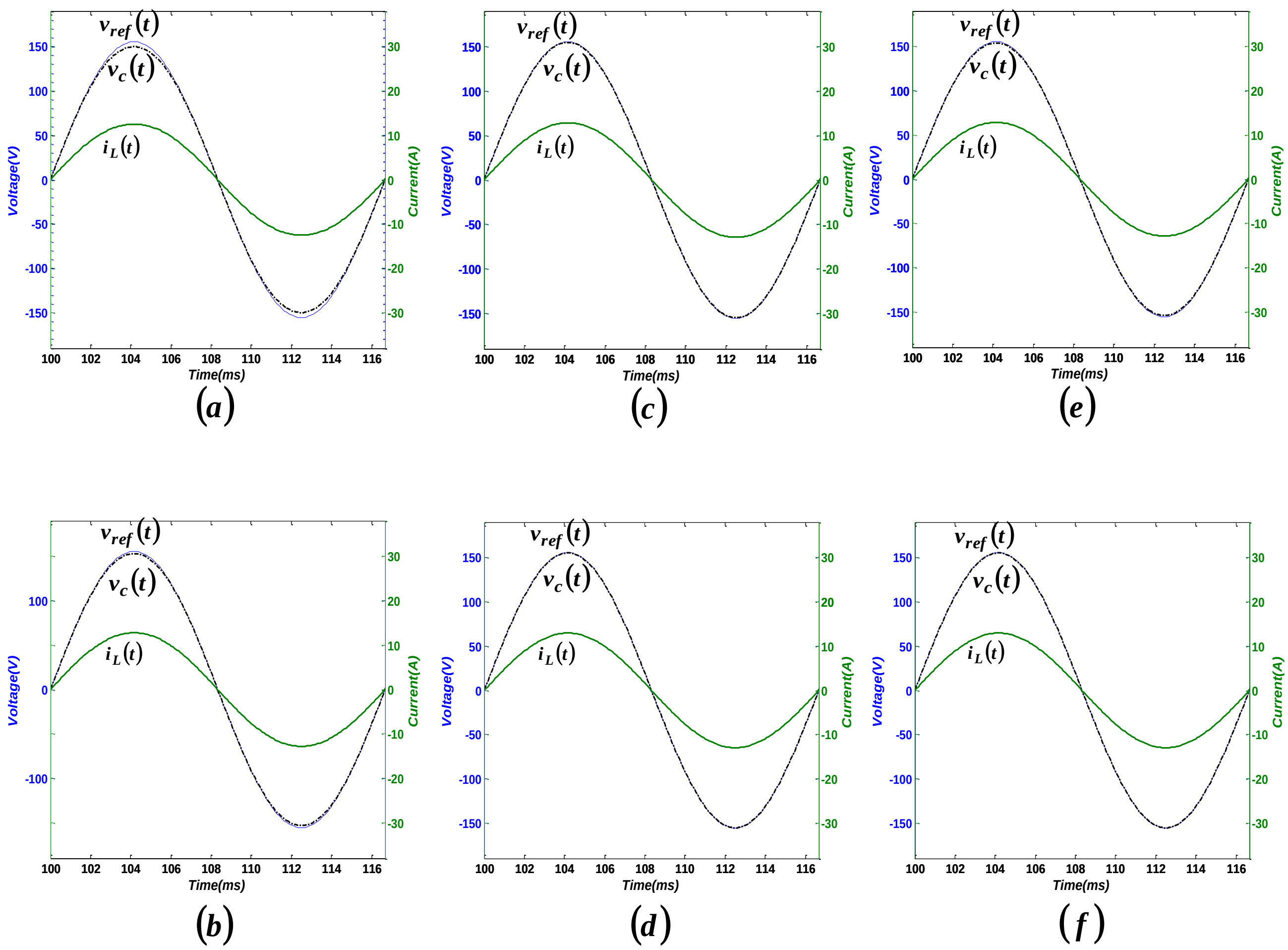

Figure (8)

Response of the developed modified OSAP controller for nominal resistive load condition $(R = 12\Omega)$ in:

(a) case(1), without repetitive controller. **(b) case(1),** with repetitive controller.
(c) case(2), without repetitive controller. **(d) case(2),** with repetitive controller.
(e) case(3), without repetitive controller. **(f) case(3),** with repetitive controller.

No – Load Condition

The simulation for the same three cases (1), (2), and (3) are shown in Figure (9). Again, better response is achieved by increasing the switching frequency in cases (2) and (3).

Figure (10) shows the total harmonic distortion (THD) to the nominal load and no-load conditions for the three cases. The influence of the repetitive integral action is clear in the consecutive cycles. Moreover, increasing the switching frequency minimizes the THD in cases (2) and (3) more than that for case (1). However, due to the integral action of the repetitive controller, THD for nominal load condition of all cases approaches zero in the latest cycles.

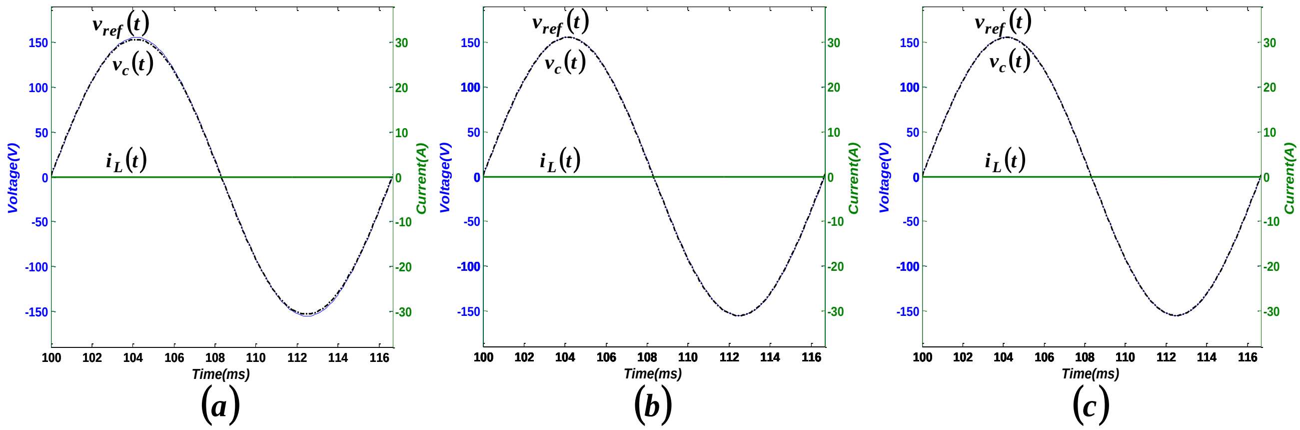

Figure (9)

Response of the developed modified OSAP controller with repetitive controller for no-load condition in: **a) case(1)**. **b) case(2)**. **c) case(3)**.

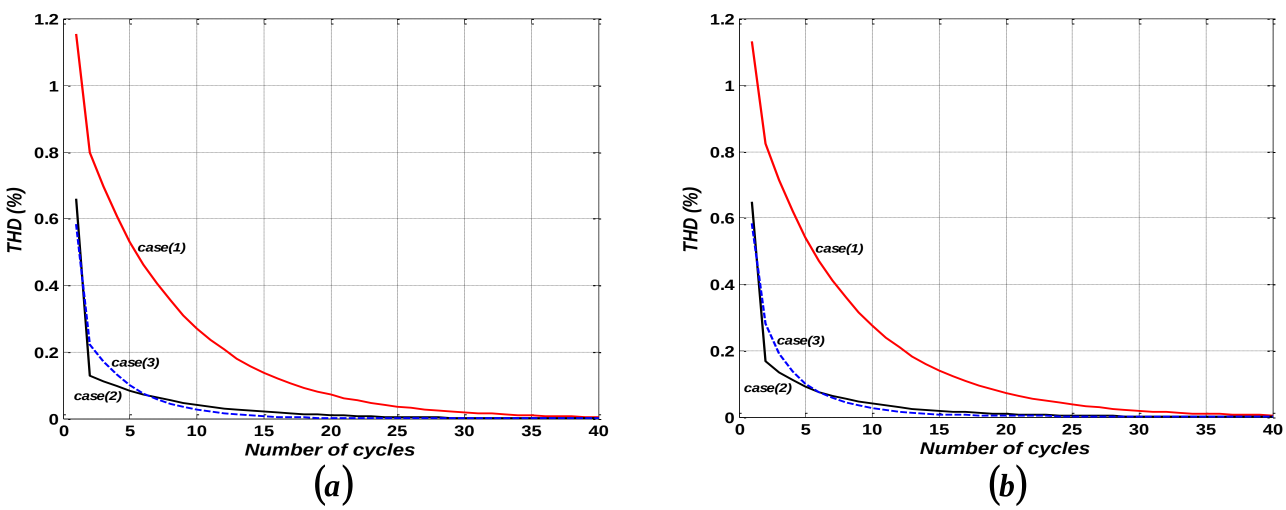

Figure (10)

Influence of repetitive integral action on the total harmonic distortion factor (THD) with the consecutive cycles for: a) Nominal load condition. b) No – load condition.

Nonlinear Load Condition

The nonlinear loads, such as AC phase – controlled loads (Triac) and rectifier loads, are considered as an output periodic disturbance on the system. Such nonlinear loads represent a challenge to evaluate the system performance. Some of nonlinear loads will be discussed here.

Triac Connected in Series with Nominal Resistive Load

Figure (11) presents the response of the proposed controller with nominal resistive load in series with a Triac commuting at ($\mathbf{72^\circ/252^\circ}$) for the three cases (1), (2), and (3).

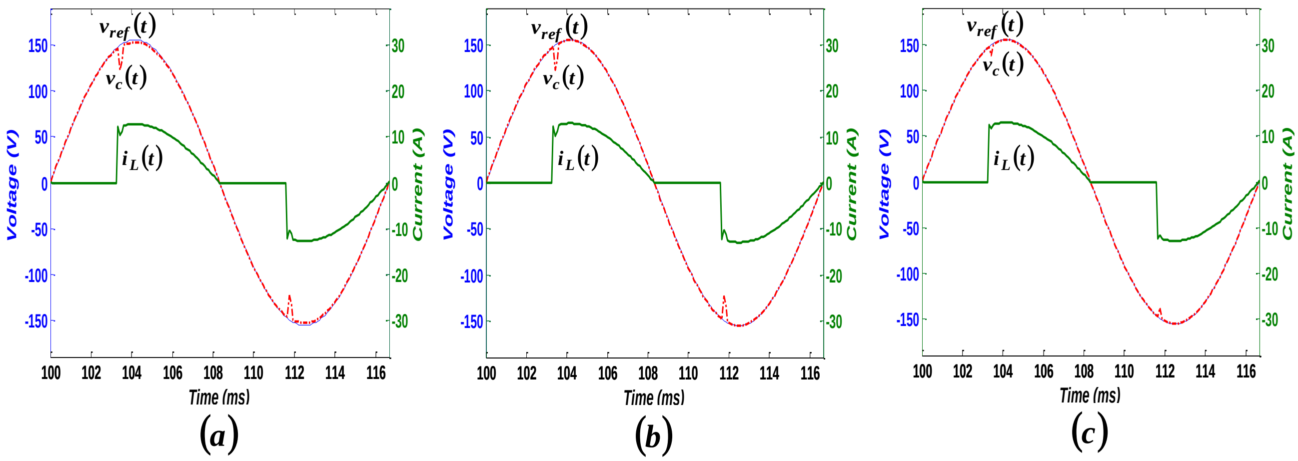

Figure (11)
Response of the developed modified OSAP controller with repetitive controller for nominal resistive load in series with a Triac commuting at $\mathbf{72^\circ/252^\circ}$ in:
a) case(1). **b) case(2)**. **c) case(3)**.

It is clear that the steady state error, caused by this nonlinear cyclic load, is minimized by adding the repetitive controller especially for case (3) in comparison with cases (1) and (2). This is due to that: the influence of reducing the filter inductance ($\boldsymbol{L_f}$) minimizes the reactance affecting current changes directly, so small inductance value is quickly compensate the drawn load current in comparison with larger values, hence less input supply voltage is needed to compensate the drop in voltage.

A comparison of (THD) for nominal resistive load with a Triac commuting at angles ($\mathbf{36^\circ/216^\circ}$, $\mathbf{72^\circ/252^\circ}$, $\mathbf{90^\circ/270^\circ}$ *, and* $\mathbf{120^\circ/300^\circ}$) each for the three different cases (1, 2, and 3) is shown in Figure (12). It is clear that the (THD) for case (1) and case (2) are very similar, while that for case (3) shows a better response. The (THD) approaches zero for Triac angles ($\mathbf{36^\circ/216^\circ}$) and case (3) of angles ($\mathbf{120^\circ/300^\circ}$) unlike for other states. This is due to the drop in the output voltage at the commuting angle that requires a low or high value of the control law (***u(k)***). High values of ***u(k)*** demanded may exceed the maximum permitted value ($\boldsymbol{V_B}$), i.e. the pulse width ($\boldsymbol{\Delta T}$) exceeds the sampling period (***T)***, according to Eq. (5), which is not possible ($\boldsymbol{\Delta T} = \boldsymbol{T}$ at saturation). In this case, the control law (***u(k)***) will be limited to the ***DC*** supply voltage ($\boldsymbol{V_B}$), and the THD may not approaches zero.

Triac Connected in Series with Nominal Resistive Load Including Unmodeled Dynamics

In this section a nominal resistive load in series with a Triac commuting at ($72^\circ/252^\circ$) connected to the developed modified OSAP controller including an unmodeled dynamics will be tested. An equivalent resistor of (0.5 Ω) in series with the filter capacitor may achieve an example for this state. From control point view, this resistor value caused an unmodeled (***stable zero***) at (-8000 rad/sec) to be added to the closed–loop transfer function of the system.

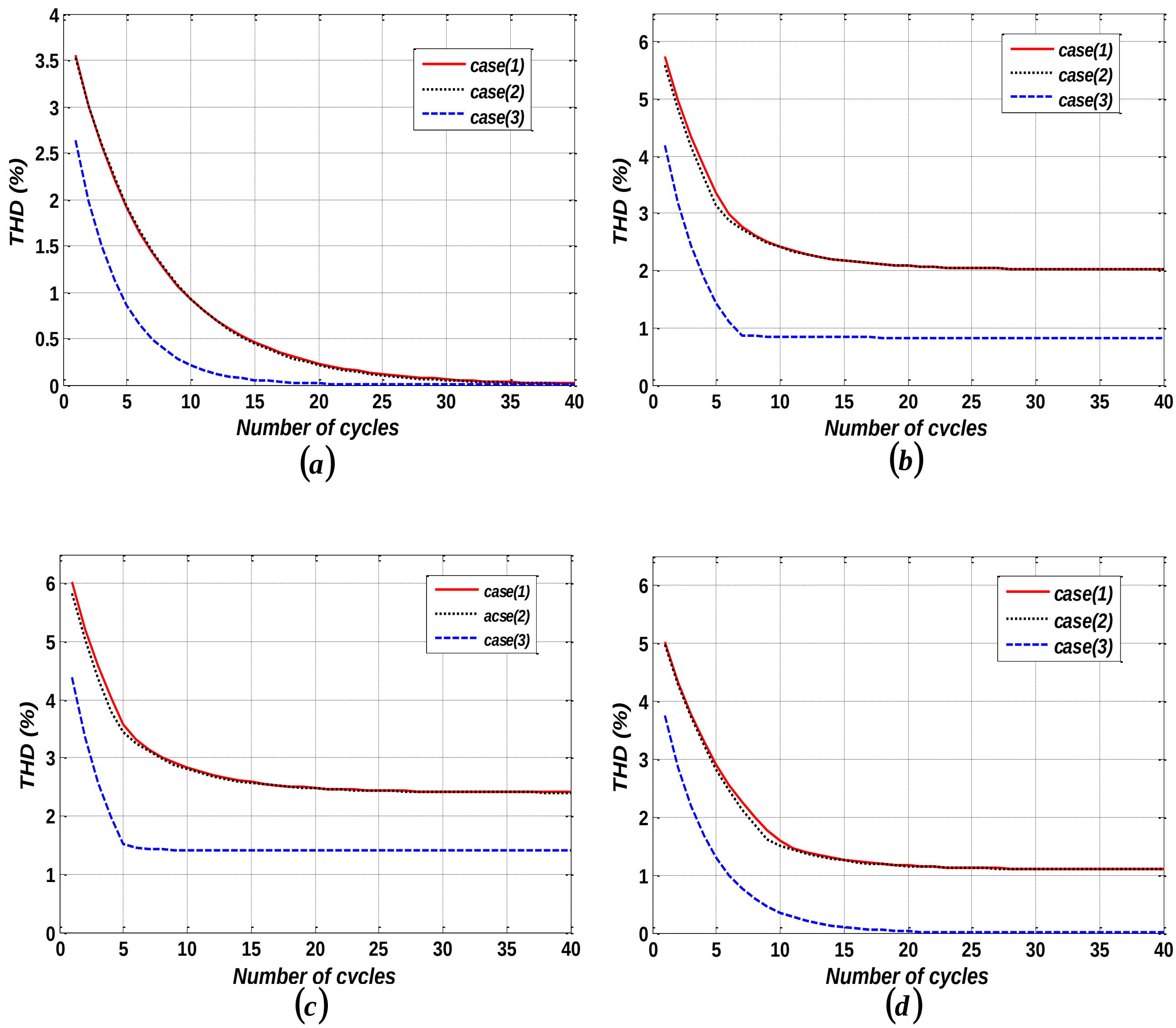

Figure (12)

Influence of repetitive integral action on the (THD) for nominal resistive load in series with a Triac commutes at:

a) ($36^\circ/216^\circ$). b) ($72^\circ/252^\circ$). c) ($90^\circ/270^\circ$). d) ($120^\circ/300^\circ$).

Figure (13) shows the output voltage and load current waveforms for the three cases defined earlier. It is clear that the proposed controller shows a good performance with the presence of this unmodeled dynamic.

Figure (14) shows the (THD) of the output voltage for the three cases. Also the (THD) for case (3), with reduced filter parameters, is better than that for cases (1) and (2).

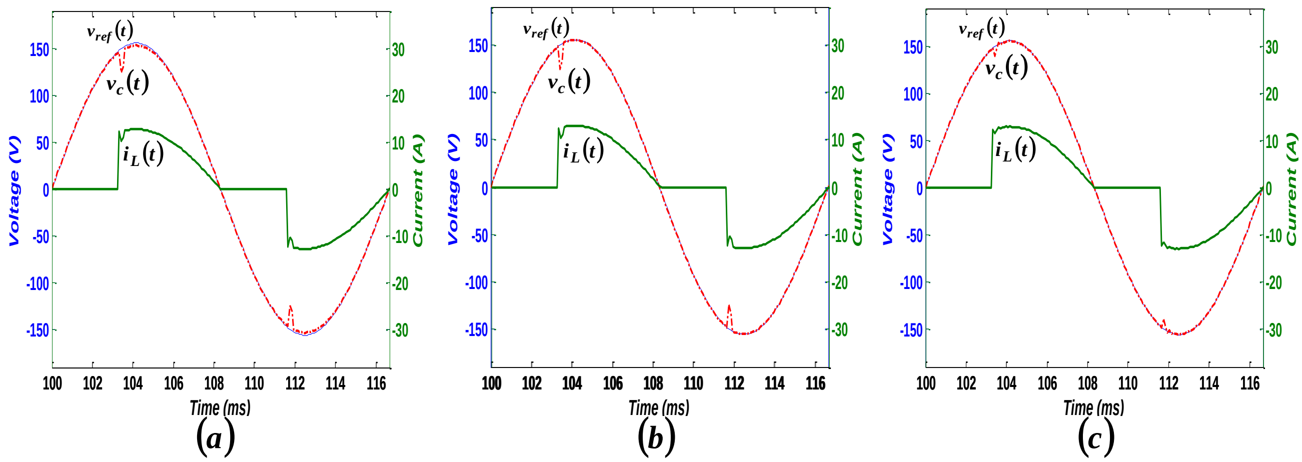

Figure (13)

Response of the developed modified OSAP controller with repetitive control action for nominal resistive load in series with a Triac commuting at $\mathbf{72^{\circ}/252^{\circ}}$ including unmodeled stable ***Zero*** at (-8000 rad/sec) : a) **case (1)**. b) **case (2)**. c) **case (3)**.

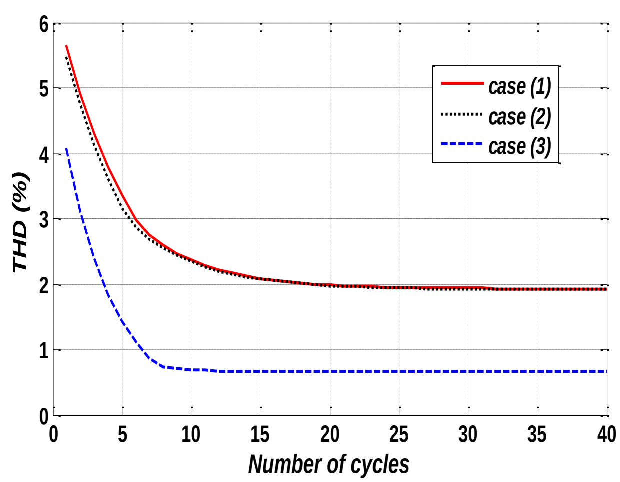

Figure (14)

THD for nominal resistive load in series with a Triac commuting at $\mathbf{72^{\circ}/252^{\circ}}$ including unmodeled stable ***Zero*** at (-8000 rad/sec).

Step Change – Load Condition

A step load changes from no – load to full load is illustrated in Figure (15) for the three cases (1), (2) and (3). The three cases show a good transient response for a step – load change.

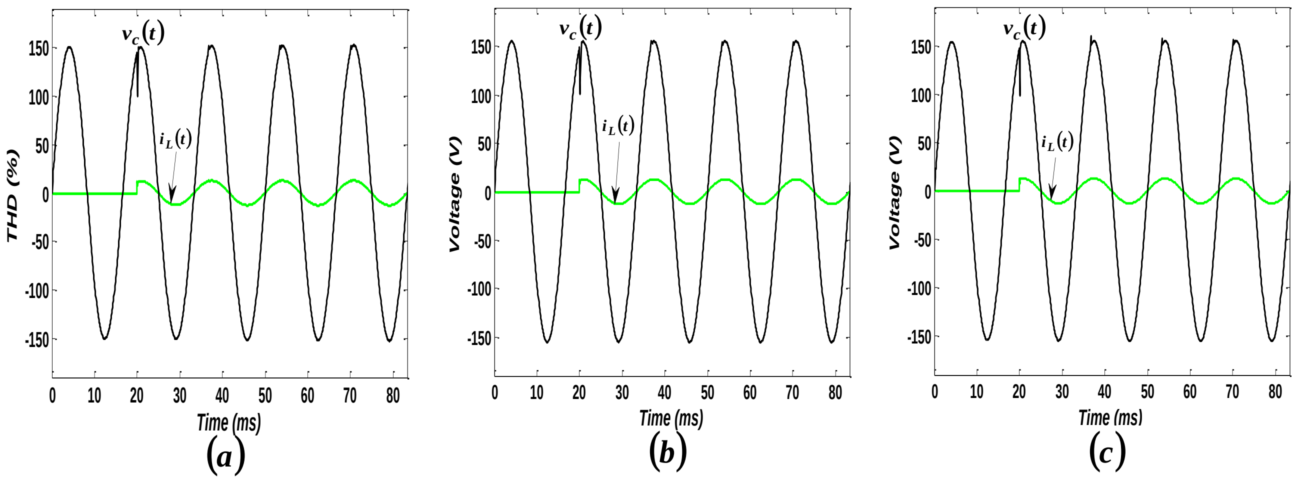

Figure (15)

Transient response for the proposed controller: a) **case (1)**. b) **case (2)**. c) **case (3)**.

CONCLUSIONS

Results show that this controller with the proposed control technique, using input pulses in the center, minimizes largely the plant modeling errors, resulted from simplification made to obtain a linear discrete - time plant model, more than that when the pulses are placed in the beginning. Moreover, increasing the switching frequency minimizes the effects of the plant modeling errors too.

Stability analysis proves that the closed-loop system for the proposed controller is stable from no-load to full load variation. In addition, an accepted stability region with a good range of output filter parameters is obtained without distinct difference between one or three pulses per sampling period states.

Simulation results assure that adding a repetitive controller to the developed modified OSAP controller minimizes the steady-state error and hence gives the advantage of low total harmonic distortion (THD).

Results show that the proposed control scheme with three pulses, each one in the center of its section from the sampling period, (MPWM pattern) improves system transient response more than the modified OSAP control system with one pulse in the center (PWM pattern) for no-load and nominal load conditions. However, there is no distinct difference in the THD of both patterns for nonlinear load conditions.

Nevertheless reducing filter parameters, which mainly reduces the cost, (especially the inductance L_f) satisfies better performance with lower (THD) for nonlinear load conditions, even in the presence of an unmodeled dynamics, appreciating that lower stability range for the repetitive controller gains is obtained.

REFERENCES

- A. Kawamura, R. Chuarayapratip, and T. Haneyoshi, “Deadbeat Control of PWM Inverter with Modified Pulse Patterns for Uninterruptible Pwoer Supply”; lEEE Trans. On lnd. Appl., Vol. 35, No. 2, May 1988, PP. 295 – 300.

- K. P. Gokhale, A. Kawamura and R. G. Hoft, “Deadbeat Microprocessor Control of PWM Inverter for Sinusoidal Output Waveform Synthesis”; IEEE Trans. On Ind. Appl., Vol. IA-23, No. 5, September/October 1987, PP. 901 – 910.

- A. Kawamura, T. Haneyoshi, and R. G. Hoft, “Deadbeat Controlled PWM Inverter with Parameter Estimation Using Only Voltage Sensor”; IEEE Trans. On Power Electronics, Vol. 3, April 1988, PP. 118 – 125.

- T. Haneyoshi, A. Kawamura, and R. G. Hoft, “Waveform Compensation of PWM Inverter with Cyclic Fluctuating Loads”; IEEE Trans. On Ind. Appl., Vol. 24, July/August 1988, PP. 582 – 588.

- Y. Nishida and T. Haneyoshi, “Predictive Instantaneous Value Controlled PWM Inverter for UPS”; IEEE Trans. On Power Electronics, Spec. Conf. Rec., PP. 776 – 783, 1992.

- Cassiano Rech, H. Pinheiro, H. A. Gründling, H. L. Hey, and J. R. Pinheiro, “Improved Modified OSAP Controller for Voltage Source PWM Inverters”; Proc. Brazilian Power Electronics Conf., PP. 329 – 334, 2001.

- Cassiano Rech, H. Pinheiro, H. A. Gründling, H. L. Hey, and J. R. Pinheiro, “Comparison of digital control techniques with repetitive integral action for low cost PWM inverters”; IEEE Trans. On Power Electronics, Vol. 18, No. 1, January 2003, PP. 401 – 410.

LIST OF SYMBOLS

The symbols repeatedly used are listed below. Other symbols are explained in the text.

c_{r1}, c_{r2}	Repetitive controller gains
f_p	Resonance frequency
f_r	Reference frequency
f_s	Sampling frequency
f_{sw}	Switching frequency

$G_d = \begin{bmatrix} g_{d11} & g_{d12} \\ g_{d21} & g_{d22} \end{bmatrix}$	State space matrix for the new linear discrete-time plant model
$G_{dMOSAP}(z)$	Transfer function of the developed modified OSAP controller system
$H_d = \begin{bmatrix} h_{d1} \\ h_{d2} \end{bmatrix}$	Input matrix for the linear discrete-time plant model
$\begin{bmatrix} h_{d_{non}1}(k) \\ h_{d_{non}2}(k) \end{bmatrix}$	Nonlinear input matrix for the discrete-time plant model
k	Counter of samples
n	Number of samples in a period of reference voltage
n_p	Number of pulses per sampling period
N	Time advance step size
$p_1,\ p_2, q_1, q_2$	OSAP controller parameters
$P_{d1}, P_{d2}, Q_{d1}, Q_{d2}, Q_{d3}$	Developed modified OSAP controller parameters
$r(k), r(z)$	Reference voltage (in control notation)
$u(k)$	Discrete system input voltage (denoted by the control law too)
$u_{dMOSAP}(k)$	Control law of developed modified OSAP controller
$u_{OSAP}(k)$	Control law of OSAP controller
$u_{RP}(k)$	Repetitive control law
$v_{in}(t)$	Inverter input voltage
$v_{ref}(t)$	Reference voltage signal
$y(t), y(s), y(k), y(z)$	System output voltage
ω	Angular frequency of the reference input
ω_p	Resonance angular frequency
ζ_p	Resonance damping ratio
$\Delta T(k)$	k-th pulse width
MPWM	Multiple Pulse Width Modulation
PWM	Pulse Width Modulation
THD	Total Harmonic Distortion
UPS	Uninterruptible Power Supply

ALLOCATION OF GENERATION PLANTS THAT GIVES MINIMUM LOSSES FOR IRAQI SUPER GRID NETWORK

Dr. Afanin A. Abood
Assistant Professor
University of Technology

Dr. Samir S. Mustafa
Assistant Professor
Technical Institute/Kirkuk

ABSTRACT

The main goal of this work is to determine optimal location for placing generating plants in the Iraqi National Super Grid which gives minimum total losses in the system. A package build under Matlab was used to allocate optimal placement of generating sets, calculating active and reactive power for these generators, .calculating system minimum losses, and determine the effect of varying the output of the generators used on losses reduction.

KEYWORDS

Allocation of the generating units, Minimum Losses, Iraqi supper grid network

تحديد مواقع إنشاء محطات التوليد التي تعطي اقل خسائر في القدرة لشبكة الضغط الفائق العراقية

ألخلاصة

تهدف هذه الدراسة إلى تحديد أفضل المواقع المستقبلية لمحطات التوليد لشبكة الضغط الفائق في العراق والتي تعطي اقل خسائر في المنظومة. استخدم لهذا الغرض برنامج جاهز بلغة Matlab حيث تم التوصل إلى تحديد أفضل الأماكن لنصب محطات التوليد، حساب القدرة الفعالة والمتفاعلة لكل محطة، اقل الخسائر التي يمكن الحصول عليها عند تحديد أماكن وقدرات تلك المحطات، و تأثير تغيير قدرات المحطات الحالية في التقليل من خسائر المنظومة .

INTRODUCTION

Electric power systems designed with generating units that are widely scattered and interconnected by long transmission lines may suffer significant losses. The losses depend on the line resistance and currents and are usually referred to as thermal losses. While the line resistances are fixed, the currents are a complex function of the system topology and the location of generation and load. Proper placement of generation units will reduce losses also free available capacity for transmission of power and reduce equipment stress, while improper placement may actually increase system losses. In this work an algorithm was applied to determine the best placement of new units for the Iraqi super grid network in order to maximize power available and minimize losses on the system for a given load (William 2002).

Mathematical representation of the problem:

The main objective is to find the partial derivatives (sensitivity) of active power loss with respect to active and reactive power injected at all buses except slack bus.

$$[SEN] = [\partial P_L / \partial P \quad \partial P_L / \partial Q]$$

Where $[SEN]$ is the sensitivity factor.

The results of sensitivity vector $[SEN]$ are used as an indicator to the efficiency of the system to reduce losses in case of installing generation units or shunt capacitors at these buses (samir2007).

The following matrix [D] is the partial derivative of real losses with respect to voltage magnitude at load buses and voltage angles at all buses except slack bus.

$$[D] = \frac{\partial f}{\partial x} = \begin{bmatrix} \partial P_{loss} / \partial \delta_2 \\ \partial P_{loss} / \partial \delta_3 \\ \\ \partial P_{loss} / \partial \delta_N \\ \partial P_{loss} / \partial V_2 \\ \partial P_{loss} / \partial V_3 \\ \\ \partial P_{loss} / \partial V_{NL+1} \end{bmatrix} \tag{1}$$

The components of $[D]$ are calculated as follows:

$$\partial P_{loss} / \partial \delta_i = 2\sum_{\substack{j=1 \\ j\neq i}}^{N} G_{ij} \left[|V_i||V_j| \sin(\delta_i - \delta_j) \right] \tag{2}$$

$$\partial P_{loss} / \partial V_i = 2\sum_{\substack{j=1 \\ j\neq i}}^{N} G_{ij} \left[|V_i| - |V_j| \cos(\delta_i - \delta_j) \right] \tag{3}$$

The mathematical analysis needs also Jacobian matrix $\left[Jac\right]$ which is used in power flow problem, then:

$$\left[Jac\right]^T\left[SEN\right]=\left[D\right] \tag{4}$$

Then $\left[SEN\right]=\left[Jac\right]^{T^{-1}}\left[D\right]$ (5)

$$\begin{bmatrix} P_{sen} \\ Q_{sen} \end{bmatrix}=\begin{bmatrix} \frac{\partial P_L}{\partial P} \\ \frac{\partial P_L}{\partial Q} \end{bmatrix}=\left[Jac\right]^{T^{-1}}\begin{bmatrix} \frac{\partial P_L}{\partial \delta} \\ \frac{\partial P_L}{\partial V} \end{bmatrix} \tag{6}$$

Where $\left[J\right]$ is the Jacobian matrix of Newton-Raphson load flow.

Then P_{sen} = $\begin{bmatrix} \frac{\partial Ploss}{\partial P_2} \\ \frac{\partial Ploss}{\partial P_{NL+1}} \end{bmatrix}$ (7)

And Q_{sen} = $\begin{bmatrix} \frac{\partial Ploss}{\partial Q_2} \\ \frac{\partial Ploss}{\partial Q_{NL+1}} \end{bmatrix}$ (8)

The following matrix represents derivative of active power losses w.r.t generation voltages:

$$\frac{\partial f}{\partial u}=\begin{bmatrix} \frac{\partial P_{loss}}{\partial V_1} \\ \frac{\partial P_{loss}}{\partial V_2} \\ \vdots \\ \frac{\partial P_{loss}}{\partial V_{NG}} \end{bmatrix} \tag{9}$$

Where $\frac{\partial P_{loss}}{\partial V_i}=2\sum_{\substack{j=1 \\ j\neq 1}}^{NG} G_{ij}\left[\left|V_i\right|-\left|V_j\right|\cos(\delta_i-\delta_j)\right]$

$$\frac{\partial g}{\partial u}=\begin{bmatrix} \frac{\partial P_2}{\partial V_1} & \frac{\partial P_2}{\partial V_2} & \cdots & \frac{\partial P_2}{\partial V_N} \\ \vdots & & & \\ \frac{\partial P_N}{\partial V_1} & \frac{\partial P_N}{\partial V_2} & \cdots & \frac{\partial P_N}{\partial V_N} \\ \frac{\partial Q_2}{\partial V_1} & \frac{\partial Q_2}{\partial V_2} & \cdots & \frac{\partial Q_2}{\partial V_N} \\ \vdots & & & \\ \frac{\partial Q_{N_{L+1}}}{\partial V_1} & \frac{\partial Q_{N_{L+1}}}{\partial V_2} & & \frac{\partial Q_{N_{L+1}}}{\partial V_N} \end{bmatrix} \tag{10}$$

Where $\left[\frac{\partial g}{\partial u}\right]$ represents partial derivative of injected power to bus voltages.

Gradient $[\nabla f] = \left[\frac{\partial f}{\partial u}\right] + \left[\frac{\partial g}{\partial u}\right]^T * [SEN]$ (11)

Where $[\nabla f]$ represent the sensitivity of losses w.r.t control variables (Manadur 1981).

$$\text{Hessian } [H] = \frac{\partial_2 P_{loss}}{\partial V_i \partial V_j} = \begin{bmatrix} \frac{\partial_2 P_{loss}}{\partial V_1^2} & \cdots & \frac{\partial P_{loss}}{\partial V_1 \partial V_{NG}} \\ \frac{\partial_2 P_{loss}}{\partial V_2 \partial V_1} & \cdots & \frac{\partial P_{loss}}{\partial V_2 \partial V_{NG}} \\ \vdots & & \\ \frac{\partial_2 P_{loss}}{\partial V_{NG} \partial V_1} & \cdots & \frac{\partial P_{loss}}{\partial V_N{}^2{}_G} \end{bmatrix} \quad (12)$$

Where $[H]$ represents the second partial derivative for P_{loss} w.r.t control variables.

$$[\Delta u] = \begin{bmatrix} \Delta V_1 \\ \Delta V_2 \\ \vdots \\ \Delta V_{NG} \end{bmatrix} = -[H]^{-1} * [\nabla f] \quad (13)$$

$[\Delta u] \leq \in$ Optimum, where $\in$ opt. = 0.001, then P_{loss} represents minimum losses in the system. Otherwise control variables have to be developed as follows:

$$\begin{bmatrix} V_1 \\ V_2 \\ \vdots \\ V_{NG} \end{bmatrix}^{K+1} = \begin{bmatrix} V_1 \\ V_2 \\ \vdots \\ V_{NG} \end{bmatrix}^{K} + \begin{bmatrix} \Delta V_1 \\ \Delta V_2 \\ \vdots \\ \Delta V_{NG} \end{bmatrix}^{K} \quad (14)$$

Where P_{sen} = partial derivative of real losses with respect to real power injected at load buses.

Q_{sen} = partial derivative of real losses with respect to reactive power injected at load Buses (Manadur 1981).

Iraqi National Super Grid (INSG) System:

INSG network consists of 19 busbars and 27 transmission lines; the total length of the lines is 3711 km., six generating stations are connected to the grid. They are of various types of generating units, thermal and hydro turbine kinds, with different capabilities of MW and MVAR generation and absorption. **Fig.1** shows the single line diagram of the INSG (400) kV system (Afaneen 2004).

The diagram shows all the bus bars, the transmission lines connecting the bus bars with their lengths in km marked on each one of them. The load and generation of INSG system on the 2nd of January 2003 are tabulated in **Table1**. Lines parameters were tabulated in **Table2** (Al-Rawi2002) and used for a program formulated under Matlab 5.3. For this study Baji was chosen as slack bus.

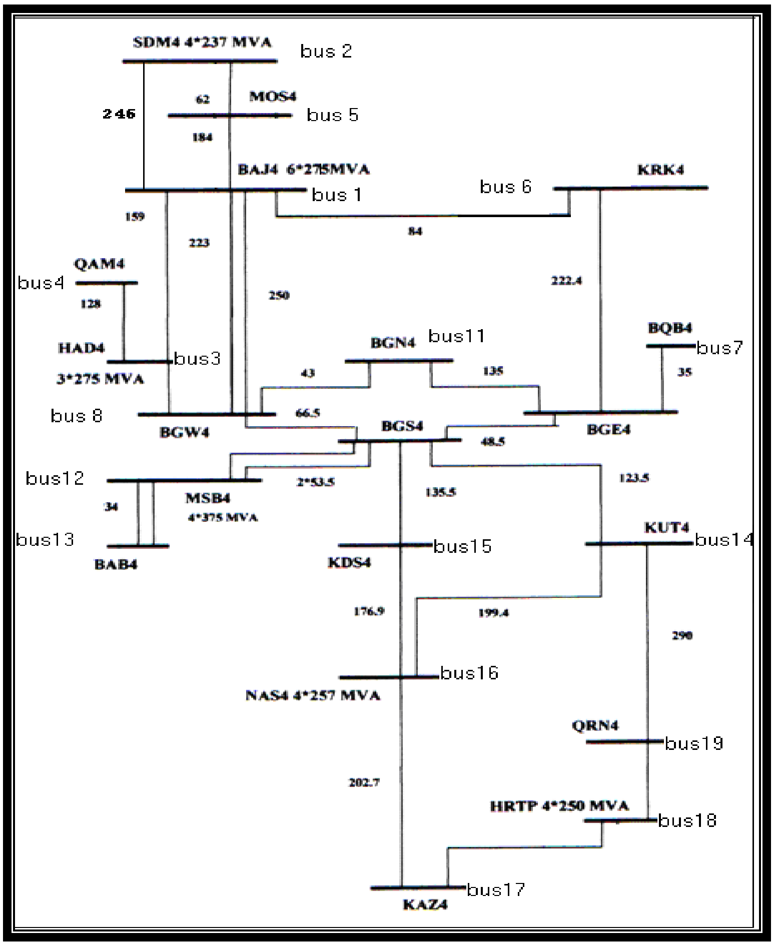

Figure1: Configuration of the 400 kV Network

Table1: The load & Generation of the Iraqi National Super Grid System (400 kV)

Bus Bar Number	Bus Bar Name	Type	Generation		Load	
			MW	M_{VAR}	MW	M_{VAR}
1	BAJ	Slack	570.592	100.4455	200.00	98.00
2	SDM	P,V	700.00	- 23.2248	5.00	2.00
3	HAD	P,V	500.00	- 0.8474	100.00	60.00
4	QAM	P,Q	.00	.00	60.00	40.00
5	MOS	P,Q	.00	.00	300.00	180.00
6	KRK	P,Q	.00	.00	70.00	40.00
7	BQB	P,Q	.00	.00	150.00	80.00
8	BGW	P,Q	.00	.00	500.00	360.00
9	BGE	P,Q	.00	.00	500.00	360.00
10	BGS	P,Q	.00	.00	100.00	50.00
11	BGN	P,Q	.00	.00	300.00	200.00
12	MSB	P,V	600.00	420.6564	120.00	70.00
13	BAB	P,Q	.00	.00	100.00	50.00
14	KUT	P,Q	.00	.00	100.00	60.00
15	KDS	P,Q	.00	.00	200.00	100.00
16	NAS	P,V	650.00	- 69.1434	100.00	54.00
17	KAZ	P,Q	.00	.00	350.00	200.00
18	HRT	P,V	380.00	35.9855	38.00	22.00
19	QRN	P,Q	.00	.00	70.00	30.00
Total	Total losses=37.592Mw		3400.592	463.8716	3363	2056

Table2: INSG System Line Data

From	To	R (P.U)	X (P.U)	B (P.U)
BAJ4	SDM4	0.00542	0.0487	1.4384
MOS4	SDM4	0.00143	0.0124	0.36439
MOS4	BAJ4	0.00399	0.03624	1.074
BAJ4	HAD4	0.00364	0.03024	0.8676
QAM4	HAD4	0.0035	0.03	0.7413
BGE4	BQB4	0.00076	0.00689	0.2043
BAJ4	KRK4	0.00182	0.01654	0.49031
BAJ4	BGW4-2	0.0055	0.05004	1.4826
BAJ4	BGW4-1	0.00483	0.04393	1.3017
HAD4	BGW4	0.00483	0.04393	1.3017
BGW4	BGN4	0.00093	0.00847	0.25099
BGN4	BGE4	0.00029	0.00265	0.0788
KRK4	BGE4	0.00481	0.04373	1.29581
BGE4	BGS4	0.00105	0.00955	0.28309
BGW4	BGS4	0.00144	0.0131	0.38816
BGS4	MSB4-1	0.00121	0.0102	0.30944
BGS4	MSB4-2	0.00121	0.0102	0.30944
BAB4	MSB4-1	0.00077	0.00648	0.19666
BAB4	MSB4-2	0.00077	0.00648	0.19666
BGS4	KUT4	0.00245	0.02236	0.6625
BGS4	KDS4	0.00292	0.02659	0.788
KDS4	NSR4	0.00383	0.03486	1.03314
KAZ4	NSR4	0.00439	0.03999	1.1849
KUT4	NSR4	0.00433	0.0394	1.1674
KAZ4	HRT4	0.00119	0.01083	0.32104
QRN4	HRT4	0.0013	0.01182	0.35022
QRN4	KUT4	0.00628	0.05713	1.6927

Results and Discussion

The values of dPloss/dPi which represents the efficiency to reduce system power losses with respect to real power injecting at the buses except the slack bus, were tabulated in **Table3**.

High negative partial derivative at any bus means that the system has high efficiency to reduce active power losses when injecting active power in that bus. On the other hand positive partial derivative for example at buses (3, 5, and 2) means that system power losses increase in case of injecting real power in these buses. The best buses to accept injecting active power are those with high negative partial derivative. **Table4** and **Fig.2** show the values of active power injection at each load bus, which gives maximum real power loss reduction. Injecting real power at bus 9 (BGE) gives max system loss reduction equal to $\frac{37.592-22.67}{37.592}\times 100\%$ = 39.69%.On the other hand

Table 3: loss sensitivities for all buses

Bus No.	Bus Name	Loss sensitivity $\partial P_{loss}/\partial P_{injection}$
7	Baquba	- 0.0392
9	Baghdad East	- 0.0361
11	Baghdad North	- 0.0359
8	Baghdad West	- 0.0279
10	Baghdad South	- 0.0258
15	Kadissia	- 0.0230
13	Babel	- 0.0214
12	Mussayab	- 0.0207
14	KUT	- 0.0188
17	Khour-Al-Zubair	- 0.0152
19	Qurna	- 0.0126
6	Kirkuk	- 0.0110
18	Hartha	- 0.0096
16	Nasiriya	- 0.0034
4	Qaim	- 0.0004
1	Baji	0.0000
3	Haditha	0.0031
5	Mousil	0.0136
2	Sed Al-Mousil	0.0268

injecting real power at bus 16 (NSR) gives min system loss reduction equal to $\frac{37.592-37.49}{37.592}\times 100\%$ = 0.27%. For the other buses, loss reduction lies between these two values.

Table (4): The Injection of Real Power which Gives Max Loss Reduction

Bus No.	Bus Name	$P_{injection}$ [Mw]	Minimum losses [Mw]	Max. loss Reduction %
9	Baghdad East	800	22.67	39.69
11	Baghdad North	825	22.83	39.26
7	Baquba	625	25.37	32.51
8	Baghdad West	825	25.83	31.28
10	Baghdad South	550	30.35	20.19
12	Mussayab	350	33.71	10.32
13	Babel	200	34.406	8.47
15	Kadissia	250	34.56	8.06
14	KUT	225	35.30	6.09
6	Kirkuk	350	35.528	5.49
17	Khour-Al-Zubair	100	36.71	2.34
19	Qurna	100	36.946	1.71
18	Hartha	75	37.197	1.05
16	Nasiriya	50	37.49	0.27

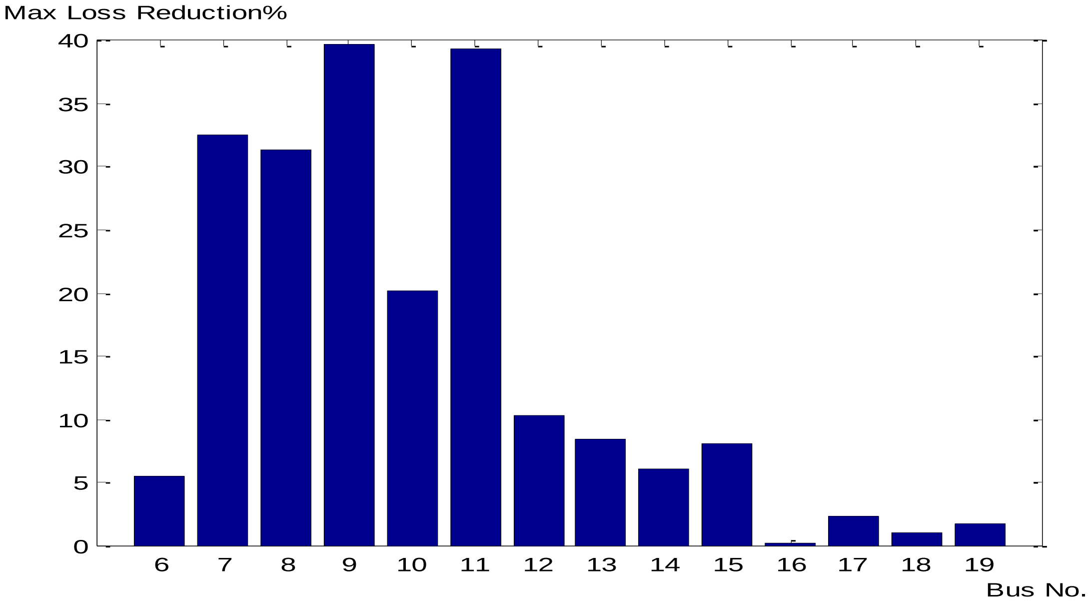

Figure2: maximum real power loss reduction

The optimal power injection at all buses is obtained by adding in steps small real power (U) equal to (5 Mw) in each step at the buses with the negative partial derivative of power losses with respect to real injection power (sensitivity) as shown before in **Table3**.

The addition of active power to each bus is stopped when sensitivity at that bus becomes zero or positive, the overall addition is stopped when sensitivity in all buses becomes zero or positive, at the same time this process must satisfy the constraints including reactive power limits of the generators as shown in **Table5** where the load bus voltage limit is pulse minus 0.05.

The injection of 180,200,210 and 300 Mw at the buses 7,8,9,11 respectively which are the best buses according to **Table3,** gives total system losses equal to 21.824 Mw. Total system losses according to **Table4** is equal to 37.592 So: Loss Reduction $= \frac{37.592 - 21.824}{37.592} \times 100\% = 41.94\%$.

Table5: INSG System Line Data Limits

Bus Bar	$Q_{generation}$ [M_{var}]		Voltage [P.V]	
	Q_{min}	Q_{max}	V_{min}	V_{max}
1	- 200	200	0.95	1.05
2	- 257.15	433.82	0.95	1.05
3	- 183.68	309.87	0.95	1.05
4	0	0	0.95	1.05
5	0	0	0.95	1.05
6	0	0	0.95	1.05
7	0	0	0.95	1.05
8	0	0	0.95	1.05
9	0	0	0.95	1.05
10	0	0	0.95	1.05
11	0	0	0.95	1.05
12	- 220.42	371.85	0.95	1.05
13	0	0	0.95	1.05
14	0	0	0.95	1.05
15	0	0	0.95	1.05
16	- 238.77	402.83	0.95	1.05
17	0	0	0.95	1.05
18	- 139.6	235.5	0.95	1.05
19	0	0	0.95	1.05
20	- 200	200	0.95	1.05
21	- 257.15	433.82	0.95	1.05
22	- 183.68	309.87	0.95	1.05
23	- 220.42	371.85	0.95	1.05
24	- 238.77	402.83	0.95	1.05
25	- 139.6	235.5	0.95	1.05

CONTROL OF ACTIVE POWER AT GENERATION BUSES:

Optimal power generation for the present six generators in INSG, were calculated using procedure similar to that implemented for the other buses. Generation at each bus is increased by (10 Mw) at each step until the sensitivity at the bus becomes zero or positive, i.e. the system losses start to increase. **Table6** show active power generation at each generation bus which gives minimum losses equal to (25.95 Mw) with optimal losses reduction equal to (30.96 %).

Table 6: Active Power Generations which Give Optimal Losses Reduction

Generation Bus Number	Generation [Mw]
1 BAJ	571
2 SDM	250
3 HAD	350
12 MSB	1000
16 NSR	500
18 HRT	400

CONCLUSIONS

Proper placement of generation units will reduce losses, while improper placement may actually increase system losses. Each bus in the system has its sensitivity to decrease losses with respect to the power injection in that bus. From the obtained results it is very clear that the best buses for the placement of generation units are (7)Baquba, (8)Baghdad West, (9)Baghdad East, (10)Baghdad South and (11)Baghdad North which give maximum loss reduction and the best case to operate the present generation plants in Iraqi power system is to operate them at optimal power generation, which gives optimal loss reduction.

REFERENCES:

- Afaneen A. Abood, "Implementation of Geographic Information System (GIS) in Real-Time
- Transient Stability", Ph.D. thesis, University of Technology, Baghdad, 2004.

- Al- Rawi M. Ali," Transient Stability Improvement Using Series Capacitors with Application to Iraqi National Super Grid" , Ph.D. Thesis, University of Mosul, 2002, Mosul.

- Manadur K. and Chenweth, "Optimal Control of Reactive Power Flow for Improvement in Voltage Profiles and for Real Power Loss Minimization". IEEE Transactions on Power Apparatus and System Vol. PAS-100, No. 7, July 1981, pp. 3185-3193.

- Samir S. Mustafa, "Minimum Power Losses Based Optimal Power Flow Iraqi National Super Grid and its Effect on Transient Stability, Ph.D thesis", University of Technology, Baghdad, 2007.

- William R., "Optimal Placement of Distributed Generation", www.pscco2.org, 2002, USA.

RECLAMATION AND REUSE OF TEXTILE DYEHOUSE WASTEWATER BY ELCTROCOAGULATION PROCESS

Assist. Lecturer Hussain M. Flayeh
University of Baghdad
Environmental Engineering Department

ABSTRACT

The present study investigates the removal of the textile dyehouse wastewater [azo dye para red(reactive dye)and M-5R200%(disperse oranges dye)] by Electrocaogulation process. The effect of nature of the anode, current density, initial pH, rate of stirring and concentration of dyes on the removal efficiency were tested.

The experimental results showed that the color of dyes in the aqueous solution was effectively removed when aluminum was used as anodes and the current density 25mA/cm^2 , initial pH (3-9),stirring rate 200rpm, and the concentration of dyes was less than 100mg/l. When the concentration of reactive dye exceeded 300mg/l iron was a more suitable anode than aluminum.

For the electrocaogulation of disperse dye in aqueous solution aluminum as anode was more suitable than iron when the concentration exceeded 300mg/l. The removal efficiency of reactive dye was increased to 90% when using iron as anode and the removal efficiency of disperse dye 96% when aluminum was used as anode at different running time (10-30) minute.

الخلاصة

يقدم هذا العمل مساهمة في تطوير تقنيات متقدمة واقتصادية لمعالجة فضلات المياه . حيث تم دراسة معالجة فضلات مياه مصنع نسيج ، باستخدام الطريقة الكهروكيميائية لإزالة اللون وباستخدام أقطاب الألمنيوم وحديد حيث تم بحث عملية التخثير الكهربائي ودراسة تأثير نوع القطب،كثافة التيار،الدالة الحامضية،معدل الخلط،وتركيز الملوث على كفاءة الإزالة.

وقد وجد أن أفضل كفاءة لإزالة الملوث عند استخدام الألمنيوم كقطب انود تكون عند كثافة تيار 25 ملیامبیر/سم^2 وقيمة الدالة الحامضية 3-9 ومعدل خلط 200 دورة بالدقيقة وتركيز ملوث(اللون) اقل من 100 ملغرام/لتر وعند زيادة تركيز الملوث عن 300 ملغرام/لتر يكون الحديد مناسب أكثر كقطب من الألمنيوم للون متفاعل كفاءة إزالة 90% ويكون الألمنيوم مناسب أكثر كقطب من الحديد للون متشتت كفاءة إزالة 96% بزمن تشغيل يتراوح بين (10-30) دقيقة .

INTRODUCTION

Increasingly stringent effluent discharge permit limitations have been put into effect(4). The textile industry generally has difficulty in meeting wastewater discharge limits, particularly with regard to dissolved solids, ionic salts, pH, COD, colour and sometimes heavy metals. The textile dyeing industry consumes large quantities of water and produces large volumes of wastewater from different steps in the dyeing and finishing processes. Wastewater from printing and dyeing units is often rich in color, containing residues of reactive dyes and chemicals and require proper treatment before being released into the environment.

The problem of color in textile dyehouse effluent and the possible problems associated with the discharge of dyes and dye degradation products are of concern. The methods for dealing this kind of wastewater are as shown in table1

Table1, Possible treatments for cotton textile wastes and their associated advantages and disadvantages

Processes	Advantages	Disadvantages	References
Biodegradation	Rates of elimination by oxidizable substances about 90%	Low biodegradability of dyes	Pala and Tokat,2002; Ledakowicz et al.,2001
Coagulation-flocculation	Elimination of insoluble dyes	Production of sludge blocking filter	Gachr et al.1994.
Adsorption on activated carbon	Suspended solids and organic substances well reduced	Cost of activated carbon	Arslan et al.,2000
Ozone treatment	Good decolorization	No reduction of the COD	Adams et al.,1995;Scott and Ollis,1995.
Electrochemical processes	Capacity of adaptation to different volumes and pollution loads	Iron hydroxide sludge	Lin and Peng,1994;Lin and Chen,1997.
Reverse osmosis	Removal of all mineral salts, hydrolyzes reactive dyes and chemical auxiliaries	High pressure	Ghayeni et al.,1988;
Nanofiltration	Separation of organic compounds of low molecular weight and divalent ions from monovalent salts. Treatment of high concentration	------	Erswell etal.,1998;Xu et al.,1999
Ultrafiltration-microfiltration	Low pressure	Insufficient quality of the treated wastewater	Watters et al.,1991;Rott and Ranieri,2001

Electro-coagulation has been successfully used to treat textile industrial wastewater. The goal is to form flocs of metal hydroxide within the effluent to be cleaned by electro-dissolution of soluble anodes. Three main processes occur during electro-coagulation; electrolytic reactions at the electrodes; formation of coagulants in the aqueous phase and adsorption of soluble or colloidal pollutants on coagulants; and removal by sedimentation and floatation. The characteristic of electrocoagulation are simple equipment and easy operation, brief reactive retention period, decreased or negligible equipment for adding chemicals and decreased amount of sludge. Therefore electrocoagulation has been widely used to treat waters containing food and protein wastes, oil wastes, synthetic detergent effluents, mine wastes, and heavy metal-containing solutions(13).

Electrocoagulation is complicated process involving many chemical and physical phenomena that use consumable electrodes to supply ions into wastewater stream(13) . Principle of EC is catins generated by dissolution of sacrificial anodes induce flocculation of the dispersed pollutants contained by Zeta potential reduction system(13).

Electrocoagulation can also be used to remove phosphate, for defluoridation of water, and treat portables water, and textile waters. A direct anodic process or an indirect anodic oxidation via the production of oxidants such as hydroxyl radicals, ozone,…etc . usually destroys the organic and toxic pollutants present in wastewater such as dyes and phenols.

Electrocoagulation is the distinct economical and environmental choice for meeting water treatment discharge standards and compliance requirement eliminating discharge fees and fines, harvesting resource, and significantly reducing water replacement costs, generally recover capital and operating costs(13).

In this paper the electrocoagulation of azo dye para red(reactive dye) and M-5R200%(disperse oranges dye) in aqueous solutions with aluminum and iron as anodes is described.

Material And Methods

Materials

The wastewater sample used was collected after a bio-filter treatment from a textile dyehouse in Tripoli . It looked red and the composition of the sample after analysis presented ADMI color unit 850, COD=175mg/l, Turbidity=18NTU, TSS=269mg/l, pH=7.2.

A aluminum and iron(6*4)cm^2 plate was used as an anode while stainless steel of the same dimension served as a cathode in this system.

Sample color was analyzed by UV-Spectrophotometer(Hitachi, Japan), Solution pH values were detected by a pH meter(Thermo orion model 420A+). The turbidity was measure by using HACH DR14000(HACH Method 10047). To measure TSS, the wasrewater sample were filtered through a standard GF/F glass fiber filter. The residue retained on the filter was dried in an oven at 105±2 C until the weight of the filter remains unchanged. The increase in weight of the filter represents the total suspended solids(APHA Method 2540d).

Methods

The electrocoagulation set-up shown in fig.1 was composed mainly of aluminum or iron and stainless steel electrodes, a DC power source(Hampden, USA), a rheostat(Engield-Middlesex,U.K.) to keep the current invariant, and a 1.5 liter capacity test beaker used as a reactor. Two Pyrex glass strips (1*0.5*15) cm attached to the inside of the glass beaker the distance between them 20cm were used as baffles to create turbulence and facilitate proper mixing of the sample using a magnetic bar stirrer. Each electrode had an active surface area 48cm^2 and a spacing of 2cm between electrodes. The electrodes are inserted in the test beaker. An ammeter was used to measure the current and electrical switch was used to change the polarity of electrodes in order to reduce the passivation phenomenon that usually occur during the process and impedes the Redox reactions.

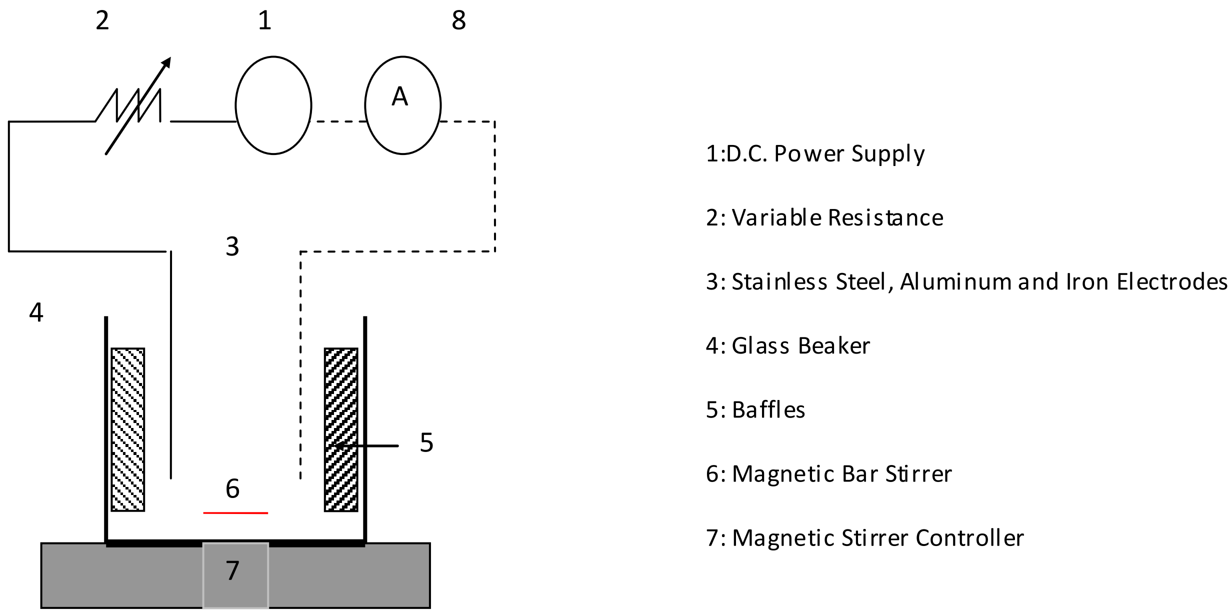

Fig. 1 (A): Schematic Diagram of Experimental Setup.

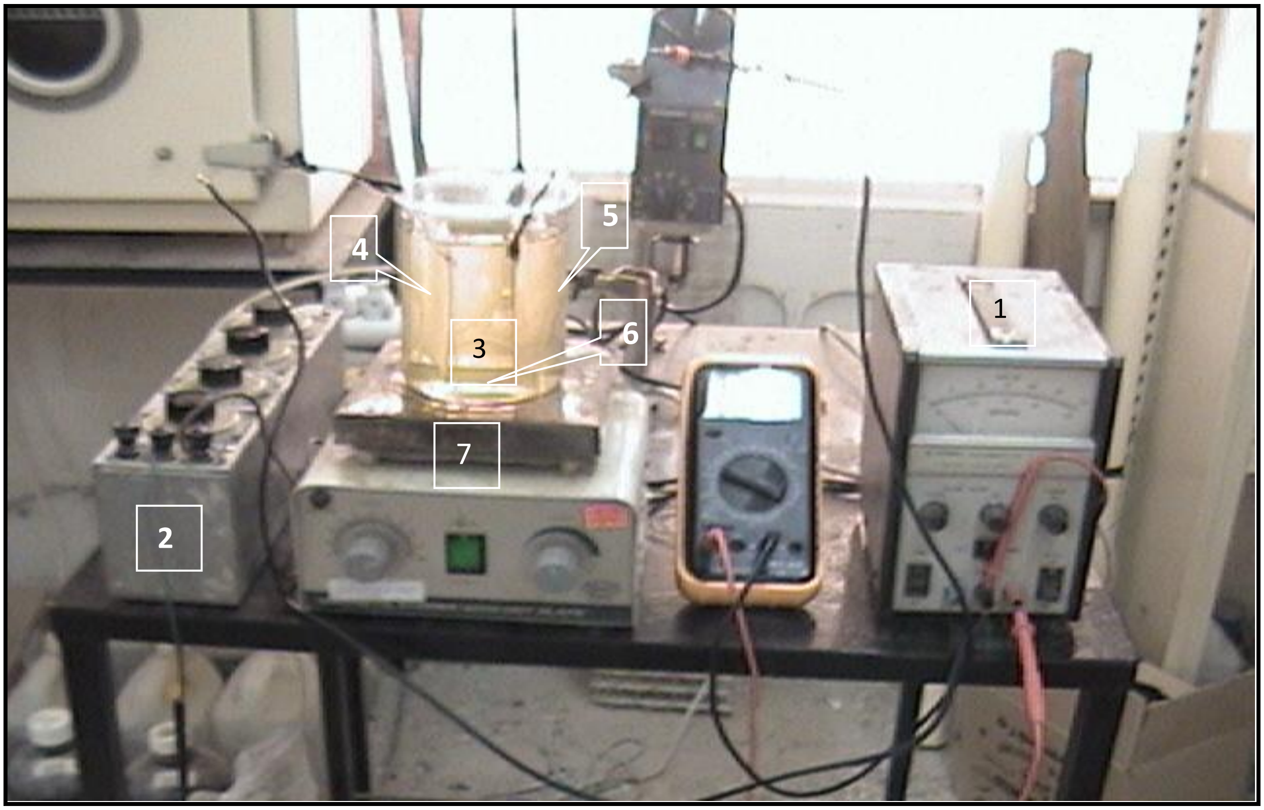

Fig. 1 (B): Photograph of Experimental Setup.

The electrocoagulation current density from 15to40mA/cm2 of dye-containing aqueous solution was carried out in a beaker. At the beginning of a run, the desired concentration of dye in the sample was fed into the reactor, and the pH was adjusted to desired value. The reaction was timed starting when the DC power supply was switched on. Samples were periodically taken ($5cm^3$, 10min.)from the reactor used pipette.

The precipitate in the sample was centrifuged at 700rpm for 10min and the filtrate was obtained. Filtrate(1ml) was added into buffer solution(pH 7, 4ml) and the residual concentration of reactive dye and disperse oranges dye were determined according to optical adsorption at 400 and 500 nm, respectively.

Results and discussion

Aluminum as Anode

Effect of current density on the electrocoagulation of dyes

Figure (2) shown that the increase in current density from 15 to 40mA/cm^2 yields an increase in the removal efficiency of reactive dye and disperse dye from 21 to 83%, from 30-80% respectively, because when the current density increase, the efficiency of aluminum production on the anode and cathode increases. Therefore there is an increase in floc production in the solution and hence an improvement in the removal efficiency. For solution with a dye concentration of 100 mg/l, the optimum current density was 25mA/cm^2 where the maximum removal efficiency 88%, 86% for reactive and disperse dyes respectively. The decay in the anode 0.0437 gm/cm^2.min .

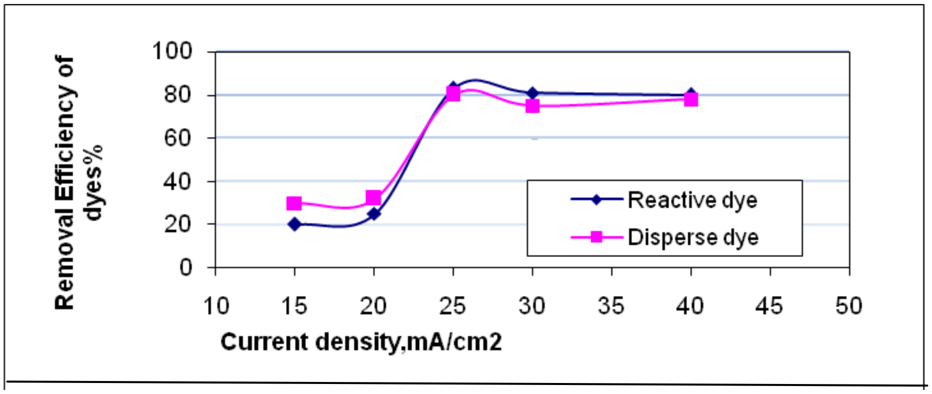

Fig.2.Effect of current density on the removal efficiency of dyes, conc.of dyes(100mg/l), using aluminum as anode

Effect of Stirring on the electrocoagulation of reactive dye

Figure(3) shown that the effect of stirring rate on the electrocoagulation of reactive dye, when the stirring rate increased from 100 to 200 rpm, the removal efficiency of reactive dye increased from 45 to 60% when the electrocoagulation period was 10min. Further increased of stirring rate to 500rpm, decreased the removal efficiency to 30%.The effect of stirring rate on electrocoagulation of reactive dye increased when the duration of electrolysis increased. In the initial state of coagulation, rapid mixing of dye and coagulant species was required. After that slowly mixing was needed for the chemical precipitate to grow large enough for removal.[10] Therefore increased stirring rate resulted in decreased coagulation/removal efficiency of reactive dye when reaction time exceeded 30min. The optimal rate of stirring of decolorization of reactive dye with aluminum as anode was 200rpm.

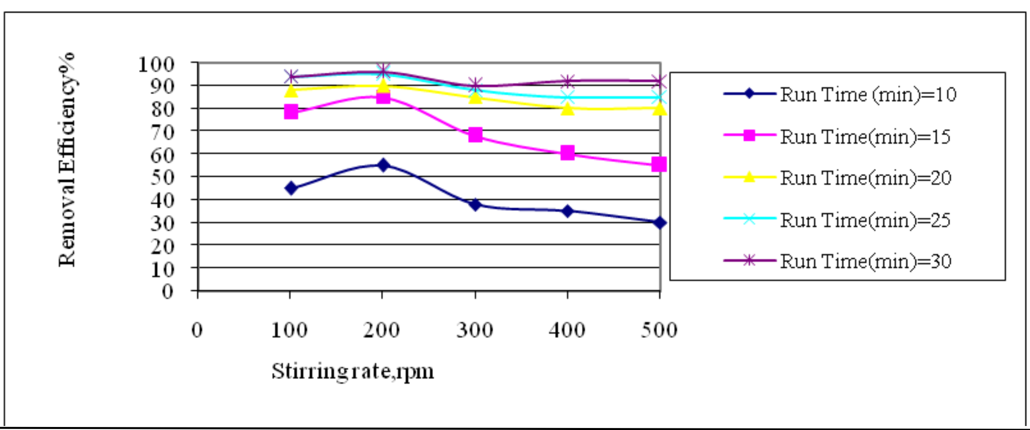

Fig.3, Effect of stirring rate on the removal efficiency of reactive dye using aluminum as anode

Effect of initial pH on the electrocoagulation of reactive dye

Figure(4) show that the decolourization of reactive dye was significantly affected by the initial pH under acidic conditions. The removal efficiency increased to 28% over thirty minutes with initial pH value 2. In contrast, the removal efficiency was increased to 90% when the initial pH exceeded 3. In this case (using aluminum as Anode), the dominant species are cationic monomers such as Al^{+3} and $Al(OH)^{-}_{2}$ when allow initial pH is applied. The main mechanism for the coagulation of dyes is double-layer compression. In this case, coagulant (Al^{+3}) at a high concentration is needed for effective removal of dyes in the aqueous solution. Hence the coagulation efficiency to removal reactive dye at initial pH 2 was small within 30 min. When the pH in the range 3-9, polymeric species (such as $Al_{13}O_4(OH)^{+7}_{24}$) and precipitate $Al(OH)_3$ (s) were formed. The dyes were effectively coagulated with the polymeric species and precipitated by the mechanisms of adsorption, charge neutralization and enmeshment. Therefore, the removal efficiency at the initial pH 2 was lower than that when the initial pH exceeded 3 in acidic solution.

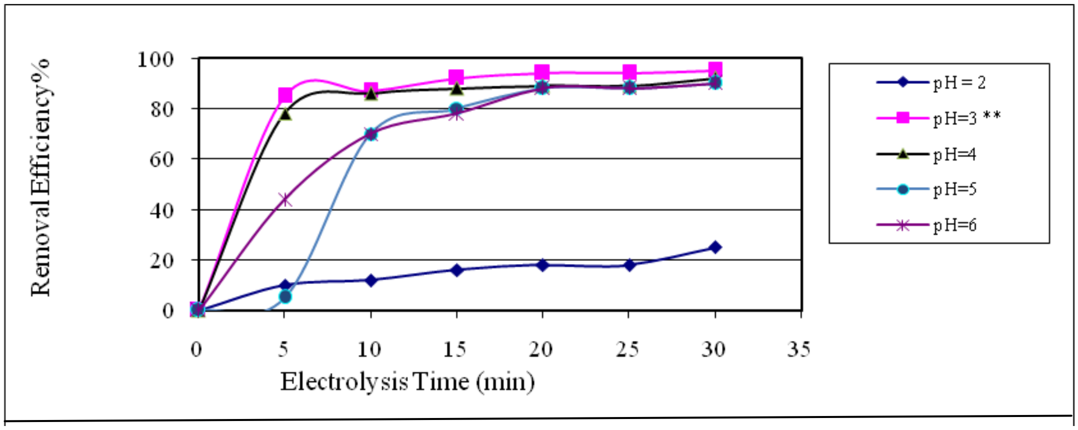

** THE BEST CASE

Fig.4.Effect of electrolysis time on the removal efficiency of reactive dye in acidic solution using aluminum as anode

When the initial pH was less than 9 in the alkaline region and the electrolysis period was 15 min., the removal efficiency of reactive dye effectively increased to 90% fig.5. The removal efficiency was 42% when the initial pH was increased to 10. As described above, the coagulation efficiency was promoted by the enmeshment of reactive dye with $Al(OH)_3$(s) in the neutral solution. When the initial pH increased to 10, the amount of $Al(OH)_3$(s) decreased and concentration of monomeric anion $Al(OH)^{-}_{4}$ increased. The efficiency of electrocoagulation of reactive dye then decreased with initial pH large than 10.

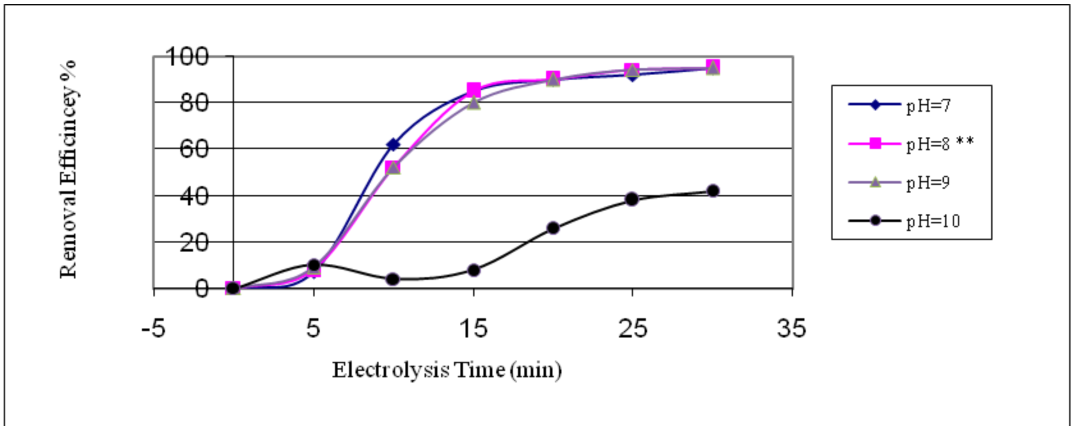

** THE BEST CASE

Fig.5.Effect of electrolysis time on the removal efficiency of reactive dye in alkline solution using aluminum as anode

Effect of initial pH on the electrocoagulation of dispresve dye

Figure(6) shown that the decolourization of M-5R200%(disperse oranges dye) was significantly affected by the initial pH under acidic conditions. Increasing the initial pH from 2 to 3 and keeping the electrolysis period at 15min resulted in increasing removal efficiency in the aqueous solution from 15-95%. Upon further increase of the initial pH to 10 the removal efficiency remained constant. The final solution pH increased from 2.5 to 8.5 and remained constant when the initial pH was increased from 2 to 10. These results revealed that the pH of electrocoagulation of disperse dye with aluminum as anode was in the range 2 to 2.5 with initial pH 2. The absence of adsorption, charge neutralization and enmeshment in the electrocoagulation of disperse dye resulted in the small coagulation efficiency at the initial pH 2. With aluminum as anode, the disperse dye M-5R200% was more readily removed and has a greater operational initial pH than that of the reactive dye.

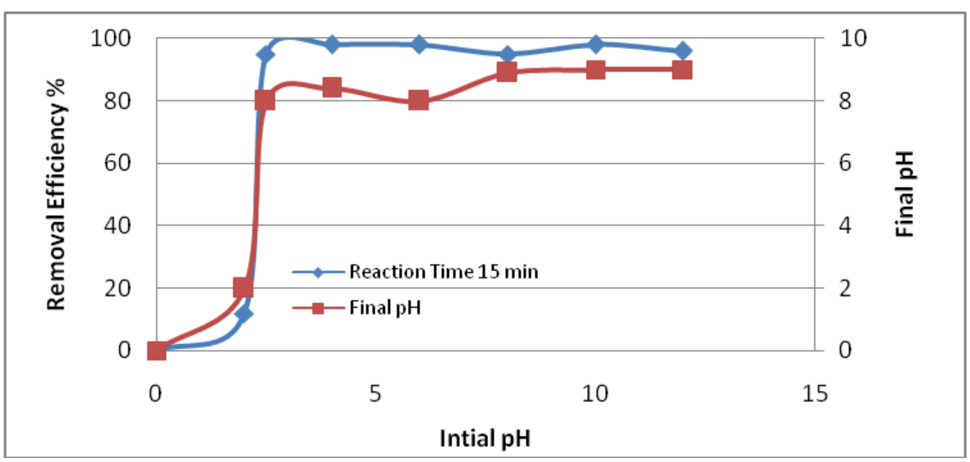

Fig.6. Effect of initial pH value on the removal efficiency of disperse dye and the final pH value using aluminum as anode

Effect of concentration of dye in aqueous solution

Fig.7.shown that, using aluminum as anode and maintaining the initial pH at 7, with the concentration of reactive dye in the range 100-600 mg/l ., the removal efficiency decreased from 95 to 40% with an electrolysis time of 15min . Under the same conditions, the removal efficiency of disperse dye decreased from 100 to35% when the initial concentration of disperse dye was increased from 100 to 600mg/l . as shown in fig.8. The amount of coagulant species for the coagulation dyes needs to be increased when the dye concentration increases. Hence the increase in dye concentration subsequently caused decrease in the removal efficiency when the electrolysis time was fixed. With the concentration of disperse dye increased from 300 to 600mg/l, the removal efficiency was increased to 96% when the electrocoagulation time 30min.Fig.8. At the same electrolysis time, the removal efficiency of reactive dye decreased from 75 to 60% when the concentration increased from 300 to 600mg/l . The results revealed that the removal of disperse dye was easier than that of the reactive dye with aluminum as anode.

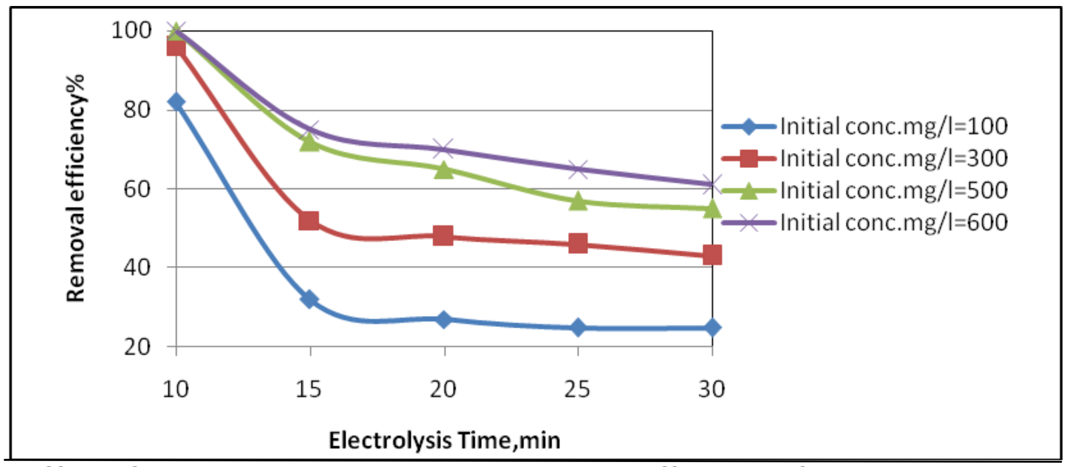

Fig.7. Effect of initial concentration on the removal efficiency of reactive dye in aqueous solution.

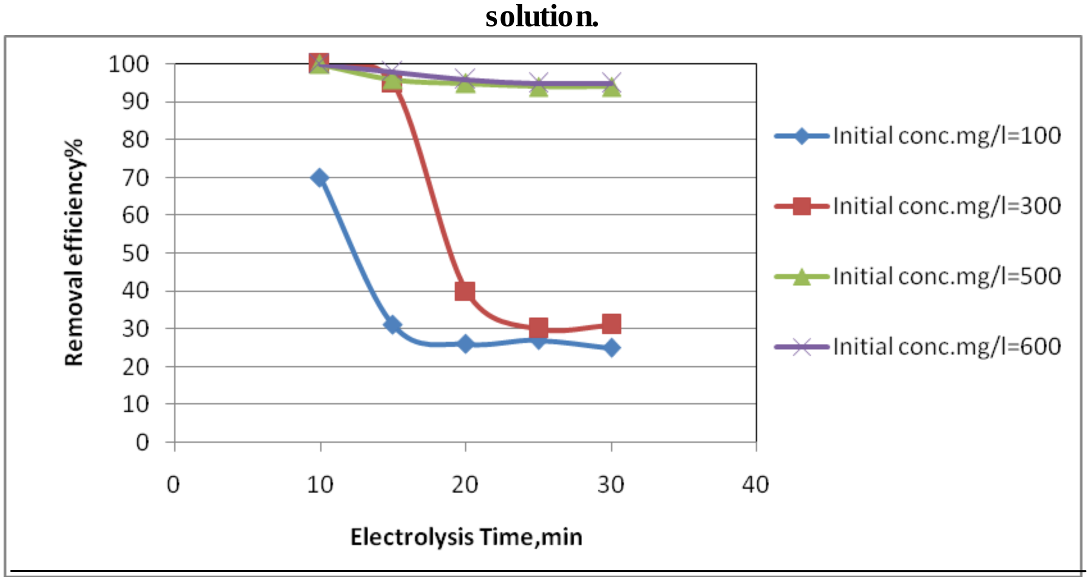

Fig.8. Effect of initial concentration on the removal efficiency of disperse dye in aqueous solution.

IRON AS ANODE

Effect of Stirring on the electrocoagulation disperse dye

Figure(9) Shown that, when stirring rate increased from 100 to 500rpm, the removal efficiency of disperse dye decrease from 80to45% at 15min. under the same conditions, the removal efficiency decrease from 90 to 70% at 30min.. As described above, the rapid mixing inhibited, thus resulting in an decrease in the removal efficiency and increased stirring rate the removal efficiency of disperse dye altered slightly Fig.(9). The results indicated that the time for electrocoagulation increased with stirring rate The optimal rate of stirring of decolorization of disperse dye with Iron as anode was 200rpm.

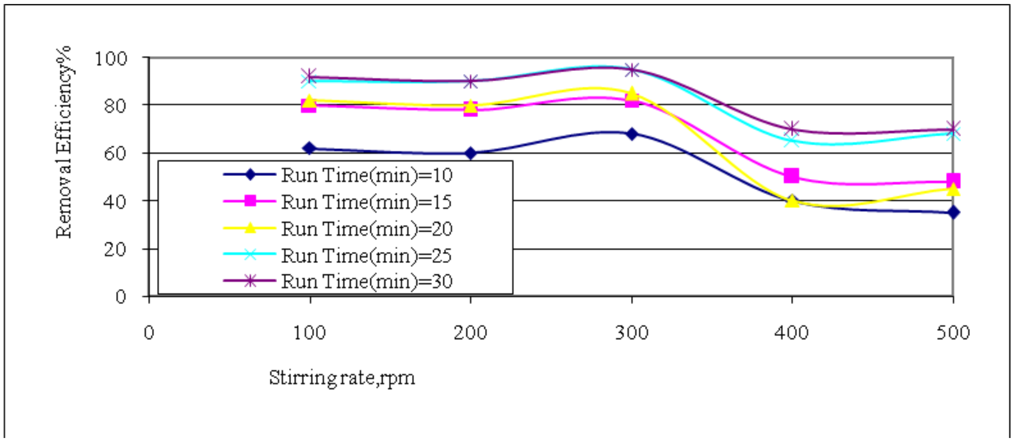

Fig.(9)Effect of stirring on the removal efficiency of disperse dye,Iron as anode

Effect of initial pH on the electrocoagulation of dyes

The removal efficiency of reactive dye increased significantly with time in the acidic range except for pH 2 as shown in fig.10. At lower pH, the dominant species of coagulant generated from iron anode were cationic monomers such as Fe^{+3} and Fe^{+2} (10). As described above, the efficiency of coagulation of dyes with cationic monomer was small. Furthermore, the increase of the concentration of Fe^{+3} and Fe^{+2} might result in the increase of light absorption in the analytical process. The importance of coagulation of reactive dye due to adsorption, neutralization and enmeshment increased when the initial pH increased in the acidic solution. Hence the electrocoagulation efficiency increased and the removal efficiency of reactive dye increase when the initial pH increased in the acidic range.

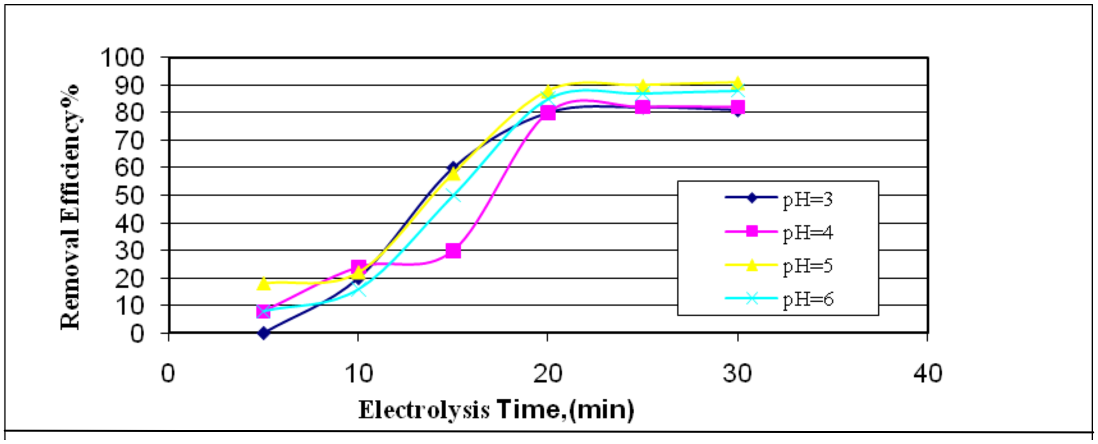

Fig.10.Effect of electrolysis time on the removal efficiency of reactive dye in acidic solution using iron as anode

The removal efficiency of disperse dye increased to 90% with initial pH greater than 2 when the electrolysis time exceeded 15min. as shown in fig.12. The removal efficiency of disperse dye increased to 10% at initial pH 2 over 15min. (fig.11) . The small electrocoagulation efficiency of disperse dye with iron as anode was due to the poor coagulation ability of cationic monomer as described above.

The removal efficiency of disperse dye significantly increased in the initial range pH 7-10 when the duration of electrocoagulation increased from 10-30min. as shown in fig.12. The apparent decrease of removal efficiency of disperse dye in the initial stage of electrocoagulation was due to light absorption by ferrous and ferric ions generated from the anode. The time for removal of disperse dye increased with initial pH increase in the alkaline range.

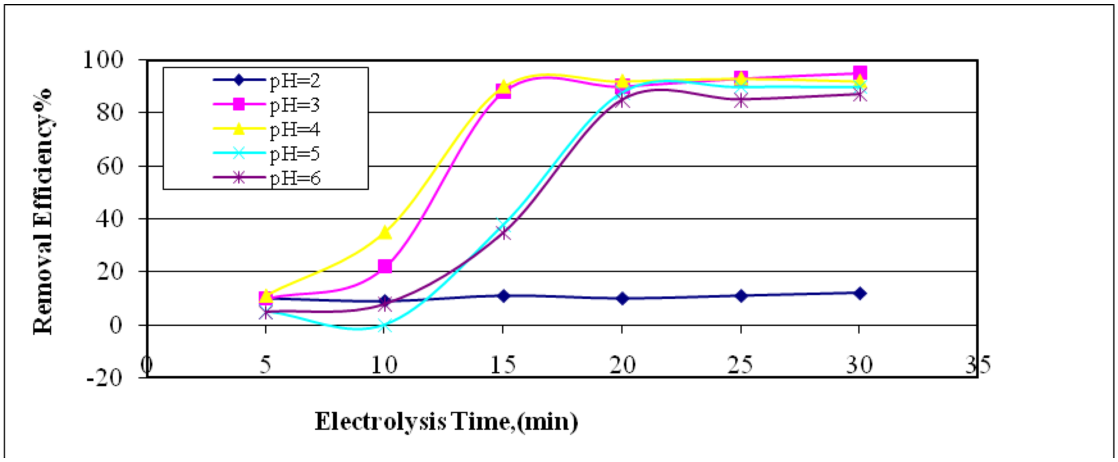

Fig.11.Effect of electrolysis time on the removal efficiency of disperse dye in acidic solution using iron as anode

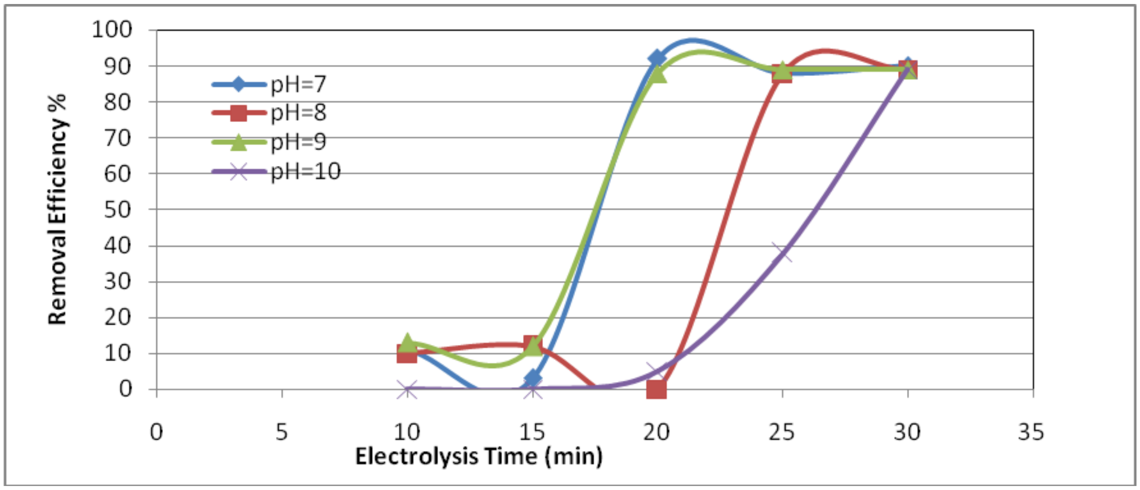

Fig. 12.Effect of electrolysis time on the removal efficiency of disperse dye in the alkaline solution using iron as anode

Effect of concentration of dyes in the aqueous solution

Using iron as anode. The removal efficiency of reactive dye was effectively increased to 90% when the initial concentration was in the range 100-600 mg/l. and the electrolysis period exceed 20 min as shown in fig.13. When the initial concentration was 100mg/l., the removal concentration was increased to90mg/l in 20min. Increasing the initial concentration of reactive dye required increased electrolysis time for electrocoagulation of reactive dye. Under the same electrocoagulation conditions, the removal efficiency of disperse dye reduced to 30% when the initial concentration of disperse dye was larger than 300mg/l and the time of electrocoagulation was 20min. as shown in fig.13. These results might be due to the high concentration of disperse dye causing an altered range of pH for removal of disperse dye with coagulant (10). The removal efficiency was increased to 95% when the initial concentration was 100mg/l. These results showed that the removal of reactive dye with iron as anode was easier than that of disperse dye, especially when the concentration of dye exceeded 300mg/l. In comparison with result in fig.7. Aluminum used as anode for the electrocoagulation of disperse dye was more suitable than iron. Comparing the results in fig.8and fig.5. ,it is seen that the electrocoagulation of reactive dye with iron as anode was superior to that with aluminum.

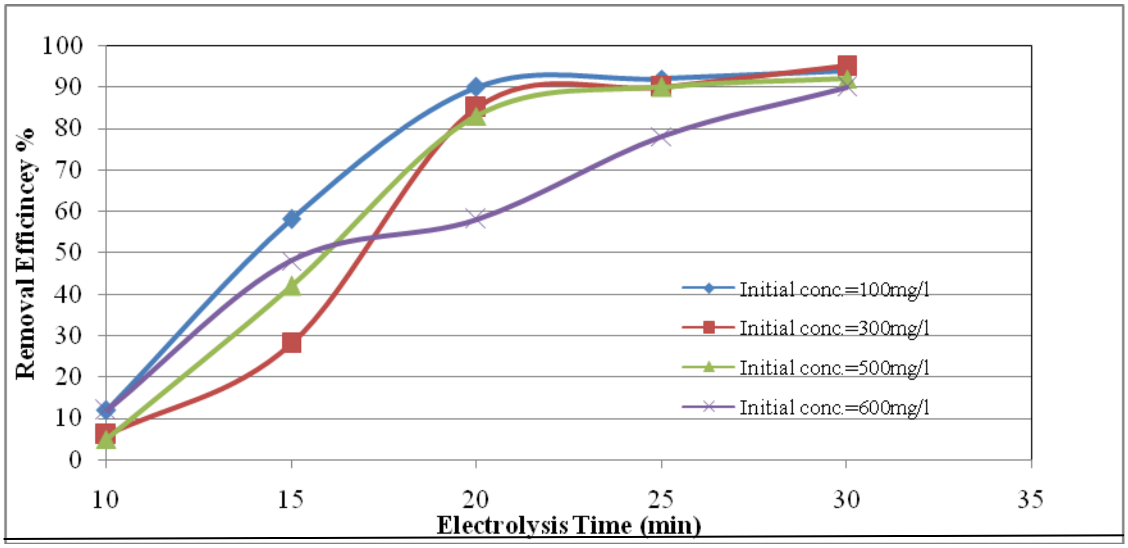

Fig.13 Effect of electrolysis time on the removal efficiency of reactive dye for various initial concentration using Iron as anode

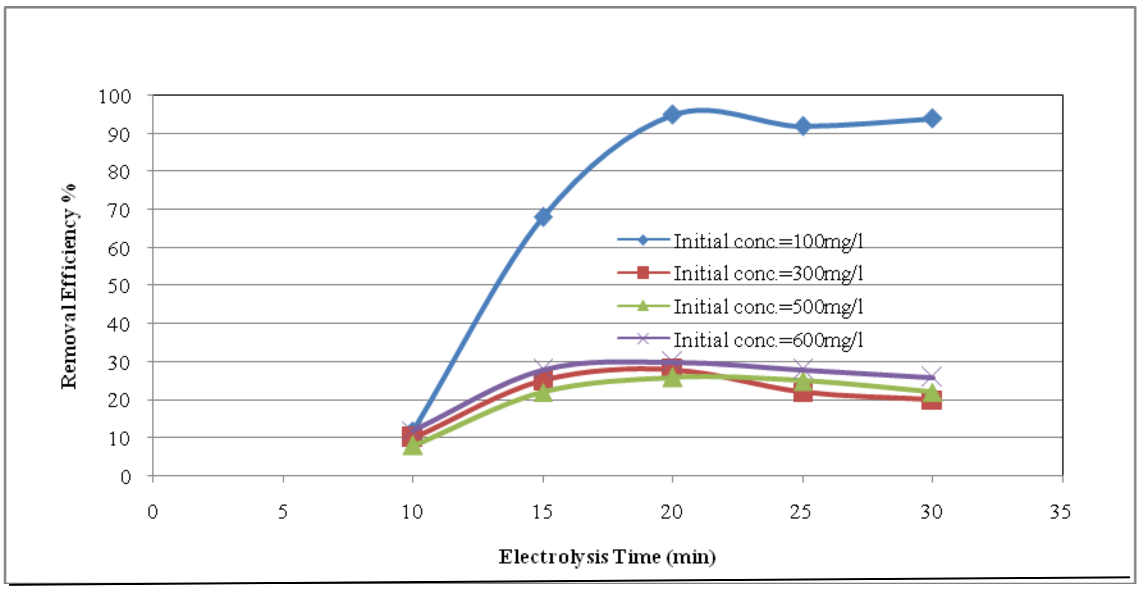

Fig.14 Effect of electrolysis time on the removal efficiency of disperse dye for various initial concentration using Iron as anode

CONCLUSIONS

The results shown that the removal of the azo dye para red(reactive dye)and M-5R200%(disperse oranges dye) by electrocoagulation was effected by the nature of the anode, current density, stirring rate, initial pH, and dye concentration. The dyes were effectively removed at initial pH 3-9 when the initial concentration of dye was 100mg/l, current density 25mA/cm2, stirring rate 200rpm. The results also indicated that the removal fraction of reactive dye was increased to 90% when iron was used as anode and the initial concentration of reactive dye exceeded 300mg/l. The removal efficiency of reactive dye exceeded 75% when aluminum was used as anode for decolonization of reactive dye was superior to aluminum. With aluminum as anode, the removal efficiency of disperse dye was increased to 95% when the initial concentration of disperse dye exceeded 300mg/l. The removal efficiency of disperse dye was less than 30% when iron was used as anode. This showed that aluminum was a suitable anode for electrocoagulation of disperse dye.

REFERENCES

- Chavan,R.B.,2001.Environmental-Friendly dyeing processes for cotton.Ind.J. Fibre Textile Res.4:239-242.
- B.Ramesh Babu.2007"Cotton Textile processing:Waste Generation and Effluent Treatment".J.Cotton Sci.11:141-153.
- Carmona,M.,M.Khemis.j.p.Leclerc,andF.Lapicque.2006.A Sample Model to predict The Removal of Oil Suspensions from water Using The Electrocoagulation Technique. Chemical E ngineering Sicence.61:1237-1246.
- Defazios and lemleyat(1999) Electrochemical treatment of acide dye waste, Sodiammeta-bisulfite addition to Anodic system.J.Environ.Sci..
- Kumar, P.R.S.Chaudhar, K.Khilar, and C.Mahajan2004. Removal of Arsenic from Water by Electrocaogulation. Chemosphere.55:1245-1252.
- Calvo, L.S.,J.P. Leclerc,G. Tnguy,M.C. Cames,G.Paternotte,G.Valentin,A. Rostan, and F.Lapicque.2003. An Electrocaogulation unit for the purification of soluble oil waste of high COD. Environmental Progress.22(1):57-65.
- Larue,O.,E. Vorobiev,C.Vu, and B.Durand.2003. Electrocaogulation and coagulation by Iron Latex particles in Aqueous suspension. Separation and purification Technology.31:177-192.
- Holt,P.K.,G.,W.Barton,M.Wark,and C.A.Mitchell.2002. A Quantitative comparision between chemical dosing and electrocaogulation. Colloids and Surfaces :A Physicochemical Engineering Aspect.211:233-248.
- T.R.Demanin andK.D. Uhrich,American Dyestuff Reporter 77(6).(1988)13.
- Chen Junshui,Liu MELCHUAN,Zhang Jidong,Kan uyezhong and Jin Litong(2003) Electrochemical degradation of bromopyrogallol red in presence of cobalt ions Chemes.5:1131-1136.
- F.W. Pontius."Water Quality and the Treatment",4th edn McGraw-Hill,New York(1990).
- Xuejun Chen, Yaobo Fan"Advanced treatment of textile wastewater for reuse using electrochemical oxidation and membrane filtration", http://www.wrc.org.za .
- Web: www.powellwater.com, 1994-2001 powell water systems inc.

WATER QUALITY OF AL-HAMMAR MARSH SOUTH IRAQ

Tariq J.Kadhem Al-Mosewi
Department of Environmental Engineering/College of Engineering/Baghdad University-Iraq

ABSTRACT

Water quality plays an important role in the restoration of marshes south Iraq, hence, in this paper water samples were taken from different sites in Hammar marsh in south of Iraq to know the variation of some water parameters with the distance along Hammar marsh. The water samples will submit to chemical and physical analyses.

Ten water samples were analysis to discuss the results of these parameters and give reasons for changing these parameters with the location along the Hammar marsh. It was found that the concentrations of Biochemical Oxygen Demand (BOD) and Dissolved Oxygen (DO) with the acceptable range for drinking and agriculture uses, DO concentrations did not decreased less than 6 mg/l.

The analyses showed that high concentrations of The Total Dissolved Solids (TDS) and Electrical Conductivity (EC) at the beginning and end of the marsh, the analyses showed a decrease in these parameters at the middle of the marsh.

The analyses showed low concentrations of Total Suspended Solids (TSS) along the Al-Hammar marsh, the concentration of TSS strongly depends on the velocity of water in marsh which is considered low at the study region. As well as the analyses showed that the Mg concentration increased above 125 mg/l level, this level may cause diarrhea.

It was also found that the concentrations of sulphates exceed allowable limits of WHO standards for drinking water (400 mg/l), these concentrations of SO_4 came from severally burned of organic matter in soils after drainage period.

الخلاصة

تعد نوعية المياه في الاهوار ذات اهمية كبيرة في عمليات انعاش الاهوار التي تجرى في الوقت الحاضر، في هذا البحث تم اخذ عدة عينات لمياه هور الحمّار في جنوب العراق لمعرفة تغيرات بعض خصائص المياه في الهور حيث تم تحليل هذه العينات كيمياوياً وفيزياوياً .

تم اخذ عشرة عينات لمناقشتها واعطاء تفسير لتغير مواصفات المياه حسب مواقع العينات داخل الهور. وجد ان قيم تراكيز المتطلب الكيمياحيوي والاوكسجين المذاب ضمن الحدود المقبولة لاستخدام المياه لاغراض الشرب او للاغراض الزراعية حيث ان قيم الاوكسجين المذاب لم تقل عن 6 ملغم/لتر.

بينت النتائج ارتفاع قيم تراكيز المواد الكلية الذائبة والتوصيلية الكهربائية خاصة في العينات الماخوذة من بداية ونهاية الهور مع انخفاض ملحوض لهذه التراكيز في العينات المأخذوة من منتصف الهور.

بينت النتائج انخفاض قيم تراكيز المواد العالقة الكلية على طول هور الحمّار حيث ان تراكيز المواد العالقة الكلية في المياه السطحية تعتمد بشكل كبير على سرعة المياه في الهور والتي تعد بطيئة نسبياً. كذلك بينت نتائج الفحوصات ارتفاع قيم تراكيز المغنيسيوم حيث وصلت اكثر من 125 ملغم/لتر حيث ان مثل هذه التراكيز في المياه السطحية قد تسبب الاسهال، بينما وصلت تراكيز الكبريتات اكثر من 400 ملغم/لتر، هذه التراكيز للكبريتات تاتي بصورة رئيسية من المواد العضوية الوفيرة في ترب الاهوار المجففة.

INTRODUCTION

Marshes in Iraq are important for economic, social and biodiversity Values characterized by frequency of water flows and quality, accumulation of nutrients and organic matter and the production of commercially important vegetation and fish, They were the permanent habitat for millions of birds and a flyway for millions more migrating between Siberia and Africa (Maltby, 1994).

Although the uncontrolled reflooding is welcome news, it presents potential problems and challenges regarding the quality of water:

1) The release of toxins from reflooded soils that are contaminated with chemicals, mines and military ordnance.
2) Flooding of local villages and farms now developed on the edges of formerly drained marshes.
3) A false sense of security regarding the volume of water that will be available to restore the marshes in future years.

Many studied were achieved from many Iraq Ministries, Organizations and Associations that related to the restoration of marshes. United Nation Environment Program (UNEP) was made many studies before and after 2003 some of them:

- **Water Quality of Marshlands,** south of Iraq(2004) in this study the team of UNEP took many water samples and analyses their to know the water quality of Abu-Zaraq marsh (40 km) east of Al-Nasria city, the results of chemical analyses compared with the upper limits of concentrations in irrigation water, the comparison shows moderate saline water and no significant effect of Na,Cl,No_3.
- **Environment in Iraq** (UNEP progress, October 2003), this study concerned on the environment status in Iraq, background materials used in the reports preparation relied on UNEP's earlier work in the region, including three studied it had carried out about the environmental impacts of the 1991 gulf war, and the 2001 report on the demise of the Mesopotamian marshlands, this study was represented the reflooded marshlands in summer 2003, in addition discussion the status of marsh Arabs. The study also was showed all the constrains that forced the restoration of marshes.

Partow (2001) Studied the hydrology of marshes of Iraq and mentioned that less than 10 % of the area of marshes in Iraq remained as functioning marshland by the year 2000; the only remaining marsh was the northern portion of Al-Hawizeh. The researcher was concluded that the idea that only 15 % to 20 % of dried wetland could be restored because of excessive salinity, environmental pollution, lack of availability high-quality water.

Curtis (2006) studied the ecology of the Iraq marshes focusing on the returned different species of animals and plants. Samples of water and soils at selected locations in marshes were analyses for Conductivity, Dissolved oxygen, dissolved solids, total nitrogen, total phosphorus and salinity. The researchers were showed that uncontrolled release of water in many areas was resulted to return of native plants and animals, including rare and endangered species of birds, mammals and plants. In addition the researchers were concluded that the poor water quality presence high saline soil and toxic materials would prevent the complete ecological restoration of marshes.

The marshes in Iraq were considered once famous for their biodiversity and cultural richness. Hammar marsh is the largest marsh on the right side of Euphrates River before it joins Tigris River at Al-Qurna to form Shut Al-Arab. After 1991 Hammar Marsh subjected to many drying processes and the reason of this drying is to increase the agriculture areas in the country (Al-Samaria 1999).

Water enters Hammar marsh from many feeders, the most important of them are Kurmishia, Um-Nakhla and Jassim rivers, all them take their water from Euphrates River. During the flood season, Hammar marsh becomes a connected lake and becomes disconnected shallow small lakes depth (0.2–0.5m) during the dry season. (Al-Samaria 1999). **Fig.1** shows satellite image of Hammar marsh area after 2003 [Google Earth].

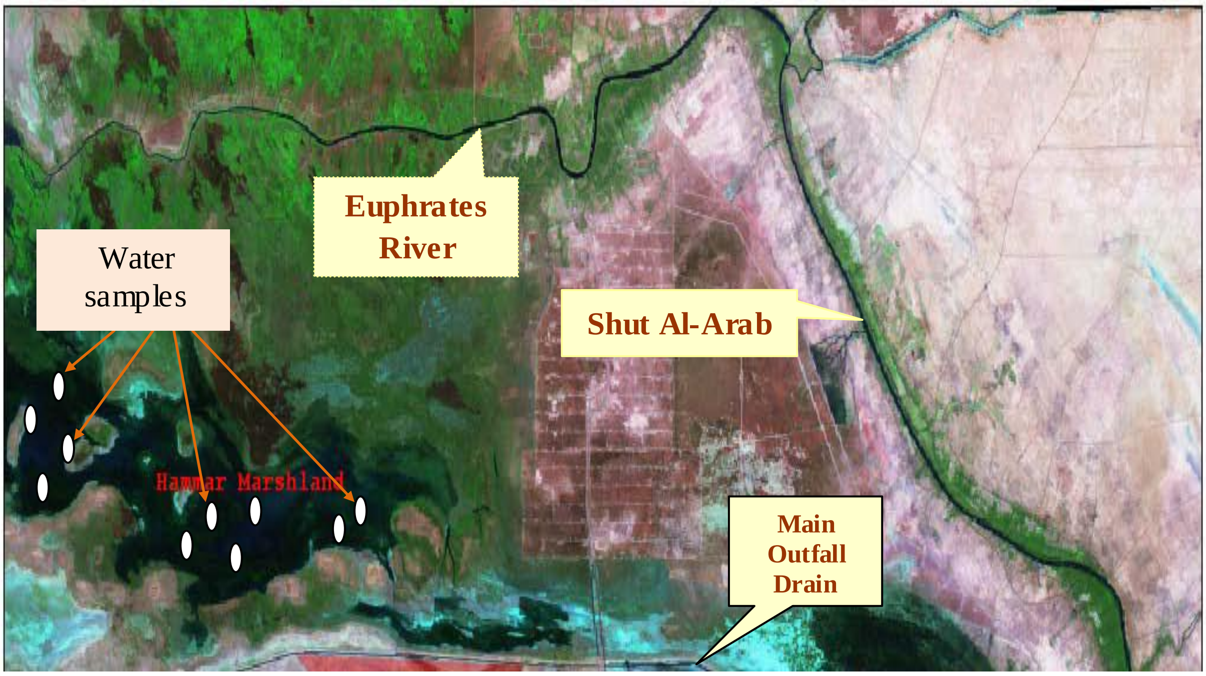

Fig.1 Satellite Image of Hammar Marsh.

Many studies showed increase in salinity in both soil and water of marshes in Iraq, the cause for increase of salinity is unknown, but it probably relates to a rise in salinity in the Euphrates River and to increase flux into the water column of ion concentrated in the soil after 10 years of drainage and evaporation. In addition the continued use of ancient methods of flooding vast agriculture field from open ditches coupled with extremely high evapotranspiration rates and result in massive losses to the atmosphere and increased soil salinity problems. Accordingly it was expected that the salinity of Hammar marsh is high.

The following table shows the physical and chemical analysis of samples taken from different locations in Al-Hammar marsh soil in Al-Basra city (Al-Hasseny,2005)

Table 1 Physical and chemical analysis of four samples from Al-Hammar marsh soils.

	Clay %	Sand %	Silt %	Organic matter %	pH	EC (Ds/m)
Al-Az	42	18	40	5.5	7.7	10.9
Al-Naser	49	19	32	7	7.7	11.2
Al-Shafi	44	20	36	10	7.7	11.5
Al-Mudel	44	16	40	7.7	7.7	11.2

RESULTS AND DISCUSSIONS

Saline irrigation water compounded with urban and industrial effluent would therefore have a major negative influence on any rehabilitation plans of marshes (Partow, 2001). Therefore, studying of water quality of marshes leads to give imagination of pollution in these marshes.

Ten water samples were taken at different locations of Al-Hammar marsh on February, 2007 to know the water quality, four of the water samples taken from at locations near the feeders of

Al-Hammar marsh and four at different locations in the middle of the marsh, the remains two taken from locations near the end of marsh.

All water samples submitted to tests that identify the tests of "Standard Methods" the details of procedures can be found in authoritative references of testing procedures in water pollution control such as (APHA, 1975). The following figure shows the locations of ten samples.

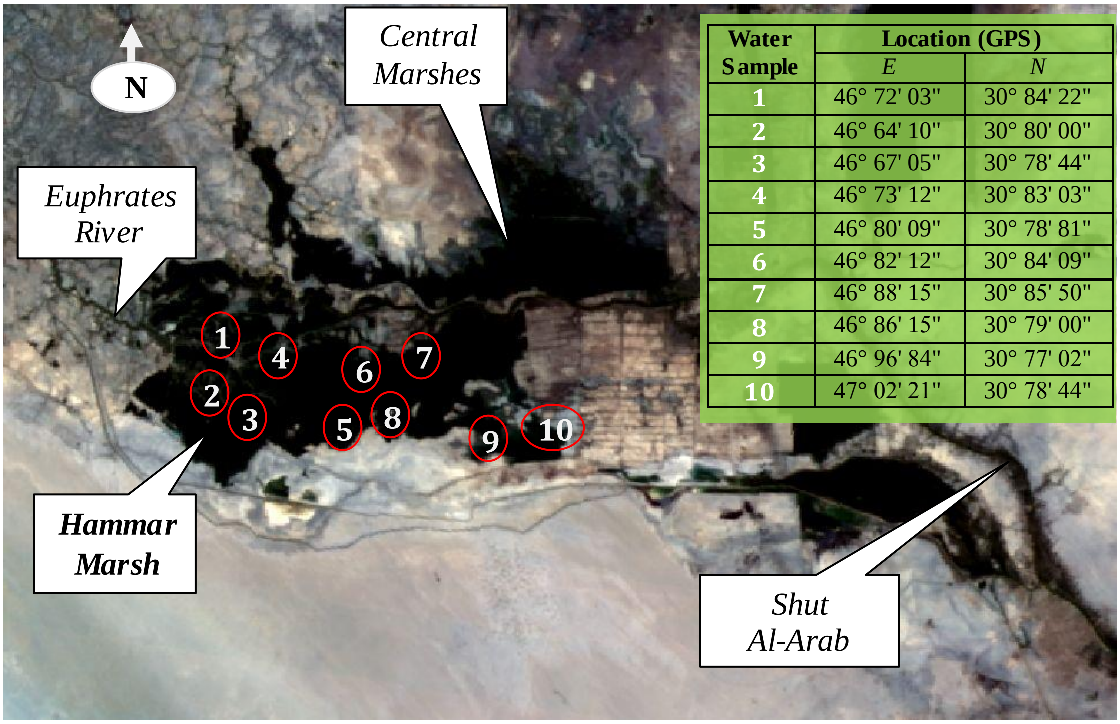

Water Sample	Location (GPS)	
	E	N
1	46° 72' 03"	30° 84' 22"
2	46° 64' 10"	30° 80' 00"
3	46° 67' 05"	30° 78' 44"
4	46° 73' 12"	30° 83' 03"
5	46° 80' 09"	30° 78' 81"
6	46° 82' 12"	30° 84' 09"
7	46° 88' 15"	30° 85' 50"
8	46° 86' 15"	30° 79' 00"
9	46° 96' 84"	30° 77' 02"
10	47° 02' 21"	30° 78' 44"

Fig.2 Locations of Ten Samples were Taken at Different Locations of Al-Hammar Marsh.

Iraqi legislations did not put water quality standards to the marshes as well as lacking information of water quality of Iraqi marshes before drying operations; all that prevent evaluation of water quality samples that taken from marshes, so that comparisons of water quality values with the requirements of different uses of water of marshes becomes important in Environmental impact assessment. The most important uses of water in marshlands are agriculture and drinking.

Fig.3 shows the results of dissolved oxygen (DO) and biochemical Oxygen Demand (BOD) analysis of the ten samples which were taken from different locations in the Al-Hammar marsh. From this figure it can be seen that the highest value of DO obtained at location 1 and then began to decrease at location 3 and reached its minimum value at location 8 before it increased at location 9, the D.O in water is related to atmospheric aeration and photosynthetic activity of aquatic plants. Many factors are effect on the concentrations of dissolved oxygen in water body among them Temperature, light penetration, water movement, available of nutrients, salinity (UNEP,WHO,UNESCO and WMO 1992). Optimal concentrations of DO required for aquatic life are over 5 mg/l, all analysis samples showed the D.O concentrations above 6 mg/l in Al-Hammar Marsh, but it should emphases that high oxygen concentrations in the first samples are slightly decreasing in other samples, the reason of that is the first samples were taken from locations near the feeders of Al-Hammar marsh, these feeders may contain high concentrations of dissolved oxygen.

Also for BOD analysis it can be noticed that there is a fluctuation for its value from one location to another, so it was clear that the highest value happened at location 4 while the lowest value at location 8. However the value of BOD is low and this due to two points, first there are no industrial activities that throw pollutants directly to the marsh, as well as the human pollution is low because of little villages in Hammar Marsh, second the spreading of plants and slow water velocity contribute to decrease BOD concentration.

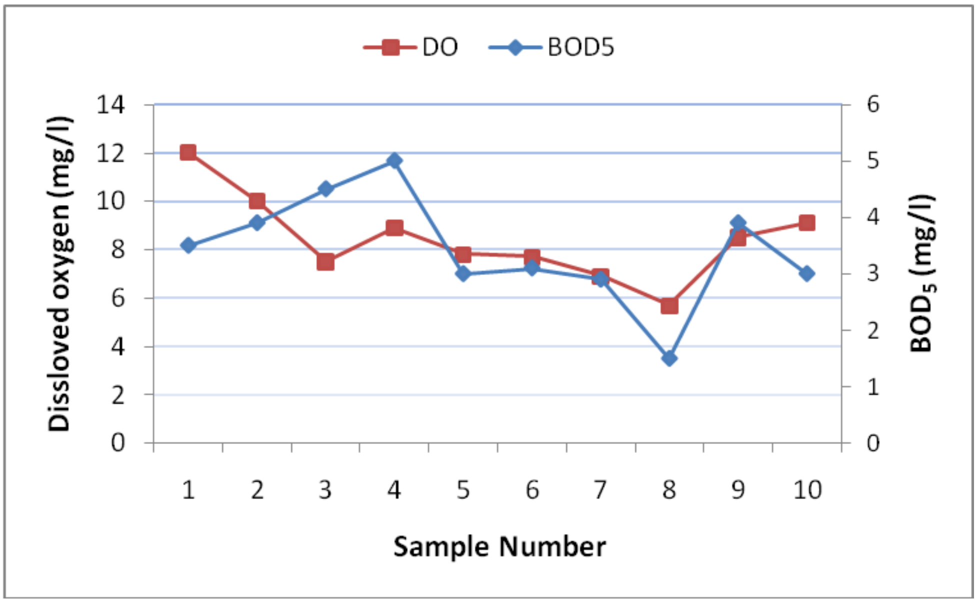

Fig. 3 Results of Dissolved Oxygen and BOD Analysis.

The changes of pH and water turbidity along Al-Hammar marsh are plotted into **Fig.4**. The pH of an aqueous solution is controlled by interrelated chemical reactions that produce or consume hydrogen ions (Hem, 1989). Dissolved gases, such as carbon dioxide, hydrogen sulfide, and ammonia have an appreciable effect on pH. The samples analysis shows that the range of pH was from 6.5-9; this range is acceptable for different uses such as drinking and agriculture. Also from the same figure it can be seen that a sharply increased in the turbidity value (samples 7 and 8) because in this area it was noticed movement of fishermen boat as well as those fishermen were using toxic materials for fishing that may cause high turbidity level. This sharply change effects on the photosynthesis in this area and leads to decrease dissolved oxygen concentration.

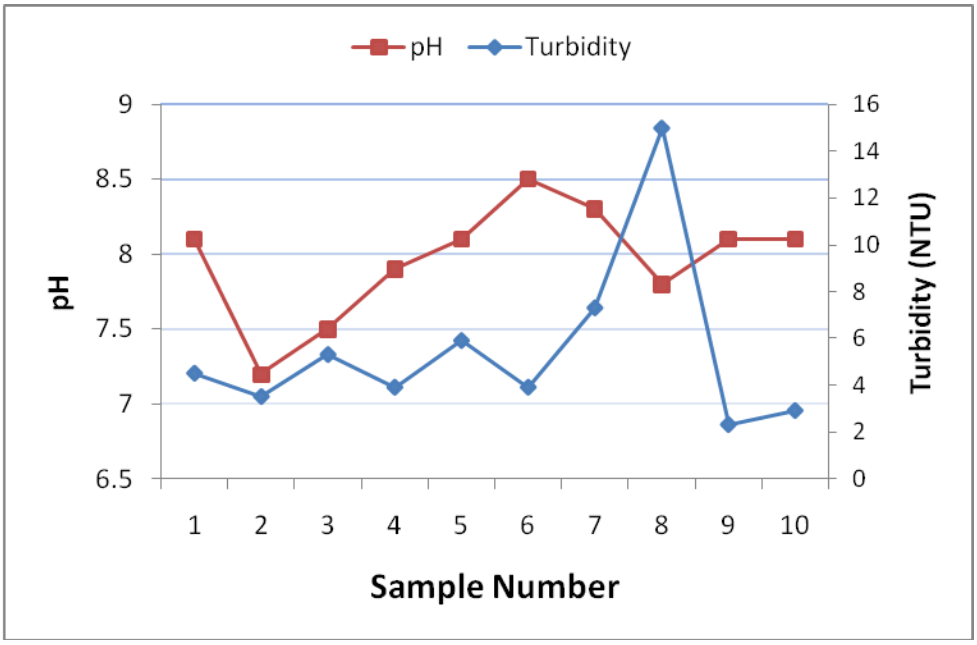

Fig. 4 Results of pH and Turbidity Analysis.

Electrical conductivity is a measure of the capacity of water to conduct an electrical current and is a function of the types and quantity of dissolved substances in water and temperature. Specific conductance of the water increases. Specific conductance measurements are good indicators of total dissolved solids and total ions concentrations, but there is no universal linear relation between total dissolved solids and specific conductance.

Fig. 5 shows the variation of electrical conductivity and total dissolved in the ten samples, it is clear that the first samples gave high concentrations of EC and TDS while the sample taken from the middle of Al-Hammar marsh gave concentrations in less degree, but in the end of the marsh the EC concentration return to high levels because of the following reasons:

- The first locations contain high concentration of total dissolved solids convey from feeders that take water from Euphrates River.
- The final samples show high concentrations of EC and TDS because of tide waves that come from shut Al-Basra which is connected with Hammar marsh by Al-Msheb and Al-Salal marshes.
- The middle samples show decreasing the EC and TDS concentration from first and end samples and that may justify that marsh plants and phytoplanktons have the ability to adsorb dissolved solids.

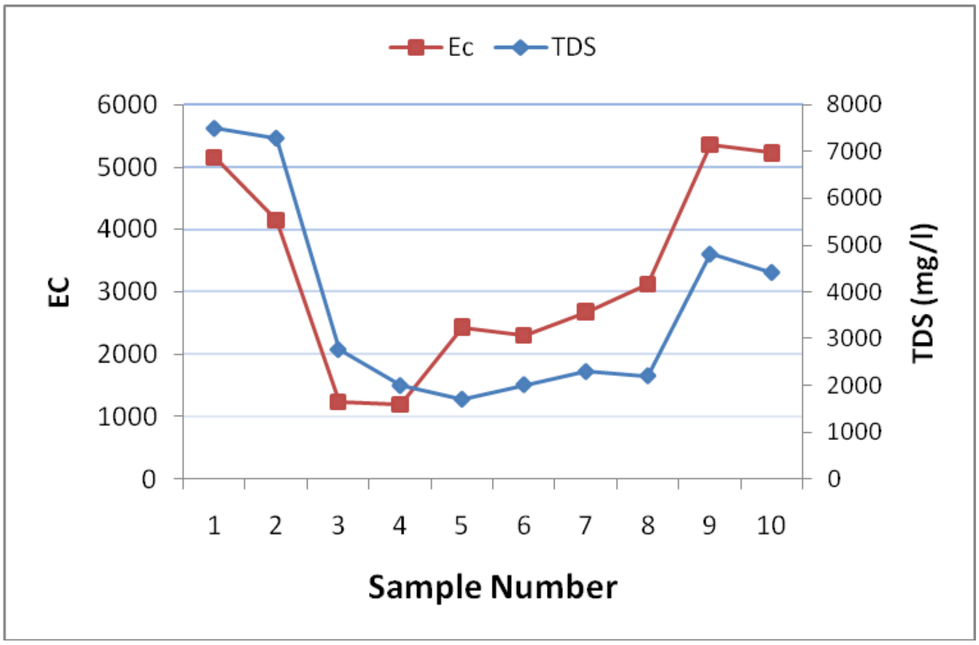

Fig.5 variation of EC and TDS.

Fig.6 shows the variation of temperature and the total dissolved solids at different locations, temperature depends on the weather and the time of taking samples, as the temperature increases, the solubility of water to carry suspended materials decreases. Stoke's law describes the velocity of settling particles in a non turbulent medium by the following equation:

$V_S=d^2g(\rho_s-\rho_w)\ /18\mu$ (1)

Where: Vs= settling velocity (m/s),d= diameter of particles(m), g=gravitational acceleration = 9.81, m/s^2,ρ_s= density of settling particles(Kg/m^3), ρ_w= density of water, (Kg/m^3), μ=viscosity of water.($N.S/m^2$).

Many Studies reoffered to that the TSS concentration in marshes considered low because of the stagnant of water, hence the samples results did not refer to increase TSS more than 35 mg/l, this value is consider low in surface water.

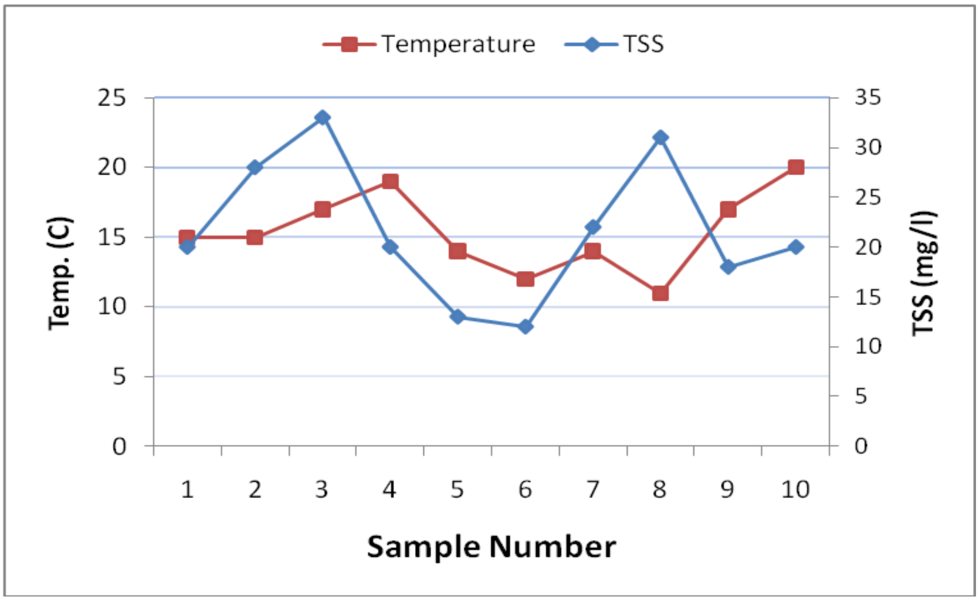

Fig.6 Variation of Temperature with the TDS.

Fig.7 shows the variation of Ca and Mg along Al-Hammar marsh. Many water rivers that flow in limestone soil may be contain (30-100) mg/l, while the rivers flow in Gypsum soils may contain hundreds concentrations. Ca concentrations contribute to raise the hardness of water.

Mg is a wide spread agent in surface water. The effects of Mg are same of Ca effects as well as Mg concentration more than 125 mg/l may be cause diarrhea (UNEP,WHO,UNESCO and WMO 1992).

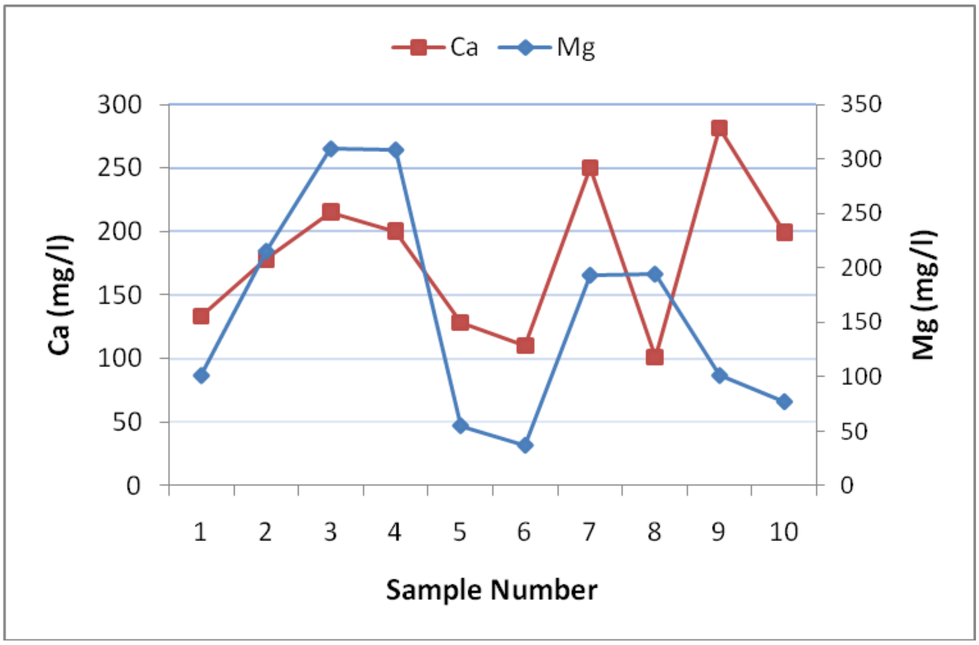

Fig.7 variation of Ca and Mg along Hammar marsh.

Fig.8 shows the concentration of total hardness and the hardness of carbonates, this hardness is strongly related to the nature of soils of Hammar marsh. From this figure it can be conclude that the total hardness is high at samples taken from the beginning of Al-Hammar marsh and may reach more than 1800 mg/l, while the other samples show decrease of hardness and don't exceed more than1000 mg/l.

The variations of concentrations of chloride and sulphates along the marsh shown in **Fig.9**. Chloride effect on agriculture and make salty taste to the water. Sulphate may be found in surface water at concentrations from little milligrams to more than thousands milligrams, the So_4 effects on the taste of water, WHO limited 400 mg/l as a maximum allowable level in drinking water.

Many areas of the marshes were severally burned after drainage. The intensity of the burns in some areas, with high surface organic matter covering sulfidic pyrite soils beneath resulted in soils being greatly altered chemically and then exposed to oxygen for decades for draining, resulting in the formation of sulphuric acid (Fitzpatrick, 2004).

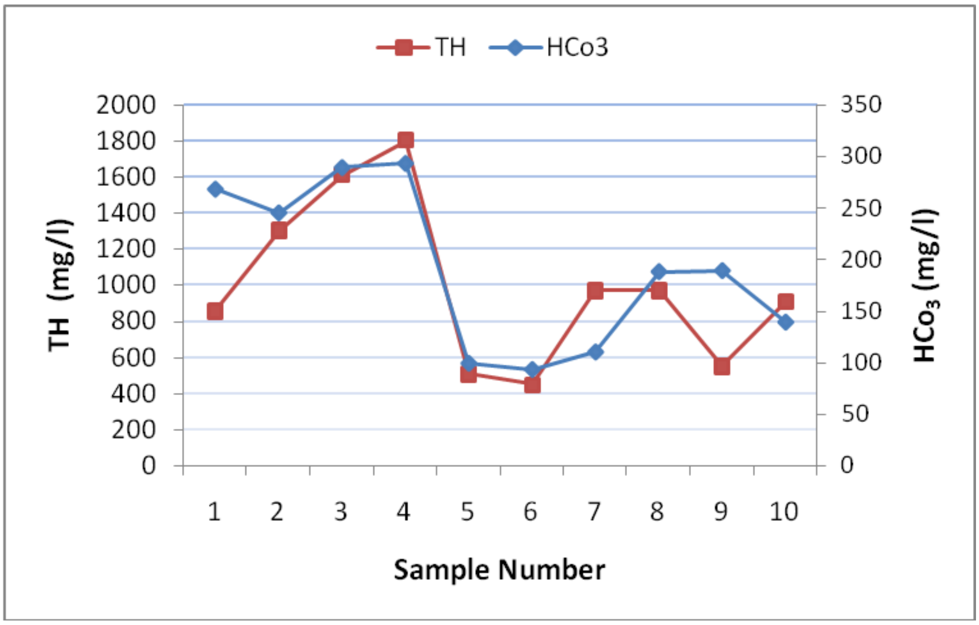

Fig.8 Concentration of Total Hardness and the Hardness of Carbonates.

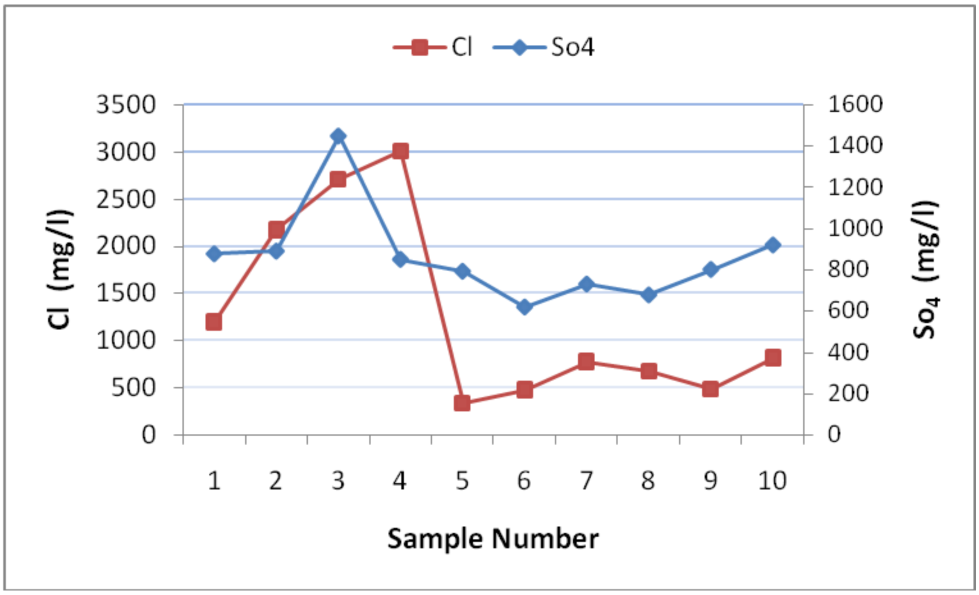

Fig.9 Variations of Concentrations of Chloride and Sulphates.

CONCLUSIONS

- Water analyses were showed that Al-Hammar marsh contains high quantity of salts; the concentration of salts sometimes exceeds the acceptable level of water for agriculture use (EC above 800 µS/cm).
- Samples of Al-Hammar marsh water were showed perceptible concentrations of Sulphate and Magnesium and calcium.
- Concentrations of TSS, BOD and pH don't exceed at significant degree along the study region.

REFERENCES

- Al-Hasseiny, Ayad Kadhim Ali, (March/ 2005), "Study the Properties of Some Dried Hore Al-Hammar Soils Southern in Iraq", M.Sc.Thesis, College of Agriculture, University of Baghdad.
- APHA,American Public Health Association,(1975)"Standard Methods for the Examination of water and wastewater". Washington,D.C.
- Curtis J.Richardson and Najah A.Husssain ,(June/ 2006) "Restoration the Garden of Eden: An Ecological Assessment of the Marshes of Iraq", Research, Bioscience Journal, Vol. 56, No.6. WWW.biosciencemag.org.
- Fitzpatrick.R.W,(2004)"Change in Soil and Water Characterisitics of some Natural, drained and Reflooded Soils in the Mesopotamian Marshlands" CSIRO land and water client report . N.P, Internet.
- Hem,J.D.,(1989)"Study and Interpretation of the Chemical Characteristics of Natural Water", US Geological Survey, Water Supply Paper, p 264.
- Maltby E,ed.(1994) "An Environmental and Ecological Study of the Marshlands of Mesopotamia" Wetland Ecosystem, Research Group, University of Exeter. London.
- Partow H.(2001) "The Mesopotamian marshlands, Demise of Ecosystem " Narobi (Kenya), UNEP publication, TR.01-3.
- UNEP,2005, " Water Quality of Marshlands, South of Iraq", UNEP publication, Internet.
- UNEP, October/ 2003," Environment of Iraq" UNEP publication, Internet.
- UNEP,WHO,UNESCO and WMO " Global Environment Monitoring System (GEMS)" Water Operational Guide/Water Research Institute, Canada, 1992.

- السامرائي، محمد جعفر جواد (شباط/1999) "مشاريع الري والبزل الحديثة في محافظات ميسان وذي قار والبصرة ، دراسة في جغرافية الموارد المائية " اطروحة دكتوراه، كلية الاداب/ جامعة بغداد.
- وزارة البيئة / دائرة الاعلام والتوعية البيئية ،"التشريعات البيئية العراقية النافذة لعام 1990/ نظام رقم 25 لسنة 1967 – صيانة الانهار والمياه العمومية من التلوث".

DIFFERENCE BETWEEN OF PWM STRATEGIES FOR INVERTER FED INDUCTION MOTOR

محمد حسين
معهد اعداد المدربين التقنيين

ABSTRACT

Several sophisticated or "optimum" modulation strategies have been suggested for voltage source pulse with modulated (PWM) inverters for ac motor control. These modulation strategies may suppress specific low – order harmonics or minimize total harmonic.

The effectiveness of these (PWM) techniques in minimizing harmonic and reducing torque pulsation is investigated analytically, and their performance is compared with that of the usual sinusoidal or sub-harmonic PWM approach. The influence of skin effect on motor (I^2R copper losses) is taken into consideration, and harmonic core losses are compared. Peak current is also an important factor in inverter design, and the various modulation strategies are again compared on this basis. Fourier analysis techniques are used in order to allow skin effect phenomena to be taken into consideration and performance criteria are developed to allow comparisons of waveform quality with respect of harmonic copper and iron losses.

الخلاصة

في هذا البحث تم اقتراح اساليب تضمين لمصدر فولتية تضمين عرض النبضة (PWM) باستخدام المبدل للسيطرة على المحرك (A.C). ان طرق التضمين المستخدمة تعمل على تشتيت التوافقيات او تقليلها الى اقل مايمكن . ان فعالية تقنية عرض النبضة (PWM) هو تقليل التوافقيات وعزم النبضات ويتحقق هذا من خلال التحليل والعمل بمقارنة الموجة الجيبية الاعتيادية والتوافقيات لعرض النبضة الترددية.

هنالك تاثيرات للقشرة الجلدية (Skin effect) في المحركات من خلال (I^2R) والتي تمثل المفاقيد النحاسية وبهذا الاعتبار يتم مقارنتها مع المفاقيد الحديدية .

ان القيمة العظمى للتيار تاخذ بالاهمية من خلال عامل تصميم الميدل (Inverter) وان اختلاف علم التضمين وبالمقارنة بالتحليل باستخدام (Basis Fourier) تم ادراك تاثيرات القشرة الجلدية (Skin effect) التي تؤخذ بنظر الاعتبارعند المقارنة وتؤخذاعتبارات العمل لتطوير جودة الموجة على اعتبار المفاقيد النحاسية والحديدية.

INTRODUCTION

Voltage source pulses with modulated (PWM) inverters for a.c motor control have conventionally employed square wave or sinusoidal PWM strategies. In recent years, more sophisticated techniques have been suggested in which specific low-order harmonics are suppressed or total harmonic content is minimized [1]-[2]-[3]

These optimized PWM strategies are extremely difficult to realize with conventional analog circuitry, but they can be effectively implemented with modern microprocessor – based control techniques [4]-[5]. Conventional modulation strategies which have been implemented by means of complex analog circuits may now be more effectively realized using a look – up table accessed by a microprocessor or digital hardware. In an ac motor drive, the modulation strategy which is most appropriate to a particular portion of the speed range is readily selected. It is therefore, of interest to compare the different modulation techniques available with regard to the additional harmonic losses in the motor and developed pulsating torque.

For the purposes of comparison, it is assumed that standard 50 or 60-Hz induction motor is fed from a standard ac supply network by a frequency converter circuit as shown in fig. (1).

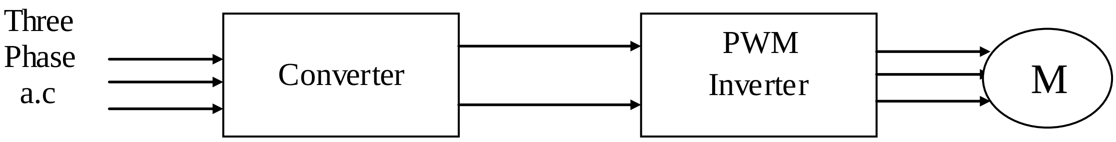

Fig. (1) Variable frequency induction motor drive

The ac supply is rectified to a fixed dc voltage by the converter and converted to variable – frequency ac by the PWM inverter which also controls the amplitude of the fundamental output voltage. If the inverter operates on un-modulated six-step voltage waveform, motor operation at rated voltage and frequency is possible. Constant-torque operation is obtained below based frequency by modulating the output voltage waveform from the PWM inverter so that the fundamental component of the output voltage is reduced proportionally with frequency, giving the usual constant volts/ hertz mode of operation.

In controlling the fundamental voltage output, the PWM strategy may introduce additional harmonic components, the presence of which detrimental to motor performance and efficiency.

A correct choice of modulation strategy is necessary for optimum drive performance.

PWM Strategies

The basic three-phase bridge inverter configuration develops an output voltage waveform as in fig. (2) which shows the inverter phase voltage (V_b) relative to the center-point of the dc supply – the amplitude of the kth harmonic voltage, assuming quarter – wave and half – wave symmetry, is[5].

$$V_k = \frac{2V_b}{K\pi}\left[1 - 2\sum_{i=1}^{m}(-1)^i \cos k\,\alpha_i\right] \qquad \ldots\ldots (1)$$

The switching angles $\alpha_1, \alpha_2, \ldots, \alpha_m$ can be determined in a number of ways,[6].

Many commercial PWM inverters have employed sinusoidal or sub-harmonic PWM in which the switching instants are determined by the intersection of a high frequency triangular carrier wave with a sine wave reference signal, which has the desired fundamental output frequency.

The triangular carrier wave usually has fixed amplitude, and the ratio of sine-wave amplitude to carrier amplitude is termed the modulation index.

The ratio of the carrier and reference frequencies is termed the carrier ratio.

In a three-phase PWM inverter, it is uses to generate a three-phase set of reference voltages, each phase of which is compared with a common triangular carrier wave.

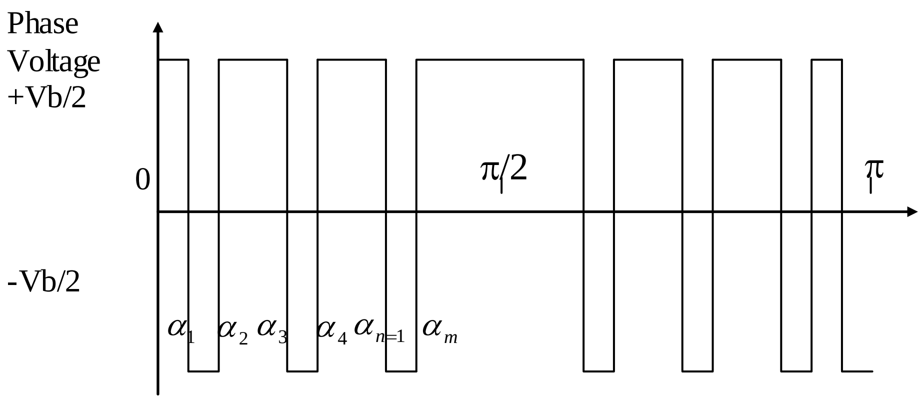

Fig. (2): Inverter phase voltage relative to center point of dc supply

It has been pointed out that harmonic elimination PWM technique can be used to determine the switching angles necessary to set the fundamental voltage at some magnitude and suppress specific harmonics. But numerical techniques are necessary to solve the non linear equations of the problem [1].

If **m** switching occurs per quarter cycle the fundamental can be controlled and (m-1) harmonics suppressed.

An alternative approach is to define a performance index related to the undesirable effects of the voltage harmonics and to select the switching angles so that the fundamental voltage is controlled, and the performance index is minimized [2]- [3]. This can be classified as a distortion minimization PWM technique.

Overall drive efficiency is the product of inverter efficiency and motor efficiency. Inverter losses are a function of the number of commutation per second, and in order to compare drive performance with different PWM strategies, it is desirable that the number of commutation per cycle should be the same in each case. For this reason, the following (PWM) techniques were selected:

a) Harmonic elimination PWM with fifth, seventh, eleventh, and thirteenth harmonics suppressed (control of fundamental voltage and elimination of these four harmonics require 22 commutation per phase per cycle, including the commutations at (0° and 180°).
b) Distortion minimization PWM with five switching angles per quarter-cycle, also requiring 22 commutations per phase per cycle.
c) Sinusoidal PWM with a carrier ratio of nine, requiring 18 commutations per phase per cycle.
d) Sinusoidal PWM with carrier ratio of 12, requiring 24 commutations per phase per cycle. Waveform c) has fewer commutations per cycle than waveform a) and b), whereas waveform d) has too many commutations.

Exact correspondence in the number of commutation is not possible, since sinusoidal PWM must have a carrier ratio which is a multiple of three.

This ensure that identical phase outputs are obtained in a three-phase system and also eliminates the dominant harmonic which is the carrier frequency, since all harmonic multiples of three are suppressed in a three-phase three wire load.

The study of sinusoidal PWM strategies is confined to the region, where the modulation index is less than unity, and pulse dropping does not occur.

Comparison of waveforms a)-d) is performed over the constant volts/hertz range of operation below base frequency.

In practice, of bourse, each modulation strategy would have an increased number of commutations per cycle at low fundamental frequencies to minimize motor losses and torque pulsations.

As base frequency is reached, the number of commutations per cycle is reduced to minimize inverter switching losses and to allow a gradual transition to six-step operation, it is possible to draw general conclusions regarding the relative merits of the PWM strategies under consideration by confining the comparison to the particular number of switching per cycle specified above.

Harmonic Copper Losses

An optimum PWM technique should minimize additional harmonic losses in the motor. These losses are primarily harmonic copper losses [6], [7]. At the harmonic frequencies, stator resistance and rotor resistance are usually negligible compared with the leakage reactance of the motor. If **x** denotes the per unit (pu) leakage reactance at base frequency, the pu kth harmonic current is given by:

$$I_k = \frac{V_k}{k f_1 \; x} \qquad \text{...... (2)}$$

Where V_k is the pu kth harmonic voltage, and f_1 is the pu fundamental frequency.

The kth harmonic copper loss is $I^2_k R_k$

Where R_k is the resistance of the motor to the kth harmonic. The total harmonic copper losses is therefore.

$$P_{loss} = \sum_{k \neq 1} I_k^2 R_k = \frac{1}{x^2} \sum_{k \neq 1} \left(\frac{V_k}{k f_1} \right)^2 R_k \qquad \text{...... (3)}$$

If R_k can be assumed constant and unaffected by frequency, the harmonic copper losses are proportional to the quantity

$$\sigma_1 = \sum_{k \neq 1} \left(\frac{V_k}{k f_1} \right)^2 \qquad \text{...... (4)}$$

This is a loss factor which ideally has a value of zero and can be used to compare the harmonic copper losses due to different PWM techniques fig. 3 compares the four PWM waveforms over the fundamental voltage and frequency range. Evidently, the harmonic elimination PWM technique:

a- Is superior to sinusoidal PWM above 0.6 pu voltage. Despit having fewer commutations per cycle, curve

(a) Shows harmonic losses of less than one-third of those for curve

(d) in the region of 0.9 pu voltage. At low fundamental voltages, however, harmonic elimination PWM has large losses.

The distortion minimization curve (b) is a composite curve consisting of a number of segments and gives the absolute minimum value of loss factor which is possible with five switching angles per quarter-cycle. Harmonic losses in the region of 2.9 pu voltage are now less than one-sixth of those for sinusoidal PWM with a carrier ratio of 12 the comparison. For six step operation, σ_1 is a horizontal straight line at a value of 2.15×10^{-3}. The constant value of σ_1 over the constant volts/hertz range is explained by the fact than the six-step wave shape is retained at all frequencies, and so the relative harmonic content and harmonic losses do not vary. The results indicate that sinusoidal PWM with a carrier ratio of nine, or less, is always inferior to the six-step wave.

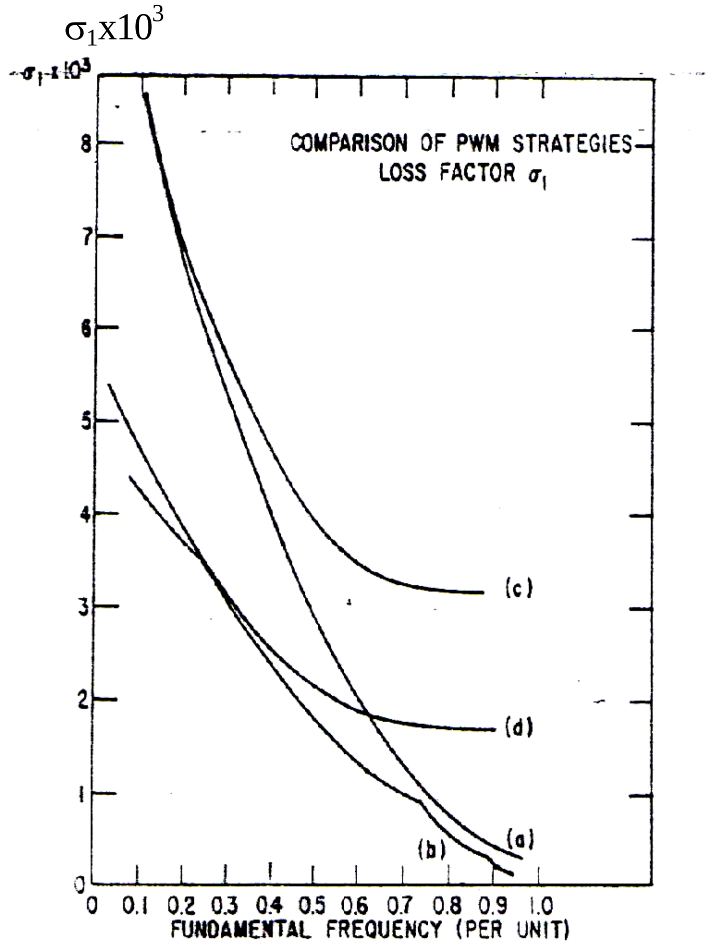

Fig. (3) Copper loss factor as function of per unit fundamental frequency.

MODIFIED LOSS FACTOR

In practice, skin effect can have a significant influence on harmonic losses, particularly if the rotor has deep-bar construction. The slot leakage component of rotor inductance decreases with frequency, but the overall reduction in the leakage inductance of the motor is less significant than the appreciable increase in rotor resistance which occurs. Because the loss factor σ_1 as defined in equation (4), ignores skin effect, it may not be a reliable criterion for comparing PWM waveforms.

Thus a fifth harmonic voltage component of (0.2 pu) makes the same contribution to the loss factor as a 25th harmonic of (1 pu) whereas in practice, the motor will offer a significantly higher resistance to the 25th harmonic, resulting in greater copper losses. The loss factor (σ_1) is therefore unduly favorable to waveforms with pronounced high-order harmonics.

Statar resistance and rotor resistance increase with frequency due to skin effect, but the additional harmonic copper losses are primarily in the rotor [6]- [7].

If f_{2k} is the rotor frequency corresponding to the kth harmonic, the rotor resistance R_{2k} taking skin effect into account, is [8].

$$R_{2k} \cong \sqrt{f_{2k}}$$

Assuming that the motor operates near its synchronous speed, then

$$f_{2k} = (k \neq 1)\ f_1 \cong kf_1$$

And hence

$$R_{2k} \cong (kf_1)^{1/2} \qquad \text{...... (5)}$$

The harmonic rotor copper losses are given by:

$$P_{2loss} = \frac{1}{x^2} \sum_{k \neq 1} \left(\frac{V_k}{kf_1} \right)^2 R_{2k} \qquad \text{...... (6)}$$

Substituting for R_{2k} from (5) gives a modified loss factor

$$\sigma_2 = \sum_{k \neq 1} \frac{V_k^2}{(kf_1)^{3/2}} \qquad \text{...... (7)}$$

Fig. (4) plots σ_1 for the previous PWM waveforms. The percentage loss reduction obtained by the use of optimum PWM techniques is slightly less than in fig. (3), but their superiority over the sinusoidal PWM strategies is again quite evident.

The distortion minimization curve is calculated for the same switching angles as used previously, although a slightly better solution is possible.

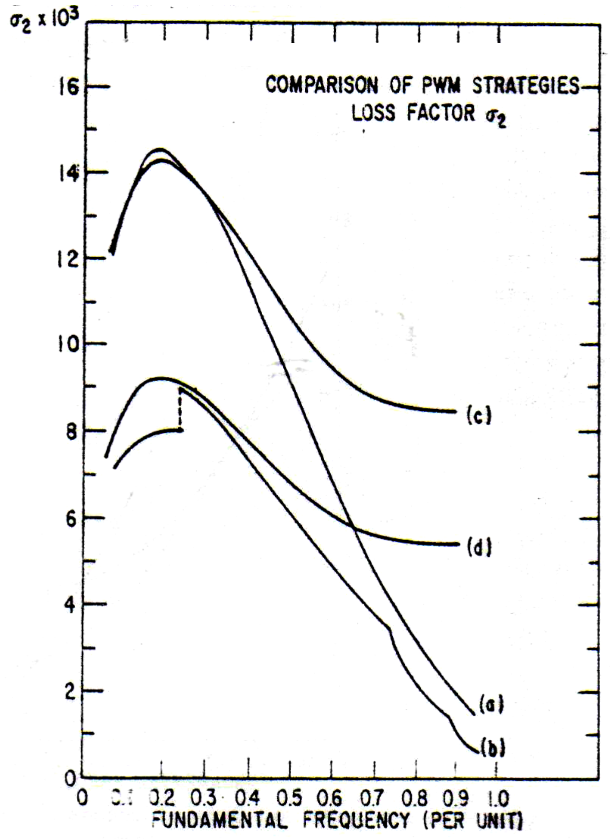

Fig. (4) Modified copper loss factor as function of per unit fundamental frequency

HARMONIC IRON LOSSES

Harmonic iron losses are significantly in fluencies by the machine construction and magnetic materials used and are difficult to predict accurately. Theoretical and experimental investigations have. Confirmed that the increase in core loss due to the harmonic main fluxes is negligible [9]- [10]. The core loss due to space harmonic fluxes is also small, but the end-leakage and skew-leakage fluxes, which normally contribute to the stray load loss, may produce an appreciable core loss at the harmonic frequencies. If an unskewed rotor construction is employed, end-leakage losses are the dominant component and may be calculated using the equation of Alger et al. [11] which indicates that these losses are proportional to frequency times current squared, hence the stator and rotor end losses associated with the kth harmonic are nearly proportional to I^2_k (kf_1) and the total harmonic end loss is give by

$$p_{end\,loss} \cong \sum_{K \neq 1} (I_k)^2 \, kf_1$$

An end loss factor can be defined for these dominant harmonic iron losses and is

$$\sigma_3 = \sum_{k \neq 1} \frac{(V_k)^2}{kf_1} \qquad \text{...... (8)}$$

Fig. (5) plots this loss factor for the four PWM techniques under consideration. The distortion minimization strategy is again seen to be the optimum despite the fact that the switching angles are chosen to minimize harmonic copper losses the total stray load (SL) losses are given more generally by

$$P_{SL\,Loss} \cong \sum_{k=1} (I_k)^x \,(kf_1)^y$$

Where the (x) only coefficients depend on the machine construction. It has been determined experimentally that the total stray load losses due to harmonics are obtained with responsible accuracy by putting x=2 and y=1.5 [10].

This gives a loss factor of

$$\sigma_4 = \sum_{k \neq 1} \frac{I_k^2}{(kf_1)^{0.5}} \qquad \text{...... (9)}$$

The stray load loss factor σ_4 is plotted in fig. (6) which confirms the concitious reached in fig. (5) regarding the superiority of distortion minimization PWM, but shows a some what less significant less reduction.

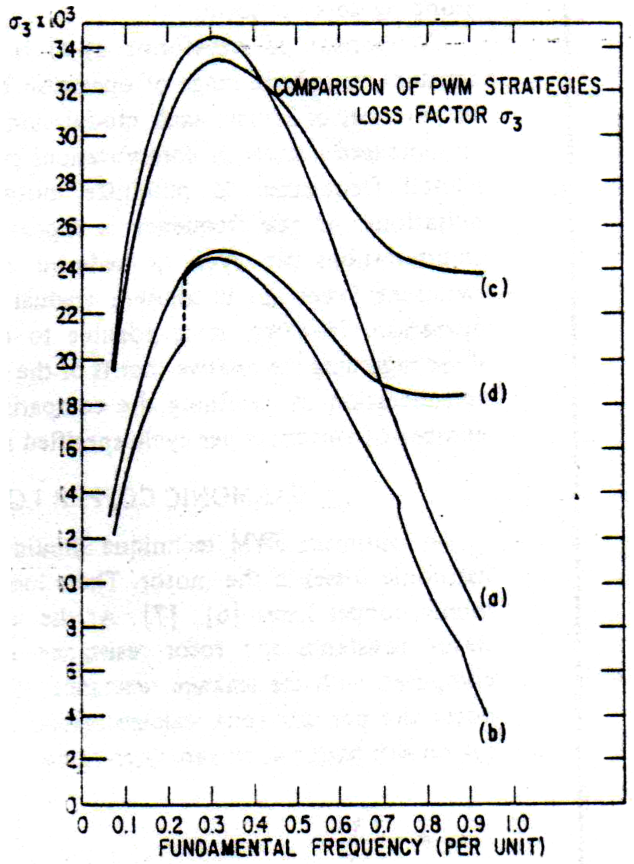

Fig. (5) End loss factor as function of per unit fundamental frequencies

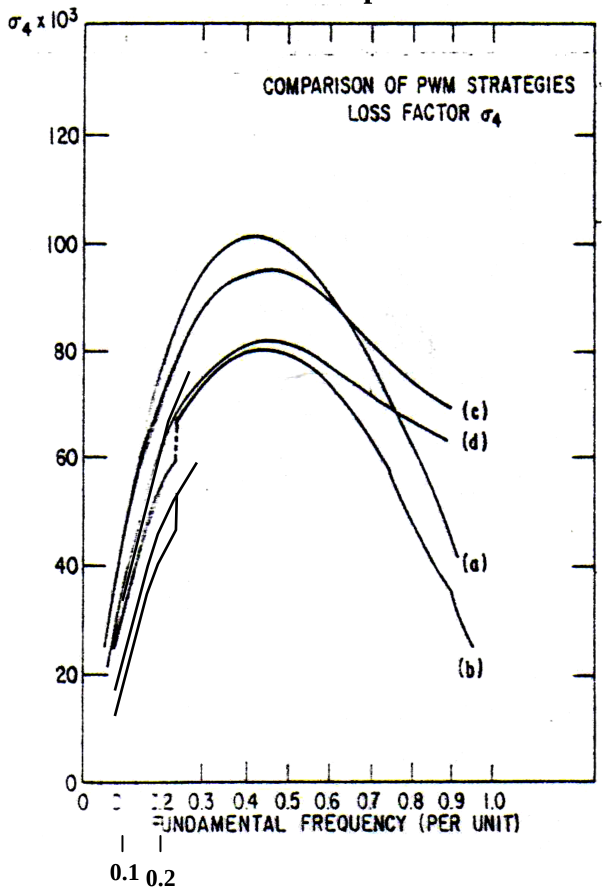

Fig. (6) Stray loss load factor as function of per unit fundamental frequency.

PEAK CURRENT

Peak current variation as function of fundamental frequency is also investigated for each of the modulation strategies. It is assumed that the inverter delivers rated fundamental current at 0.85 power factor over the full costant volts/hertz range.

The leakage reactance of the motor is 0.15 pu at base frequency. The resulting peak current (I_{max}) is expressed in per unit with peak fundamental current as its base under these conditions, the six-step inverter has a constant peak current of (1.32 pu) as shown in fig. (7) for the PWM strategies a small value of loss factor in general also implies a low peak current value.

It is evident that above a fundamental frequency of about 0.6 pu, the optimum PWM techniques again display improved performance as compared with conventional analog modulation strategies.

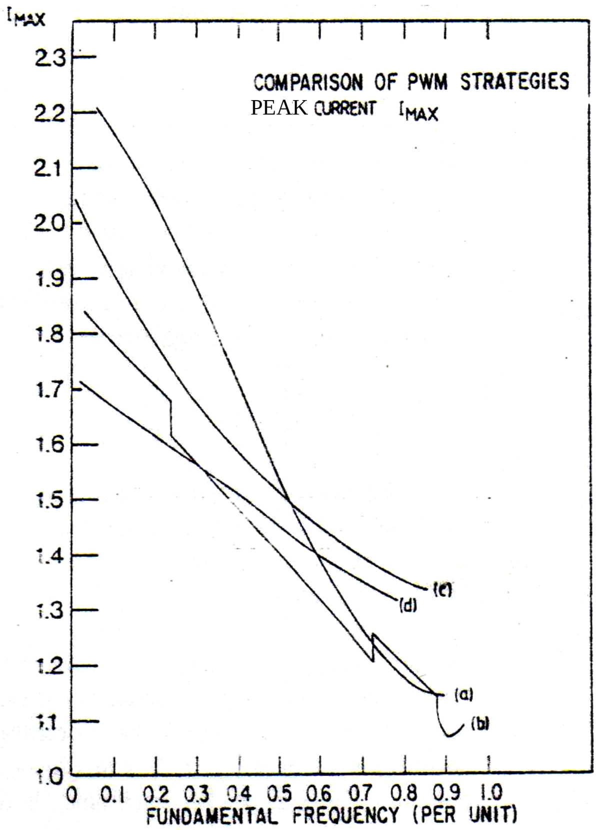

Fig. (7) Peak current variation as function of per unit fundamental frequency.

PULSATING TORQUES

Low-frequency pulsating torques is detrimental to low-speed rotation of a.c motor. It is characteristic of a PWM strategy that low-frequency cogging torques can be eliminated at the expense of large-amplitude high-frequency torque harmonics [9]-[10]-[11].

This is advantageous if the pulsating torque frequencies lie above the shaft mechanical resonances. In order to compare the low-speed capability of various PWM techniques, the dominant pulsating torques developed by each waveform is calculated [9].

Possible amplification of the harmonic torques due to rotor speed fluctuation and d.c link voltage variations is not taken into consideration [12].

It is well-known that a pulsating harmonic torque is developed by the interaction of an air gap flux harmonic with a rotor current harmonic of a different order.

Air gap flux levels at harmonic frequencies are very small, and the dominant torque fluctuations are those due to the interaction of the fundamental flux in the air gap with the harmonic rotor currents. Thus the (Kth) harmonic rotor current I_k reacts with the fundamental flux ϕ_1 to produce a pulsating torque component whose per unit amplitude is given by:

$$T_{k\mp1} = \phi_1 I_k \qquad \ldots\ldots (10)$$

The torque harmonic is of order (k+1) for negative-sequence rotor currents and of order (k-1) for positive-sequence currents

Base torque corresponds to one pu fundamental rotor current at unity power factor and is therefore some what larger than the rated torque of the motor.

Subsitting from (2) into (10) for I_k gives the per unit harmonic torque amplitude as:

$$T_{k\mp1} = \frac{\phi_1 V_k}{k f_1 X} \qquad \ldots\ldots (11)$$

The dominant pulsating torque component may be calculated using (11) moor operation is at 0.2 pu, fundamental frequency and voltage is assumed, as is a typical induction motor leakage reactance of 0.15 pu.

Sinusoidal PWM with a carrier ratio (p) is characterized by huge-amplitude voltage harmonics at (p±2) and (2p±1) times the fundamental frequency [13]. The harmonics of order (p-2) and (2p+1) have positive sequence while the harmonics of order (p+2) and (2p-1) have negative sequence.

The (2p ±1) harmonics both develop pulsating torques at (2p) times the fundamental frequency. There two torque component are approximately in phase so that a major hunting torque component of order (2p) is present.

Fourier analysis shows that the amplitude of the (2ρ±1) the harmonics are 0.18 pu and are independent of harmonic order (ρ) for ρ>p. For a carrier ratio of (12), assuming that the fundamental flux is close to 1 pu, the dominant pulsating torque is therefore of order (24) and has an amplitude of 0.513 pu. For a carrier ratio of the amplitude is 0.684 p.u and the harmonic order is (18). The harmonics of order (ρ±2) cause lower order harmonic torques. In the case of ρ=12 there are additional ninth and fifteenth harmonic torques of amplitude 0.065 pu and 0.067 pu respectively. For ρ=9 there are sixth and twelfth harmonic torques with amplitudes of 0.094 pu and 0,060 pu respectively [13].

Harmonic elimination of PWM seeks to suppress the specific lower order torque harmonics which cause speed fluctuation is reduced. Elimination of the fifth, seventh, eleventh and thirteenth harmonic voltages removes the sixth and twelfth harmonic pulsating torques, but higher order hunting torques may be significant. For 0.2 pu fundamental voltage harmonic analysis shows that the seventeenth and nineteenth harmonic voltages have amplitudes of 0.157 pu and 0.218 pu respectively [13].

Each of the resulting current harmonic reacts with the fundamental air gap flux to produce an eighteenth harmonic pulsating torque. The two torque components are additive, giving resulting torque amplitude of 0.69pu which is approximately the same as that for sinusoidal PWM with p=9 lower order torque are absent so that low-speed capability may be some what improved as compared with sinusoidal PWM distortion minimization PWM can not be seriously considered for low-frequency operation. The overall harmonic distortion is minimized, but no specific attention is paid to the lower order harmonic so that large low-frequency hunting torques is developed.

CONCLUSIONS

- Based on results the following aspects are concluded:
- General loss factors have been developed which permit a rapid comparison of PWM waveform quality with respecte to harmonic motor losses. Loss factors are derived from harmonic copper loss (with and without skin effect), harmonic end-leakage loss, and total harmonic stray load loss.
- Loss factor (σ_r) has been shown to be a general measure of waveform "badness" with respect to all types of harmonic motor loss. Despite the fact that it is based only on harmonic copper loss and ignores skin effect. A large value of σ_1 is also an indicator of high peak current. Using this loss factor, an appropriate choice of

modulation strategy can be quickly made for each portion of the constant volts/hertz range of operation without performing detailed loss calculations for a particular machine. Conversely, if minimization of loss factor σ_1 adopted as a criterion for the derivation of an optimum PWM waveform, the resulting solution gives near optimum results for all harmonic motor losses and also for peak current amplitude.

- For low-speed operation with a high switching frequency sinusoidal PWM is perfectly satisfactory.
- At these low frequencies computation of the numerous switching angles for the optimum PWM techniques is very tedious, and subsequent implementation does not yield a significant improvement in efficiency.
- As motor speed increases, the number of switching angles per cycle must be reduced to avoid an excessive number of commutation per second and allow a gradual transition to six-step operation at about base frequency. At these higher speeds, the optimum PWM strategies have been shown to be superior to sinusoidal PWM in respect to harmonic motor losses and peak current amplitude.
- The PWM strategies used immediately prior to the change to six-step operation have few commutations per cycle and must be carefully selected, whether an analog or digital approach is used for waveform generation. A poor choice of transition strategy can result in very light harmonic losses and rapid overheating of the motor in this region, loss factor σ_1 is of great benefit in selecting correct transition strategies.

REFERENCES

- H.S. Patel and R.G. Hoft, " Harmonic elimination and voltage control in thyristor inverters: Part1 – Harmonic elimination IEEE trans. 1nd. Appl., vol. IA-13. PP. 310-317 May/ June 2002.
- G.S. Baja and G.B. Indri, "Design Pulse width modulation for fed induction motor", IEEE trans. 1nd. Appl., vol. IA-13, pp.38-44 Ian/Feb. 2001.
- Haasz. "Design of control voltage source inverters feeding induction motors," in proc 2nd IFAC symp. On. Control in power electronic and electrical drives. Oct. 2002. pp. 379-385.

- j.M.O. Murphy, L.S. Howard. And R.G. Hoft, "microprocessor control of PWM inverter induction motor drive," in proc IEEE 2003 power electronic specialist conf., pp. 344-348.
- J.M.O. Murphy. R.G. Hoft and L.S. Howard , "controlled-slip operation of an induction motor with optimum PWM waveforms." In proc inst. Elect. Eng. Conf. on Electrical variable speed drives Sept. 2004. pp. 157-160.
- A.H.kadhim, "Control of an inverter drive reluctance motor," Ph.D Thesis submitted to the electrical and electronic engineering Department Bradford university,1990.
- E.A. Khistirm and H.E. Jordan. "polyphase induction motor performance and losses on nonsinusoidal voltage sources" IEEE Trans proc. App. Syst. Vol. PAS-87, pp. 624-631- Mar. 1988.
- C.W. Lander . "Induction mtors," New York: Gordon and Breach. 2004.
- B.J. Chaimes and B. R. Sarakar, " Additional losses due to nonsinusoidal supply waveforms with machines, "proc. Inst. Elect. Eng. Vol. 115, pp. 1782 Dec. 2005.
- G.K.Dubey, "Design aspects of AC machine application with supply variable static frequency," Brown Bovers Apr. 1999.
- P.L. Alger. G. Angest, and E.I Davies, " stray-load losses in polyphase noncation machines," AIEE trans. Power App. Syst. Vol. 78, pp. 349-357. 1999
- Mika Salo and Heiki Tuusa," control of the PWM current source inverter fed induction motor drive," 2005.
- J.W. A. Wilson and J.A. Yeamans. "intrinsic harmonics of idealized
- Inverter PWM system," inconf.Rec.1987. pp.973-976

ENTROPY METHOD AS CRITERIA FOR ANALYSIS A STEAM POWER PLANT

Dr. Moayed Razoki Hasan / University of Technology – Mech. Engr. Dept.

ABSTRACT

In this paper a theoretical analysis of South Baghdad and Dura power plant is carried out according to second law of thermodynamic depending on entropy (irreversibility coefficient or lost work) method instead of exergy (availability) method. In the used entropy method. The power plant is divided into main blocks (boiler, turbine, condenser, and feed water heater and pumps). The irreversibility losses and coefficient for each block are calculated and then the overall irreversibility and thermal efficiency of the plant are calculated. The results of this work are compared with previous results, that depending on exergy method. The comparison of results show that both methods give approximately the same results since both of them rely the 2nd law of thermodynamic. Entropy method is simple and intellectually and intuitively satisfying and giving direct relationship between components losses of power plant and its overall efficiency.

الخلاصة

يتناول البحث الحالي تحليل محطة جنوب بغداد ومحطة الدورة الحرارية باعتماد طريقة الانتروبي (معامل اللانعكاسية او الشغل المفقود) بدلا من طريقة المتاحية. في طريقة الانتروبي المستخدمة، يتم تقسيم محطة القدرة الى اجزاء رئيسية (المرجل، التوربين، المكثف، و المسخنات و مضخات ماء التغذية). يتم حساب معاملات و خسائر اللاانعكاسية لكل جزء ثم بعد ذلك يتم حسلب اللاانعكاسية الكلية للمحطة و كفاءتها الحرارية. اظهرت مقارنة النتائج مع نتائج الاعمال السابقة لتحليل المحطتين باعتماد طريقة المتاحية. لقد اشارت النتائج بان الطريقتين تعطيان نتائج متقاربة جداً مع افضلية لطريقة الانتروبي التي تمتاز بسهولتها مع امكانية الربط المباشرلخسارات كل جزء من اجزاء المحطة مع الكفاءة الكلية للمحطة.

KEYWORDS: Steam Power Plant, Analysis, Entropy Method

INTRODUCTION

With increasing fuel prices and the possibility of diminishing supplies in the years a head, the importance of developing systems which make efficient use of energy is apparent. The second law of thermodynamic method of analysis is particularly suited for furthering the goal of more efficient energy use, for it identifies the locations, types, and the true magnitudes of energy resources waste and loss, such method can also be used to guide steps taken to reduce inefficiencies.

According to this second law different criteria are defined for analysis the performance of power plants based on the concept of exergy (availability). If all of these criteria are used, they must all give the same results. Although availability pinpointed the real losses of a steam power plant, it is difficult, complex and can not gives direct relationship between component losses and overall efficiency of plant. Thus, the criteria for selecting the best procedure to evaluate thermodynamic analysis should be, best ease of use, best degree of correspondence with the viewpoint and background of intended users and greatest breadth of application. On these grounds, the entropy method (lost work) approach was believed to be superior to other approaches in common use **(Seader 1986).**

The purpose of this work is to analyze performance of South Baghdad and Dura power plants according to 2^{nd} law of thermodynamic depended on the concept of entropy method instead of exergy method. Then compare the results with that which obtained previously by other researches **(Hashem and Murad 1998) and (Mathure et.al. 2000)** depending on exergy method.

EXERGY METHOD ANALYSIS OF THE THERMAL POWER PLANT

The processes in steam turbine plant are steady flow processes .Where the general form of the exergy value was calculated from the following formula **(Hashem and Murad 1998)**, **(Moran 1982) and (Yunus 1994)** :

$$e = (h - T_o.s) - (h_o - T_o.s_o)$$

For exergy analysis the plant was divided in to the following main blocks: steam boiler, steam turbine, steam condenser, feed water heaters and feed water pump. The exergy losses in each block can be defined as follows **(Hashem and Murad 1998) and (Mathure et.al. 2000)** :

Steam Boiler

The total exergy losses of boiler are given,

$$E_{Lb} = E_f - \Delta E_w \qquad (1)$$

This total exergy losses of boiler are divided into three main losses,

a- Combustion Losses

$$E_{Lc} = m_g.T_o.C_{pg}.\ln(\tfrac{T_c}{T_o}) \qquad (2)$$

Where, combustion temperature (T_c) is roughly given by,

$$m_f.C.V. = m_g.C_{pg}.(T_c - T_o)$$

b- Exhaust Losses

$$E_{Lex} = m_g.(h_{ex} - h_o) - T_o.(S_{ex} - S_o) \tag{3}$$

Where, $h_{ex} = C_{pg}.T_{ex}$, $s_{ex} = C_{pg} \ln(T_{ex} / T_o)$

c- Heat Transfer Losses

Exergy losses due to heat transfer (E_{Lht}),

$$E_{Lht} = E_f - \Delta E_w - E_{Lc} - E_{Lex} \tag{4}$$

Thus, the total exergy losses of boiler can be calculate from,

E_{Lb} = **Eq .(2) + Eq . (3) + Eq . (4)**

And the second law efficiency of boiler can be calculated as,

$$\eta = \frac{\Delta E_w}{E_f} \tag{5}$$

Steam Turbine

$$E_{Lt} = \Delta E_t - W_{out} \tag{6}$$

And 2nd law efficiency of turbine,

$$\eta = \frac{W_{out}}{\Delta E_t} \tag{7}$$

Steam Condenser

Condenser effectiveness = (exergy gain by surrounding) /(exergy losses by steam through the condenser) (8) exergy gain by surrounding = $Q_{rej} \left(\frac{T_{max} - T_{min}}{T_{max}} \right)$ (9)

Where,
T_{max} – steam temperature at condenser inlet
T_{min} – surrounding temperature
Whereas, exergy losses through the condenser is equal to the exergy losses by steam.

Feed Water Heater

Exergy losses = Σ exergy input - Σexergy output (10)

the effectiveness of feed water heater = (exergy gain by cold water)/(exergy lost by steam) (11)

feed water pump

Exergy losses = W_{input} – exergy increasing of working fluid (12)

Effectiveness of pump = (exergy increase of working fluid)/(W_{input}) (13)

According to 2nd law steam cycle efficiency is given as,

$$\eta_{IIc} = \frac{W_{output}}{m_s . \Delta e_w} \quad (14)$$

So from **Eq. (5)** $\eta_{IIb} = m_s . \Delta e_w / E_f$,

then the 2nd law efficiency of the power plant is given as,

$$\eta_{IIplant} = \eta_{IIc} . \eta_{IIb} \quad (15)$$

The schematic diagram of one unit of South Baghdad power plant is shown in **Fig.1** . The description data of its steam cycle is given in **Table.1 (Mathur et.al. 2000)**. Whereas, the schematic diagram of one unit of Dura power plant and the description data of its steam cycle are shown in **Fig.2** and **Table .2,** respectively **(Hashem and Murad 1998)** .

Using **Tables. 1** and **2** and above equations, exergy analysis of each component was calculated for South Baghdad **(Mathur et.al. 2000)** and Dura **(Hashem and Murad 1998)**and the results are summarized in **Tables. 3** and **4** , respectively.

ENTROPY METHOD

According to **(Gashteen and Varkevker 1986)** and **(Yunus 1994)** irreversibility losses (lost work) are given as, Irreversibility losses = W_{is} - W_{act}

Irreversibility losses = $(Q_{add} - Q_{rej})_{rev} - (Q_{add} - Q_{rej})_{ire}$

Irreversibility losses = $(Q_{rej})_{irre} - (Q_{rej})_{rev}$ (16)

But for reversible engine,

$$\Delta s_{sys} = \Sigma \Delta s = \frac{(Q_{rej})_{rev}}{T_o} - \frac{Q_{add}}{T_1} = 0$$

Then,

$$\frac{(Q_{rej})_{rev}}{T_o} = \frac{Q_{add}}{T_1} \tag{17}$$

For irreversible engine,

$$\Delta s_{sys} = \Sigma \Delta s = \frac{(Q_{rej})_{irre}}{T_o} - \frac{Q_{add}}{T_1}$$

From **Eq. (17)**, $\dfrac{Q_{add}}{T_1} = \dfrac{(Q_{rej})_{rev}}{T_o}$, then

$$\Delta s_{sys} = \frac{(Q_{rej})_{irre}}{T_o} - \frac{(Q_{rej})_{rev}}{T_o}$$

$$T_o.(\Delta s)_{sys} = (Q_{rej})_{irre} - (Q_{rej})_{rev} \tag{18}$$

Sub**. Eq. (16)** in **Eq. (18)**, then

Irreversibility losses = $T_o\ (\Delta s)_{sys} = T_o\ \Sigma\ \Delta s$ (19)

For example for the arbitrary system shown below the irreversibility losses can be calculated as follows,

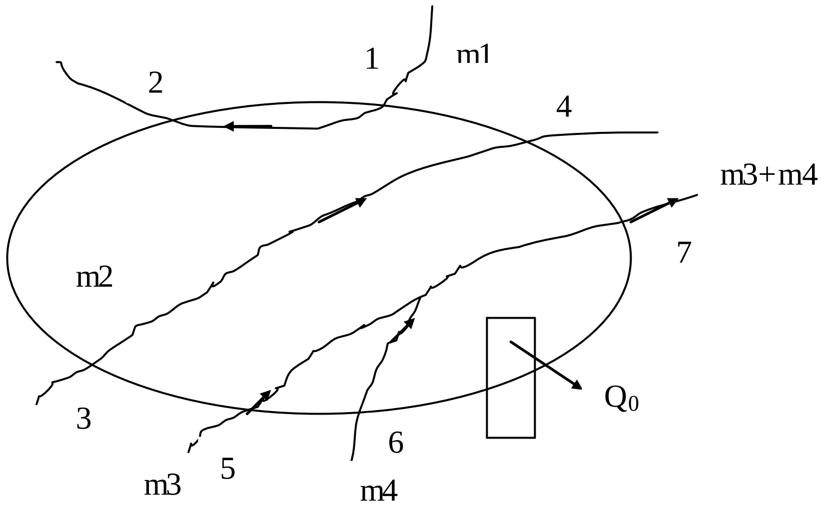

Irreversibility losses (Φ) = T_o [$m_1.s_2 + m_2.s_4 + (m_3 + m_4).s_7 - m_1.s_1 - m_2.s_3 - m_3.s_3 - m_4.s_6 + Q_o / T_o$]

$$\Phi = T_o.[\Sigma_{i=1}^{n}(m_i.s_i)_{out} - \Sigma_{i=1}^{m}(m.s_i)_{in}] + Q_o \tag{20}$$

If there is no heat transfer across the boundary (Q_o = o) then,

$$\Phi = T_o [\ \Sigma_{i=1}^{n}(m_i s_i)_{out} - \Sigma_{i=1}^{m}(m_i s_i)_{in}\ ] \tag{21}$$

From **Eq.(21)** irreversibility losses can be calculated depending only on the change of entropy. This is why this method was given name of entropy by **(Gashteen 1963)** . Irreversibility coefficient (Ω) for each component of the power plant is equal to,

$$\Omega_i = \Phi_i/(\text{exergy input to the plant}) \tag{22}$$

And the overall irreversibility coefficient for any power plant,

$$\Omega_{total} = \frac{\sum_{i=1}^{n}\Phi}{input}$$

$$\Omega_{total} = \Omega_1 + \Omega_2 + \Omega_3 \ \ldots\ldots\ldots\ldots \Omega_n = \Sigma_{i=1}^{n}\Omega_i \tag{23}$$

Plant thermal efficiency is defined as,

$$\eta = \frac{output}{input} = \frac{input - \Sigma losses}{input}$$

$$\eta = \frac{input - \Sigma_{i=1}^{n}\Phi_i}{input} = 1 - \Sigma_{i=1}^{n}\Omega_i \qquad (24)$$

By using entropy method to analyze thermal power plant, the plant was divided into main blocks and irreversibility losses for each block was calculated according to **Eqs.(20) or (21)** and then irreversibility coefficient for each block was calculated from **Eq. (22)** . The overall irreversibility coefficient of the plant was found from **Eq. (23)** and then from **Eq. (24)** the thermal efficiency of plant can be calculated **(Gashteen and Varkevker 1986)**.

The main blocks of thermal power plants and their irreversibility coefficient are as the following,

Steam Boiler

The total irreversibility losses of steam boiler are divided into three parts,
(a) Exhaust losses (b) combustion losses (c) heat transfer losses.

(a) Exhaust losses
These losses are calculated as follows,

Irreversibility exhaust losses = $Q - Q.\eta_b$

Irreversibility exhaust losses = $Q(1-\eta_b)$ (25)

Where $Q = (m_s.\Delta h_w)/\eta_b$

(b) Combustion losses
Combustion leads to appearance irreversibility losses which are depended on temperature of combustion.
Thus when this temperature increases the irreversibility losses decreases as shown on T-S diagram below :

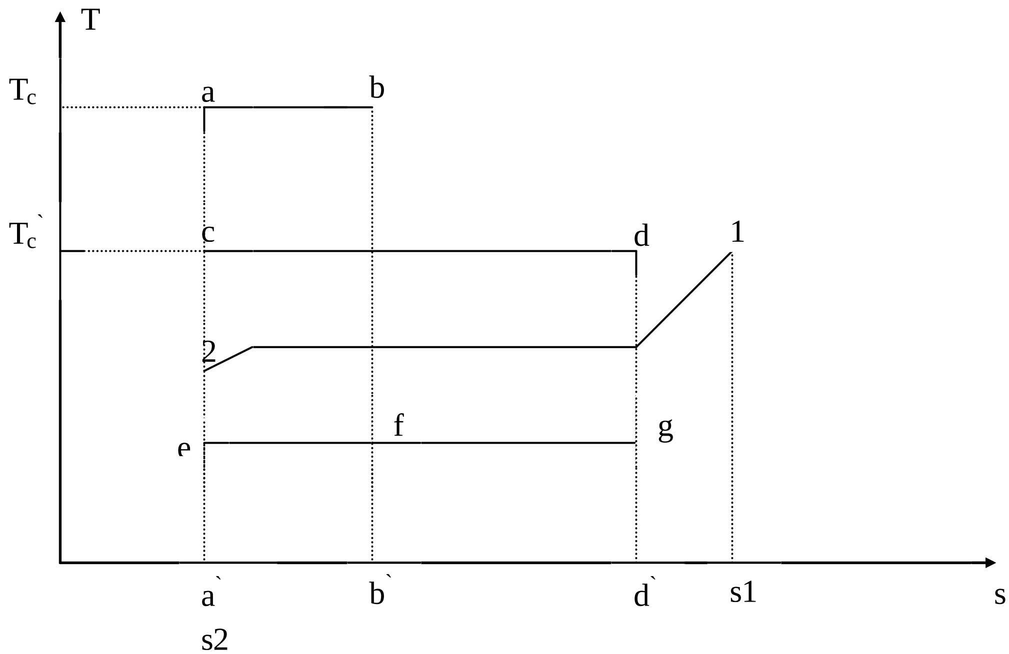

The area abb`a`a represents the heat released during combustion at T_c. The equal area cdd`a`c represents the same heat released when combustion occurs at T_c`.

Irreversibility losses of combustion at (T_c) $= Q - Q.[\frac{T_c - T_o}{T_c}] = Q.\frac{T_o}{T_c}$ (26)

Irreversibility losses at temperature (T_c`) = $Q.\frac{T_o}{T_{c`}}$ (27)

So T_c` < $T_c$ , then irreversibility losses at $T_c$ are less than that at $T_c$`. These losses are shown on T-s diagram which are equals to area efb`a`e and egd`a`e at T_c and T_c` respectively.

(c) Heat transfer losses
Irreversibility losses= $T_o.(m_s.(s_1 - s_2) - \frac{Q}{T_c}]$ (28)

When combustion temperature is T_c. whereas these losses at T_c` become,

$$T_o.(m_s.(s_1 - s_2) - \frac{Q}{T_{c`}} \quad (29)$$

From **Eqs.(28)** and **(29)** it is clear that these losses are increasing when combustion temperature is increasing.Thus, **Eq.(26) + Eq.(28)** and **Eq.(27) + Eq.(29)** give the sum of irreversibility losses due to combustion and heat transfer at different combustion temperatures. From which a conclusion can be achieved that irreversibility losses due to combustion and heat transfer are given as,

$$m_s.T_o.(s_1 - s_2) \quad (30)$$

Where s_1&s_2 are the entropy of working fluid at outlet and inlet of boiler respectively **Eq.(30)** is valid whatever the temperature of combustion is.
Thus, the total irreversibility losses of steam boiler can be calculated as follows,

Total irreversibility losses of boiler = **Eq.(25) + E q. (30)**

Steam Turbine

Irreversibility losses of turbine can be calculated from **Eq. (21).**

Steam Condenser

This irreversibility losses can be calculated from **Eq.(20)** in which $Q=m_s\ \Delta h_s$

Feed Water Heaters And Pumps

This can be calculated from **Eq. (21)**

Mechanical And Generator Losses

These can be calculated as follows,

$$\text{Mechanical irreversibility losses} = w_t - \eta_m . w_t \tag{31}$$

$$\text{Generator irreversibility losses} = \eta_m .\ w_t - \eta_m . \eta_g .\ w_t \tag{32}$$

For all above components the irreversibility coefficient (Ω) for each component can be calculated by dividing $\Phi_{component}$ by fuel exergy, which is in our calculated equal to m_f.C.V. Then,

$$\eta = 1 - \sum_{i=1}^{n} \Omega_i$$

The results obtained from entropy method are summarized in **Table.5** and **6** for South Baghdad and Dura power plant respectively.

CONCUSION

- Both exergy and entropy methods give approximately the same results **Figs.3** and **4** ,since the second law of thermodynamic is unambiguous.
- Entropy method (irreversibility) independent on dead state except for the value of T_o. Whereas the exergy is determined in relative to restricted dead state, which can be some what misleading.
- Entropy method which is simple and easy to apply is superior to exergy method. Since the former method requires only one property (entropy) to obtain the results, while the later method requires two properties (entropy and enthalpy).

- The entropy method is pinpointing the real losses in each component and giving direct relationship between them and the overall efficiency of the plant. By this the effect of inefficient components can be directly reduced to improve the performance of plant.

- The entropy method show that combustion temperature not posses influence on the irreversibility losses of the boiler. This is in contrast with what **(Hashem and Murad 1998)** previously concluded.

REFERENCES

- Goshteen D.P. (1963), Entropy method for calculation irreversibility losse. Mocko pp.111. (in Russion)

- Goshteen D.P.,verkhevker G.P. (1986), Analysis heat cycles for nuclear power plants. Mocko P.285 (in Russion)

- Hashem H.H, Murad N.K., (1998) Pinpointing the real losses of a steam power plant by using exergy method. (Accepted for publication) in Technical research journal.

- Mathur M.L., sinha S.P. and Oda S.D., 2000, First and second law analysis of a steam power plant" steam and fuel users Association od India, vol.33, No.2.pp.31-36.

- Moran M.J. (1982), Availability analysis: a guide to efficient energy use. America p.260.

- Seader J.D. (1980), Lost work: :a measure or thermodynamic efficiency. Energy.vol.5 pp.757-769.

- Yunus A.C. (1994), thermodynamics an engineering approach. America p.-986.

NOTATION

C.V. caloric value of fuel (kJ /kg)
h specific enthalpy (kJ /kg)
s specific entropy (kJ /kg.K)
e,E specific exergy (kJ /kg) , power (W)
C_p Specific heat at constant pressure (kJ /kg K)
T temperature (K)
Q total heat (kJ)
W work (kJ)

GREEK

η efficiency
Φ irreversibility loss

Ω irreversibility coefficient
Δ difference

SUBSCRIPTS

add	added	irre	irreversible
act	actual	is	isentropic
b	boiler	L	losses
c	combustion	m	mechanical
ex	exhaust	max	maximum
f	fuel	min	minimum
g	gas, generator	o	ambient
ht	heat transfer	rej	rejected
II	second law	rev	reversible
s	steam	sys	system
w	water	t	turbine

Table.1: Description Data Of Steam Cycle For South Baghdad Power Plant **(Mathur et.al. 2000)**

Pt	mass kg/s	pressure bar	x%	saturation tem.c^0	h kJ/kg	s kJ/kg.K
1	74.433	87.2	510	301	3414.5	6.7085
2	0.0756	87.2	510	301	3414.5	6.7085
3	74,358	87.2	510	301	3414.5	6.7085
4	0.1767	87.2	510	301	3414.5	6.7085
5	0.051	87.2	510	301	3414.5	6.7085
6	0.1106	71.02	482.222	286.722	3367.3	6.742
7	0.1616	75.84	493.333	291.277	3382.2	6.7336
8	0.0504	75.84	493.333	291.277	3382.2	6.7336
9	0.0315	75.84	493.333	291.277	3382.2	6.7336
10	0.0797	75.84	493.333	291.277	3382.2	6.7336
11	0.8343	71.02	482.222	286.722	3367.35	6.742
12	73.1855	87.2	510	301	3397.3	6.7253
13	5.418	32.9	388.888	239	3199.87	6.83417
14	67.766	32.9	388.888	239	3199.87	6.83417
15	3.9858	16.81	308.888	203.666	3046.129	6.8886
16	63.781	16.81	308.888	203.666	3046.129	6.8886
17	3.377	7.177	215.555	165.888	2876.5	6.9388
18	60.403	7.177	215.555	165.888	2876.5	6.9388
19	4.012	2.7	132.222,0.995	130	2713.5	7.0016
20	56.391	2.7	132.222,0.995	130	2713.5	7.0016
21	4.845	0.792	92.22,0.967	92.888	2539.99	7.1105

22	51.545	0.792	92.222,0.967	92.888	2539.99	7.1105
23	51.545	0.0677	38.333,0.89	38.333	2303.67	7.4246
24	9.0449	0.106	46.788	46.855	195.895	0.6603
25	51.545	0.067	36.15	38.333	151.376	0.5201
26	60.64	0.072	38.388	52.277	160.726	0.5502
27	60.64	14.734	38.388	197.222	160.726	0.5502
28	0.0756	87.2	510	301	3412.24	6.7211
29	0.0756	27.58	224.833	229.222	988.55	2.6143
30	60.64	14.73	39.111	197.244	163.75	0.56
31	8.969	0.103	45.191	45.5	189.21	0.6407
32	0.0315	0.827	97.71	99.555	417.28	1.18509
33	60.64	14.734	39.444	197.222	165.146	0.5645
34	4.925	0.8411	98.111	94.444	2553.7	7.1189
35	8.938	0.102	45	45.233	188.4	0.6382
36	4.0122	0.6895	87.883	89.555	394.95	1.1641
37	60.64	14.245	88.611	195.72	370.997	1.1809
38	60.64	13.755	124.944	194.222	524.28	1.5787
39	4.21166	10.342	266.666	181.333	2973.79	6.9765
40	74.433	8.511	172.222	172.944	686.63	2.0519
41	74.433	122.5	179.2	325.666	703.615	2.0594
42	4.1626	14.479	312.777	196.44	3061.7	6.8969
43	9.581	8.136	171.05	171.055	722.223	2.0469
44	74.433	122.0	197.5	325.372	844.8	2.4091
45	5.4188	17.237	197.5	205	866.435	2.3576
46	74.433	121,60	234.9	325	1014.67	2.6038

Table.2: Description Data Of Steam Cycle For Dura Power Plant **(Hashem and Murad 1998)**

Pt	t (C^0)	pressure (bar)	m kg/s	h kJ/kg	s kJ/kg.K
1	535	133.4	135.95	3426	6.549
2	360.7	39.11	19.03	3124	6.645
3	361.9	40.45	115.1	3124	6.627
4	535	36.29	115.1	3528	7.253
5	374	11.13	4.837	3208	7.345
6	269.8	4.435	6.557	3004	7.387
7	164.1	1.603	5.548	2800	7.232
8	X=0.995	0.563	6.789	2639	7.52
9	X=0.922	0.068	91.38	2384	7.688
10	------	0.068	91.38	161.7	0.553
11	38.6	0.068	105.5	161.6	0.554
12	38.8	15.57	105.5	163.7	0.552
13	45.1	-------	12.34	188.8	0.639
14	81.4	6.886	105.5	341.2	1.089
15	113.4	-------	5.548	475.6	1.456
16	110.4	6.396	105.5	463.5	1.421

17	147.4	4.435	135.95	620.9	1.815
18	150	160.4	135.95	641.8	1.825
19	157	--------	23.862	662.8	1.912
20	184.8	159.5	135.95	790.9	2.163
21	249	--------	19.03	1081	2.785
22	248	158.5	135.95	1077	2.748

Table.3: Exergy Analysis Summary Of South Baghdad Power Plant **(Mathure et. Al. 2000)**

No	Components	Exergy loss %	η_{II}%
1	Boiler	56.8	Boiler-43.2
2	Turbine	7.4	Steam cycle-74.76
3	Condenser and hot well	2.08	Overall efficiency-29.61 take to account
4	Pumps	--------	power use facter =0.917
5	Feed water heaters	--------	

Table.4: Exergy Analysis Summary Of Dura Power Plant **(Hashem and Murad 1998)**

No	Components	Exergy loss %	η_{II}%
1	Boiler	50.00	Boiler – 50.0
2	Turbine	4.17	Steam cycle-84.0
3	Condenser	2.05	Overall efficiency-42.0%
4	Feed water heating	1.45	
5	Feed water pump	0.105	
6	Mec.&generator	0.65	

Table.5: Entropy Method Analysis Summary Of South Baghdad Power Plant

No	Components	Irreversibility coefficient Ωi %	η
1	Boiler	58.0	
2	Turbine	6.60	

3	Condenser and hot well	2.3	
4	Feed water heaters	4.8	
5	Mechanical	0.3	
6	Generator	0.4	Overall efficiency=27.6
7	total	72.4	

Table.6: Entropy Method Analysis Summary Of Dura Power Plant

No	Components	Irreversibility coefficient Ω_i %	η
1	Boiler	51.03	
2	Turbine	4.12	
3	Condenser	1.998	
4	Feed water heaters	1.6	
5	Mechanical	0.4	
6	Generator	0.4	Overall efficiency=40.2
7	total	59.8	

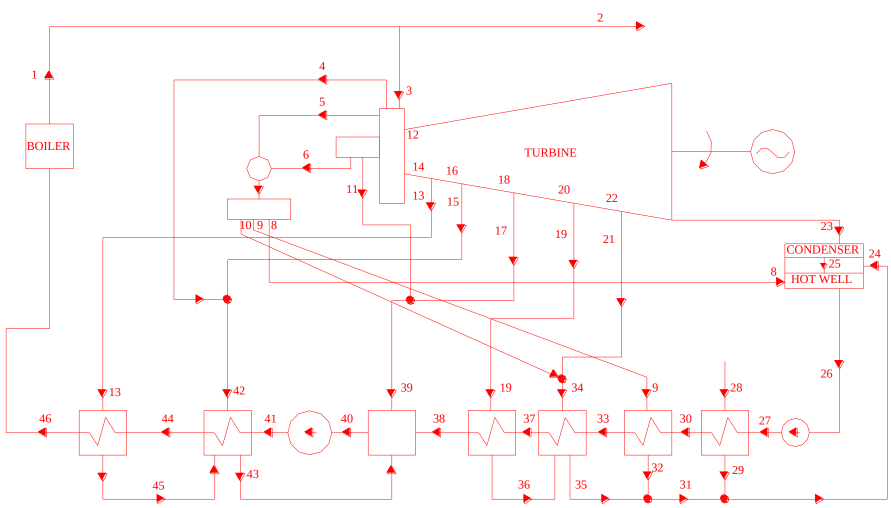

Fig. 1: The Heat Cycle Of The Unit Of South Baghdad Power Plant

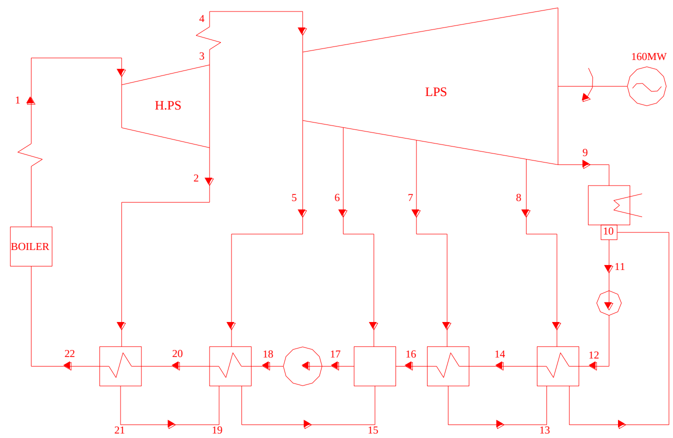

Fig.2: The Heat Cycle Of The Unit Of Dura Power Plant

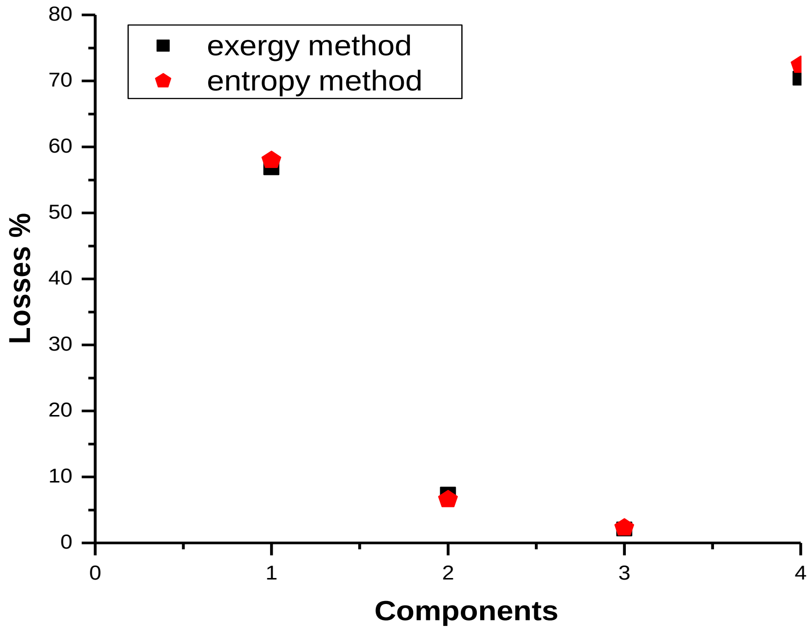

Fig3: Exergy And Entropy Method Analysis For South Baghdad Power Plant
X-Axis:- 1- Boiler 2- Turbine 3- Condenser And Hot Well 4- Overall Plant

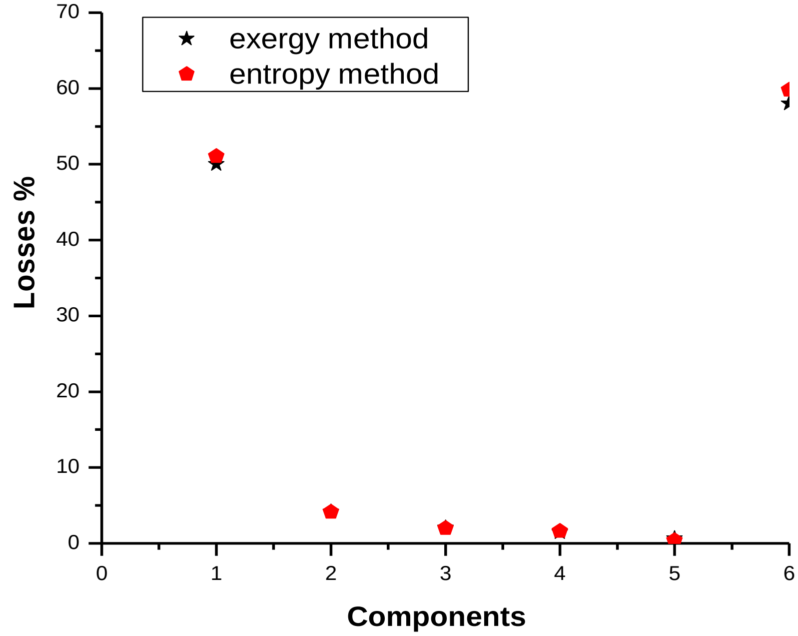

Fig.4: Exergy And Entropy Method Analysis For Dura Power Plant
X-Axis: 1- Boiler 2- Turbine 3- Condenser 4- Feed Water Heaters
5- Mec.& Gen. 6- Overall Plant

PANEL METHOD CACULATIONS OF WING - TAIL INTERFERENCE EFFECTS

Asst. Lec. Maki H. Majeed
University of Baghdad., College of Engineering, Mechanical Eng. Dept.

ABSTRACT

A low-order panel method was used to predict the flow characteristics between two sets of wings representing wing and tail. Constant source and doublet singularities with Drichlet boundary condition are used on the body surfaces. Distance and setting angle changes of the tail are studied to predict the air flow characteristics. Since the flow is incompressible non-viscous (potential flow), the results obtained contain a large physical evidence and may give a good design tool for aircraft stability consideration. A **FORTRAN** program was built to calculate the flow characteristics and then validated with published data. Highly acceptable results are obtained as compared with these data, so that; the program can be used for discussing the design or control parameters of such aerodynamical problems.

الخلاصة

طريقة الالواح ذات الدرجة الواطئة استخدمت لتخمين خواص الجريان مابين جناحين يمثلان الجناح والذنب. استخدم مصدر وقطب مع تطبيق شرط دريشلت على سطح الجسم. تغيير البعد وزاوية التثبيت للذنب تمت درستها لتخمين خواص جريان الهواء. رغم ان الجريان لا انضغاطي وغير لزج (جريان كامن)، فان النتائج المتحصلة منه كانت تحمل الكثير من الملاحظات الفيزيائية والتي من الممكن ان تكون اداة جيدة لدراسة استقرارية الطائرات. برنامج بلغة الفورتران تم بناءه لحساب خواص الجريان وتحقيق هذه النتائج مع بيانات منشورة. النتائج المتحصلة كانت مقبولة الى حد عالي مع هذه البيانات المنشورة، ولذلك فان البرنامج يمكن استعماله لمناقشة عوامل التصميم والسيطرة لمسائل الديناميكا الهوائية.

KEYWORDS: Wing-Body-Tail Interference, Potential Flow, Panel Method

INTRODUCTION

While the present work is dealt with the interference between wing and tail, it could be regarded as lifting surface –vortex interference. Vortices passing close to a lifting surface can cause significant changes in the aerodynamics characteristics of the lifting surface. An important example is the loss of tail effectiveness, which results from wing vortices pass in close proximity to the tail. **Fig (1)** shows the physical situation that give rise to such wing tail interference.

Changing the wing and tail angle of attack is very effective aspect of controlling the airplane. For the design aspect, the distance between the wing and tail, their shapes and sizes would make a large change in aerodynamics of the airplane.

If complete configuration without the wing is first considered the tail wing will then develop lift that is mostly generated by the tail and tail body interference. The addition of wing to the previous configuration will cause a general down wash field in the region of tail panels, and thereby reduces their lifting effectiveness. The loss of tail lift can be directly ascribed to the modification of the flow field produced by the vortices shed by the wing. It is clear that any vortices regardless of their origin will in passing close to the tail produced interference effect similar to those produced by the wing vortices.

Several methods were established to investigate the flow field behavior upon and around bodies moving inside fluids. The researchers always try to implement numerical methods that solve engineering problems with a satisfactory agreement with experimental data. This led to introduction of the panel method, which is reliable potential solution for a wide range of a complex geometries compared with actual measured data. Articles on this method were published since 1967 up to date which indicate the justification of such method in the field of aerodynamic design.

Many previous works studied the interference problem between different parts of airplanes like wing-body-tail components. Most of these studies used panel method as a tool to analyze the interference problem due to simplest form of this method and its ability to deal with complex configuration. The first beginning with **(Hess and Smith 1967**) used the panel method in solving the problem of lifting and non-lifting bodies by distribution of constant sources and vortices on them. Neuman boundary condition was used with kutta condition to find the strength of these singularities .The flow is incompressible and the results were in good agreement with both analytical and experimental data, the method still to be an efficient tool in aerodynamic problems especially on the interaction between air plane components like wing, body and tail components. After them **(Morino and Kuo 1974)** present a general method for steady and unsteady linearized subsonic flow around arbitrary shape. A distribution of constant source strength with constant doublet was used with the Drichlet boundary condition. **(Morino 1975**) extend this method for linearized supersonic flow. These results for different body's interactions agree well with experimental data and available exact solution of selected bodies. (**Tinoco 1984)** use higher order panel method represented by **PANAIR** commercial program to predict complex configuration like wing-body-tail. Good results are obtained as compared with experimental data.

(Bandyo pahyay 1989) developed a numerical method to calculate the aerodynamic characteristics of wing-canard configurations by considering both the attached and separated flow over the canard surface using horse-shoe vortex technique. Experimental test have been conducted in a low Speed wind tunnel to compare the theoretical results. The comparison shows good agreement up to 16^o incidences.

(Arnott and Berstin 2000) made an analysis for aerodynamic interference at the forward swept wing and plate interaction region with a fully developed turbulent boundary layer. Flow visualization and surface pressure distribution have been made for Reynold Number 1.03×10^6 based on the wing chord and free stream velocity equal 30m/s. For low stall angles, boundary layer separation was wake at plate while a higher angles many separation regions have been noticed with a large three-dimensional vortex region.

The present work deals with the aerodynamic characteristics of wing and tail interaction in low speed region. Wing wake is considered to be a flat vortex sheet and the reaction of the tail section is then calculated. Low-order panel method is used to predict the flow characteristics due to complex shapes and incompressible potential flow were assumed for the flow.

PANEL METHOD FORMULATION

Panel method is commonly used for analyzing subsonic and supersonic inviscid flows about Configurations of arbitrary geometries, and is widely use throughout the areo-space industry. A major advantage of panel methods is that they are not encumbered by the need for a field grid for numerical solution, and as thus free of most of the geometric limitations which today limit the non-linear method to simpler configuration **(Katz and Plotkin 1999).**

The flow outside the boundary layer is assumed to be incompressible, besides it is irrotational. The continuity equation in terms of the potential function (Φ) is:

$$\nabla^2\Phi = 0 \tag{1}$$

The general solution of equation (1) can be constructed by assuming a source (σ) and doublet (μ) distribution placed on the boundary of the body assigned as (s);

$$\Phi = \phi_\infty + \frac{1}{4\pi}\int_s \left[\mu\,\hat{n}\times\nabla\left(\frac{1}{r}\right) - \sigma\left(\frac{1}{r}\right)\right]ds \tag{2}$$

Where ($\hat{n}$) is the normal vector on the surface (s) and in the direction of the potential (μ) and (ϕ_∞) is the free stream potential;

$$\phi_\infty = Q_{l\infty}x + Q_{m\infty}y + Q_{n\infty}z \tag{3}$$

If the wake of the body is modeled with a doublet **eq. (2)** will be;

$$\Phi = \frac{1}{4\pi}\int_{body+wake}\mu\,\hat{n}\times\nabla\left(\frac{1}{r}\right)ds - \frac{1}{4\pi}\int_{body}\nabla\left(\frac{1}{r}\right)ds + \phi_\infty \tag{4}$$

The boundary condition of **eq. (1)** can directly be specified as zero normal velocity component $\left(\partial\Phi/\partial n\right)$=0 on the surface (s) in which case this direct formulation is called the Neuman problem. It is possible to specify the potential (Φ) on the boundary, so that the zero normal flow condition will be met, this is called Drichlet problem. The second boundary condition are used, so that; the distributing of singularity elements on the surface and placing the point (x, y, z) inside the surface (s) the inner potential (Φ_i) in terms of the surface singularity distributions is obtained;

$$\Phi_i = \phi_\infty + \frac{1}{4\pi}\int_{B+W}\mu\,\hat{n}\times\nabla\left(\frac{1}{r}\right)ds - \frac{1}{4\pi}\int_b\nabla\left(\frac{1}{r}\right)ds \tag{5}$$

B+W means body and wake surface. For enclosed boundary e.g. (s), $\left(\partial\Phi/\partial n = 0\right)$ as required by the boundary condition of zero normal velocity ($\nabla(\phi_p + \phi_\infty)\times\hat{n} = 0$) then the potential inside the body (without internal singularities) will not change **(Katz and Plotkin 1999)**.

$$\boldsymbol{\Phi_i = const.} \tag{6}$$

Now let the source be;

$$\sigma = \vec{Q}_\infty \bullet \hat{n} \tag{7}$$

Then **eq. (5)** can be written as;

$$\frac{1}{4\pi}\int_{B+W}\mu\hat{n}\times\nabla\left(\frac{1}{r}\right)ds-\frac{1}{4\pi}\int_{B}\sigma\left(\frac{1}{r}\right)ds=0 \qquad (8)$$

NUMERICAL SOLUTION

The body is divided into NB surface panels and NW wake panels. The Drichlet boundary condition will be specified at each body panel at a "collocation point" which for the Drichlet boundary condition must be specified inside the body. In most cases though, the point may be left on the surface without moving it inside the body.

$$\sum_{K=1}^{NB}\frac{1}{4\pi}\int_{B}\mu\hat{n}\times\nabla\left(\frac{1}{r}\right)ds+\sum_{L=1}^{NW}\frac{1}{4\pi}\int_{W}\mu\hat{n}\times\nabla\left(\frac{1}{r}\right)ds-\sum_{K=1}^{NB}\frac{1}{4\pi}\int_{B}\sigma\left(\frac{1}{r}\right)ds=0 \qquad (9)$$

Element of constant source strength (σ) and doublet strength (μ) are assumed thus, **eq. (9)** can be written as;

$$\sum_{k=1}^{NB}c_k\mu_k+\sum_{l=1}^{NW}c_l\mu_l+\sum_{K=1}^{NB}B_K\sigma_K=0 \qquad (10)$$

Where the result of integration for a quadrilateral panel can be found in **(Katz and Plotkin 1999**) as;

$$C_k=\frac{1}{4\pi}\int_{panel}\frac{\partial}{\partial\hat{n}}\left(\frac{1}{r}\right)ds_k$$

$$B_k=\frac{1}{4\pi}\int_{panel}\left(\frac{1}{r}\right)ds_k \qquad (11)$$

The source strength of (σ) is selected from **eq. (7),** then the coefficients (B_k) are known and can be moved to the right side of the **eq. (10)** by using Kutta condition, the wake doublet can be expressed as follows;

$$\mu_w=\mu_u-\mu_l \qquad (12)$$

So that the **eq. (10)** can be simplified as follows:

$$C_w\mu_w=C_w(\mu_u-\mu_l) \qquad (13)$$

$$\sum_{k=1}^{NB}A_k\mu_k=-\sum_{K=1}^{NB}B_K\sigma_K \qquad (14)$$

Where

$A_K=C_K$ If the panel not at T.E

$A_K=C_K\pm C_W$ If the panel is at T.E

It could be written in matrix notation as;

$$[A]\{\mu\} = -[B]\{\sigma\} \tag{15}$$

AERODYNAMIC LOADS

Once **eq. (15)** is solved and the unknown singularities values are obtained; the velocity components are evaluated from local coordinate's derivation, the two tangential perturbation velocities are;

$$q_l = \frac{\partial \mu}{\partial l} \tag{16}$$

$$q_m = \frac{\partial \mu}{\partial m} \tag{17}$$

Where the differentiation is made numerically using the values on the neighbor panels, the normal component of the velocity is obtained from the source

$$q_n = -\sigma \tag{18}$$

The total velocity in the local direction of panel (k) is

$$Q_K = \left(Q_{\infty L}, Q_{\infty m,} Q_{\infty n}\right) + \left(q_l, q_{m,} q_n\right) \tag{19}$$

The pressure coefficient can be computed at each panel using panel Bernaullies equation;

$$C_{pk} = \frac{p_k - p_\infty}{\frac{1}{2}\rho_\infty Q_\infty^2} = 1 - \frac{Q_K^2}{Q_\infty^2} \tag{20}$$

The total aerodynamic forces are calculated from

$$\begin{aligned} F_x &= -\frac{1}{2}\rho_\infty Q_\infty^2 \sum_{k=1}^{NB} C_{pk} A_k n_{xk} \\ F_z &= -\frac{1}{2}\rho_\infty Q_\infty^2 \sum_{K=1}^{NB} C_{pk} A_k n_{zk} \end{aligned} \tag{21}$$

Where A_k = area of each body panel and n_{xk}, n_{zk} = Component of unit normal vector ($\hat{n}$) in X and Z directions.

The lift and induced drag forces are calculated by:

$$\begin{aligned} F_l &= F_z \cos\alpha - F_x \sin\alpha \\ F_D &= F_z \sin\alpha + F_x \cos\alpha \end{aligned} \tag{22}$$

The moment at reference point is;

$$M = 0.5\rho Q_\infty^2 \left[\sum_{k=1}^{NB} \left(C_p A n_x\right)_k (Z_{ck} - Z_{ref}) + \left(C_p A n_z\right)_k (X_{ck} - X_{ref})\right] \tag{23}$$

In which $\left(X_{ck,}Z_{ck}\right)$ are the global coordinates of each collocation point and (X_{ref}, Z_{ref}) are the reference moment point of the body.

A combination between rectangular wing and tail in potential flow is patterned by changing the space between them and the angle of setting of the tail as shown in **Fig (2).** The interference between the wing and tail can be clearly seen from the pressure coefficient distribution along the mid stream line on wing and tail and from dynamic forces on them. The other parameter like wing and tail aspect ratio and cross-sectional airfoil are selected constant for all cases studied in the present work.

It must be noted that the wake will be assumed straight (flat wake shape) and deflected with an angle of attack of the wing, to prevent wake to go inside tail which may cause an error in pressure distribution on the tail due to presence of singularity inside it, so that; there will be difference in height level between them. This approximation is done in real case where most of aircraft place the tail at higher or lower level from wing position and never placed in the same level.

The procedure discussed in the numerical method is used to build a computer program in Fortran 90 power station and modified to predict complex configurations like wing-body-tail system. To insure that program give reasonable results, the program results must be verified with other dependent published results.

RESULTS AND DISCUSSION

Figs (5, 6, 7, and 8) show a comparison between the present code and the results of software program called **PANAIR** pilot code **(Tinoco 1984)** which is a commercial potential flow program predicts subsonic and supersonic flow over complex bodies. The discretization of a selected case (swept back tapered wing) is shown in **Figs (3 and 4).** Also the control point is clear in **Fig (4).** Other figures **(5, 6, 7 and 8)** show pressure distribution (upper and lower surfaces) on the wing surface of two angles of attack and two span wise stations**.** Good agreement between present works with pilot code is clear.

To simplify the interference between wing and tail problem the consideration will be concentrated on some parameters like the distance between them and the tail setting angle. Wing and tail is considered as a rectangular wings as shown in **Fig (9)** where all the dimensions are assumed with respect to chord length of the wing. The reference area and length which is used in calculation of the aerodynamic coefficients are calculated with respect to wing area and its chord length. Also **Fig (9)** shows the discretized wing and tail configuration, it is seen that dense panels are used at leading and trailing edge for both wing and tail. This type of discretization is used due to rapid change in flow characteristics at these regions and it gives approximately constant aspect ratio for each panel.

Fig (10) illustrates the influence of tail on the wing by considering the lift coefficient distribution along the span of wing with tail and without tail at 5^{o} angle of attack. The figure shows the influence of tail on the wing which clearly increasing the load slightly on it. Pressure distribution on the wing surface is shown in figures (**11 and 12).** A comparison with tailness wing shows no major difference between them. The figures shows small tail effect on the wing and it could be neglected.

Fig (13) shows that lift distribution along the tail. Two cases are studied, the first consideration predicts the tail without wing at angle of attack of 5^{o} where a free stream goes on its surface and the other consideration the effect of wing on the tail is considered. The difference is clearly shown in the figure, by decreasing the lift distribution along the span wise of the tail. The decreasing in lift could be represented by decreasing in angle of attack at tail. The down wash behind the wing acted as a normal velocity in the down ward direction which tries to decrease the angle of attack on the tail.

Fig (14) shows a comparison between lift distribution along the span of wing and tail at 5^o angle of attack. It is clear that the wing carry most of lift and the tail used mainly to control. Pressure distribution on the tail surface with and without wing is shown in **Figs (15 and 16)**. The figures show a difference in two cases, which lead to a difference in load on the tail.

An important figure which illustrates the relation between wing and tail effect is shown in **Fig (17)** where lift coefficient is considered with and without interference between them. The most important notice that is the wing load increased due to presence of tail while tail load decrease from tail alone due to presence of wing. The overall wing tail load shows an increase in lift coefficient with angle of attack for them. **Fig (18)** shows another notice for them, the figure illustrates that the induced drag coefficient decreased for wing and tail simultaneously due to interference effect on wing and tail with that when take them alone.

Fig (19) represents the stability curve of the wing-tail system, because it represents a relation between moment coefficient variations with lift coefficient. The figure constructed from four curves representing wing-tail combination and wing moment alone. The reference moment point is located at 0.5 of wing chord length behind wing leading edge. It could be seen that the wing moment tends to cause a positive moment coefficient at a reference point. While the tail causes a reverse action on this point, the figure is separated with a vertical line at zero moment coefficients to illustrate the stability behavior. Due to large lift produced on the wing as compared with tail, the moment of the system (wing-tail) tend to be a positive behavior i.e. nose up. This mean the system is not stable i.e. at the right side of the figure and the inclination of the overall curve is positive as clearly illustrated in the figure.

To consider a different parameter and its effects on the system which contain wing and tail, the distance and setting angle of the tail is illustrated in foregoing discussion. The distance of the tail from the wing increased gradually from the wing to consider the interference effect between them. **Fig (20)** shows this effect by considering the lift coefficient on the tail and wing. Clearly there is no major effect on the lift coefficient with increasing the distance. But **Fig (21)** shows an increasing in the induced drag of the wing as the tail goes far from the wing, and this satisfied **Fig (18)** which illustrates that the induced drag of the wing without tail is larger than that with tail. The far distance means that there is no effect between two set of wings.

Fig (22) is an important graph where the moment coefficient vs. distance between wing and tail is presented at angle of attack 5^o. The moment coefficient changes its behavior as the tail reached to a distance equal approximately to 3.56 of wing chord length measured from wing leading edge to the leading edge of the tail. At this position the stability is satisfied and the moment tends to make a nose down for the wing-body system.

Other parameter considered here is the setting angle of the tail. This angle is added or subtracted to the angle of attack of the wing and tail system. **Fig (23)** shows the lift coefficient of the wing and tail, it could be seen that the lift coefficient of the tail increased rapidly with the setting angle of the tail while the wing lift coefficient is constant with this angle. The overall lift coefficient increased with this angle as shown in figure.

Fig (24) shows that the increasing in induced drag due to increasing in the tail induced drag. The other notice is the wing induced drag which is decreased due to interference effect as it is clear in the figure.

Fig (25) shows the wing will be stable at angle of attack equal to 3.5^o approximately. The tail is stable for all setting angle which overcome the unstable wing moment coefficient.

CONCLUSIONs

The results show that there is an interference causing a change in longitudinal characteristics of each wing and tail. The increase distance between wing and tail decrease the interference effect and increase the stability of wing-tail system. It is found also that for the system suggested in the present work the moment stability occurred at distance 3.5 times wing chord make the system stable. The results can be seen in the transport aircraft where the tail at a far distance from wing. The increasing of setting angle of tail will cause an increasing in stability of wing-tail system. The interaction between them causes an increasing in lift coefficient for the whole system (wing and tail) also in the induced drag. The moment coefficient prediction shows that the system will be stable at 3.5^o setting angle of tail. These results could be applied in military aircraft where the length of aircraft is small.

REFERENCES

- **Arnott A. D. and Berstein L., "**Aerodynamic Interaction at the Junction Between A forward Swept Wing and Plate," Aeronautical Journal, Vol. 104, No. 1023, 2000.

- **Bandyopadhyay G., "**Low-Speed Aerodynamics of Canard Configurations," Aeronautical journal, January 1989.

- **Hess J. L., and Smith A. M. O., "**Calculation of Potential Flow about Arbitrary Bodies," Progress in Aeronautical Science Journal, Vol. 8, Pergamon Press 1967.

- **Katz J. and Plotkin A., "**Low Speed Aerodynamics From Wing Theory To Panel Method," McGraw Hill, 1999.

- **Morino L., and Kuo C., "**Subsonic Potential Aerodynamic for Complex Configuration: A General Theory," AIAA journal, Vol. 12, No. 2, 1974.

- **Morino L., Chen L. T., and Emil O. Suciu, "**Steady and Oscillatory Subsonic and Supersonic Aerodynamics around Complex Configuration," AIAA journal, Vol. 13, No. 3, 1975.

- **Tinoco E. N., "**PANAIR Analysis of Supersonic/Subsonic Flow about Complex Configurations," the University of Tennessee Space Institute, Tullahoma, Tenessee 37388, March 1984.

NOMENCLATURE

A	Panel Area	m^2
A	Doublet influence matrix	
AR	Aspect ratio	
B	Source influence matrix	
b_w b_T	Wing and Tail Span	m
c	Wing Chord length	m
c_T	Tail Chord Length	m
C_l	Section Lift Coefficient	m
C_L	Total Lift Coefficient	m
C_m	Pitching Moment Coefficient	m
C_p	Pressure Coefficient	

F_D	Drag Force	N
F_L	Lift Force	N
F_x	Axial Force	N
F_z	Normal Force	N
l, m, n	Local directional unit	
M	Moment	N.m
n_x,n_y,n_z	Normal direction unit	
NW	Number of Division on the wake	
NB	Number of division on the body	
Q	Total velocity	m/s
x_{ref}, z_{ref}	Reference point	m
x_t	Distance between wing and tail leading edge	m
α	Angle of attack	Deg
ϵ	Tail Setting Angle	Deg
Φ	Total velocity potential	$m^2/2$
μ	Doublet Strength	$m^2/2$
μ_w	Doublet Strength of wake	$m^2/2$
Φ_∞	Free Stream Velocity Potential	$m^2/2$
σ	Source Strength	$m^2/2$
ρ_∞	Free Stream Density	Kg/m^3

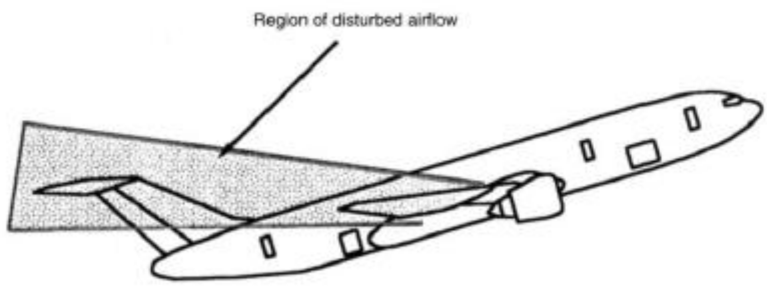

Fig (1): Interaction Problem Between Wing and Tail in Flying Aircraft.

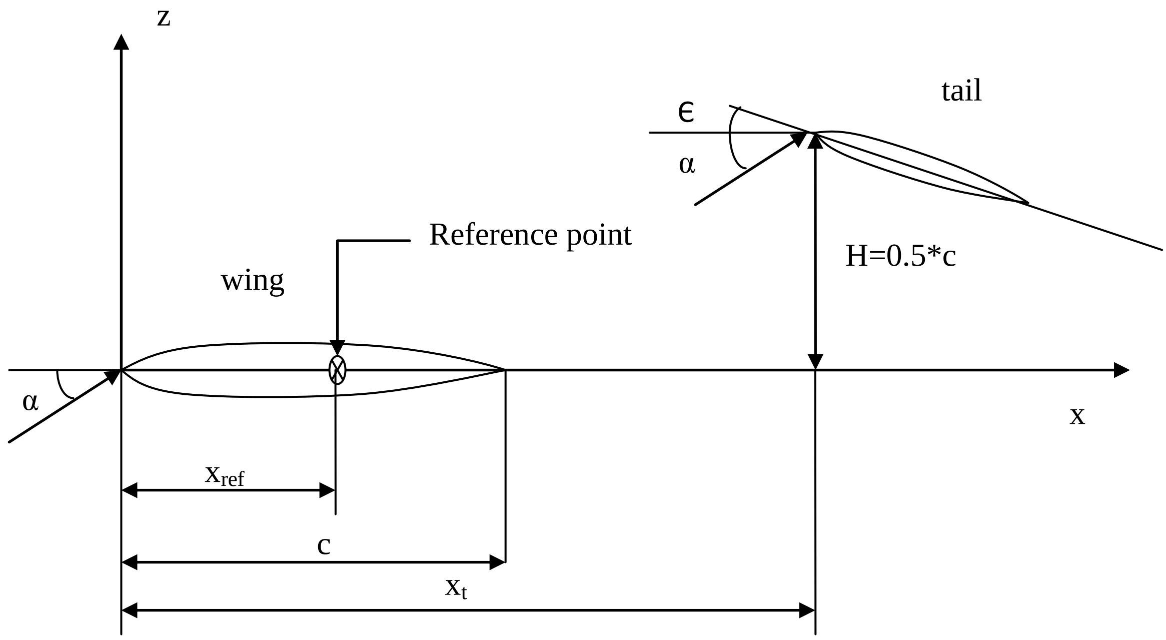

Fig (2): Terminology of Wing-Tail Interaction Problem.

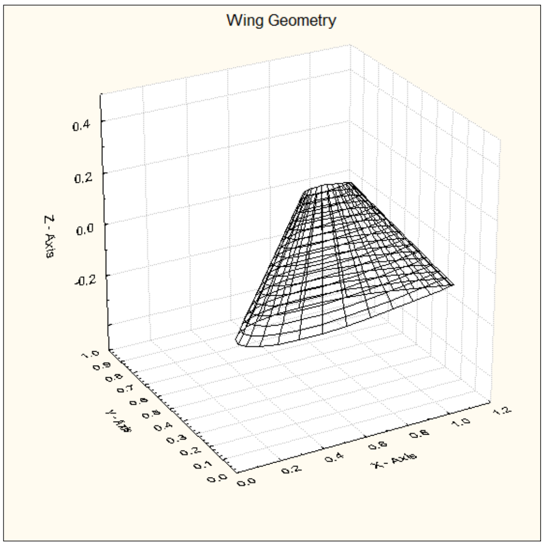

Fig (3): Wing Geometry.

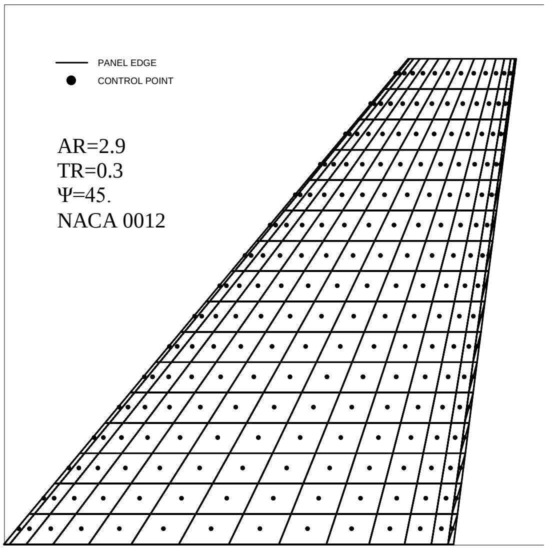

Fig (4): Wing Panels and Control Point.

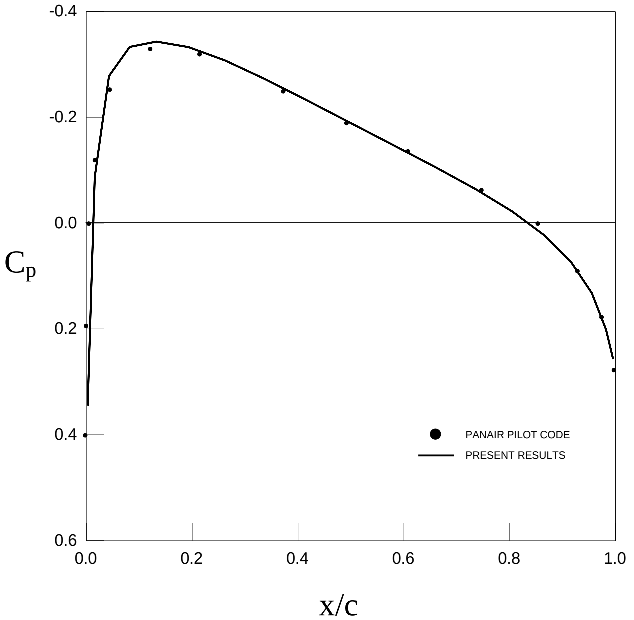

Fig (5): Pressure Distribution at 2y/b=0.19 and α=0.

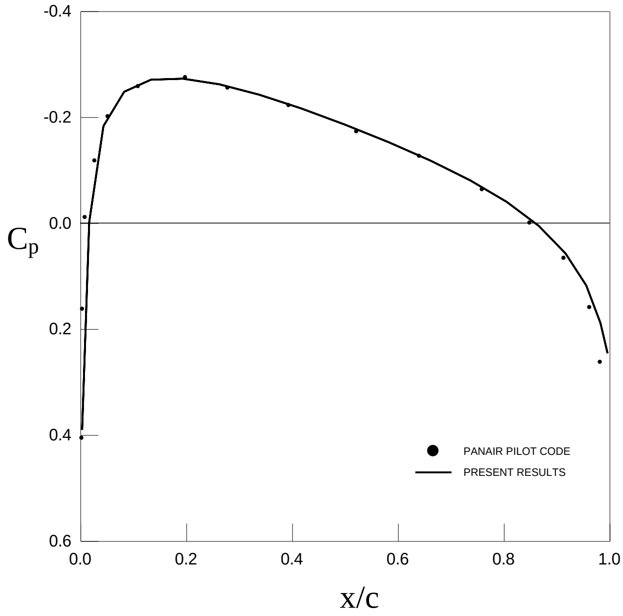

Fig (6): Pressure Distribution at 2y/b=0.81 and α=0.

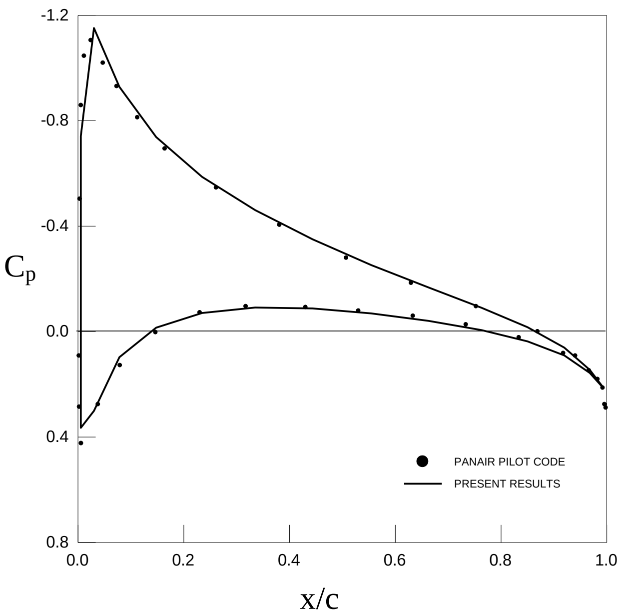

Fig (7): Pressure Distribution at 2y/b=0.19 and α=5^o.

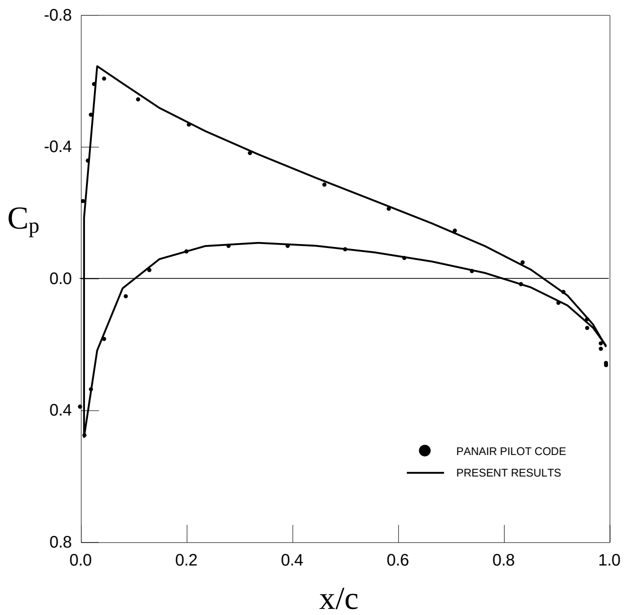

Fig (8): Pressure Distribution at 2y/b=0.81 and α=5^o.

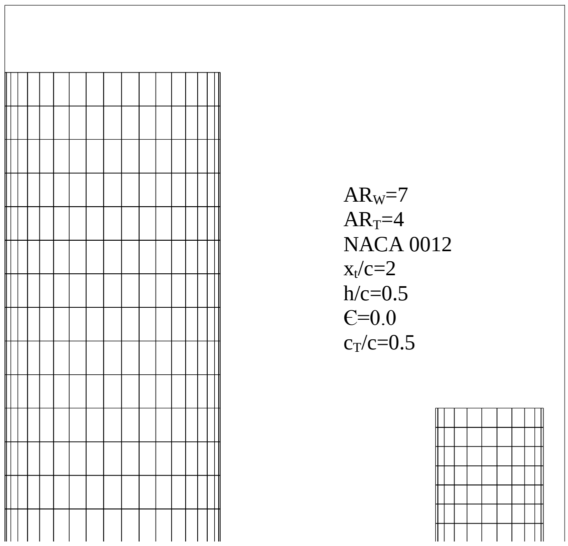

Fig (9): Wing-Tail Geometry.

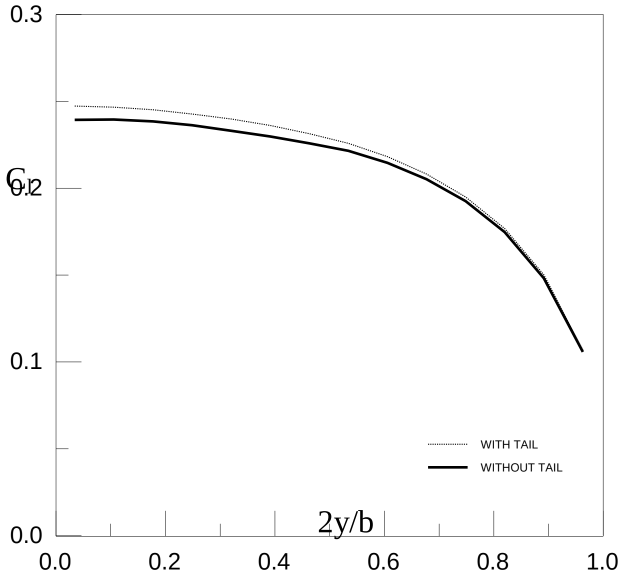

Fig (10): Lift Distribution along Span Wise Direction of Wing

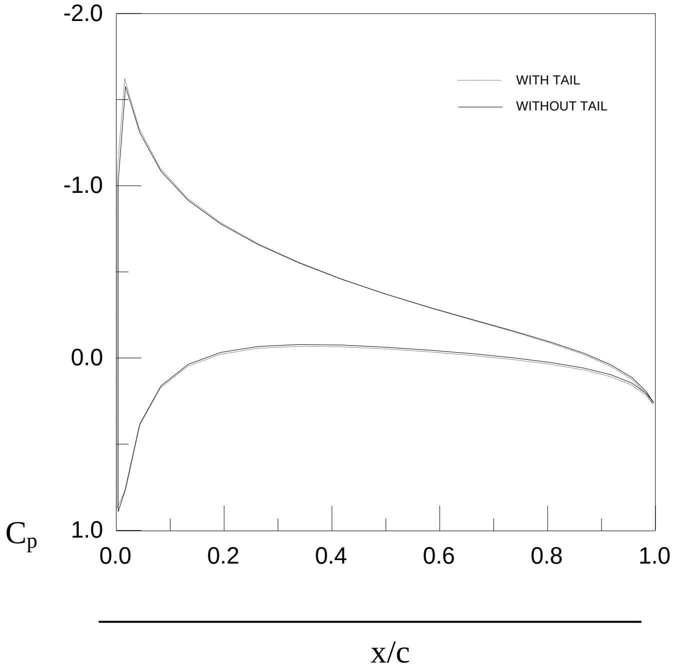

Fig (11): Pressure Distribution on the Wing at 2y/c=0.19.

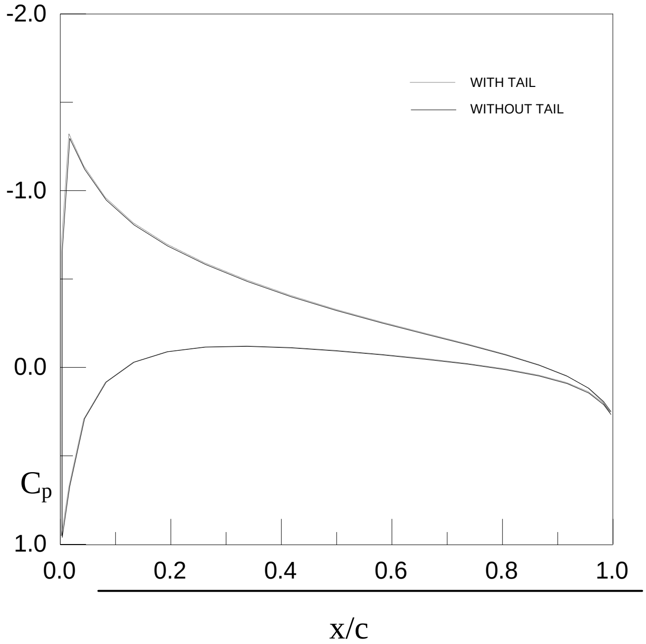

Fig (12): Pressure Distribution on the Wing at 2y/c=0.81.

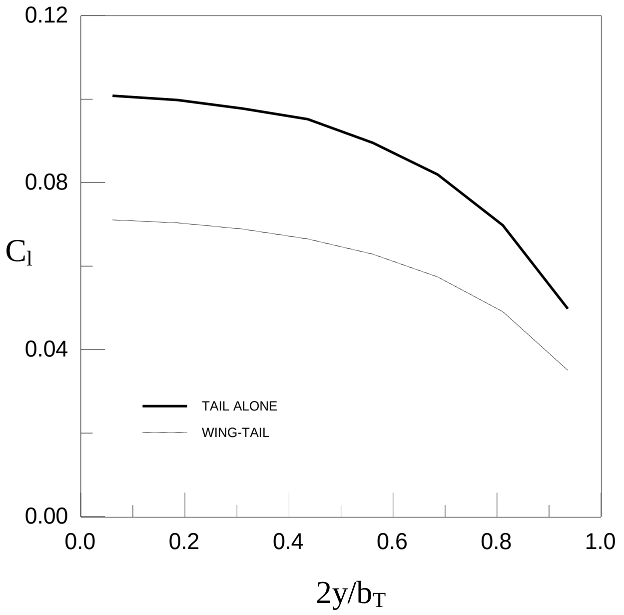

Fig (13): Lift Distribution a Long Span Wise Direction of Tail α=5°.

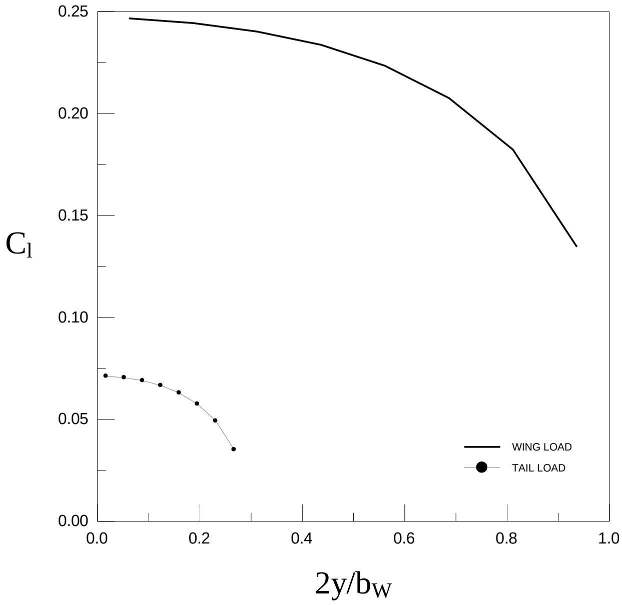

Fig (14): Lift Distribution a Long Span Wise Direction for Wing and

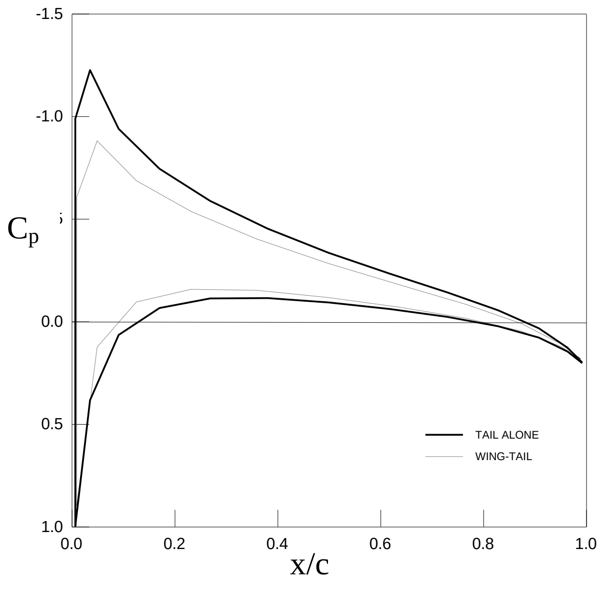

Fig (15): Pressure Distribution on the Tail at 2y/c=0.19.

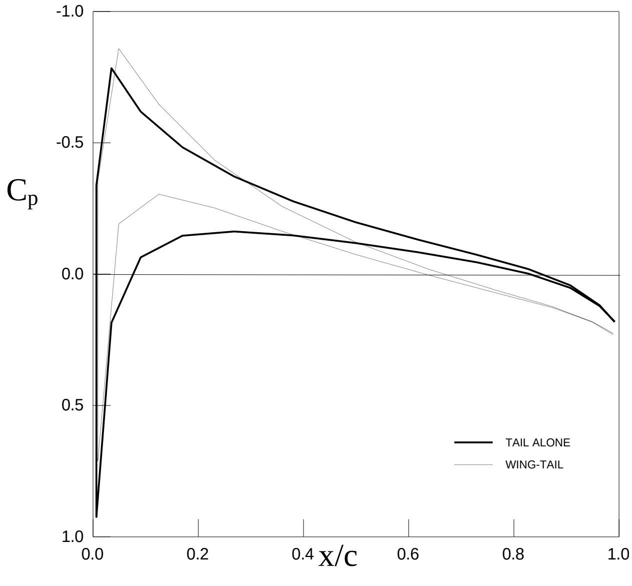

Fig (16): Pressure Distribution on the Tail at 2y/c=0.81.

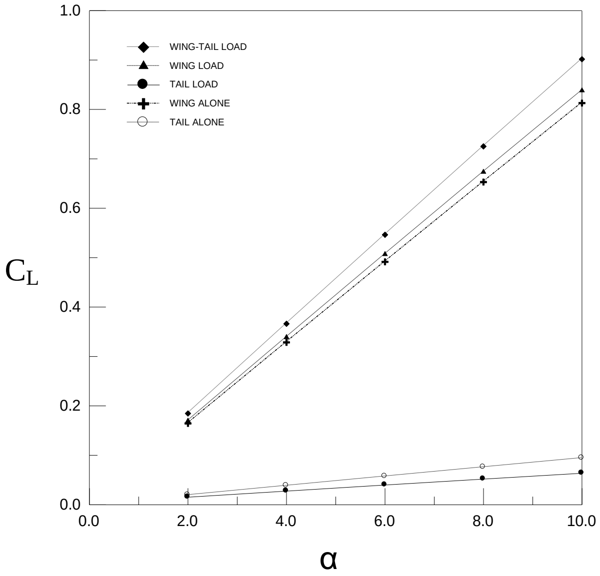

Fig (17): Wing-Tail Lift Coefficients with Angle of Attack.

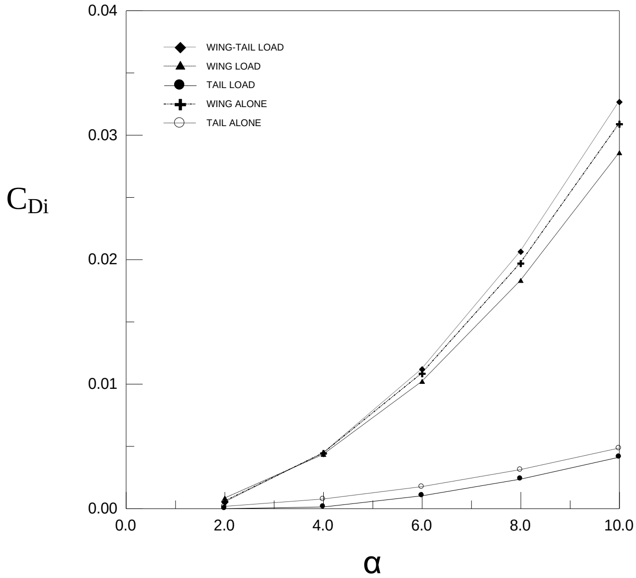

Fig (18): Wing-Tail Induced Drag Coefficients with Angle of Attack.

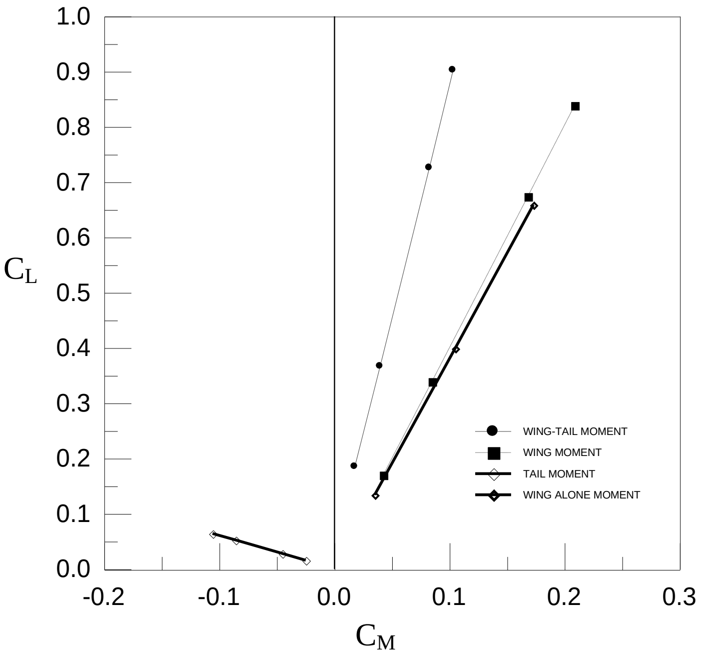

Fig (19): Wing-Tail Moment Coefficients with Lift Coefficient.

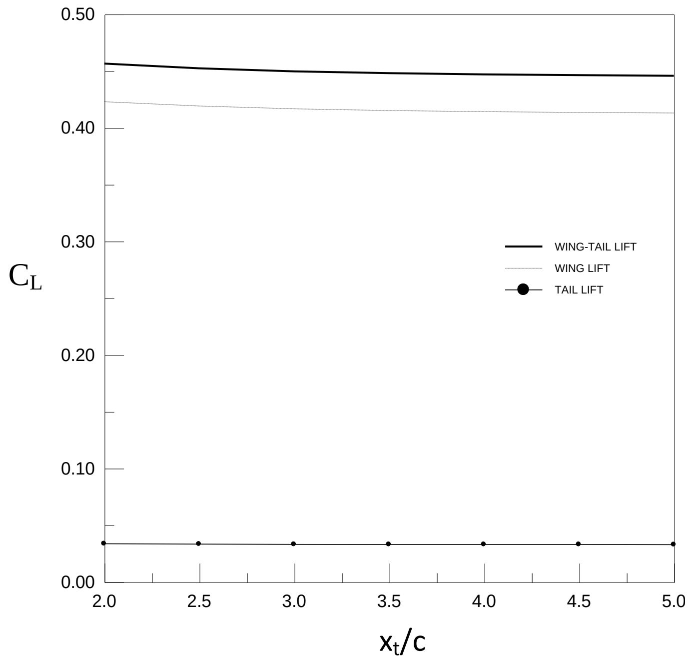

Fig (20): Wing-Tail Lift Coefficients with Distance Between Wing and Tail $\alpha=5^o$.

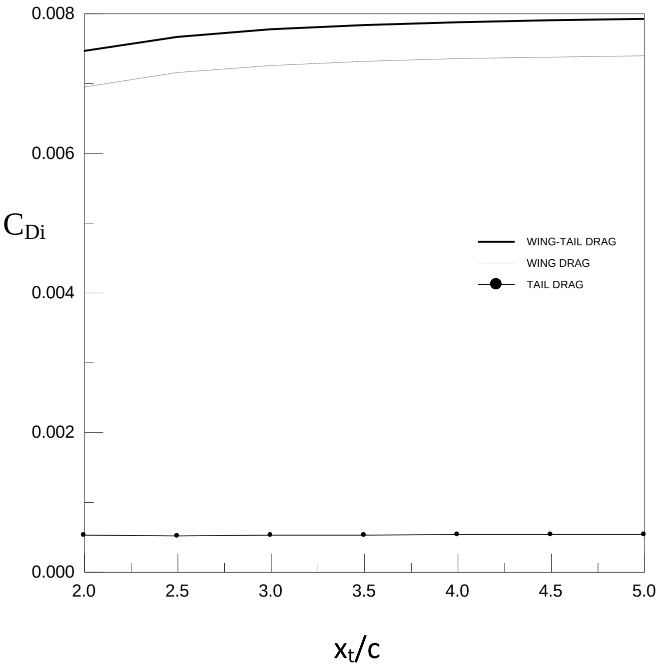

Fig (21): Wing-Tail Induced Drag Coefficients with Distance Between Wing and Tail, α=5^o.

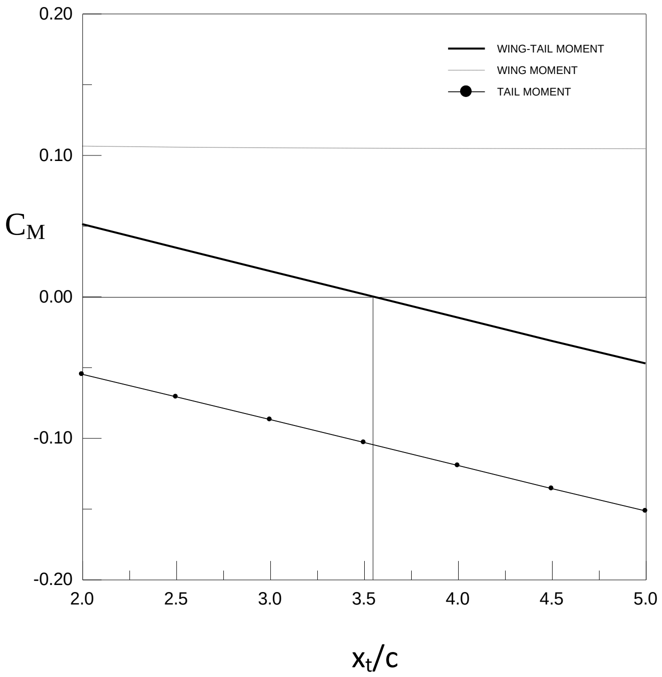

Fig (22): Wing-Tail Moment Coefficients with Distance Between Wing and Tail, α=5^o.

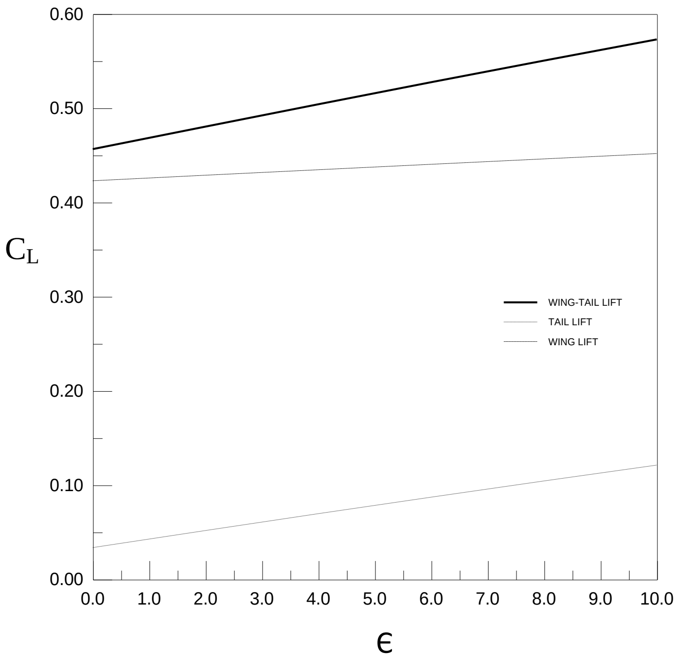

Fig (23): Wing-Tail Lift Coefficients with Tail Setting Angle, α=5^o.

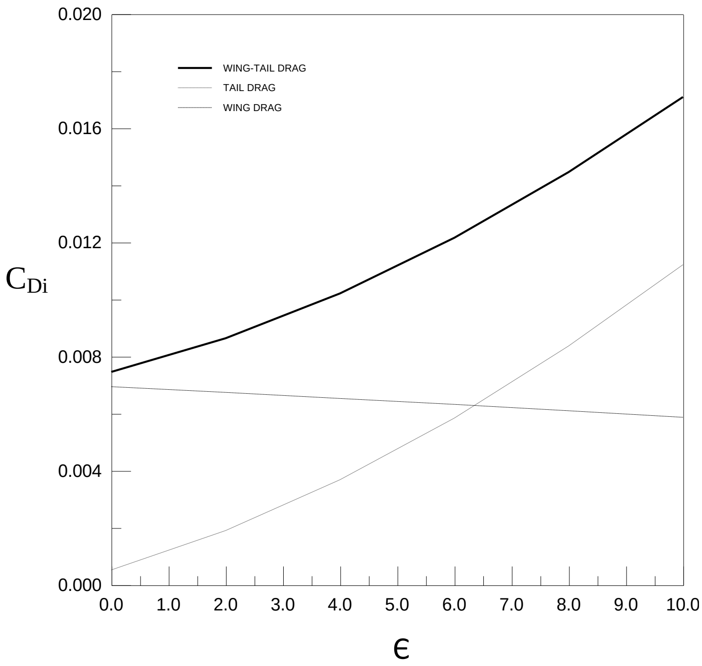

Fig (24): Wing-Tail Induced Drag Coefficients with Tail Setting Angle, α=5^o.

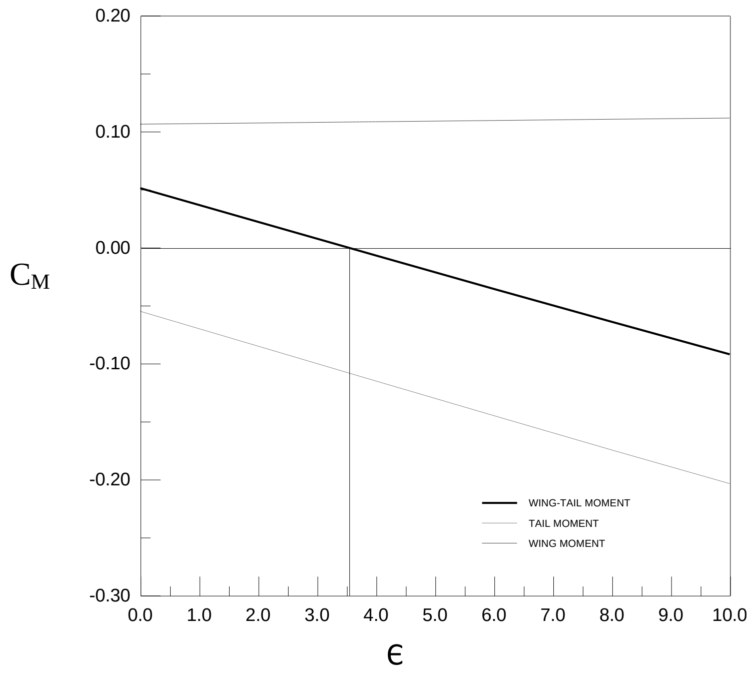

Fig (25): Wing-Tail Moment Coefficients with Tail Setting Angle, $\alpha=5^o$.

REVIEW AN IMPROVEMENT ON TECHNICAL OPERATION IN DRINKING WATER SYSTEM FOR WATER SUPPLY STATION

Ms. Iman Q. Alsaffar
Mech. Eng. Dep.
College of Eng.
University of Baghdad
Baghdad – Iraq

ABSTRACT

Water plays a strategic role in the development of many facilities in our country. Still, the biggest construction projects in the world take place in Iraq with the creation of the most ambitious architectural centers. Great water production plants and distribution networks are constructed and management of available water resources is an important issue. This paper includes the identification of the hazards and introduction of control points that serve to minimize these potential hazards that providing more effect control for drinking water quality. We can conclude that end-product testing is a reactive rather than preventive way to demonstrate confidence in good and safe drinking water. This justifies the need for the formulation of a new approach in drinking water *Quality Control* QC based on understanding of system defense reduces for contamination and on preventive means and actions necessary to guarantee the safety of the water supplied to the consumer. *Water safety plan* WSP is a concept for risk assessment and risk management throughout the water cycle from the catchments to the point of consumption. This work outline and presents an overview of the first year occurrences in the developing and implementing a WSP in the multi- municipal water supply system for a city area of Baghdad. Since key personnel had contributed to the assessment of hazards and evaluation of corrective actions for control points, a greater understanding of water QC and improvements on technical operation and performance have been register, demonstrating good value for the methodology.

الخلاصة

يلعب الماء دورا استراتيجيا في جميع ميادين الحياة المتطورة في بلادنا ومع مواكبة مشاريع البناء والأعمار في العراق، فان عملية بناء وإدارة مشاريع إنتاج الماء وشبكات التوزيع تعد مسالة مهمة. يهتم البحث بالتعريف بالمخاطر المحتملة وإدخال نقاط سيطرة تؤدي إلى التقليل من تلك المخاطر وتوفير رقابة أكثر فاعلية لنوعية مياه الشرب. يمكن أن نستنتج إن اختبار الناتج النهائي يكون فاعلا أكثر مما هو وقائيا لاعتماد الثقةِ في ماء جيد وامن وصالح للشربِ. هذا يُبرّرُ الحاجةَ لصياغةِ وإيجاد معالجة جديدة في إدارة الجودة للماء الصالح للشربِ الذي يستند على فهم نظامِ المناعة ضد التلوثِ والإجراءات الوقائية المطلوبة لضمان صلاحية الماء المجهز للمستهلكِ. خطة ضمان سلامة الماء **(WSP)** هو مفهوم لتقديرِ الخطر والسيطرة عليه, خلال دورة الماء الكاملة من المصدر ولحد الاستهلاك. يقدم هذا العمل ملخص أعمال

التحسين والتطوير للسنة الأولى للأسلوب التقني في تطبيق السيطرة النوعيةِ في منظومة شبكة ماء متعددة الامتدادات لمدينةٍ مثل بغداد. إن المساهمة في تقييم الأخطار والإجراءات التصحيحية لنقاط السيطرة المسجلة أدت إلى فهم وتحقيق قيمة جيدة في استخدام طريقة التحسين في أسلوبQC .

KEY WORDS: drinking water quality control, End- product test risk assessment, source water protection

INTRODUCTION

Drinking water QC is a key issue in public health policies. Special attention and efforts were taken on surveillance and safety of water supply systems that the water as major route of cholera transmission. Later, much legislation published focused on standards for treated drinking water and on compliance monitoring. Water quality was guaranteed by the so called end-product testing, based on spot sampling of the water produced. With this procedure, it was possible to bring the very widespread water-borne diseases under control, especially those of bacterial origin.

Over the years, several shortcomings and limitations of the end-product testing methodology have been identified. Some of them related to the following aspects:

- There is a multitude of water-borne pathogens that cannot be detected or they can be detected insecurely that occurred through water supply systems that met the standard for absence of indicator microorganisms.
- Often, monitoring results are available out of time of intervention needed to maintain the safety of a supply system. End-product testing only allows checking if the water delivered was good and safe (or unsafe) after distributed and consumed.
- End-product testing hardly can be considered a sound method for representative water quality *status*. A very small fraction of the total volume of water produced and delivered is subject to microbiological and chemical analysis. Moreover, the monitoring frequency does not guarantee representative results in time and space, as well.
- End-product testing does not provide safety in itself. Rather is a mean of verification that all the supply system components and installed control measures are working properly.

In recognition of these limitations, primary reliance on end-product testing is presently considered not to be sufficient to provide confidence in good and safe drinking-water, moving towards to process monitoring by introducing a management framework for safe water [Bartram *et al.*, 2001].

Problems

Drinking water research and practice has focused mostly on water delivery infrastructure, treatment technology, specific contaminants, end-product quality and poorly perceived or uncertain understanding of health risks. It is necessary to ask if this focus on technology, engineering practice, end-product quality and immediate reactions to a few specific contaminants is really a rational basis for managing drinking water health risks. Is it the highest or main priority in the provision of safe water? Is the decision making process about drinking water research and practice focused on the most important issues to consumers and their communities? Furthermore, who decides what the issues and priorities are, and are all stakeholders represented or adequately represented in the decision-making processes? It must be asked if the process of setting priorities for drinking water research and good practice is “scientific”, rational, preventative and visionary? Most importantly, is safe drinking water consistently available to everyone?

ANSWERS

Actually, the answers to all of these questions are: "No". The reality is we need to:

- address more of the key issues and questions which influence the condition of safe drinking water,
- re-evaluate and set new and better priorities for drinking water research and practice,
- include more stakeholders in the processes of identifying key issues and setting priorities,
- become more rational and scientific in the overall approach to drinking water research and the provision of safe drinking water,
- become more visionary and anticipatory of the risks to drinking water safety, and
- do a better job of making safe water available, accessible and affordable for all.

In addressing water and health, it is necessary to focus on the fact that water is a fundamental human right for all people, communities and societies, and that human behavior and the process of daily living is inextricably linked to drinking water. These aspects of drinking water and their implications for human health need to be addressed by appropriate research and practice.

THE METHODOLOGY

The proposed methodology request to move away from single dependence on end product testing, which will be integrated into a control strategy for consistently ensuring the safety of a drinking-water supply system, applying a comprehensive risk assessment and risk management approach. The safety of drinking-water depends on a number of factors, including quality of source water, effectiveness of treatment and integrity of the distribution system. System-tailored hazard identification and risk assessment must be considered as a starting point for system management, so a general flow diagram can be represented in figure (1) for risk assessment.

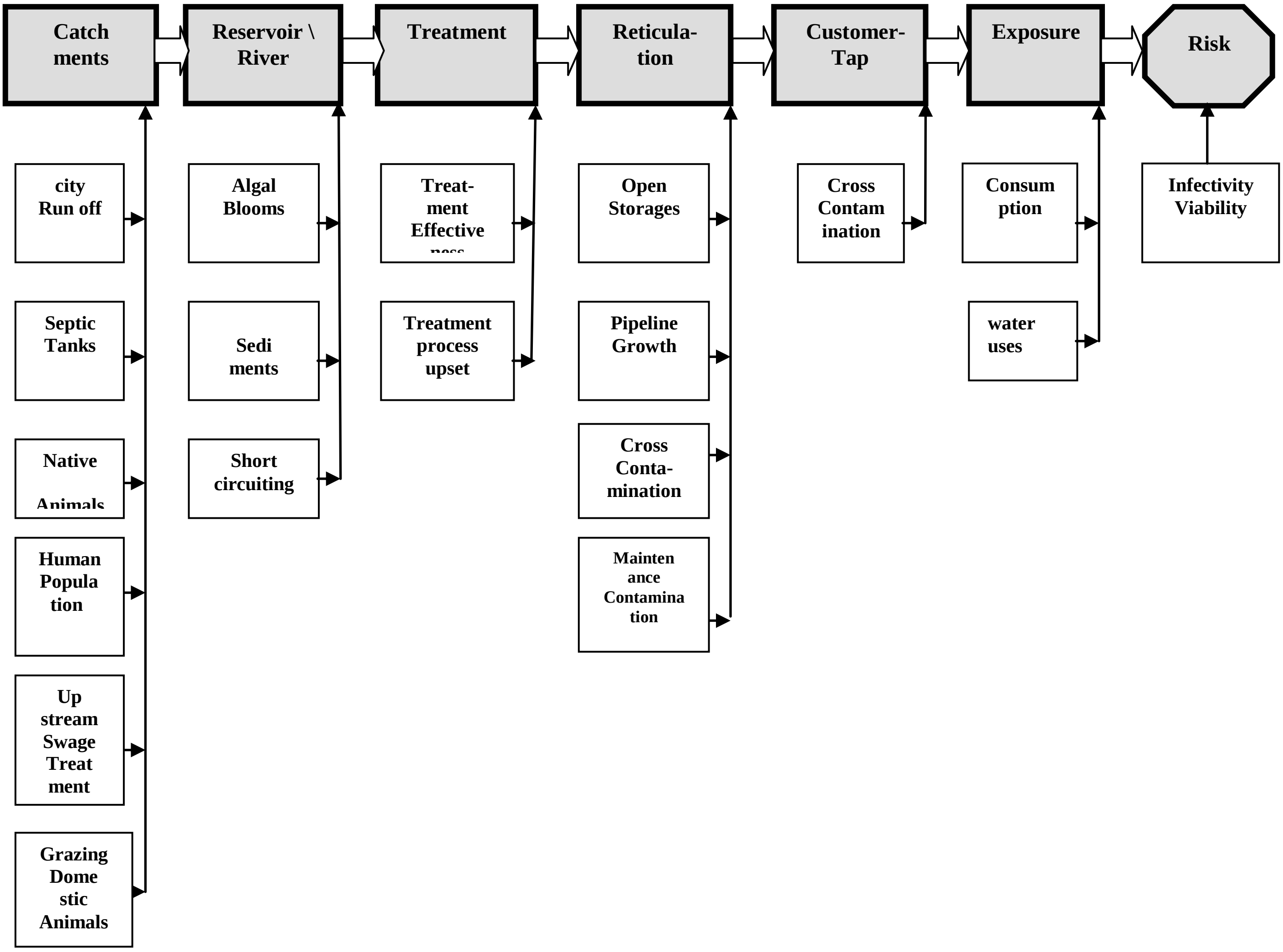

Fig.1 General flow diagram for risk assessment [Stevens *et al*., 1995]

END - PRODUCT TESTING

The traditional approach to water quality management placed a great emphasis on the routine monitoring of water quality. The results of analysis were compared against acceptable concentrations in order to evaluate performance of the water supply and to estimate public health risks (Helmer *et al*., 1999).

The focus of attention was on end-product standards rather ensuring that the water supply was managed properly from catchments to consumer. Although operation and maintenance of water supplies has been recognized as important in improving and maintaining water quality, the primary aim of water suppliers, regulators and public health professionals has been to ensure that the quality of water finally produced met these standards. This reliance on end-product testing has been shown to be ineffective for microbiological quality of water, as evidence has emerged of significant health impact from the consumption of water meeting national standards (Payment *et al*., 1991).

The quality of the source protection measures is an important component in controlling whether pathogens may be present in the final drinking water.

End-product testing has a further weakness in that the number of samples taken is typically very small and not statistically representative of the water produced in a domestic supply. The focus on end-product testing has meant that action is only initiated in response to a failure in relation to the specified water quality standard. However, this typically means that the water has been supplied and may have been consumed before the results of the test are known and the increased risk to health identified. As a result, outbreaks occur and rates of endemic disease remain higher when good practice in relation to water quality management is emphasized. The reliance on end-product testing is therefore not supportive of public health protection and whilst it retains a role in assessing water safety, it should not the sole means by which risks are managed (Davison *et al.*, 2004).

WATER SAFETY PLAN WSP

The objective of the WSP is to supply water of a quality that will allow health-based aims to be met so; the success of the WSP is assessed through drinking-water supply observation including the three key components:

- ***System Assessment*** : Which involves assessing the capability of the drinking-water supply chain (from water source to the point of consumption) to deliver water of a quality that meets the identified targets, and assessing design criteria for new systems;
- ***Detection of Control Measures in a Drinking-Water System***: For each control measure identified, an appropriate means of *operational monitoring* should be defined that will ensure that any deviation from required performance is rapidly detected in a timely manner.
- ***Management Plans****:* Describe actions to be taken during normal operation or extreme and incident conditions, and that document system assessment (including upgrade and improvement), monitoring, communication plans and supporting programs. Figure (2) shows a comparison summery between Historical and WPS approaches to assuring the drinking safety water.

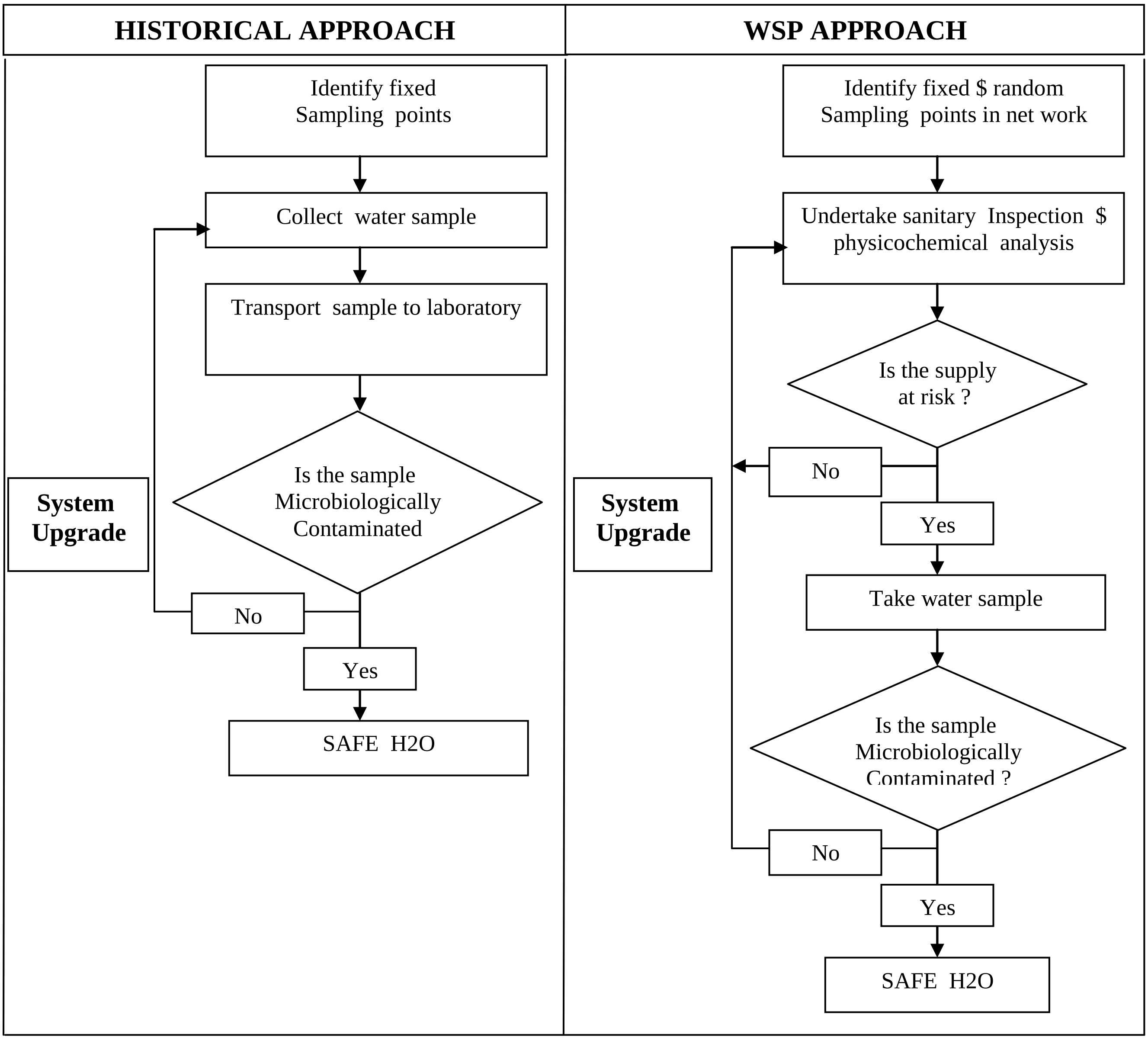

Fig. 2 Summary of approaches to assuring safe drinking water
[Tibatemw A, Nabasirye and Godfrey 2003]

PROCEDURE SYNTHESIS FOR WSP DEVELOPMENT

The structure of the methodology in developing and implementing the WSP was represented in three parts: ***Basics***: corresponding to the development phase, in which the basic aspects needed for risk assessment and risk management are described; ***Operational Aspect:***, where, for each element of the water supply step (source, treatment, and distribution), a synthesis of risk management, control measures and corrective actions in *Critical Control Points* CCP are established; ***WSP Practical Application***: where, for operational monitoring and reporting is stated.

BASICS

The assessment of risk and management, from catchments to the customer, constitute the key issues for the whole process. This was made identifying risks and assessing their significance, and stating systematic management of the control measures and corrective actions needed for their control [Vieira, 2004]. So, three working stages can be defined: preliminary tasks (technical inventory of the system); hazards identification and risk assessment; and performance reporting. For each of the working stage, supplementary forms were designed, as described in Table (1).

The WSP approach represent in the principles and steps that have been established in *Hazard Analysis and Critical Control Point* HACCP preventive risk management methodology [Dewettink *et al*., 2001; Nokes & Taylor, 2003]. Figure (3) gives a diagrammatic overview with the key steps for (WSP) development.

Table - 1 Procedure synthesis for WSP development for water system in a station [Vieira, 2004]

Working Stage	Supplementary Forms	Contents
Preliminary Tasks	**Form 1** – Water company general organization.	Flowchart with a summary description of the hierarchical structure and functioning. Includes a brief description of manager tasks and responsibilities for each functional area
	Form 2 – Overview of the water supply system	List and brief description of the main water supply system steps.
	Form 3 – Team constitution for WSP development	Identification of the WSP team: contacts, functions and responsibilities.
	Form 4 – Flux diagram construction and validation.	Construction and validation of the flux diagram from catchments to service reservoirs.
Hazards Identification and Risk Assessment	**Form 5** – Hazards identification and critical control points CCP definition.	Assessment of hazards that can occur in the water supply system. Establishment of CCP.
	Form 6 – Critical limits CL definition and monitoring procedures	Definition of CL. Establishing of monitoring procedures to confirm if CLs are respected
	Form 7 – Corrective actions establishing.	Hazards removal or reduction. For each CCP corrective actions and related procedures have been defined.
	Auxiliary Form 8 – Definition of instructions for CCP control.	Working instructions for CCP control. Upgrade existing or establish new instructions.
Performance Reporting	**Form 9** – WSP compliance.	Instructions for the daily functioning of the WSP (instructions for maintenance and control of CCP). Reports on daily activities and data collected.
	Form 10 –WSP validation and verification.	Assessment of WSP in an annual basis. Analysis of external and internal factors and their influence on system performance.

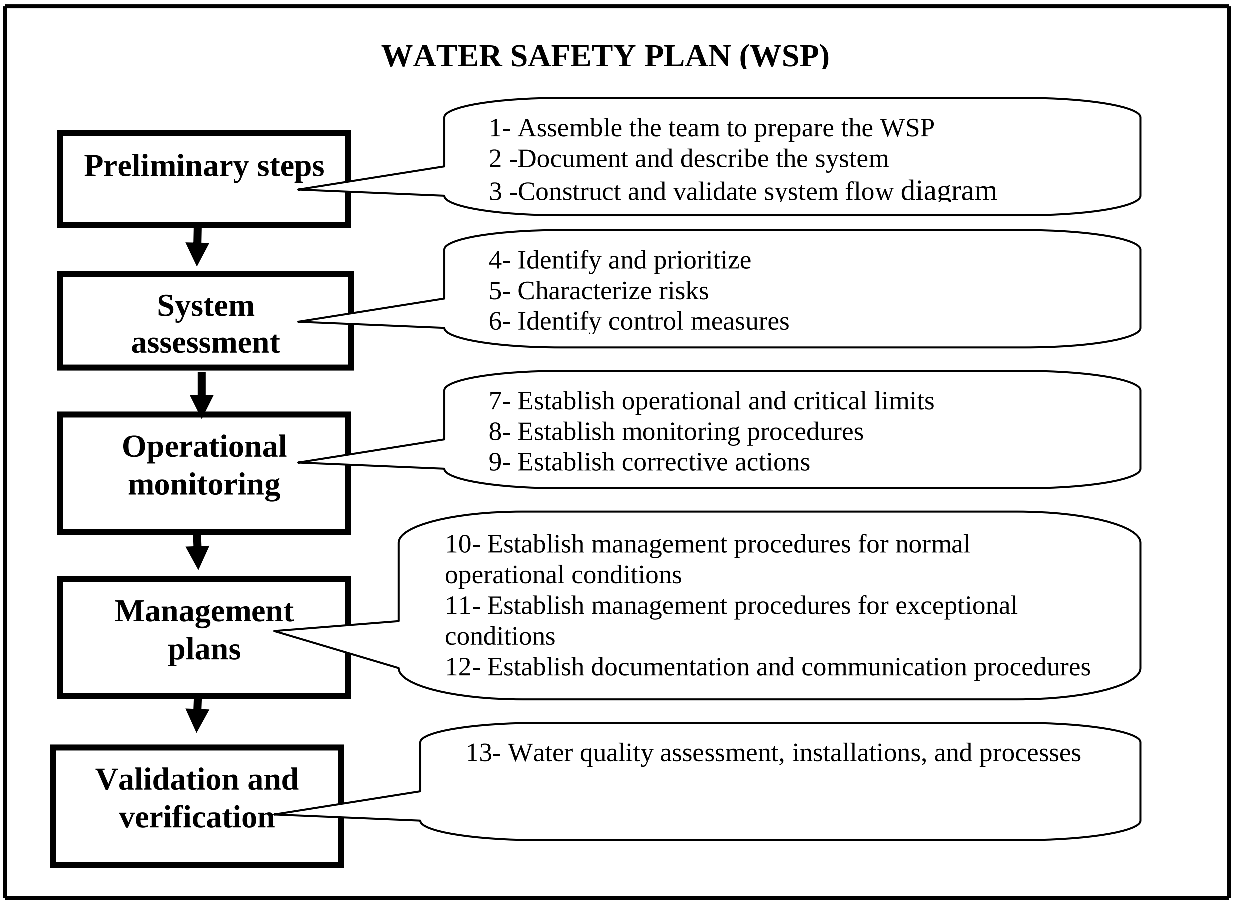

Fig. 3 Overview of the key steps in the development of WSP
[Dewettink *et al*., 2001; Nokes & Taylor, 2003]

WATER SUPPLY SYSTEM IN BAGHDAD

Service water formations of Baghdad responsible for processing water for the city of Baghdad (Baghdad consists of 13 municipalities). The Department of Water Baghdad water processed through the first two systems network processing net water for human consumption and for a second network for the processing of raw water for purposes of watering plants, and the only source of water for the city is the eternal Tigris River. Serving the water area of Baghdad, an estimated 5, 917 square kilometers, including the city of Baghdad and surrounding areas such as (Abu Ghraib and Taji) ..

Situation: We have been tasked with taking a risk assessment for a town of Anywhere *Contaminated Drinking Water System*. The main components of the system consist of two stations and a water storage tank.
(Station No.1) is for example 50 year old that was recently determined to be under the direct influence of supply water with effective filtration. As such, the town had a system installed with duty and standby units.

Additional disinfection is provided by chlorine addition with contact time provided in the water previous to the first user. It is aware that the pumping system for this station is old and has been experiencing frequent breakdowns. A recent inspection of the station has also determined that the casing has some small cracks.

(Station No.2) is a 10 year old with good water. Treatment is provided by chlorination contact time in the section of water main before the first customer. The facilities and equipment for this station are in good working order.

Each station system has chlorine analyzers in place and monitoring equipment to notify the operator (at the site or remotely) on low/high chlorine residual and pumping system failure. The system at (station No.1) is also alarmed. There is no standby power at either station location. The system operates with (station No.2) as the duty. (Station No.1) is usually only brought online during peak demand periods.

However, the town has been noticing that increased usage in the system has required the use of both stations more often. If necessary the water tank in town is capable of providing about a day and a half worth of storage in emergency situations (assuming it is full and there are up normal occurring). Given the problems with (station No.1) and increasing demand, the town has decided to develop the stations in a different setting, however, it is anticipated this process could take a year or more to complete.

SYSTEM ASSESSMENT

The system assessment stage of the WSP development uses the information gained in the system description and hazard analysis and is designed as a first step in determining whether the water supply is able to meet the water quality targets and if not, what investment of human, technical and financial resources would be required to improve the supply. At this stage, specific control measures need not to be defined, but rather the system is looked at in terms of whether it will be possible to define control measures that will allow water safety to be assured.

For example, if the system at (station No.1) a significant not ensured zone, with limited human development over the pumping system and the potential to use legislation to control activities, the system is theoretically capable of meeting established targets and control measures in the catchments can be identified. By contrast, if a supply water from (station No.1) where there is extensive human development and there is no disinfection, the system may not be able to meet the targets without investment at least in a treatment step. The system assessment, therefore, may identify immediate investment requirements essential for meeting the targets and which may become control measures. It is unlikely that all control measures will rely on infrastructure improvements and therefore even in situations when improvements are needed, some control measures can be identified, monitored and managed.

IDENTIFICATION OF HAZARDS AND PREVENTIVE MESURES

The information given by the water supply flow diagram (figure 4) and the deep knowledge of the system performance are the basic conditions for hazards identification and risk assessment. Occurrences of biological, physical and chemical hazards linked with the different steps of the system were investigated.

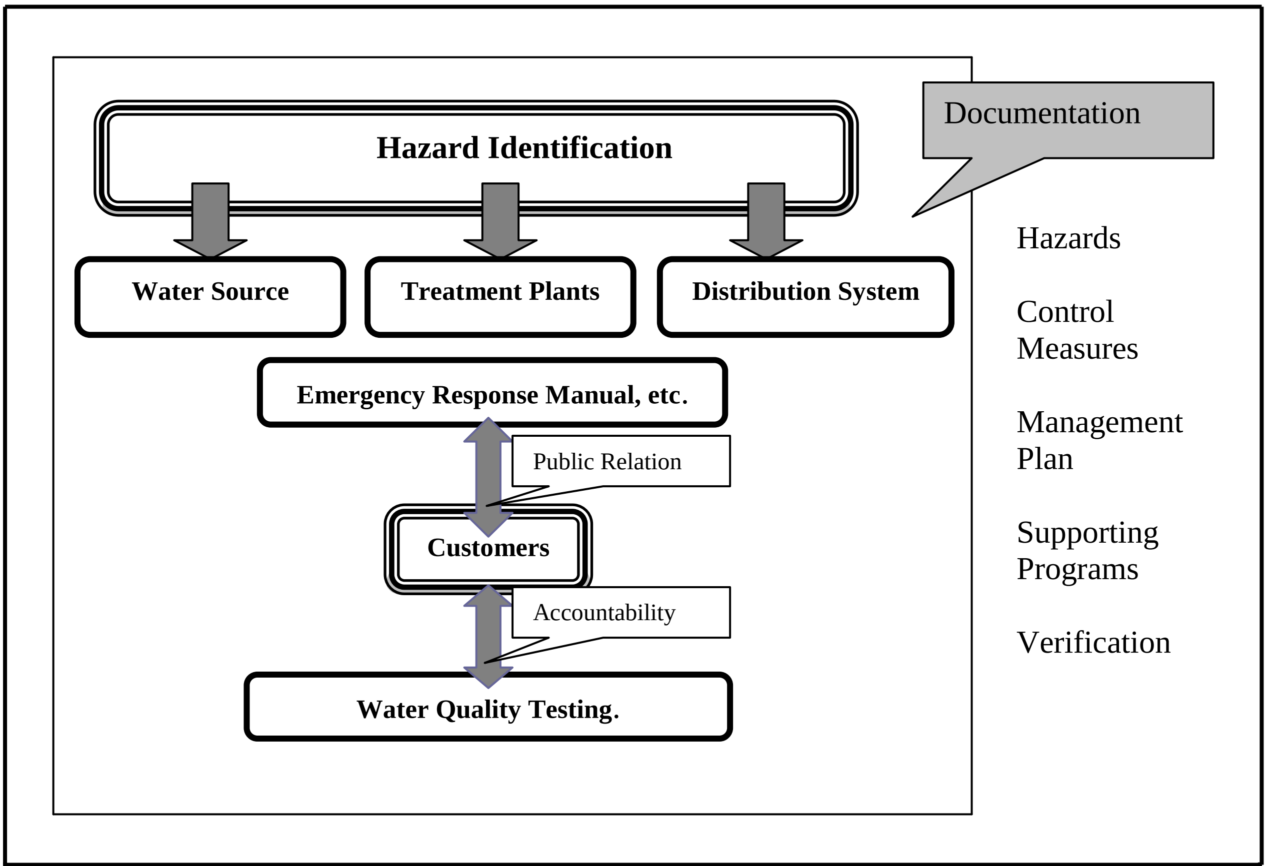

- R river surface water
- Raw water reservoir
- Ozone contactor
- Lime mixing tank
- CO2 mixing tank
- Rapid mixing chamber
- Sedimentation tank
- Rapid sand filter
- Chlorine contact tank

- Treated water reservoir
- Service reservoir
- Ozone production & application
- Residual ozone removal
- Lime solution production & application
- CO2 dosing
- Coagulant application
- Activated carbon application

- Flocculants aid application
- Chlorine-water solution application
- Lime solution production & application
- Sludge hopper
- Sludge pumping station
- Sludge thickener
- Sludge equalization tank
- Mechanical dewatering sludge

Fig. 4 Flow diagram of the water supply system

PRIORITIZING HAZARDUOS EVENTS FOR CONTROL

The definition of control measures should be based on a ranking of risks associated with each hazard or hazardous event. A risk is the likelihood of identified hazards causing harm in exposed populations in a specified time frame, including the magnitude of that harm and/or the consequences. Those hazardous events with the greatest severity of consequences and highest likelihood of occurrence should receive higher priority than those hazards whose impacts are mild or whose occurrence is very uncommon.

There are a variety of means by which prioritization can be undertaken, but most rely applying expert judgment to a greater or lesser degree. The approach discussed below uses a semi quantitative risk scoring matrix to rank different hazardous events. Within this approach, severity of impact is categorized into three major types of event: lethal (i.e. significant mortality affecting either a small or large population); harmful (i.e. primarily morbidity affecting either a small or large population); and, little or no impact. Table 2 and 3 shows the definition of a set of variables for likelihood/frequency of occurrence and combined severity/extent assessment with appropriate weighting of variables, and Table 4 indicates the final overall score of all possible combinations of the conditions. The approach recognizes that qualitative rather than quantitative information may be all that is available for decision making. However, the qualitative level of relative risk determined based on the likelihood and potential impacts of an event is evaluated using a matrix shown in Table 5, gives an example of that approach for the scenario in a chlorine analyzers for water supply.

The risk analysis model shown in tables is used by the HACCP to calculate the risk factor (i.e. score) for each identified hazard (s) arising from a hazardous event. The risk factor is defined as:

Risk Factor = Severity of Consequences (S) * Likelihood (L)

Table - 2 Risk assessment likelihood or frequency of occurrence scale.

Description	Definition	Weighting
Almost certain	Once per day	**5**
Likely	Once per week	**4**
Moderate	Once per month	**3**
Unlikely	Once per year	**2**
Rare	Once per 5 years	**1**

Table - 3 Risk assessment Severity of consequence or impact scale.

Description	Definition	Weighting
Catastrophic	Potentially lethal to large population	**5**
Major	Potentially lethal to small population	**4**
Moderate	Potentially harmful to large population	**3**
Minor	Potentially lethal to small population	**2**
Insignificant.	No impact or not detectable	**1**

Table – 4 A Simple risk ranking matrix

		Severity of Consequences or impact				
		Catastrophic *Rating: 5*	**Major** *Rating: 4*	**Moderate** *Rating: 3*	**Minor** *Rating: 2*	**Insignificant** *Rating: 1*
Likelihood or frequency of occurrence scale	**Almost Certain** *Rating: 5*	**25 (Very High)**	**20 (Very High)**	**15 (Very High)**	**10 (High)**	**5 (Moderate)**
	likely *Rating: 4*	**20 (Very High)**	**16 (Very High)**	**12 (High)**	**8 (High)**	**4 (Moderate)**
	Moderate *Rating: 3*	**15 (Very High)**	**12 (Very High)**	**9 (High)**	**6 (Moderate)**	**3 (Low)**
	Unlikely *Rating: 2*	**10 (Very High)**	**8 (High)**	**6 (Moderate)**	**4 (Low)**	**2 (Low)**
	Rare *Rating: 1*	**5 (High)**	**4 (High)**	**3 (Moderate)**	**2 (Low)**	**1(Low)**

We can used both a scoring approach as indicated by the numbers in table 4, and others which prefer non-numerical classifications describing the risk (as indicated Low, Moderate, High , and Very High). It should be stressed that when using the scoring approach it is the relative ranking based on the numerical categories rather than the numbers themselves that is important. Furthermore, in applying such approaches common sense is important to prevent obvious discrepancies arising from applying the risk ranking, for instance events that occur very rarely but have catastrophic effects should also be a higher priority for control than those events that have limited impact on health, but occur very frequently.

Table –5 hazardous events identified and assessed for the pumping system

Process Step	Hazardous Event	Hazard Type	Likelihood	Severity	Risk Score
Pumping System	Water pumped during an earthy storm event results in contaminated surface water from catchments that being pumped	Microbes and Chemicals (nutrients and potential pesticides from agricultural practices)	Unlikely (2)	Catastrophic (5)	10
	Cattle grazing near The resource and rain events result in contaminated surface water entering the resource	Microbes and chemicals (mainly nutrients)	Moderate (3)	Catastrophic (5)	15
	The pumped water from the resource causing naturally occurring chemicals for entering water	Chemicals	Rare (1)	Major (4)	4

CONTROL MEASURES

The approach provides a relative measure of potential risk that allows hazards present in a system to be prioritized for evaluation. Filtering was applied to distinguish significant hazards from those considered to be of less significance, and to separate hazards related to aesthetic concerns, which did not result in potable water becoming unsafe to consume. Risks with a risk factor equal to or greater than moderate were classified as significant risks to water quality and were assigned a higher priority for further investigation. Risks with a risk factor less than moderate (i.e. risks with a risk factor score of “low”) were classified as risks that did not pose a significant risk to water quality. These hazards were assigned a lower priority for further investigation.

After *Critical Control Points* CCPs identification, *Critical Limits* CL are established based on scientific or operational information. In this case, CLs. have been set according to internal standards, operating procedures, and performance targets of the Quality Management System. Some of the CLs were taken on the safety side of legal standards parameters, in order to guarantee the overall water quality of the system.

The observance of CLs is verified through a wide range of parameters that are monitored with on-site determination. A sampling and laboratory analysis program at different points of the system has also been included. It is expected that the control measures and monitoring activities are effective enough to smoothly control the routine functioning of the system. However, if and when a CL destruction is detected, corrective actions must be considered.

Performance reporting has been established by setting instructions for the daily functioning of the WSP (instructions for maintenance and control of CCP) as well as for the assessment of WSP in an annual basis. Analysis of external and internal factors and their influence on system performance, with special focus on communication, were also included.

As presented in figure (5), a structuring procedure for hazard identification of Treatment Stage and for set up control measures can be proposed for applying , CCPs, CLs and corrective actions.

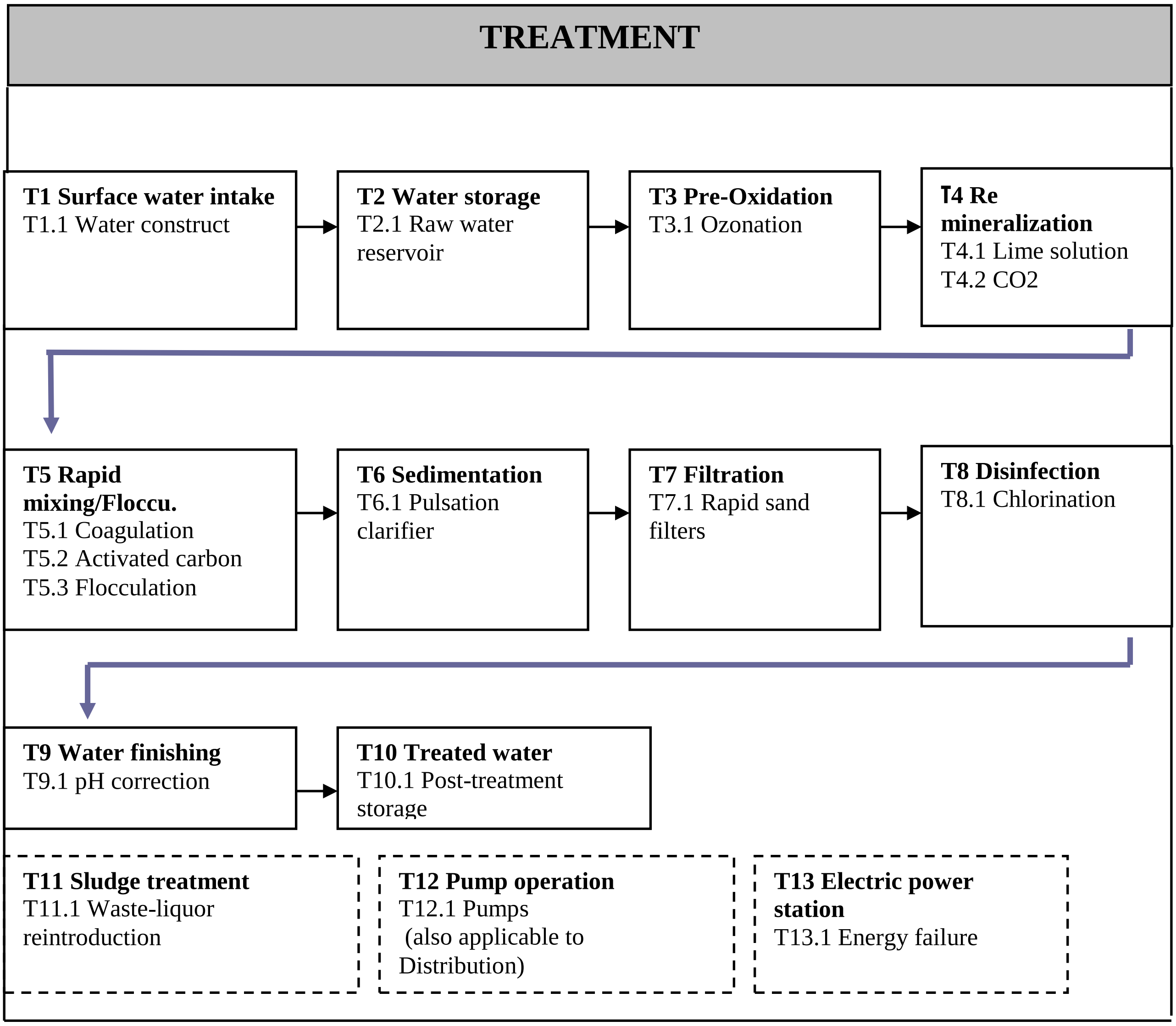

Fig.5 Water supply elements for WSP development

In the development of the (WSP) there were (16) CCPs identified but it is realized that many of the controls initially identified as CCP will not be further considered if the risks are adequately managed with “good management practices” or if effective subsequent control exists. This will be an obligatory point of revision after one year of (WSP) implementation.

OPERATIONAL ASPECTS

For each of the CCPs identified, a synthesis of risk management, control measures and corrective actions was established. As an example of the (Event T7 Filtration) in figure 5, which represent the (10th) CCPs, a designing of operational tables is given in Table 6, where the case of rapid sand filtration is considered. It shows an easy way to understand the major facts associated to this (CCP): particles and organic matter passing through the porous filter media are considered physical and biological hazards; control measures are implemented in order to guarantee the quality of filtered water; corrective actions consist of operational adjustments in previous treatment steps or higher dosing of chlorine at the disinfection step.

Table -6 CCP. Of Event T7 (Example for rapid sand filtration)

<table>
<tr><td>EVENT</td><td colspan="5">T 7.1.1 Filter bed supernatant water out of control</td></tr>
<tr><td>CCP. 10</td><td colspan="5">Hazard: physical and microbiological
Level of risk: high</td></tr>
<tr><td>Hazard</td><td colspan="5">T7.1.1.1: Organic matter and turbidity not removed</td></tr>
<tr><td>Control measures</td><td colspan="5">Develop a filter analyzer maintenance plan. Adjust the pumping system according to the flow rate to treat. Control backwash water recirculation. Establish an equipment calibration procedure</td></tr>
<tr><td colspan="6">Operational Monitoring</td></tr>
<tr><td>What?</td><td>Unity</td><td>CL</td><td>Who?</td><td>When?</td><td>Corrective Actions</td></tr>
<tr><td>Turbidity of treated water</td><td>NTU</td><td>0.695</td><td>A</td><td>On – Line</td><td rowspan="7">Adjust previous steps in order to optimize filtration efficiency. Higher disinfectant dosing</td></tr>
<tr><td>Color</td><td>mg/L Pt-Co</td><td>22</td><td>B</td><td>Weekly</td></tr>
<tr><td>Clogging optimal point</td><td>mm</td><td>2350</td><td rowspan="2">A</td><td rowspan="2">Whenever a criterion is reached</td></tr>
<tr><td>Filtration time</td><td>hour</td><td>70</td></tr>
<tr><td>Residual Aluminum</td><td>mg/L Al</td><td>0.2</td><td rowspan="2">B</td><td rowspan="2">Daily</td></tr>
<tr><td>Ammonia - N</td><td>mg/L NH4</td><td>0.7</td></tr>
<tr><td>Cryptosporidium</td><td>n.º/100 mL</td><td>0</td><td>B</td><td>Weekly</td></tr>
</table>

WSP PRACTICAL APPLICATION

The secretariat of Baghdad set up a special operations room to follow up (cholera) and take all measures to prevent the arrival in Baghdad and a follow-up laboratory tests on water and the product on a daily basis to ensure its fitness for human consumption and free of any distress pollution.

The results of the examination in all water projects demonstrated the safety net product water from pollutants and fitness for human consumption with an appropriate amount of chlorine disinfectants and to eradicate all kinds of microscopic bacteria and microbes. Table (7) shows the results of laboratory tests of water [2008 ,أمانة بغداد].

After one year of (WSP previous situation) practical application, a series of monthly reports are already available. From them it is possible to have the first understandings of capabilities, vulnerabilities and difficulties for an efficient system management. Figure 6 present example of turbidity removal efficiency by adding the chlorine proportions that mentioned the previous data and the results of laboratory tests of water in the system.

Table – 7 The results of laboratory tests of water[2008 ,أمانة بغداد]

Bacteriological Result	نسبة الكلورين mg / L	المشروع	التاريخ	
صالح للاستهلاك البشري	1.50	مشروع الكرخ/الطارمية	6/12/2008	1
صالح للاستهلاك البشري	1.60	مشروع شرق دجلة/سبع ابكار	6/12/2008	2
صالح للاستهلاك البشري	2.00,2.00,3.70	مشروع الوثبة/باب المعظم	6/12/2008	3
صالح للاستهلاك البشري	4.00,4.00	مشروع الكرامة/العطيفية	6/12/2008	6
صالح للاستهلاك البشري	3.30,2.62	مشروع القادسية/القادسية	6/12/2008	7
صالح للاستهلاك البشري	5.25	مشروع الدورة/الدورة	6/12/2008	8
صالح للاستهلاك البشري	2.00	مشروع الكرخ/الطارمية	7/12/2008	9
صالح للاستهلاك البشري	0.60	مشروع شرق دجلة/سبع ابكار	7/12/2008	10
صالح للاستهلاك البشري	3.42,3.21,3.52	مشروع الوثبة/باب المعظم	7/12/2008	11
صالح للاستهلاك البشري	5.00,4.00	مشروع الكرامة/العطيفية	7/12/2008	12
صالح للاستهلاك البشري	2.80,0.98	مشروع القادسية/القادسية	7/12/2008	13
صالح للاستهلاك البشري	3.00	مشروع الدورة/الدورة	7/12/2008	14
صالح للاستهلاك البشري	5..36,2.47	مشروع الوحدة/المسبح	7/12/2008	15
صالح للاستهلاك البشري	4.06	مشروع الرشيد / معسكر الرشيد	7/12/2008	16
صالح للاستهلاك البشري	2.00	فحص مشترك مع الصحة فقط /مركز صحي بلاط الشهداء	4/12/2008	17
صالح للاستهلاك البشري	3.25-3.50	فحص مشترك مع الصحة فقط /حي الحضر م / ٨٢٤	4/12/2008	18
صالح للاستهلاك البشري	1.50-2.10	فحص مشترك مع الصحة فقط /حي الحضر م / ٨٢٦	4/12/2008	19
صالح للاستهلاك البشري	2.01-2.72	مدينة الصدر م / ٥٢٣	4/12/2008	20
صالح للاستهلاك البشري	1.74-1.93	مدينة الصدر م / ٥٥٣	4/12/2008	21
صالح للاستهلاك البشري	1.73-2.81	مدينة الصدر م / ٥٣٢	4/12/2008	22
صالح للاستهلاك البشري	1.80-2.73	مدينة الصدر م / ٥٢٦	4/12/2008	23
صالح للاستهلاك البشري	1.28-1.54	حي الاورفلي م / ٥٥٥	4/12/2008	24
صالح للاستهلاك البشري	3.10-3.30	حي القادسية م / ٦٠٢	4/12/2008	25
صالح للاستهلاك البشري	2.80-3.00	حي القادسية م / ٦٠٤	4/12/2008	26
صالح للاستهلاك البشري	2.00	حي الكرادة / مستشفى عبد المجيد	4/12/2008	27
صالح للاستهلاك البشري	1.84	حي الكرادة م / ٩٠٩	4/12/2008	28
صالح للاستهلاك البشري	2.07-2.10	حي الكرادة م / ٩٠٥	4/12/2008	29
صالح للاستهلاك البشري	3.74-4.82	حي الكرادة م / ٩٠٧	4/12/2008	30
صالح للاستهلاك البشري	1.50-2.00	فحص مشترك مع الصحة فقط /حي الحرية م / ٤٢٦	4/12/2008	31
صالح للاستهلاك البشري	2.00-2.25	فحص مشترك مع الصحة فقط /حي الحرية م / ٤٢٤	4/12/2008	32
صالح للاستهلاك البشري	2.00-2.25	حي الربيع م / ٣٤٢	4/12/2008	33
صالح للاستهلاك البشري	2.00	حي الربيع م / ٣٤٠	4/12/2008	34
صالح للاستهلاك البشري	2.25	حي الربيع م /٣٣٨	4/12/2008	35
صالح للاستهلاك البشري	2.25	حي الربيع م /٣٣٢	4/12/2008	36

Process	Efficiency of Filtration% 04/12/2008	Efficiency of Filtration% 07/12/2008
Raw Water	0	0
Sedimentation	67.08	97.5
Filtration	100	98.33
Treated Water	95.65	98.33

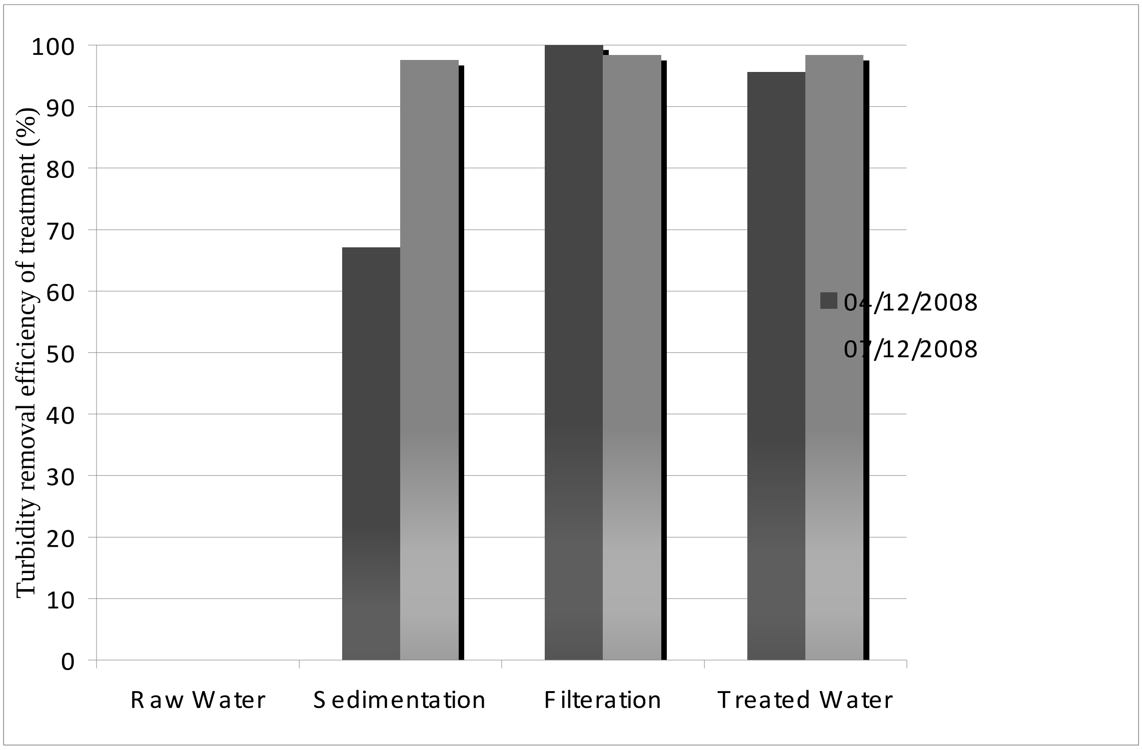

Fig. 6 Turbidity removal efficiency through the water supply system

CONCLUSIONS

WSP is a process control oriented management system that can help water suppliers to produce and deliver good and safe drinking-water, contributing in this way to improve public health protection.

Development and implementation of a WSP in The Department of Water Baghdad water, have also demonstrated that water suppliers can successfully adopt methodologies for risk assessment and risk management in drinking-water systems. This water company has already quality management systems according to ISO standards (for water quality monitoring, and for preventive maintenance of the water system). Performance reporting has been established by setting instructions for the daily functioning of the WSP (instructions for maintenance and control of CCP) as well as for the assessment of WSP in an annual basis.

Analysis of external and internal factors and their influence on system performance, with special focus on communication, were also included.

REFERENCES

- BARTRAM, J., FEWTRELL, L., STENSTRÖM, T. (2001) *Harmonized Assessment of Risk andRisk Management for Water-related Infectious Disease: An Overview*. *In* Water Quality: Guidelines, Standards and Health (edited by Fewtrell L. and Bartram J.), IWA Publishing, London.

- Davison A, Howard G, Stevens M, Callan P, Kirby R, Deere D and Bartram J. (2004). *Water*
- *Safety Plans.* WHO, Geneva.

- DEWETTINCK, T., VAN HOUTTE, E., GEENENS, D., VAN HEGE, K., VERSTRAETE, W. (2001) *Hazard Analysis and Critical Control Point (HACCP) to Guarantee Microbial Safe Water Reuse and Drinking Water Production: A Case Study*. (1998), Water Science and Technology 43, nº 12, European Community Directive 98/83/EC.

- Helmer, R, Bartram, J and Galal-Gorchev, H, (1999). *Regulation of drinking-water standards. Water Supply*, 17(3/4): 1-6.

- NADEBAUM P., CHAPMAN, M., MORDEN, R. and RIZAK, S. (2004), A guide to *Hazard Identification and Risk Assessment for Drinking Water Supplies*, CRC for Water Quality and Treatment Research Report Number 11.

- NOKES, C., TAYLOR, M. Towards public health risk management plan implementation in New Zealand. In Schmoll, O. and Chorus, I. Water Safety Conference Abstracts, Umweltbundesamt. Text 74/03, Berlin. SNOW, J. (1855), (2003), *On the Mode of Communication of Cholera*, John Churchill. England.

- Payment, P, Richardson, L, Siemiatycki, J, Dewar, R, Edwardes, M and Franco, E.(1991). *A*
- *Randomized trial to evaluate the risk of Gastrointestinal disease due to consumption of*
- *drinking water meeting current microbiological standards.* American Journal of Public
- Health 81(6): 703-708.

- STEVENS, M., McCORNELL, S., NADEBAUM, P., CHAPMAN, M., ANANTHAKUMAR, S., and McNEIL, J. (1995), *Drinking Water Quality and Treatment Requirements: A Risk-based Approach*. Water **22**, November/December.

- TIBATEMW, S.M., GODFREY, S., NABASIRYE, L., NIWAGABA, C. (2003). *Water safety Plans for utilities in developing countries – a case study from Jinja, Uganda*. WEDC, Loughborough, UK.

- VIEIRA, J.M.P. (2004), *Risk Management in Drinking-water (in Portuguese). In* Proceedings of XI Portuguese-Brazilian Symposium on Sanitary and Environmental Engineering. Natal-Brazil.

- أمانة بغداد ، دائرة السيطرة النوعية ، نتائج الفحوصات المختبرية للماء الصالح للشرب ،2008

NOMENCLATURES

Symbol	Description
CCPs	Critical Control Points
CLs	Critical Limits
HACCP	Hazard Analysis and Critical Control Points
L	Likelihood
QC	Quality Control
S	Severity
WSP	Water Safety Plan

HEAT AND MASS TRANSFER DURING AIR DRYING OF SWEET POTATO

Manal H. AL-Hafidh
Ass. Prof. /University of Baghdad

Shaimaa Mohammed Ameen
Mechanical Engineer

ABSTRACT

This study included the convective air drying of a single sweet potato sample which is taken as an ellipsoid with (40mm) in the longitudinal direction and (20mm) in the thickness direction. Convective heat and mass transfer takes place between the sample surface and its drying environment; while, unsteady heat conduction and moisture diffusion take place within the drying body without phase change for liquid (evaporation occurs at the surface only). The numerical solution of the mass, energy conservation equations was used; by applying the finite difference technique after using the body fitted coordinate system with grid generation techniques. A set of empirical correlations have been employed to determine the product properties and the important affecting factors on the drying process were studied. The results showed that the product temperature is increased and its moisture content is decreased with time and the increase in air velocity caused an increase in the heat transfer coefficient and as a result moisture content will decrease and this accelerates the drying process. The numerical results were compared with experimental results and showed good agreement.

الخلاصة:

تضمنت هذه الدراسة استخدام الهواء كوسط تجفيف لعينة مفردة من البطاطا الحلوة ذات شكل بيضوي ذات (40) ملم طول و(20) ملم سمك. يحصل ا نتقال الحرارة بالحمل بين سطح العينة ومحيط تجفيفها بينما يحصل انتقال الحرارة بالتوصيل وانتقال الرطوبة بالانتشار داخل العينة بدون حدوث تغير بالطور للسائل الرطوبي (التبخر يحصل على السطح فقط). تم استخدام الحل العددي لمعادلات حفظ الطاقة والكتلة باستخدام طريقة الفروقات المحددة بعد استخدام نظام مطابقة احداثيات الجسم مع تقنيات التوليد الشبكي. الحسابات العملية استخدمت في هذا البحث مجموعة من المعادلات التجريبية لحساب خواص المنتج مع دراسة اهم العوامل المؤثرة على عملية التجفيف بينت النتائج زيادة درجة حرارة المنتج ونقصان محتواه الرطوبي مع الزمن وان زيادة سرعة هواء التجفيف تسبب زيادة معامل انتقال الحرارة بالحمل وكنتيجة لذلك يتناقص المحتوى الرطوبي وهذا يعجل من عملية التجفيف.قورنت النتلئج العددية مع النتائج العملية وبينت توافق جيد.

KEY WORDS:
Heat and mass transfer, Convective drying, Conduction, Diffusion, Potato

INTRODUCTION:

Drying, in general, usually means removal of relatively small amounts of water from material. The purpose of drying food products is to allow longer periods of storage with minimized packaging requirements and reduced shipping weights .In the chemical industries, drying or dehydration is one of the most important processes used in the processing of food and in the storage of grains [Mulet, 1994].
Drying is a complex operation involving transient transfer of heat and mass along with several rate processes, such as physical or chemical transformations, which, in turn, may cause changes in product quality as well as the mechanisms of heat and mass transfer. Physical changes that may occur include: shrinkage, puffing, crystallization, glass transitions. In some cases, desirable or undesirable chemical or biochemical reactions may occur leading to changes in color, texture, odor or other properties of the solid products, many of these changes are functions of temperature, moisture content, and time. Therefore, undesirable effect could be better controlled, if temperature and moisture distributions in food as a function of drying time could be accurately predicted [Arun and Devahastin, 2004].

Food materials such as grains, fruits, and vegetables have microscopic capillaries and pores which cause a mixture of transfer mechanisms to occur simultaneously when subjected to heating or cooling. The complex interactions of various phenomena occurring within a material undergoing heating, solution dependent properties and the strong coupling between processes make modeling the transient moisture and temperature within the material a difficult task, so some simplified assumptions should be taken, like ignoring capillary action, all physical changes, chemical or biochemical reactions.
[Hassini and Azzouz, 2004], performed two models of diffusion to evaluate the moisture diffusion coefficient of potato during convective drying by using perforated tray. The first model was analytical solution based on Fick′s law. The diffusion coefficient was found to vary with air temperature and also increase with the thickness of the slab at a constant temperature level. The second model consist of solving numerically the equation of conservation of mass of both solid and liquid phase which was more adequate because it take into account the shrinkage phenomena.
In modeling drying, the most widely used mass transport model in Fick′s second law of diffusion using the moisture concentration difference as the driving force and Fourier's law for heat transport model. The heat and moisture transfer within individual particles of the material should be understood and accurately represented by a mathematical model .In the most general case, the transfer of heat and moisture must be considered simultaneously in order to accurately describe the transport processes within the material.

MATHEMATICAL MODEL:

The goal of the present model is to describe the drying process for a single sample of a sweet potato. This model is based on the fact that during the single-particle drying processes, moisture diffusion and heat conduction dominate inside that particle and convective heat and moisture transfer take place on the surface.

<u>Governing Equations:</u>

The assumptions are as follows:

1. the potato sample was taken as an ellipsoid having a known initial temperature and moisture distribution and subjected to a uniform convective environment of hot air as in **Fig1**
2. No phase changes occurs within the drying material i.e. evaporation occurs only at the surface.
3. Shrinkage phenomenon is not considered.

Based on the above assumptions, the 2-D governing equations in Cartesian coordinate system(x, y) can be expressed as [Yang, 2004]:

$$\rho\ c_p \frac{\partial\ T}{\partial\ t} = k\ \left(\frac{\partial^2 T}{\partial\ x^2} + \frac{\partial^2 T}{\partial\ y^2} \right) \tag{1}$$

$$\frac{\partial\ M}{\partial\ t} = D\ \left(\frac{\partial^2 M}{\partial\ x^2} + \frac{\partial^2 M}{\partial\ y^2} \right) \tag{2}$$

Initial and Boundary Conditions:

$$T(x, y, 0) = T_\circ \tag{3}$$

$$M(x, y, 0) = M_\circ \tag{4}$$

$$K\ \left(\frac{\partial\ T}{\partial\ x} + \frac{\partial\ T}{\partial\ y} \right) = h\ \ (T_{air} - T\ ) + h_{fg}\ h_m\ (\ M\ \rho\ - M_{air}\ \rho_{air}\ ) \tag{5}$$

$$D\ \rho\ \left(\frac{\partial\ M}{\partial\ x} + \frac{\partial\ M}{\partial\ y} \right) = h_m\ (\rho_{air} M_{air} - M\rho) \tag{6}$$

Material Properties and Methods of Calculation:

The sweet potato was the food material used in this study because the material properties calculation of the potato is available in different literatures. The calculation of these properties was as follows:

Specific Heat Calculation:

An empirical equation proposed by [Chemkhi and Zagroba, 2005] to calculate specific heat which takes into account the composition of food:

$$C_p = 4184\ (0.406 + 0.00146\ T + 0.203\ M - 0.0249\ M^2) \tag{7}$$

Thermal Conductivity Calculation:

An empirical equation developed by [Raisul and Mujumdar, 2005] for solid and liquid foods to calculate thermal conductivity:

$$K = \frac{0.049}{1\ +\ M}\ \exp\left[- \frac{47}{8.3143\ \times\ 10^{-3}} \left(\frac{1}{T} - \frac{1}{333.15} \right) \right] + \frac{0.611\ M}{1\ +\ M} \tag{8}$$

Moisture Diffusivity Calculation:

An empirical equation proposed by [Chemkhi and Zagroba, 2005] and [Kiranoudis and Maroulis, 1995] to calculate moisture diffusivity as follow:

$$D = a \exp\left(-\frac{b}{M}\right) \exp\left(-\frac{c}{T}\right) \tag{9}$$

Where:

a = 1.29×10^{-6}
b = 0.0725
c = 2044

Heat Transfer Coefficient Calculation:

The heat transfer coefficient is given by the following empirical equation [Tang and Cenkowski, 2000]:

$$h = 16.09 + 8.87 \times V^{0.53} \tag{10}$$

Mass Transfer Coefficient Calculation:

The mass transfer coefficient is given by the following empirical equation [Tang and Cenkowski, 2000]:

$$h_m = 0.01959 + 0.08073 \times V^{0.553} \tag{11}$$

Material Density Calculation:

[Raisul and Mujumdar, 2005] proposed an empirical equation to calculate the density of potato sample and as follow:

$$\rho = -10^{-3} M^4 - 6.4 M^3 + 55 M^2 - 154 M + 1253 \tag{12}$$

The thermal and physical properties for the heating media (air) are calculated according to the equations that are mentioned in different researches and as shown in **Table1**.

Transformation of Coordinate System:

The determination of the coordinate transformation is called grid generation. Once the coordinate transformation has been determined differential equations must be transformed from physical space (x,y) as shown in **Fig.(3)** to computational space (ξ, η) which is shown in **Fig. (4)**. The transformation relating the physical space and the computational space is specified by the direct transformation:

$$\zeta = \zeta(x, y),\ \eta = \eta(x, y) \tag{13}$$

Equation (13) can now be solved on a uniform grid in computational plane. The derivatives of ξ_x, η_x, ξ_y and η_y are called the metrics of the direct transformation. The Jacobean determinant J of the direct transformation is defined as

$$J = \frac{\partial(x,y)}{\partial(\xi,\eta)}$$
(14)

Transformation of the Governing Equations:

Equation (1) will now be used for transform the conduction equation from Cartesian (x, y) coordinate to (ξ, η) coordinate

$$\alpha \frac{\partial \psi}{\partial t} = \left(\lambda . \frac{\partial \psi}{\partial \xi} + \sigma \frac{\partial \psi}{\partial \eta} + \alpha \frac{\partial^2 \psi}{\partial \xi^2} - 2.\beta \frac{\partial^2 \psi}{\partial \xi \eta} + \gamma \frac{\partial^2 \psi}{\partial \eta^2} \right) \Big/ J^2 \tag{15}$$

$$D \frac{\partial \psi}{\partial t} = \left(\lambda . \frac{\partial \psi}{\partial \xi} + \sigma \frac{\partial \psi}{\partial \eta} + \alpha \frac{\partial^2 \psi}{\partial \xi^2} - 2.\beta \frac{\partial^2 \psi}{\partial \xi \eta} + \gamma \frac{\partial^2 \psi}{\partial \eta^2} \right) \Big/ J^2 \tag{16}$$

Where:

$$\sigma = \left[\left(\frac{\partial y}{\partial \xi} \right) Dx - \left(\frac{\partial x}{\partial \xi} \right) Dy \right] \Big/ J \tag{17}$$

$$\lambda = \left[\left(\frac{\partial x}{\partial \eta} \right) Dy - \left(\frac{\partial y}{\partial \eta} \right) Dx \right] \Big/ J \tag{18}$$

$$Dy = \alpha \frac{\partial^2 y}{\partial \xi^2} - 2\beta \frac{\partial^2 y}{\partial \xi \eta} + \gamma \frac{\partial^2 y}{\partial \eta^2} \tag{19}$$

$$Dx = \alpha \frac{\partial^2 x}{\partial \xi^2} - 2\beta \frac{\partial^2 x}{\partial \xi \eta} + \gamma \frac{\partial^2 x}{\partial \eta^2}$$
(20)

$$\alpha = \left(\frac{\partial x}{\partial \eta} \right)^2 + \left(\frac{\partial y}{\partial \eta} \right)^2 \tag{21}$$

$$\beta = \left(\frac{\partial x}{\partial \xi} \right)\left(\frac{\partial x}{\partial \eta} \right) + \left(\frac{\partial y}{\partial \xi} \right)\left(\frac{\partial y}{\partial \eta} \right) \tag{22}$$

$$\gamma = \left(\frac{\partial x}{\partial \xi}\right)^2 + \left(\frac{\partial y}{\partial \xi}\right)^2 \tag{23}$$

Finite-Difference Form of the Governing Equations:

The line successive over relaxation form of the finite-difference equation for the interior node i, j will be as follow:

$$\frac{\psi_{i,j}^{n+1}-\psi_{i,j}^{n}}{\Delta t} = \Gamma_{\phi}\left(\lambda\frac{\psi_{i+1,j}^{n}-\psi_{i-1,j}^{n}}{2.\Delta\xi} + \sigma\frac{\psi_{i,j+1}^{n+1}-\psi_{i,j-1}^{n+1}}{2.\Delta\eta} + \alpha\frac{\psi_{i+1,j}^{n}-2\psi_{i,j}^{n}+\psi_{i-1,j}^{n}}{\Delta\xi^2}\right.$$
$$\left. -2.\beta\frac{\psi_{i+1,j}^{n}-\psi_{i,j-1}^{n+1}-\psi_{i,j+1}^{n+1}+\psi_{i-1,j}^{n}}{4.\Delta\xi.\Delta\eta} + \gamma\frac{\psi_{i,j+1}^{n+1}-2\psi_{i,j}^{n+1}+\psi_{i,j-1}^{n+1}}{\Delta\eta^2}\right) \tag{24}$$

$$\begin{aligned}\psi_{i,j}^{n+1}\left(\frac{1}{\Delta t}+2\Gamma_{\psi}\gamma/J^2\right) &= \psi_{i+1,j}^{n}\left(\Gamma_{\psi}\lambda/J^2/2+\Gamma_{\psi}\alpha/J^2\right)+\psi_{i-1,j}^{n}\left(-\Gamma_{\psi}\lambda/J^2/2+\Gamma_{\psi}\alpha/J^2\right)\\ &+\psi_{i,j+1}^{n+1}\left(\Gamma_{\psi}\sigma/J^2/2+\Gamma_{\psi}\gamma/J^2\right)+\psi_{i,j-1}^{n+1}\left(-\Gamma_{\psi}\sigma/J^2/2+\Gamma_{\psi}\gamma/J^2\right)\\ &+\psi_{i,j}^{n}\left(\frac{1}{\Delta t}-2\Gamma_{\psi}\gamma/J^2\right)-2\beta\ \Gamma_{\psi}\psi_{\eta\xi}/J^2\end{aligned} \tag{25}$$

$$\begin{aligned}AP(i,j) &= \left(\frac{1}{\Delta t}+2\Gamma_{\psi}\gamma/J^2\right)\\ AE(i,j) &= \left(\Gamma_{\psi}\lambda/J^2/2+\Gamma_{\psi}\alpha/J^2\right)\\ AW(i,j) &= \left(-\Gamma_{\alpha\psi}\lambda/J^2/2+\Gamma_{\psi}\alpha/J^2\right)\\ AN(i,j) &= \left(\Gamma_{\psi}\sigma/J^2/2+\Gamma_{\psi}\gamma/J^2\right)\\ AS(i,j) &= \left(-\Gamma_{\psi}\sigma/J^2/2+\Gamma_{\psi}\gamma/J^2\right)\\ SU(i,j) &= \psi^{n}(i,j)\left(\frac{1}{\Delta t}-2\Gamma_{\psi}\gamma/J^2\right)\end{aligned} \tag{26}$$

Where Γ_{ψ} denotes ($k/\rho\ c_p$) or D.

$$\begin{aligned}AP(i,j)\psi_{i,j}^{n+1} &= AE(i,j)\psi_{i+1,j}^{n}+\psi_{i-1,j}^{n}AW(i,j)+AN(i,j)\psi_{i,j+1}^{n+1}\\ &+AS(i,j)\psi_{i,j-1}^{n+1}+Su\,\psi_{i,j}^{n}\end{aligned} \tag{27}$$

RESULTS AND DISCUSSION

Fig (4) shows the temperature distribution as a function of location. It can be seen that the temperature of the product drops sharply at the beginning of the drying process .This drop indicates that the heat convected from the drying air to the product surface can not sustain the higher evaporation rate of moisture during the initial period of drying (initial cooling period of the product). Consequently, product surface temperature increases rapidly after fifteen minutes which is clearly seen in **Fig (4)** but the temperature inside remains at low values. Also **Fig (4)** clearly shows that the product temperature in thickness direction increased more quickly than that in the longitudinal direction.

Evaporation of liquid moisture takes place from the product surface by absorbing the heat of vaporization as well as heat of desorption when removing bound moisture. As the initial moisture content at the drying surface of the product is high, it can evaporate rapidly at the beginning of the drying process. In **Fig (5)** Product moisture in thickness direction decreased more quickly than that in the longitudinal direction starting from the center to the surface due to the small diffusion distance of the product in thickness direction (20mm) relative to the distance in longitudinal direction (40mm). Also **Fig (5)** shows profiles of moisture content which have a parabolic shape before flatting at end of drying.
The convective heat transfer coefficient is directly related to the air flow velocity by **eq.(10).**An increase in air velocity directly influences this coefficient, which promotes a higher product temperature and larger moisture loss for a higher air velocity and this higher temperature increases the diffusivity of mass transfer**.** **Fig. (6) & (7)** is clearly shown moisture will be decreased and temperature will be increased more fast when the heat transfer coefficient value is high and that will accelerate the drying process .This can be explained by the fact that the air flow is responsible for decreasing moisture content; while increasing this velocity this favors the transport phenomenon.

Table (1) The physical and transport properties for the drying air [Raisul Islam and Mujumdar, (2005].

Property	Expression
ρ_{air}	$\rho_{air} = -3.5101\times10^{-8}T_{air}{}^{3} + 1.58398\times10^{-5}T_{air}^{2} - 4.6995\times10^{-3}T_{air} + 1.2921$
μ_{air}	$\mu_{air} = 1.7676\times10^{-13}T_{air}{}^{3} - 5.541110^{-11}T_{air}^{2} + 4.9832\times10^{-8}T_{air} + 17.1964\times10^{-6}$
$\Pr_{air}$	$pr_{air} = -2.2727\times10^{-8}T_{air}^{3} + 4.1991\times10^{-6}T^{2air} - 3.5335\times10^{-4}T_{air} + 0.719$
K_{air}	$K_{air} = 6.8181\times10^{-10}T_{air}^{3} - 1.474\times10^{-7}T_{air}^{2} + 8.0291\times10^{-5}T_{air} - 0.024$

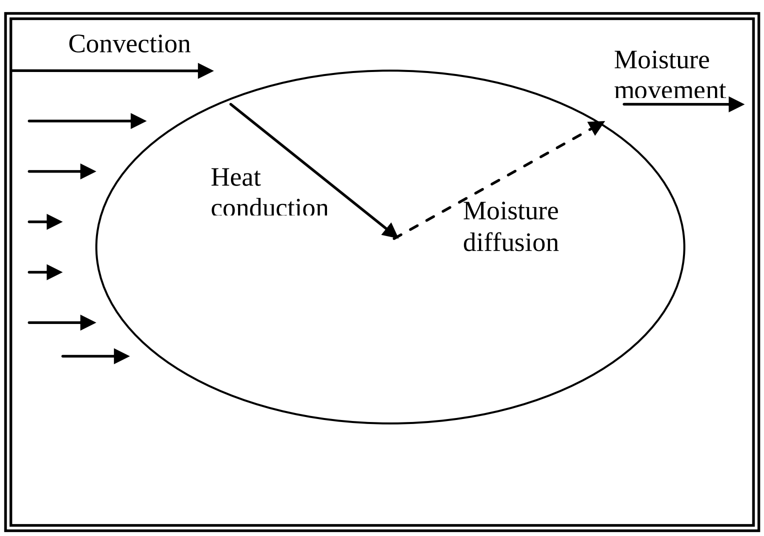

Fig 1 heat and mass transfer during drying of the product

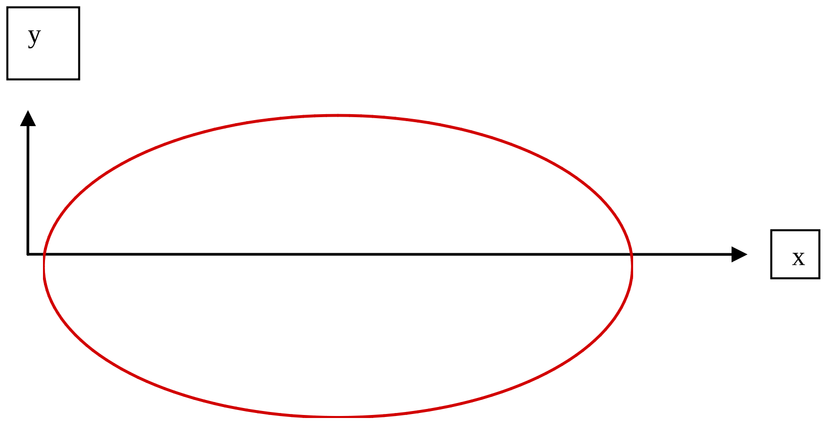

Fig. (2) Solution region in (x, y) plane

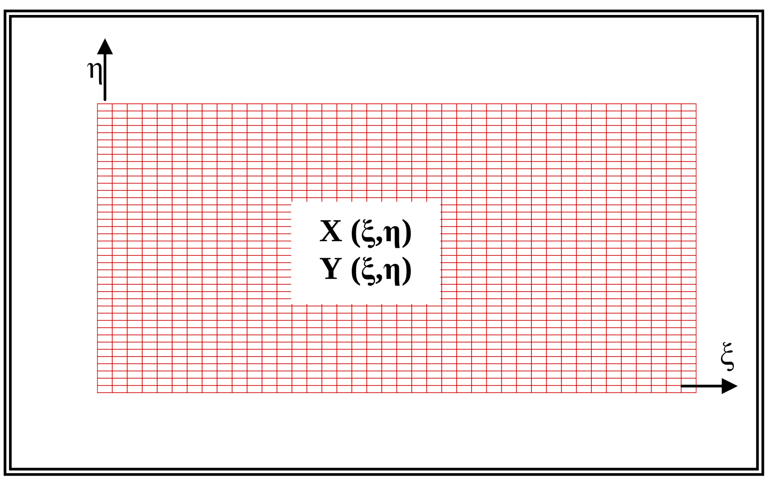

Fig (3) Transformed region in (ξ, η) plane

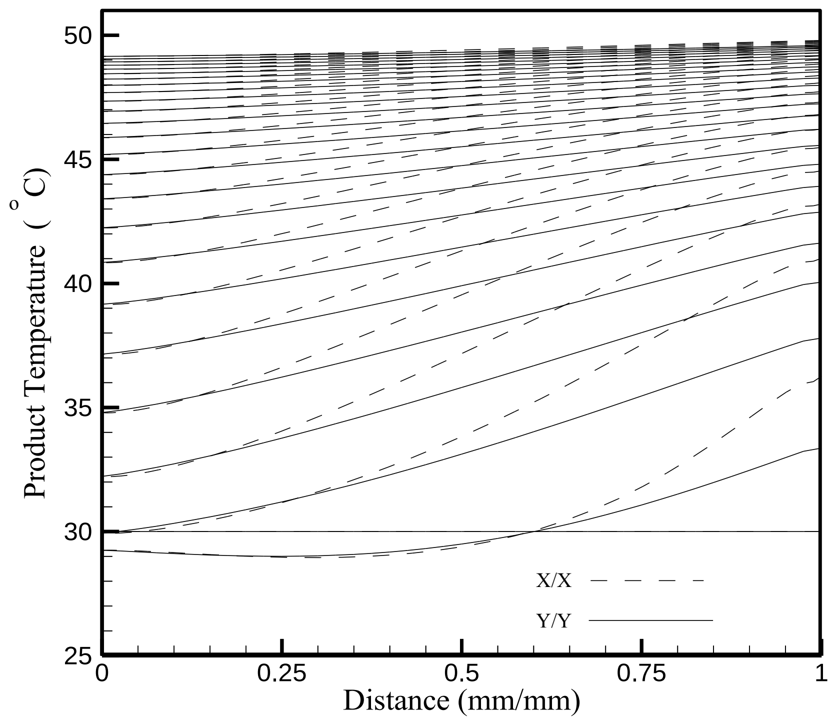

Fig (4) Temperature profiles at time intervals of 15 minutes.

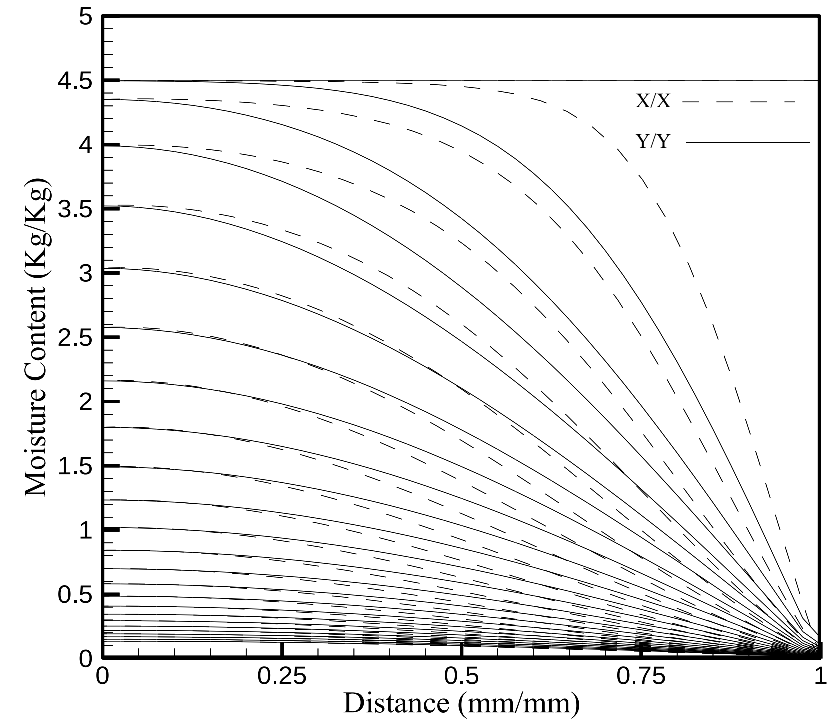

Fig. (5) Moisture content profiles at time intervals of 15 min

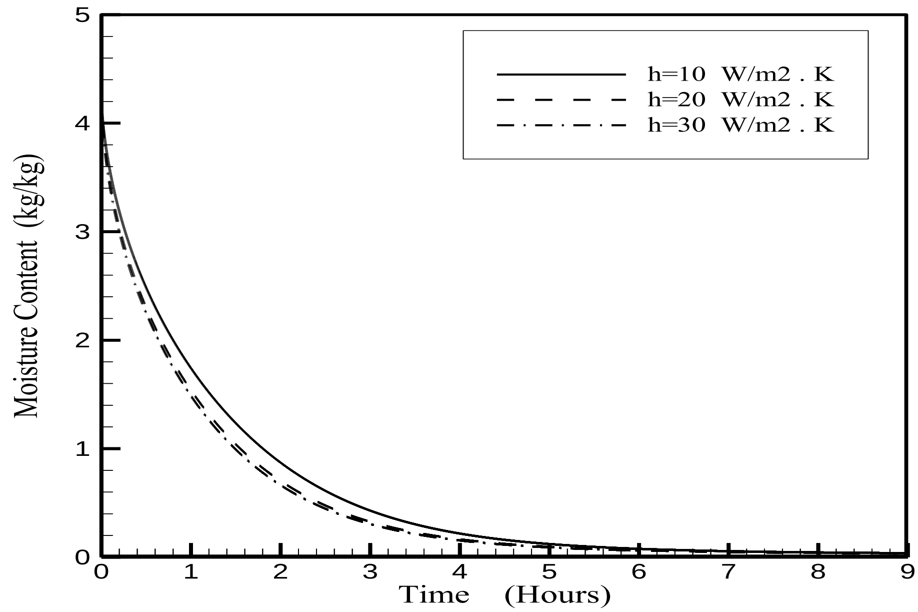

Fig. (6) The effect of convective heat transfer coefficient on moisture loss during drying

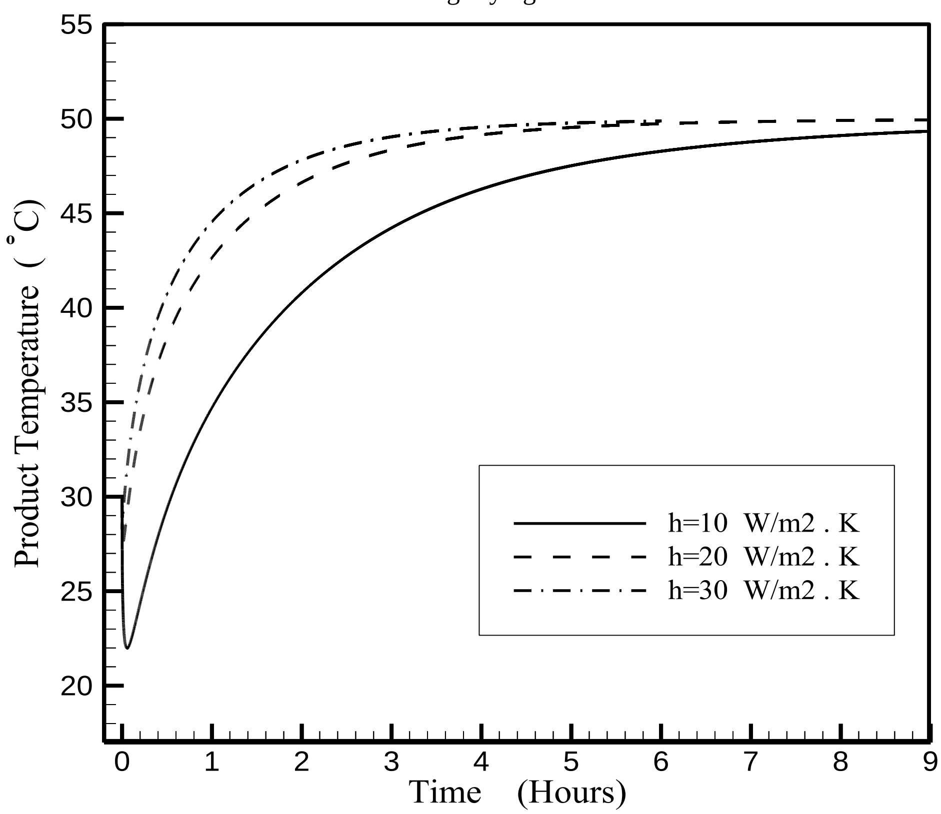

Fig. (7) The effect of convective heat transfer coefficient on product temperature during drying

CONCLOUSIONS

From the present work results, the following conclusions can be obtained:

- The product temperature in thickness direction increased more quickly than that in the longitudinal direction.
- Product moisture in thickness direction decreased more quickly than that in the longitudinal direction starting from the center to the surface.
- Moisture decreased and temperature increased more fast when the heat transfer coefficient value is high and that will accelerate the drying process.

REFERENCES

- Arun S. Mujumdar and Devahastin (2005), Fundemantal Principle of Drying, Chapter One, Taylor And Francis, New York.

- Chemkhi S., Zagroba F. and Bellagi A. (2005), Modeling and Simulation of Drying Phenomena with Rheological Behaviour, Brazilian journal of Chemical Engineering, Vol. 22, no.02, pp153-163, April-June.

- Hassini L. and Azzouz S. (2004), Estimation of the Moisture Diffusion Coefficient of Potato During Hot Air Drying, Proceeding of the 14th International Drying Symposium, Brazil, 22-25 August, Vol. B, pp. 1488-1495.

- Kiranoudis and Maroulis C. T. (1995), Heat and Mass Transfer Model Building In Drying, Int. J. of Heat Transfer, Vol. 38, pp.463-480

- Mulet A. (1994), Preservation of Fruits and Vegetables by Drying” J. of Food Eng., Vol. 22, pp329-348.

- Raisul Islam Md. and Mujumdar A. S. (2005), Periodic Multi Mode Batch Drying of Heat-Sensitive Materials-Engineering Application of the Diffusion Equation, Int. J., Vol.09, no.2, pp.325-347.

- Tang Z. and Cenkowski S. (2000), Dehydration Dynamic of Potatoes in Superheated Steam and Hot Air, Canadian Agricultural Engineering, Vol.42, no.1.

- Wu B. and Yang W. (2004), A Three Dimensional Numerical Simulation of Transient Heat and Mass Transfer Inside a Single Rice Kernel During The Drying Process, Silsoe Research Institute , Biosystems Engineering, Vol. 87, no.2, pp.191-200.

NOMENCLATURE

Symbol	Definition	Units
C_P	Specific heat of product at constant pressure	J/kg.°K
D	Moisture diffusion coefficient in product	m^2/ s
h_m	Mass transfer coefficient of vapor in air	m/ s
h	Convective heat transfer coefficient in air	W/m^2. °K

h_{fg}	Latent heat of vaporization of water	J/kg
k	Thermal conductivity	W/m.°K
k_{air}	Thermal conductivity of air	W/m.°K
M	Moisture content	kg of water/kg of dry solid
M_o	Initial moisture content	kg of water/kg of dry solid
M_{air}	Air moisture content	kg of water/kg of dry solid
Pr_{air}	Prandtl number of air	-
T	Product temperature	°K
T_o	Initial temperature of the product	°K
T_{air}	Drying air temperature	°K
t	Time	sec
V	Air velocity	m/ s
X	Axis along product length	m
Y	Axis along product thickness	m

GREEK SYMBOLS

Symbol	Definition	Units
ρ	Density of product	kg/m^3
ρ_{air}	Density of air	kg/m^3
μ_{air}	Dynamic viscosity of air	kg/m. s
ξ, η	General coordinates	-

SUBSCRIPTS

Symbol	Definition
air	Drying air
o	Initial

EXPERIMENTAL AND FINITE ELEMENT INVESTIGATION ON THE LOAD – SLIP BEHAVIOR OF COMPOSITE PUSH OUT SEGMENTS USING VARIOUS SHEAR CONNECTORS

by
Laith Khalid Al- Hadithy [1] (Ph.D.) , Khalil Ibrahim Aziz [2] (Ph.D.) , Mohammed Raji M. AL-Alusi [3] (M .Sc)
[1] Department of Civil Engineering , Nahrain University , Iraq
[2] Department of Civil Engineering , Al-Anbar University , Iraq
[3] Department of Civil Engineering , Al-Anbar University , Iraq

ABSTRACT

The study described herein deals with experimental and finite element modeling of a variety of composite steel-concrete column segments using shear connectors of different shapes and sizes to provide resistance to slip at steel – concrete interfaces . Hence , it represents a qualitative transition in the experimental and analytical investigations on shear connectors effectivity at steel – concrete interfaces , as most studies in the field of shear connectors were devoted to composite beam and slab – systems .

Three types of shear connectors – with four concrete grades for each type – were used in fabricating composite specimens . The twelve composite prototypes were subjected to push – out test individually to examine their behavior by measuring the slip values for each load incremental till failure , thus determining the resistance extent of each connectors type and specifying the failure mode at interface .

A nonlinear three – dimensional finite element analysis have been carried out on twelve composite column segments using **ANSYS** computer program (5 th version , 2002) to investigate their behavior and predict their load – slip relationships , equivalent stress distributions and concrete cracking patterns . The defined numerical modeling included using the eight node isoparametric brick element with smeared reinforcement (**SOLID** 65) and the eight node isoparametric steel brick element (**SOLID**45) , to model the reinforced concrete medium and the steel section and shear connectors , respectively , considering perfect bond between concrete and steel reinforcing bars . Nonlinear properties including cracking and crushing of concrete , yielding of steel section and reinforcement , and nonlinear bond – slip at interface were also considered .

Comparison of the experimental and theoretical results has shown good agreement that verifies the accuracy of the finite element model based on the smeared crack model of concrete .

Results have detected the development of the relative movement (slip) be at all ranges of the load-slip relationship at interface even with using effective shear connection and /or high quality concrete.

The headed studs have revealed the highest slip resistance and ultimate load over the channel and the L-shaped studs . The high strength concrete has also revealed the same superiority over the other three tested types of concrete .

التحري التجريبي وبالعناصر المحددة لسلوك الحمل- الانزلاق للقطع المركبة ذوات الأنواع المختلفة من روابط القص

الخلاصة :

تعنى الدراسة الموصوفة أدناه بالفحص المختبري والتمثيل بالعناصر المحددة لمجموعة متنوعة من قطع الأعمدة المركبة الحديدية – الخرسانية ذوات روابط القص بمختلف الأشكال والمقاسات لإعطاء مقاومة الانزلاق عند أسطح التلامس بين الحديد والخرسانة .

تمثل هذه الدراسة انتقاله نوعية في الأبحاث العملية والتحليلية في مجال فعالية روابط القص عند أسطح التملس الحديدية – الخرسانية لكون الأبحاث في مجال روابط القص منذ ثمانينات القرن الماضي ولهذا الحين – تختص في مجال البلاطات وأنظمة السقوف والعتبات المركبة .

تم استخدام ثلاثة أنواع من روابط القص – مع أربعة أنواع من الخرسانة لكل واحد منها - في تصنيع وتحميل وفحص قطع الأعمدة المركبة .

تم إخضاع نماذج الأعمدة المركبة الاثني عشر تلك إلى فحص الانضغاط push –out test بشكل منفرد لاختبار سلوك كل منها بواسطة قياس مقدار الانزلاق لكل قيمة حمل إضافية ولحين الفشل ، وبهذا يتم تحديد مدى مطاولة كل نوع من أنواع رباطات القص في مقاومة التحميل وتحديد شكل الفشل عند سطح التماس لكل نموذج .

تم استخدام تحليل لاخطي ثلاثي الأبعاد بطريقة العناصر المحددة باستخدام برنامج الحاسوب (ANSYS)(الإصدار الخامس ، 2002) في دراسة السلوك الإنشائي لقطع الأعمدة المركبة الاثني عشر واستقراء علاقة الحمل – الانزلاق لكل منها ، مع استقراء توزيع الإجهاد المكافئة وأنماط التشققات خلال الأوساط الخرسانية المسلحة ، يتضمن النموذج الرقمي المذكور استخدام العنصر الطابوقي الايزوبارامتري الخرساني ثماني العقد ذي التسليح الموزع (**SOLID** 65) ، العنصر الطابوقي الايزوبارامتري الحديدي ثماني العقد (**SOLID**45) لتمثيل الوسط الخرساني المسلح ، و مقطع الحديد الإنشائي ، وروابط القص على التوالي مع افتراض ترابط تام بين الخرسانة وحديد التسليح .

تم أيضا الأخذ بنظر الاعتبار تأثيرات الخصائص اللاخطية للمواد والمشتملة على التشقق والتهشم للخرسانة ، إجهاد الخضوع لمقاطع الحديد الإنشائي ولقضبان التسليح ، وظاهرة الانزلاق اللاخطي عند الترابط في أسطح التماس .

بينت المقارنة بين النتائج النظرية والنتائج العملية توافقاً جيداً وبذلك يتم إثبات دقة نموذج العناصر المحددة المستخدم والمبني على نمط التشقق المنتشر في الخرسانة .

أثبتت النتائج أيضاً وجود حركة نسبية (انزلاق) على امتداد أسطح التماس بين الحديد والخرسانة لغاية الفشل مع تحديد التطور عبر مراحلها لجميع النماذج الاثني عشر حتى مع استخدام روابط قص كفوءة او خرسانة عالية الخصائص .

أبدت روابط القص من نوع القضبان ذوات الرؤوس الكبيرة (headed studs) تفوقاً على النوعين الآخرين المستخدمين من روابط القص

(مقطع ساقية ومقطع L) في مقاومة الانزلاق والحمل الأقصى . كما أعطت النماذج ذات الخرسانة من نوع

خرسانة عالية المقاومة
(HSC) تفوقاً في نفس الخصائص – على الأنواع الثلاث الأُخرى من الخرسانة المستخدمة .

NOTATION:

A_{co} Cross sectional area of stud shear connector.

Ac Cross section area of concrete.

As Cross section area of steel .

Ast Cross section area of steel in tension .

E_c Concrete modulus of elasticity.

E_s Steel modulus of elasticity.

f_{cu} Cube compressive strength of concrete.

f_y Yield strength of steel beam .

G_s Shear modulus of steel.

h_c Thickness of concrete block

K_n Normal stiffness of connector.

Ks Stiffness of connectors per unit length (kN/mm2)

N Number of shear connectors

R.C Reinforced concrete .

S Spacing between shear connectors.

Ss Slip at the steel-concrete interface

β_c , β_o Shear transfer coefficient for closed and opened crack.

γ Slip.

ε Strain.

ε_y Yielding strain of steel plate.

ABBREVIATION:

LWAC Light weight aggregate concrete

NWC Normal weight concrete

FGC Fine grain concrete

HSC High strength concrete

CHBDC Canadian Highway Bridge Design Code

INTRODUCTION:

Numerous amount of research work was done in the filed of composite steel- concrete beams since the early fifties of the last century. However the most important ones in the last six years are denoted here.

In 2002, partial interaction analysis of beam - column members was made by Wu et al. **[1]** , by extending the classic linear elastic partial interaction theory to allow for axial forces and also boundary conditions associated with plastic hinges . Najem **[2]** , in 2003, carried out two theoretical models on partially layered beams to simulate a multi- layer beam with interlayer slip. The difference between the two models concerns the neglect (or regard) of both slip and separation between the layers of the beam . Validation of those models was verified by previous experimental evidentce. A model for predicting the stiffness behavior of the steel- concrete composite beam under negative bending at the serviceability limit state with different degrees of shear interaction was developed by Nile et al. **[3]** , in 2004 . Accuracy of the proposed analytical method in predicting deflection of a cantilever beam was verified on the bases of comparison with finite element modeling and experimental investigation. In 2005 Aziz **[4] ,** conducted a theoretical analysis and an experimental investigation of multilayer composite steel – concrete beams of partial interaction that permits slip and separation between layers. The developed method of analysis led to a set of differential equations for separation and slip which were solved numerically by the finite difference method **[4]** . Recently , in 2006 , the behavior of ten steel - concrete – steel sandwich (SCSS) beams of fully threaded bars (connected to upper and lower steel plates by nuts) as shear connectors was studied by Zebun **[5]** , in addition to twelve push-out tests using threaded bars of different sizes –as shear connectors . His experimental results showed that the procedure of calculating the ultimate load of sandwich beams based on plastic analysis can safely be used with a reduction factor of o.8 for the shear connectors ultimate force obtained from the push –out test **[5] .**

Parallel to the investigative effort defined above, several researches in the field of shear –connector behavior and push - out test have been performed . The most recent ones are highlighted herein.

Slobodan and Dragoljub **[6]** , in 2002 reviewed the most important analytic expressions for the strength of shear connectors with special attention to the recommendation given by the European standard Ec(4) **[7]**, and gave a commentary in that field. In 2004 , Deanna and Rambo –Roddenberry **[8]** , performed a comprehensive experimental study including 117 push- out tests on solid and composite slabs , whose results, along with 61 other beam tests were used to propose and veriefy a new stud strength reduction model. Experimental investigation on shear connection between steel and high strength light weight concrete (HSLWC) was performed by Valente and Cruz **[9]** , in 2005, to evaluate load-slip behavior . Larose et al **[10]** , conducted , in

2006, an experimental testing regime using push-out test specimens constructed with precast concrete panels connected to steel flanges with steel studs within a circular grout pocket to investigate the reduction in ultimate strength after cyclic loading. That study was done to examine the validity of embedding clustered shear studs in high strength grout for construction using precast deck panels according to the Canadian Highway Bridge Design Code (CHBDC) requirements . An investigation on the effect of confining reinforcement on the shear capacity and ductility of polypropylene concrete –steel composite systems was made by Maleki and Mahoutian **[11]**, in 2007 through several monotonic push -out test on this concrete type with channel shear connectors . Based on comparisons with result of the specified test setup comprising ordinary concrete specimens or polypropylene concrete specimens of confining reinforcement they concluded that the polypropylene fibers have no significant effect on the ductility of steel-plain concrete composite system , while stirrups in concrete blocks cause this property to increase . Lastly ,Thorsten **[11]** , studied the behavior of light weight aggregate concrete (LWAC) in composite specimens of headed studs in push-out test setup in 2008. He concluded that the empirical basic design rules given in EC(4) **[7]** , for headed studs in normal NWC underestimate the real shear resistance considerably in the case of LWAC. Hence it will be necessary to work out new design formulas for the application of LWAC **[11]**.

The privilege of the present study over the preceeding ones in the specified scope comes firstly from its embodiment to a wide and comprehensive experimental investigation of the shear –slip behavior for steel - concrete composite segments under push –out test including stiffness, ductility and ultimate resistance of those segments for three main types of shear connectors and for four types of concrete NWC , LWAC , FGC and HSC separately (thus forming twelve autonomous cases), and making comparisons to show effects of shear connectors and concrete types. Moreover, the present study has recorded an antecedence in the finite element modeling of such composite segments under push-out test using ANSYS finite element program which has given accurate results as in comparison with experimental results.

SHEAR TRASFER MEANS AND TESTING

<u>Definition</u>:

In steel-concrete composite structural members (primarily beams) the force applied to the interface between the two components is mainly, but not entirely, longitudinal shear. The interface is an origin of severe and complex stresses that require accurate analysis , therefore methods of connection have been developed empirically and verified by tests.

<u>Shear Connector Types and Behavior</u>*:*

Shapes of shear connectors in common use are specially established to provide adequate resistance to uplift as well as slip. They may be divided into two categories :(i) rigid connectors (bars or tees with hoops);and(ii)flexible connectors (studs and channels). The two groups differ in the mode of failure . While rigid connectors tend to cause higher stress concentrations in the surrounding concrete or even weld failure, the failure mode of flexible connectors is more consistent and less catastrophic as they derive their resistance essentially through bending of the connectors. Some commonly used types of connectors are shown in Fig 1. The rigid bar, tee and channel connectors are limited to shear transfer in one direction only ,while the headed stud

connectors can resist and transfer shear in any direction perpendicular to the shank, making it the more useful connector. Adding its simple fastening and little obstruction to reinforcement in concrete medium it has become the most common type in practice. It was recommended **[12]** , for that connector , that the shank diameter should not exceed twice the thickness of the steel part so that the full static strength of the stud can be utilized. In the present study the headed stud, channel and L-shaped types of shear connectors –shown in Fig1 **a**) and **c**) – have been used

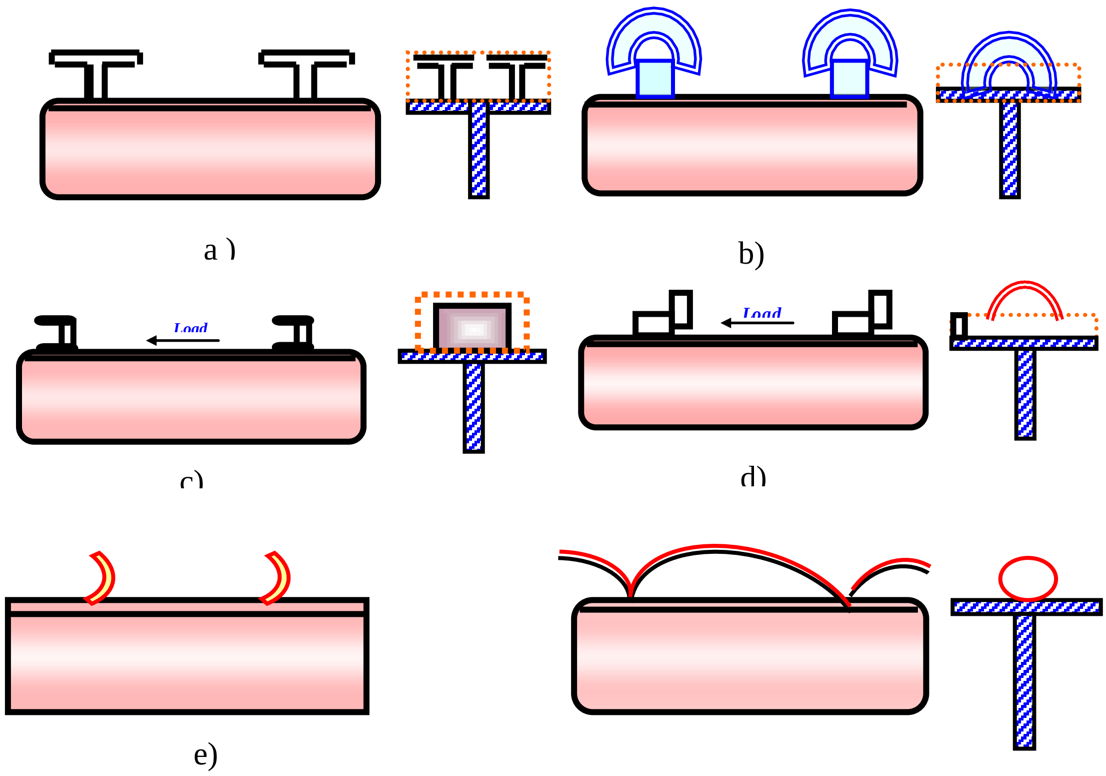

Fig.1: Types of Shear Connectors [4]

a) Headed Stud Connector , b) Bar Connector , c) Channel Connector , d) Tee Connector e) (L –shape Connector , f) Helical Connector .

Fig. 2 shows variation of the bearing stress on the shank of a headed stud connector with stress concentration near its base reaching four times the concrete cube strength owing to the concrete restraint there by the steel part, the shank of stud and the reinforcement [13]. The two major modes of failure are crushing of the concrete surrounding the connector (for sutds with large diameter)and connector shearing off at the base (for slender studs)

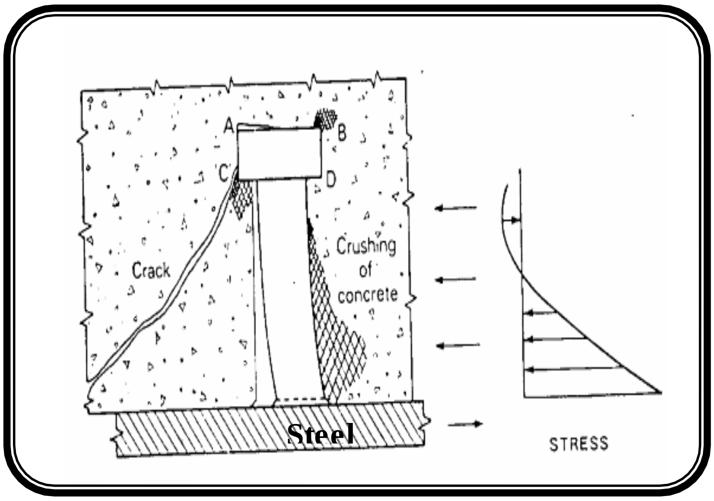

Fig.2 : Stress distribution on the Shank of a headed stud [13]

Push - out Test :

The shear connector property of most design relevance is the relationship between the transmitted shear force and the slip at interface. The load - slip curve should ideally be found from tests on composite beams . However , most of such data on shear connectors can be obtained from various types of " Push-out " tests shown in Fig. 3 in which the flanges of a short steel I-section segments is connected to two small reinforced concrete blocks [7, 12].

EXPERIMENTAL WORK :

Description and Classification of the Tested Prototypes :

With reference to Fig. 3 , the typical push –out test prototype of the present research work consists of a 560 mm long 254mm*147mm*43mm UB standard I-section connected at its two flanges to two 460mm *300mm*150mm reinforced concrete blocks by means of shear connectors welded to its flanges . The concrete blocks are reinforced by 10-mm diameter deformed steel reinforcing bars of mechanical properties shown in Table 1 . Their anchorage ends were made according to the ACI318-2002 sections 7.1 and 7.2

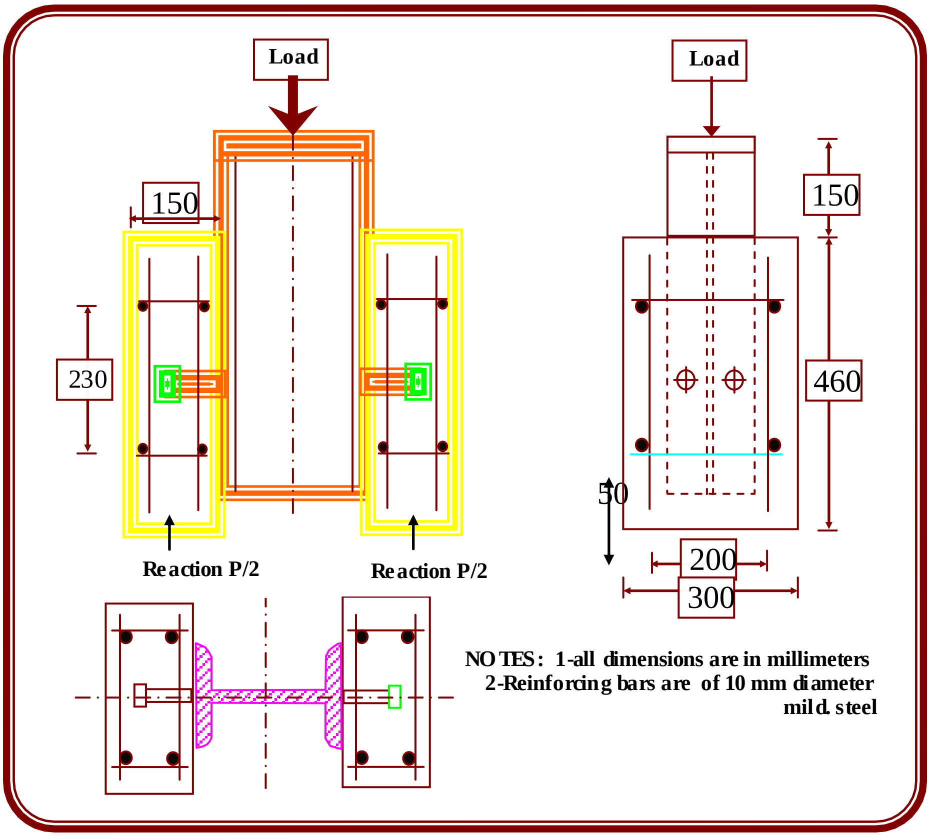

Fig .3: Schematic diagram for the typical push – out test prototype of the present work

i) Based on shear connector type :

headed stud shear connector containing prototypes : S- connector type .

channel shear connector containing prototypes : C - connector type .

L- shaped shear connector containing prototypes : L- connector type .

	Yield Stress (Fy) MPa	Ultimate Strength (Fu) Mpa	%Elongation at Rupture	Modulus of Elasticity (E) GPa
Ø10mm Reinforcing Bars	**285**	**510**	**20**	**203**
Ø19mm Smooth Bars for Stud L-connectors	**290**	**580**	**24**	**202**
UNP Channel for C-connectors	**240**	**540**	**24**	**205**
I-section	**248**	**400**	**17**	**205**

The S- and L- type connectors are made of 19mm diameter smooth bars whose lengths are 100mm and 210mm , respectively . Stud head of the S-type connector is of 30mm diameter . The C-type connector is a 60mm in length of UPN 100 standard channel section whose web depth , flange width and thickness are 80mm ,40mm and 4mm respectively . Mechanical properties of the specified steel bar and channel are given in Table 1 .

Any prototype of S-or L-type connectors contains two connectors –in one row welded to each flange , while each flange of any C- type connector prototype contains one connector only . Geometries , numbers , location and configurations of the three types of shear connectors are shown in Plate 1 .

Table 1 : Mechanical properties of the reinforcing bars , smooth bar and channel section used to form the three types of shear connectors , and the used steel I- section .

a) b) c)

Plate 1 : Typical prototypes before casting of concrete showing :
a) S- types connector , b) C- types connector , c) L- types connector

ii) Based on concrete type .
- Normal Weight Concrete (NWC) block containing prototypes .
- Light Weight Aggregate Concrete (LWAC) block containing prototypes .
- Fine Grained Concrete (FGC) block containing prototypes .
- High Strength Concrete (HSC) block containing prototypes .

Designations :

According to the two defined bases of classification , twelve different prototypes have been manufactured , fabricated , tested and analyzed in the present investigation .
Their designations are given herein :
SNWC, SLWAC , SFGC , SHSC , CNWC , CLWAC , CFGC , CHSC , LNWC , LLWAC , LFGC and LHSC .
The first character of each designation refers to the type of shear connector , while the remaining characters denote the concrete type .

Properties of Concrete Types and their Constituents :

General :

With reference to Table 2 the participated constituents of the used concrete types are the tap water , cement and natural silica sand .
Ordinary Portland cement (type I) [14] of chemical and physical properties conformable to the associated Iraqi specifications No.5 / 1984 [15] and presented in literature [16] was used thoughout this work .

Table 2 : Quantities of constituents and average compressive strength of cubes at 28 days for

		CONSTITUENTS AND QUANTITIES (Kg/ M^3)									
		Tap Water	O.P Cement	Ordinary Sand	Crushed Natural Gravel	Crushed Porcelinite	Silica Fume	Super Plasticizer	Silica Sand < 0.4mm	Average[1] Compressive Strength for Cubes at 28 days (MPa)	Modulus of Elasticity (GPa) [2]
CONCRETE TYPE	NWC	210	500	652	1022	0	0	0	0	44.2	31.26
	LWAC	210	500	500	0	520	15	2		39.55	29.56
	HSC	233	971.5	320	0	0	271.5	2	747	49	32.9

(1) Average cubic compressive strength for FGC at 28 days is 43 MPa .

(2) Concrete modulus of elasticity = 4700 (F_c) ^ $^{0.5}$, E for FGC = 30.82 GPa

The physical and chemical tests and the sieve analysis for the normal weight sand used as fine aggregate were all conducted in this work according to their associated specifications (17, 18 , 19, 20) Their results are shown in Table 3 .

Table 3 : Physical and chemical properties and grading parameters of the natural sand used in

	Property	Specification	Test Results	Award
1	Bulk specific gravity	ASTM C128-88[17]	2.55	Conformable to the associated specification
2	Absorption %	ASTM C128-88	2.1%	
3	Dry loose unit weight (Km/m3)	ASTM C29-89[18]	1600	
4	Sulphate content (SO_3)%	I.O.S No.45-84 [19]	0.14%	
5	Material finer than 0.075 mm%(*)	B.S882—1965 [20]	0.7%	
6	Fineness modulus (*)	B.S882—1965	4.3	

Normal Weight Concrete :

Crushed natural gravel of 10mm maximum size was used as course aggregate for this type of concrete . Its specific gravity , absorption ratio and grading were all tested , measured and recorded [16] . They were found to be conformable to the I.O. S. No. 45-84 [19] .

From the present experimental work

*** These two properties are obtained from the sieve analysis done in this work [16]**

Light weight aggregate concrete :

Porcelinite crushed particles of 12.5 mm maximum size were used as coarse aggregate in this type of concrete to give a unit weight value of 1747 kg/m^3 . It also contains a superplasticizer and a hardener (as shown in Table 2) . Physical , chemical and mineral analysis for porcelinite were done by the State Company of Geological Survey and Mining " in Baghdad and were recorded [16] . They were conformable with the associated specifications (18, 21 , 22) . The grading of course porcelinite aggregate was conformable to ASTM(330-87) [23] as concluded from the sieve analysis results [16] .The " Tuf Flow 603 " superplasticizer used for (LWA , FG and HS)concretes in this work was classified into types (F) and (G) in ASTM – (494 (65) with properties presented in Ref. [16] .The hardener used in this mix is silica fume (SF) which is a pozzolanic material of very fine spherical particles and amorphous silicon dioxide . Its chemical and physical properties are documented [16] .

High strength concrete *:*

With reference to Table 2 , silica sand (SS) is the substitute constituent of porcelinite particles for the HSC mix relative to the LWAC mix . It is an inexpensive extremely hard fine granular material (0.15-0.40mm). Its chemical composition and physical properties are recorded [16] . Table 2 also refers to the rather low w/c ratio of HSC mix .

Fabrication of Prototypes :

The associated shear connectors for each of the twelve specified push –out tested prototypes previously described previously were welded to the two flanges at the appropriate locations by using the electrical resistance welding process of E70 electrodes [25] as shown in Plate 1.

The four concrete types were mixed in a horizontal rotary type mixer of 0.1 m3 capacity according to the ASTM C192-995[26] . Coarse and fine aggregates were first soaked and blended for sixty seconds in two – thirds of the required water quantity . For NWC , cement and rest of water quantity were then added and mixed for three minuted followed by additional three minutes of waiting for cement hydration . For LWAC , FGC and HSC Ohama's procedure [27] was followed by formerly mixing the required quantities of silica fume (SF) in dry state with the required quantities of cement for 15 minutes to ensure the thorough disperse of (SF) powder amongst the cement particles , then water was added with continuous mixing until uniform mix was obtained .

The four concrete mixes were then poured into their lightly oiled moulds which were vibrated for 30 seconds on a vibrating table . Except for NWC the risk of segregation is present by floating light weight aggregate particles which was extremely reduced by the application of silica fume . Curing of the prototype concrete blocks was realized by submerging in water . The 28 –day age average compressive strength values for the four concrete types were obtained from test results of three (150*150*150 mm) cubes for each of the NWC and LWAC mixes , and three (100*100*100mm) cubes for each of the
FGC and HSC mixes . Those Values are given in Table 2 .

Loading Scheme and Testing Procedure *:*

The twelve push –out tests were excuted using a testing machine of a loading frame and 2500 kN Capacity hydraulic jacks which was recently calibrated by the " Iraqi Central Organization of Standardization and Quality Control " . Each tested prototype was centrally loaded with two wood blocks placed under its two concrete blocks . 5-kN load was initially applied in order to settle down the loading system , then released within ten seconds . 3-kN incremantal loading series was then applied up to failure and the vertical slip value of the steel I – section relative to the two concrete blocks were measured at the level of shear connectors by means of calibrated dial gauge readings to 0.002 mm precision as shown in Plate 2 for each load increment .

The downward concentric load was applied to the end of the steel I-section by the crosshead of the machine acting through a ball seating , with care being taken each time in centering the load . The total duration of the test up to the failure point is about 45 minutes . If the prototype remained intact , loading was continued until severe cracking in the concrete block or fracture at the connectors occurred .
Measurements of the slip all the twelve push-out tests are plotted against the applied loads in figure to come later 7 and 8 . Values of the secant shear stiffness Ks for the twelve prototypes were calculated by dividing values of half's of the ultimate loads by the corresponding slip values and given in Table 4 that comes later .

Plate 2 : Typical prototype and push – out test machine with dial gauges attached to the concrete

FINITE ELEMENT ANALYSIS– "ANSYS" MODEL

Definition :

The commertial finite element package ANSYS [28] (Analysis System Version 5.4) was set up-with its parameters calibrated - and used in the analysis of the present twelve composite segments . The computer program has the capacity of solving linear and nonlinear reinforced concrete problems including the effects of cracking , crushing , shrinkage and creep of concrete , yield , placticity , creep , swelling , large deflection and large strain capabilities of steel sections , connectors and reinforcing bars , bond slip between shear connector (or steel rebar's) and the surrounding concrete medium , and temperature changes .

ANSYS Main Features

Concerning the present composite steel - concrete segments with steel shear connectors , the features for the program are specified :

Material Nonlinearities :

Nonlinearity properties of materials , namely cracking and crushing of concrete in tension and in compression , respectively and yield of the steel I-section , shear connectors and reinforcing bars were taken into account through ANSYS operations .

Element Types :

i) Steel I-section and shear connectors :

SOLID45 isoparametric element was used for three dimensional modeling of the mentioned steel parts . The element is defined by eight nodes each having three translational degrees of freedom as shown in Fig.4 .The element has plasticity , creep , swelling , large deflection and large strain capabilities .

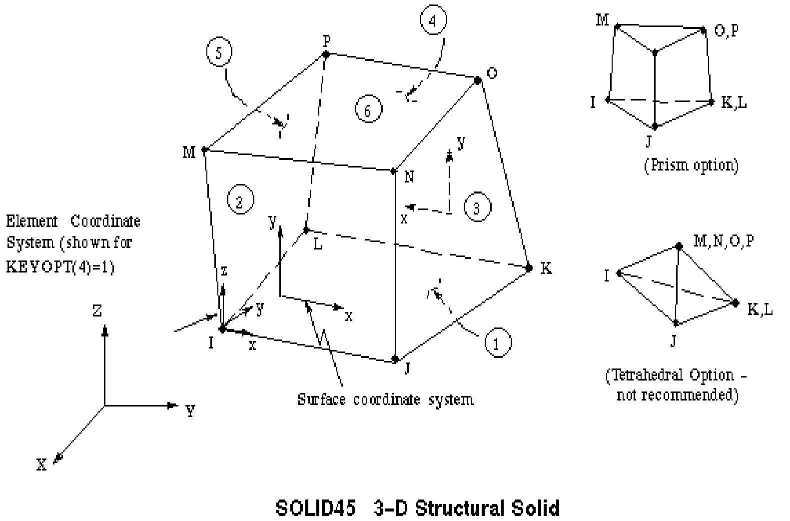

Fig. 4 : Solid 45 three dimensional structural solid elements [28]

ii) Reinforced concrete blocks :

SOLID65 isoparametric element was used for three dimensional modeling of the reinforced concrete blocks . The element is also defined by eight nodes each having three translational degrees of freedom as shown in Fig.5 . It is capable of plastic deformation , cracking in three orthogonal directions , and crushing . The steel reinforcement was introduced into this element by assuming it smeared throughout the element . Any orientation of the steel rebars is permitted . Use of this approach is supported by the fine – meshing of the concrete blocks , especially at locations of the reinforcing bars as recommended by the computer program [28] .

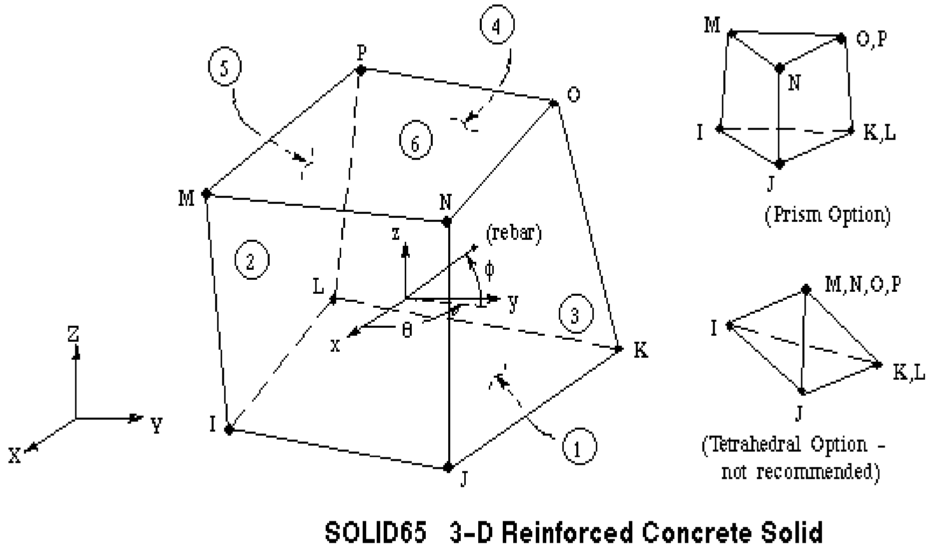

Fig. 5 : Solid 65 three dimensional structural solid elements [28].

Meshing :

Mesh controls of the computer program , if used , allow to establish the element shape , midside node placement , and element size to be used in meshing the solid model . This operation is one of the most important steps of the entire analysis . Volume elements (like SOLID45 and SOLID65) can often be either hexahedral (brick) or tetrahedral shaped , but a mixture of the shapes in the same model is not recommended . Hence , the tetrahedral shape was found to be suitable for meshing the steel I-section , shear connectors and the reinforced concrete block of the present composite segments .

Interfaces :

Bonds between the reinforcing bars (or the shear connectors) and the surrounding concrete of the two blocks of each prototype were all assumed to be perfect . Bond slips at those specified surfaces were then not allowed Accordingly , the defined contact locations were represented by participated nodes and the use of interface finite elements becomes unwarrantable .

Nonlinear Solution Algorithm :

The nonlinear equations of equilibrium were solved using an incremental – iterative technique under load procedure . The full Newton –Raphson method was used for the nonlinear solution algorithm and the displacement criterion is used as a convergence criterion [28] .

Modeling of the Composite Prototype :

The steel I-section , the two concrete blocks and the steel shear connectors of each of the twelve studied composite prototypes were divided by ANSYS computer program into numbers of small tetrahedron SOLID45 and SOLID65 elements as appropriate . After load application , stresses and strains were calculated at integration points of those elements . An important step in the finite element modeling is the selection of the mesh density . The appropriate mesh densities for the twelve composite members were selected on the bases of a convergence study that determined the level of mesh reinforcement at which an increase in the mesh density was of a negligible effect on the results .

Based on that principle the degree of mesh refinement for each of the twelve composite segments was determined , then the number of the three dimensional elements for each component of the composite segment was obtained . The finite element mesh pattern, and the applied load and reaction simulations by ANSYS package for three typical composite prototypes comprising the three used types of shear connectors are shown in **Fig. 6 .**

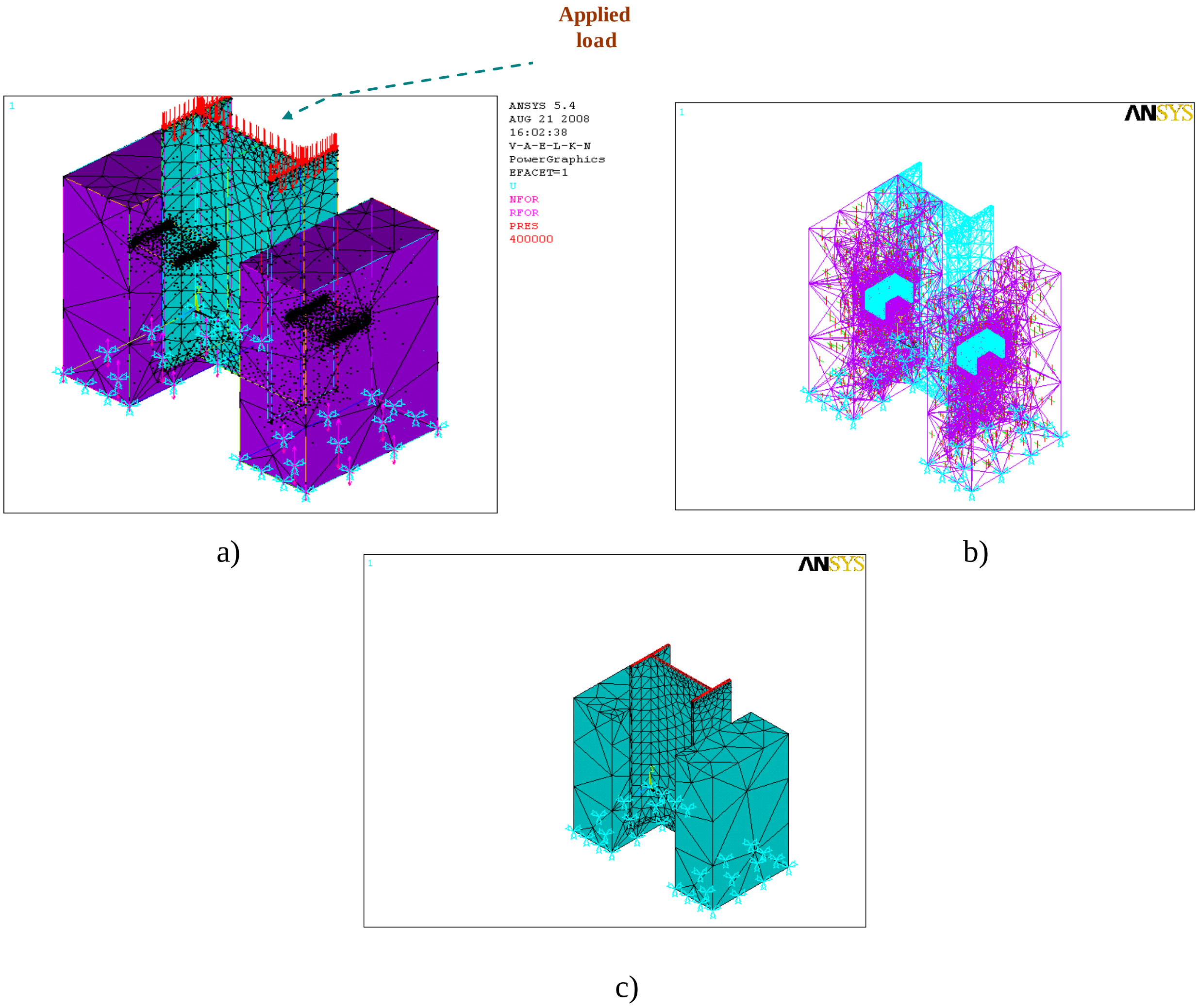

Fig . 6 : Finite element meshes and the load and reaction simulations for three typical composite segments of the twelve prototypes comprising the three used types of shear connectors as modeled by ANSYS . a) case of headed stud . b) case of channel stud . c) case of L- shape stud .

PRESENTATION AND DISCUSSION OF RESULTS:

Outline *:*

The main objective of this study is to examine experimentally and assess theoretically the structural behavior and strength of concrete – steel – concrete composite segments with partial shear connection. Varying degrees of shear connection were realized by introducing different shapes and penetration depths of shear connectors and different types of concrete into the twelve composite segments subjected to push – out tests. The general behavior and test observations of those degrees of shear connection have then been discussed , with special attention to the correlation between the finite element prediction and the experimental evidence.

Inspection of Experimental Results :

General load – slip behavior :

Figs.7 and **8** explain the characteristics and stages of the load – slip behavior along test history of the twelve tested composite prototypes. Regardless of the difference between the degrees of shear interaction (represented by the types of shear connectors and concrete) of the twelve prototypes, the test history (load – slip relation) can be subdivided into three ranges.

The first range was the serviceability stage in which the load increases almost linearly up to about 60 – 68 % of the ultimate (maximum) load and the vertical shear force acting at the steel – concrete interface was tramitted principally by the connector root . Because of the load concentration at the weld collar of the connector , only small deformations occured . Therefore , it is reasonable to regard full shear connection in that stage .

The second range extends from end of the previous range till the ultimate stage for which a significant nonlinear increase of the deformation was inspected . That loss of stiffness was caused by the local crushing of concrete around the foot of the shear connector and thus by a load distribution from the weld collar to the shank of the stud (or web of the channel –connector) , resulting in flexural and shear deformations of the connectors which depend wholly on the modulus of elasticity of concrete [11] . At this range the first cracks in the concrete blocks were observed .

The third range extends from the ultimate state till failure , where lower load levels were reached step by step . A ductile behavior was detected (especially for Stud and L-connectors) because as one stud failed , there was enough capacity in the neighbouring studs to absorb the load .

Effect of Shear Connector Type :

With reference to Fig. 7 , it is obvious that the stud – type connector revealed the highest values of the seviceability stiffness and the ultimate load capacity , followed by the L- type connector . Experimental work proved that the channel – type connector is the weakest in the two defined flexural parameters , which may primarily attributed to its relatively narrow cross-sectional dimensions and penetration depth , then to its be inability to absorb the load shed after the first yield (as only one channel – type connector was attached to a flange) . Percentages of excess in the values of the ultimate load capacity for the tested composite prototypes with Stud- type connectors over the corresponding values for the associated prototypes with L- type connectors were 40% , 20% , 29.5% and 57% , for NWC, LWAC , FGC and HSC concrete types , respectively , while the corresponding percentages of excess for the case of Stud – type connectors relative to the channel – type connectors were 78% , 40% , 65% and 92% for NWC , LWAGC , FGC and HSC concrete types , respectively .

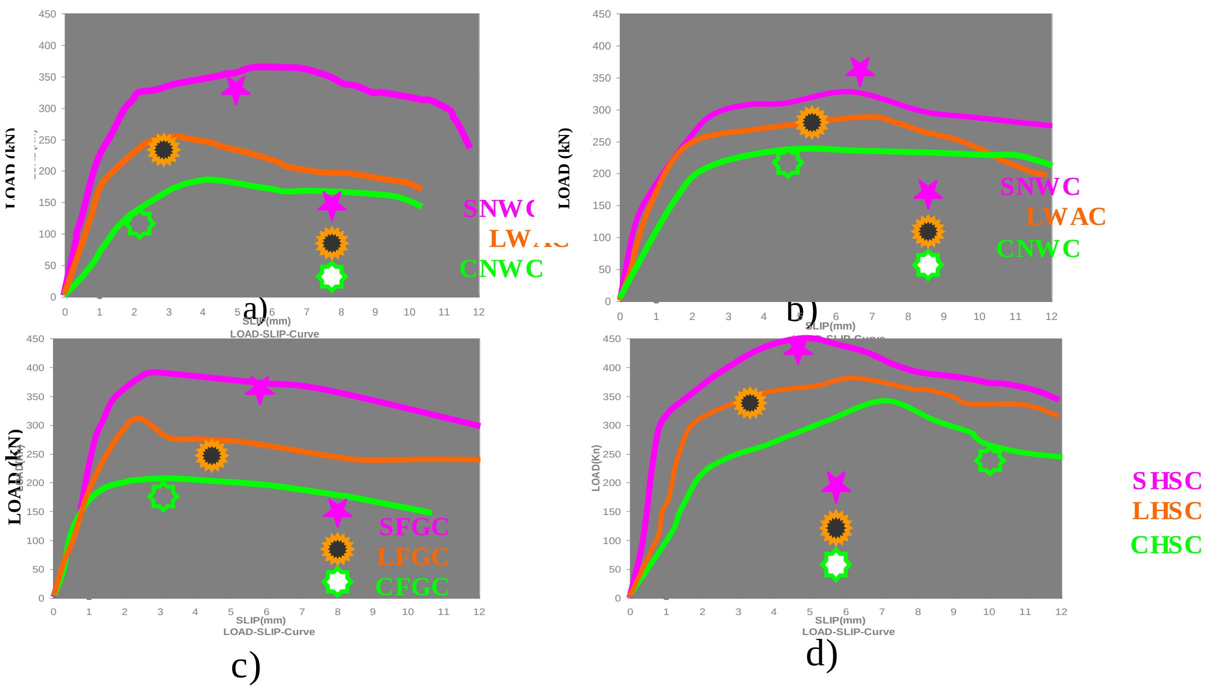

Fig.7 : Load – slip relationships obtained experimentally for the three tested types of shear connectors embedded in each of the four used types of concrete . a) in NWC, b) in LWAGC , c)in

EFFECT OF CONCRETE TYPE:

Recalling the difference between values of the E- modulus for the four used concrete types NWC , LWAGC , FGC and HSC, the inspection of **Fig.8** (which shows the load – slip relationships for each type of shear connectors embedded in the four concrete types in one graph for the sake of comparison) leads to the following remarks :

i) In general the same trend of this relationship (formerly subdivided into three ranges) is detected for the four concrete types .

ii)In the first (serviceability) range of that relationship the behavior of the two stronger types of concrete (NWC , and HSC) under working loads differ only irrelevantly from those of the two less strong concrete types (LWAGC and FGC) because of the bigger initial – stiffness of the two stronger types by about 40-56% . This fact is not of great significance because of the small deformations at this load level .

iii) In the second range (extending from first yield up to ultimate stage) wide difference is shown in the development of the load - slip curves for the two weaker concrete types (LWAGC and FGC) relative to the two stronger types (NWC and HSC) . This is mainly because of the loss of stiffness due to local crushing the concrete around the foot of the shear connector .

iv) In the third range (from the maximum load stage till failure where lower load levels were reached gradually) similar wide difference between development of the relationships for the two weaker and the two stronger concrete types resulted . This is mainly due to the difference in the elastic bedding between the cases of the stronger and the weaker concrete types [11] .

From another point of view the effect of concrete type on load-slip relationship can be evaluated on the bases of the **shear stiffness parameter Ks** value which is defined as the load –slip ratio at a load level of 50% of the ultimate load , thus representing slope of the secant stiffness at that load level of the relationship and giving an indication to the average load- slip relationship and the level of the ultimate load . Referring to **Table 4** (which gives values of the Ks parameter for the twelve tested prototypes) it can be noticed that the effect of concrete compressive strength (which decreases monotonicly for HSC to NWC to FGC to LWAGC by the evidence of Table 2) on the Ks parameter is vital . In its absolutely maximum particular case the reduction in the Ks parameter reaches 66% when the concrete type is changed from HSC to LWAGC with channel – type connector .

Table 4: Variation in the values of shear stiffness parameter Ks for the twelve tested prototype) relative to the NW concrete type for each of the three types of shear connectors obtained experimentally

Connector type used with concrete type	50%Ultimate load (kN)	Slip corresponding at 50% (mm)	Ks (kN/mm)	% difference (Ks) with in NWC
SNWC	196.8	0.734	268.122	0
SLWAC	165.2	1.48	111.623	-58.4
SFGC	174.7	1.21	144.38	-46.2
SHSC	219.3	0.64	342.65	27.8
LNWC	152.1	1.01	149.7	0
LLWAC	138.8	1.76	78.86	-47.3
LFGC	98.4	1.31	75.12	-49.9
LHSC	174.4	0.82	212.7	42.08
CNWC	112.5	1.18	95.334	0
CLWAC	89.6	1.88	47,658	-50
CFGC	103.3	1.42	72.7	-23.75
CHSC	144.6	1.04	139.03	45.8

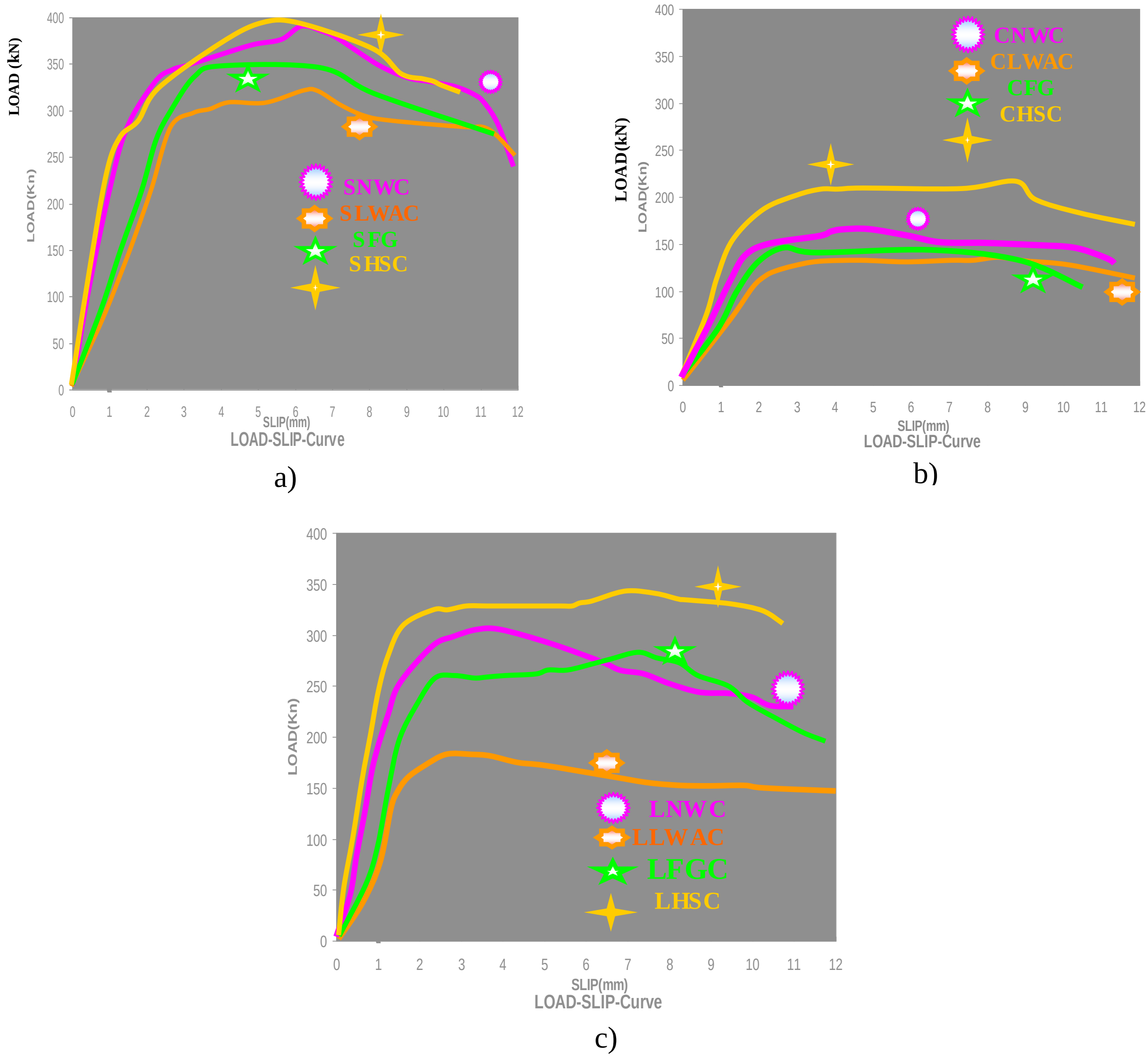

Fig. 8 : **Load – slip relationships obtained experimentally for the four used types of concrete with each of the three tested types of shear connectors : a) with Stud-type connector , b)) with channel-type connector , c) with L-type connector**

Correlation between Finite – Element Prediction and Experimental Evideuce :

With reference to Fig. 9 which shows the load – slip relationship determined by the ANSYS model (according to the formerly mentioned concepts and fundamentals) beside the corresponding results obtained from the present experimental testing for each of the twelve composite prototypes , the following concluding remarks are recorded :

i) Good agreement between the experimental and numerical investigations in describing and evaluating the charactaristics of the first stage (linear serviceability range) is obtained , mainly the initial stiffness .

ii) The numerical model was accurate in predicting the ductile elasto-plastic trend of the load – slip relationship . This remark was confirmed by the complete coincidence between the experimental and theoretical values of the deflection at failure for all prototypes .

iii) The numerical model gave no distinct transition from the second to the third fiormerly defined ranges of the studied relationship .

iv) According to the last remark no distinct ultimate stage point was detected from the load – slip relationship of the finite element model , leading to a noticable difference in the maximum load resistance values given by the experimental and theoretical analysis .

v) The unability of the present numerical model in describing the third range of the load- slip relationship (beyond the maximum load stage till failure load where low load levels were attained gradually) , has led to failure values not in coincidence with the corresponding experimental ones .

vi) The view drawn from Tabel 5 , which shows that the percentage difference between the theoretical and experimental values of the Ks factor , is fairly positive . The maximum defined difference is 19.05% for SHSC prototype (the absolutely strongest one) , while the minimum difference is 3.318% for CLWAC prototype (the absolutely weakest one) . The avarege difference for the twelve prototypes is 7.58% , a quantity reflecting the accuracy of the present finite element model in simulating the tested composite segments .

Table 5 : Experimental and theoretical values of the shear stiffness parameter Ks and the percentage difference between them for the twelve studied composite segments .

		Prototype Designation											
		SNWC	**SLWAC**	**SFGC**	**SHSC**	**LNWC**	**LLWAC**	**LFGC**	**LHSC**	**CNWC**	**CLWA**	**CFGC**	**CHSC**
Shear stiffness parameter kN/mm	**Experimental**	268.12	111.62	144.38	342.65	149.7	78.86	75.12	212.7	95.334	47.658	72.7	139.03
	Theoretical	252.9	107.2	138.8	323.6	142.87	74.65	70.001	202.09	89.7	44.34	69.123	131.8
	%difference	15.22	4.2	5.58	19.05	6.83	4.03	5.119	10.61	5.63	3.318	3.577	7.23

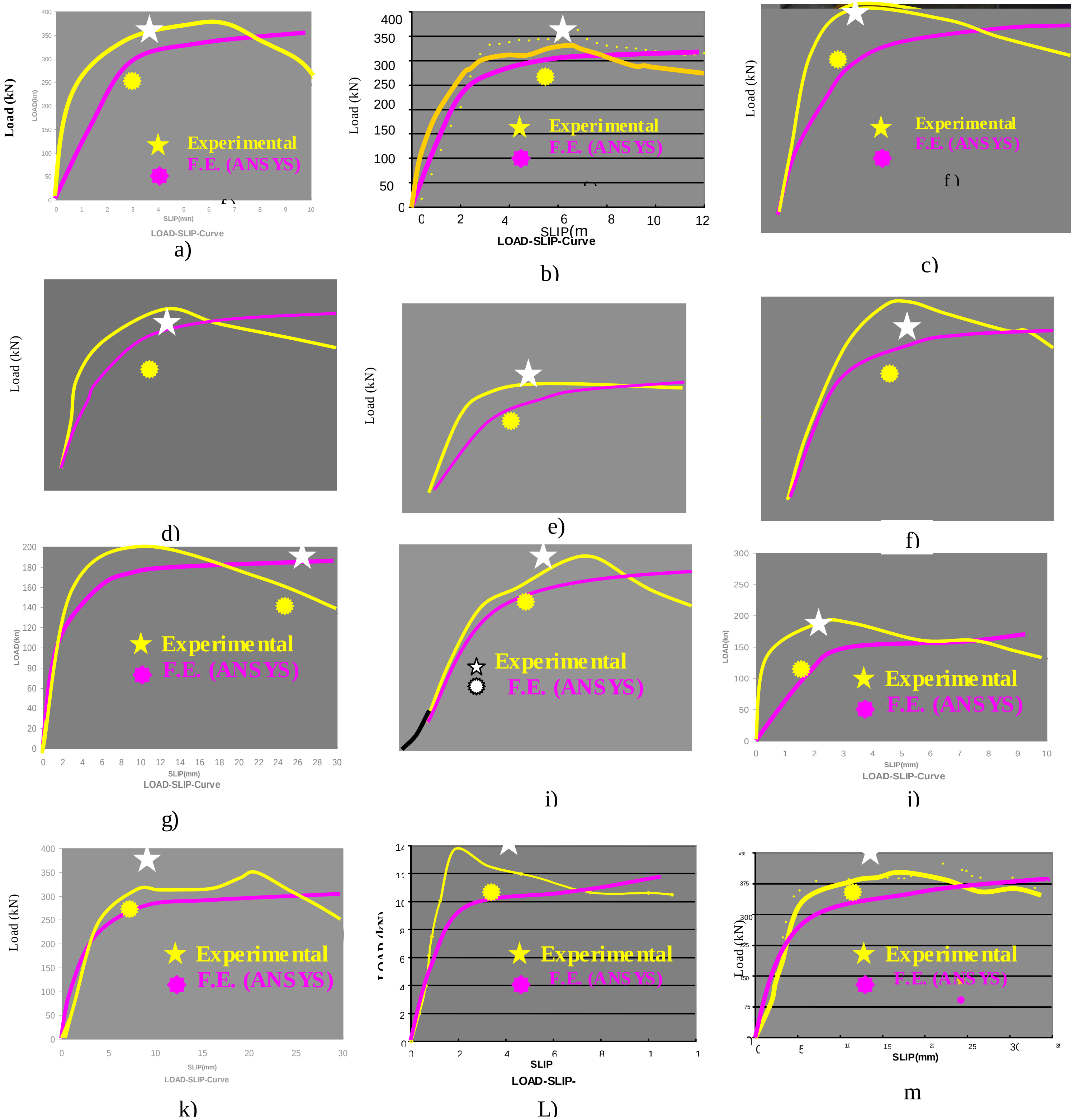

Fig. 9: Experimentally and theoretically obtained load -slip relationships for the twelve studied composite prototypes : a)SNWC , b) SLWAC , c)SFGC d) SHSC , e) CNWC , f) CLWAC , g) CFGC , h) CHSC , i) LNWC , j) LLWAC , k) LFGC , l) LHSC

CONCLUSIONS :

The following conclusions have been reached in this study so far :

- Regardless of the degree and state of partial interaction at the steel-concrete interfaces the twelve tested composite prototypes have given the same general trend , features and characteristics of the load – slip relationship consisting of the main three ranges detected in few recent experimental researches , especially the linearly , high stiffness and precise limit of the serviceability stage (60-68%) of the ultimate load).

- Further comparative inspection of the load-slip curves for the twelve tested composite prototypes shows the significant and quantitively - organized differences between their ultimate load values at ends of the second ranges of their curves accompanied by slight differences in the corresponding slip values .

- The comparative inspection also shows the same general signpost of differences in levels of load – slip curves in the third range (from ultimate stage till failure) for the twelve tested prototypes . More significant differences in the extensions of slip beyond ultimate stages for the twelve prototypes are attained , referring to significant differences in ductility .

- The shear connector shape , penaration depth and configuration are of major effects on serviceability stiffness and extension , ultimate load capacity , and ductility of the shear in partially interacted steel- concrete composite segments . The S- type connector comes in the vantage followed by L-type one .

- Quantitatively speaking with regard to connector type effect on ultimate load capacity of composite segments , the average excess percentages in that property values for segments with S-type connectors over segments with L- type ones are 48.5% and 24.8% for the stronger (NW and HS) and for the weaker (LWA and FG) types of concrete , respectively . The corresponding average excess percentages for the case of S-type connectors relative to C-type ones are 85% and 52.5 % for the stronger and weaker types of concrete , respectively .

- The first (serviceability) range of load- slip relationships for the composite segments revealed relatively slight effect of the concrete elasticity modulus (E-value)on stiffness of segments under working loads (in spite of the rather large differences in the initial stiffness values of about 40-56% between the two stronger and the two weaker tests types of concrete . This is due to the small deformations at the service load levels .

- The ultimate compressive strength of concrete directly affects the development of the load-slip curve in the second range (from end of service stage to ultimate stage). The higher the difference in concrete strength this property values of concrete types , the wider are the differences between levels and extensions of those curves in that range , a criterion confirming the prediction of stiffness loss due to local crushing of the concrete surrounding the connector foot .

- Similar wide differences between levels and extensions of the load –slip curves for the two stronger and the two weaker tested types of concrete are obtained .

- The shear stiffness parameter Ks of a composite segment of partial shear interaction at steel-concrete interfaces is solely affected by the concrete compressive strength . The present work shows that 66 % reduction in Ks value is attained when replacing HSC by LAWC in composite segments of C- type connectors .

-In regard to the correlation between the finite element prediction and the experimental issue for the steel – concrete segments of various types and levels of partial shear interaction at interfaces , the numerical model has proved its efficiency and accuracy in predicting characteristics of the serviceability stage and the ductile elasto- plastic trend of the load-slip relationship , which appears precisely in the highly accurate computation of slip value at failure .

- On the other hand , ability of the present finite element model in giving distinct border between the second and third range of the load-slip relationship and in protruding the ultimate stage was limited , this has led to discrimination between the third range of the load-slip relationships of the numerical model and the experimental work .

– The present finite element model has proved its efficiency in computing the shear stiffness parameter Ks values as compared with the corresponding experimentally obtained values . 7.58% comprehensive average difference between the two methods is attained .

REFERENCES :

* Wu, Y.F., Ohelers, D.J. and Griffith, M.C., "Partial-Interaction Analysis of Composite Beam/Column Members", Mechanics of Structures and Machines, Vol. 30, No. 3, 2002, pp.309-332 .

* Najem, M.A., "Behaviour and Strength of Multi-Layer Composite Beams with Unequal Length Components", M.Sc. Thesis, Al- Mustansiriya University, 2003, 132 p.

* Nie, J., Fan, J. and Cai, C.S., "Stiffness and Deflection of Steel-Concrete Composite Beams under Negative Bending", Journal of Structural Engineering , ASCE, Vol. 130, No. 11, November 1, 2004, pp.1842-1851.

* Aziz, K.I., "Behaviour of Multi-Layer Composite Beams with Partial Interaction", Ph.D. Thesis, University of Technology, 2005, 170 p.

* Zebun .M.A. " Structural behaviour ofSteel –Concrete –Steel Sandwich Panels " , Ph.D. Thesis, University of Technology, 2006, 110 p

* Slobodan ,R. and Dragoljub , D. , " Static Strength of The Shear Connectors in Steel-Concrete Composite Beams Regulations and Research Analysis -UDC 624.072.2(045)" Architecture and Civil Engineering Vol. 2, No 4, 2002, pp. 251 – 259.

* Eurocode 4 , Part -14 , German Draft ENV 1994 -1-1 :1992 .

* Deanna , M. and Roddenberry. R " Static Strength of the Shear Connectors in Steel-Concrete Composite Beams Regulations and Research Anlysis " Architecture and Civil Engineering Vol. 2, No 4, 2002, pp. 252.

* Valente and Cruz P. J. S. " Experimental Studies on Shear Connection Between Steel and Light Weight Concrete " Civil Engineering Department, University of Minho, Azurém, 4800-058 Guimarães , pp1 .

* Larose, . K. and Elwood .K.J . " Performance of Headed Shear Stud Clusters for Precast Concrete Bridge Deck Panels " web site .

* Faust , Thorsten, "Headed Studs in Composite Structures With LWAC" , web site .

* BS 5400, Part 5, "Steel, Concrete and Composite Bridges", British Standards Institution, London, 1979.

* Johnson, R.P., " Composite Structures of Steel and Concrete" Vol.1, Beams, Columns , Frames, Applications in building ", Crosby Lockword Staples, London, 1975, pp 210.

* ASTM C150-86 , " Standard Specification for Portland Cement" Annual Book of ASTM Standards , Vol .04.02 , 1988,pp.89-93 .

* Al-Alusi , Mohammed Raji .M , " Experimental and Finite Element Investigation on the Structural Behavior of Different Shear Connectors within Different Types of Concrete" M.Sc Theses , Al-anbar Univercity , 2008 , 150p.

* ASTM C128-84, " Standard Test Method for Specific Gravity and Absorption of Fine Aggregate " , Annual Book of ASTM Standards , Vol .04-02 , 1988 ,pp.69-72 .

* ASTM C29-87, " Standard Test Method for Unit Weight and Voids in Aggregate", Annual Book of ASTM Standards , Vol .04-02 , 1988, pp 1-3 .

* BS 882 ,1965 " Specification for Aggregate from Natural Sources for Concrete " British Standards Institution , London , 98 pp

* ASTM C127-84, " Standard Test Method for Specific Gravity and Absorption of Coarse Aggregate " , Annual Book of ASTM Standards , Vol.04-02 , 1988,pp. 64-68 .

* BS 812 , Part 110 ,1990 , " Method for Determination of Aggregate Crushing Value (ACV) " , British Standards Institution , London , 8pp

* ASTM C330-87 , " Standard Specification for Light Weight Aggregates for Structural Concrete " , Annual Book of ASTM Standards , Vol . 04-02, 1988,pp,.187-189 .

* Standard Specification for Chemical Admixtures for Concrete. ASTM –C494-05) , American Society for Testing and Materials, 2005.

* Manual of Steel Construction :Allwable Stress Design , 9th ed. , American Institute of Steel Construction (AISC) , Chicago , 1989 .

* American Specification for Testing and Materials, "Making and Curing Concrete Test Specimens in the Laboratory", C192-1990 .

* Ohama , Y. , "Recent progress in Concrete-Polymer Composition". Advance in Cement -based Materials, Elsevier Science Ltd., New York, 1997, pp.31-40.

* ANSYS Manual , version 5.4 , 1997 .

* المواصفة القياسية العراقية للسمنت البورتلاندي ، رقم 5 لسنة 1984 ، الجهاز المركزي للتقييس والسيطرة النوعية ، بغداد ، 8 صفحات

* الجهاز " ركام المصادر الطبيعية المستعمل فـي لخرسانة والبناء ") رقم (45) لسنة 1984 I.O.S المواصفة القياسية العراقية
*المركزي للتقييس والسيطرة النوعية ، بغداد ، 4 صفحات

الأمثلية في توقيع الخدمات باستخدام تقنيات مناطق التأثير

(دراسة في توزيع مدارس التعليم الثانوي لقطاع الدورة)

الدكتور فراس ثامر حمودي

المعهد العالي للتخطيط الحضري و الإقليمي

Optimum Sit Selection of Services by means buffer zones techniques

(Study of secondary school distribution for Al_Dorraa sector)

ABSTRACT

Optimization in the distribution of services is one of the fundamental requirements for the urban and regional planners, so that the researchers interested to find many instruments to help them to achieve perfect allocation of services on the city.

Many of difficulties for urban and regional planner's tasks were reduced by using of geographic information system, especially for spatial distribution of services or other things of urban and regional planning elements. Through exact allocated for geographic site and achievement of many requirements of the planner works in a rapid way and for diverse data and locations in the same time.

Buffering so-called (zone of influence) one of the important tool in the geographic information system , this research came to present some of common method of buffering structure in the field of urban and regional planning use the distribution of secondary school in one of the Baghdad sector.

الخلاصة ...

تعد العدالة في توزيع الخدمات مكانيا من المتطلبات الرئيسة ضمن عمل المخطط الحضري و الإقليمي ، لذا فقد شغل بال هذه الفئة من الباحثين إيجاد او الاعتماد على سبل عديدة تساعد في تحقيق هذا التوزيع المثالي لمناطق الخدمة المختلفة في المدينة .

و كان لنظام المعلومات الجغرافية (GIS) دورا بارزا في تذليل العديد من صعوبات العمل التي يواجهها واضعو الخطط الحضرية و الاقليمية على حد سواء ، وخصوصا فيما يتعلق بعمليات التوزيع المكاني سواء للخدمات ام لغيرها من مقومات الهيكل الحضري او الإقليمي ، و ذلك من خلال التحديد الدقيق للمواقع الجغرافية و اجراء العديد من متطلبات عمل المخطط

بصورة سريعة و دقيقة و للعديد من المواقع و البيانات في أن واحد ، و من بين هذه الوسائل المهمة في نظام المعلومات الجغرافية هو بناء الحواجز Buffering او ما يدعى (بنطاق التاثير او التاثر) ، و جاء هذا البحث ليوضح بعض طرق استخدام عملية بناء الحواجز في منهجية التخطيط الحضري و الاقليمي ، مستعينا باحدى الظواهر المهمة المتمثلة في توزيع مدارس التعليم الثانوي في احدى بلديات مدينة بغداد .

المقدمة ...

هذه الدراسة توضح مدى الاهمية التطبيقية في عملية التخطيط و اتخاذ القرار لاحدى تقنيات نظام المعلومات الجغرافية المتمثلة بالحواجز(مناطق التاثير) ، و اثرها في تسهيل و تسريع قراءة الخارطة التوزيعية لاية ظاهرة جغرافية ام غير جغرافية و في جميع مستويات التخطيط (محلية ، حضرية ، اقليمية و قومية) و تبيان مدى تاثيرها او تاثرها بمحيطها الخارجي و ايجاد الخلل في توزيع هذه الظواهر على المستوى المدروس ، و من بين هذه الظواهر هو توزيع الخدمات في الحيز الحضري و التي تتطلب عناية فائقة الغرض منها ايجاد المكان المثالي الذي يحقق افضل منفعة لأكثر عدد من الناس ويغطي حاجات و متطلبات اغلب المناطق الممكنة من سكان المدينة المنشودة ، و تعد المدارس الثانوية واحدة من هذه الخدمات التي يتطلب توزيعها ضمن مناطق المدينة عناية خاصة لغرض تحقيق توازن في عملية التوزيع من اجل خدمة كل اجزاء المدينة بصورة متقاربة دون تمييز فائق ، لذا فقد درست خدمات التعليم الثانوي لقطاع الدورة من مدينة بغداد في هذا البحث بعدها إحدى التطبيقات الممكن توظيف هذه الميزة من ميزات برامج نظام المعلومات الجغرافية عليها.

هدف الدراسة...

الهدف من هذه الدراسة هو ابراز اهمية احدى تقنيات نظام المعلومات الجغرافية المتمثل بنظام الحواجز، في تحديد الموقع الامثل لخدمة معينة عن طريق استخراج مدى جودة التوزيع الحالي لمدارس التعليم الثانوي في قطاع الدورة من مدينة بغداد و تتبع البيانات الممثلة مكانيا وفق خرائط تتسلسل بشكل منطقي وصولا الى التوزيع المثالي لتلك المدارس.

مشكلة البحث...

المدارس بشكل عام و مدارس التعليم الثانوي بشكل خاص ، حالها حال معظم خدمات الحيز الحضري لمدينة بغداد تعاني من رداءة في التوزيع المكاني على مستوى تخطيط المدينة نتيجة عدم اتباع او تبني اساليب علمية و عملية في عملية التوزيع المكاني الصحيح و ان نظام المعلومات الجغرافية واحد من ابرز هذه التقنيات الحديثة المتاحة .

فرضية البحث ...

من الممكن التوصل الى ايجاد نقاط الضعف في توزيع الخدمات بشكل عام و خدمات مدارس التعليم الثانوي منها بشكل خاص من خلال تطبيق تقنيات نظام المعلومات الجغرافية ، و اقتراح صيغ جديدة للتوزيع تساهم في تحسين مستوى تلك الخدمات المختلفة .

منهجية البحث...

سيتبنى البحث المنهج التحليلي المكاني Spatial Analytical Methodology باستخدام تقنيات نظام المعلومات الجغرافية GIS اداة تحليلية مكانية ، و بالاعتماد على المسوحات المكتبية و المكانية ، و قد استخدم نظام ال Arcgis 9.2 في عملية تنظيم البيانات مكانيا و من ثم ادارتها و تحويلها الى اشكال كارتوكرافية اعتمادا على البيانات الوصفية المرتبطة بها من جهة و تطبيقات ذلك النظام من جهة اخرى و انتهاء بعرض الخرائط المطلوب تصميمها بوصفها مخرجات نظام المعلومات الجغرافية .

مصادر البيانات ...

تتعدد و تتنوع مصادر البيانات المدخلة في نظام المعلومات الجغرافية ، فقد تكون ذات مرجعيات مكانية Spatial مثل الخرائط و الصور الجوية او قد تكون ذات مرجعيات غير مكانية مثل الإحصاءات و البيانات الوصفية ، و اعتمد في تمثيل و تحديد منطقة الدراسة و بناء قاعدة البيانات لهذا البحث على مجموعة من مصادر البيانات تمثلت في :

- خارطة توزيع المدارس الثانوية في مدينة بغداد بمقياس رسم 50000/1 .
- مخططات للمحال السكنية في منطقة الدراسة بدون مقياس رسم عين من خلالها الاستعمال السكني للأرض .
- صورة جوية لمدينة بغداد من نوع Mr. Sid Extension ، و هذا النوع من الامتداد للصور يستخدم مع الصور المأخوذة بالطائرات تكون فيها دقة التمييز الارضي Resolution ما بين 1-5 متر لكل عنصر صورة Pixel .
- اعداد السكان في قطاع الدورة لسنة 2008 ، وفق تقديرات الجهاز المركزي للاحصاء .

طريقة مناطق التاثير(الحواجز) Buffer Zones...

طريقة الحواجز عبارة عن منطقة او مناطق ذات ابعاد محدد او معرفة توضع حول المعلم ، و هي تستخدم للتحليلات التقريبية على سبيل المثال استخراج نطاق التاثير لسوق او خدمة معينة اخرى (Birkin,1996,p33) ، و بناء الحواجز واحدة من اكثر العمليات الشائعة الاستخدام في النماذج الخرائطية ، و منطقة التاثير كما اسلفنا مساحة قطرية بمسافة محددة

لظاهرة خرائطية (نقطة ، خط ، شكل معين) تستخدم هذه الحواجز لتعريف مساحة محيطة بهذه الظواهر (Demers,2003,p309)، على سبيل المثال ينبغي ابقاء مياه الصرف الصحي على بعد اكثر من 100 م بعيد عن الانهار و الجداول ، او تعيين موضع المساكن على بعد نصف كيلو متر عن طرق المرور السريعة الموجودة ، او التأكد ان معظم اجزاء المدينة تقع ضمن المسافة العظمى لمختلف الخدمات مثل محطات الاطفاء او المستشفيات و المراكز الصحية او محطات تعبئة الوقود وغيرها من الخدمات (الشافعي،2009،ص354) .

عندما توضع الحواجز لمجموعة ظواهر ستكون المخرجات مجموعة اشكال تمثل هذه الظواهر مضاف لها مسافة الحاجز المحددة و التي تمثل منطقة تاثير او تاثر هذه الظاهرة (زرقطة،2007،ص342) ، و بعبارة اخرى هي تعيين اقليم الظاهرة و الذي يمثل المساحة المشمولة بمسافة الحاجز المحدد لتلك الظاهرة ، فإذا حدد منطقة تاثير لنهر بمسافة 300م فان المنطقة التي تزيد عن 300م تمثل المسافة الخارجة عن اقليم هذا النهر في حالة الدراسة تلك شكل (1) .

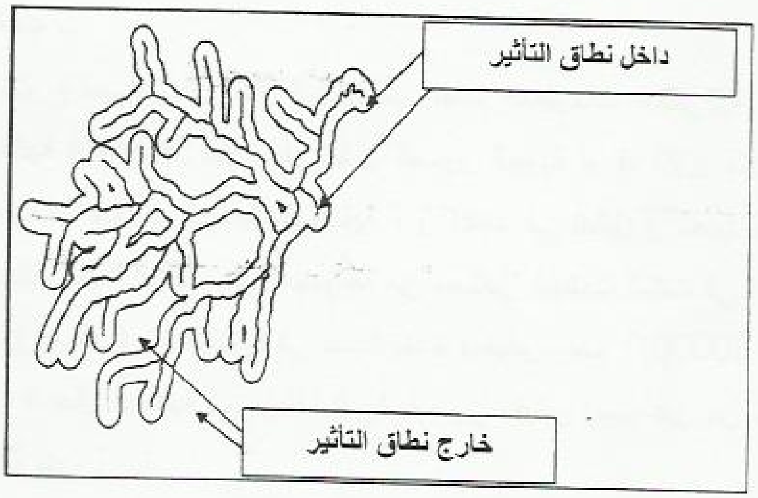

شكل (1) حاجز خطي لنهر بني على اساس المسافة المحددة من قبل المستخدم

المصدر: (M.Smith,2002,p43)

و الحواجز انواع منها الاعتيادية و التي تطرقنا اليها و منها (المتراكبة Compound or Nested Buffers) وهنالك (المتغايرة Variable Buffers) و الحواجز المتراكبة او المتداخلة غالبا ما تكون مطلوبة في أي تحليل ، لانها تقوم بتعيين مناطق تاثير لمسافات مختلفة من أي ظاهرة مدروسة (Chang,2002,p75) ، على سبيل المثال اذا رغب في تحديد الارض المناسبة لاقامة منطقة سياحية جوار احدى البحيرات و كان من متطلبات التوقيع انها تبعد عنها بمسافة 100م لتجنب حركة المد و كذلك تجنب عملية التلوث للبحيرة ، لكن المكان ينبغي ان لا يبعد اكثر من 200م ليتيح سهولة في الوصول للتمتع بالبحيرة ، و

الشكل (2) يوضح المنطقة التي تقع على مسافة اكثر من 100م و اقل من 200م من البحيرة.

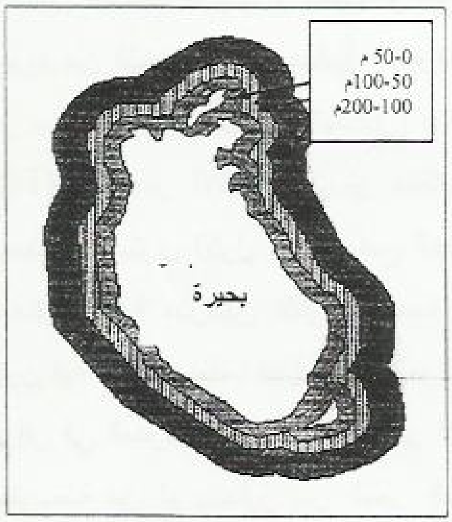

شكل (2) اختيار المكان الامثل باستخدام الحواجز المتراكية

المصدر : (M.Smith,2002,p45)

اما الحواجز المتغايرة فهو نوع جديد من الحواجز يختلف في مسافة الحاجز باستقلالية مع خواص الظاهرة المدروسة (Demers,2003,p313) ، فأذا تطلب مشروع لنظام المعلومات الجغرافية GIS لمجموعة بحيرات انشاء انطقة تاثير حول هذه البحيرات لايجاد المسافة الدنيا لتوقيع فتحات مجاري الصرف الصحي Septic Systems من ساحل تلك البحيرات ، و كانت متطلبات توقيع هذه الفتحات مختلفة من حيث المسافة اعتمادا على حجم تلك البحيرات ، فان الحواجز المرسومة ستكون مختلفة المسافة مع اختلاف البيانات الرقمية المعطاة في طبقة خواص حجم البحيرات شكل (3) .

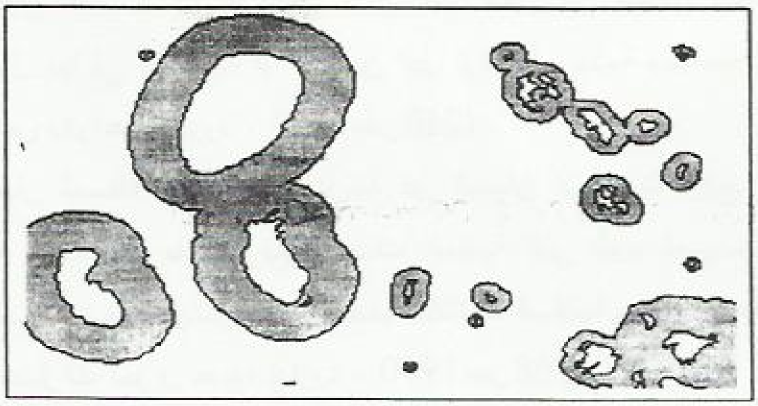

شكل (3) مجموعة من البحيرات رسمت حولها حواجز متغايرة تبعا لخواص الطبقة التي تمثل حجم البحيرات

المصدر : (Demers,2003,p313)

التعليم الثانوي...

التعليم الثانوي مرحلة مكملة للتعليم الابتدائي يتضمن محور الدراسة فيه تعليما يتيح للناشئين اكتشاف قابليتهم و تنميتها و التوسع اكثر في الثقافة و العلوم و التدرج للحصول على المزيد من التخصص في ميادين المعرفة ، مدة الدراسة في هذه المرحلة ست سنوات تنقسم الى مستويين (المتوسط و الاعدادي) بواقع ثلاث سنوات لكل منهما (مزعل ، 1990 ، ص 145)، و تجدر الاشارة الى ان هنالك مدارس تضم المستويين تسمى المدارس الثانوية ، ويستمر المستوى الاول في البرامج الخاصة بالمرحلة الابتدائية مع التركيز بشكل اكبر على المادة بواسطة مدرسين اكثر تخصصا ، اما المستوى الثاني الذي يمثل المرحلة الاعدادية يكون فيه التعليم منظما فيما يخص المواد الدراسية اكثر منه في المستوى الاول ، و ينبغي ان تتوافر في المدرسين مؤهلات اعلى و اكثر تخصصا من المستوى الاول ، ويقبل في المرحلة المتوسطة من لم يتجاوز من العمر السادسة عشر بالنسبة للذكور و الثامنة عشر بالنسبة للاناث ، ويقبل من الذكور في المستوى الاعدادي من لم يتجاوز الحادية و العشرين والثالثة و العشرين بالنسبة للاناث (رزوقي،1987،ص27)

معايير توقيع مدارس التعليم الثانوي ...

تخضع المدارس بصورة عامة و منها مدارس التعليم الثانوي حالها حال بقية الخدمات في المدينة الى معايير معينة عند توقيعها و تتعدد هذه المعايير التي تهدف الى تحقيق اغراض النشاطات التعليمية بالصيغ المقبولة و الممكنة لذا يمكن عرض اهم الاعتبارات التي تؤخذ عند وضع معايير التوقيع كما يلي :

- معيار حجم السكان : ينبغي توافر عدد معين من السكان بحسب المعايير المعمول بها في أي مدينة او اقليم من اجل توقيع أي خدمة مجتمعية جديدة ومنها المدارس بانواعها (داؤود ، 1990،ص268) .
- معيار المسافة : أي بعد المدرسة عن المسكن اذ يرتبط توقيع المدرسة في منطقة معينة بخارطة توزيع الوحدات السكنية التي تقوم المدرسة بخدمتها و لمسافات تحددها الجهات المعنية بحسب الكثافات السكانية و البيئة الحضرية فضلا عن اعتبارات اخرى عديدة (داؤود ، 1990،ص268) .
- الاعتبارات البيئية: تعد البيئة من اهم العوامل المؤثرة في اختيار مواقع المدارس على نحو عام ، اذ تؤدي البيئة غير الصحية للمدرسة الى انتشار الامراض البدنية و النفسية لذا يراعى عند اختيار موقع المدارس الشروط الاتية :

أ- ان تكون المدرسة في منطقة هادئة بعيدة عن الضوضاء و الاماكن المزدحمة مثل المصانع و سكك الحديد و تقاطعات الشوارع العامة اذ تؤثر الضوضاء على الجهاز العصبي للطالب و المدرس الامر الذي يؤدي الى قلة في التركيز و العطاء و انخفاض في المستوى العلمي (ديكس ، 1988 ،ص282-283) .

ب- ان تكون المدارس في منطقة بعيدة عن الرياح المحملة بالروائح و الادخنة و الاتربة و قريبة من مناطق الخدمات .

4-سهولة الوصول : ينبغي ان تكون المدارس قريبة من مناطق السكن و ان لا يقطع الطالب في الوصول اليها الكثير من المناطق المزدحمة و الطرق العامة السريعة .

معايير توقيع المدارس الثانوية في العراق ...

ظهر اهتمام مبكر للنهوض بواقع المدن و تنظيم عمرانها يتجلى من خلال القوانين التي صدرت في هذا المجال ، و اولها قانون ادارة البلديات رقم 84 لسنة 1931 ، ومن ثم نظام الطرق و الابنية رقم 44 لسنة 1935 (الفتلي ، 1998، ص38) ، وبعدها قانون ادارة البلديات رقم 165 لسنة 1964 .

اما فيما يتعلق بالمعايير التخطيطية المحلية فقد تم وضع انموذجين من المعايير التخطيطية العراقية من قبل الجهات التخطيطية المسؤلة و هي معايير هيئة التخطيط الاقليمي عام 1977 و معايير مخطط الاسكان العام في سنة 1982 ، وهذا الاخير يعد اخر التحديدات التي حددت في مجال تنظيم المناطق السكنية و هي تطوير للدراسات التي اعدت للمخطط عام 1977 بالتعاون مع المجموعة الاستشارية البولندية بولسيرفس (الفتلي ، 1998 ،ص39-44) .

وقد تضمن منهاج الخدمات في معايير هيئة التخطيط الاقليمي لعام 1977 تامين الخدمات الضرورية للسكان و منها مدارس التعليم الثانوي (المتوسط و الاعدادي) ، من خلال تحديد مساحة كل خدمة ضمن المستوى المطلوب سواء كان (محلة ، حي ، قطاع) فكان نصيب المدارس المتوسطة اثنان مدرسة بمساحة 9000-10000م2 لكل مدرسة في الحي و الاعدادية مدرسة واحدة بمساحة 10000-12000م2 ، (وزارة التخطيط ، 1977،ص117) اما معايير مخطط الاسكان العام في سنة 1982 ، جدول (1) فقد كان اكثر تفصيلا اذ تكون برنامج الخدمات من مجموعة من مباني التسهيلات و الخدمات الاجتماعية التي تخدم سكان المحلة حسب عدد سكانها ، و من ضمن هذه الخدمات مدارس التعليم الثانوي و حددت المعايير المتعلقة بها على الاسس الاتية :

1- مساحة قطعة الارض التي يشغلها المبنى لكل 1000 من السكان.
2- عدد السكان المستفيدين من المبنى لكل 1000 من السكان .
3- المساحة الصافية لكل مستفيد (م2 /شخص) .
4- الحد الاعلى للمسافة المقطوعة بين الوحدات السكنية و موقع المبنى .

جدول (1) التركيب الديمغرافي للمستفيدين من خدمات التعليم الثانوي و معايير توقيع هذه الخدمات

المستوى الدراسي	المتوسط	الاعدادي
الفئة العمرية للمستفيدين	14-12	17-15
نسبة المستفيدين الى مجموع السكان %	7,5	6,8
نسبة الطلبة الذين يستخدمون المبنى من حجم السكان %	90	90
عدد الطلبة في المدرسة	360	360
عدد السكان المطلوب توفرهم لانشاء مدرسة	4800	4800
مساحة قطعة الارض م2 / 100 شخص	2000-1600	1700-1400
مسافة الوصول بين المسكن و المدرسة (م)	800	800

المصدر : (Minstry of Housing , 1982 , part 2, p174)

و نلاحظ ان واضعو المعايير قد حددوا مسافة 800م حدا اقصى للمسير من المسكن الى المدرسة الثانوية (المتوسطة و الاعدادية) ، دون ان يكون هنالك مرونة في هذا المعيار على غرار المعايير العالمية مثل المعيار الامريكي الموضح في الشكل (4) و الذي حدد مسافة للمسير تتراوح بين (0.5 - 0.75) ميل أي (0.8 - 1.2) كم بالنسبة للمدارس المتوسطة و (0.75 - 1) أي (1.2 - 1.61) كم بالنسبة للمدارس الاعدادية (De Chiara,1969,p182-183) و هي بالتاكيد لا تنطبق على واقع المدينة العراقية لاختلاف الاعتبارات مثل المناخ و الخصائص الاجتماعية الاقتصادية و غيرها الا انه ينبغي الاخذ بالحسبان مستوى المرونة المحددة في المعيار و التي تساهم بشكل او باخر في اعطاء خيارات اوسع و مرونة اكبر للمخطط الحضري في تحديده لموقع الخدمة ضمن الحيز

الحضري و خصوصا في تصاميم المدن الجديدة ، و هنا ينبغي الالتفات الى مسالتين هامتين عند تحديد المعايير الاولى تتعلق بعمر الطالب و الثانية بجنسه اذ ان طالب المرحلة الاعدادية ذو بنية اقوى منها عند طالب المرحلة المتوسطة و كذلك ملكته العقلية و الفكرية مما يتيح له الانتقال الى مسافة اطول منها عند طالب المتوسطة ، و كذلك فان للذكور القدرة على المسير و الانتقال الى مسافة اطول منها بالنسبة للاناث و خاصة في مجتمع مثل المجتمع العراقي ، لذا يقترح البحث تخصيص معايير تراعي هذه المسائل من اجل التوصل الى توزيع يقترب من الصيغة الاكثر عدالة على مستوى هذه الخدمات علما انه قد اعتبر معيار 800م المعيار الاعلى و على اساسه صيغت بقية النسب جدول (2) .

جدول (2) معيار المسافة الاقصى لتوقيع المدارس المتوسطة و الاعدادية المقترحة

الجنس / المرحلة	المتوسط	الاعدادي
ذكور	750م	800م
اناث	700م	750م

شكل (4) التنظيم النموذجي لمواقع المؤسسات التعليمية بحسب المعيار الامريكي

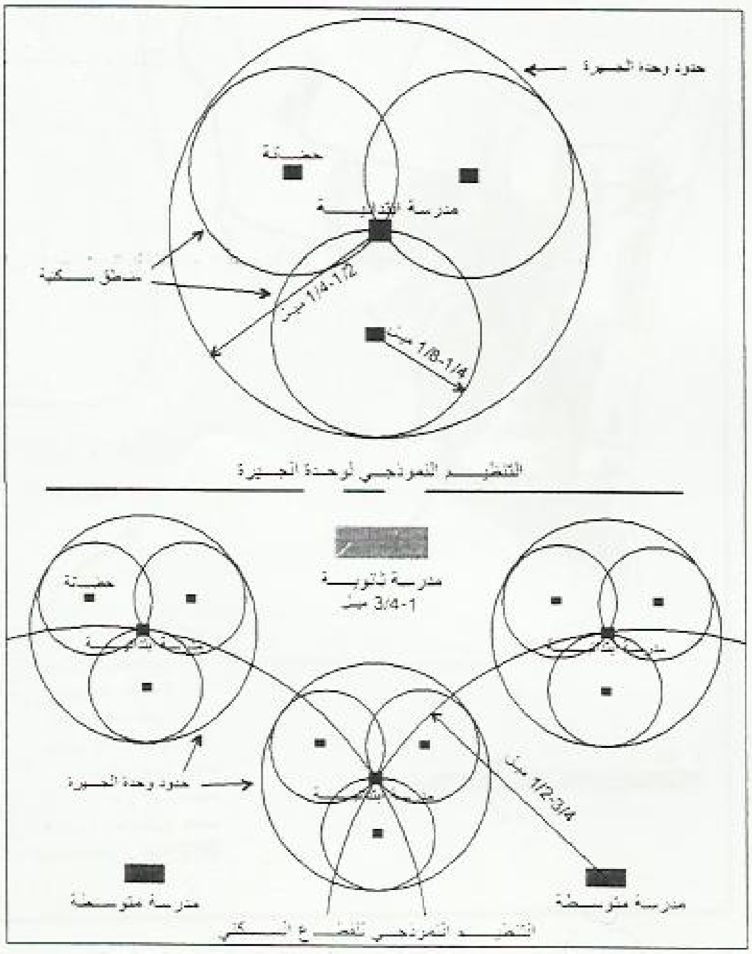

مصدر (De Chiara,1969,p179)

منطقة الدراسة ...

قطاع الدورة جزء من مدينة بغداد يقع جنوب الى جنوب شرق المدينة بمساحة تقدر بحوالي (82) كم2 يحدها من الشمال و الشرق نهر دجلة و من الغرب قطاع الرشيد اما من الجنوب فهي تحادد المناطق الجنوبية من محافظة بغداد ، توجد في منطقة الدراسة (46) مدرسة للتعليم الثانوي للعام الدراسي 2008-2009 خارطة (1) ، جدول (3) و(4) ، منها (14) مدرسة ثانوية أي تشمل المستويين المتوسط و الاعدادي (10) منها للاناث و (4) للذكور ، كما و تحوي على (24) مدرسة متوسطة (16) منها للذكور و (8) للاناث ، فضلا عن (8) مدارس اعدادية (4) للذكور و مثلها للاناث ، و سجل في منطقة الدراسة (25903) طالب في التعليم الثانوي (9025) طالب في المرحلة المتوسطة بالنسبة للذكور و (7249) بالنسبة للاناث ، و كذلك (5230) طالب في المرحلة الاعدادية بالنسبة للذكور و (4199) بالنسبة للاناث .

خارطة (١) توضح توزيع مدارس التعليم الثانوي في قطاع الدورة لعام ٢٠٠٩م

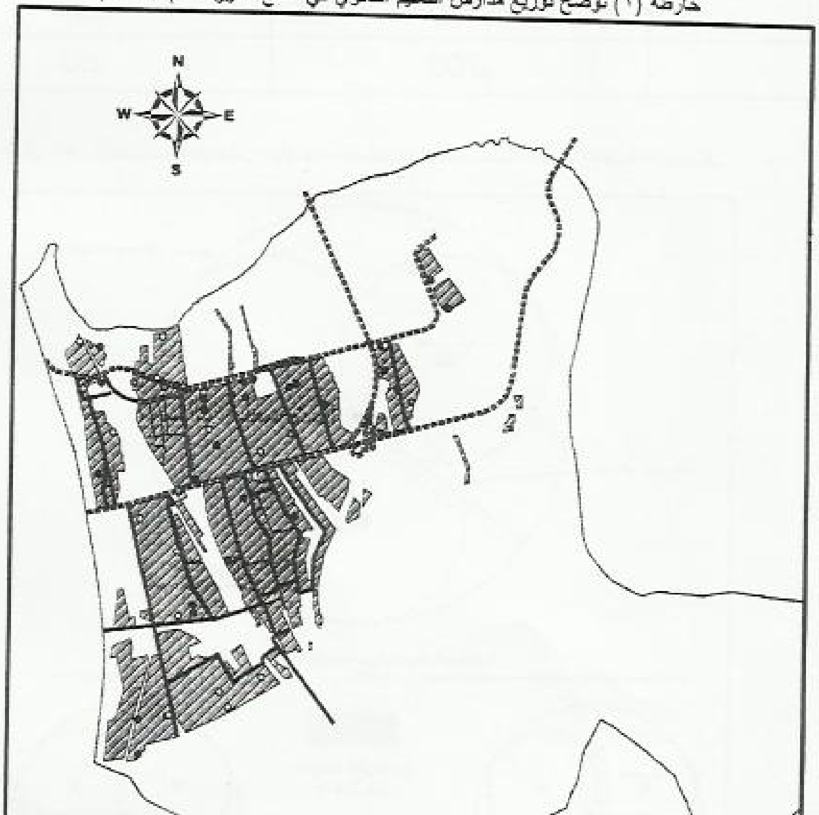

جدول (3) المدارس المتوسطة في قطاع الدورة للعم الدراسي 2008-2009

	اسم المدرسة	متوسطة ذكور	متوسطة اناث	اعدادي ذكور	اعدادي اناث	المجموع
1	م/بيروت	675	0	0	0	675
2	م/ام المومنين	0	411	0	0	411
3	م/الفاروق	656	0	0	0	656
4	م/الشيماء للبنات	0	256	0	0	256
5	م/ حمورابي للبنين	650	0	0	0	650
6	م/العفة للبنات	0	400	0	0	400
7	م/سكينة بنت الحسين	0	536	0	0	536
8	م/ انس ابن مالك	470	0	0	0	470
9	م/بنت الهدى	0	450	0	0	450
10	م/ضرار بن الازور	475	0	0	0	475
11	م/ السراج	319	0	0	0	319
12	م/دجلة	0	285	0	0	285
13	م/نابلس	433	0	0	0	433
14	م/ النجاح للبنين	600	0	0	0	600
15	م/طه حسين	510	0	0	0	510
16	م/النيل المسائية	225	0	0	0	225
17	م/معاذ بن جبل	755	0	0	0	755
18	م/الصابر للبنين	692	0	0	0	692
19	م/الخرطوم الا ساسية	0	265	0	0	265
20	م/حفصة	0	825	0	0	825
21	م/امنة بنت وهب	0	1050	0	0	1050
22	م/خالد بن الوليد	770	0	0	0	770
23	م/النسر العربي	165	0	0	0	165
24	م/علي بن ابي طالب	140	0	0	0	140
	المجموع	7535	4478	0	0	12013

المصدر: المديرية العامة لتربية الكرخ الثانية، 2009.

جدول (4) المدارس الاعدادية و الثانوية في قطاع الدورة للعام الدراسي 2008-2009

	اسم المدرسة	متوسطة ذكور	متوسطة اناث	اعدادي ذكور	اعدادي اناث	المجموع
1	ع/دمشق	0	0	710	0	710
2	ع/رقية	0	0	0	231	231
3	ع/نبوخذ نصر للبنين	0	0	1050	0	1050
4	ع/الامال	0	0	0	734	734
5	ع/التقى	0	0	0	815	815
6	ع/ تطوان للبنين	0	0	620	0	620
7	ع/ النهرين للبنين	0	0	1700	0	1700
8	ع/خديجة الكبرى	0	0	0	851	851
9	ث/الجمهورية	0	465	0	375	840
10	ث/ابن سينا للبنات	235	0	515	0	750
11	ث/ البتول للبنات	0	225	0	310	535
12	ث/مريم العذراء	0	235	0	520	755
13	ث/ ذو النورين للبنين	360	0	280	0	640
14	ث/العقيدة	0	340	0	283	623
15	ث/فاطمة الزهراء	0	250	0	201	451
16	ث/ذات النطاقين	0	187	0	160	347
17	ث/النهضة للبنات	0	376	0	129	505
18	ث/العلا المسائية	504	0	260	0	764
19	ث/المعينية	320	0	295	0	615
20	ث/عشتار للبنات	0	285	0	165	450
21	ث/ الطاهرة للبنات	0	190	0	50	240
22	ث/الزهور للبنات	0	245	0	140	385
	المجموع	1419	2798	5430	4964	14611

المصدر :المديرية العامة لتربية الكرخ الثانية ، 2009

و من الجدول (3) و (4) نلاحظ ارتفاع اعداد الطلبة المسجلين في معظم مدارس منطقة الدراسة فوق المعيار العراقي الذي حدده مخطط الاسكان العام لسنة 1982 ، الذي بلغ 360طالب/المدرسة لكل من المتوسطة و الاعدادية ، اذ ان هنالك 19 مدرسة متوسطة في منطقة الدراسة و 9 مدارس اعدادية دون مستوى هذا المعيار ، و يعود ذلك الى ارتفاع حجم السكان في هذا القطاع مقارنة مع انخفاض عدد مدارس التعليم الثانوي فيه ، اذ بلغ عدد سكان قطاع الدورة سنة 2008 (324000) نسمة حسب تقديرات الجهاز المركزي للاحصاء (وزارة التخطيط ،2007،ص53) و قد تم تقدير عدد السكان لسنة الهدف المتمثلة في سنة 2018 بالاعتماد على معدل النمو لمدينة بغداد البالغ 3% ، و ظهر ان عدد السكان لهذا القطاع ستكون (435429) نسمة ، و من خلال عدد السكان الحالي و المستقبلي (سنة الهدف) يمكن حساب عدد المدارس الثانوية المطلوبة لسد النقص في عدد مدارس منطقة الدراسة وفق المعايير التي وضعتها دراسة مخطط الاسكان العام المشار اليها ، و ذلك في الجدول (5).

جدول (5) مقدار العجز في عدد مدارس التعليم الثانوي لكلا الجنسين في منطقة الدراسة

المستوى		نسبة المستفيدين الى مجموع السكان	نسبة الطلبة الذين يستخدمون المبنى من حجم السكان	المدارس المطلوبة	المدارس المتاحة	العجز في عدد المدارس
متوسط	2008	24300	21870	60	38	22
اعدادي		22032	19828	55	20	35
المجموع		46332	41698	115	58	57
متوسط	2018	32657	29391	81	38	43
اعدادي		29609	26648	74	20	54
المجموع		62266	56039	155	58	97

من خلال الجدول (5) ظهر ان عدد المستفيدين من مدارس التعليم الثانوي في منطقة الدراسة قد بلغ (46332) شخص بواقع (24300) متوسط (22032) اعدادي ، اما عدد المستخدمين فعلا فقد بلغ (41698) طالب (21870) متوسط (19828) اعدادي ، و كان عدد المدارس المطلوبة في منطقة الدراسة و حسب المعيار (115) مدرسة علما ان المدارس

المتاحة هي (58) مدرسة متوسطة و اعدادية ، اما العجز فقد بلغ (57) مدرسة (22) متوسطة و (35) اعدادية موزعة على منطقة الدراسة هذا فيما يخص واقع الحال ، اما بالنسبة لسنة الهدف فسوف يبلغ العجز في مدارس التعليم الثانوي (97) مدرسة (43) متوسطة و (54) اعدادية ، و يمكن تحديد مواقع مدارس التعليم الثانوي المطلوبة في الوقت الراهن اما فيما يخص سنة الهدف 2018 فلا يمكن تحديد اماكن هذه المدارس الا بعد تحديد مناطق التوسع العمراني المحتملة حتى سنة الهدف ، و لتحديد الاماكن التي ينبغي توقيع هذه المدارس فيها بواسطة تقنية مناطق التاثير في نظام المعلومات الجغرافي من خلال تطبيق مجموعة من الطبقات المنتجة في برنامج ال Arcgis 9.2 بالاستعانة بصورة جوية لمدينة بغداد من نوع Mr. Sid وقد تمثلت هذه الطبقات في :

الاولى : تشمل مناطق الاستخدام السكني للارض في قطاع الدورة و الذي يمثل المنطقة المراد توفير خدمة المدارس الثانوية فيها .

الثانية : مواقع المدارس الحالية و انطقة التاثير لها و التي تمثل مسافة المسير من المسكن الى موقع الخدمة (المدرسة) فان المناطق السكنية الواقعة ضمن منطقة التاثير هذه في الحواجز تعد مناطق مخدومة بمدارس التعليم الثانوي و التي هي في الغالب لا تحتاج لتوقيع مدارس اضافية الا في حالات معينة مثل مناطق الكثافات السكانية العالية ، على سبيل المثال لا الحصر منطقة العمارات السكنية ، و هو امر لم تتطرق اليه هذه الدراسة بسبب عدم توفر معلومات دقيقة عن كثافات السكان في منطقة الدراسة كي تدخل ضمن اعتبارات توقيع المدارس الثانوية الجديدة ، حالها حال اهمية اعتبار توفر الاراضي الفارغة غير المستغلة و التي يمكن استغلالها في توقيع مدارس للتعليم الثانوي في المناطق غير المخدومة و التي لم تتوفر بيانات بخصوصها أيضا ، و يوصي البحث ان تؤخذ هذه الاعتبارات بالحسبان عند المحاولة الجادة في توقيع هذه الخدمات بشكل دقيق و تؤشر على هيئة طبقات ضمن طبقات برنامج المعلومات الجغرافية الاخرى ، كذلك ينبغي تاشير طبقة اخرى تمثل المحددات التي لا يمكن مع وجودها توقيع مدارس التعليم الثانوي فيها مثل المناطق المعرضة للتلوث بانواعه و مناطق الطرق السريعة و الاسواق المزدحمة ، و غيرها من المحددات المختلفة و التي تختلف باختلاف المنطقة المدروسة .

و من خلال عملية دمج مجموعة الخرائط المنتجة في برنامج Arcgis 9.2 و المتمثلة بالطبقات المختلفة الداخلة في عملية التحليل (مناطق الاستعمال السكني و أي متغيرات اخرى ممكن ان تدخل في عملية التحليل فضلا عن طبقات مناطق التاثير (الحواجز) المنتجة في البرنامج) ، يمكن تحديد المناطق التي تصلح في عملية توقيع الخدمات الجديدة من مدارس

التعليم الثانوي ، لتلبية حاجة المنطقة من النقص في هذه الخدمات و لتغطية حالتي العجز المتمثلة في :

- حالة العجز العددية من حيث الفرق بين العرض من هذه الخدمات و كمية الطلب عليها في منطقة الدراسة .
- حالة العجز الموقعية من حيث عدم شمول مناطق معينة بهذه الخدمة يكون فيها معدل مسافة المسير بصورة مناسبة و حسب المعيار .

و تعد مناطق الاستعمال السكني غير المغطاة بانطقة التاثير لمختلف مدارس التعليم الثانوي في الخرائط (5،4،3،2) هي المناطق ذات الاولوية في عملية توقيع خدمات التعليم الثانوي المقترحة الجديدة و التي تم تأشيرها في الخرائط (9،8،7،6)، في المستويات المختلفة المتوسطة و الاعدادية للذكور و الاناث كل على حدة و كما مؤشر في الخارطة الخاصة بكل صنف منها .

خارطة (٢) توضح نطاق التاثير للمدارس المتوسطة للذكور في قطاع الدورة لعام ٢٠٠٩م

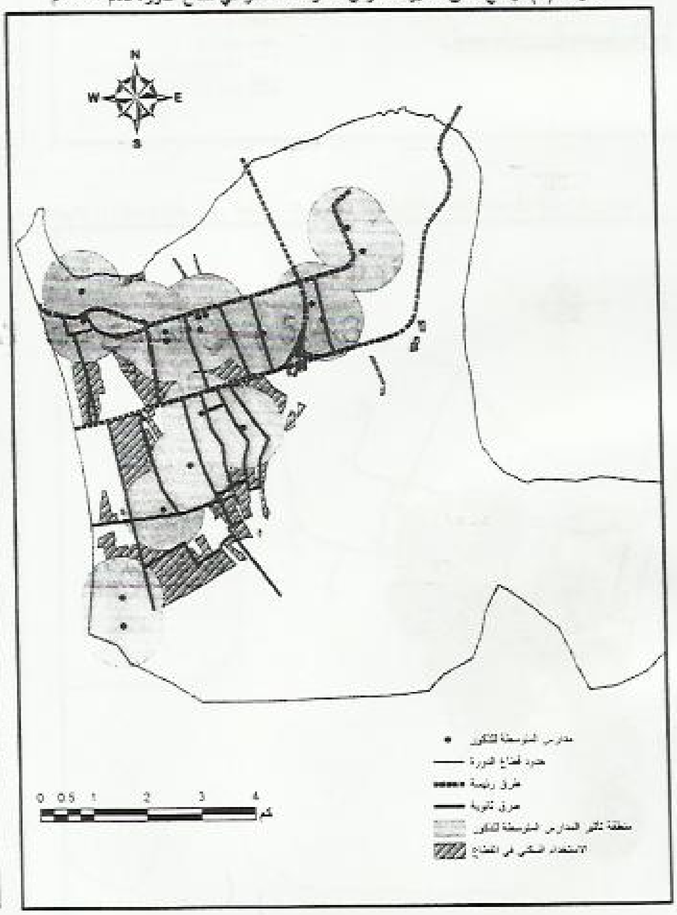

خارطة (٣) توضح نطاق التاثير للمدارس المتوسطة للاناث في قطاع الدورة لعام ٢٠٠٩م

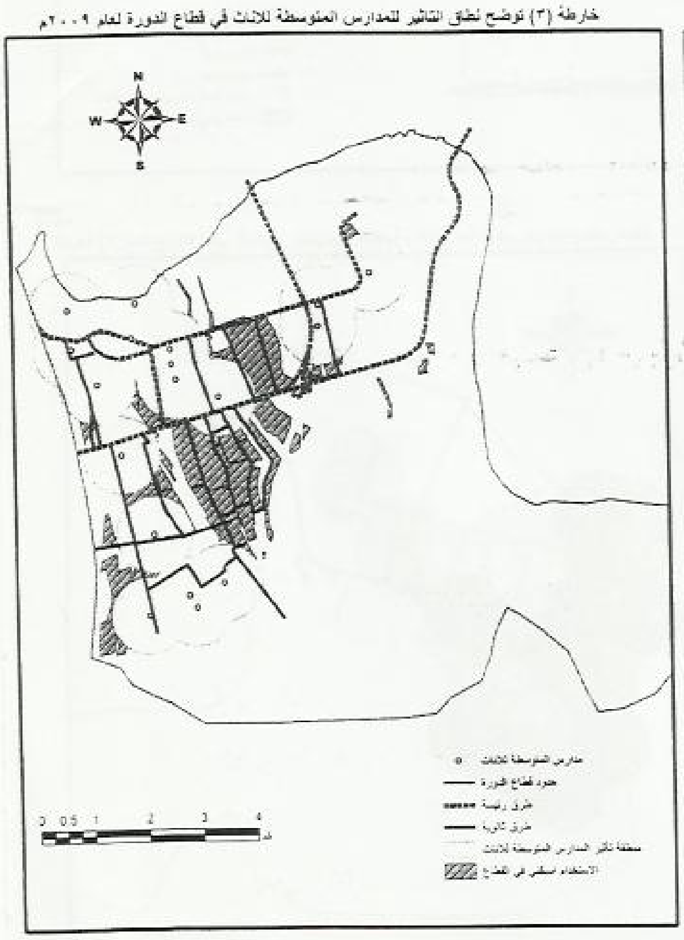

خارطة (٤) توضح نطاق التأثير للمدارس الاعدادية للذكور في قطاع الدورة لعام ٢٠٠٩م

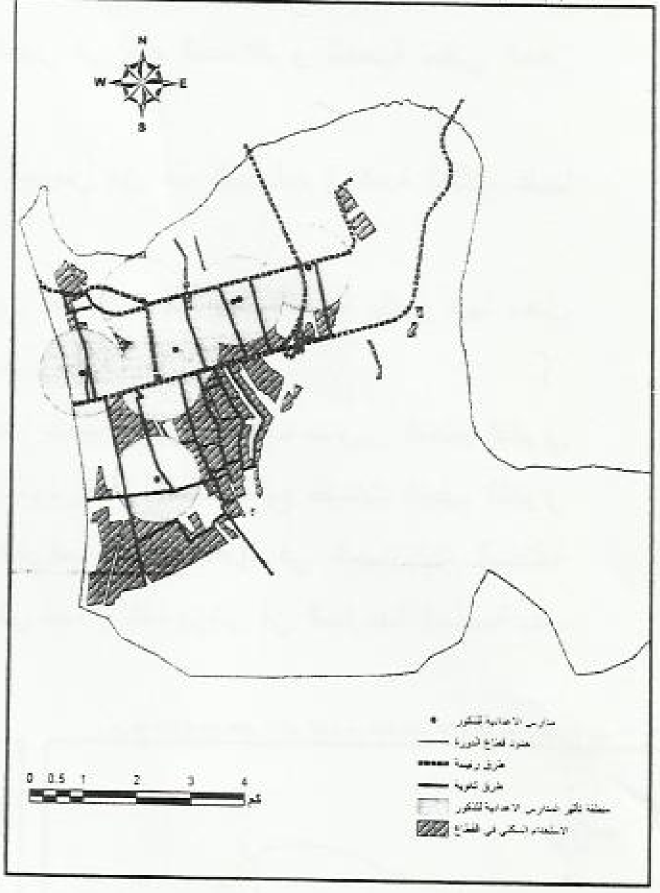

خارطة (٥) توضح نطاق التأثير للمدارس الاعدادية للاناث في قطاع الدورة لعام ٢٠٠٩م

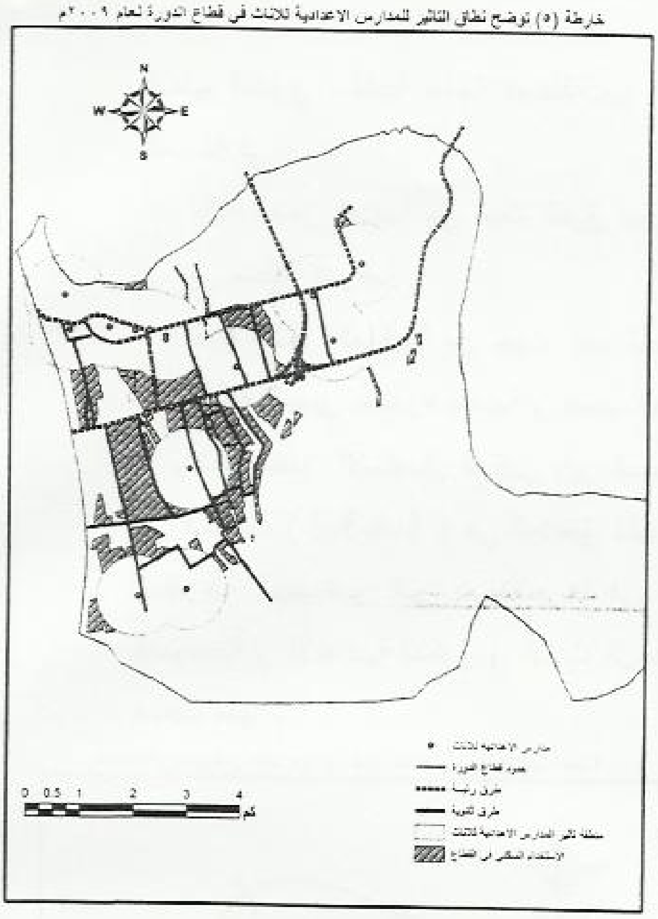

خارطة (٦) توضح نطاق تاثير المدارس المتوسطة الحالية و المقترحة للذكور في قطاع الدورة لعام ٢٠٠٩م

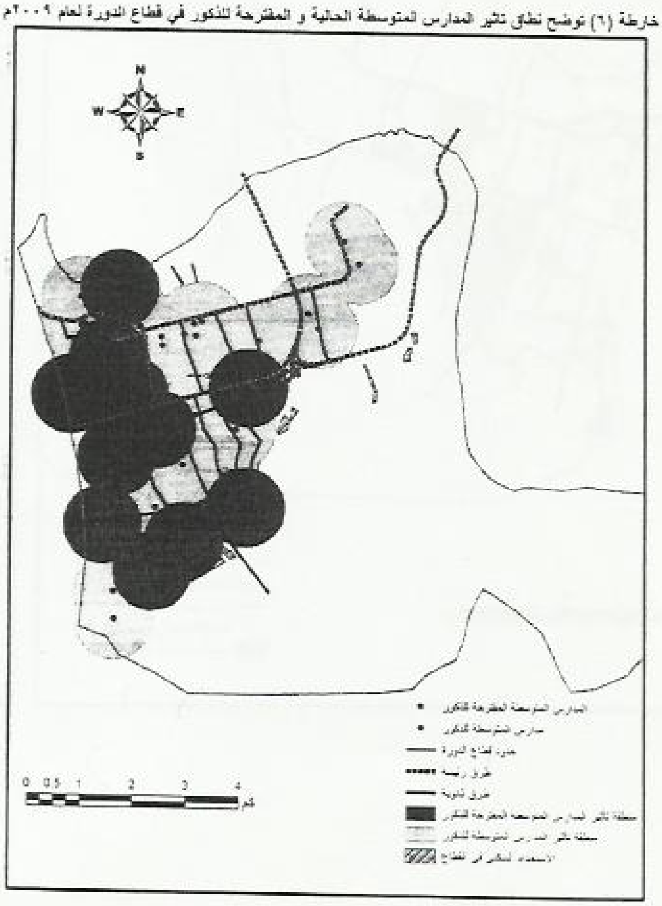

خارطة (٧) توضح نطاق تاثير المدارس المتوسطة الحالية و المقترحة للاناث في قطاع الدورة لعام ٢٠٠٩م

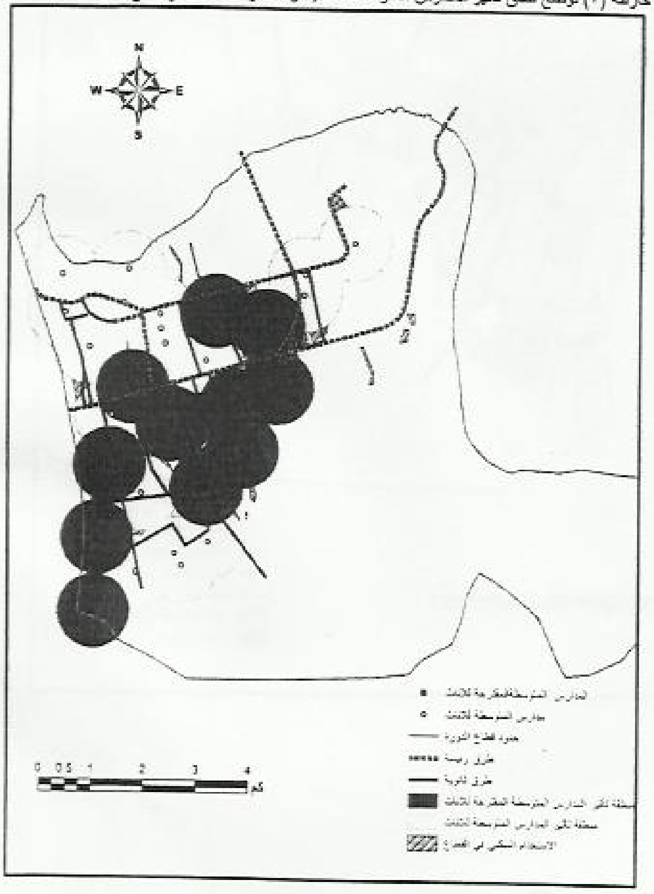

خارطة (٨) توضح نطاق تاثير المدارس الاعدادية الحالية و المقترحة للذكور في قطاع الدورة لعام ٢٠٠٩م

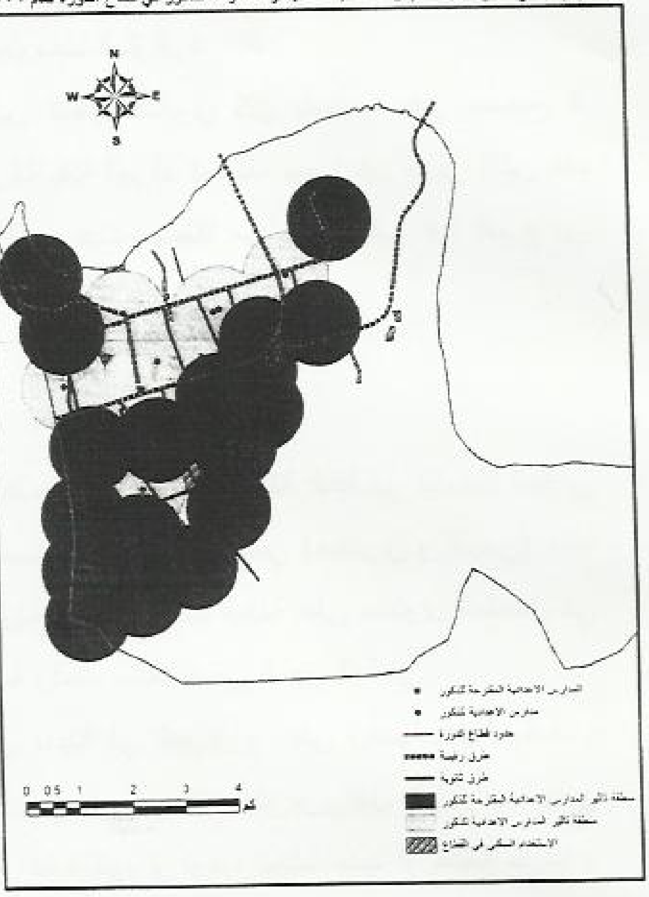

خارطة (٩) توضح نطاق تاثير المدارس الاعدادية الحالية و المقترحة للاناث في قطاع الدورة لعام ٢٠٠٩م

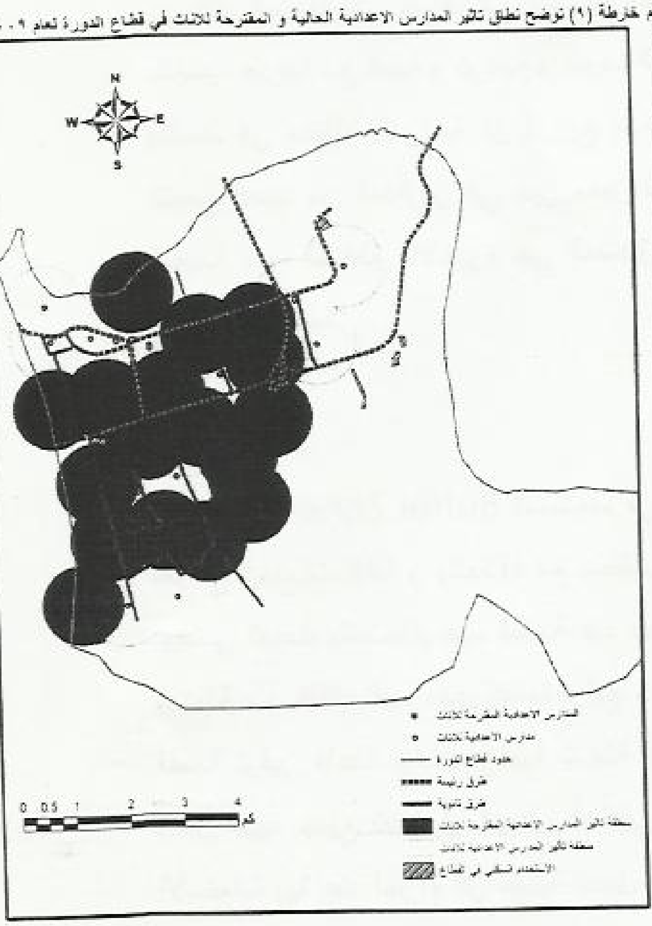

الاستنتاجات ...

- ان دور التقنيات الحديثة مثل نظام المعلومات الجغرافي GIS في مجال التخطيط الحضري و الاقليمي يكمن في دور المخطط لتحديد مشاكل المجتمع و تمريرها الى متخذ القرار مع النتائج المترتبة عليها و البدائل التي تؤمن حلها .
- يساعد نظام ال GIS في التحديد الدقيق للمواقع الجغرافية و اجراء العديد من متطلبات عمل المخطط بصورة سريعة و دقيقة للعديد من المواقع و البيانات في ان واحد ، و ذلك مما ساعد على تذليل العديد من الصعوبات التي يواجهها واضعو الخطط الحضرية و الاقليمية .
- تساعد برامج الGIS كل من المخطط الحضري و الاقليمي و الجغرافي و المهندس و غيرهم من المهتمين بالتحليلات و العلاقات المكانية ، على قراءة الخارطة التوزيعية لاية ظاهرة جغرافية ام غير جغرافية و في جميع المستويات (محلية ، حضرية ، اقليمية ، قومية) .

- ان الخطوة الاولى لاعداد قاعدة بيانات عن أي منطقة ما هو توفير البيانات الضرورية الكاملة عن تلك المنطقة لكي تساهم في استنباط العلاقات فيها ، و مما لا شك فيه ان كفاءة اداء النظام يتناسب طرديا مع كمية و نوعية و جودة المعلومات المتوافرة.
- يلاحظ في منطقة الدراسة ان توزيع مدارس التعليم الثانوي كان باسلوب غير صحيح اذ تتجمع العديد من المدارس في حيز معين تاركة بقية اجزاء المنطقة بعيدا عن نطاق تاثير هذه الخدمة ، و المناطق الاخيرة هي المناطق التي عدت مناطقا مرشحة لتوقيع هذا النوع من الخدمات مستقبلا .

التوصيات ...

- يوفر نظام Buffer Zone المستخدم في هذه الدراسة امكانية فائقة الدقة في التحديد المكاني لمواقع الخدمات كافة و بالعلاقة مع مختلف مستويات الهيكل المكاني (حضري و اقليمي) ، لذا يوصي البحث باستخدام هذه التقنية عند محاولة توقيع خدمات معينة على مستوى المناطق في المدينة ، و كذلك تقييم مدى كفاءة توقيع خدمة وقعت سابقا ضمن الحيز المكاني .
- اهمية توفير قاعدة بيانات رقمية شاملة لاي مدينة في العراق و على رأسها مدينة بغداد ، تتمثل فيها جميع تفاصيل الهيكل المكاني و من ضمنها الخدمات من اجل الرجوع اليها و الاستعانة بها عند اجراء أي عملية تحليل او اعادة تقييم او توقيع لمنشأ جديد او خدمة جديدة و بحسب متطلبات و معايير التوقيع المرغوبة .
- عند اجراء دراسات تهتم بتوقيع الخدمات المجتمعية في أي مدينة ينبغي الانتباه الى جميع المؤثرات التي لها العلاقة في تحديد الموقع الامثل لهذه الخدمة من اجل تحقيق افضل منفعة ممكنة لهذه الخدمة و باقل كلف .

المصادر ...

- داؤود ، سالم داؤود ، التوزيع الجغرافي للمدارس المتوسطة في مدينة الموصل ، مجلة التربية و العلوم ، العدد التاسع ، 1990.
- ديكس،اج،ام،التلوث البيئي،ترجمة كوركيس عبد ال ادم،مطبعة جامعة البصرة ، 1988.
- رزوقي ، دريد موسى ، الاسس التخطيطية و التصميمية و تاثيرها على الاداء الوظيفي لابنية المدارس في العراق ، رسالة ماجستير ، جامعة بغداد ، كلية الهندسة ، 1987.
- زرقطة ، هيثم يوسف ، نظام المعلومات الجغرافية GIS الدليل العملي الكامل لنظام Arcview9 ، الطبعة الاولى ، دار شعاع للنشر ، سوريا ،2007.

- الشافعي ، شريف فتحي،الدليل العلمي لادارة نظام المعلومات الجغرافية GIS باستخدام المجموعة البرمجية Arcgis Desktop ، دار الكتب العلمية للنشر ، القاهرة ، 2009 .
- الفتلي ، باسل احمد خلف ، تقويم كفاءة التصميم الاساسي لمدينة الحلة ، اطروحة دكتوراه ، جامعة بغداد ، مركز التخطيط الحضري و الاقليمي ، 1998 .
- المديرية العامة لتربية الكرخ الثانية ، احصاءات المدارس الثانوية ، بيانات غير منشورة ، 2009.
- مزعل ، جمال اسد ، نظام التعليم في العراق ، مديرية دار الكتب للطباعة و النشر ، بغداد ، 1990.
- وزارة التخطيط ، الجهاز المركزي للاحصاء ، نتائج تقديرات السكان لعام ، 2007.
- وزارة التخطيط ، هيئة التخطيط الاقليمي ، قسم الاسكان و المستوطنات البشرية ، اسس و معايير الاسكان الحضري ، حزيران ، 1977.

- Birkin , Mark & Others , Intelligent GIS Location Decisions & Strategic Planning , Co published in the American with John wiley , and sons Inc 605 Third avenue , New York , NY10158,1996.
- Chang , kang-Tusng ,Introduction to Geographic Information System , McGraw-Hill comp.Inc , New York ,2002 .
- DE Chiara , joseph and Lee Koppelman , planning design criteria , Van Nostrand Reinhold company , New York , Litton Educational publishing , Inc. , 1969 .
- Demers , Michael , N , Fundamentals of Geographic Information Systems , Second Edition , John Wiley , and sons , Inc , 2003 .
- M. Smith , Jason , Arcgis-Buffering , (www.pop-psu/gis-cove/pdts/gis-rd-o2-50/2002).
- Ministry of Housing &Construction , state organization for housing , Housing Technical & Codes of Practice , Part2 , Baghdad , 1982 .

الادراك البصري للفضاء الداخلي في مستشفيات الاطفال

د.هدى عبد الصاحب العلوان
استاذ مساعد
كلية الهندسة/جامعة بغداد

وديان هشام عبدالله الخالدي
ماجستير هندسة معمارية

مستخلص البحث:-

يمثل الأطفال شريحة مهمة في المجتمع بوصفهم أهم مقومات بنائه، ومن ثم فإن مسؤولية توفير أفضل خدمات الرعاية الصحية لهم على وفق الطريقة الملائمة لاعمارهم تقع على عاتق المجتمع بكافة مؤسساته. لذا إنصب اهتمام المخططين والمهندسين المعماريين وعلماء النفس والإجتماع على حد سواء في طرح الإعتبارات الرئيسة عند تصميم البيئة الداخلية لمرافق الرعاية الصحية للأطفال، لتحقيق بيئة علاجية تسهم في التخفيف من حدة الالم والخوف والقلق عند الطفل فضلا عن تعزيز الإحساس بالأمن والسلامة لديه مما يسهم في سرعة شفائه وتقليل مدة اقامته في المستشفى.

وتلعب المثيرات (Stimuli) دوراً رئيسياً في تصميم الفضاء الداخلي في مستشفيات الاطفال لما لها من تأثير مباشر على الحواس يسهم في خلق الاجواء الصحية والنفسية الملائمة للعلاج الطبي.ان توظيف المثيرات الحسية ولاسيما البصرية (الضوء،اللون،الاعمال الفنية،المناظر الطبيعية،الاشارات والرموز...الخ) في الفضاءات الداخلية يحفز الاطفال على حب المكان والحركة واللعب والتخيل فيه فضلاً عن خلق جو آمن مرح يطمئن فيه الطفل وينسى مخاوفه وألامه..

لقد تحددت مشكلة البحث بالحاجة العلمية للتعرف على دور المثيرات الحسية البصرية في إدراك البيئة الداخلية لمستشفيات الأطفال، إذ يهدف البحث الحالي الى الكشف عن اسس تأثير تلك المثيرات الحسية، والوصول الى انموذج معماري مستقبلي لابنية مستشفيات الاطفال بشكل خاص والابنية الخاصة بالاطفال بشكل عام، مفترضاً تأثر إدراك البيئة الداخلية لمستشفيات الأطفال بالمثيرات الحسية عامة والمنبهات البصرية خاصة، التي لها أثر نفسي إيجابي عند الأطفال يسهم في تسريع العملية الشفائية.

لقد تطلب تحقيق الهدف بناء الاطار النظري للبحث ومن ثم تطبيق الاطار على بيئات معمارية منتخبة بهدف اختبار صحة الفرضية ثم استخلاص اسس تأثير المثيرات الحسية البصرية وآلياتها..وأظهرت نتائج الدراسة الاهمية الفاعلة لمؤشرات اللون و الضوء الطبيعي و المناظرالطبيعية ووجود الاشارات في ممرات المستشفى واثرها في ايجاد الطفل لطريقه واستخدام التعابير البصرية للتقليل من مخاوف الطفل. كما افرزت الاستنتاجات النهائية اهمية الدور التصميمي للبيئة المحيطة في اماكن العلاج الذي يساعد الاطفال على تحمل الضغط والتوتر الناجم عن المرض. وبما يحقق الاجواء الملائمة للتكامل بين العقل والجسد والروح ضمن بيئة المستشفى.

VISUAL PERCEPTION OF INTERIOR SPACES IN PAEDIATRIC HOSPITALS

ABSTRACT:

Children represent an important category in any society being the most important basis of its structure.Thence the society is utterly responsible for providing children with the healthiest services. Architects, planners, psychologists and sociologists have taken into account major considerations when designing the interior spaces in health institutions to help reinforce a curing environment. This is hoped to decrease pain, fear and anxiety, which in turn would enhance the feeling of security and safety in the child and fasten his cure and decrease the period of his stay in the hospital.

Stimuli play a significant role in designing the interior space of paediatric hospitals as they have a direct influence on the senses and would create the required psychological environment for medical treatment. The use of various sensory stimuli especially visual ones (light, color, artworks, signs, natural scenes …etc) would create a love relation between the child & the place and encourage movement, playing and imagination. In addition it would create a pleasant and secure environment for children to feel secure and forget their fears and pain.

The problem, the research will tackle, is limited to the scientific need to explore the role that visual stimuli play in the perception of the interior environment in paediatric hospitals. The research seeks to discover the influence of the visual stimuli to create an ideal architectural design for the future building of paediatric hospitals. Assuming that visual perception would have apositive, psychological effect on sick children which is hoped to accelerate healing.

To achieve the aim of the study, a theoretical framework has been set up first and then applied to selected architectural environments in order to verify the hypothesis adopted in this research and to infer the influence of the visual stimuli hoping to get an ideal architectural design for the future building of paediatric hospitals. The final conclusion reveal the importance of the role played by the visual stimuli: color, natural light and natural scenery as well as the presence of signs in the hospital corridors which have an effect on helping children find their way and reducing fear.The final conclusion also emphasize the importance of the role played by the surrounding environment in the treatment area, to help sick children endure pressure resulted from pain. And create a suitable place where the mind, body and spirit incooperate with the hospitals environment .

المقدمة

تلعب الاجواء الداخلية لمستشفى الاطفال دوراً مهماً في التأثيرعلى نفسية الطفل وسير العملية العلاجية وقد ينعكس تأثيرها سلباً أو ايجاباً على الاطفال المرضى . وتلعب المثيرات (Stimuli) دوراً رئيساً في تصميم الفضاء الداخلي لما لها من تأثير مباشر في الحواس يسهم في خلق الاجواء الصحية والنفسية الملائمة للعلاج الطبي .

إن من اهم الجوانب التي يجب تأكيدها هو تداخل المثيرات الحسية مع الجانب المعماري إذ إن اصعب مايتعرض له المصمم هو خطأ الوقوع في العمارة الجامدة دون ادنى مراعاة للمثيرات الحسية مما ينعكس سلبا على التحديد الفراغي والتشكيل والتأثيرالبصري السيكولوجي للاطفال وفهم الابعاد الحقيقية وقيود الحواس تمكن المصمم من ايجاد بيئات يستجيب اليها الطفل المريض.

ويتناول البحث دراسة دور المثيرات الحسية البصرية في إدراك الفضاء الداخلي في مستشفيات الاطفال إذ يلعب الإدراك البصري دوراً أساسياً في الإدراك الحسي للفضاء من خلال مثيرات اللون والاضاءة والطبيعة والاعمال الفنية

والرموز والإشارات .كما يتناول البحث دور المثيرات الحسية البصرية في تشكيل صورة ذهنية واضحة ومتماسكة للفضاء الداخلي تشعر الطفل بالراحة والاطمئنان والأمان.

الدراسات السابقة

*** دراسة (National Health Services: NHS)**

"Hospital Accommodation for Children and Young People",2004.

تصف هذه الدراسة أفضل شكل للممارسة المعمارية في البيئة العمرانية من منظور الطفل نفسه، كما تتضمن وجهات نظر وأفكار ذوي الأطفال، إذ تكمن الاعتبارات الرئيسة للمخططين والمهندسين المعماريين عند تصميم مرافق الرعاية الصحية للأطفال في التخفيف من حدة الخوف والقلق وتعزيز الأمن والسلامة، والحد من الملل لديهم، وتهيئة بيئة شفائية، فضلاً عن تلبية تلك المرافق الصحية احتياجات المرافقين للطفل.

وتتوصل الدراسة إلى أن تصميم المدركات الحسية أمر أساس في عملية شفاء الطفل، إذ إن الأطفال يفهمون محيطهم من خلال حواسهم الخمس. كما تؤكد أيضاً أن تأخذ الاعتبارات التصميمية في الحسبان العلاقة مع الطبيعة والمشتتات عن الآلام مثل الموسيقى والفن والترفيه وتجنب الإجهاد البيئي ، فضلاً عن أهمية الإرشادات الفنية العامة.

*** دراسة (Al Aynsley Green)**

"Friendly Healthcare Environment for Children and Young People",2003.

تتبنى هذا الدراسة توجها استرتيجيا بعنوان تحسين تجربة المريض "Improving the Patient Experience"، لتصف كيفية تحسين الخدمات المقدمة للأطفال الصغاروالاستراتيجات التخطيطة عبر تحديد احتياجاتهم لتصميم المرافق الصحية والمبادئ الرئيسة لأفضل الممارسات التصميمة من خلال دراسة عملية لمجموعة من مستشفيات الأطفال، ليضع بموجب تلك النتائج الخطوط العريضة الرئسية لإيجاد الاعتبارات التصميمية التي تخاطب كلاً من الصغار والبالغين.

وتشير الدراسة بوضوح الى أنَّ تصميم فضاءات المستشفى وآستخدام الإضاءة ، واللون والصوت الخفيف، وتفصيلات المواد والملمس تعد أساسية للشفاء المباشر للطفل والحصيلة النهائية للعملية الشفائية،ليضع في النهاية المبادئ التوجيهية التصميمية بالارتباط بالحواس الخمس كلها.

3.دراسة (Rosalyn Cama)

"Art in Children's Environment" ,1999.

ترى الدراسة أن مستشفى الأطفال ليس بناءً مجرداً، إنمّا مكاناً لتلبية حاجاتهم الصحية. وتطرح الدراسة بموجب ذلك الاعمال الفنية بوصفها مفردة من مفردات التخطيط الشاملة لعوامل الرعاية الصحية. وتوصلت الدراسة إلى أن مستشفيات الأطفال هي مراكز للاستشفاء والرعاية وعامل مساعد للتطوير السليم للأطفال ونموهم ولا بد من العمل الفني لتحقيق ذلك.

4. دراسة (John Pangrazio)

" Healing Environemnts",1999.

تبدأ الدراسة بوصف البيئة العلاجية للطفل،وتشدد الدراسة على أهمية إدراك مصممي البيئات العلاجية، مدى تأثير تصاميمهم في تطور العملية العلاجية، إذ إن هناك عوامل عديدة تسهم في تعزيز الشفاء، فمن الضروري أن يكون هناك تكامل في العقل والجسد والروح لخلق أجواء ملائمة تصون خصوصية المريض ووقاره وهويته وأمنه ومكانته الاجتماعية، ويمكن تحقق هذا كله بتصميم بيئات علاجية تعزز الآتي:

1 . فرص الحركة التي تسمح للأطفال للتنقل بحرية والوصول إلى مواقع معينة ورسم تصورات واضحة للمبنى.

2 . الراحة والأمان والتحفيز والتنوع الحسي.

3. التحكم والإدراك اللذان يسمحان للطفل بضبط مستويات الرؤيا والصوت.

4. دعم الطفل اجتماعياً من خلال توفير المرافق المريحة لعائلته وأقربائه.

5. توافر الملهيات الإيجابية التي تزيل التوتر مثل الموسيقى والمشاهد الكوميدية والعناصر الطبيعية ومشاهدة الحيوانات الأليفة.

فالمراكز العلاجية على وفق الدراسة ليست ملزمة بتزويد المرضى بأسباب العلاج، لكنها ملزمة أيضاً بتفقد حاجاتهم الاجتماعية والنفسية والتنموية.

*** دراسة John I.Plappert and Linda M.Gabel**

"Interior Design, (Furnishing α Way Finding)",1999.

تهتم الدراسة بمسألة البيئة الداخلية لمستشفيات الأطفال وعلاقتها بتقديم الدعم النفسي لكل من الطفل وعائلته ومن ثم خلق البيئة الشفائية.وتناقش الدراسة العوامل الفاعلة في إيجاد بيئة شافية، فضلاً مفاهيم تخص توافر الملهيات الإجابية للأطفال وتوافر المناظر الطبيعية واستخدام ألوان الطيف ومصادر الضوء، لما لها من تأثيرات نفسية إيجابية، كما أنها تنعش الأجواء وتفعل الحركة الداخلية، وتزود المرضى وعائلاتهم بإحساس الزمان والمكان.وعليه فإنه عند تصميم مستشفيات الأطفال وبنائها يجب مراعاة حاجة الطفل للعب وأن توفرالفرصة له لإشباع رغباته وميوله وتحفيزه على الحركة والتخيل مع خلق بيئة امنة.

يتبين من آستكشاف الطروحات المعمارية السابقة، أنها طرحت جوانب معرفية متعددة ومتنوعة ومتباينة في سعتها المعرفية فيما يخص دور المثير الحسي البصري في إدراك البيئة الداخلية لمستشفيات الأطفال ليتضح النقص المعرفي المتمثل بأن بعض الدراسات السابقة تناولت جوانب معرفية عامة دون التطرق الى جوانبها التفصيلية، او انها ركزت على بعض الجوانب التفصيلية دون الخوض في أطرها العامة.

المحور الاول:الاطار النظري

المثيرات الحسية البصرية

تعد حاسة البصر الحاسة الأولية التي يجمع الانسان من خلالها المعلومات عن بيئته، لذلك يكون احساسه بالمكان في البداية مرئي ولايحد الاحساس البصري بالبيئة سوى مجال الرؤيا.فالعين هي امتداد الدماغ و يستمر نموها وتطورهـــا بعد الولادة . لذلك هناك مثيرات بصريه وجب الاهتمام بها لاهميتها للاطفال. (Grauer,1989,p.53).

ويعدالضوء واللون الجانبان الرئيسان المؤثران في البصر ولهما أكبر الاثر في بهجة المريض ،فضلاً عن العمل الفني في المستشفى والتواصل مع الطبيعة و الرموز والإشارات. لهذا يتوجب الاهتمام بالتحفيز البصري المستمر بتوظيف مجموعة متنوعة من اللون ومستويات الاضاءة بما يضمن عدم اصابة الاطفال بالضجر ،إذاً عدم وجود التحفيز الكـــافي يسبب رتابة البيئات البصرية.

وعليه فإن حاسة البصر هي من أهم الحواس ولها الأهميه الكبرى في إدراك الفضاء باعتبارها الحاسة الأولى التي يجمع بها الطفل معلوماته عن بيئته.لذا سيتم القاء الضوء على المؤشرات التي تخاطب المثير البصري التي قد يكون تأثيرها ايجابيا إذا صممت بعناية او قد تكون سلبية مؤدية الى إزعاج المريض.

* الضوء

في مستشفيات الاطفال يمكن ان يوفر الاهتمام البصري من خلال الاضاءة والتنوع بها لخلق التحفيز البصري . وكماأن للاضاءة ايجابيات فأحياناً تكون لها سلبياتها فمثلا الاطفال الصغار(حديثي الولادة) الذين ولدوا قبل أوانهم يكونوا حساسين للضوء الساطع الذي يمكن ان يسبب الإجهاد وأيضاً أضرار في شبكية العين ولكنهم أيضاً يحتاجون الى الضوء لتميز الليل من النهار ولتنشيط الحواس.

وأستعملت الاضاءة كعلاج في الأماكن الطبية كعلاج للاطفال حديثي الولادة بمرض (الصفراء) و في مكان عمليات نقل الدم .ويستخدم الضوء البنفسجي لمعالجة مرض (الصدفية)،كما يعالج طيف الضوء الكامل الاضطرابات العاطفية الموسمية التي تعتقد انها تنجم عن تقليل انتاج الملانين خلال الظلام في أشهر الشتاء إذ يتعرض الناس في ذلك الوقت الى الاضاءة الصناعية المنقوصة الاطوال الموجية وينتج عن هذا النقص الكآبة والمزاجية والرغبة بأكل الكاربوهيدرات .(Green ,2003,p.49) .

جدول(1-1) يشير الى الاعتبارات التصميمية للاضاءة في انطقة المستشفى المختلفة.

اولاً:الانطقة العامة

- منطقة المداخل :

ينبغي ان تتدرج مستويات الاضاءة في المدخل بعناية، فالمنطقة القريبة من المدخل يجب ان تنال قيمة عالية من الاضاءة كي تعطي الانطباع بالترحيب من الخارج حتى يتمكن الناس من التكيف عند الدخول الى المستشفى كما يمكن ان تكون مستويات الاضاءة المختلفة دليلا على تحديد الطرق الرئيسة من المدخل الى مناطق آخرى .

ويراعى تجنب الكثير من الاضاءة الساقطة (Downlighting) لان الهدف هو اضاءة الاسطح الرأسية بما في ذلك الإشارات ووجوه الناس. و في الليل هناك حاجة الى الاضاءة لجعل الفضاء اكثر حيوية ومرحاً اما مخارج الطوارىء فيجب ان تكون مضاءة دوماً.(Dalke et al.,2004, p.51)

- منطقة الاستقبال:

ان فضاء الاستقبال بحاجة الى مستوى عالٍ من الاضاءة الرأسية وخصوصا على موظف الاستقبال لتوفير الترحيب. فضلاً عن كونه وسيله للاتصال بالزوار الذين يستخدمون قراءة الشفة.و ينبغي وضع الاضاءة على كاونتر الاستقبال بين الزائر وموظف الاستقبال مع تجنب الاكثار من الاضاءة الساقطة من مكتب الاستقبال لأنها يمكن ان تجعل موظف الاستقبال يبدو مخيفاً بالنسبة للاطفال. ان موظف الاستقبال يحتاج أيضاً الى القراءة والكتابة فضلاً عن أستخدام الحاسوب ، لذا يفرض توفير الاضاءة المناسبة للقيام بهذه المهام.(NHS Estates, 2003 ,p.22)

- مناطق الانتظار:

يجب توفير الاضاءة الجيدة بأستخدام اضاءة السقف وأستكمالها بالاضاءة الجدارية لإعطاء جو الفضاءالمنزلي.ويجب الأخذ بعين الاعتبار النمطية في توجيه الرؤيا والطريقة التي يتم فيها أستخدام الفضاء. في كثير من الأحيان يتم استدعاء المرضى للعلاج السريرى الى منطقة الرعايه او غرفة الاستشارة الطبية لذا يجب حدوث توازن جيد خال من وهج الاضاءة بحيث من المهم ان يرى المرضى الموظفين بسهولة والعكس صحيح و تشكل مناطق الانتظار أيضاً جزءاً من عملية الخروج في كثير من المستشفيات .(Mahnke et al., 1987,p.12)

غالبا ما يستخدم التلفاز أو شاشات الكمبيوتر ضمن مناطق الانتظار للترفيه وإعطاء المعلومات الى المرضى.وينبغي ان تصمم الاضاءة لتجنب الاشعة المباشرة أووهجها على الشاشة. وقد يتم في أحيان كثيرة إبقاء الاضاءة الكهربائية عاملة من دون داع في مناطق الانتظار لذا من المفيد النظر في برمجة الاضاءة لضمان اغلاقها خارج ساعات العمل وان يكون مقرونا بضوابط الافادة من الاضاءة النهارية أينما وجدت.(Michel,1996,p.23)

- **الحمامات والمرافق الصحية:**

تحتاج الحمامات الى أستخدام عدد من المصادر الضوئية الصغيرة بدلاً من مصدر ضوئي واحد في منتصف السقف .وإنّ أستخدام الاضاءة الجانبية المعلقه تفي بالاحتياجات الخاصة بالمناطق المبلولة،وهي احد الحلول الممكنة. فضلاً عن ذلك ،وجود اضاءة جانبية إلى جانب المرآة تشجع على الاهتمام بالمظهر, كما ان توفير الاضاءة الممتعة و المدروسه يمكن أيضاً أن يشجع على تحسين الصيانة والتنظيف .

ومن الشائع ان تترك الاضاءة في هذه الغرف ، لذا فإن تركيب مفتاح الاضاءة على وفق الاشغال يمكن ان يكون ميزة لتوفير الطاقة. ولكن يجب التأكد من انه يشمل مدة زمنية معقولة قبل ان تعمل فيه تأخير،للسماح للمستخدمين بالخروج بشكل أمن. (CIBSE,2002,p5)

ثانياً:انطقةالعناية الطبية

- **مناطق الحركة في الردهات:**

تعد مناطق الحركة اول نقطة اتصال مع جناح المرضى والزوارو يفترض أن تنقل شعوراً بالتفاؤل والكفاية الطبية . في أثناء النهار تكون مناطق الحركة بحاجة إلى ان تبدو مشرقة وسارة و يفضل استعمال ضوء النهار كلما كان ذلك ممكنا. وتعالج الجدران والسقوف لتكون غير لامعة , اما الارضيات فينبغي ان تكون متوسطة الى عالية الانعكاس و تكون لامعة مع تفادي انعكاس صور تجهيزات الاضاءة الذي يمكن ان يسبب بقعاً مشرقة على الارض (Figueiro,2001,p30).

وفي النهار ينبغي ان تتلقى الارضية من الاضاءة الجيدة لضمان الحركة الأمنة ولكن في الليل ينبغي ان تخفض لمساعدة الموظفين على التكيف مع انخفاض مستويات الاضاءة , في مناطق الاسّرة ،كما تؤدي الى الاقتصاد في أستخدام الطاقة.و يمكن ان تكون الاضاءة الكهربائيه مثبتة على الجدارأو السقف بأستخدام مصابيح الفلوروسنت ، لكنها تحتاج الى اختيار مواقعها بعناية وتحديد درجة السطوع ، لتجنب إزعاج المرضى وخاصة اللذين يتم نقلهم على الاسّرة .وهناك حاجة الى اختيار الاضاءة التي تضمن اضاءة بعض الجدران لتبدو مشرقة.(Lovett et al., 1991,p.62)

- **محطة التمريض:**

يجب ان تكون هناك كمية كافية من الضوء على وجوه الممرضين العاملين في هذة النقطة. كما إن اسقاط الضوء على جانب الجدار أو على الجزء الخلفي يمكن ان يكون مفيداً مما يجعل هذه المنطقة بارزة بصريا.ويمكن أستخدام الاضاءة الساقطة فوق مكتب الممرضين لانجاز المهام المطلوبة ومنع انعكاس المصابيح في شاشات الكمبيوتر. وإنّ احد البدائل هو أستخدام الاضاءة المعلقه على المكتب.و في أثناء الليل فإن مستويات الاضاءة بحاجة الى تقليل. (Dalke et al.,2004, p.63)

- **منطقة الاسّرة:**

في فضاء الاسّرة يكون ضوء النهاروالمشاهد الخارجية مهمة وحاسمة لاستعادة المريض عافيتة.وإنّ عتبة النافذة ينبغي الا تكون على ارتفاع مرتفع جداً في الجدار ليكون الطفل في سريرة قادراً على النظر الى الخارج ، ادنى متوسط لمعامل الانارة الطبيعية هو 3 ٪ ويجب ان يتحقق كلما كان ذلك ممكنا. ولانتاج نمط جذاب يتم الجمع بين النوافذ مع اضاءة السقف مع الحرص كي لا تتسبب بأي إزعاج بصري للمرضى الراقدين على الاسّرة. (Rosenfield 1971,p58)

ويجب ان تكون الاضاءة الاصطناعية مريحه للسماح للمرضى بالقراءة وبالنسبة للموظفين لاجراء الفحوصات المناسبة او توفير العلاج.وفي أثناء الليل يحتاج الموظفون الى ان يكونوا قادرين على التحقق من المرضى دون إزعاجهم إذ يتطلب مستوى منخفض جدا من الضوء.في الردهات فأن أحد الحلول التي توفر مجموعة من الشروط هي أستخدام مصابيح الفلوروسنت مثبتة على الجدار و التي تجمع بين الضوء الموجه للاعلى و للاسفل . ان الضوء الموجه للاسفل يحتاج الى مفتاح تحكم في شدة الاضاءة حتى يمكن أستخدامه في الليل ويفترض ان تكون قادرة على توفير الاضاءة ما لا يقل عن(300) لوكس على سريرالمريض للفحص اولأغراض العلاج.

إن الاضاءة الموجهه للاعلى(غير مباشرة) يمكن ان توفر الاضاءة الخافته للفضاء بشكل عام وتكون بديلاً للاضاءة الموجهه للاسفل في الليل .ويمكن اضاءة الردهات في الليل عن طريق تركيب وحدة انارة صغيرة مثبتة على السقف مجهزة بمصباح الفلوروسنت الذي يوجه معظم الضوء، نزولا الى المنطقة الوسطى للسماح بالحركة الأمنة للممرضات وحجب الاضاءة عن المريض وهو يرقد على سريره. وثمة نهج بديل يتمثل في أستخدام مصدر ضوء على الجدار ولكن يجب تجنب وجود حاجز.ان توفير شعور بالاضاءة المنزلية في مستشفيات الاطفال في بعض الأوقات سيكون خطوة كبيرة لتحسين البيئة المباشره للمرضى.(Lovett et al., 1991,p.63)

- **الغرف اليومية المستخدمة للاستجمام أو اللعب او القراءة:**

يستخدم المرضى (الذين لا يلزم بقاءهم في السرير) هذه الغرف للقراءة و مشاهدة التلفزيون او الاجتماع مع الزوار أو اللعب. وهذا الفضاء يحتاج الى جو منزلي محبب للطفل .وإن وجود الاضاءة الطبيعية ضروري في فضاءات لعب الاطفال لتحفيزهم على النشاط ويمكن أستخدام النوافذ الملونة اووضع ملصقات لإعطاء البهجة للفضاء و يمكن ان تكون الاضاءة الكهربائية وحدات لمصابيح قياسية مثبتة على الحائط مع مراعاة عنصر الأمان لامكانية عبث الاطفال بها لذا يجب تجنب اسلاك الكهرباء الطويلة عبر الغرفة و تزويد النقاط الضرورية بقواطع الكهرباء من الارض .و في حالة صعوبة توفير مصدر في الأرض فبالامكان توفير المصدر نفسه من السقف.(Ibid.,p.66)

ثالثاً:انطقةالحركة

يجب ان تكون الاضاءة مصممة لتوجيه الانتباه الى العلامات وليس لالهائهم عنها.فالاضاءة المناسبه مطلوبة في مناطق الحركة ويفضل استغلال الاضاءة النهارية في الممرات للحد من أستخدام الاضاءة الاصطناعية.
(Dalke et al.,2004, p.59)

- **الممرات:**

الممرات ينبغي ان تكون اضاءتها زاهية لكنها لا تتطلب مستويات عالية من الاضاءة الافقيه كما انها لا تحتاج الى التوحيد في مستوى الاضاءة. وهناك حاليا اتجاه لأستخدام الاضاءة الساقطة (Down lighting) ولكن بعض الاضاءات الساقطة يمكن ان تنتج إزعاجا كبيرا، كما ان توجيهها للضوء غير جيد ويمكن ان تكون صارخة ومثيرة للقلق للاطفال المستلقين على عربات المرضى .ويمكن حل هذه المشاكل بالتخفيف من أستخدام الاضاءة المركبة على الجدار وانارة السقف لانارة الاسطح العموديه و يمكن ترتيبها كي تتناسب مع الأبواب والمداخل الآخرى على الممر.إن الاضاءة الخطيه عبر الممر تجعلها تبدو أوسع.ولكن هي اقل ملائمة مع الممرات التي يتم استعمال العربات فيها بشكل كثيف و قد يكون هناك انعكاس خفيف لصور وحدات الاضاءة على الارض اللامعه. إنّ أستخدام الاضاءة المخفية (غير المباشرة) التي تضيء الجدران تعد حلاً بديلاً يمكن ان يعطي فضاءً متجدداً.(Ibid, p.61) .

ان معاملة سقف الممر أمر مهم بالنسبة لكيفية إحساس الشخص في الفضاء فالاضاءة الموجهة الى اعلى التي تنعكس الى الاسفل تعطي الشعور بضوء النهار. ومع ذلك فإن بعض الاساليب البصرية (كما في نمط السقوف) يمكن ان تسبب القلق. وعند استعمال أرضية الممر من مواد عالية اللمعان(polished) يمكن ان يسبب الوهج وهذا ليس مفيدا

للاشخاص المصابين بضعف البصر. ويمكن اُستخدام السجاد ولكن يحتاج الى تصميم ليتناسب مع الاضاءة لتجنب المزج السيء للالوان مما يؤثر سلبا في المريض.

إنّ إضاءة مناطق معينة على الجدار وسيلة جيدة لتوفيرالتوجيه الى جانب إيجاد مناطق مثيرة للاهتمام بدلاً مما يمكن ان يكون مملاً جداً للمناطق نفسها .(Mahnke et al.,1987,p.14)

- السلالم والسلالم المتحركة والمنحدرات:

تحتاج السلالم الى معالجة جيدة بالاضاءة كي نتمكن من اُستخدامها بسلام وخصوصا في الليل .إنّ كثيراً من الناس الذين يعانون من ضعف البصر يودون الافادة من الاضاءة اسفل الدرجات.إذ إن نقاط الضوءتقوم بإعطاء ثقة للمستخدمين عند اُستخدام السلالم المتحركة . وعلى رغم من ان العديد من التوجهات لاتحبذ اُستخدام الحديد بسبب الوهج ، فإن ضعاف البصر كثيرا ما يستفيدون من لمعان المعادن لمساعدتهم على معرفة اتجاهاتهم .(Ruiold,2000,p.116)

- المصعد:

ان الاضاءة يجب ان تجعل المصعد يبدو مشرقا وواسعا ؛ ويمكن ان يتم ذلك عن طريق القاء الضوء على الجدران والسقف.كما ان لوحات التحكم يجب ان تكون جيدة الاضاءة كذلك اللافتات مع تجنب الاضاءة الساقطة Down (lighting) لانها تجعل المصعد يبدو ضيقا كذلك فانها ستجعل النظر للاعلى يعطي شعوراً بأن المصعد محصور ومظلم. لذا فإن المصعد من الداخل ينبغي ان يكون مشرقا بدرجة متوسطة لان الاشراق الحاد سيؤدي الى عرقلة الاضاءة خارج المصعد.(Dalke et al .,2004, p.59)

لقد وضع(CIBSE)* تعليمات تصميم الضوء الطبيعي و الاصطناعي في مستشفيات الاطفال وكما يأتي:

- المساحات جميعها التي تشغل من الاطفال ومرافقيهم والموظفين لمدة طويلة من الزمن ينبغي ان تعطى ضوءاً طبيعياً مع منظر خارجي .
- اختيار موقع لاسّرة الاطفال والمهود بالقرب من الشرفات او البلكونات . واضاءة اجنحة المرضى بشكل أكبر بالضوء الطبيعي مع عتبات منخفضة للشبابيك للارتباط مع الطبيعية ولتحسين الروح المعنوية للمرضى.ان هذا يساعد في إعطاء المرضى و الموظفين سيطرة على الطبيعة .
- تصميم النوافذ المنخفضة و النوافذ العميقة التي توحي بالجاذبيه للاطفال .
- أينما ما أمكن تخفض الحواجز الصلبة أو تستبدل بالزجاج أو جزء منها بالزجاج أوجعلها جداراًمصغراً. ان هذا سيساعد على نقل ضوء النهار وتوزيعه من خلال الاقسام .
- ضمان التوجيه الافضل للنوافذ.
- المعالجة التصميمية للواجهات التي تستقبل اشعة الشمس القوية مع معالجة شكل الشباك وحجمه وتفاصيله للسيطرة على نور الشمس المفرط والوهج الحراري الذي يمكن ان يكون خطراً ويسبب مضايقة حادة وخصوصاً الاطفال في الاسّرة أوالحاضنات .
- ان الزجاج العاكس للشمس قد يشوه الضوء الطبيعي لذا ينبغي تجنبه كلما أمكن لانه يعيق التشخيص الدقيق .
- الاضاءة غير المباشرة يجب اُستخدامها على نطاق واسع في المناطق العامة .
- يجب ان يطور المصممون برنامج اضاءة يساعد على تقرير الجودة العالية وخلق صورة غير مهددة وبيئة مريحة في مناطق المستشفى.

* Chartered Institute of Building Services Engineers :CIBSE

- ان تركيب الاضاءة بمسافات متساوية على طول ممر المستشفى قد يكون لـــه تأثيرسلبي كالـشعور بـسرعة الدوران(Stroboscopic) في المريض الذي يسير في إحدى هذا الممرات ــ إذ إن تشتت الـضوء يعـد حـلاً افضل.
- ان وحدات الاضاءة الكهربائية (Luminaries) يجب ان لا تعلق بالسقف فوق المريض مباشرة أو في الحاضنة أو المهد أو السرير أوفوق العربة أو الاريكة .(BS EN 60598-2-25:1995,p.27)
- يجب ان يصمم الضوء بحيث ينعكس من جدار السقف .
- ايلاء العناية بالاضاءة الموجودة فوق رأس المريض وخصوصاً في مقصورة الانعاش والفحص وأماكن العـلاج إذ يجب ان تكون خالية من الوهج وتسمح بالتشخيص الصحيح ،فالاطفال عموماً لهم جلد عاكس إذ يمكـن مـن تغيير لون الجلد معرفة حالته الصحية .
- مستوى الاضاءة ينبغي ان يصمم مع مراعاه ارتفاع الاطفال ومستخدمي الكراسي المتحركة.
- يجب ان تكون النوافذ كبيرة بما يكفي لتوفير مشاهد جيدة وبمساحة لاتقل عن 20% من الجدار لإعطاء نظـرة واسعة وجيدة .(CIBSE,2002,p4)

*** اللون:-**

اللون اداة قوية لمخاطبة المدركات الحسية للطفل وبالذات المثير البصري إذ يجب ان يكون مـصمماًبعناية لكـل عمر معين ويستخدم ليعطي معناً لبيئة المستشفى .كما يمكن أستخدامه كأداة توجيه بين الفضاءات لتعرف الاطفـال علـى بيئاتهم الجديدة وتمكنهم من ايجاد الطريق .فالاطفال قد يجدوا الاقامة في المستشفى أمرا مرهقاً الا أن تصميم اللون بـشكل جيد يمكن ان يجعل المستشفى اكثر ترحابا ولطافة وقبولاً من قبلهم إذ يلعب اللون دوراً في العملية الشفائية واضفاء شعور بالرفاهية ويؤدي الى صرف انتباههم.

ان المواليد الجدد تكون عيونهم غير ناضجة التكوين إذ يتعرفوا على الالوان الأساسية و المـشبعة كـالاحمر و الازرق و الاصفرو الاخضر بدلاً من الاشكال غير الملحوظة و يظهر الرضيع استجابة للرسوم المعقدة وغالبية الاطفـال قبل سن المدرسة يركزون على اللون بدل الشكل اما الاطفال الذين تترواح اعمارهم بين 7-9 سنوات يصبح اللون والشكل بالأهمية نفسها. وفي سن 9 الى المراهقة يكون تركزيهم على الشكل. ، وعند الاطفال مـن 6-14 شـهراً يكـون اللـون المفضل هو الاحمر يليه الاصفر فالازرق فالاخضر فاللون البرتقالي و الاحمر والوردي هي الالون المفضلة للاطفال الذين تترواح اعمارهم بين 3-6 سنوات و يكون تفضيليهم نحو الالوان الساخنة ويقل اهتمامهم بالألوان الباردة وكلمـا زاد نمـو الطفل ينتج تأرجح في المزاج الى عمر التفكير المنطقي و السيطرة العاطفية . (Green ,2003,p.48)

ويظهر لدى الاطفال تناغم بالاحساس بالالوان بعمر ال 4 سنوات وكلما كبر الطفل يصبح لديه اهتمام بـالمظهر اكثر من اللون المشبع والساطع . فالفتيات اللاتي تتراوح اعمارهن بين(6-17) سنة يفـضلن الالـوان الدافئـة والأولاد يفضلون الالوان الباردة .وإنّ الاطفال الأكبر سناًوالمراهقون عموماً يفضلون الخلفية المحايدة التـي يمكـن ان يظهـروا بصورة جزئية زينتهم عليها.(Ruiolds,2000,p.213)

إنّ اللون له تأثيرات نفسيه على الاطفال فمثلاً :اللون الاصفر المشبع قد يؤثر في نشاط حركة العين فـي أثنـاء النوم. واللون الاخضر قد يجعل طفل السرطان يشعر بالغثيان و أظهرت التجارب في مستشفي بريستول (Bristol) فـي لندن ،ان اللون الارجواني له تأثير مقرف على الاطفال كما ان للون الاحمر قد يجمع بالدم بالنسبة لبعض الاطفال.

فالاطفال بمختلف الاعمار يحفزون ويثارون بالالوان المختلفة ومزج الرسوم .وإن أستخدام الوان الباستيل الناعمة مع قليل من الالوان المشبعة هو الافضل في منطقة اللعب ومنطقة الفعاليات الهادئة . وفـي جنـاح مانشيـستر(Manchester

Booth) طورت بيئة لونية بصرية جيدة مع (فضاءات الغرفة السعيدة التي تم ذكرها سابقاً)من ظلال الاصفرو البرتقالي والاحمر وغرفة الهدوء من ظلال الازرق والبنفسجي.(Marberry et al .,1995,p.43)

اولاً:الانطقة العامة:-

- منطقة المداخل:

تحتاج الالوان الداخلية أن تكون جذابة وتدعو الى الاسترخاء دون إعطاء جو صارخ جداً .ان اختيار الألوان لهذا الفضاء ليس سهلاً ، لأن الالوان جميعها يتم اختبارها إذ يتغير تأثيرها بالاضاءة فمثلاً بعض درجـات البـيج أوالالـوان المحايدة يمكن ان تظهراللون الاخضر أو البرتقالي بشكل غير جذاب تحت مختلف أنواع الاضاءة.وما يبدو انه خفيف جدا ومحايد في النهار يمكن أن يتحول الى غير مريح في الليل.

ان اللون الاصفر على الرغم من انه غير محبذ اّستخدامه في كثير من اجزاء مبنى المستـشفى الاانـه يمكـن اّستخدامه لتوفير جو مشمس ودافئ في منطقة المدخل.وإنّ استعمال اللون بشكل ظاهر على الزجاج في حالـة التـزجيج بمساحات كبيرة ضروري لابرازه وخصوصا بالنسبة الى الاطفال الذين يعانون من ضعف البصر إذ إن ذلك سيساعد على تجنب وقوع الحوادث.(NHS Estates, 2003 ,p.22)

- منطقة الاستقبال:

أنّ اّستخدام مزيج من اللون والاضاءة الموجهه يساعد في ابراز و تحديد المعالم مثل مكاتب المساعدة و مكتـب الاستعلامات ومناطق الجلوس. وسيكون من المعقول الى حد ما البدء في اّستخدام الوان محايدة و امكانية استيعاب الـوان آخرى مستخدمه في مختلف المناطق . ان اللون المستخدم في منطقة الاستقبال ينبغي ان يكون امتدادا من لـون المـدخل وادخال ما هو خارج المستشفى الى الداخل وإنّ الالوان ينبغي ان تستخدم لمساعدة المرضى اللذين يعانون مـن ضـعف البصر من أجل التوجية الفوري .(Ibid.,p.23)

- مناطق الانتظار:

ينبغي ان تكون مناطق الانتظار بعيدة عن جو المؤسسات الذي يدعو الى الملل وان تكون مثيرة للاهتمام، فـاللون يمكن ان يوفر الجو الجذاب و الممتع.كما ان استعمال ارضية جميلة و سهلة الصيانة وتوظيف الالوان الفاتحة و المفـضل الالوان الدافئة. ان اّستخدام الالوان الهادئة التي تميل الى اللون الرمادي تدعو الى الاسترخاء وتوفيرعنصر تصميم داخـل صالة الانتظار وهذه الألوان المحايده يمكن ان تشكل خلفية لأقوى انواع الألوان ، وتـستخدم علـى سـبيل المثـال فـي المفروشات والاثاث وتحتاج هذه الفضاءات الى التنوع بالالوان من أجل شد انتباه الطفل وتقليل شـعوره بالملـل نتيجـة الانتظار المرهق له.(Dalke et al .,2004, p.53)

- المرافق الصحية:

ان اختيار الالوان في المرافق الصحية ينبغي ان يوفر دائما تناقض بين الأدوات الصحية والجـدران لمـساعدة الزوار جميعهم على رؤية واّستخدام المرافق بثقة.وإنّ الالوان التي يمكن اّستخدامها لمقابض الأبـواب أوالأبـواب تكـون بشكل يتباين مع لون الجدارالمحيط بها لمساعدة الناس على العثور على المرافق بسهولة ، دون الحاجة الى لمس السطوح.

ثانياً:انطقةالعناية الطبية

- مناطق الحركة في الردهات:

ان تنوع الالوان في مناطق الحركة مرغوب من أجل تصميم نقاط مثيرة للاهتمام وخلق وتيرة متغيرة من أجـل الزوار والاطفال.إنّ اّستخدام الألوان الزاهية لهذه المناطق سيساعد على تعويض النقص في الضوء الطبيعي . ويمكـن ان

تستخدم الألوان في عملية البحث عن الطريق والحصول على المعلومات ، لايجاد أو تحديد المعالم ، وتأكيد الوصول الى الردهة المطلوبة. وهذا مفيد بوجه خاص للاطفال الذين لا يدركون الموقع أو اللغة المستخدمة في اللافتات.

وتمتازهذه الفضاءات غالباً بالضوضاء البصريه إذ تحتوي على الملاحظات و اللافتات ، والعربات ، واتجاهات للمرافق والمعدات. وفي غياب تصميم مساحة التخزين على نحو كاف ، فقد يكون من الافضل تصميم بعض المناطق كي تأخذ الجزء الأكبر من هذه المواد ، مع المحافظة على هدوء بعض المناطق بصرياًويفضل وضع الحدود والالوان على حواف الطوابق إذ يتم اًستخدامها الى حد كبير بوصفها اداة عملية في البحث عن الطريق.وينبغي ان تكون الارضيات فاتحة لتعكس و لتجنب عدم وضوح النفايات .(Mahnke et al.,1987,p.18)

- محطة التمريض:

يمكن في بعض الأحيان تنسيق اللون لمراكز الممرضين مع الألوان المستخدمة في الممر وليس الردهات.ان اًستخدام درجة لون أقوى من أي مكان آخر في القسم من أجل تأكيد مركز الممرضين كما تعمل على ايجاد خلفية مميزة لمنطقة العمل.

و قامت بعض الهيئات في الولايات المتحدة بدراسات حول اللون و وجدت ان الإجهاد يحدث في المكاتب البيضاء التي لاتستعين بالألوان الأخرى.و بشكل عام تم هجر الفضاءات البيضاء التي تتطلب التركيز والملاحظه.ان نوعية وتصميم محطات الممرضين يمكن ان تؤثر على كفاية العمل ومعنويات الموظفين والمرضى على حد سواء.

وفيما يخص اسطح العمل فينبغي ان تكون مريحة و لا تحتاج العين الى كثير من سطوع اللون للتكيف مع مهام مراقبة المسافة الطويلة في الردهات أو منطقة المريض . فاللون يجب اختياره ليناسب نوع العمل . إذ كان المطلوب اًستخدام ورق ملون بلون الكريمة في المكتب ،فإن اللون الازرق-الرمادي الباهت سيكون مثاليا كلون الخلفية لسطح العمل .(Dalke et al.,2004, p.62).

اما السقوف فيمكن ان تكون بيضاء لضمان التوزيع الأمثل للاضاءه. ووجود مساحة بدرجة لون اخف على الجدار الواحد سيسمح لتجول العين من التركيز على نقطة عمل قريبة الى النظر لمسافة بعيدة.ان محطة التمريض يمكن في الوقت نفسه ان تكون مبهجة ومجهدة للغاية. وإن تصميم مخطط الالوان ينبغي ان يستخدم الالوان الحية واللطيفة وعلى سبيل المثال الازرق والرمادي والاخضر و الاصفر.

- منطقة الاسرة:

تحتاج منطقة الاسرة الى اًستخدام الالوان الفاتحة لتوفير الاضاءة المنعكسة.فالسقوف البيضاء ليست دائما مثاليه على الرغم من قابليتهاعلى عكس الضوء إذ إن الاطفال الذين يقضون اوقات طويلة في السرير يحتاجون الى اسقف ملونة تشعرهم بالبهجه وتقلل الملل.ويحتاج اختيار اللون هنا الى عناية في الانتقاء إذ إن بعض الالوان قد تسبب الهلوسة للطفل.

يفضل اختيار الوان الجدار بمعامل انعكاسية بحدود 50-60 ٪وللجدران البعيدة عن النافذة للتعويض عن قله الضوء ويتم اختيار اللون بمعامل انعكاس 70 ٪ .ويفضل ان تكون الجدران بلون فاتح وإذا كانت النوافذ صغيرة فإن الجدار ينبغي اضاءتة ليتعارض مع الظلمه الموجودة حوله. اما الارضية فيجب ان تكون بلون فاتح و لكن قيمة معامل الانعكاس 15-20 ٪ بين الجدران والأرضيات كاختيار أمثل لضعاف البصر. (HBN23,2004,p.36)

ويمكن استعمال الالوان الدافئة و الباردة أو المحايدة بالقرب من سرير المريض ويستخدم اللون وفقا لنوع الردهة.و فيما يخص الردهات التي يمكث فيها المريض زمناً قصيراً تكون الحاجة الى الالوان التي تبعث المرح والاستبشار وتساعده على التعافي و الانتعاش. و عند البقاء لمدة طويلة ، يكون المريض بحاجة الى الألوان الباردة إذ أنها المفضلة لدى الاكثرية وتعد الواناً مريحة للعين.وهذه الألوان من شأنها ان تحول دون حصول التناقض بين اليقظة العقلية واعتلالها الجسدي.

وفيما يخص المريض غير القادر على التحرك والذي قد يكون محاطاً بمستوى عال من التكنولوجيا الطبية وقد يحصل على مشهد محدود جداً للخارج ، لذا فإن هذا الفضاء الذي يشغله يتطلب اقصى درجة من الحرص على توفير الجو الممتع مع الحفاظ على العناصر البصريه الممتعة. ففي الاجنحه العامة قد يتم استعمال خليط من اللون الحار والبارد بالتناوب لإعطاء التوازن بين مشاعر الاثارة والاكتئاب. وثمة استراتيجية آخرى تتمثل في أستخدام اثنين أو اكثر من الالوان وتختلف المجموعات في الغرف المجاورة لتوفير التحفيز البصري.(Ruiolds,2000,p.226)

إنَّ أستخدام الالوان القوية في الردهات يمكن ان يؤدي الى اشغال المرضى. ومع ذلك ، قد يكون من المناسب أستخدام مساحة محدودة لاستعمال لون قوي لترميز الردهة ليتمكن الطفل من معرفه لردهته. وكقاعده عامة:الألوان التي لا تملك الكثير من ظل الباستيل ولها درجة لون رمادية تؤدي الى خلق جو مريح. وهي أيضاً عملية مقاومة للتلوث والتخريب. ان أستخدام الالوان بانصاف يساعد على تجنب بعض الاثارة العاطفية. وينبغي اتخاذ الحذر في أستخدام الازرق في ردهات القلب إذ إن هذه المناطق قد تعوق تشخيص الأزمات القلبية. وبالمثل الألوان الصفراءالقوية في ردهات الاطفال حديثي الولادة قد تعوق تشخيص اليرقان.

وينبغي ان يؤخذ الحذر في اختيار اللون في ردهات الأمراض الجلديه .فالالوان الباردة ذات الموجات القصيرة مثل الازرق يظهر انها تساعد على تخفيف الحك للمرضى الذين يعانون من اضطرابات البشرة.إنَّ اللون الاخضر هو أيضاً جيد من حيث أستخدامه في تشطيب الارضيات ، إذ تظهرالسوائل ، مما يساعد على منع وقوع حوادث بسبب الارضيات المنزلقة.(Marberry et al.,1995,p.45)

وهناك حاجة لبذل الجهود من أجل جعل المكان جذاباً وملوناً و موضع تقدير من جانب المرضى والأسر والموظفين والزوار.و في كثير من الأحيان فأن قرارات الكبار حول ما يحبه الاطفال تكون خاطئة. وإنَّ مزيجاً جيداً من درجات الالوان الحارة والباردةهي نقطة الانطلاق لمخطط الالوان ..

- الغرف اليومية المستخدمة للاستجمام او اللعب او القراءة:

ينبغي ان تكون الغرفة اليومية مختلفة كثيرا عن مناطق الردهات لتوفير ما يكفي لتحفز العقل و يمكن تحقيقه بالتناوب بين أستخدام الالوان الحارة والباردة بالتناوب بين الردهات و الغرفة اليومية . و من المتوقع ان هذا الاختلاف يحافظ على الاثارة و يعمل على راحة المريض من مظهر غرف المرضى . ويجب ان تكون درجات اللون المستخدمة ذات قيمة انعكاسيه عالية و تحتوي على مجموعات متجانسه من المفروشات ، والسجاد والمنسوجات.
(Dalke et al.,2004, p.68)

<u>ثالثاً:انطقةالحركة</u>

إنَّ اللون في أماكن الحركة مهم إذ من خلاله يمكن ان يستدل الاطفال على طريقهم كما يمكن إعطاء فضاءات الحركة المتعة البصرية في أثناء الحركة ويعمل اللون مع الاضاءة على إعطاء الشعور بالرغبة في الحركة ويمكن أستخدام اللون في الفضاء كأداة تمييز بين أجزاء المستشفى . (HBN23,2004,p.36)

- الممرات:

الممرات هي الوسيلة المثالية لتطبيق فكرة أستخدام اللون في عملية البحث عن الطريق . إذ يمكن أستخدام اللون والرسوم في الجدار للإشارة الى الاتجاه الصحيح. فألون الابواب يمكن ان يستعمل في كثير من الأحيان كشكل من اشكال الترميز باللون أو التقسيم لتميز الاقسام.لكن الكثرة في أستخدام الالوان غير المدروسة يمكن ان يؤدي الى إرباك بصري.وينبغي أستخدام الالوان الحيوية المشجعة على الحركة في الممرات التي تساعد على التوجيه .و ينبغي وضع خطة استراتيجية حول النغمه التوافقيه للالوان ومن الافضل تجنب أستخدام لون واحد في الممرات وخصوصا الطويلة . ومن الحكمة ادخال اللون المكمل كنوع من الراحة البصرية. (HBN23,2004,p.50)

- السلالم والسلالم المتحركة والمنحدرات:

ينبغي وضع علامات جيدة في أعلى السلالم واسفلها عند الاقتراب منها لتحذير الناس ذوي المشاكل البصرية بأن هناك تغير قريب في السطح.كأستخدام التناقض في الالوان بين خطوات الدرج أوحواف الادراج وإنّ الالوان المتناقضة الأكثر شيوعاً هي الاسود والاصفر أوالابيض أو اضائتها لتساعدعلى السلامة ومن المهم التأكد من وضوح لون الدرجة وتوفر النقيض الكافي لاسطح الدرجات في الليل.كما يجب تصميم السطح الجانبي الى بيت الدرج ليكون بلون متناقض مع الدرج ليساعد المستخدمين على توقع إيقاع الخطوات،ولا يجب وضع النوافذ على خط البصر للاشخاص الذين ينزلون بيت الدرج فقد يسبب الوهج ويؤدي الى وقوع حوادث. (Dalke et al.,2004,p.59)

- المصاعد:

يمكن استغلال عنصر الحركة العمودية للتحفيز البصري للاطفال وأستخدامه كعنصر ممتع وحركي من خلال اللون وتوظيف الشكل.ويفضل تصميم الوان متناقضة بين الأزرار و السطح الخلفي وأبواب المصعد كي تبرز جيدا عن الجدران المحيطة كذلك عن الارضية بحيث تكون مرئية لجميع المستخدمين للبناء. وإذا جاءت المصاعد في المنطقة الوسطية لخطوط الالوان المستخدمة في التصميم الكلي فإن ذلك قد يحدد الالوان المستخدمة للمصعد ولكن ينبغي لها أن تعمل من داخل المصعد و خارجه بشكل متكافل. (Ibid,p.60)

وعلى ضوء ماتقدم ذكره،يمكن استخلاص اهم الاعتبارات التصميمية للمثيرات البصرية (الاضاءة واللون)في انطقة المستشفى ضمن الجدول الآتي:

جدول(1-1) يوضح الاعتبارات التصميمية للاضاءة واللون في انطقة المستشفى

ت	الانطقة	الفضاء	الاضاءة	اللون
1	**الانطقة العامة**	1.منطقة المدخل	1. خلق تدرج في مستويات الاضاءة.	1. أستخدام الالوان الجذابة التي تدعوا الى الاسترخاء دون إعطاء جو صارخ جدا.
			2.أستخدام الاضاءة لتحديد الطريق الرئيسة.	2.اختيار الألوان لهذا الفضاء بعناية ، إذ يتغير تأثيرالالوان بالاضاءة وما يبدو انه خفيف جدا ومحايد في النهار يمكن أن يتحول الى غير مريح في الليل.
			3. تجنب الكثير من الاضاءة الساقطة (Downlighting).	3. يمكن أستخدام اللون الاصفر لتوفير جو مشمس ودافئ في منطقة المدخل على الرغم من انه غير محبذ أستخدامه في كثير من اجزاء مبنى المستشفى .
			4. وجود الحاجة الى الاضاءة لجعل الفضاء اكثر حيوية ومرحاً في ساعات الليل. 5. اضاءة مخارج الطوارئ.	4. استعمال اللون بشكل ظاهر على الزجاج في حالة التزجيج بمساحات كبيرة وهو ضروري لابرازه وخصوصا بالنسبة الى الاطفال الذين يعانون من ضعف البصر إذ إن ذلك سيساعد على تجنب وقوع الحوادث.
		2. منطقة الاستقبال	1. الحاجة الى مستوى عالٍ من الاضاءة الرأسية وخصوصا على موظف الاستقبال لتوفير الترحيب.	1. وجوب أستخدام الالوان لمساعدة المرضى الذين يعانون من ضعف البصر من أجل التوجية الفوري.

			2. يفترض توفير الاضاءة المناسبة لقيام موظف الاستقبال بمهامه.	2. ينبغي ان يكون اللون المستخدم في منطقة الاستقبال امتدادا من لون المدخل
		3. مناطق الانتظار	1. توفير الاضاءة الجيدة لإعطاء جو الفضاءالمنزلي مع مرعاه وجود توازن جيد خال من وهج الاضاءة.	1. ينبغي ان تكون مناطق الانتظار بعيدة عن جو المؤسسات الذي يدعو الى الملل وان تكون مثيرة للاهتمام.
			2.ينبغي ان تصمم الاضاءة لتجنب الاشعة المباشره أووهجها على شاشات التلفاز في حالة وجودها.	2. استعمال ارضية جميلة و سهلة الصيانة وتوظيف الالوان الفاتحة و المفضل الالوان الدافئة.
			3. يفضل وجود برمجة للاضاءة لضمان اغلاقها عند عدم الحاجة اليها.	3. أستخدام الالوان الهادئة التي تميل الى اللون الرمادي التي تدعو الى الاسترخاء
				4.الحاجة في هذه الفضاءات الى التنوع في الالوان من أجل شد انتباه الطفل وتقليل شعور الملل نتيجة الانتظار المرهق له.
		4.الحمامات والمرافق الصحية	1.الحاجة الى أستخدام عدد من المصادر الضوئية الصغيرة بدلا من مجرد مصدر ضوئي واحد في منتصف السقف.	1. اختيار الالوان في المرافق الصحية ينبغي ان يوفر دائما تناقضاً بين الأدوات الصحية والجدران لمساعدة الزوار جميعهم على رؤية وأستخدام المرافق بثقة.
			2. وجود اضاءة جانبية إلى جانب المرآة تشجع الاهتمام بالمظهر.	2.الالوان التي يمكن أستخدامها لمقابض الأبواب أوالأبواب تكون بشكل يتباين مع لون الجدار المحيطة بها لمساعدة الناس على العثور على المرافق بسهولة.
			3.ان توفير الاضاءة الممتعة و المدروسه يمكن أيضاً ان يشجع على تحسين الصيانة والتنظيف.	
2.	انطقةالعناية الطبية	1. مناطق الحركة في الردهات	1.الحاجة إلى ان تبدو مشرقة وسارة و يفضل استعمال ضوء النهار كلما كان ذلك ممكنا.	1. يفضل وجود تنوع الالوان في مناطق الحركة لتصميم نقاط مثيرة للاهتمام وخلق وتيرة متغيرة من أجل الزوار والاطفال.
			2. معالجة الجدران والسقوف لتكون غير لامعة , اما الارضيات فينبغي ان تكون متوسطة الى عالية الانعكاس	2.أستخدام الألوان الزاهية لهذه المناطق سيساعد على تعويض النقص في الضوء الطبيعي.
			3. ينبغي ان تتلقى الارضية من الاضاءة (150) لوكس لضمان الحركة الأمنة في ساعات النهار اما في الليل فينبغي ان تخفض لمساعدة الموظفين على التكيف مع انخفاض مستويات الاضاءة في مناطق الاسّرة.	3.يمكن ان تستخدم الألوان في عملية البحث عن الطريق والحصول على المعلومات ، لايجاد أو تحديد المعالم. وهذا مفيد بوجه خاص للاطفا الذين لا يدركون الموقع أو اللغة المستخدمة ف اللافتات.
		2.مركز عمل الممرضين	1. يجب ان يكون هناك كمية كافية من الضوء على وجوه الممرضين العاملين في هذة النقطة.	1.أستخدام درجة لون أقوى من أي مكان آخر في القسم من أجل تأكيد مركز الممرضين كما

			تعمل على ايجاد خلفية مميزة لمنطقة العمل.
		2. الابراز البصري لهذه المنطقة من خلال اسقاط الضوء على جانب الجدارأو على الجزء الخلفي.	2. ينبغي ان تكون اسطح العمل مريحة و تحتاج العين الى كثير من سطوع اللون للتكيف مع مهام مراقبة المسافة الطويلة في الردهات أو منطقة المريض.
		3. الحاجة الى تقليل مستويات الاضاءة في أثناء الليل.	3. لضمان التوزيع الأمثل للاضاءه يمكن ان تكون السقوف بيضاء.
			4.وجود مساحة بدرجة لون اخف على الجدارالواحد ستسمح لتجول العين من التركيز على نقطة عمل قريبة الى النظر لمسافة بعيدة.
	3.منطقة الاسرّة	1. ينبغي وجود ضوء النهاروالمشاهد الخارجية في منطقة الاسّرة لاستعادة المريض عافيتة.	1.تحتاج منطقة الاسرة الى أستخدام الالوان الفاتحة لتوفير الاضاءة المنعكسة.
		2. عتبة النافذة ينبغي الا تكون على ارتفاع مرتفع جداً في الجدار ليكون الطفل في سريرة قادراً على النظر الى الخارج.	2.السقوف البيضاء ليست دائما مثالية على الرغم من قابليتهاعلى عكس الضوء إذ إن الاطفال الذين يقضون اوقات طويله في السرير يحتاجون الى اسقف ملونه تشعرهم بالبهجة وتقلل الملل.ويحتاج اختيار اللون هنا الى عناية في الانتقاء إذ إن بعض الالوان قد تسبب الهلوسة للطفل
		3. ادنى متوسط لعامل ضوء النهارهو 3 ٪ ويجب ان يتحقق كلما كان ذلك ممكنا.	3.يفضل اختيار الوان الجدار بقيمه انعكاسية بحدود 50-60٪وللجدران البعيدة عن النافذة للتعويض عن قله الضوء و يتم اختيار اللون بخاصية 70 ٪.
		4. لانتاج نمط جذاب يتم الجمع بين النوافذ مع اضاءة السقف مع الحرص كي لا تتسبب باي إزعاج بصري للمرضى الراقدين على الاسّرة.	4.يفضل ان تكون الجدران بلون فاتح وإذا كانت النوافذ صغيرة فإن الجدار ينبغي اضاءتة ليتعارض مع الظلمه الموجودة حوله. اما الارضيه فيجب ان تكون بلون فاتح و لكن قيمة الانعكاس 15-20 ٪ بين الجدران والأرضيات كاختيار أمثل لضعاف البصر.
		5. الاضاءة الاصطناعية يجب ان تكون مريحه للسماح للمرضى بالقراءة أو الموظفين لاجراء الفحوصات المناسبة أو توفير العلاج.	5.يمكن استعمال الالوان الدافئة, الباردة أو المحايدة بالقرب من سرير المريض ويستخدم اللون وفقا لنوع الردهة. وفيما يخص الردهات التي يمكث فيها المريض زمناً قصيراً تكون الحاجة الى الالوان التي تبعث المرح والاستبشار وتساعده على التعافي و الانتعاش
		6. أحد الحلول التي توفر مجموعة من الشروط	6.عند البقاء لمدة طويلة ، يكون المريض بحاجة

		في الردهات هي أستخدام مصابيح الفلوريسنت مثبتة على الجدارالتي تجمع بين الضوء الموجه للاعلى و للاسفل.	الى الألوان الباردة إذ إنها المفضلة لدى الاكثرية وتعد الالوان المريحة الى العين. وهذه الألـــوان من شأنها ان تحول دون حصول التناقض بين اليقظه العقلية واعتلالها الجسدي.
		7. ان الضوء الموجه للاسفل يحتاج الى مفتاح تحكم في شدة الاضاءة حتى يمكن أستخدامه في الليل ويفترض ان يكون قـادراً علـى تـوفير الاضاءة ما لا يقل عـن(300) لـوكس علـى المريض للفحص أو اغراض العلاج.	7. قد يتم استعمال خليط من اللون الحار والبارد في الاجنحة العامة بالتناوب لإعطاء التوازن بين مشاعر الاثارة والاكتئاب.
		8. إن الاضاءة الموجهه للاعلى يمكن ان توفر الاضاءة الخافته للفضاء بشكل عام وتكون بديلاً للاضاءة الموجهه للاسفل في الليـل .ويمكـن اضاءة الردهات في الليل عن طريق تركيـب وحدة انارة صغيرة مثبتة على السقف ومجهزة بمصباح الفلوريسنت الذي يوجه معظم الضوء، نزولا الى المنطقة الوسطى للسماح بالحركـة الأمنة للممرضـات وحجـب الاضـاءة عـن المريض وهو يرقد على سريره.	8. يمكن أستخدام اثنين أو اكثر مـن الالـوان وتختلف المجموعات في الغرف المجاورة لتوفير التحفيز البصري.
			9.أستخدام الالوان القوية في الردهات يمكن ان تؤدي الى اشغال المرضى. ومع ذلك ، قد يكون من المناسب أستخدام مساحة محدودة لاسـتعمال لون قوي لترميز الردهة ليـتمكن الطفـل مـن معرفه ردهته.
			10.وكقاعده عامة: الألوان التي لا تملك الكثيـر من ظل الباستيل ولها درجة لون رمادية تـؤدي الى خلق جو مريح.
			11. ينبغي اتخاذ الحذر في أستخدام الازرق في ردهات القلب إذ إن هذه المنـاطق قـد تعـوق تشخيص الأزمات القلبيـة. وبالمثـل الألـوان الصفراءالقوية في ردهـات الاطفـال حـديثي الولادة قد تعوق تشخيص اليرقان.
	4.الغرف اليوميـة المـــستخدمة للاســـتجمام أو اللعب أو القراءة	1. إن وجود الاضاءة الطبيعية ضروري فـي فضاءات لعب الاطفال لتحفيز النشاط ويمكـن أستخدام النوافذ الملونـه أو وضـع ملـصقات لإعطاء البهجة للفضاء.	1.الغرفة اليومية ينبغي ان تكون مختلفة كثيـرا عن مناطق الردهات لتوفير ما يكفي لتحفز العقل و يمكن تحقيقه بالتناوب بين أسـتخدام الالـوان الحارة والباردة بالتناوب بين الردهات و الغرفة اليومية.
		2. ان تكون الاضـاءة الكهربائيـة وحـدات لمصابيح قياسية مثبتة على الحائط مع مراعـاة عنصر الأمان لامكانية عبث الاطفال بـه لـذا يجب تجنب اسلاك الكهربـاء الطويلـة عبـر الغرفة و تزويد النقـاط الـضرورية بقواطـع الكهرباء من الارض.	2.درجات اللون المستخدمة يجب ان تكون ذات قيمة انعكاسيه عالية.

3	انطقةالحركة	1.الممرات	1. ان تكون اضاءتها زاهيه لكنها لا تتطلب مستويات عالية من الاضاءة الافقيه كما انها لا تحتاج الى التوحيد في مستوى الاضاءة.	1.الممرات هي الوسيلة المثاليه لتطبيق فكر أستخدام اللون في عملية البحث عن الطريق .
			2. يمكن ترتيبها كي تتناسب مع الأبواب والمداخل الآخرى على الممر.	2. يمكن ان تستعمل الالوان للابواب في كثير من الأحيان كشكل من اشكال الترميز باللون أ التقسيم لتميز الاقسام.
			3. الاضاءة الخطيه عبر الممر تجعلها تبدو أوسع.ولكن هي اقل ملاءمة مع الممرات التي يتم استعمال العربات فيها بشكل كثيف و قد يكون هناك انعكاس خفيف لصور وحدات الاضاءة على الارض اللامعة.	3. الكثرة بأستخدام الالوان غير المدروسة يمكن ان يؤدي الى ارباك بصري.
			4. أستخدام الاضاءة المخفية التي تضيء الجدران تعد كحلاً بديلاً يمكن ان يعطي فضاءاً متجدداً.	4. ينبغي وضع خطة استراتيجية حول النغم التوافقية للالوان ومن الأفضل تجنب أستخدا لون واحد في الممرات وخصوصا الطويلة.
			5.معاملة سقف الممر أمر مهم بالنسبة كيفية احساس الشخص في الفضاء فالاضاءة الموجهة الى اعلى التي تنعكس الى الاسفل تعطي الشعور بضوء النهار.	5.الحكمة ادخال اللون المكمل كنوع من الراح البصرية.
			6.استعمال ارضية الممر من مواد عالية اللمعان(polished) يمكن ان يسبب الوهج وهذا ليس مفيداً للاشخاص المصابين بضعف البصر.	6.ينبغي أستخدام الالوان الحيوية المشجعة على الحركة في الممرات التي تساعد على التوجيه.
			1.7 إضاءة مناطق معينة على الجداروهي وسيلة جيدة لتوفيرالتوجيه الى جانب إيجاد مناطق مثيرة للاهتمام بدل ان يكون مملاً جدا للمناطق نفسها.	
		2.السلالم والسلالم المتحركة	1.تحتاج السلالم الى معالجة جيدة بالاضاءة للتمكن من أستخدامها بسلام وخصوصا في الليل.	1.ينبغي وضع علامات جيدة في أعلى السلالم واسفلها لتحذير الناس ذوي المشاكل البصرية بأن هناك تغير قريب في السطح.كأستخدام التناقض بالالوان بين خطوات الدرج أوحواف الادراج والالوان المتناقضة ليساعدعلى السلامة.
				2.التأكد من وضوح لون الدرجة وتوفر النقيض الكافي لاسطح الدرجات في الليل.كما يجب تصميم السطح الجانبي الى بيت الدرج ليكون بلون متناقض مع الدرج ليساعد المستخدمين على توقع إيقاع الخطوات.

	3.المصعد:	1. أستخدام الاضاءة لجعل المصعد يبدو مشرقاً وواسعاً ؛ ويمكن ان يتم ذلك عن طريق القاء الضوء على الجدران والسقف.	1.أستخدام المصعد كعنصر ممتع وحركي من خلال اللون وتوظيف الشكل.
		2.ان لوحات التحكم يجب ان تكون جيدة الاضاءة و كذلك اللافتات مع تجنب الاضاءة الساقطة (Down lighting) لأنها تجعل المصعد يبدو ضيقا كما انها ستجعل النظر للأعلى يعطي شعوراً بأن المصعد محصور ومظلم.	2.يفضل تصميم الوان متناقضة بين الازرار و السطح الخلفي وأبواب المصعد كي تبرز جيداً عن الجدران المحيطة و كذلك عن الارضية بحيث تكون مرئية لمستخدمين المبنى جميعهم.
		3. ينبغي ان يكون المصعد من الداخل مشرقا ولكن ليس بالاشراق الكبير إذ سيؤدي ذلك الى عرقلة الاضاءة خارج المصعد.	

المصدر (الباحثتين)استناداً على المصادر الاتية (Lovett et al., 1991,/ NHS Estates, 2003/Dalke et al.,2004 / CIBSE,2002/Mahnke et al., 1987)

* <u>الاعمال الفنية:-</u>

الصورة والمنحوتة في المستشفى يمكن ان تهدئ الاطفال وتقلل من مخاوفهم وقد تسليهم وتجعلهم يضحكون كما انها قد تصرف انتباههم لمدة طويلة من الوقت. ويجب ان تكون حاملة لرسائل باعثة للامل والبهجة والحب والراحة والأمن والنمو والحياة ويمكن أستخدامها للاستجابة الحسية كما يمكن ان تستخدم كمعالم لايجاد الطريق داخل المستشفى كأستخدام التماثيل أو المياه بالاشتراك مع الإشارات والرسومات لتكون في النهاية حافزاً بصرياً يمكن الاطفال من التجوال في المستشفى والسيطرة على بيئتهم . والعمل الفني مفيد للاطفال خصوصا في الغرف اليومية ومناطق المعالجة و الردهات كما يكون مفيداً في أماكن العناية طويلة المدى مثل الوحدات القلبية وكذلك التجبير.(NHS,2002,P.7)

وأثبتت الدراسات ان العمل الفني يمكن أن:

- يقلل الإجهاد البيئي .
- يخلق الاحساس بالأمان و الأمن .
- يرفع القيد بين المريض و الكادر الطبي .

كما ان العمل الفني في السقوف ضروري للاطفال الذين يقضون مدة طويلة من الوقت في السرير أو على العربات المتحركة فيمكن سرد قصة بواسطة سقف الغرفة وقد اثبت ان الاشكال الحركية للفن مثل الهواتف النقالة جيدة جداًو فعالة في صرف انتباه الاطفال في الردهات ومناطق المعالجة و الفحص فضلاً عن مناطق الممرات كما في مستشفي لورناليندا أمريكا إذ استخدمت صور الحيوانات الاليفة وصورة لتخفيف المخاوف لدى الاطفال . (Green ,2003,p.43)

* <u>الطبيعة الخارجية والنباتات الداخلية:-</u>

لايمكن إهمال الطبيعة في صحة المرضى ودورها الايجابي في إزالة الضغط النفسي وخلق بيئة انسانية والتقليل من الإجهاد والشعور بالسرور وإعطاء مشاعر ايجابية والتقليل من الافكار المجهدة ومن ثم تسريع العملية الشفائية .كما لايمكن إهمال مدى تأثير محفزات البيئة الطبيعية في الانسان سيكولوجيا وفسيولوجيا، و أظهرت الدراسات اثر المناظر الطبيعية على المريض إذ وضعوا مرضى بعد اجراء عملية المرارة في ردهات تطل على مناظر طبيعية وتحتوي على

نباتات وحيوانات فأظهروا استجابه للشفاء أسرع وقضوا وقتاً اقل في المستشفى واستخدم المسكنات بنسبة اقل من مرضى تم وضعهم في ردهات تحتوي فقط على جدران من طوب.وهذا نتيجة لحب الانسان للطبيعة .التي لها تأثيرحسي – بصري على المريض. (Leger, 2003 ,P.174) كما ان أستخدام النوافذ في الممرات يمكن ان يساعد في الاستدلال على الطريق وإنَّ وجود النباتات الداخلية يساعد على الراحة النفسية ويجب ان يراعى أستخدام النباتات التي لها قيمة علاجية على النفسية وأيضاً غير السامة أوالشائكة لان الطفل في كثير من الأحيان يرغب في الامساك بها أو وضعها في فمه ،وأستخدام النباتات التي تهدف الى اشراك حواس الطفل جميعها من اختلاف قوام ورائحة ولون إذ يعزز بالاخص الإدراك البصري من خلال التباين كذلك اشراك نافورة الماء بتصميم الفضاء الداخلي لما للماء من تأثير في ابهاج الطفل كما أنَّ صوت الماء له التأثير المهدى .

* **الرموز والإشارات:–**

إنَّ أستخدام الرسوم كإشارات عملية مهمة فالاطفال الصغار الذين لايستطيعون القراءة يمكن ان يتذكروا من خلال الرسوم ولهذا يتوجب أستخدام الإشارات بشكل يخاطب عقل الطفل فمثلا تستخدم الرسومات لشخصيه كارتونية معينة كرموز ضمن القسم الواحد بحيث يدرك انه مازال في القسم نفسه وأيضاً من خلالها يتم إعطاء التوجيه الصحيح للحركة ويمكن ان تحذر الطفل من التوجه الى أماكن معينة من خلال احتواء العلامات على رموز تحذيرية . (Cowgill et al.,2003,p.8)

ويتوجب وضع الإشارة في مكان يجذب انتباه المشاهدين فهي نوع من الدعاية والاعلان ،ولكن كثرة الإشارات وتنوعها في اللون والشكل تعمل على ارباك المشاهد وعدم تقديم أية معلومة ومن ثم إهمال وجود الإشارة ،فكثرة الإشارات تؤدي الى صعوبة الحصول على المعلومة ومن ثم صعوبة في الإدراك البصري.(شقوارة،1998،ص52)

إنَّ اللون و الإضاءة يمكن أستخدامهما لجذب انتباه الطفل للوحات الإرشادية في مبني المستشفي كماتساعد لتكون المعلومات واضحة ومقروءة ،ويساعد أستخدام التباين بين النصوص والارضية في العلامات من قراءتها من مسافات بعيدة وخصوصاً لضعاف البصر. (Dalke et al.,2004, p.26)

استخلاص مؤشرات الاطار النظري

توصل البحث الى وضع مؤشرات للمثير الحسي البصري في البيئة الداخلية لمستشفيات الاطفال بصيغته النهائية وكما موضح في الجدول(2-1)

الجدول (2-1): مؤشرات الاطار النظري

1. الضوء	1. توفيراهتمام بصري من خلال الضوء
	2.وجود اضاءة مريحة في فضاءات النوم واللعب
	3.إعطاء التوجيه وتحديد الطرق من خلال تصميم الضوء
	4.إعطاء الانطباع بالترحيب والجو المنزلي
	5.وجود توازن جيد خالي من وهج الضوء
	6.ابراز أماكن الاستعلامات ومحطة التمريض ومكتب الاستقبال من خلال الضوء
	7.وجود الاضاءة الطبيعية الكافية في فضاءات المستشفى
	8.وجود نمط جذاب للاضاءة يجمع بين الاضاءة الطبيعية والاصطناعية
2.اللون	1. وجود اللون للتحفيز البصري والاثارة ولاضفاء شعور بالرفاهية

	2.مراعاة التأثير النفسي للألوان على الاطفال.
	3.أستخدام اللون لابراز مصادر المعلومات كمكتب الاستقبال ومحطات التمريض
	4.أستخدام اللون كإشارة دالة على الحركة والتوجيه وكمصدر للمعلومات
	5.إعطاء المتعة البصرية في أثناء الحركة من خلال اللون
	6.وجود خطة حول درجة اللونية التوافقية للألوان لمنع ظهور الأرباك البصري
	7.أستخدام الالوان الاكثر تذكرا لدى الاطفال
	8.أستخدام الالوان المحببة لكل فئة عمرية
3. الاعمال الفنية	1.وجود العمل الفني كحافز بصري لتهدئة الاطفال وتقليل الإجهاد البيئي
	2.تصميم العمل الفني كرسائل باعثة للأمل و البهجة
	3.أستخدام العمل الفني كمعالم لإيجاد الطريق
	4.إحتواء سقف غرف الاطفال على الأعمال الفنية للتقليل من الشعور بالملل
4.الطبيعة الخارجية والنباتات الداخلية	1.تعزيز التواصل مع الطبيعية بوجود نباتات داخلية
	2.وجود منافذ رؤية مطلة على الفضاءات الخارجية
	3.أستخدام النوافذ في الممرات للمساعدة في الاستدلال على الطريق
	4.وجود الملهيات البصرية التي تشعر الطفل بالسعادة كنافورت الماء
5.الرموز والإشارات	1.وجود الرموز لتحديد الوجهة وإرسال المعلومات للناس
	2.بساطة رسالة الرموز لتسهيل أستقبالها بصرياً
	3.موضوعة بشكل مدرك في الفضاء
	4.أستخدام الرسوم الكارتونية بوصفها إشارات لايصال رسالة معينة
	5.وجود هوية للإشارات
	6.أستخدام اللون والضوء لجذب الانتباه للوحات الارشادية

المحور الثاني: الدراسة التطبيقية ونتائجها

لقد تضمنت الدراسة العملية مرحلتين :

المرحلة الاولى: تحليل الواقع الفيزيائي والادراكي الحسي للمواقع المختارة من خلال الزيارات الميدانية المتكررة والمسح الفعلي لهذه المواقع وأعتماد الملاحظة الحسية الدقيقة مع اعداد المخططات التفصيلية للتنظيم الفضائي لها.

المرحلة الثانية: إجراء الاستبانة (Questionnaire) لأفرادالعينة البحثية بهدف استخلاص المعلومات المتكونة لديهم حول البيئة الفيزيائية من الجانب الادراكي الحسي البصري وتجسيد الصورة الذهنية لهذه البيئة لدى مستخدميها .ومقارنة النتائج المستخلصة من الاستبانة مع نتائج تحليل الواقع الفيزيائي بهدف التحقق من العلاقة بين المثيرات الحسية البصرية وادراك الفضاء الداخلي في مستشفى الأطفال وذلك بأعتماد الاساليب الاحصائية الملائمة.

أمّا اسلوب معالجة البيانات فتم الأعتماد على:

- التحليل الحسي والبصري .
- التحليل الاحصائي.

1. **انتخاب مواقع الدراسة العملية:**

بعد إجراء الزيارات الميدانية لعدد من المستشفيات في مواقع مختلفة من القطر الأردني الشقيق ، تم انتخاب كل من:

* مستشفى الأميرة رحمة التخصصي في طب الأطفال في مدينة اربد
* مستشفى الأردن في عمان / قسم الأطفال التخصصي (الحاصلة على جائزة أفضل تصميم لمستشفى في المملكة الأردنية).

تم اختيار هذين المستشفيين كمواقع لإجراء الدراسة الميدانية والكشف من خلالها عن دور المثيرات البصرية في الادراك الحسي للفضاء الداخلي .وقد تم انتخاب هذه المواقع للأسباب الآتية:-

- صعوبة إجراء الدراسة العملية على مستشفيات الأطفال في العراق لعدم تلبيتها المواصفات العالمية في المجال الادراكي الحسي البصري فضلاً عن الظروف الراهنة والاوضاع الصعبة ومانتج عنها من اضرار وتغيرات كبيرة لحقت بالمستشفيات الأمر الذي جعل من الصعب إجراء الدراسة الميدانية واستخلاص المعلومات اللازمة.
- التقارب الجغرافي والثقافي بين العراق والقطر الأردني ،وعليه فإن نتائج الدراسة العملية (فيما يخص الجوانب الادراكية) يمكن اعتمادها كمؤشرات في وضع تصاميم أو تطوير واقع الحال لمستشفيات العراق.
- ان المواقع المختارة مصممة كمستشفيات تخصصية للأطفال على وفق أسس تخطيطية وتصميمية مدروسة ولها مبدأ تنظيمي واضح وتمتلك المقومات كافة التي تتطلبها الدراسة الحالية.
- تمثل المواقع المختارة تبايناً في تلبيتها للمتطلبات الادراكية الحسية التي تم استخلاصها من الاطار النظري مما يتيح مجالاً واضحاً للمقارنة والخروج بنتائج موضوعية وأكثر شمولية حول موضوع البحث.

– **وصف العينة الدراسية:**

تتطرق هذه الفقرة الى تقديم شرح موجز عن المستشفيين الممثلتين للعينة البحثية وهي:

- **مستشفى الأميرة رحمة التخصصي في طب وجراحة الأطفال :**

تم افتتاح المستشفى بتاريخ 1995/11/20 كمستشفي تخصصي لطب الأطفال وجراحتها ويعد المستشفي الوحيد المتخصص في المملكة الأردنية الهاشمية . ويقع المستشفى في مدينة اربد على قطعة أرض تبلغ مساحتها (114) الف متر مشتركة مع مستشفى الأميرة بديعة للنساء والولادة و بلغت مساحة المباني (4000) متر مربعاة ويعمل في المستشفى (40) طبيباً و(287) موظفاً إدارياً وتمريضياً،وتتكون المستشفى من ثلاثة طوابق كما هو موضح بالشكلين (1-1),(1-2).

- **مستشفى الأردن**

أنشئ مستشفى الأردن في ضوء حاجة ماسة لإنشاء مؤسسة طبية تخصصية عصرية توفر للطبيب الأمكانيات الفنية والعلمية كلها من أجل الممارسة الكاملة لمهنة الطب وتؤمن للمريض الافادة من آخر ما توصلت إليه التقنية الطبية الحديثة.

بوشر العمل به في 1996/11/20ويقع المستشفى في وسط مدينة عمان على قطعة أرض تبلغ مساحتها (14) الف متر و بلغت مساحة المباني (22000) متر مربع ويعمل في المستشفى (39) طبيباً و(460) موظفاً إدارياً وتمريضياً.

ويتكون مستشفى الأردن والمركز الطبي من ثلاثة أجزاء رئيسة: المستشفى و العيادات الخارجية و سكن الممرضات.الشكل(1-3) يوضح اقسام المستشفى والشكل (1-4) يوضح مخطط موقع مستشفى الاردن

- **اختيار العينة البحثية وتصميم استمارة الاستبانة**

احتوت استمارة الاستبانة على مجموعة من الاسئلة على وفق المؤشرات التي تم الخروج بها من الاطار النظري في المحور الثاني وتم تقسيم العينة البحثية الى قسمين :

القسم الاول: الأطفال في المستشفى وتم تثبيت العينة التي تبلغ (30) طفلاً من كل مستشفى اي مجموع (60) للحصول على نتائج أقرب للصحة (الملحق- 1-) وجاءت الاسئلة بصيغة مخاطبة للأطفال واستخدمت الصور وطلب منهم تلوينها في الاستمارة الصور

القسم الثاني: استمارة الكادر الطبي في المستشفى(الملحق-2-) وتم أخذ (30) شخصاً من كل مستشفى أي بمجموع (60) شخصاً بشكل عشوائي بإذ يضم أشخاصاً من مختلف الأعمال ومختلف التخصصات

*** نتائج تحليل الواقع الادركي الحسي البصري للبيئات المنتخبة**

نتائج تحليل الواقع الادراكي الحسي لمستشفى الأميرة رحمة

- مثير الضوء

تم الأعتماد على الاضاءة الطبيعية بشكل كبير خلال مدة النهار نتيجة وجود النوافذ الكبيرة المتوزعه في أرجاء المستشفى كما في الشكلين(1-5)، (1-6). أمّا في ساعات الليل فكانت اضاءة فضاء المدخل زاهية لكنها لاتحتوي على تدرج بين الخارج والداخل وعدم ابراز أماكن الاستعلامات من خلال الاضاءة. أمّا اضاءة غرف المرضى كانت الاضاءة الاصطناعية ضمن المديات المقبولة ولا تحتوي على إزعاج بصري للأطفال ولقد لحظ ان اضاءة الممرات كانت اضاءة ساقطة من السقف تولد إزعاج للمرضى الراقدين في أسرّتهم أثناء نقلهم في الممرات والاضاءة بصورة عامة خالية من توفير اهتمام بصري.

- مثير اللون

تم رصد عدم توظيف اللون لمخاطبة المدركات البصرية للطفل أوأستخدامه كأدارة للتوجيه بين الفضاءات فقد كان هناك لون واحد سائد وهو اللون الابيض لنصف الجدار العلوي والنصف السفلي هو اللون الرصاصي الفاتح المائل الى البياض وعولجت الارضيات باللون التبني والسقف باللون الابيض كما في الشكل (1-7) ولحظ هناك محاولات لاضافة بعض التغيير في اللون في مناطق الردهات بأستخدام الزركشة على الجدران وبصورة عامة يمكن القول ان الخصوصية اللونية كانت غائبه في الفضاءات ولم تؤخذ في الحسبان أو تراعي المتطلبات النفسية للأطفال لدى تواجدهم في فضاءات المستشفى.

- الاعمال الفنية في المستشفى

لم يظهر الأستخدام الكبير للعمل الفني ضمن فضاءات المستشفى إذ اقتصر على وجود بعض الاشرطة الملونة المعلقة بالسقف ضمن فضاء المدخل والانتظاركما في الشكل(1-8) فضلاً عن تواجد صورعدة موضوعة بشكل غير منظم ولا تحمل أي معنى مخاطب للطفولة أمّا بقية الفضاءات فقد خلت من الاعمال الفنية مع وجود لوحتين في ممر الطابق الاول كما استخدمت الاشرطة الملونة في الممر المؤدي الى الغرف الادارية وهو قليل الأستخدام من قبل الأطفال

- الطبيعية الخارجية والنباتات الداخلية

تعزيز التواصل مع الخارج من خلال منافذ الرؤية الموجودة في أغلب الفضاءات نتج من شكل المستشفى الطولي وان وجود حديقة على جانبي المستشفى أوجد بيئة داخلية انسانية مشجعة على الشفاء وفي الوقت نفسه افتقرت المستشفى الى النباتات الداخلية ونوافير الماء واقتصر التواصل مع الطبيعة على الحديقة الخارجية والاطلالة عليها.

5.الرموز والإشارات

تم ملاحظة وجود الإشارات والرموز في فضاءات المستشفى إلاأنها موضوعة بشكل مربك وغير منظم . إنّ عدم إمكانية معرفة المشاهد أين سيتلقى المعلومه ادى الى حالة من الضجيج البصري وعدم القدرة على تميز المعلومات فضلاً عن كثرة عددها كما في الشكل (1-9) مما ولد حالة من الارباك كما لحظ انعدام أستخدام اللون و الإضاءة التي تجذب انتباه الطفل للوحات الإرشادية في مبني المستشفي وجاءت الرموز مخاطبة للكبار بأحتوائها على كتابات فقط.

نتائج تحليل الواقع الادراكي الحسي لمستشفى الأردن

- مثير الضوء

الانارة الطبيعية التي كانت الاساس في فضاء المدخل والمزج بين الاضاءة الطبيعية والاصطناعية عند مكتب الاستقبال الموضحة في الشكل (1-10) كما واضاءةغرف النوم ومناطق الادراج بالاضاءة الطبيعية الوافرة ولكن خلو الممرات بين الاقسام من آية نافذه وأعتماده كليا على الاضاءة الاصطناعية.

أمّا في ساعات الليل كانت اضاءة فضاء المدخل زاهية ومتنوعة منها المنعكسة ومنها الساقطة فضلاً عن تنوع شكل الضوء مع ظهور منطقة الاستعلامات بصوره بارزه من خلال الضوء كما في الشكل (1-11) كذلك الحال بالنسبة لمركز عمل الممرضين كما في الشكل (1-12) إذ ظهر بوضوح ضمن الفضاء أمّا اضاءة غرف المرضى فخلال النهار تكون بالأعتماد على ضوء النهار وفي الليل كانت الاضاءة الاصطناعية جيده وودودة ولا تحتوي على إزعاج بصري للأطفال أمّا بالنسبة لاضاءة الممرات فكانت ساقطة وأيضاً منعكسة و أستخدم نمط جيد للاضاءة مع توفير اهتمام بصري للمناطق التي يمكن ان يحصل الشخص منها على المعلومات واستغلال الاضاءة في اعطاء توجيه وتحديد للأماكن .

- مثير اللون

تم ملاحظة توظيف اللون كمثير بصري ولتمييز فضاءات المستشفى وخصوصاً في الممرات الرابطة بين الاقسام فضلاً عن أستخدام اللون لابراز الابواب في الممرات كذلك استخدم مساند على جانبي الممر كما في الشكل (1-13) وروعي أستخدام اللون بشدة في قسم الأطفال لاظفاء المتعة والبهجة في نفوسهم كما في الشكلين (1-14) و(1-15) أمّا بالنسبة للسقف والارضيات فكانت موحده لكل فضاءات المستشفى فاستخدم للاسقف اللون الابيض والارضيات جاءت باللون الابيض وأحتوت على خطوط ومربعات زرقاء غامقة باستثناء منطقة الادارة إذ كانت الارضية باللون الابيض.وتم ابراز منطقة المصاعد بأستخدام الرخام الملون حول المصعد وعند الحركة في الممرات يمكن الاحساس باختلاف الاقسام من إذ تغيير الالوان مما يشير الى دخولك ضمن قسم.

- الاعمال الفنية في المستشفى

امتازت فضاءاتها بوفرة الاعمال الفنية واللوحات منذ اللحضة الاولى لدخول المستشفى فيمتاز المدخل بلوحة فنية ملهمة كبيرة فضلاً عن اللوحات الموجودة على جدران الممرات والفضاءات وخصوصا في قسم الأطفال إذ اغتنى الممر باللوحات عن الرسوم الكارتونية والفراشات والأزهار والحيوانات المحببة لدى الأطفال.كما موضح بالشكل (1-16)

- الطبيعية الخارجية والنباتات الداخلية

امتازت مستشفى الأردن بوفرة الاضاءة الطبيعية والنوافذ المطلة على الفضاءات الخارجية وأستخدام مدخل زجاجي كبير كما في الشكل (1-17) ، وجعل فضاء المدخل والدرج الموجود في منطقة المدخل في تواصل مع الخارج .فضلاً عن وجود حديقة داخلية تفتح علية طوابق المستشفى الثلاثة كما استخدمت النباتات في فضاء الانتظار.و في غرف نوم الأطفال لحظ وجود منافذ رؤية مطلة على الفضاءات الخارجية و منظرطبيعي يخلق تواصلاً بصرياً بينماافتقرت فضاءات المستشفى الى وجود عنصر الماء أو النافورات في فضاءاتها التي تساعد الأطفال على الهدوء وصرف الانتباه عن الأمهم.

- الرموز والإشارات

لحظ ان المستشفى تضمن ثلاثة انواع من الإشارات هي: الإشارات التعريفية التي تعرف استعمال الفضاء والإشارات التوجيهية التي تحوي على أسهم تدل على الاقسام الرئيسة والإشارات التأكيدية عند التقاطعات المهمة . كما تم ملاحظة توحيد الإشارات الرئيسة للاقسام من ناحية شكل الكتابة ونوعهاوتوقيعها بشكل منظم والقدرة على تميزها .وأستخدام اللون كرمز للقسم بلون الابواب نفسها الموجودة في ممرات كل قسم كاستعمال اللون الاحمر لقسم الطوارئ والاخضر للكلى والبنفسجي الفاتح لقسم الأطفال وازرق سمائي للمختبرات والابيض للعمليات وغيرها مما يمكن الأطفال الذين لايجيدون القراءة من التعرف على قسم الأطفال من خلال اللون المصاحب للإشارة فضلاً عن احتواء بعضها على رسوم توضيحية مخاطبة للطفل.

* **<u>التحليل المقارن بين المستشفيين</u>**

بعد ان تم تحليل المستشفيين وفق الزيارة الميدانيةوأعتماد الملاحظة الموقعية الدقيقة تبعاًللمؤشرات الادراكية الحسية البصرية والحصول على المعلومات.و أستخدام رمز (•) للدلالة على تحقيق تأثير المثير الحسي البصري وفقاً لما يأتي:

الجدول(1-3) نتائج تحليل المثيرات البصرية

ت			مستشفى رحمة	مستشفى الأردن
1.	1.الضوء	1. توفير اهتمام بصري من خلال الضوء		•
		2.وجود إضاءة مريحة في فضاءات النوم واللعب	•	•
		3. اعطاء التوجيه وتحديد الطرق من خلال تصميم الضوء		•
		4.اعطاء الانطباع بالترحيب والجو المنزلي		•
		5. وجود توازن جيد خالٍ من وهج الضوء.		•
		6.ابراز أماكن الاستعلامات ومحطة التمريض ومكتب الاستقبال من خلال الضوء		•
		7.وجود الاضاءة الطبيعية الكافية في فضاءات المستشفى	•	•
		8.وجود نمط جذاب للاضاءة يجمع بين الاضاءة الطبيعية والاصطناعية		•
2.	اللون	1. وجود اللون للتحفيز البصري والاثارة ولاضفاء شعور بالرفاهية		•
		2.مراعاه التأثير النفسي للالوان على الأطفال		•
		3.استخدلم اللون لابراز مصادر المعلومات كمكتب الاستقبال ومحطات التمريض		•
		4.أستخدام اللون كإشارة دالة على الحركة والتوجيه وكمصدر للمعلومات		•
		5.اعطاء المتعة البصرية في أثناء الحركة من خلال اللون		•
		6.وجود خطة حول النغمة التوافقية للالوان لمنع ظهور ارباك بصري.		•

		7.أستخدام الالوان الأكثر تذكرا لدى الأطفال		•
		8.أستخدام الالوان المحببة لكل فئة عمرية		•
3.	الاعمال الفنية	1.وجود العمل الفني كحافز بصري لتهدئة الأطفال وتقليل الاجهاد البيئي		•
		2.تصميم العمل الفني كرسائل باعثة للامل والبهجة		•
		3.أستخدام العمل الفني كمعالم لايجاد الطريق		•
		4.احتواء سقف غرف الأطفال على اعمال فنية للتقليل من الشعور بالملل.		
4.	الطبيعية الخارجية والنباتات الداخلية	1.تعزيز التواصل مع الطبيعة بوجود نباتات داخلية		•
		2.وجود منافذ رؤية مطلة على الفضاءات الخارجية.	•	•
		3.أستخدام النوافذ في الممرات للمساعدة في الاستدلال على الطريق		
		4.وجود الملهيات البصرية التي تشعر الطفل بالسعادة كنافورت المياه		
5.	الرموز والإشارات	1.وجود الرموز لتحديد الوجهة وإرسال المعلومات للناس		•
		2.بساطة رسالة الرموز لتسهيل استقبالها بصرياً		•
		3.موضوعة بشكل مدرك في الفضاء		•
		4.أستخدام الرسوم الكارتونية كإشارات لايصال رسالة معينة		•
		5.وجود هوية للإشارات		•
		6.أستخدام اللون والضوء لجذب الانتباه الى اللوحات الارشادية		•

*** نتائج تحليل استمارة الاستبانة**

تهدف هذه الفقرة الى تحليل بيانات الدراسة العملية ونتائجها في تحقيق بيئة شفائية للطفل وعرض النتائج ومناقشتها .وكما ذكر سابقاً فقد شملت استمارة الاستبانة نوعين:استمارة مخصصة للأطفال ،وأستمارة مخصصة للكادر الطبي.

نتائج تحليل استمارة الاطفال

اولاً:الاضاءة

وأظهرت النتائج انه في كلتا المستشفيين ان الاضاءة كانت جيدة وضمن المديات المقبولة إذ لم يشتكِ منها الأطفال سؤاء أكانت في غرفة اللعب أم في غرف النوم وذلك لأعتمادها الكبير على الاضاءة الطبيعية ووجود النوافذ الكبيرة التي فسحت لنور الشمس بالدخول ومداعبة احاسيس الأطفال ولم تحتوي على إزعاج بصري ملحوظ .

ثانياً:اللون

وعند مقارنة النتائج وجد أن كلتا العينتين اجمعتا على الرغبة بوجود اللون في المستشفى ويعود السبب للتأثيرات السيكولوجية والفسيولوجية للون في حياة الفرد مما يلعب دوراً علاجيا كبيرا في الابنية الصحية كذلكَ امتاع البصر وراحة النفس والعقل .

وعند الاستفسار عن الالوان التي يتذكرها الطفل في المستشفى جاءت النتائج على وفق النسب الآتية:

ومن مقارنة النتائج يظهر ان اللون الذي يتذكره الطفل يعتمد على درجة توقيعه في الفضاء ففضلاً عن اللون السائد، يمكن ان يتذكر الطفل اللون القوي إذا ظهر بمساحات قليلة وكان من الالوان القوية وسيلفت الانتباه له أكثر من اللون السائد ويمكن استخدام هذه الميزة في توجيه الطفل في الفضاء وإمكانية الاستدلال على الطريق.

وعند الاستفسار من الأطفال عن اللون الذي يحب ان يكون لون غرفته جاءت اجاباتهم كما يأتي:

ومن مقارنة النتائج نلحظ تقارب الالوان التي يرغب الأطفال بتواجدها وهي كل من الاحمر والوردي والازرق إذ إنها من الالوان المحببة للاطفال التي تبعث فيهم الطاقة والنشاط مما يخلق لهم بيئة رائعة تعزز شعورهم بالشفاء ويمكن إيعاز السبب في هذا التقارب بالذوق الى تقارب الفئات المنتخبة للعينية البحثية ووقوعهم ضمن المرحلة العمرية نفسه.

ثالثاً:**الاعمال الفنية**

ومن المقارنة نجد ان الرسوم الكارتونية تمثل عنصراً رئيسياً يؤثر في الادراك الحسي سواء للطفل الزائر أو المقيم فهي قريبة من الأطفال ويمكن استيعابها من قبلهم كما انها تغني المبنى حسياً ومن ثم تنعكس تأثيراتها على الجانب النفسي إذ تقلل من مخاوفهم وتسليهم وتصرف انتباههم لمدة طويلة من الوقت .

رابعاً:**الطبيعة الخارجية والنباتات الداخلية**

ومن مقارنة النتائج تظهرالرغبة بوجود تواصل مع الخارج فالطفل بفسلجته يكره العزلة ويرغب بتواصله مع الخارج إذ يعد هذا المؤثر مهماً ويزود الطفل بالاحساس المكاني ويمنحه التحكم والادراك لبيئته.

خامساً:**الرموز والإشارات**

وأظهرت النتائج ان الأطفال في كلتا المستشفين يرغبون بوجود الإشارات ويمكن تفسير ذلك ان الإشارات متغير رئيسي يساعد على التوجيه إذا ما وضعت في موقع اتخاذ القرار وتكون عاملاً مساعداً في معرفة الطريق إذ إن وجود الإشارات يوفر للطفل ولعائلته السيطرة على البيئة والراحة وسهولة الحركة والمقدرة على فهم فضاء المستشفى.

نتائج تحليل استمارة الكادر الطبي

اولاً:**الاضاءة**

ومن نتائج المقارنة نلحظ اجماع الكادر الطبي في كلتا المستشفيين على الاثر الكبير للاضاءة على الاحساس بالراحة وما يعكسه من تأثيرات صحية في الاطفال نتيجة تواجد النوافذ الكبيرة في أرجاء غرف الاطفال في كلتا المستشفيتين .

ثانياً:**اللون**

نلحظ تفاوتاً في ملاحظات الكادر لتأثير اللون في الاطفال ويعود السبب الى عدم توظيف اللون كمثير حسي بصري في مستشفى الأميرة رحمة بينما جاء رأي الكادر الطبي في مستشفى الأردن على عكس ذلك إذ اكدوا تأثير تنوع اللون في نفسية الطفل واظفاء شعور بالراحة و يخلق متعة بصرية في أثناء التجوال في المستشفى ويبعد عن نفوس الاطفال القلق والرهبة لدخولهم المستشفى.

ثالثاً:**الاعمال الفنية**

وتقاربت النتائج إذ يرى الكادر الطبي ان وجود الرسوم الجدارية ضروري في تبديد مخاوف الاطفال وخلق جو منزلي للاطفال ويسهم في أستدلالهم على الطريق و كان ذلك واضحاً في مستشفى الأردن إذ وجدت الرسوم على جدران المستشفى بصورة واضحة.

رابعاً:**الطبيعة الخارجية والنباتات الداخلية**

ومن مقارنه النتائج ظهر وجود تقارب بالنسب في كلتا المستشفين على ان وجود اطلالة على الخارج تؤثر في نفسية الطفل وان لها فعالية عالية كمثيرات حسية بصرية بطريقة تساعد الطفل على تحمل الضغط والتوتر الناجم عن المرض وقلل من أهمية كل من النافورات والنباتات الطبيعية ويمكن ايعاز السبب الى انعدام تواجدهما في مستشفى رحمة فضلاً عن عدم تواجد نافورات الماء في مستشفى الأردن مما ادى الى عدم ملاحظة التأثير الكبير لهما

خامساً:**الرموز والاشارات**

ومن مقارنة النتائج ظهر ان كلتا المستشفين أكد كادرها الطبي ضرورة وجود الاشارات فهي عناصر مهمة بالفضاء تساعد على ارشاد الطفل سواء عن طريق الكتابة الموجودة عليها أو عن طريق الرسوم وتعد من المتغيرات الرئيسة اذا ماتم توظيفيه بصورة صحية.

وعند الاستفسار عن الوسائل الارشادية التي يفضلها الطفل في ايجاد طريقة جاءت الاجابة كما يأتي:

ومن نتائج المقارنة ظهر ان أستخدام التعابير البصرية سواء الاشرطة الملونة أو الرسوم هي التي يفضلها الاطفال ويمكن تفسير ذالك ان الاعمال الفنية والاشرطة اقرب للطفل واسهل للفهم وتخاطب عقله وتمكنه من السيطرة على بيئته إذ إنّ الاطفال يحتاجون الى ان يجدوا المعلومات السريعة لترشدهم وعائلتهم في المستشفى لذا فإن البناء العصري الناجح يجب ان يكون مزودا بعلامات ودلالات تعرف بمرافق المستشفى وتسهل الحصول على المعلومات ومعرفة الاتجاه.

استنتاجات البحث

- احدى العوامل التي ساعدت على انجاح التصميم الداخلي وخلق بيئة مثيرة في مستشفى الأردن هو التنوع والغنى اللوني في فضاءات المستشفى والتي بدورها ساعدت على التميز الفضائي على عكس مستشفى رحمة التي اكتفت باللون الابيض واستخدمته كلون سائد.
- اغناء المبنى حسيا من خلال اثرائه بالاعمال الفنية في مستشفى الأردن وافتقار مستشفى رحمة اليها واقتصارها على بعض الاشرطة الملونة في منطقة الانتظار.
- تعزيز التواصل مع الخارج يساعد في تحسين الحالة الصحية وقد كان واضحاً وجود النوافذ بصورة كبيرة في كلا المستشفيين في حين افتقارهما الى نوافير المياه.
- تساعد الاشارات في الأستدلال على الطريق وتستخدم كمثير في الفضاء اذا امكن تمييزها عما حولها بالموقع أو اللون أو الحجم وإمكانية قراءتها بسرعه وظهرت الاشارات بوضوح في مبنى مستشفى الأردن ولكنها كانت مربكة في مستشفى الأميرة رحمة.
- كفاءة المعرفة المطروحة على حاسة البصره التي تعد من أهم الحواس ولها الأهميه الاكبر في إدراك الفضاء بوصفها الحاسة الاولى التي يجمع بها الطفل معلوماته عن بيئته.

- كفاءة المعرفة المطروحة لأهمية الاعمال الفنية في مستشفيات الأطفال اذ ان من الضرورة استخدامها في فضاء المستشفى إذ إنها تخاطب عقل ومشاعر الطفل وتكون قريبة منه .
- كفاءة المعرفة المطروحة للدور الرئيس لعناصر الطبيعية في تنشيط المريض حسياوذلك من خلال توفير اضاءة طبيعية واستغلال المصمم للفرص التي تتيحها الشمس من تلاعب بالضوء وتحقيق اطلالة نحو الخارج ترافقهـا اضافة نافورات الماء واستخدام النباتات كل ذلك يسهم في تحسين الحالة الصحية والعلاجية للطفـل ومخاطبـه احاسيسه إذ تساعده في خلق الملهيات وتشعره بالسعادة والابتعاد عن الجو المخيف للمستشفيات.
- تأكيدالمعرفة المطروحة على دور اللون في العملية الشفائية واضفاء شعور بالرفاهية كما ويؤدي الى صـرف انتباههم و يمكن استخدامه كأدات توجيه بين الفضاءات للتعرف على بيئات الأطفال الجديدة.
- بيان المعرفة المطروحة لمعايير استخدام الرسوم والعلامات والرموز التي تحتوي على رسوم وصور تخاطـب الأطفال ومدركة من قبل حواسهم تساعدهم في السيطرة المكانية على الفضاء وتمكنهم من معرفة طريقهم وايضا تساعد في تحفيز الحواس لديهم وتنميها على الاستكشاف
- كفاية المؤشرات المطروحة في الكشف عن دور المثيرات الحسية في مستشفيات الأطفال.
- تطابق وتلاؤم المعرفة النظرية مع نتائج الدراسة التطبيقية حول دور المثير البصري الحسي في الادراك الحسي للفضاء.

التوصيات

- إدراك دور مستشفيات الأطفال في أنظمة الرعاية الصحية بوصفها الجوهرة الثمينة التي يرصع بها التاج ، لذا وجب الارتقاء بها وإعطائها أهمية كبرى من مشاركة السوق وتزويدها بالكفاءات العليا والمتطوعين المتحمـسين لإظهارها بحلة جيدة ، كما ويجب مدها بالدعم المجتمعي المتواصل.
- ضروره مراعاة الانطباعات البصرية داخل مستشفيات الأطفال واعتبارها معيارا لكفايـة العمـل المعمـاري ،فالمصمم المعماري لايصمم فضاءاً معمارياً فقط بل يصمم سلوك المستعمل.
- وضع معايير تصميمية للفضاءات الداخلية لمستشفيات الأطفال والأهتمام بتأثير فضاءات المبنى علـى نفـسية الطفل.
- ضرورة رفد العملية التصميمية بالابحاث والدراسات العلمية المتخصصة في مجال علم نفس البيئة والدراسـات السايكولوجية المرتبطة بالطفل.
- رفع كفاية المستشفيات الحالية من خلال تصاميم احيائية يقوم بها فريق متخصص من المعماريين ومهندسـي الفضاءات الداخلية مستندا على الأسس التي تناولها البحث بعد اعداد دراسة جدوى لامكانيـة التنفيـذ واعـادة الصيانة واعتماد ذلك كشرط اساسي لاستمرارية المستشفيات .

المصادر والمراجع

- **BS, British Standards Institution** EN 60598-2-25 :(1995). **"Particular Requirements. Luminaires for Use in Clinical Areas of Hospitals and Health Care Buildings"**. U.K
- **CIBSE, Chartered Institute of Building Services Engineers,** (2002) **"Lighting Guide LG3 – The Visual Environment for Display Screen Use"**, London.
- **Cowgill,** J., Bolek, J., (2003), **"Symbol Usage In Health Care Settings For People With Limtted English Roficiency"**, JRC Design, Arizona

- **Dalke**, H. , Littlefair, P.& Loe, D., (2004), "**Lighting and Color for Hospital Design**", Her Majesty's Stationery Office, London
- **Figueiro**, M.,(2001), "**Lighting the Way: A Key to Independence**". Lighting Research Center, Rensselaer Polytechnic Institute. New York
- **Grauer**, T., (1989) "**Environmental Lighting, Behavioral State and Hormonal Response in the Newborn**". Scholarly Inquiry into Nursing Practice, London. Pp.53–66
- **Green**, A., (2003) "**Improving the patient experience: Friendly Healthcare Environments for Children and young people**", The Stationery Office, London
- **Hospital building note HBN** 23, (2004),"**Hospital Accommodation for Children and Young People**", The Stationery Office, London. NHS Estates.
- **Komiske**, B., (1999),"**Designing the World's best: Children's Hospital**", Images Publishing. Australia
- **Leger**, L., (2003). "**Health and Nature—New Challenges for Health Promotion**", Health Promote. Oxford Journals Oxford University Press, Int. 18
- **Lovett**, P., Halstead, M.& Hill, A.., (1991), "**The Effect on Clinical Judgments of New Types of Fluorescent Lamp**". Lighting Research and Technology. Vol. 23 No. 1, New York.
- **Mahnke**, F., and Mahnke, R. 1987,"**Colour and Light in Man-made Environments**", Van Nostrand Reinhold. New York.
- **Marberry** , S. , Zagon, L., (1995), "**The Power of Color: Creating Healthy Interior Spaces**", John, Canada
- **Michel**, L., (1996), "**Light: The Shape of Space**", Van Nostrand Reinhold., New York.
- **NHS** ESTATES, (2002) "**The Art of Good Health: Using Visual Arts in Healthcare**", the Stationery Office
- **NHS** Estates, (2003),"**Welcoming Entrances and Reception Areas**", The Stationery Office, London
- **Rosenfield**, I. , Rosen field, Z., (1971) **Hospital Architecture: Integrated Components**. Van Nostrand Reinhold Company, Michigan
- **Ruiolds**, A.., (2000),"**Child Care Design Guide",** MC Graw-hill professional. U.S.

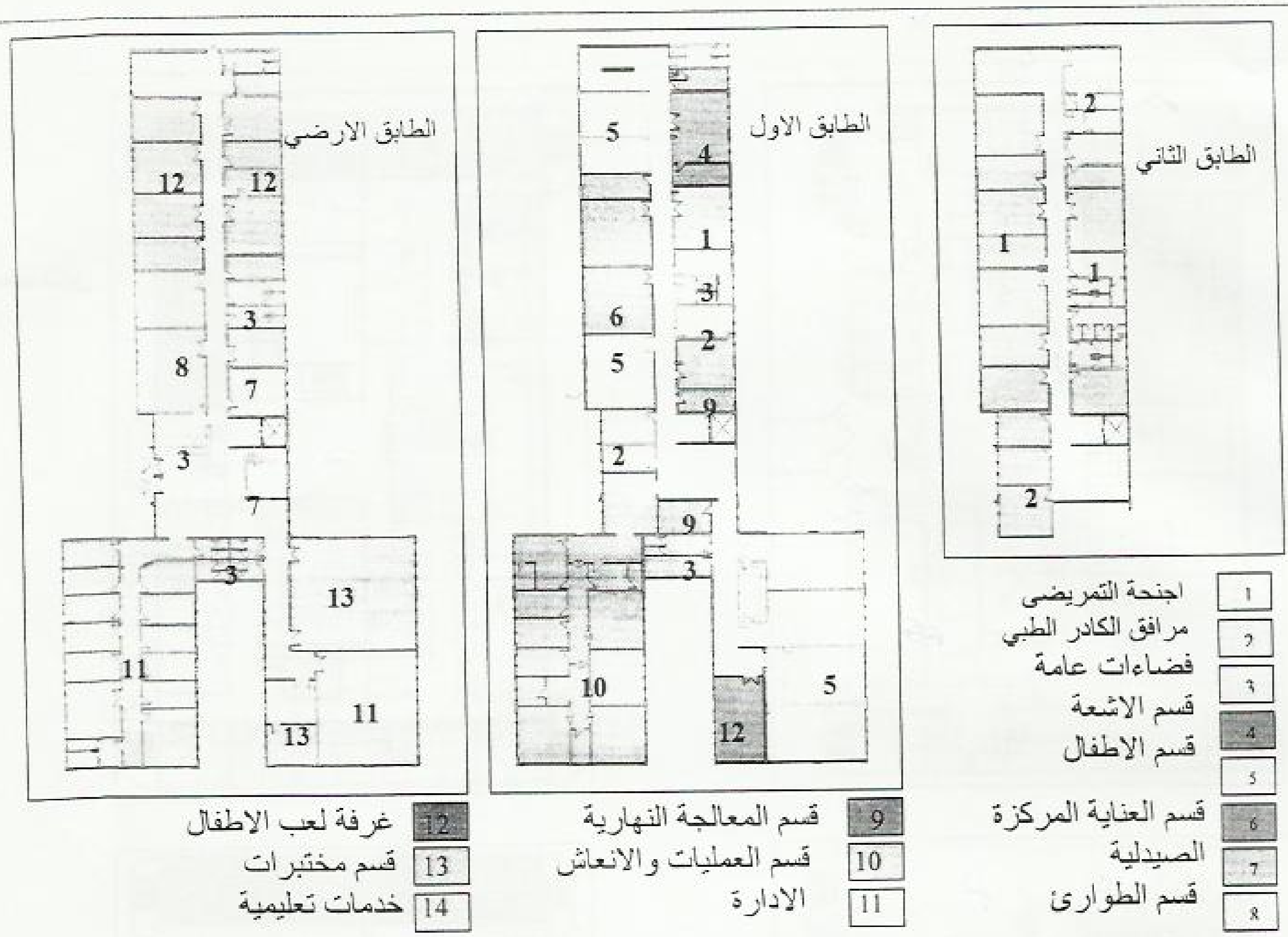

شكل (1-1) يوضح الاقسام في مستشفى الاميرة رحمة

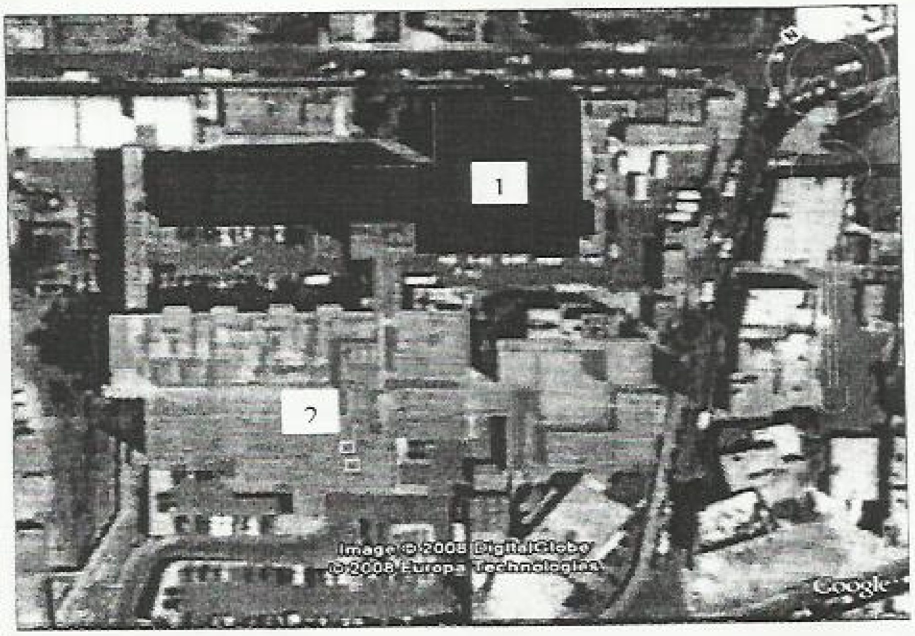

الشكل (1-2) يوضح مخطط موقع مستشفى رحمه وعلاقتها مع مستشفى الاميرة بديعة

1.مستشفى رحمه ،2.مستشفى الاميرة بديعة .(Google earth,2008)

مخطط طابق الاول

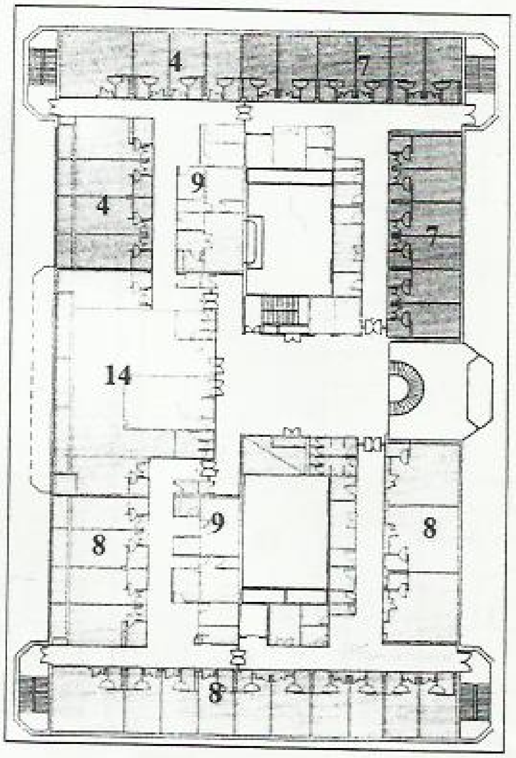

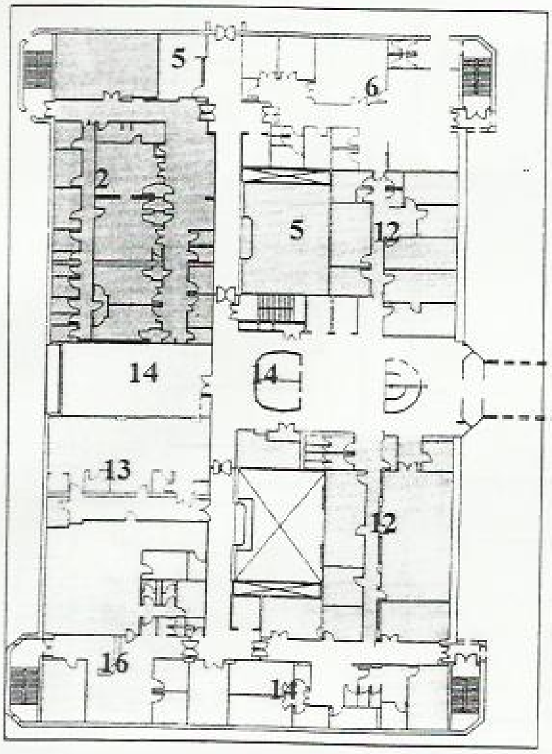

مخطط الطابق الثالث

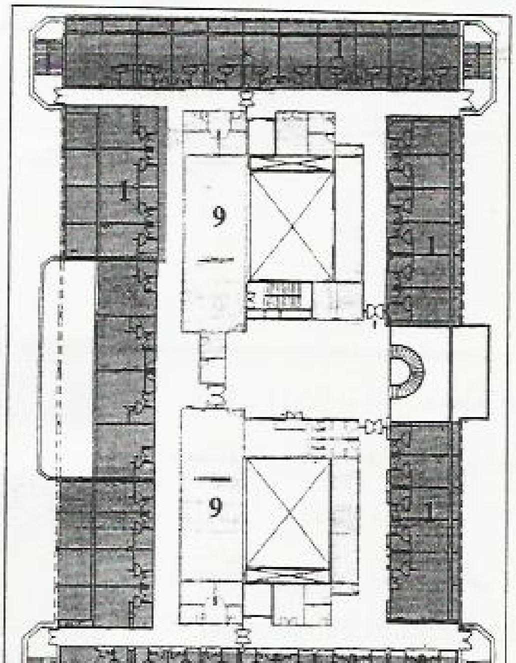

مخطط الطابق الثاني

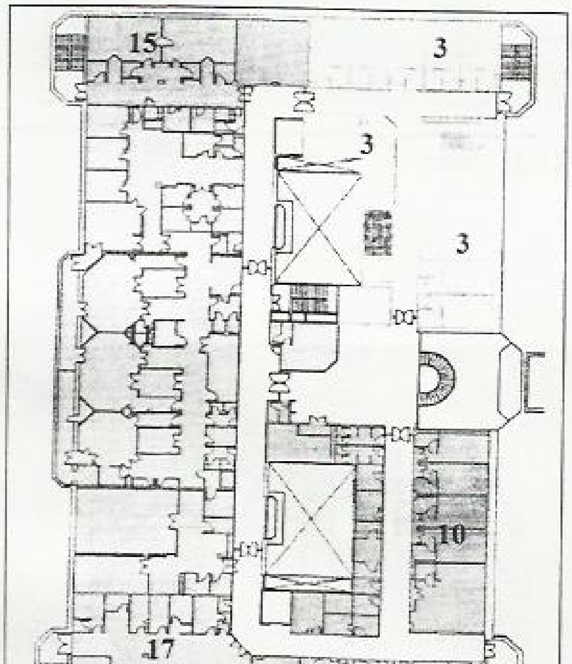

1	اجنحة مرضى
2	قسم الاشعة
3	قسم الاطفال
4	قسم العناية المركزة
5	الصيدلية
6	قسم الطوارئ
7	غرف الدرجة الثالثة
8	اجنحة الاطفال
9	مرافق الكادر الطبي
10	قسم المعالجة النهارية
11	قسم العمليات والانعاش
12	الادارة
	غرفة اللعب
13	تعقيم مركزي
14	فضاءات عامة
15	قسم الخدج
16	قسم مختبرات
17	عناية حثيثة

الشكل (1-3) يوضح تسقيط الاقسام في مستشفى الاردن(المصدر /الباحث)

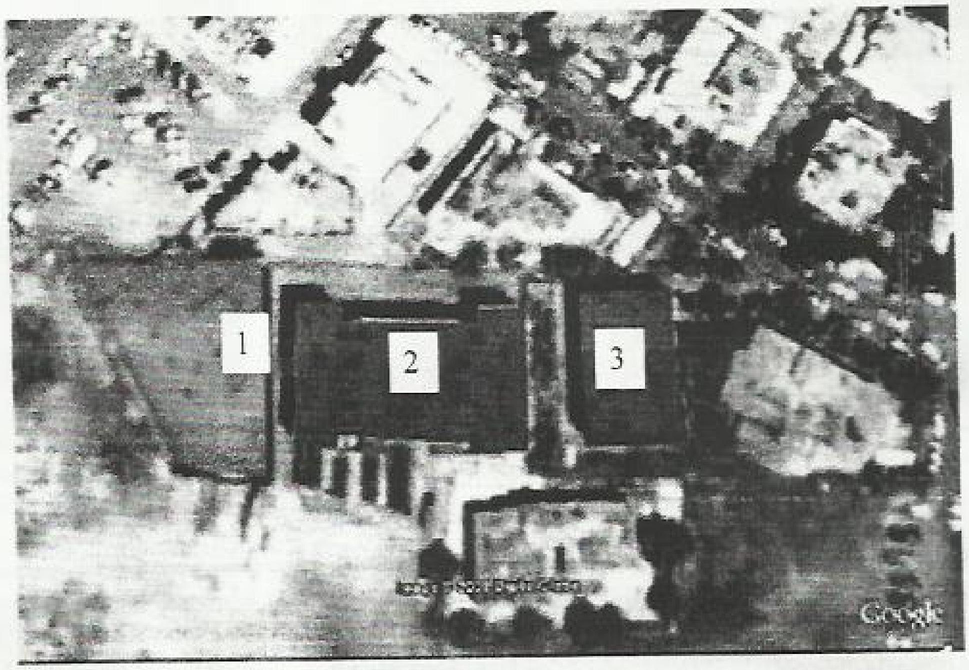

الشكل (1-4) يوضح مخطط موقع مستشفى الاردن ومكوناتها التي هي 1.المستشفى و 1.العيادة الخارجية و 3.سكن الممرضات. (Google earth,2008)

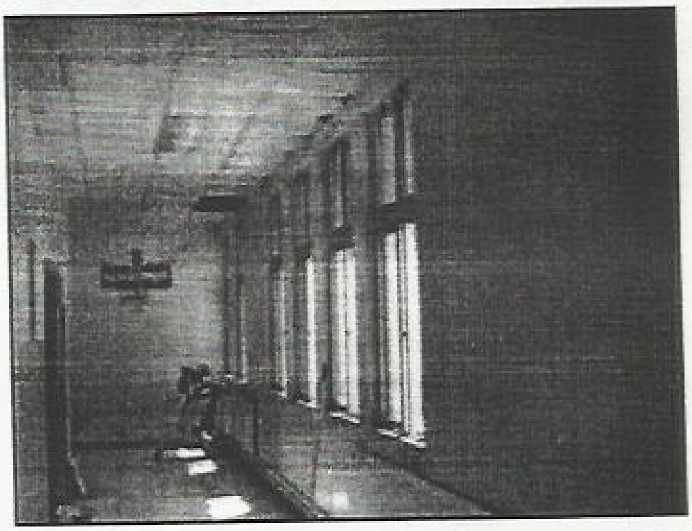

الشكل (1-5) يوضح الاضاءة الطبيعية الوافرة في الممرات.(مستشفى رحمه)

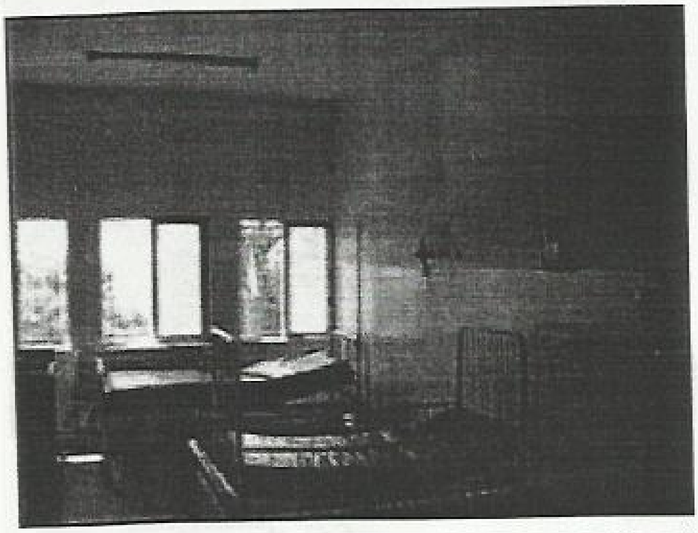

الشكل (1-6) يوضح غرفة المرضى.(مستشفى رحمه)

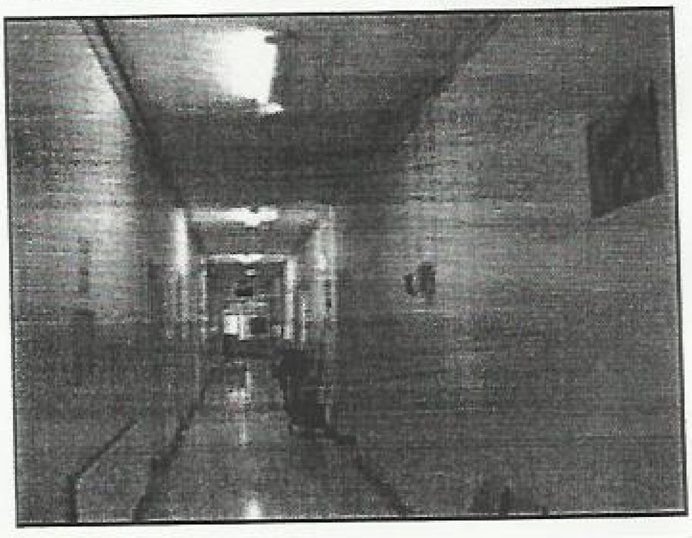

الشكل (1-7)يوضح الاضاءة الساقطة في الممرات وكذلك استخدام اللون الرصاصي الفاتح لنصف الجدار السفلي واللون الابيض للنصف العلوي والسقف.(مستشفى رحمه)

الشكل(1-8) يوضح استخدام الاشرطة الملونة في فضاء المدخل محاولة لاظفاء روح للفضاء (مستشفى رحمه)

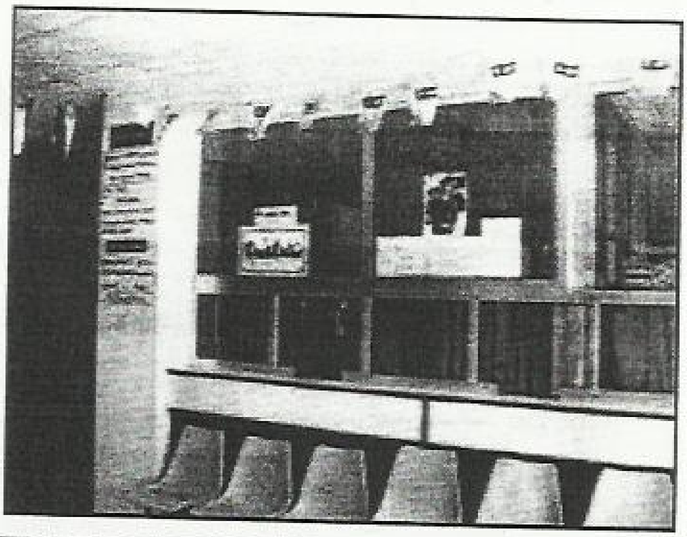

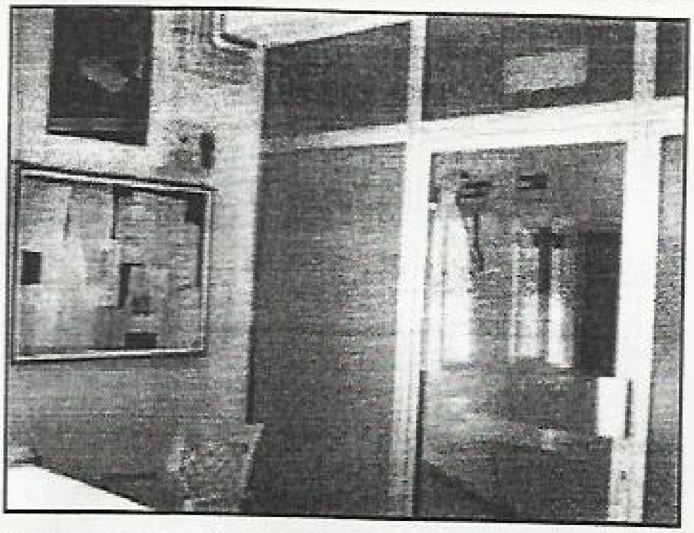

الشكل (1-9) يوضح منطقة المدخل والتوزيع المربك للاعلانات الموجودة مما قلل من اهمية وخلق حالة من التشويش لدى الزائر (مستشفى رحمه)

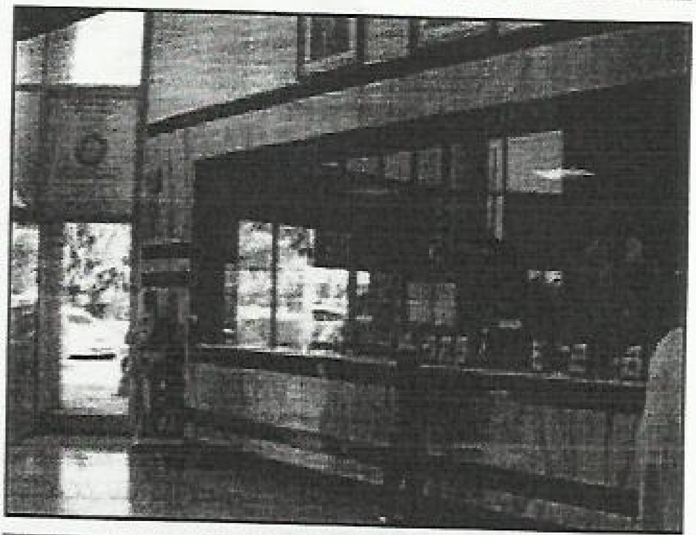

الشكل (1-10) المزج بين الاضاء الطبيعية والاصطناعية في منطقة الاستقبال(مستشفى الاردن)

الشكل (1-11) استخدام عدة انواع من الاضاءة في فضاء المدخل (مستشفى الاردن)

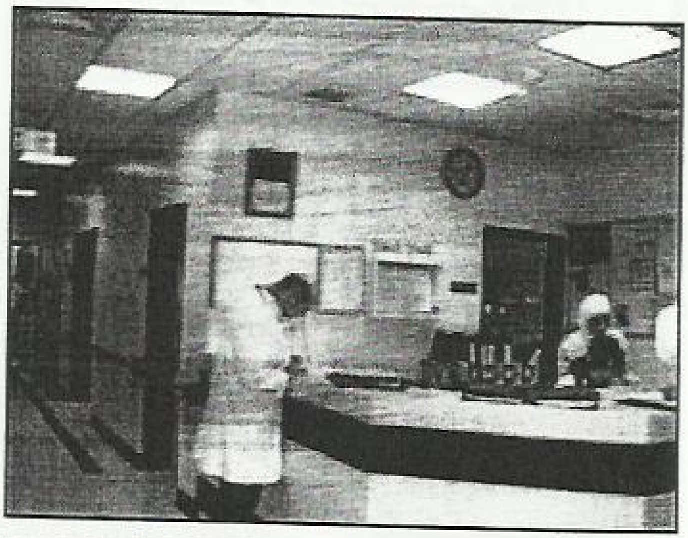

الشكل (1-12) ابراز منطقة عمل الممرضين في الاقسام من خلال الاضاءة. (مستشفى الاردن)

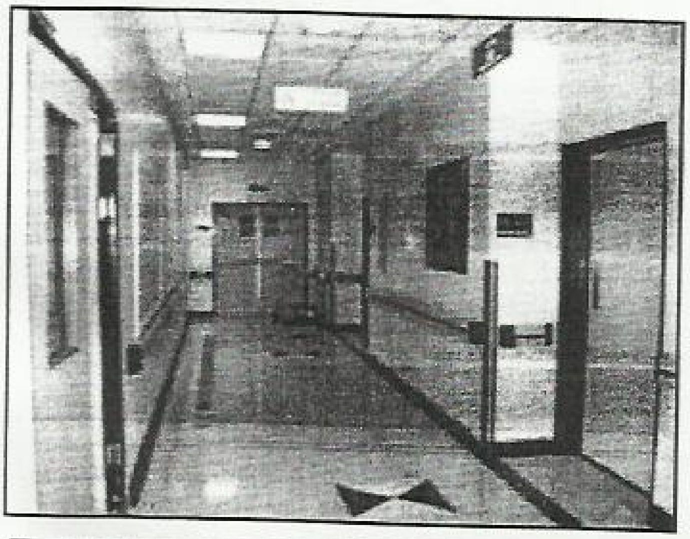

الشكل (1-13) استخدام الاصفر الفاتح والبنفسجي للابواب في ممرات قسم الاطفال. (مستشفى الاردن)

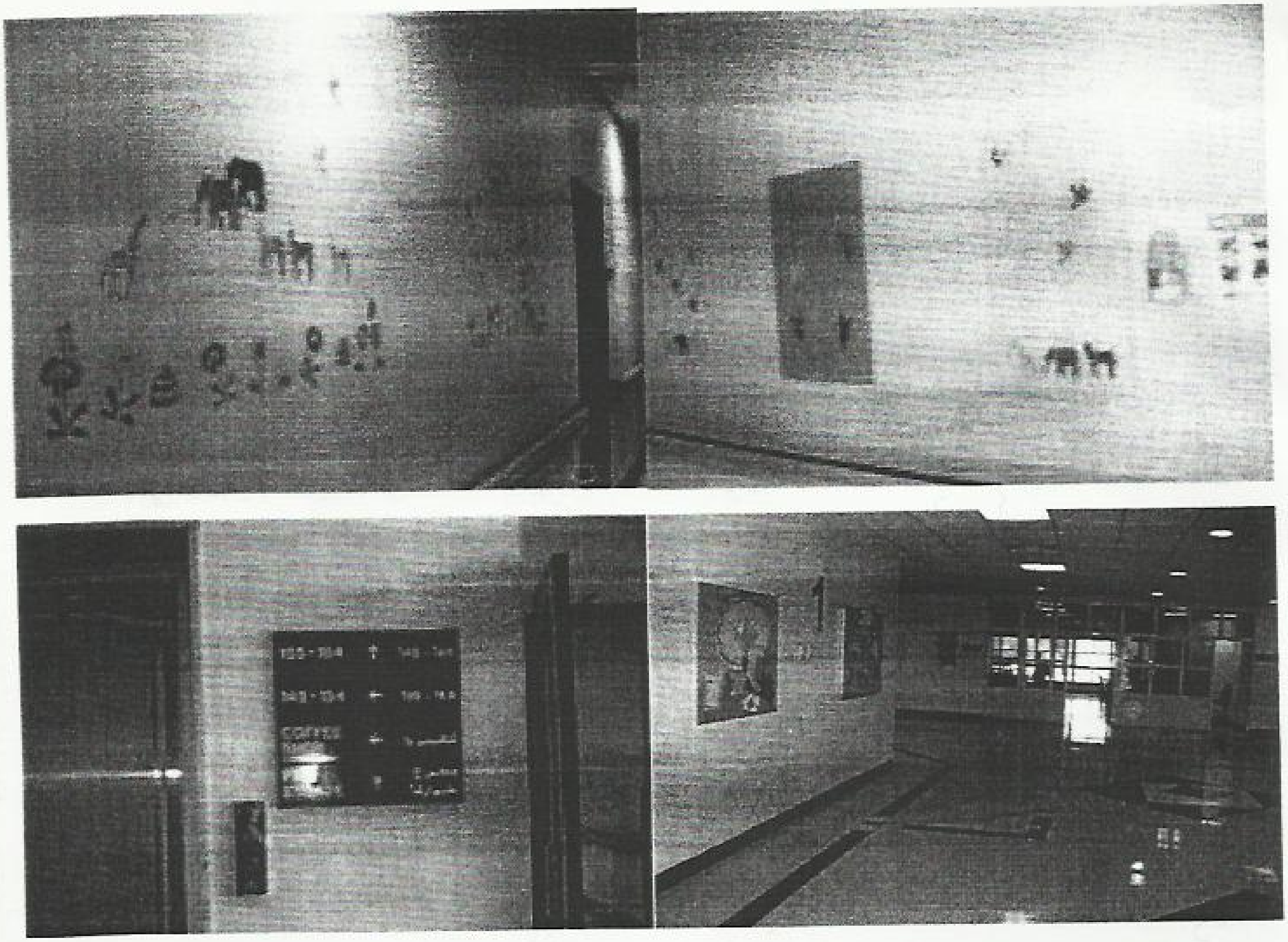

الشكل (1-16) يوضح الاعمال الفنية في الممرات و توقيع الاشارات بصورة بارزة. (مستشفى الاردن)

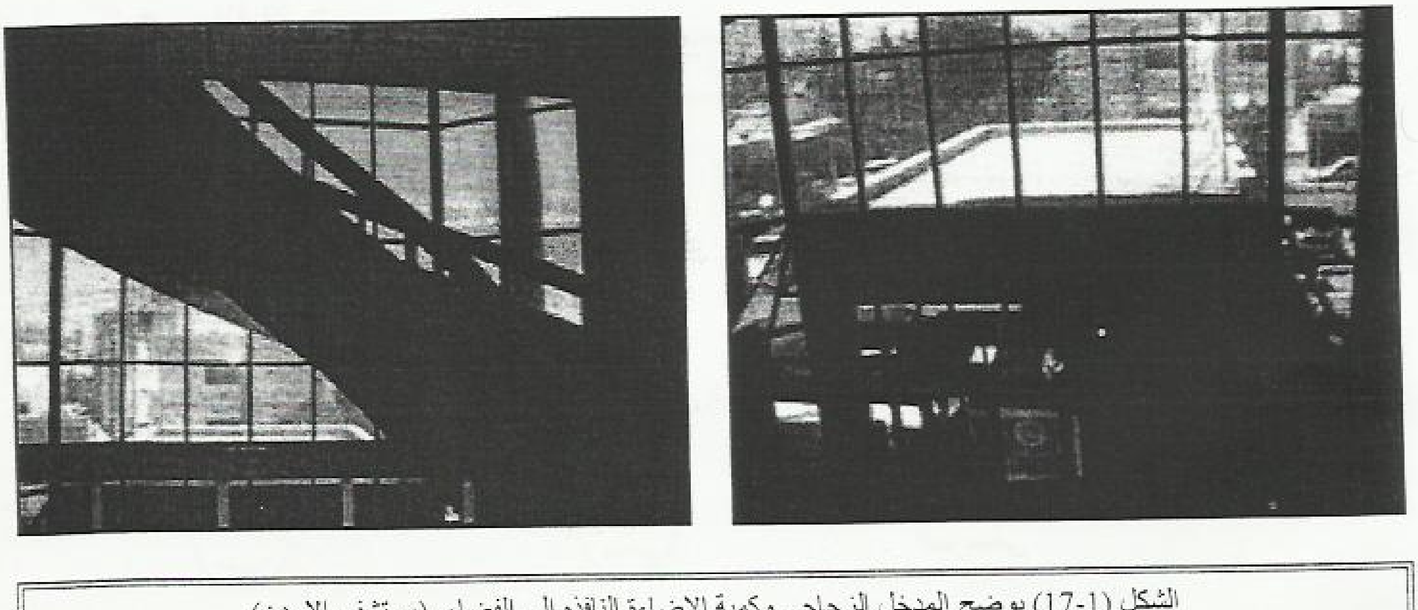

الشكل (1-17) يوضح المدخل الزجاجي وكمية الاضاءة النافذه الى الفضاء. (مستشفى الاردن)

ملحق رقم (1)

استمارة استبيان الاطفال

جامعة بغداد/كلية الهندسة

قسم الهندسة المعمارية

الدراسات العليا /ماجستير

الى الاطفال واهاليهم الاعزاء

تقوم الباحثة باعداد رسالتها الموسومة (الادراك الحسي للفضاء الداخلي في مستشفيات الاطفال)

لون وارسم حول الذي تره يطابق حالتك

1.المعلومات العامة

- الجنس :  ذكر  انثى
- العمر : 6 ، 7 ، 8 ، 9 ، 10
- التردد على المستشفى : اول مرة ☐ اكثر من مرة ☐
- مهنة الام :
- مهنة الاب:
- نوع المريض: مريض خارجي ☐ مريض مقيم ☐

2.المثيرات الحسية

1.المثيرات السمعية

- احب وجود الاصوات التالية في المستشفى:

  الموسيقى

الاشجار

الطيور

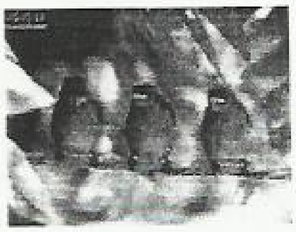

المياه

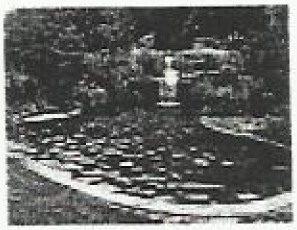

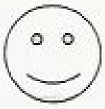

- لااحب وجود الاصوات التالية في المستشفى:

بكاء الاطفال

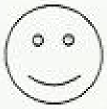

صوت الاجهزة

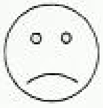

صوت حركة
العربات والاسرة

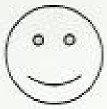

2. مثيرات الشم

- احب وجود رائحة :

الزهور

روائح التعقيم

3. مثيرات البصر

اولاً:الاضاءة

- تريحنى انارة غرفتى

- جميلة انارة غرفة اللعب

ثانياً:اللون

- احب الالوان في المستشفى

- اتذكر الالوان التالية في المستشفى:

الاحمر , الاصفر , الازرق , الاخضر
الوردي , الابيض , البرتقالي , البنفسجي

- احب ان يكون لون غرفتي في المستشفى:

الاحمر , الاصفر , الازرق , الاخضر
الوردي , الابيض , البرتقالي , البنفسجي

ثالثاً:الاعمال الفنية في المستشفى:

- احب الشخصيات الكارتونية المرسومة على جدران غرفتي في المستشفى



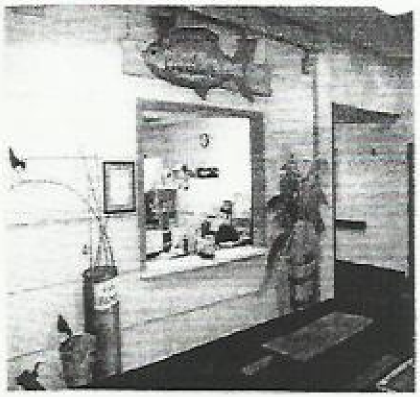

رابعا:الطبيعية الخارجية والنباتات الداخلية:

- يفرحنى النظر من نافذة غرفتى



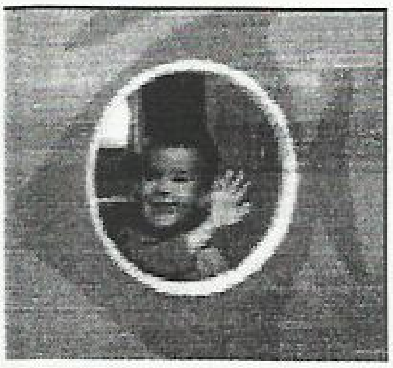

خامساً:الرموز والاشارات:

- احب الاشارات الموجوده في ممرات المستشفى


3. مرتاح في الاقامة في هذه المستشفى


ملحق رقم(2)

استمارة استبيان الكادر الطبي

جامعة بغداد/كلية الهندسة

قسم الهندسة المعمارية

الدراسات العليا /ماجستير

تقوم الباحثة باعداد رسالتها الموسومة (الادراك الحسي للفضاء الداخلي في مستشفيات الاطفال) كجزء من متطلبات درجة الماجستير لذا نرجو تعاونكم بملء هذه الاستمارة وان تكون الاجابات عن هذه الاسئلة محددة ودقيقة قدر الامكان وشكرا

1.المعلومات العامة

- الجنس : ☐ ذكر ☐ انثى
- العمر : ☐ اقل من 20 ☐ 20-40 ☐ من 41 فما فوق
- المهنة:
- فترة العمل ☐ اقل من 3 اشهر
  ☐ 3 اشهر الى السنة
  ☐ سنة فما فوق

2.المثيرات الحسية

1.المثيرات السمعية

- هل وجدت ان الاصوات التالية سببت الازعاج للطفل

☐ نعم ☐ لا صوت المرضى المراجعين

☐ نعم ☐ لا صوت الاجهزة

☐ نعم ☐ لا صوت حركة العربات والاسرة

☐ نعم ☐ لا صوت بكاء الاطفال

- اي الاصوات الاتية كانت اكثر تقليلاً من مخاوف الطفل

☐ صوت الموسيقى الهادئ

☐ صوت الاشجار

☐ صوت العصافير

☐ صوت المياه المتساقطة

2. مثيرات الشم

- هل يؤثر الروائح على نفسية الطفل

☐ نعم ☐ لا

3. مثيرات البصر

اولاً:الاضاءة

- هل يؤثر الضوء الطبيعي على نفسية الطفل

☐ نعم ☐ لا

- هل يؤثر الضوء الاصطناعي على نفسية الطفل

☐ نعم ☐ لا

ثانياً:اللون

- هل يؤثر تنوع الالوان في ممرات ومحجرات وابواب المستشفى على الطفل

☐ نعم ☐ لا

ثالثاً:العمل الفني في المستشفى:

- هل يؤثر استخدام التعابير البصرية التالية في تقليل مخاوف الطفل:

☐ نعم ☐ لا مواد مجسمة قابلة للمس

☐ نعم ☐ لا صور جدارية

رابعا:التواصل مع الطبيعية:

- اي المؤشرات التالية اكثر تأثيراً على نفسية الطفل

☐ نافورة ماء

☐ نبات وزروعات

☐ وجود اطلالة على الخارج

خامساً:الاشارات والرموز:

- هل توثر الاشارات الموجودة في ايجاد الطريق بين غرفة اللعب وغرفة اقامته

☐ نعم ☐ لا

- ماهي الوسائل التي يفضلها الطفل في ايجاد طريقه

☐ سؤال الكادر العامل في المستشفى

☐ استخدام بعض الرسوم والاعمال الفنية

☐ استخدام الاشرطة الملونة

☐ اختلاف الالوان والتدرج فيها

☐ استخدام الاضاءة الموجهة للاستدال على الطريق

3. هل يجد الطفل البيئة الداخلية للمستشفى مثيره

☐ نعم ☐ لا